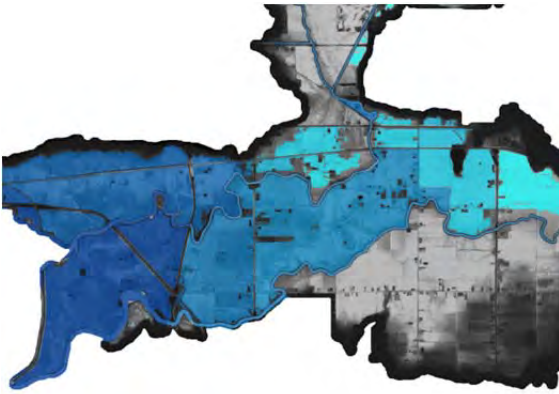




## SERPENTINE & NICOMEKL RIVER CLIMATE CHANGE FLOODPLAIN REVIEW PHASE 2

### FINAL DRAFT REPORT



Prepared for:



Surrey, British Columbia



6 March 2015

NHC Ref. No. 300319

**SERPENTINE & NICOMEKL RIVERS  
CLIMATE CHANGE FLOODPLAIN REVIEW - PHASE 2**

**FINAL DRAFT REPORT**

Prepared for:

**City of Surrey**  
Surrey, British Columbia

Prepared by:

**Northwest Hydraulic Consultants Ltd.**  
North Vancouver, British Columbia

6 March 2015

NHC Ref No. 300319

**Prepared by:**

Vanessa O'Connor, PEng.  
Hydrotechnical Engineer

Patty Dillon, PE  
Hydrologic Engineer

**Reviewed by:**

Monica Mannerström, PEng.  
Principal

Malcolm Leytham, PEng.  
Principal

**DISCLAIMER**

This document has been prepared by Northwest Hydraulic Consultants Ltd. in accordance with generally accepted engineering practices and is intended for the exclusive use and benefit of the City of Surrey and their authorized representatives for specific application to the Serpentine & Nicomekl Rivers, Climate Change Floodplain Review – Phase 2 in Surrey, British Columbia, Canada. The contents of this document are not to be relied upon or used, in whole or in part, by or for the benefit of others without specific written authorization from Northwest Hydraulic Consultants Ltd. No other warranty, expressed or implied, is made.

Northwest Hydraulic Consultants Ltd. and its officers, directors, employees, and agents assume no responsibility for the reliance upon this document or any of its contents by any parties other than the City of Surrey.

## CREDITS AND ACKNOWLEDGEMENTS

The NHC team would like to thank the City of Surrey for initiating this study, making available extensive background information and providing advice and support through-out the study. Key City representatives were:

- Matthew Osler, PEng. Project Manager
- Carrie Baron, PEng. Drainage & Environment Manager

The following Northwest Hydraulic Consultants Ltd (NHC) personnel participated in the study:

- Monica Mannerström, PEng. Project Manager
- Vanessa O'Connor, PEng. Project Engineer – Hydraulic Modelling
- Sarah North, GISP GIS Specialist
- Malcolm Leytham, PhD., P.E. Senior Engineer – Hydrology & Review
- Patty Dillon, P.E. Senior Engineer – Hydrologic Modelling
- Vaughn Collins, P.E. Senior Engineer – Hydraulics
- Mariza Costa-Cabral, PhD. Climate Scientist
- David McLean, PEng., PhD. Specialist Input
- Clayton Hiles, PEng. Project Engineer – Ocean Modelling
- Jenna Paul Junior Engineer – Hydraulic Modelling

The following Thurber Engineering Ltd (TEL) personnel provided geotechnical sub-consultant services:

- David Smith, PEng. Senior Geotechnical Engineer

## EXECUTIVE SUMMARY

Inundation of the Serpentine/Nicomekl River floodplain is a complex function of: 1) the volume and temporal pattern of storm rainfall and the watershed’s hydrologic response; 2) the time varying sea level in Mud Bay coincident with a storm event; and, 3) the hydraulic response of the watersheds (comprising storage and various hydraulic infrastructure) to the hydrologic inputs and the sea level boundary condition. In the lower areas of the floodplain the most severe floods occur during winter storms when high ocean levels coincide with intense rainfall events. The joint probability of sea level and rainfall events cannot be characterized by direct statistical analysis. Therefore, a continuous simulation approach was adopted where long-term (approximately 50 year) simulations were conducted of the system’s hydraulic performance, and the simulated annual peak water levels were subject to conventional frequency analysis.

Phase 1 of the Climate Change Floodplain Review (NHC 2012) developed a scientifically defensible modelling approach to characterizing flood hazards under sea level rise and undertook a preliminary assessment of infrastructure vulnerability and flood risk from ocean and riverine sources. The current Phase 2 CCFR project refined and expanded on NHC’s previous study and incorporated climate change impacts on precipitation and recently updated subsidence estimates. In addition to the base year (2010) and year 2100, the modelling was extended to include years 2020, 2040, 2070 and 2200. Floodplain extents corresponding to estimated 200-year flood levels were evaluated for all modelling scenarios and preliminary vulnerability assessments were completed. Based on 2-dimensional modelling, water depths and flow velocities caused by select dike breaches were simulated.

### Coastal flooding

The Phase 2 coastal modelling calculated Designated Flood Levels, Flood Construction Levels and Dike Crest Elevations (DCEs) assuming that the coastal dikes remain as currently constructed. Also, the water level return period corresponding to the current dike crest elevations at nine locations for different time frames were estimated.

#### Return Period (Years) when dike crest levels will be exceeded:

Site	Location	DCE (m)	2010	2020	2040	2070	2100
1a	Colebrook - Serpentine	2.84	22	8	2	<1	<1
1b	Crescent Beach East	2.88	220	70	7	<1	<1
1c	Mud Bay - Serpentine	3.00	28	11	2	<1	<1
1d	Mud Bay - Nicomekl	2.98	350	110	10	<1	<1
2	Colebrook (Highway 99)	3.15	22	10	2	<1	<1
3	Crescent Beach North	2.90	2	1	<1	<1	<1
4	Crescent Beach South	3.30	70	22	3	<1	<1
5	BNSF Railway	3.20	7	3	<1	<1	<1
6	8 <sup>th</sup> Avenue at Campbell	2.30	4	1	<1	<1	<1

Most of the City's coastal dikes currently provide inadequate protection against flooding and immediate attention is required to reduce the risk of overtopping and breaching. With sea level rise, conditions are expected to continuously worsen. For 2010 conditions, the return period ranges from 2 to 350 years, with only two of the dikes meeting 200-year ocean level standards. Provincial guidelines have adopted a 1 m rise in sea level between 2010 and 2100 and assume the rate of rise will be linear during this period. Based on these assumptions, by year 2020, none of the dikes will meet the 200-year standard; by 2040, the return period event the dikes can withstand without overtopping will be less than 10 years; and, by 2070, it is expected that all dikes will be inundated multiple times per year. The dikes are not designed for overtopping and would likely fail if ocean waters washed over the crests or, potentially as soon as the dike freeboard is compromised.

Key recommendations are for first developing an emergency response plan and as soon as possible perform critical dike upgrades where most needed. A long-term flood management strategy for coastal flooding should also be developed. The plan will require assessment of the feasibility, costs and benefits of various coastal protection options such as: 1) improved diking; 2) coastal protection (jetties, breakwaters, beach nourishment and different edge treatments such as riprap and sheet piling); 3) introduction of adaptation measures to increase the resilience of affected areas; 4) introduction of landuse changes; or, 5) a combination of the options. Potential impacts of a tsunami generated flood wave should also be considered.

### **Precipitation, Runoff and Climate Change Impacts**

The Phase 2 hydrologic model reproduced observed calibration storm volumes within about 5% and event peaks within 10%. Some uncertainty continues to surround reported flows at WSC Station 08MH155, Nicomekl at 203<sup>rd</sup> Street.

Climate change is expected to affect precipitation, with winters generally becoming wetter but the number of wet days becoming fewer. A unique approach was developed to assess climate change impacts on future precipitation. Two alternative synthetic time series of hourly precipitation were developed to reflect a moderate and a severe climate change scenario based on downscaled results from Global Climate Models. The analyses suggest that at the 200-year return period level the moderate scenario may increase the daily precipitation by roughly 33% and the severe scenario by 50% over the period from 2010 to 2100. The projections reflect plausible representations of the future, given the best current scientific information, but do not represent specific predictions. As climate science improves, the estimates will need refinement.

### **Inland Flooding**

Phase 2 enhanced the HEC-RAS hydraulic model developed in Phase 1 and the model validations to the January 2014 and January 2013 flood events showed good agreement at most locations. Flood levels were output at 97 locations for the near 50 year simulation time period and annual peak levels were extracted for frequency analyses to estimate the 200-year flood level at each location.

The lower river reaches are more susceptible to flooding caused by increases in sea level than the upper reaches. The floodplain cells experiencing the largest increases in peak 200-year water levels are those connected to the river channels with spillways. The upper reaches are more sensitive to increases in runoff. Revised subsidence rates fall within the accuracy of modelling and were not assessed in detail.

In the lower floodplain (above the sea dams), the present 200-year flood level will have a return period of less than 2 years by year 2100. In the upper Nicomekl and upper Serpentine reaches, the present 200-year flood level will have a return period of roughly 75 years in year 2100, assuming no changes in precipitation. With the estimated precipitation increases corresponding to a moderate or severe climate change scenario, the present 200-year water level would occur on average every 5 to 10 years.

The vulnerability assessment of the sea dams, dikes, bridges, roads and railroads indicated that at the present 200-year flood condition, freeboard would be compromised at the Serpentine Sea Dam; the Serpentine left bank dike downstream of the sea dam would be inundated and freeboard would be compromised at all of the lowland dikes; bridge decks would be inundated at three of the bridges and the low chords submerged at nine other bridges; a portion of Highway 99 would be inundated and freeboard compromised at Colebrook Road, with a few sections of railroad having compromised freeboard as well. Infrastructure upgrades are clearly required for current flood conditions.

In 2100 at the 200-year flood, ignoring potential precipitation increases, both the Serpentine and Nicomekl Sea Dams would be inundated; the lowland dikes upstream and downstream of the sea dams would also be inundated and nearly all other dikes would have compromised freeboard; the bridge decks would be inundated at seven bridges and the low chords submerged at 10 other bridges; major roads would have either compromised freeboard or some degree of inundation, similarly railroads.

The US Corps' RAS2D software was used for an initial assessment of flood depths and velocities following a dike breach. The impacts of breaches were last modelled 30 years ago and did not include any SLR projections. Results are sensitive to the selected breach locations, adopted parameters and water levels. The breach modelling simulated: 1) a storm induced failure of coastal dikes under 2010 and 2100 conditions; 2) a future seismic failure of an inland dike; and, 3) conditions following failure of the sea-dams. Sea dike failures produced flow velocities in the order of 4-5 m/s at the breach, dropping to 1.5 – 2.5 m/s on the floodplain. At present conditions, breaches could potentially result in some loss of life and extensive damage, whereas future breaches would be catastrophic with flood depths reaching over 3 m in some locations. Based on the particular inland seismic breach modelled during typical winter conditions (the Coast Meridian dike) inundation depths and velocities were moderate. However, impacts of a seismic breach occurring during a period with high river level are anticipated to be severe. The post sea-dam scenario modelled, reflecting moderate tidal conditions in 2008 to 2010, did not result in dike overtopping but freeboard was compromised in several locations. It is anticipated that impacts would have been more severe under higher tide conditions. The greatest impact of the sea dam failure will be the upstream migration of salt water which will impact the ability to irrigate agricultural lands. Further breach modelling is required to better understand the impacts to the City's many valuable assets in the at risk areas.

With the steep rise in topography bordering the near horizontal floodplain, inundation extents for the different model scenarios showed relatively minor variation. Year 2100, in combination with a severe precipitation scenario, had the largest increase in floodplain compared to present conditions, showing a total area increase of 25% (with main expansions in floodplain south of the Erickson and Burrows pump stations and by the Latimer and Bear Creek tributaries).

The City's current flood construction levels (FCLs) are based on design water levels computed by KPA (1994). Considering the different approaches adopted for the present modelling, simulated 200-year flood levels plus freeboard were expected to vary from the FCLs. In general, the CCFR Phase 2 flood levels for both 2010 and 2100 are lower than KPA levels in the floodplain storage cells but higher where flood levels are directly influenced by the ocean and in some of the upper river reaches as well. There is a need for updating the FCLs but further refinement of the model is necessary before developing official floodplain maps and setting FCLs.

The current work focussed on year 2010 and 2100 flood conditions. Tentative projections were made for year 2200 flood conditions; however, the associated climate change projections are highly uncertain.

Recommendations were developed for collecting additional information to improve the performance of the hydrologic and hydraulic models and for developing a long-term flood management strategy. The strategy must be flexible and allow for adjustment based on the observations of actual changes to sea levels, runoff, subsidence and land use. Development of the strategy will involve assessing the status of the existing flood protection and developing potential improvements, identifying flood hazards in more detail, and prioritizing upgrades based on sustainability, socio-economic and cost/benefit perspectives.



## TABLE OF CONTENTS

LIST OF TABLES.....	IX
LIST OF FIGURES.....	X
LIST OF MAPS.....	XI
<b>1 INTRODUCTION .....</b>	<b>1</b>
1.1 Background.....	1
1.2 Scope of Work .....	3
1.3 Project Goals and Objectives.....	3
1.4 Report Organization .....	5
<b>2 OCEAN LEVEL ANALYSIS .....</b>	<b>7</b>
2.1 Introduction.....	7
2.2 Ocean Level Analysis.....	7
2.2.1 Designated Flood Levels .....	7
2.2.2 Relative Sea Level Rise.....	8
2.2.3 Dike Geometry.....	8
2.2.4 Wave Conditions.....	9
2.2.5 Dike Crest Elevation.....	10
2.3 Frequency Analysis .....	11
2.3.1 Return Periods Associated with Current Dike Crest Elevations .....	11
2.3.2 Return Periods Associated with Current 200 Year Event .....	13
2.4 Coastal Flood Mitigation.....	14
<b>3 HYDROLOGIC MODELLING .....</b>	<b>16</b>
3.1 HSPF Model Refinement.....	16
3.2 HSPF Model Calibration.....	21
3.2.1 Review of Nicomekl at 203 Street Gauge Record.....	22
3.2.2 Calibration Adjustments and Results .....	26
3.3 Climate Change Precipitation Scenarios.....	31
3.3.1 Methodology for Developing Future Precipitation Time Series.....	32
3.3.2 Uncertainty in Future Precipitation Projections.....	33
3.4 HSPF Long-Term Simulations.....	33
<b>4 HYDRAULIC MODELLING .....</b>	<b>35</b>
4.1 Purpose of Hydraulic Modelling .....	35
4.2 HEC-RAS Model Enhancements.....	35
4.2.1 Model Geometry .....	35
4.2.2 Model Inflows and Water Level Boundaries .....	38
4.3 Model Validation .....	38
4.3.1 January 2014 Flood.....	39
4.3.2 January 2013 Flood.....	42
4.4 Sensitivity Analysis.....	44
4.4.1 Model Roughness Coefficients .....	44
4.4.2 Inflow Values .....	44
4.5 HEC-RAS Model Simulations.....	47

4.5.1	Run 1: Simulation of Present (2010) Conditions .....	49
4.5.2	Run 2, 3, and 4: Simulation of Intermediate Future (2020, 2040, and 2070) Conditions with Sea Level Rise .....	49
4.5.3	Run 5: Simulation of Projected Future (2100) Conditions with Sea Level Rise .....	49
4.5.4	Run 6 and 7: Simulation of Projected Future (2100) Conditions with Changes in Precipitation... ..	49
4.5.5	Run 8: Simulation of Projected Future (2100) Conditions with Subsidence .....	50
4.5.6	Run 9: Simulation of Projected Future (2200) Conditions with Sea Level Rise .....	50
4.6	Model Limitations.....	50
5	VULNERABILITY ASSESSMENT .....	52
5.1	200-year Flood Levels.....	52
5.1.1	Inputs to Frequency Analyses.....	52
5.1.2	Frequency Analysis Results.....	56
5.2	Flood Construction Levels .....	67
5.3	Floodplain Extents .....	70
5.4	Vulnerable Infrastructure .....	72
5.5	System Capacity.....	76
6	DIKE BREACH MODELLING .....	79
6.1	Breach Mechanisms.....	79
6.2	Model Selection .....	79
6.3	Model Development.....	79
6.4	Model Calibration and Validation.....	80
6.5	2D Model Runs .....	80
6.5.1	Coastal Dike Breach, 2010 (Run 10) .....	82
6.5.2	Coastal Dike Breach, 2100 (Run 11) .....	85
6.5.3	Seismic Inland Dike Failure (Run 12) .....	88
6.5.4	Post Sea Dam Failure (Run 13) .....	91
6.6	Breach Flood Levels .....	93
6.7	Breach Flood Hazard.....	95
7	SUMMARY AND CONCLUSIONS .....	99
7.1	Coastal Flooding .....	99
7.2	Precipitation, Runoff and Climate Change Impacts.....	99
7.3	Inland Flooding .....	100
7.3.1	Hydraulic Modelling.....	100
7.3.2	Frequency Analyses .....	100
7.3.3	Vulnerabilities.....	101
7.3.4	Dike Breaches .....	101
7.3.5	Flood Extents and FCLs .....	101
8	RECOMMENDATIONS.....	103
8.1	Recommendations for Developing a Flood Management Plan.....	103
8.1.1	Coastal Flooding .....	103
8.1.2	Precipitation, Run-off and Climate Change Impacts .....	103
8.1.3	Inland Flooding .....	104
8.2	Recommendations for Modelling .....	105
9	REFERENCES .....	107

APPENDIX A	GIS Data Table
APPENDIX B	Ocean Analysis
APPENDIX C	Hydrologic Analysis Report: Two 21 <sup>st</sup> Century scenarios of hourly precipitation for City of Surrey, BC.
APPENDIX D	Hydraulic Analysis Validation, comparison plots of modelled and observed water levels January 2014 and January 2013 Sensitivity analysis , longitudinal profiles of peak water levels Q $\pm$ 10% and n $\pm$ 20%
APPENDIX E	Frequency Analysis Boundary conditions, selected timeseries of ocean levels and rainfall Frequency distribution plots Run 1 to Run 5 Run 5 to Run 9
APPENDIX F	Vulnerability Analysis Vulnerability Figures Bridges, Run 1 to Run 5 Dikes, Run 1 to Run 5 Rail Lines, Run 1 to Run 5 Major Roads, Run 1 to Run 5
APPENDIX G	Dike Breach Analysis Water Surface Elevations Run 10, Run 11, Run 12

## LIST OF TABLES

Table 1. DFL corresponding to a 200-year combined tide and storm event. ....	8
Table 2. SLR and subsidence rates at each coastal location. ....	8
Table 3. Current maximum elevations of dike crests as per 2010 LIDAR Survey. ....	9
Table 4. DFL and storm runoff for each coastal location for selected years from 2010 to 2100.....	10
Table 5. Summary of DCE values for selected years 2010 – 2100. ....	11
Table 6. Total water level return periods (years) associated with the current DCE for selected years from 2010 to 2100.....	12
Table 7. Return periods (years) associated with the 2010 DFL for selected years from 2010 to 2100.....	14
Table 8. HSPF drainage area summary. ....	18
Table 9. Discharge Calibration Gauges .....	22
Table 10. Calibration event summary.....	26
Table 11. Summary HSPF model calibration results. ....	30
Table 12. Precipitation exceedance frequency comparison.....	33
Table 13. Agreement between maximum observed and modelled peak water levels (Jan 2014).....	40
Table 14. Agreement between maximum observed and modelled river water levels (Jan 2013).....	43
Table 15. Model sensitivity to changes in bed roughness. ....	44
Table 16. Model sensitivity to changes in inflow hydrographs. ....	45
Table 17. Floodplain cell sensitivity to changes in inflow hydrographs.....	46
Table 18. List of hydraulic model simulations.....	48
Table 19. 200 year flood extents area. ....	71
Table 20. Summary of system capacity for year 2010. ....	77
Table 21. Summary of breach scenarios .....	81
Table 22. Summary of breach parameters .....	81
Table 23. Maximum modelled water levels and velocities at Nicomekl and Serpentine bridges. ....	92
Table 24. Flood hazard ratings (source: UK DEFRA/EA 2006).....	95

## LIST OF FIGURES

Figure 1. Study area. ....	2
Figure 2. Approximate projected annual subsidence isolines. ....	5
Figure 3. Return period of total water level associated with current DCEs.....	12
Figure 4. DCE for existing, 2010, and 2100 scenario using joint probability approach. ....	13
Figure 5. Drainage areas, storage cells and flow input for simplified hydraulic model.....	17
Figure 6. Existing land use for Serpentine and Nicomekl river basins. ....	20
Figure 7. Projected future land use for Serpentine and Nicomekl river basins.....	20
Figure 8. Surficial geology for Serpentine and Nicomekl river basins. ....	21
Figure 9. Hydrometric stations used for hydrologic model development and calibration.....	22
Figure 10. Stage-discharge measurements and rating curves, Nicomekl River at 203 Street.....	23
Figure 11. Stage-area measurements, Nicomekl River at 203 Street.....	24
Figure 12. Stage-velocity measurements, Nicomekl River at 203 Street.....	25
Figure 13. HSPF precipitation zones .....	27
Figure 14. Simulated vs. gauged flows for Nicomekl River at 203 St, January 2013 and January 2014. Observed flow is shown in red, simulated flow in blue, and Surrey Municipal Hall precipitation in green on the upper axis. ....	28
Figure 15. Flow frequency comparison for Upper Nicomekl River.....	34
Figure 16. Model reaches extended using 2014 survey data or MIKE11 cross-sections.....	37
Figure 17. Observed (red) and modelled (blue) discharge (m <sup>3</sup> /s) at the Nicomekl sea dam for January 1 to 17, 2014. ....	40
Figure 18. Model key output locations .....	53
Figure 19. Serpentine River (sea dams = 0 km), longitudinal profiles of peak water levels from various types of events for Run1, year 2010.....	54
Figure 20. Top ranking events for Run 1 (year 2010).....	55
Figure 21. Longitudinal profiles of 200-year water levels for Serpentine River for years 2010 to 2100....	57
Figure 22. Longitudinal profiles of 200-year water levels for Nicomekl River for years 2010 to 2100. ....	58
Figure 23. Increase in 200 year floodplain water levels from 2010 to 2100 (Run 5 – Run 1).....	59
Figure 24. Frequency distributions (Runs 5 to 9) for Nicomekl River immediately upstream of sea dam. 61	
Figure 25. Frequency distributions (Run 5 to 9) for Serpentine River 17 km upstream of sea dam. ....	62
Figure 26. Frequency distributions (Run 5 to 9) for Bear Creek at a distance of 3850 m upstream from East Newton pump station. ....	63
Figure 27. Longitudinal profiles of 200-year water levels for Serpentine River for year 2100 (Run5 to Run 9).....	64
Figure 28. Longitudinal profiles of 200-year water levels for Nicomekl River for year 2100 (Run5 to Run 9).....	65
Figure 29. Sensitivity of 200 year water levels in 2100 to changes in precipitation (severe precipitation scenario) (Run 7 - Run 5). ....	66
Figure 30. Modelled 200-year flood levels for year 2010 (Run 1), year 2100 (Run 5) and KPA levels. ....	68
Figure 31. Modelled 200-year flood levels for year 2200 (Run 9) and KPA levels.....	69
Figure 32. Areas where floodplain extents change due to climate change.....	72

Figure 33. Vulnerability of dikes (current dike design elevations) to 2010 200-year water levels. .... 74

Figure 34. Vulnerability of dikes (current dike design elevations) to 2020 200-year water levels. .... 74

Figure 35. Vulnerability of dikes (current dike design elevations) to 2040 200-year water levels. .... 75

Figure 36. Vulnerability of dikes (current dike design elevations) to 2070 200-year water levels. .... 75

Figure 37. Vulnerability of dikes (current dike design elevations) to 2100 200-year water levels. .... 76

Figure 38. Maximum modelled flood depths from coastal dike breaches (Run 10). .... 83

Figure 39. Maximum modelled water levels from coastal dike breaches (Run 10). .... 84

Figure 40. Maximum modelled flow velocities from coastal dike breaches (Run 10). .... 85

Figure 41. Maximum modelled flood depths from coastal dike breaches (Run 11). .... 86

Figure 42. Maximum modelled water levels from coastal dike breaches (Run 11). .... 87

Figure 43. Maximum modelled flow velocities from coastal dike breaches (Run 11). .... 88

Figure 44. Maximum modelled flood depths from coastal dike breaches (Run 12). .... 89

Figure 45. Maximum modelled water levels from coastal dike breaches (Run 12). .... 90

Figure 46. Maximum modelled flow velocities from coastal dike breaches (Run 12). .... 91

Figure 47. Modelled 200-year flood levels for year 2100 (Run 11) and KPA levels. .... 94

Figure 48. Flood hazard mapping for coastal dike breaches (Run 10). .... 96

Figure 49. Flood hazard mapping for coastal dike breaches (Run 11). .... 97

Figure 50. Flood hazard mapping for inland seismic dike failure (Run 12). .... 98

## LIST OF MAPS

- Map 1. Hydraulic Model Overview Map
- Map 2. Flood Extents Including Freeboard – Year 2010 Design Levels (Run 1)
- Map 3. Flood Extents Including Freeboard – Year 2100 Design Levels, SLR 0.97 m (Run 5)
- Map 4. Flood Extents Including Freeboard – Year 2100 Severe Precipitation, SLR 0.97 m (Run 7)
- Map 5. Flood Extents Including Freeboard – Year 2200 Design Levels, SLR 1.97 m (Run 9)

# 1 INTRODUCTION

## 1.1 Background

In 2012, Northwest Hydraulic Consultants Ltd. (NHC) completed an initial Climate Change Floodplain Review (Phase 1 CCFR) for the City of Surrey (City), assessing potential flooding and infrastructure vulnerability along the Serpentine and Nicomekl Rivers and in Mud Bay, resulting from projected local climate change. This previous work developed a scientifically defensible modelling approach to characterizing flood hazards under sea level rise and climate change, and undertook a preliminary assessment of infrastructure vulnerability and flood risk from ocean and riverine sources. The current Phase 2 CCFR work described in this report, refined and expanded on NHC's previous study and incorporated the findings of work conducted by others since the initial study.

Figure 1 shows a map of the study area and the surrounding region. Potential flood hazards in the Serpentine-Nicomekl system are:

- Floods generated from upland runoff;
- Interior flooding behind dikes due to local precipitation;
- Interior flooding resulting from lack of outflow during times when the sea dams are closed due to high ocean levels;
- Interior flooding caused by breaching of the river dikes (seismic);
- Breaching of the sea dikes along Mud Bay during extreme high water conditions (high tide, storm surge and wave runup); and,
- Breaching of the sea dikes along Mud Bay due to seismic events or tsunami waves.

NHC (2012) contains a summary of historic flood events.

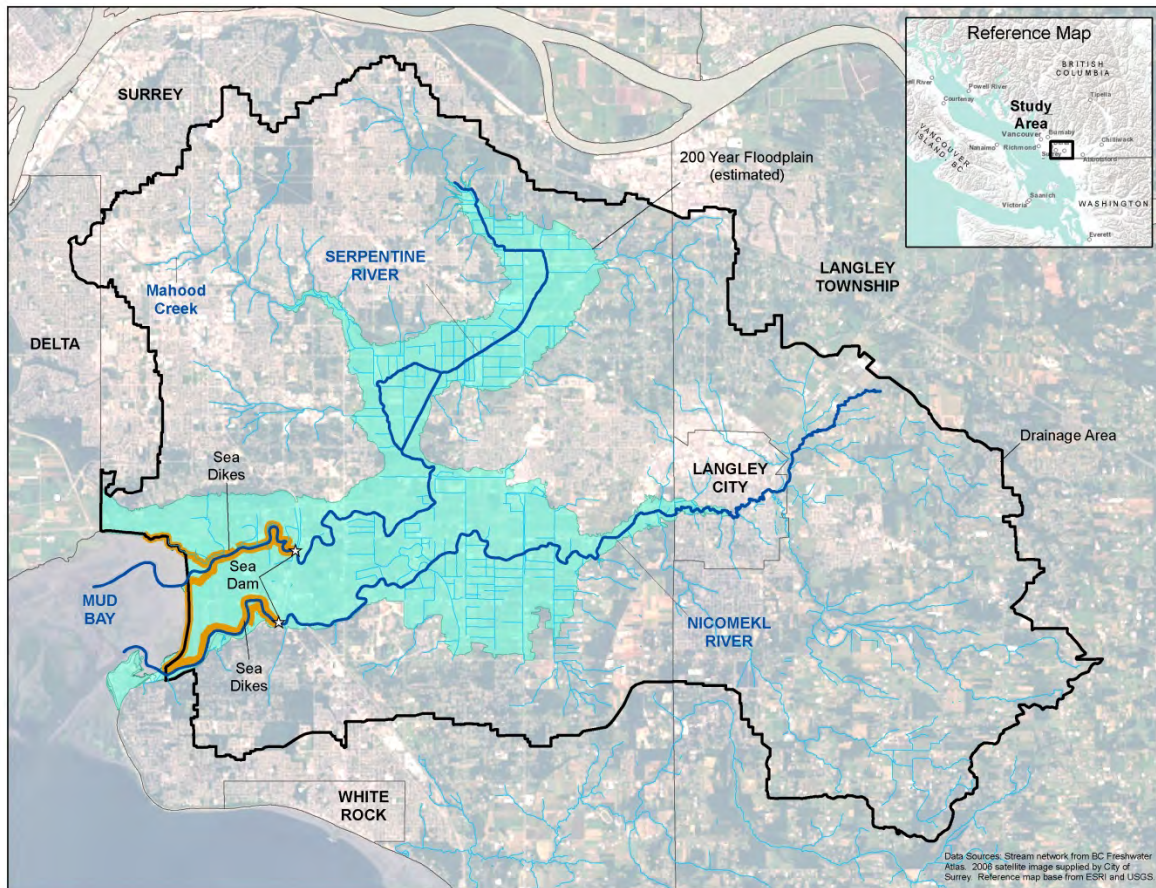


**Figure 1. Study area.**

For the Serpentine/Nicomekl River floodplain, inundation is a complex function of:

- The volume and temporal pattern of storm rainfall and the watershed’s hydrologic response to rainfall;
- The time varying sea level in Mud Bay coincident with the storm event; and,
- The hydraulic response of the system (comprising storage and various hydraulic infrastructure) to the hydrologic inputs and the sea level boundary condition.

This complex system is not amenable to direct statistical analysis; i.e. it is not possible to state a priori with any reasonable confidence what combination of tidal conditions and storm rainfall event will result in peak floodplain inundation with an annual exceedance probability (AEP) of 0.5%, equivalent to a return period of 200-years.



To avoid the difficulties of a direct statistical approach to joint probability analysis, a continuous simulation approach was adopted where long-term (approximately 50 year) simulations were conducted of the system's hydraulic performance, and the simulated annual peak floodplain water levels were subject to conventional frequency analysis. Details of the approach are outlined in NHC 2012.

Some key assumptions of the approach are that:

- The joint occurrence of extreme sea levels and severe rainfall contained in the historic record will be maintained in the future; and,
- Future sea level time series can be adequately constructed by simply increasing all water levels by a uniform amount and scaling storm surges contained in the historic record.

## 1.2 Scope of Work

As per the City of Surrey (City) terms of reference, the scope of services for the Phase 2 CCFR comprised:

- Review of past work and new data available;
- Phase 1 CCFR enhancements;
- Dam and dike breach assessments for 2010 and 2100 scenarios;
- Analysis of climate change impacts;
- Preparation of a summary report;
- Data exchange; and,
- Overall project management.

## 1.3 Project Goals and Objectives

To improve the assessment of climate change impacts on the Serpentine-Nicomekl River floodplains up to year 2100 (with a cursory review of conditions in 2200), the Phase 1 ocean, hydrologic and hydraulic models needed to be refined. Some of these refinements included adjusting model parameters and geometries, further assessing the impacts of subsidence rates, looking at the sensitivity to changes in rainfall, improving the hydraulic model calibration, establishing flood levels and flow velocities caused by dike breaches and assessing infrastructure vulnerabilities at various milestones over the next 90 years. The results are intended to provide a framework for future policy

and design standard development within the flood prone area. Specific goals and objectives included:

1. Refine the Phase 1 CCFR models by including more detailed information. Significantly more detailed spatial data was compiled for Phase 2 and is documented in Appendix A. The spatial data categories included:
  - Hydrology
  - Flood model inputs
  - Flood model inputs specific to infrastructure
  - Base mapping
  - Flood mapping results
  - Flood mapping results – vulnerable infrastructure
2. Refine subsidence estimates based on TEL (2014) results. Subsidence varies significantly with location and TEL developed an approximate isoline map (Figure 2) which showed an average subsidence rate of 1mm/year for the floodplain or half of the value assumed for Phase 1.
3. Expand ocean level modelling to include years 2020, 2040, 2070 and 2200.
4. Assess potential increases in precipitation by year 2100 due to climate change. A moderate and a severe climate change scenario was selected and corresponding long-term hourly precipitation time series generated to be used in the hydrologic model and produce inflows for the hydraulic model.
5. Improve the hydrologic and hydraulic model calibrations/ validations and rerun the models to assess impacts of present and projected future flood conditions on the lands upstream and downstream of the sea dams.
6. Determine floodplain extents/zones of influence from the estimated 200-year flood levels.
7. Assess vulnerabilities and their critical timing throughout the 21st century to determine the order of anticipated impacts.
8. Based on 2-dimensional modelling, assess water depths and flow velocities caused by various dike breaches and overtopping scenarios. A number of possible dike breach combinations could occur during a flood/seismic event. KPA (1994) outlined a variety of sea and river dike breach scenarios that were adopted for the modelling.

Although Phase 2 reflects significant improvements in modelling, it is expected that future refinements will be necessary. Given the uncertainty in climate change projections, the City will

need to further adjust the model configurations, boundary conditions and model parameters based on future observations and new research on climate change projections as they become available. Also, as the City upgrades flood control infrastructure, additional changes or enhancements will need to be made to the models.

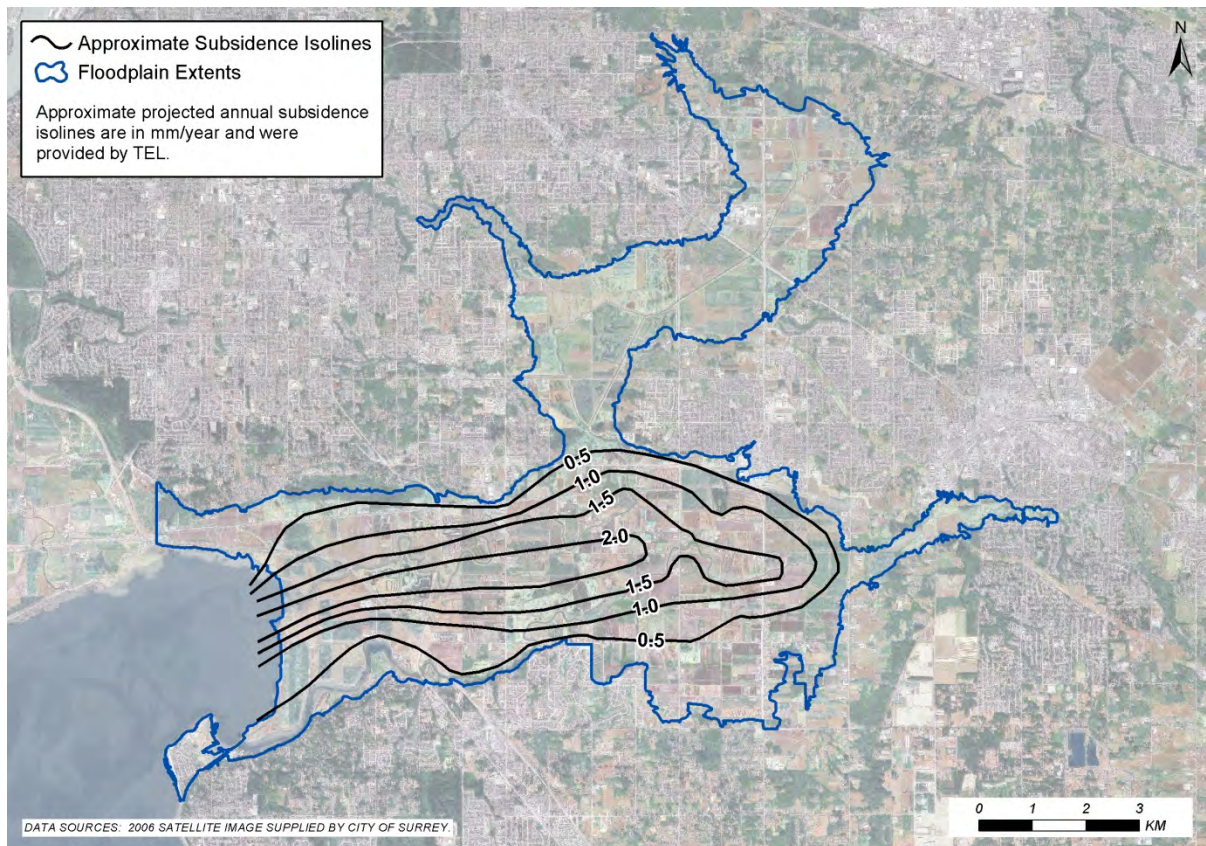


**Figure 2. Approximate projected annual subsidence isolines.**

## 1.4 Report Organization

In addition to this introductory Section 1, Section 2 provides a description of the ocean level analysis. The hydrologic and hydraulic modelling is outlined in Sections 3 and 4 while Section 5 includes the anticipated flood level increases and the vulnerability assessment. The dike breach modelling is detailed in Section 6 followed by conclusions and recommendations in Section 7. Suggested further investigations are described in Section 8, followed by references.

Five appendices are contained in the report:

- Appendix A lists available background information and data;

- Appendix B contains coastal analysis results;
- Appendix C supplements the hydrologic work;
- Appendix D provides graphical output from the hydraulic modelling;
- Appendix E contains frequency analysis output;
- Appendix F contains vulnerability figures and flood extent maps; and,
- Appendix G contains breach modelling output.

## 2 OCEAN LEVEL ANALYSIS

### 2.1 Introduction

The Phase 2 ocean level analysis built on the Phase 1 findings and this Section documents the additional analyses undertaken.

The Phase 1 Designated Flood Level (DFL), Flood Construction Level (FCL) and Dike Crest Elevation (DCE) were calculated at nine locations along Surrey's shorelines for 2010 and 2100. The calculations were based on a 50 year hind-cast of water levels in the area, storm wave conditions, expected sea level rise and subsidence. The water level hind-cast was also used to provide boundary conditions to the Serpentine and Nicomekl hydraulic model.

Phase 2 expanded on Phase 1 with the following deliverables:

- Calculation of DFL, FCL and DCE for years 2020, 2040 and 2070 assuming that the dikes remain as currently constructed.
- The water level return period corresponding to the current dike crest elevation at each of the nine coastal locations for current (2010) conditions and for the years 2020, 2040, 2070 and 2100 (with their expected relative sea level rise).
- The return period associated with the current (2010) 200-year DFL to show how the probability of occurrence of the water level associated with the current 200-year DFL increases with time due to projected sea level rise.

### 2.2 Ocean Level Analysis

Calculating DCE requires information about the Designated Flood Level, relative sea level rise (RSLR), storm wave conditions and the dike geometry.

#### 2.2.1 Designated Flood Levels

Designated Flood Levels (DFL) were calculated during Phase 1 based on the extreme value analysis of a synthesised time-series of water levels (including effects of tides, storm surge and local wind setup). The Phase 1 DFLs corresponding to the 200 year combined water level event are listed in Table 1 and are unchanged for Phase 2 (see Phase 1 report for details).

**Table 1. DFL corresponding to a 200-year combined tide and storm event.**

Site	Location	DFL (m)
1a	Colebrook - Serpentine	2.94
1b	Crescent Beach East	2.70
1c	Mud Bay - Serpentine	2.94
1d	Mud Bay - Nicomekl	2.70
2	Colebrook (Highway 99)	2.94
3	Crescent Beach North	2.70
4	Crescent Beach South	2.70
5	BNSF Railway	2.94
6	8 <sup>th</sup> Avenue at Campbell	2.58

### 2.2.2 Relative Sea Level Rise

For Phase 2, Relative Sea Level Rise (RSLR) was calculated at each site based on a Eustatic Sea Level Rise (SLR) of 0.01 m/year and newly available site specific estimates of subsidence from TEL (2014). The figure provided by Thurber was interpreted to estimate the subsidence rates at each of the coastal locations as shown in Table 2.

**Table 2. SLR and subsidence rates at each coastal location.**

Site	Location	Eustatic SLR (mm/yr)	Subsidence (mm/yr)	Combined RSLR (mm/yr)
1a	Colebrook - Serpentine	10	2.0	12.0
1b	Crescent Beach East	10	0.0	10.0
1c	Mud Bay - Serpentine	10	2.0	12.0
1d	Mud Bay - Nicomekl	10	0.5	10.5
2	Colebrook (Highway 99)	10	0.0	10.0
3	Crescent Beach North	10	0.0	10.0
4	Crescent Beach South	10	0.0	10.0
5	BNSF Railway	10	2.0	12.0
6	8 <sup>th</sup> Avenue at Campbell	10	0.0	10.0

### 2.2.3 Dike Geometry

Dike geometry is required to calculate the wave runup on each dike. In Phase 1, the geometry of each dike was idealized from a dike cross section extracted from high density LIDAR data. The maximum elevation (per cross-section) of the current dikes at each of the selected dike locations is given in Table 3 (also refer to Appendix B).

**Table 3. Current maximum elevations of dike crests as per 2010 LIDAR Survey.**

Site	Location	Dike Elevation (m)
1a	Colebrook - Serpentine	2.84
1b	Crescent Beach East	2.88
1c	Mud Bay - Serpentine	3.00
1d	Mud Bay - Nicomekl	2.98
2	Colebrook (Highway 99)	3.15
3	Crescent Beach North	2.90
4	Crescent Beach South	3.30
5	BNSF Railway	3.20
6	8 <sup>th</sup> Avenue at Campbell	2.30

### 2.2.4 Wave Conditions

Wave conditions were estimated for 5 large storms using a numerical wave model forced by measured winds. Significant wave height, mean period and direction were output at the toe of each dike location. (For a discussion of the storm selection process and the numerical model see Phase 1 report.)

Because wave propagation is sensitive to water depth and because many of the sites are subsiding at different rates, each storm scenario had to be run many times (22 times to be specific) with different water depths to cover all possible scenarios.

The final runup calculations were completed using the PC-Overtopping software available through the European Overtopping Manual. This software requires as input the dike geometry, wave height, wave angle, and wave periods. The 2% storm runup values for each of the coastal locations for years 2010, 2020, 2040, 2070 and 2100 are listed in Table 4.

In many cases the still water level exceeded the crest of the dike resulting in inundation. Where the dike is inundated, runup cannot be calculated; these cases are indicated in Table 4 by a dash ('-'). Even in cases where inundation is not expected, overtopping is likely to occur. Where the sum of the DFL and the runup exceeds the existing dike elevation, significant overtopping is anticipated.

**Table 4. DFL and storm runup for each coastal location for selected years from 2010 to 2100.**

Site #	Existing Dike Elev.	2010		2020		2040		2070		2100	
		DFL	Runup	DFL	Runup	DFL	Runup	DFL	Runup	DFL	Runup
1a	2.84	2.94	-	3.06	-	3.30	-	3.66	-	4.02	-
1b	2.88	2.70	0.17	2.80	0.17	3.00	-	3.30	-	3.60	-
1c	3.00	2.94	0.33	3.06	-	3.30	-	3.66	-	4.02	-
1d	2.98	2.70	0.23	2.81	0.20	3.02	-	3.33	-	3.65	-
2	3.15	2.94	0.51	3.04	0.55	3.24	-	3.54	-	3.84	-
3	2.90	2.70	0.65	2.80	0.63	3.00	-	3.30	-	3.60	-
4	3.30	2.70	0.69	2.80	0.69	3.00	0.74	3.30	0.76	3.60	-
5	3.20	2.94	0.70	3.06	0.71	3.30	-	3.66	-	4.02	-
6	2.30	2.58	-	2.68	-	2.88	-	3.18	-	3.48	-

**Notes:**

1. All values are in metres.

### 2.2.5 Dike Crest Elevation

The Dike Crest Elevation is calculated as the sum of the RSLR, DFL, wave effect and freeboard (0.6m). The wave effect is typically taken as the 2% wave runup. The DCE elevation at each coastal location and each study year are listed in Table 5. It is assumed that the dikes remain as currently constructed through to 2100.

With present dike elevations, it is estimated that during the 200 year storm all sites save Crescent Beach South will be inundated by 2040, and all sites will be inundated by 2100. The fact that many of the dikes are inundated complicates the accounting of the wave effect.

Wave runup depends on both the wave characteristics and the geometry and surface of the dike. Where the dike is inundated, the runup cannot be calculated because there is no dry dike surface for the wave to runup on.

In Phase 1, the problem of dike inundation for the 2100 scenario was handled by arbitrarily raising the dike crests by 1.5m. Without a future dike design it is difficult to estimate what the appropriate wave effect and resulting DCE should be.

The Phase 2 terms of reference specified that, for consistency, the dikes would remain as constructed for DCE calculation in 2010, 2020, 2040, 2070 and 2100. In cases where the dike is inundated, the wave effect in the DCE calculation was taken as 70% of the significant wave height at the toe of the dike.

DCE results based on an inundated dike should be used with caution. The results shown here for year 2100 are in some cases significantly lower than the Phase 1 values and the reason for this is the different ways the dike inundation was handled. The '70% of the significant wave height' metric typically results in lower wave effect values than the 2% runup.



If the dikes were raised to prevent inundation by 2100, the dike crest elevations would likely need to be higher than the level specified in Table 5. For this reason the DCE results based on an inundated dike should be used with caution. However, it should also be noted that any modification of the dikes would necessitate re-evaluation of the wave runup.

**Table 5. Summary of DCE values for selected years 2010 – 2100.**

Site	Location	2010	2020	2040	2070	2100
1a	Colebrook - Serpentine	<b>3.74</b>	<b>3.87</b>	<b>4.12</b>	<b>4.47</b>	<b>4.84</b>
1b	Crescent Beach East	3.47	3.57	<b>3.79</b>	<b>4.09</b>	<b>4.40</b>
1c	Mud Bay - Serpentine	3.87	<b>3.83</b>	<b>4.06</b>	<b>4.41</b>	<b>4.80</b>
1d	Mud Bay - Nicomekl	3.53	3.61	<b>3.74</b>	<b>4.07</b>	<b>4.29</b>
2	Colebrook (Highway 99)	4.05	4.19	<b>4.54</b>	<b>4.89</b>	<b>4.96</b>
3	Crescent Beach North	3.95	4.03	<b>3.96</b>	<b>4.29</b>	<b>4.60</b>
4	Crescent Beach South	3.99	4.09	4.34	4.66	<b>5.18</b>
5	BNSF Railway	4.24	4.37	<b>4.46</b>	<b>4.85</b>	<b>5.24</b>
6	8 <sup>th</sup> Avenue at Campbell	<b>3.19</b>	<b>3.30</b>	<b>3.49</b>	<b>3.80</b>	<b>4.20</b>

**Notes:**

2. Bold-italics indicate scenarios where inundation occurs.

## 2.3 Frequency Analysis

### 2.3.1 Return Periods Associated with Current Dike Crest Elevations

The return period of total water level corresponding to the dike crest elevations (DCE) as currently constructed were calculated for each of the nine coastal locations for current (2010) conditions and for the relative sea level rise associate with the years 2020, 2040, 2070 and 2100. The total water level is calculated as the sum of RSLR, DFL and wave effect; this is equivalent to DCE without freeboard allowance.

The existing crest elevations of the dikes or beaches at the coastal locations are given in Table 3. The wave allowance for all sea level rise scenarios is based on the 2% wave runup for the design storm in 2010. At sites 1a and 6, inundation occurs so 70% of the significant wave height is used as the wave allowance instead of runup. These values are given in Table 4. The 2010 design storm is used because at later years the design storm causes inundation of most of the dikes which pre-empts the calculation of runup.

For each location and year the RSLR and wave effect were added to the mean fit distribution describing the relationship between water level and return period (see Figure 5.6 of the Phase 1 report for example distribution). The adjusted distribution was then used to estimate the return period associated with the current elevation of the dike. The estimated return periods of total water level associated with the current DCEs are given in Table 6 below. Where a zero value is given

it is expected that the ocean level will exceed the DCE multiple times each year. The data in Table 6 is plotted in Figure 3. Values for the existing, 2010, and 2100 scenarios are also shown in Figure 4. As a result of sea level rise the level of protection afforded by the current dikes reduces to less than a 10 year return period (or >10% AEP) by the year 2040. Also notable is the very low return period associated with many of the dikes for current (2010) conditions.

**Table 6. Total water level return periods (years) associated with the current DCE for selected years from 2010 to 2100.**

Site	Location	DCE (m)	2010	2020	2040	2070	2100
1a	Colebrook - Serpentine	2.84	22	8	2	<1	<1
1b	Crescent Beach East	2.88	220	70	7	<1	<1
1c	Mud Bay - Serpentine	3.00	28	11	2	<1	<1
1d	Mud Bay - Nicomekl	2.98	350	110	10	<1	<1
2	Colebrook (Highway 99)	3.15	22	10	2	<1	<1
3	Crescent Beach North	2.90	2	1	<1	<1	<1
4	Crescent Beach South	3.30	70	22	3	<1	<1
5	BNSF Railway	3.20	7	3	<1	<1	<1
6	8 <sup>th</sup> Avenue at Campbell	2.30	4	1	<1	<1	<1

**Notes:**

1. Total water levels do not include freeboard.
2. DCE values will change if dike geometry is modified or updated.

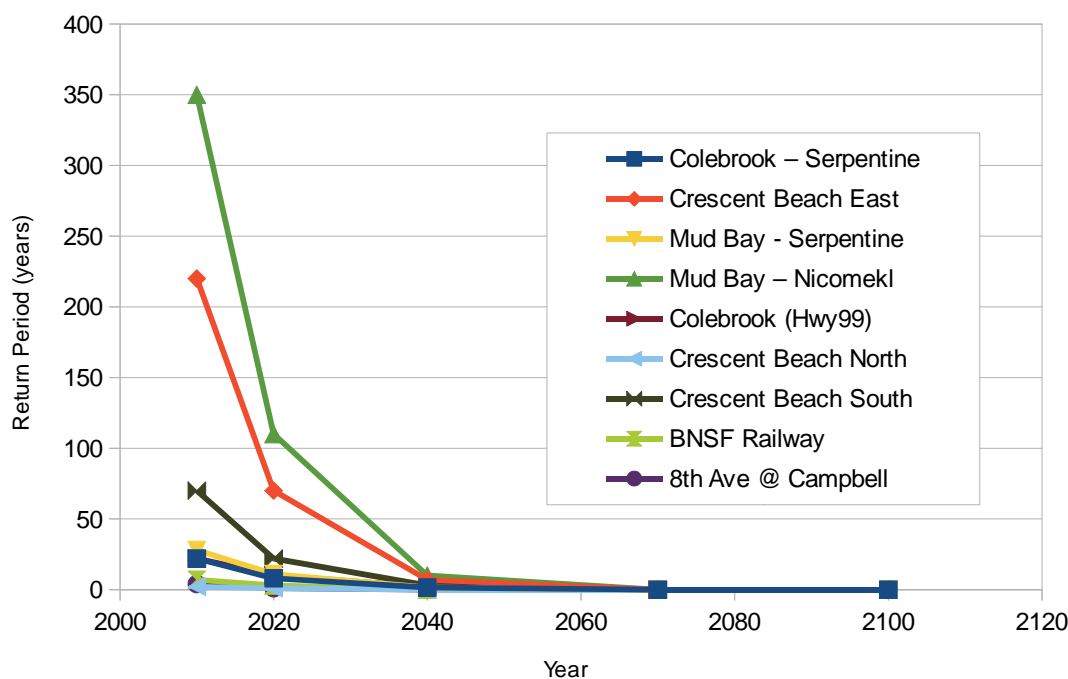


**Figure 3. Return period of total water level associated with current DCEs.**

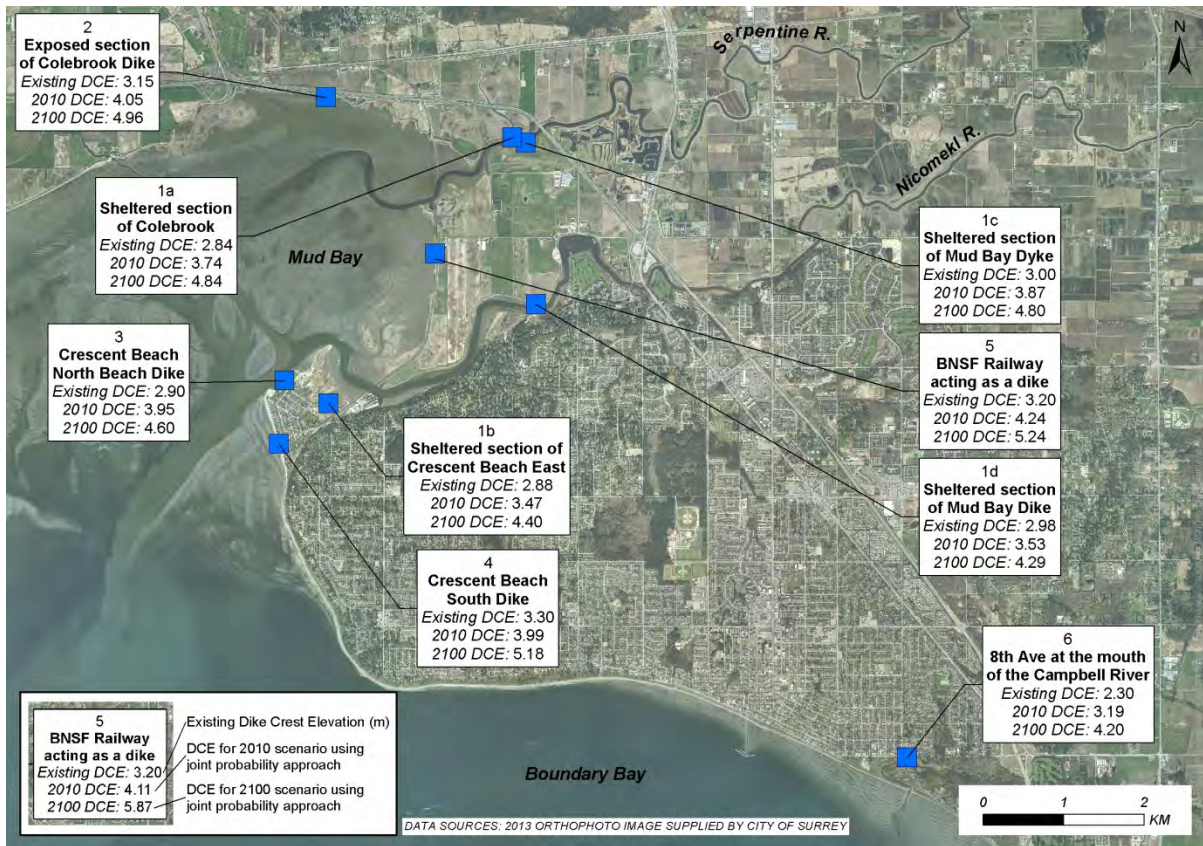


Figure 4. DCE for existing, 2010, and 2100 scenario using joint probability approach.

### 2.3.2 Return Periods Associated with Current 200 Year Event

A similar procedure was used to estimate the return periods associated with the current DFL based on the 200 year event. The estimated return period associated with the 2010 DFL is given below in Table 7 for the years 2010, 2020, 2040, 2070, 2100. It shows how the water level event associated with the current DFL occurs much more often in the future due to sea level rise.

**Table 7. Return periods (years) associated with the 2010 DFL for selected years from 2010 to 2100.**

Site	Location	2010 DFL (m)	2010	2020	2040	2070	2100
1a	Colebrook - Serpentine	2.94	200	85	14	1	0
1b	Crescent Beach East	2.70	200	60	7	0	0
1c	Mud Bay - Serpentine	2.94	200	85	14	1	0
1d	Mud Bay - Nicomekl	2.70	200	60	7	0	0
2	Colebrook (Highway 99)	2.94	200	100	22	2	0
3	Crescent Beach North	2.70	200	60	7	0	0
4	Crescent Beach South	2.70	200	60	7	0	0
5	BNSF Railway	2.94	200	85	14	1	0
6	8 <sup>th</sup> Avenue at Campbell	2.58	200	50	4	0	0

## 2.4 Coastal Flood Mitigation

Sea level rise will present a significant challenge for the City. Without intervention, storms and high tides will increasingly inundate the insufficient coastal defences surrounding Mud Bay and Boundary Bay. Coastal flood management falls into the broad categories of protection, adaptation and retreat. The following is a high level discussion of these options.

**Coastal protection** involves physically altering the coastal zone to minimize the impacts of high waters, waves, currents and sedimentation. Construction of coastal structures are the most commonly used mechanism for protection. Coastal protection structures include jetties, breakwaters, dikes, beach nourishment and edge treatments such as rip-rap, concrete sea walls and sheet piles. Coastal protection can also involve rehabilitation of shoreline vegetation.

The existing coastal dike system can potentially be improved to withstand higher ocean levels. The synthetic record of water levels and extreme wave scenarios produced in Phases 1 and 2 will help guide the design process but additional work is necessary to fully characterize the range of wave occurrences and erosion protection requirements. Site specific geotechnical investigations will be needed to understand the soil bearing capacity and seismic characteristics of sub-surface materials. Establishing right-of-ways and legal access will also be necessary. It may be possible to limit wave action on the current shoreline by constructing off-shore breakwaters. However, the thickness and instability of the sediment covering most of Mud Bay and Boundary Bay may limit the feasibility of off-shore break-waters.

**Adaptation** is a broad category of actions that increase the resilience of coastal communities to the hazards posed by sea level rise. Such actions could include ensuring that essential services are constructed to guarantee continued operation during a flood event, installing pumping systems to quickly remove water from critical transportation corridors, or measures such as elevating transportation corridors and buildings. In terms of catastrophic flood waves caused by coastal dike breaching, adaptation is likely to be a challenge.

**Retreat** involves limiting land use to minimize the risk associated with coastal hazards. This could involve the purchase of coastal properties by the City for conversion to park, wet lands and nature reserves. Retreat should be considered where the costs of protecting the lands is greater than the economic and social benefits provided by the lands over a selected time period. A rule of thumb in planning for retreat is that 1cm in sea level rise may cause about 1m of horizontal erosion. In general, land costs are relatively high even where agriculturally zoned, and purchasing land may not be feasible.

The long term costs, benefits and feasibility of various coastal protection options must be assessed and it is recommended that this work be commenced as soon as possible. Coastal structures are not permanent, require ongoing maintenance and will eventually need to be replaced. Structures may also need to be increased in height if sea level rise is greater than projected for the time period considered. Adaptation actions may be effective only for a limited range of sea levels, requiring strategies to be reconsidered within relatively short time frames. Retreat may limit the economic productivity of coastal lands, but provide environmental and societal benefit of increased public lands. Coastal flood management is highly location and time specific and strategies will need to be fine-tuned over time.

### 3 HYDROLOGIC MODELLING

Hydrologic analysis in this phase of the work focused on refinement and recalibration of the HSPF hydrologic model and development and simulation of two future climate change scenarios. This section documents changes to the HSPF model developed in Phase 1 of this study; for complete documentation of model development, the reader is referred to NHC's 2012 Phase 1 report.

#### 3.1 HSPF Model Refinement

Based on a need for additional refinement of the floodplain as represented in the hydraulic model (Section 5), NHC subdivided the 33 subbasins used in the original Phase 1 modelling into 66 subbasins, shown in Figure 5. The HSPF model provides input to the HEC-RAS model as either point inflows (upstream flow boundary conditions) or lateral inflows (added along a reach). There are nine point inflow locations—Upper Nicomekl (combining inflow from the Upper Nicomekl River and Murray Creek), the Cloverdale Canal (West Cloverdale C), the 168<sup>th</sup> Street Canal (North West Cloverdale D), Latimer Creek North and South (Latimer/Clayton<sup>1</sup>), Upper Serpentine A, Bear Creek (combined routed Mahood and Enver/Burke Creek flows), Fleetwood Creek B, and Hyland Creek—and the remaining subbasins provide lateral inflows to the river reaches or floodplain storage cells in the hydraulic model. Drainage area information is summarized in Table 8.

The updated HSPF model uses the same land use (existing and future) and surface geology data and assumptions as the Phase 1 model. Existing land use, future land use and surficial geology maps, showing the revised subbasin boundaries, are included as Figure 6, Figure 7 and Figure 8. In order to try to improve hydrograph timing at the Nicomekl River at 203 Street gauge, the stage-storage-discharge ratings (or FTABLEs) for the Upper Nicomekl River were adjusted using information from the extended HEC-RAS model (Section 5) and from a coarse upstream HEC-RAS model (based on MIKE11 cross sections) that was used previously for FTABLE development. FTABLEs for other stream reaches were not modified from the Phase 1 model.

As part of the Phase 2 update, the precipitation and evaporation input datasets for HSPF were extended through March 2014 to allow for HSPF model calibration against more recent flow data on the Nicomekl River. Precipitation was extended using data collected by the City of Surrey at Surrey Municipal Hall, and evaporation was extended using average monthly values from the historic record.

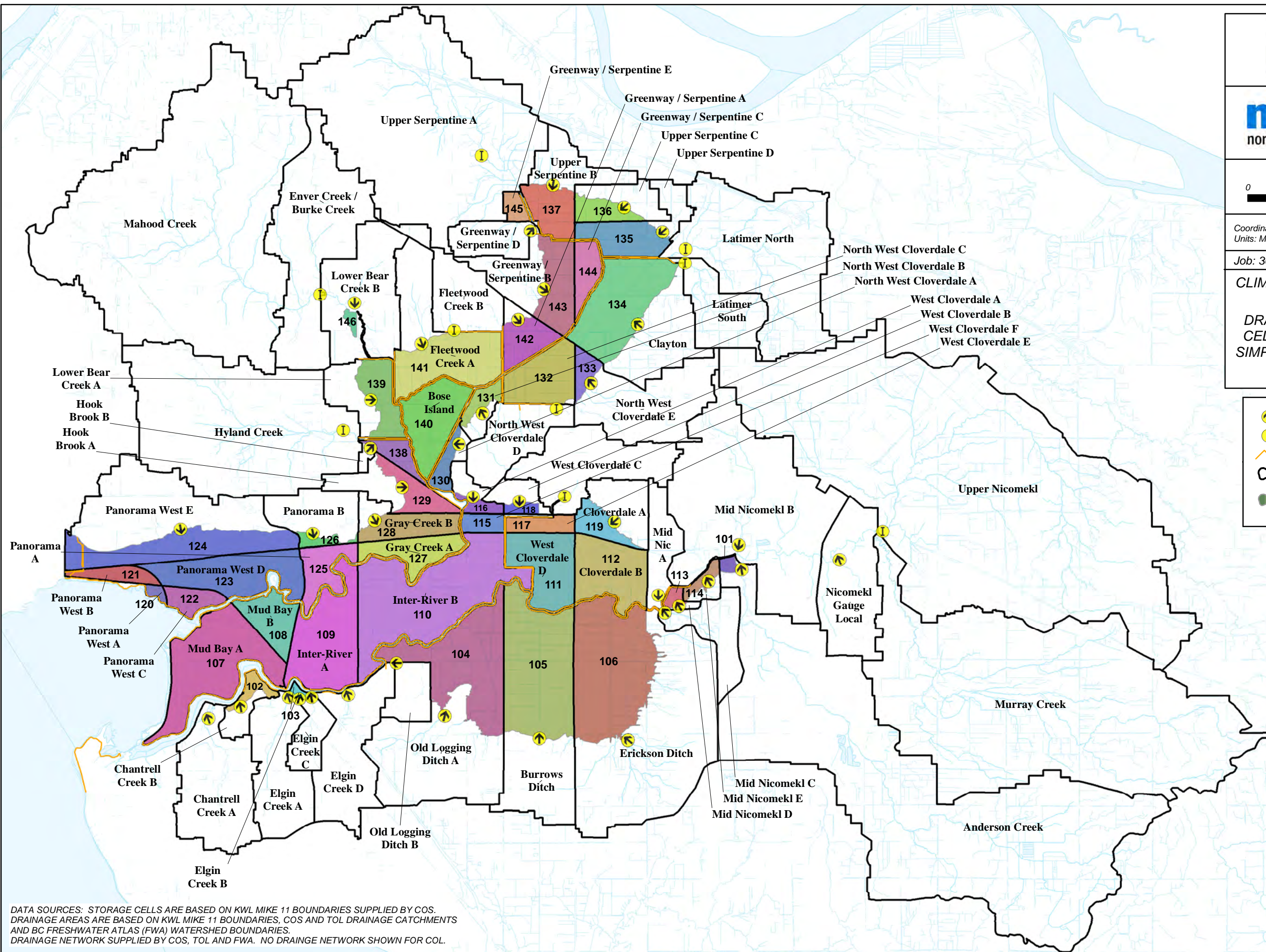
---

<sup>1</sup> The Latimer/Clayton subbasin was split into North and South Latimer drainage areas following development of the HSPF model. For HEC-RAS inputs, the combined flow is split proportionately by contributing basin area.

**CLIMATE CHANGE FLOODPLAIN  
REVIEW PHASE 2**  
DRAINAGE AREAS, STORAGE  
CELLS AND FLOW INPUT FOR  
SIMPLIFIED HYDRAULIC MODEL

FIGURE 5

- Lateral Inflow
- Point Source Inflow
- Dikes
- NHC Drainage Areas
- NHC Storage Cells  
Labelled with cell number.



DATA SOURCES: STORAGE CELLS ARE BASED ON KWL MIKE 11 BOUNDARIES SUPPLIED BY COS.  
DRAINAGE AREAS ARE BASED ON KWL MIKE 11 BOUNDARIES, COS AND TOL DRAINAGE CATCHMENTS  
AND BC FRESHWATER ATLAS (FWA) WATERSHED BOUNDARIES.  
DRAINAGE NETWORK SUPPLIED BY COS, TOL AND FWA. NO DRAINAGE NETWORK SHOWN FOR COL.

**Table 8. HSPF drainage area summary.**

<b>HSPF ID</b>	<b>Drainage Area Name</b>	<b>Short Name</b>	<b>Area (ha)</b>	<b>River Basin</b>	<b>Inflow Type</b>	<b>HSPF Routing?</b>
10	Hyland Creek	HYLD	1,323	Serpentine	Point	Yes
15	North West Cloverdale D	NWCD	252	Serpentine	Point	No
20	Lower Bear Creek B	LBRB	448	Serpentine	Lateral	No
25	Enver Creek / Burke Creek	ENVR	714	Serpentine	Point <sup>1</sup>	Yes
30	Mahood Creek	MAHD	2,536	Serpentine	Point <sup>1</sup>	Yes
35	Fleetwood Creek B	FLTB	257	Serpentine	Point	No
40	Latimer / Clayton <sup>†</sup>	LTMR	1,143	Serpentine	Point	Yes
45	Greenway / Serpentine D	GRND	143	Serpentine	Lateral	No
50	Upper Serpentine A	USRA	1,740	Serpentine	Point	Yes
102	Chantrell Creek B	CHNB	83	Nicomekl	Lateral	No
103	Elgin Creek B	ELGB	10	Nicomekl	Lateral	No
104	Old Logging Ditch A	LOGA	952	Nicomekl	Lateral	No
105	Burrows Ditch	BURR	760	Nicomekl	Lateral	No
106	Erickson Ditch	ERCK	1,400	Nicomekl	Lateral	No
107	Mud Bay A	MUDA	380	Nicomekl	Lateral	No
108	Mud Bay B	MUDB	122	Nicomekl	Lateral	No
109	Inter-River A	INTA	312	n/a	Lateral	No
110	Inter-River B	INTB	576	n/a	Lateral	No
111	West Cloverdale D	WCLD	205	Nicomekl	Lateral	No
112	Cloverdale B	CLVB	217	Nicomekl	Lateral	No
113	Mid Nicomekl D	MIDD	25	Nicomekl	Lateral	No
114	Mid Nicomekl E	MIDE	50	Nicomekl	Lateral	No
115	West Cloverdale F	WCLF	41	Serpentine	Lateral	No
116	West Cloverdale A	WCLA	69	Serpentine	Lateral	No
117	West Cloverdale E	WCLE	58	Nicomekl	Lateral	No
119	Cloverdale A	CLVA	210	Nicomekl	Lateral	No
120	Panorama West A	PAWA	13	Nicomekl	Lateral	No
121	Panorama West B	PAWB	56	Nicomekl	Lateral	No
122	Panorama West C	PAWC	61	Nicomekl	Lateral	No
123	Panorama West D	PAWD	263	Nicomekl	Lateral	No
124	Panorama West E	PAWE	785	Nicomekl	Lateral	No
125	Panorama A	PANA	103	Serpentine	Lateral	No
126	Panorama B	PANB	220	Serpentine	Lateral	No
127	Gray Creek A	GRYA	118	Serpentine	Lateral	No
128	Gray Creek B	GRYB	149	Serpentine	Lateral	No
128	Gray Creek B	GRYB	149	Serpentine	Lateral	No



HSPF ID	Drainage Area Name	Short Name	Area (ha)	River Basin	Inflow Type	HSPF Routing?
130	North West Cloverdale A	NWCA	60	Serpentine	Lateral	No
131	North West Cloverdale B	NWCB	72	Serpentine	Lateral	No
132	North West Cloverdale C	NWCC	175	Serpentine	Lateral	No
133	North West Cloverdale E	NWCE	456	Serpentine	Lateral	No
134	Clayton	CLAY	590	Serpentine	Lateral	No
135	Upper Serpentine D	USRD	204	Serpentine	Lateral	No
136	Upper Serpentine C	USRC	160	Serpentine	Lateral	No
137	Upper Serpentine B	USRB	268	Serpentine	Lateral	No
138	Hook Brook B	HOKB	68	Serpentine	Lateral	No
139	Lower Bear Creek A	LBRA	223	Serpentine	Lateral	No
140	Bose Island	BOSE	194	Serpentine	Lateral	No
141	Fleetwood Creek A	FLTA	431	Serpentine	Lateral	No
142	Greenway / Serpentine A	GRNA	115	Serpentine	Lateral	No
143	Greenway / Serpentine B	GRNB	303	Serpentine	Lateral	No
144	Greenway / Serpentine C	GRNC	72	Serpentine	Lateral	No
145	Greenway / Serpentine E	GRNE	30	Serpentine	Lateral	No
150	Chantrell Creek A	CHNA	454	Nicomekl	Lateral	No
155	Elgin Creek A	ELGA	341	Nicomekl	Lateral	No
160	Elgin Creek C	ELGC	109	Nicomekl	Lateral	No
165	Elgin Creek D	ELGD	395	Nicomekl	Lateral	No
170	Old Logging Ditch B	LOGB	116	Nicomekl	Lateral	No
175	West Cloverdale B	WCLB	81	Nicomekl	Lateral	No
180	West Cloverdale C	WCLC	407	Nicomekl	Point	No
195	Mid Nicomekl C	MIDC	189	Nicomekl	Lateral	No
200	Mid Nicomekl A	MIDA	148	Nicomekl	Lateral	No
205	Mid Nicomekl B	MIDB	1,196	Nicomekl	Lateral	No
210	Anderson Creek	ANDR	2,908	Nicomekl	Lateral	Yes
220	Nicomekl Gauge Local	NICO	411	Nicomekl	Lateral	Yes
230	Murray Creek	MURR	2,694	Nicomekl	Point <sup>2</sup>	Yes
240	Upper Nicomekl	UNIC	3,865	Nicomekl	Point <sup>2</sup>	Yes

**Notes:**

† Flow split into Latimer North and Latimer South for HEC-RAS model input.

3. Combined routed flow from Mahood Creek and Enver/Burke Creeks input to HEC-RAS Bear Creek reach.
4. Upper Nicomekl and Murray Creek inflows combined for HEC-RAS Upper Nicomekl reach inflow.

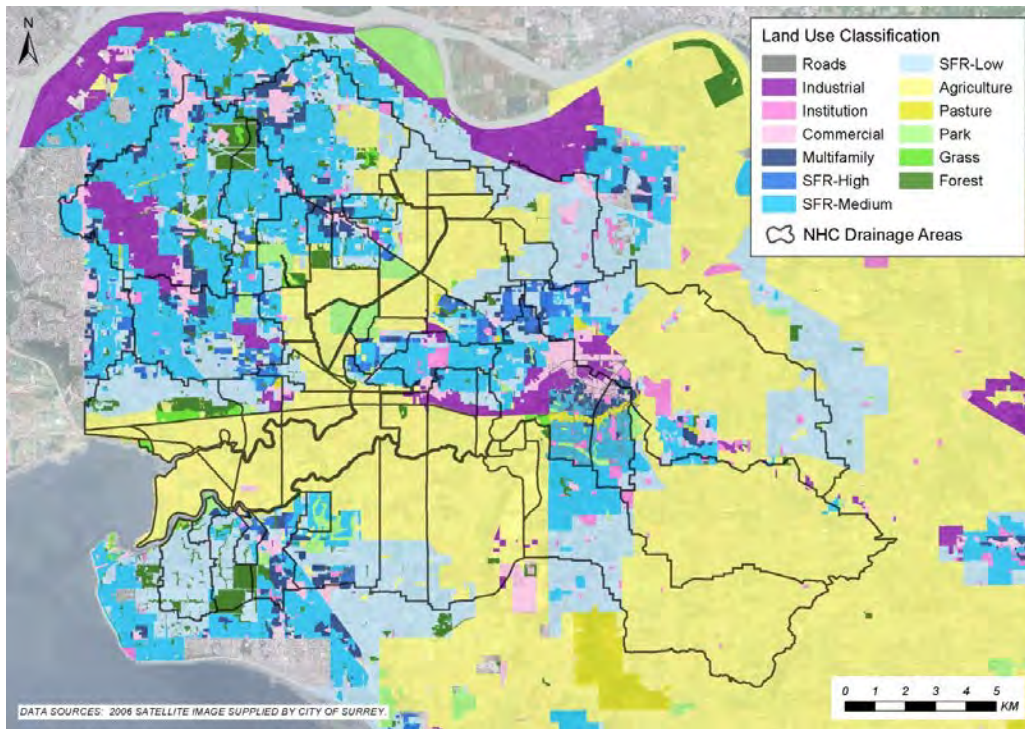


Figure 6. Existing land use for Serpentine and Nicomekl river basins.

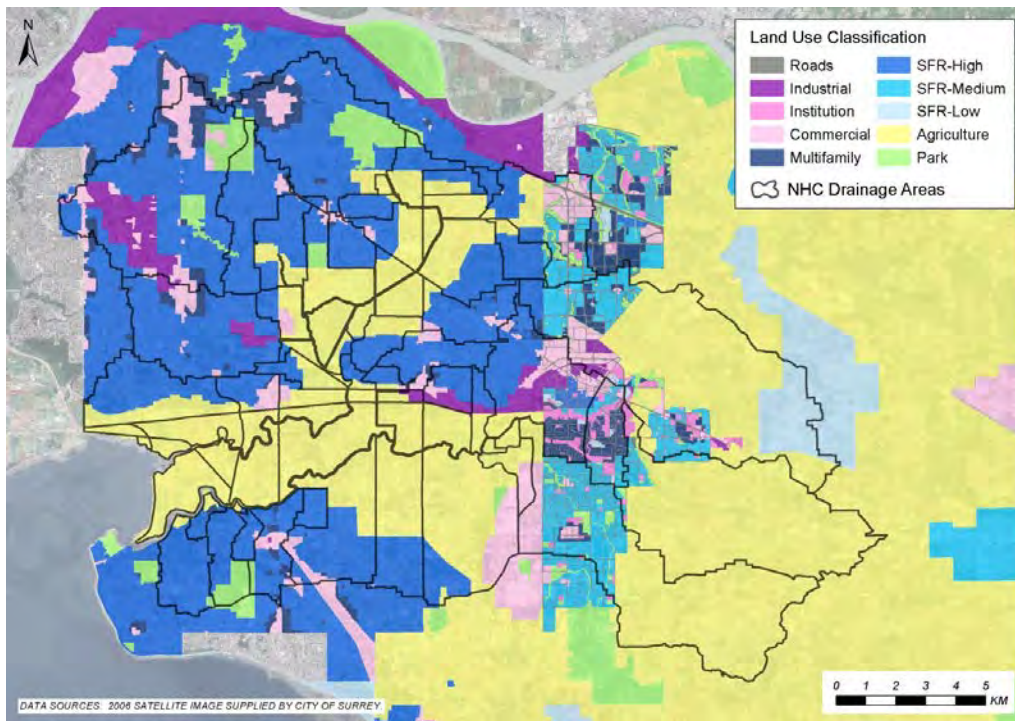
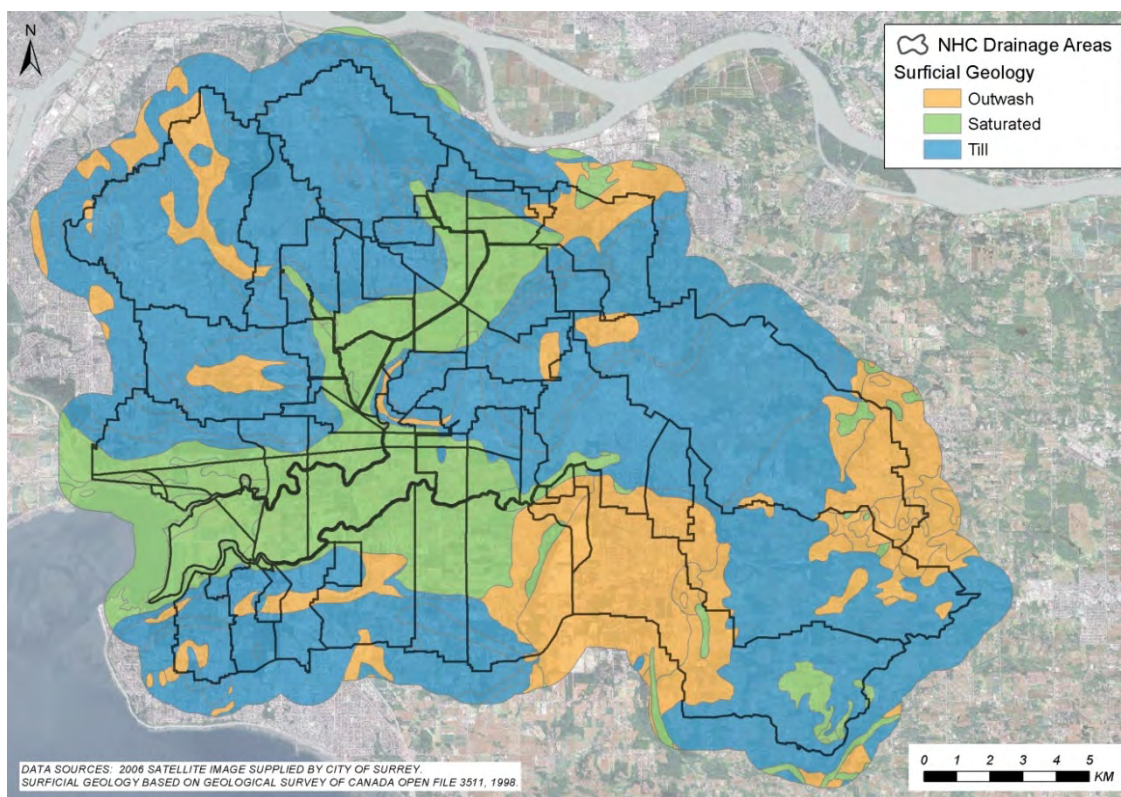


Figure 7. Projected future land use for Serpentine and Nicomekl river basins.



**Figure 8. Surficial geology for Serpentine and Nicomekl river basins.**

### 3.2 HSPF Model Calibration

In the Phase 1 modelling, NHC attempted to calibrate the HSPF model to flows on Mahood Creek and the Nicomekl River at 203 Street, focusing on matching flood event peaks and volumes. Results were mixed, with significant undersimulation of flows on the Nicomekl and a tendency to oversimulate flows on Mahood Creek. There was also a consistent timing shift on the Nicomekl, with simulated peaks at 203 Street leading gauge peaks by about six hours.

The Phase 2 work included further review of the Nicomekl at 203 Street gauge data and recalibration of the model with an emphasis on more recent large storm events in January 2013 and January 2014. No new data were available for the Mahood Creek gauge, so recent events were compared only for the Nicomekl River. Gauge information is summarized in Table 9. Locations of the flow gauges, as well as other hydrometric stations used in model development are shown in Figure 9.

**Table 9. Discharge Calibration Gauges**

Station Name	Operated By	ID	Drainage Area (ha)	Data Available <sup>1</sup>	
				from	to
Nicomekl River at 203 St.	Environment Canada	08MH155	6,970	10/2002	3/2014
Mahood-Bear Creek at 144 St.	City of Surrey	08MH154	2,536	10/1997	1/2012

**Notes:**

1. Significant gaps within period of record for both stations.

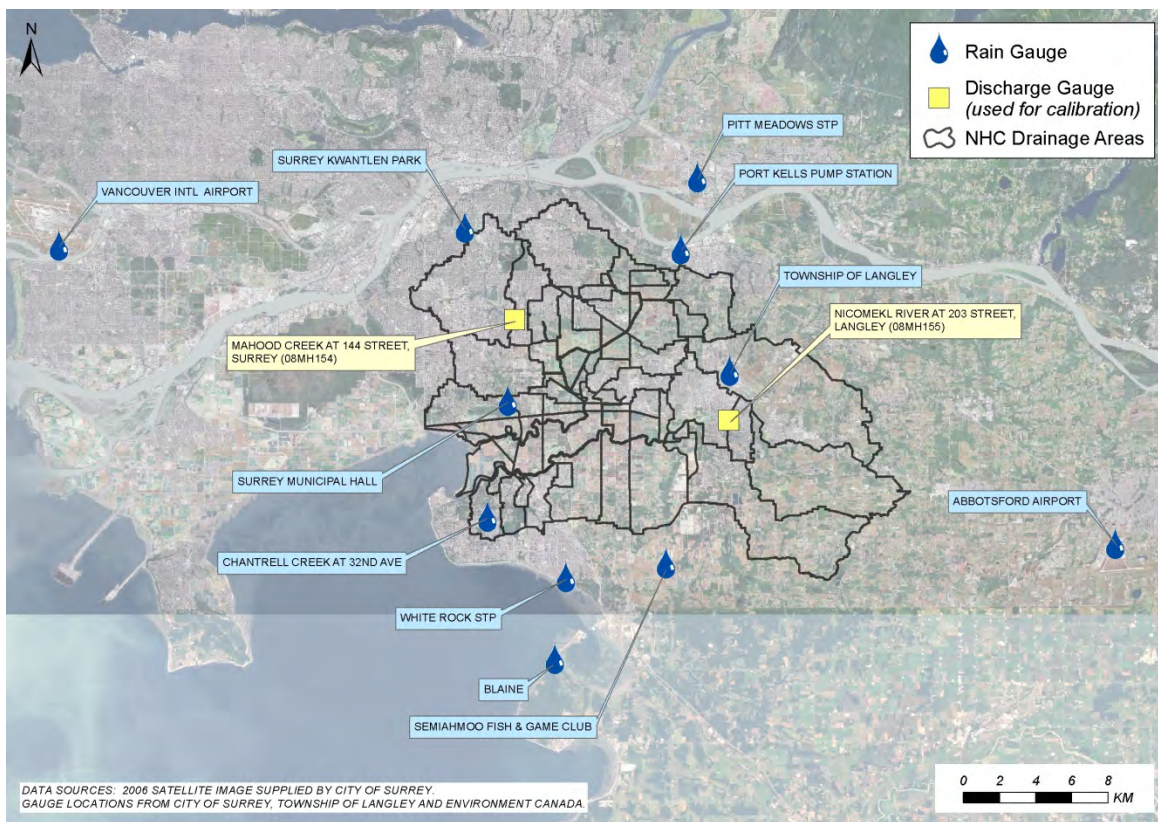


**Figure 9. Hydrometric stations used for hydrologic model development and calibration.**

### 3.2.1 Review of Nicomekl at 203 Street Gauge Record

As noted above, Phase 1 HSPF model calibration results were mixed, with a tendency to oversimulate flows on Mahood Creek and significant undersimulation of flows on the Nicomekl River

at 203 Street. The difficulties in simulating flows on the Nicomekl at 203 Street prompted an initial review which identified potential inconsistencies in the published discharge data. These included:

- Runoff volumes during some flood events that exceeded estimated rainfall inputs, and
- Maximum annual peak flows greater than would be expected from examination of peak flow data from other gauges.

Details of this initial review were provided in the Phase 1 report. Additional review was conducted under Phase 2, focusing specifically on the stage-discharge ratings for the Nicomekl River at 203 Street.

WSC developed some 13 stage-discharge rating tables for the Nicomekl at 203 Street (WSC gauge 08MH155) between 2000 and present. These can be split into two groups: those applied before 7 January 2009 (Ratings Tables 16 through 25) and those applied from 7 January 2009 to present (Rating Tables 26 through 28). Differences between rating tables in the two groups are minor. The two groups of rating tables, together with the direct discharge measurements from which the ratings were developed, are plotted in Figure 10.

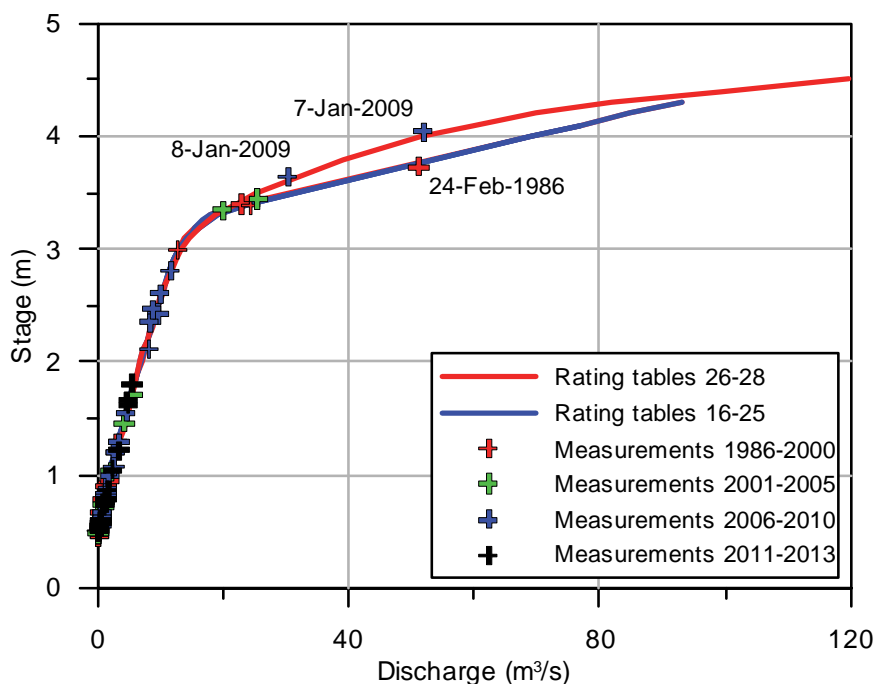


**Figure 10. Stage-discharge measurements and rating curves, Nicomekl River at 203 Street.**

As can be seen from Figure 10, all stage-discharge rating curves for this site are more or less identical for stage up to about 3.3 m (discharge about 19 m<sup>3</sup>/s). The upper end of the rating curve for Rating Tables 16 through 25 (effective through 6 January 2009) is defined by the following discharge measurement:

1986-02-24 00:00:01 Stage 3.726 Discharge 51.2

The upper end of the rating curve for Rating Tables 26 through 28 (effective from 7 January 2009 onward) is defined by two high flow measurements

2009-01-07 14:54:00 Stage 4.035 Discharge 51.9

2009-01-08 12:33:00 Stage 3.641 Discharge 30.3

The basis for extrapolating the two curves above their highest discharge measurements is not known. The curve for Rating Tables 16 through 25 appears to have relied on linear extrapolation. One would normally expect the curves to flatten off with increasing stage (as for Rating Tables 26 through 28). However, we have no information to indicate which, if either, form of extrapolation is more appropriate for this site.

For a stage of 4 m, Rating Tables 16 through 25 give a discharge of 69.15 m<sup>3</sup>/s while Rating Tables 26 through 28 give 51.5 m<sup>3</sup>/s, an approximately 25 percent reduction.

To further investigate changes at the gauge site, we examined relationships between stage and wetted area (Figure 11) and between stage and mean velocity (Figure 12) using data reported with the WSC stage-discharge measurements. The stage-area plot indicates a possible minor reduction in wetted area at high stage between the 1986 and 2009 measurements, but the relationship between stage and area appears to have been quite stable over time.

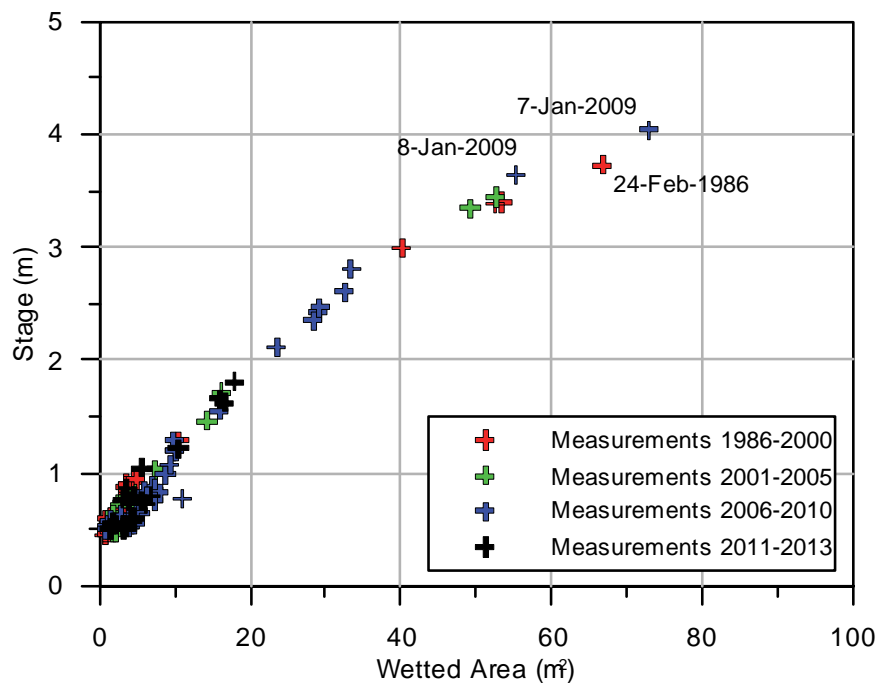


**Figure 11. Stage-area measurements, Nicomekl River at 203 Street.**

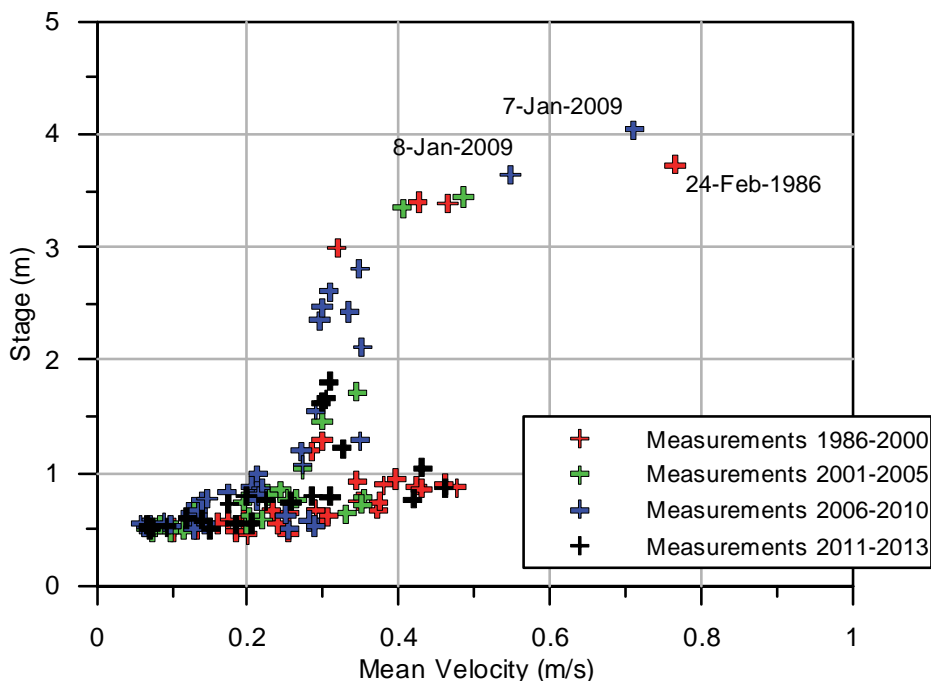


**Figure 12. Stage-velocity measurements, Nicomekl River at 203 Street.**

The stage-velocity plot shows a significantly higher mean velocity for the 1986 measurement than for the comparable stage in 2009. The reason for the wide spread in mean velocities at low stages (below about 1 m) is not known.

We have no information to suggest that the upper end of the stage-discharge relationship for the Nicomekl at 203 Street changed abruptly as a result of the high flow on 6-7 January 2009, as would be implied by the WSC rating tables. Possible explanations for the increased stage for a given flow in 2009 relative to 1986 could be diking of the river downstream from the gauge site or change in flood plain conveyance.

Google Earth images were reviewed, a site visit was conducted, and staff from the City of Langley was contacted in an attempt to identify any changes over time in flood plain conditions that could have affected the gauge rating. One relatively recent change is construction of a trail under the 200 Street bridge, approximately 0.8 km downstream from the gauge site. This may have reduced conveyance through the bridge opening slightly, but the change is not sufficient to explain the shift in gauge rating between the 1986 and 2009 discharge measurements.

In the absence of information to justify revisions to the pre-January 2009 rating tables and the difficulties encountered in model calibration under Phase 1, HSPF recalibration for the Nicomekl at 203 Street under Phase 2 focused on post-January 2009 events.

### 3.2.2 Calibration Adjustments and Results

Model calibration focused on improving simulation of hydrograph peaks and volumes for the January 2013 and January 2014 events on the Nicomekl River. These two calibration events are shown in **bold** in Table 10, which also summarizes events between 2003 and 2010 used in the Phase 1 calibration. In general, and for two recent events in particular, Nicomekl River flows based on the post-January 2009 rating curve matched simulated results much more closely than earlier flows, even prior to calibration adjustments. NHC targeted a handful of key model parameters to improve simulation of the target January events on the Nicomekl River at 203 Street. Simulations using the final parameter set were then verified against previous calibration events from the Mahood Creek data as well.

**Table 10. Calibration event summary.**

Event	Event Dates	Surrey MH Rain (mm)		Nicomekl Flow (cms)		Mahood Flow (cms)	
		Max Hr	Event	Peak	Event Avg	Peak	Event Avg
November 2003	27-30	8.2	78	85.0	22.5	38.1	8.4
January 2005	16-23	8.0	217	95.7	19.7	Missing	
November 2006	5-7	9.6	65	62.2	14.1	25.2	5.5
January 2007	1-4	9.0	75	81.3	18.3	27.9	5.2
March 2007	10-14	10.2	104	93.5	18.6	Missing	
January 2009	5-14	6.3	233	89.6	Missing <sup>2</sup>	24.8	6.2
December 2010	11-13	6.5	63	No Data		27.2	4.5
<b>January 2013</b>	<b>6-10</b>	<b>6.8</b>	<b>88</b>	<b>41.1</b>	<b>12.8</b>	<b>No Data</b>	
<b>January 2014</b>	<b>10-12</b>	<b>8.3</b>	<b>73</b>	<b>47.6</b>	<b>16.8</b>	<b>No Data</b>	

**Notes:**

1. The two calibration events are shown in bold.
2. <sup>2</sup> Gauge record includes peak but is sporadic through event.

Starting from the calibrated parameters in the Phase 1 HSPF model, NHC first increased the rainfall multipliers for the high and moderate rainfall zones (Figure 13), which encompass the tributary area to the Nicomekl gauge, to improve volume simulation over the 2013-2014 calibration period. As discussed in the Phase 1 report (NHC 2012), there is significant variability in precipitation distribution and gradients from storm to storm in this area. The increased multipliers are still well within the range of observed precipitation differences between rain gauges for historic storm events. Increasing upland rainfall improved overall runoff volume simulation for the upper Nicomekl River over the 2012-2014 period.



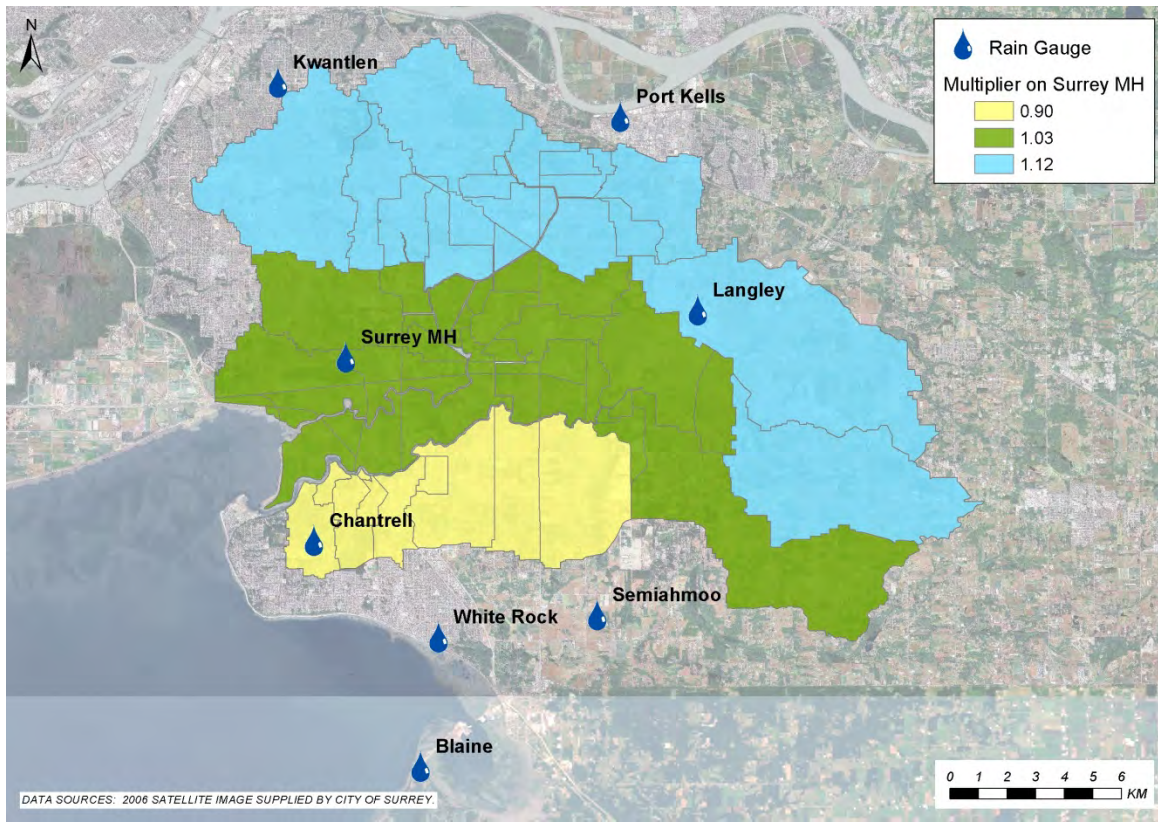


**Figure 13. HSPF precipitation zones**

Storm event hydrograph peaks and volumes were tuned by adjusting surface infiltration rates, overland flow surface lengths, and interflow parameters that control the split between fast-response surface runoff and intermediate-response interflow (or shallow subsurface flow). These adjustments were made to the parameters for till and outwash soil types, which dominate the upland areas. Plots of simulated versus gauged Nicomekl River flows for the two January events are shown in Figure 14. In the plots, gauge flows are shown in red, simulated flows in blue, and Surrey Municipal Hall precipitation is shown on the upper axis in green.

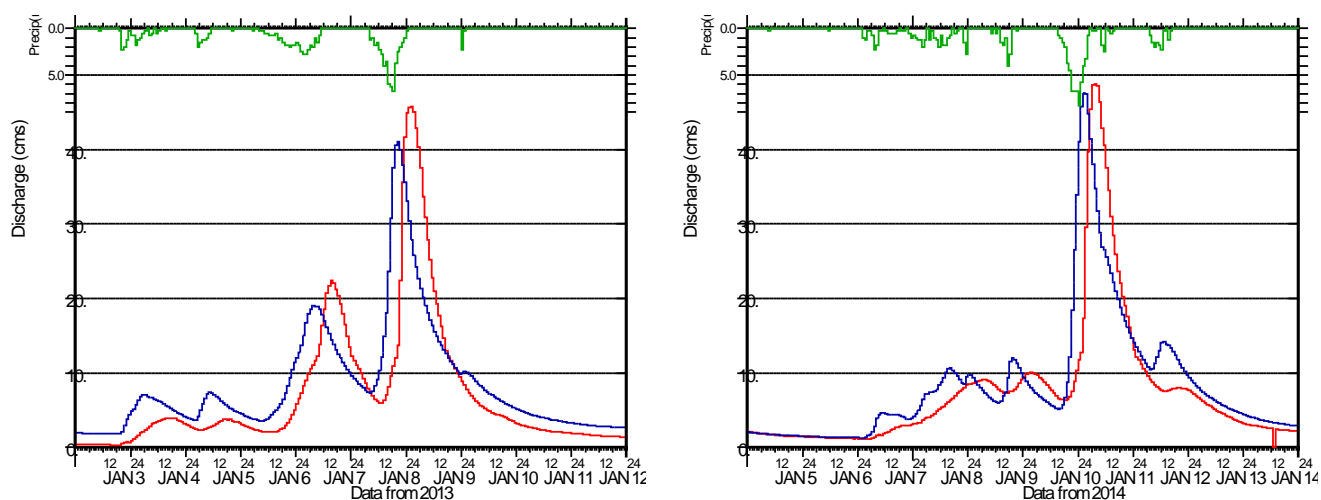


**Figure 14. Simulated vs. gauged flows for Nicomekl River at 203 St, January 2013 and January 2014. Observed flow is shown in red, simulated flow in blue, and Surrey Municipal Hall precipitation in green on the upper axis.**

Despite adjustments to FTABLEs and surface runoff parameters, we were not able to significantly improve timing of the simulated Nicomekl event hydrographs. As previously, gauge event hydrographs typically lag simulated hydrographs by about six hours. Having verified gauge data timing against recorded discharge measurements and current real-time gauging, it is not clear what mechanism within the drainage area would delay surface runoff so significantly without attenuation. Given the variable interplay between runoff timing and tide levels, this timing shift would not be expected to bias results of the extended simulations, so no further attempts were made to resolve the timing issue.

Initial HEC-RAS model simulations of the January 2013 and January 2014 events using flows simulated with the updated HSPF calibration produced flow hydrographs at the Nicomekl River gauge site similar to the HSPF calibration results. However, water levels in the downstream floodplain cells were consistently low. Most of the floodplain lies in areas with saturated soils subject to high groundwater, particularly during the winter wet season. Historic storm precipitation distributions did not support increasing precipitation volume over the southern portion of the basin, covering much of the Nicomekl River floodplain, so further rainfall adjustments were not appropriate to increase volumes. However, we judged that high groundwater conditions associated with tidal boundary conditions and land subsidence would likely limit soil infiltration and storage in these low-lying areas. To represent this condition, infiltration rates and soil storage capacity were reduced for saturated soil areas in the HSPF model<sup>2</sup>, resulting in much higher runoff production

<sup>2</sup> This change was applied to saturated soils throughout the model. It is unlikely that the same conditions would apply to upland wetlands, but upland saturated soil areas in this model are negligible, so further distinction was not warranted for this effort.

during the wet season. It should be noted that this approach will likely under-represent summer runoff in the floodplain areas, since the model does not account for the “external” high groundwater that would likely contribute to dry season baseflow.

As noted in the Phase 1 report, it is likely that some upland storage exists in most of the subbasins, and hence peak flows and hydrograph shapes for the unrouted drainage areas (e.g. local runoff to floodplain cells) are not accurate. However, the lower basin adjustments appear to have improved simulation of overall volumes, which is the more critical component given the significant dampening effects of the sea dams, pump stations, and floodplain storage.

Table 11 provides a summary of simulation results with the final calibration parameters, for both the current calibration events (January 2013 and January 2014) and the other large storm events evaluated under Phase 1. Considering all of the listed storm events for Mahood Creek and the post-January 2009 events for the Nicomekl River (earlier data on the Nicomekl were discounted due to rating curve uncertainties), the HSPF model reproduces storm event volumes within about 5 percent and event peaks within about 10 percent.

**Table 11. Summary HSPF model calibration results.**

Flood Event			Mahood Creek at 144 Street						Nicomekl River at 203 Street						Surrey MH
Month	From	To	Volume (mm)			Peak (m3/s)			Volume (mm)			Peak (m3/s)			Rain (mm) Observed
			Gauged	Simulated	% Diff	Gauged	Simulated	% Diff	Gauged	Simulated	% Diff	Gauged	Simulated	% Diff	
Nov 2003	27	30	81.5	68.5	-16%	38.1	38.0	0%	77.4	56.6	-27%	85.0	53.2	-37%	78.0
Jan 2005	16	23	m	206.4	m	m	35.6	m	195.1	182.2	-7%	95.7	58.8	-39%	216.6
Nov 2006	5	7	52.0	53.0	2%	25.2	21.2	-16%	60.8	36.4	-40%	62.2	25.1	-60%	64.6
Jan 2007	1	4	68.7	67.8	-1%	27.9	34.8	24%	87.6	57.8	-34%	81.3	42.8	-47%	74.8
Mar 2007	10	14	m	100.7	m	m	41.3	m	106.6	88.2	-17%	93.5	66.0	-29%	104.4
Dec 2007	2	5	84.9	79.9	-6%	25.4	32.2	27%	126.4	61.9	-51%	90.6	36.2	-60%	99.1
Jan 2009	5	14	188.6	233.4	24%	24.8	32.4	31%	m	202.8	m	m	49.6	m	233.0
Dec 2010	11	13	46.8	56.4	20%	27.2	27.5	1%	m	46.7	m	m	41.4	m	62.6
<b>Jan 2013</b>	<b>6</b>	<b>10</b>	<b>m</b>	<b>86.9</b>	<b>m</b>	<b>m</b>	<b>31.6</b>	<b>m</b>	<b>73.4</b>	<b>77.6</b>	<b>6%</b>	<b>45.8</b>	<b>41.1</b>	<b>-10%</b>	<b>88.3</b>
<b>Jan 2014</b>	<b>10</b>	<b>12</b>	<b>m</b>	<b>71.9</b>	<b>m</b>	<b>m</b>	<b>36.3</b>	<b>m</b>	<b>58.9</b>	<b>62.6</b>	<b>6%</b>	<b>48.8</b>	<b>47.6</b>	<b>-3%</b>	<b>73.0</b>
Average 2013-14 events			n/a			n/a			6%			-6%			
Average all events			4%			11%			-20%			-36%			

### 3.3 Climate Change Precipitation Scenarios

For the Phase 2 study, flooding and inundation in the Serpentine and Nicomekl watersheds were evaluated for both historic climate conditions and for two different future climate scenarios. This section of the report summarizes the approach used to develop future climate scenarios.

Our selected approach was to develop future climate scenarios in the form of hourly precipitation time series that could be used as input (“forcing”) to the HSPF hydrologic model. The hourly precipitation time series were created in a manner consistent with projections of global climate models, as summarized in Section 3.3.1 below. A full description of the detailed methodology is given in Appendix C.

Two alternative methodologies were suggested for possible use in this study but were discounted:

- Extrapolation into the future of observed trends in precipitation amounts, and,
- Reliance on rainfall intensity-duration-frequency (IDF) curves representative of future climate scenarios.

Dillon Consulting (2013) analysed recent precipitation trends for the City of Surrey and identified significant increases in extreme precipitation for the month of January, which is among the region’s wettest months. We agree with Dillon Consulting’s statement in their report that observed trends may not be reliably extended into the future. Such trends can have different explanations. Precipitation is a variable with high natural variability at all timescales. The term *natural* is used here to qualify this variability because it is observed to occur in the absence of any external forcings, i.e., no changes in greenhouse gas concentrations, solar intensity, etc. are required for there to be precipitation trends over time. Therefore, the detection of a precipitation trend over time is not easily attributable to anthropogenic climate change. Scientific research has led to identification and some degree of understanding of a few sources of climate variability, such as the Pacific Decadal Oscillation (Zhang et al. 1997; Mantua et al. 1997), which transitioned from a negative to a positive phase circa 1976 and may have again initiated a negative Phase in the early 21st century. Any precipitation trends over time that are the result of the atmospheric accumulation of anthropogenic greenhouse gases are currently difficult or impossible to isolate from trends explained by natural variability.

The second alternative suggested for this study, but also discounted, was the use of precipitation IDF curves. IDF curves by definition only provide a relationship between precipitation intensity, duration (i.e., accumulation period), and frequency. Given that this project uses a continuous hydrologic simulation approach, there is no method by which to translate a change in an IDF curve under future climates into a change in the rainfall time series that is used to drive the simulations. If one were to seek to develop such a method, there would be the difficulty that IDF curves do not allow for changes in rainfall intensity during longer duration events or back-to-back storms. Thus, IDF curves are most suitable for event-based analysis, where a critical duration can be defined that

is sufficiently short that the assumption of a constant intensity is plausible. In this application, which requires evaluation of independent forcings and responses over a range of time scales, such an event-based approach does not capture system variability.

### 3.3.1 Methodology for Developing Future Precipitation Time Series

Under the selected approach, two alternative synthetic time series of hourly precipitation were developed covering the 21st century. Each time series was developed to be consistent, in a statistical sense, with the projections of a particular global climate model (GCM) run, selected from the most recent runs that served as the basis for the IPCC Fifth Assessment Report, i.e., the CMIP5 climate projections.

The approach consisted of the following steps:

- 1) GCM precipitation projections downscaled by the Pacific Climate Impacts Consortium (PCIC) were obtained and analysed. Data from twelve GCMs are available from PCIC, nearly all of which project future increases in daily precipitation intensity accompanied by declines in the mean number of precipitation days in a year.
- 2) Two GCM runs were identified that represented, in the context of all the PCIC projections, an “extreme scenario” and a “moderately high scenario” in terms of flood risk.
- 3) The observed historical time series of hourly precipitation at the Surrey Municipal Hall gauge was altered so as to create two new hourly time series, representative of projected precipitation regimes toward the end of the 21st Century, one of which is statistically consistent with the “moderately high” GCM run, and the other representing a “severe” scenario situated between the “moderately high” and “extreme” GCM runs.

To create each future precipitation time series, the observed historical time series was first modified to reduce the number of precipitation days. Precipitation days were removed from the end of randomly selected storm events from the observed time series until the number of precipitation days was consistent with the GCM projections. The daily precipitation totals on the remaining wet days were then adjusted so that the distribution of daily precipitation on wet days would be consistent with the GCM-projected increases. To this end, the return period of each daily observed precipitation value was estimated, and that value was then replaced by a higher value having the same return period in the future distribution. Table 12 summarizes the number of wet days and daily intensities for selected return intervals for the historic and two climate change scenarios.

**Table 12. Precipitation exceedance frequency comparison.**

Precipitation Scenario	Average Wet Days per Year	Daily Precipitation (mm/day) for Selected Return Interval		
		10-year	100-year	200-year
Historic (WY 1963-2009)	171	81	159	200
Moderate (CanESM)	162	105	213	267
Severe	162	106	294	402

Once the future daily time series were developed, the daily precipitation values were disaggregated to hourly values using the same temporal distribution as in the observed data.

### 3.3.2 Uncertainty in Future Precipitation Projections

While there is a need to provide quantitative information for flood risk management planning, the underlying projections of climate change are subject to large and unquantifiable uncertainty (see e.g. Kundewicz et al. 2013). The main sources of uncertainty are unknown future emissions of greenhouse gases, uncertain response of the global climate system to increases in anthropogenic greenhouse gas concentrations, and incomplete understanding of regional manifestations that will result from global changes (e.g., Hawkins and Sutton 2010). Additionally, precipitation processes are very complex and difficult to simulate accurately in models. The downscaling, in space and time, of GCM-projected climate variables, the extrapolation of frequency analyses to extreme return periods, and the disaggregation from future daily precipitation to hourly precipitation represent additional sources of uncertainty. The precipitation projections developed in this work should therefore be considered to be plausible representations of the future, given the best current scientific information, but do not represent specific predictions. The actual future realizations of precipitation at Surrey will differ from any of the scenarios developed under this study, and their difference compared to historical precipitation may be greater or smaller than the differences projected in this work.

### 3.4 HSPF Long-Term Simulations

The HSPF parameters developed through calibration to the Nicomekl River and Mahood Creek discharges were applied basin-wide to generate long-term hydrologic inputs to the HEC-RAS hydraulic model of the Nicomekl and Serpentine Rivers. Hydrologic modelling was conducted for existing and future land use for the period of meteorological record from October 1962 through March 2014. In addition, the alternate precipitation inputs representing the two future climate change scenarios (discussed in Section 3.3.1) were applied with future land use conditions to

generate “moderate” and “severe” future climate change scenarios.<sup>3</sup> Flows generated by HSPF were written at an hourly time step to a HEC-DSS database for import to the HEC-RAS hydraulic model. The final HSPF model parameters are provided in the User Control Input (UCI) files in Appendix C.

Figure 15 presents a sample comparison of flow frequency curves for the Upper Nicomekl River downstream of Murray Creek for the four scenarios.

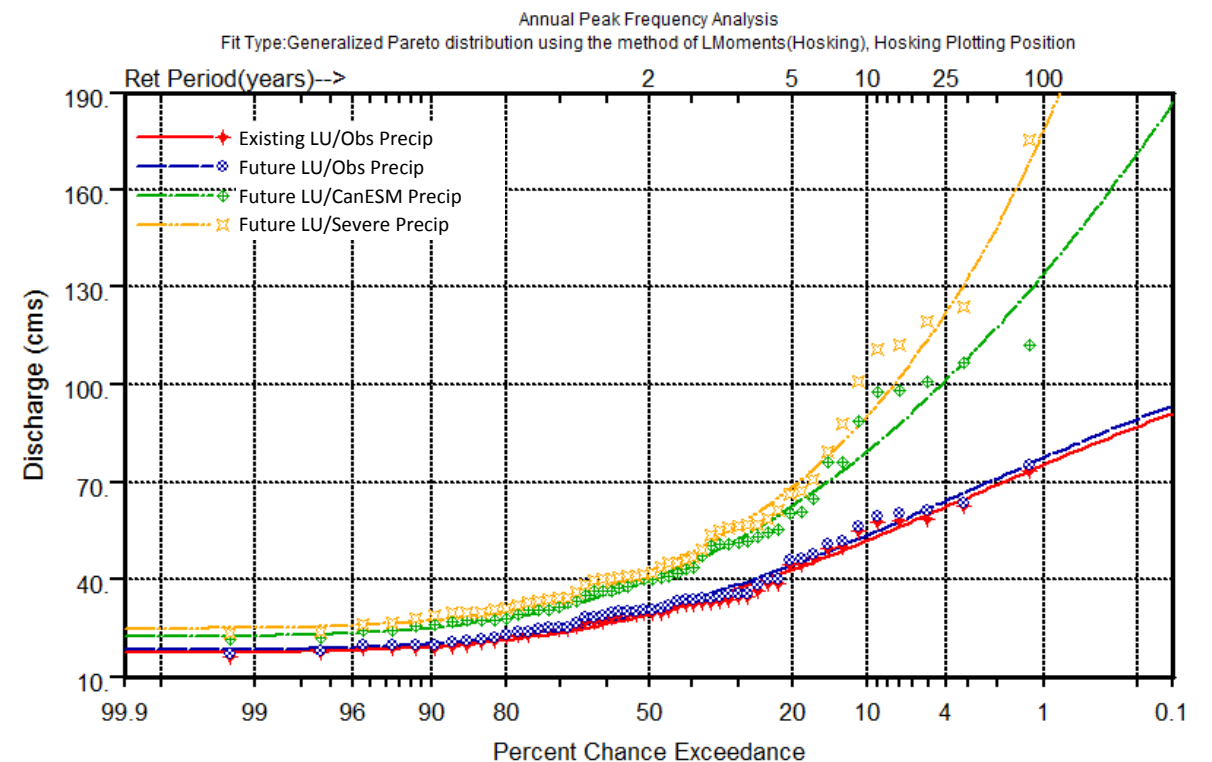


Figure 15. Flow frequency comparison for Upper Nicomekl River

<sup>3</sup> Note that evaporation data were not adjusted to account for future temperature changes. Climate models are fairly consistent in demonstrating increased evaporation associated with global warming, so this assumption may be problematic in looking at longer term flows. However, over the course of a large storm event occurring during the cool season, evaporation effects are not likely to be significant.



## 4 HYDRAULIC MODELLING

### 4.1 Purpose of Hydraulic Modelling

Sections 2 and 3 described the development of ocean level and inflow boundary conditions for continuous simulation hydraulic modelling, spanning the period 1964 to 2011. The purpose of the hydraulic modelling was to generate time-series of flood levels at a number of locations in the Serpentine and Nicomekl basins. A frequency analysis of annual peak levels was then carried out to estimate the 200-year flood levels as described in Section 5. The 200-year levels derived in this manner reflect the joint probability of high ocean levels and precipitation.

This section of the report outlines the enhancements that were done to the Phase 1 HEC-RAS hydraulic model and model verification to recent flood events. The model limitations, required simulations and final results are presented.

Background information about previous studies and hydraulic models are described in the Phase 1 report (NHC 2012). Considerations for software selection for the Phase 1 model and a summary of available data are also included in the Phase 1 report.

### 4.2 HEC-RAS Model Enhancements

The Phase 1 HEC-RAS model consisted of an idealized representation of the floodplain with a minimum number of storage cells and hydraulic structures. For Phase 2, significant enhancements were made to the Phase 1 model to improve the model's representation of the physical system.

The river network, channel cross-sectional geometry, floodplain topography and the hydraulic structures, such as the sea dams, spillways, pumps, floodboxes, bridges and culverts were reviewed and updated as required. The additional geometry data included in the model was either provided by the City, or extracted from the existing MIKE11 model. The Phase 2 model schematic is shown in Map 1. Effort was made to represent the drainage system as accurately as possible without substantially increasing model run-times. The different model inputs were pre-processed in a GIS database which allowed the use of scripts to input hydraulic structures in the HEC-RAS geometry.

An updated Digital Elevation Model (DEM) was developed for the floodplain area based on 2013 LiDAR.

#### 4.2.1 Model Geometry

The following sections describe the model geometry and lists the Phase 2 enhancements. Complete geometry information is included in GIS shapefiles and details are summarised in Appendix A.

#### Network

The rivers, creeks, and canals in the Serpentine and Nicomekl River floodplain are represented in the model. Network chainages are set to increase in the upstream direction. All branches have a downstream chainage value of zero except for the Serpentine and Nicomekl Rivers which have their zero chainage at the sea dams and negative chainages on the ocean side of the sea dams.

In the Phase 2 model, the Serpentine River, Bear Creek, Latimer Creek, and Hyland Creek reaches were extended in the upstream direction.

### **Cross-sections**

The model channel geometry reflects 2011 or 2012 channel cross-sections in reaches where recent survey data was available for the Phase 1 work. Cross-sections in all other reaches are based on the existing MIKE11 model data. It is recommended that these cross-sections be resurveyed and the model geometry updated as part of future work.

In the Phase 2 model, the upstream reaches of Serpentine River, Bear Creek, and Hyland Creek were updated using data surveyed by the City in 2014 (Figure 16). Topographic data from design drawings (dated Nov 2001) were used to represent Surrey Lake. All cross-sections were reviewed and where required, cross-sections were extended to include topography above the highest anticipated water levels.

Additional cross-sections were interpolated as necessary. The HEC-RAS model has a total of 970 cross-sections of which 354 were interpolated.

### **Floodplain**

The floodplain, which has minimal slope and is compartmentalised by roads and dikes, was represented in the model using storage areas. Flood waters can pass between the floodplain storage areas and the river based on the hydraulic capacity of the interconnecting links and the head difference across these.

In the Phase 2 model, the floodplain was treated as 46 storage areas (Map 1) and the storage areas were connected to the channels either through lateral weir structures (representing dikes and spillways), floodboxes, and/or pump stations. Connectivity between storage areas through culverts running under roads or road overtopping was also included.

The hydraulic geometry of the floodplain cells was established by developing volume-stage curves using the developed DEM updated using 2013 LiDAR data.

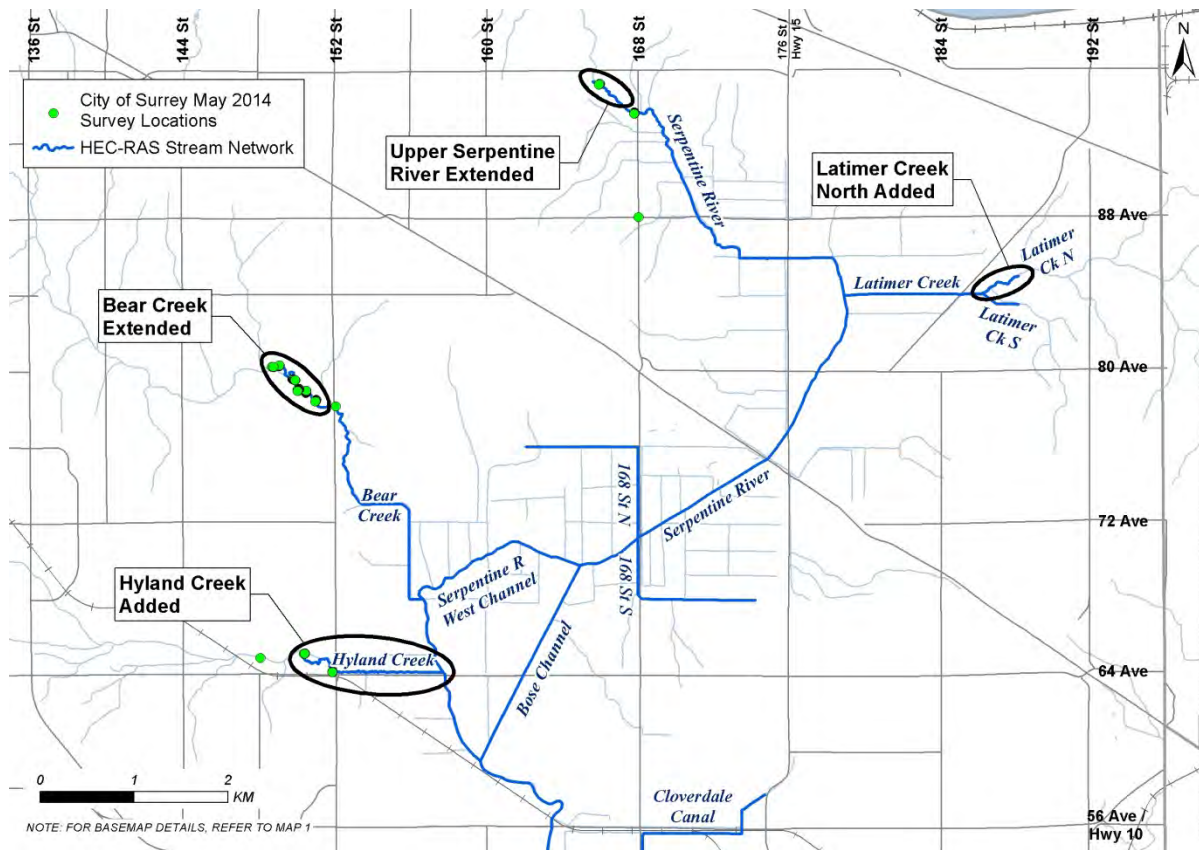


**Figure 16. Model reaches extended using 2014 survey data or MIKE11 cross-sections.**

### Hydraulic Structures

Hydraulic structures included in the model consisted of sea dams, spillways, floodboxes, bridges, culverts (floodplain and in-stream) and pump stations. The structures in the model were selected based on their hydraulic significance on water levels and the availability of data to represent their geometry and operation.

The sea dams on the Serpentine and Nicomekl Rivers were represented as flap-gated culverts that were controlled by the difference in water levels across the dams. This ensured that the sea dam gates were closed whenever the water level on the ocean side was higher than on the river side. In the Phase 2 model, the parameters controlling the gate operation were modified slightly.

Temporary and permanent spillways have been constructed (or are planned) to control the locations and volume of spills onto the floodplain. In the Phase 2 model, a total of 25 spillways (temporary and permanent) were included in the RAS model using updated geometry and location information. Spillway dimensions and elevations were entered in the model to reflect the spillways present in 2013/2014 (for calibration) and those expected for future build-out conditions (for 200-yr simulations).

Floodboxes allow water to drain by gravity from the floodplain back into the river channel once the water levels in the river have receded. For the Phase 2 model, complete information was compiled for a total of 195 floodboxes based on correlating data found in the City database and information stored in the MIKE11 model.

The most recent available information was used to represent bridges and instream culverts in the model. In the Phase 2 model, a total of 35 bridges and 28 culverts were included across creeks, canals and the Serpentine and Nicomekl Rivers.

Pump stations in the model transfer water from the floodplain to the river channel based on a specified pumping capacity curve and specified on/off reference water levels on the floodplain. A total of 21 pump stations were included in the HEC-RAS model. Pump capacity curves were copied from the MIKE11 model and adjusted as necessary to reflect recent pump tests. Pump on/off reference levels were set to the winter operation levels. In the Phase 2 model, pumps were turned off after spillway activation and resumed pumping once river water levels had receded to a target level.

Dikes were represented in the model as lateral structures. To establish design water levels, the dikes were raised to confine the flow. For breach simulations when dikes were allowed to overtop, the dike crests were set to the City's current dike design elevations.

Many of the roads and rail embankments located on the floodplain have culverts that convey water from one side to the other. A total of 51 culverts were included in the Phase 2 model to provide hydraulic connectivity between floodplain storage areas. Road elevation profiles were also included in the model to simulate overtopping of roads at high water levels.

#### **4.2.2 Model Inflows and Water Level Boundaries**

Inflows and water level boundaries for the model are shown in Map 1. The hydrologic analyses in Section 3 provided inflow time series for the floodplain cells (precipitation and/or runoff), lateral inflows to the rivers or creeks and point source inflows at the upstream end of modelled reaches. The ocean analyses of Section 3 provided ocean level time series (incorporating tide, surges and wind setup) for the downstream water levels on the Serpentine and Nicomekl Rivers.

### **4.3 Model Validation**

Model calibration typically forms an important step of hydraulic model development. It involves gradually fine-tuning initially selected channel/floodplain Manning's roughness coefficients and other model parameters to make sure simulated water levels match observed levels for a particular flood event. Once the coefficients have been fine-tuned, the model is typically used for simulating a second independent flood event with known flows and observed water levels to validate that the model is also accurate for a different magnitude event. For the present HEC-RAS model, this procedure was modified somewhat.

Considering the complex nature of the hydraulic network, the water levels, particularly in the floodplain, are largely a function of the spilling, draining and pumping capacity of the drainage system rather than the channel and floodplain roughness coefficients, which are the parameters typically adjusted during calibration. On the other hand, it was not possible to represent all hydraulic structures in exact detail and fine-tune these to provide a perfect fit, resulting in model validation being done on a somewhat broader scale.

Although MIKE11 and HEC-RAS roughness values and loss coefficients are not exactly equivalent, the coefficients from the MIKE11 model, calibrated to a 2003 flood (UMA 2004), were transferred to the HEC-RAS model as a starting point. Manning's roughness values ( $n$ ) for the channels varied from 0.060 for the upstream reaches (narrow channels flowing on moderately steep slopes) to 0.022 in Mud Bay.

The model was then validated to the two most recent storms; in January 2013 and January 2014. These two recent flood events were of lower magnitude than the 2003, 2009, and 2005 flood events. However, significant construction work was undertaken by the City between 2009 and 2011, resulting in the current infrastructure (select dikes, spillways, pump stations, bridges, etc.) being different from the infrastructure that was in place during those earlier flood events. Since the current infrastructure is in a state that more closely resembles the future infrastructure there was more value in validating the model to the more recent storm events.

#### **4.3.1 January 2014 Flood**

The 2014 flood was simulated from January 9 to 16, with peak water levels occurring on January 11. The Mud Bay water level boundaries were specified as the reconstructed water level time series for January 2014. The inflow boundaries (both point and distributed) were specified as the HSPF modelled inflow hydrographs from 2014 (existing land uses). Spillway locations, dimensions and elevations included in the RAS model were set to be representative of available data for January 2014.

The 2014 event was well documented by the City. During the 2014 event, the City's SCADA system went offline between 1AM and 8AM on January 11, thereby missing the event's peak water levels. A field survey was conducted on January 17 to identify high water marks (HWM) along the Nicomekl and Serpentine Rivers to confirm or complement the water level records. The available observed data for January 2014 are summarized in Table 13 along with differences between simulated water levels and recorded levels. Comparison plots of modelled and observed time series are included in Appendix D.

Agreement on the lower reaches of the Serpentine and Nicomekl Rivers are within 0.1 m (4 HWMs and 2 gauges) while agreement in the upper reaches (3 HWMs and 3 gauge) is within 0.2 to 0.7 m. The larger differences in the upper reaches are at HWMs. Better agreement was achieved at these locations in January 2013. At the Nicomekl sea dam, peak modelled discharge agreed to within 0.5% of the peak observed discharge. The timeseries plot of modelled and recorded discharge is shown in Figure 17.

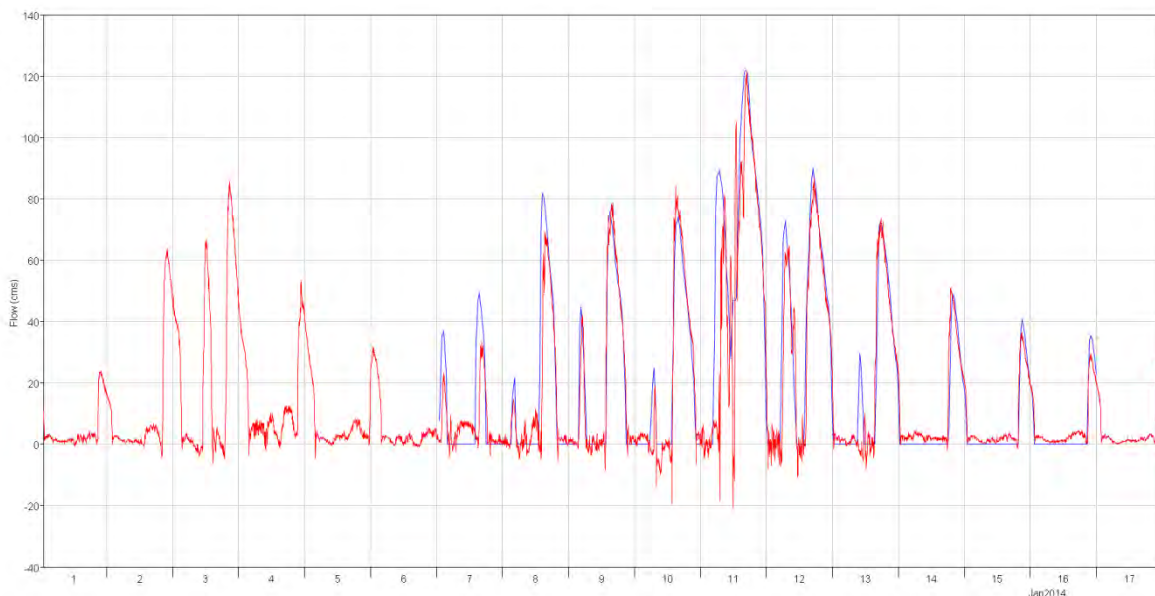


**Figure 17. Observed (red) and modelled (blue) discharge (m<sup>3</sup>/s) at the Nicomekl sea dam for January 1 to 17, 2014.**

On the floodplain, modelled water levels were generally within  $\pm 0.2$  m of observed levels (7 HWMs) except for Cell 140 where modelled levels were 1 m lower than observed. The floodplain inundation in January 2014 was limited and mostly confined to floodplain ditches. It is anticipated that the model would be better at simulating peak water levels for larger events when water overflows the ditches. The storage areas in the model assume a horizontal water level across each storage cell. In some instances, the simulated water level for the storage cell was compared with the observed water level in a local ditch near a pump station - locations perhaps unrepresentative of conditions for the entire cell. Model limitations are discussed in Section 4.6

**Table 13. Agreement between maximum observed and modelled peak water levels (Jan 2014).**

Gauge Name	HEC-RAS Location	Peak WLS (m GD)			
		Type	Obsv	Mod	Diff
<b>Floodplain</b>					
N_LOGGING DITCH PS	CELLS 104	STAGE	n/a	-0.45	n/a
N_BURROWS PS	CELLS 105	STAGE	n/a	-0.32	n/a
N_ERICKSON PS	CELLS 106	STAGE	n/a	-0.22	n/a
S_150 ST PS	CELLS 109	STAGE	n/a	-0.1	n/a
N_40 AVE PS	CELLS 110	STAGE	n/a	-0.14	n/a
N_40 AVE PS	CELLS 110	HWM	-0.33	-0.14	0.19
N_NICOMEKL PS	CELLS 110	STAGE	n/a	-0.14	n/a
N_NICOMEKL PS	CELLS 110	HWM	-0.40	-0.14	0.26
S_48 AVE PS	CELLS 110	STAGE	n/a	-0.14	n/a

S_48 AVE PS	CELLS 110	HWM	-0.22	-0.14	0.08
N_HALLS PRAIRIE PS	CELLS 112	STAGE	n/a	-0.38	n/a
N_HALLS PRAIRIE PS	CELLS 112	HWM	-0.52	-0.38	0.14
S_COLEBROOK PS	CELLS 122	STAGE	n/a	0.02	n/a
S_PANORAMA PS	CELLS 125	STAGE	n/a	-0.12	n/a
S_GRAY PS	CELLS 127	STAGE	n/a	-0.13	n/a
S_COAST MERIDIAN PS	CELLS 132	STAGE	n/a	-0.5	n/a
S_FRYS CORNER PS	CELLS 134	STAGE	n/a	0.06	n/a
S_U SERPENTINE PS	CELLS 135	STAGE	n/a	0.58	n/a
S_U SERPENTINE PS	CELLS 135	HWM	0.36	0.58	0.22
S_HOOKBROOK PS	CELLS 138	STAGE	n/a	-0.35	n/a
S_E NEWTON PS	CELLS 139	STAGE	n/a	-0.22	n/a
S_E NEWTON PS	CELLS 139	HWM	-0.03	-0.22	-0.19
S_64 AVE PS	CELLS 140	STAGE	n/a	-1	n/a
S_64 AVE PS	CELLS 140	HWM	-0.03	-1	-0.97
S_FLEETWOOD PS	CELLS 141	STAGE	n/a	-0.03	n/a
S_FLEETWOOD PS	CELLS 141	HWM	0.04	-0.03	-0.07
S_N FRYS CORNER PS	CELLS 143	STAGE	n/a	-0.1	n/a
<b>Channel</b>					
CANAL 168 ST SOUTH	CANALS 168 ST SOUTH 28.5	STAGE	1.96	1.71	-0.25
S_E NEWTON PS	CANALS BEAR CREEK 134	STAGE	n/a	1.88	n/a
S_E NEWTON PS	CANALS BEAR CREEK 134	HWM	1.84	1.88	0.04
BEAR CREEK AT SURREY LAKE	CANALS BEAR CREEK 2856.5	STAGE	4.10	3.3	-0.80
N_S CLOVERDALE PS	CANALS CLOVERDALE 96	STAGE	n/a	-0.11	n/a
LATIMER AT HARVIE RD	CANALS LATIMER CREEK 1308.5	STAGE	1.99	1.87	-0.12
N_SEA DAM DS	NICOMEKL RIVER MAIN DS -10.7	STAGE	n/a	1.71	n/a
N_SEA DAM US	NICOMEKL RIVER MAIN DS 20	STAGE	n/a	1.62	n/a
N_SEA DAM US	NICOMEKL RIVER MAIN DS 20	FLOW	121.18	121.7	0.57
N_LOGGING DITCH PS	NICOMEKL RIVER MAIN DS 5577.4	STAGE	n/a	1.68	n/a
N_S CLOVERDALE PS	NICOMEKL RIVER MAIN DS 7950.9	STAGE	n/a	1.72	n/a
N_BURROWS PS	NICOMEKL RIVER MAIN US 8642.3	STAGE	n/a	1.74	n/a
N_ERICKSON PS	NICOMEKL RIVER MAIN US 10394.5	STAGE	n/a	1.79	n/a
N_HALLS PRAIRIE PS	NICOMEKL RIVER MAIN US 10394.5	HWM	1.85	1.79	-0.06
NICOMEKL RIVER AT 192	NICOMEKL RIVER MAIN US 14415.1	STAGE	2.78	2.44	-0.34
NICOMEKL RIVER AT 203 ST	NICOMEKL RIVER MAIN US 17336.5	STAGE	n/a	4.01	n/a
NICOMEKL RIVER AT 203 ST	NICOMEKL RIVER MAIN US 17336.5	HWM	4.72	4.01	-0.71
S_SEA DAM DS	SERPENTINE RIVER MAIN -12.8	STAGE	n/a	1.73	n/a
S_SEA DAM US	SERPENTINE RIVER MAIN 13.2	STAGE	n/a	1.72	n/a
SERPENTINE RIVER AT HWY10	SERPENTINE RIVER MAIN 7500.9	STAGE	1.84	1.79	-0.05
S_64 AVE PS	SERPENTINE RIVER BOSE 9824.7	STAGE	n/a	1.82	n/a
S_64 AVE PS	SERPENTINE RIVER BOSE 9824.7	HWM	1.90	1.82	-0.08

S_FLEETWOOD PS	SERPENTINE RIVER WEST US 11817.8	STAGE	n/a	1.85	n/a
S_FLEETWOOD PS	SERPENTINE RIVER UPPER DS 11909.9	HWM	1.91	1.84	-0.07
S_FRY'S CORNER PS	SERPENTINE RIVER UPPER MID 13762	STAGE	n/a	1.85	n/a
S_N FRY'S CORNER PS	SERPENTINE RIVER UPPER MID 13845.9	STAGE	n/a	1.85	n/a
S_U SERPENTINE PS	SERPENTINE RIVER UPPER US 15940.2	STAGE	n/a	1.87	n/a
S_U SERPENTINE PS	SERPENTINE RIVER UPPER US 15940.2	HWM	2.09	1.87	-0.22
SERPENTINE RIVER AT 168 ST	SERPENTINE RIVER UPPER US 19171.5	HWM	6.40	5.81	-0.59

Notes: Differences between observed and modelled water levels are colour coded based on magnitude.

The above results (Table 13) were compared with UMA's model calibration to the 2003 flood (UMA 2004). By fine-tuning roughness coefficients, UMA achieved an agreement of  $\pm 0.08$  m at most gauges on the Serpentine with a somewhat poorer fit on the Nicomekl. For the floodplain cells, the simulated water levels were generally higher than the observed levels by 0.2 to 0.3 m although large discrepancies were also noted.

### 4.3.2 January 2013 Flood

The 2013 flood was simulated from January 6<sup>th</sup> to 13<sup>th</sup>, with peak water levels occurring between January 8<sup>th</sup> and 9<sup>th</sup>. Again, the downstream water level boundaries in Mud Bay were specified as the reconstructed water level time series from January 2013. The upstream boundaries and inflows (point and distributed) were specified as the HSPF modelled inflow hydrographs from 2013 (existing land uses). Spillway locations, dimensions and elevations included in the RAS model were set to be representative of available data for January 2013 (same as 2014).

The available observed data for January 2013 are summarized in Table 14 along with differences between simulated water levels and recorded levels. Comparison plots of modelled and observed time series are included in Appendix D.

Agreement on the Nicomekl River is within  $\pm 0.05$  m (4 gauges) except downstream of the sea dam (difference = 0.21 m) and at 192<sup>nd</sup> street gauge (difference = -0.37 m). On the Serpentine River, agreement is within  $\pm 0.06$  m (6 gauges) except at 2 gauges where peak water levels are within  $\pm 0.15$  m). Agreement at three tributary/canal gauges is within 0.1 m except for Bear Creek at Surrey Lake (difference = -0.44 m).

On the floodplain, modelled water levels are within  $\pm 0.1$  m of observed levels at 7 gauges. At the remaining gauges (11 gauges) modelled water levels are generally within  $\pm 0.35$  m of observed levels. Similarly to January 2014, the floodplain inundation in January 2013 was limited and mostly confined to floodplain ditches. It is anticipated that the model would be better at simulating peak water levels for larger events when water overflows the ditches. The storage areas in the model assume a horizontal water level across each storage cell. In some instances, the simulated water level for the storage cell was compared with the observed water level in a local ditch near a pump station, locations perhaps unrepresentative of conditions for the entire cell.



**Table 14. Agreement between maximum observed and modelled river water levels (Jan 2013)**

Gauge Name	HEC-RAS Location	Peak WLs (m GD)			
		Type	Obsv	Mod	Diff
<b>Floodplain</b>					
N_LOGGING DITCH PS	CELLS 104	STAGE	-0.42	-0.49	-0.07
N_BURROWS PS	CELLS 105	STAGE	-0.28	-0.33	-0.05
N_ERICKSON PS	CELLS 106	STAGE	-0.01	-0.24	-0.23
S_150 ST PS	CELLS 109	STAGE	-0.25	-0.22	0.03
S_48 AVE PS	CELLS 110	STAGE	-0.45	-0.25	0.20
N_40 AVE PS	CELLS 110	STAGE	-0.07	-0.25	-0.18
N_NICOMEKL PS	CELLS 110	STAGE	n/a	-0.25	n/a
N_HALLS PRAIRIE PS	CELLS 112	STAGE	-0.81	-0.42	0.39
S_COLEBROOK PS	CELLS 122	STAGE	-0.53	-0.24	0.29
S_PANORAMA PS	CELLS 125	STAGE	-0.13	-0.24	-0.11
S_GRAY PS	CELLS 127	STAGE	-0.27	-0.2	0.07
S_COAST MERIDIAN PS	CELLS 132	STAGE	-0.46	-0.57	-0.11
S_FRY'S CORNER PS	CELLS 134	STAGE	-0.06	-0.09	-0.03
S_U SERPENTINE PS	CELLS 135	STAGE	0.62	0.36	-0.26
S_HOOKBROOK PS	CELLS 138	STAGE	-0.42	-0.55	-0.13
S_E NEWTON PS	CELLS 139	STAGE	-0.06	-0.41	-0.35
S_64 AVE PS	CELLS 140	STAGE	-0.90	-1.1	-0.20
S_FLEETWOOD PS	CELLS 141	STAGE	-0.01	-0.23	-0.22
S_N FRY'S CORNER PS	CELLS 143	STAGE	0.00	-0.27	-0.27
<b>Channel</b>					
CANAL 168 ST SOUTH	CANALS 168 ST SOUTH 28.5	STAGE	1.67	1.65	-0.02
S_E NEWTON PS	CANALS BEAR CREEK 134	STAGE	1.72	1.63	-0.09
BEAR CREEK AT SURREY LAKE	CANALS BEAR CREEK 2856.5	STAGE	3.52	3.08	-0.44
N_S CLOVERDALE PS	CANALS CLOVERDALE 96	STAGE	-0.22	-0.28	-0.06
LATIMER AT HARVIE RD	CANALS LATIMER CREEK 1308.5	STAGE	n/a	1.64	n/a
N_SEA DAM DS	NICOMEKL RIVER MAIN DS -10.7	STAGE	1.54	1.75	0.21
N_SEA DAM US	NICOMEKL RIVER MAIN DS 20	STAGE	1.80	1.76	-0.04
N_LOGGING DITCH PS	NICOMEKL RIVER MAIN DS 5577.4	STAGE	1.75	1.78	0.03
N_S CLOVERDALE PS	NICOMEKL RIVER MAIN DS 7950.9	STAGE	n/a	1.8	n/a
N_BURROWS PS	NICOMEKL RIVER MAIN US 8642.3	STAGE	1.85	1.8	-0.05
N_ERICKSON PS	NICOMEKL RIVER MAIN US 10394.5	STAGE	1.84	1.81	-0.03
NICOMEKL RIVER AT 192	NICOMEKL RIVER MAIN US 14415.1	STAGE	2.68	2.31	-0.37
S_SEA DAM DS	SERPENTINE RIVER MAIN -12.8	STAGE	1.87	1.84	-0.02
S_SEA DAM US	SERPENTINE RIVER MAIN 13.2	STAGE	1.46	1.61	0.15
SERPENTINE RIVER AT HWY10	SERPENTINE RIVER MAIN 7500.9	STAGE	1.65	1.62	-0.03
S_64 AVE PS	SERPENTINE RIVER BOSE 9824.7	STAGE	1.57	1.63	0.06
S_FLEETWOOD PS	SERPENTINE RIVER WEST US 11817.8	STAGE	1.67	1.63	-0.04

S_FRYS CORNER PS	SERPENTINE RIVER UPPER MID 13762	STAGE	1.67	1.63	-0.04
S_N FRYS CORNER PS	SERPENTINE RIVER UPPER MID 13845.9	STAGE	1.66	1.64	-0.02
S_U SERPENTINE PS	SERPENTINE RIVER UPPER US 15940.2	STAGE	1.76	1.64	-0.12

Notes: Differences between observed and modelled water levels are colour coded based on magnitude.

## 4.4 Sensitivity Analysis

A sensitivity analysis was carried out to assess the model response to variations in roughness and upstream inflows.

### 4.4.1 Model Roughness Coefficients

The model was re-run with the roughness coefficients increased and decreased by 20% to assess the effect on the maximum 2014 flood profile. Overall, the model was insensitive to channel roughness in the lower – tidally influenced – reaches of the Serpentine and Nicomekl Rivers. A 20% change in roughness results in less than 0.1 m of change along the water level profile for the river reaches starting at the ocean up to river chainage 13+000 on the Nicomekl and up to river chainage 18+000 on the Serpentine River. However, the upper reach of the Nicomekl River appears to be more sensitive to changes in roughness values, resulting in variations from  $\pm 0.1$  m to  $\pm 0.25$  m. For the upper Serpentine, the reach from chainage 17+000 to 19+000 is sensitive ( $\pm 0.1$  to  $\pm 0.22$ ) to changes in roughness. Values for the entire river reaches are summarized in Table 15. Longitudinal plots of modelled water levels are included in Appendix D.

**Table 15. Model sensitivity to changes in bed roughness.**

Parameter	Nicomekl River (m)		Serpentine River (m)	
	(+20%)	(-20%)	(+20%)	(-20%)
Average =	0.06	-0.07	0.02	-0.02
Median =	0.02	-0.03	0.01	-0.01
Max =	0.21	0.02	0.17	0.04
Min =	-0.01	-0.24	-0.01	-0.22
St. Dev. =	0.07	0.08	0.04	0.04

### 4.4.2 Inflow Values

The model was re-run with both a 10% increase and a 10% decrease applied to input inflow hydrographs in order to assess the model's sensitivity to the upstream boundaries (inputs from HSPF model results).

Overall, the lower – tidally influenced – reaches of the Serpentine and Nicomekl Rivers are insensitive to changes to inflow hydrographs. A 10% change in inflows results in less than 0.10 m of change along the water level profile for the river reaches starting in the ocean, up to river chainage 13+000 on the Nicomekl, and going all the way up on the Serpentine River (chainage 19+600). However, the upper

reach of the Nicomekl River appears to be more sensitive to changes in inflows values (corresponding variations ranging from  $\pm 0.1$  m to  $\pm 0.15$  m).

Values for the entire river reaches are summarized in Table 16 and for the floodplain cells in Table 17. Longitudinal plots of modelled water levels are included in Appendix D.

**Table 16. Model sensitivity to changes in inflow hydrographs.**

Parameter	Nicomekl River (m)		Serpentine River (m)	
	(+10%)	(-10%)	(+10%)	(-10%)
Average =	0.04	-0.04	0.02	-0.06
Median =	0.02	-0.02	0.02	-0.07
Max =	0.12	0.00	0.10	0.01
Min =	0.00	-0.13	-0.01	-0.11
St. Dev. =	0.04	0.04	0.03	0.03

**Table 17. Floodplain cell sensitivity to changes in inflow hydrographs.**

Cell	Max WSE (m)		
	Base Case	(+10%)	(-10%)
101	1.79	0.04	-0.04
102	0.53	0	0
103	0.45	0	-0.01
104	-0.45	0.01	0
105	-0.32	0	-0.01
106	-0.22	0.01	0
107	0.31	0	0
108	0.31	0	0
109	-0.1	0	0
110	-0.14	0.01	0
111	-0.38	0	0
112	-0.38	0	-0.01
113	0.09	0.02	-0.02
114	1.08	0.08	-0.07
115	-0.11	0	-0.01
116	-0.07	0	0
117	-0.38	0	0
118	0.1	0.06	-0.07
119	0.23	0	0
120	0.02	0	0
121	0.18	0	0
122	0.02	0	0
123	0.04	0	0
124	0.16	0	0
125	-0.12	0.01	0
126	-0.11	0.01	0
127	-0.13	0.01	0
128	-0.12	0	-0.01
129	-0.34	0.01	-0.02
130	-0.16	0	0
131	0.09	0.04	-0.04
132	-0.5	0.01	-0.01
133	0.35	0	0
134	0.06	0.03	-0.03
135	0.58	0.01	-0.03
136	0.61	0.02	-0.02
137	0.77	0	0
138	-0.35	0.01	-0.02

139	-0.22	0.02	-0.01
140	-1	0.01	0
141	-0.03	0.03	-0.03
142	-0.24	0.01	-0.01
143	-0.1	0.03	-0.03
144	-0.35	0	0
145	1.82	0.01	-0.02
146	2.59	0.07	-0.07

#### 4.5 HEC-RAS Model Simulations

Following verification and sensitivity analyses, the model was used to generate nine time series of simulated water levels at key locations in the river channels and floodplain. The list of simulations is included in Table 18. For all nine simulations, spillways were set to ultimate elevations, dikes were raised to prevent overtopping (except at spillways) and dikes were not allowed to breach.

For each simulation, water level output (corresponding to a period of 47 years) were written to a HEC-RAS DSS file at 30 minute time intervals at 97 key locations in the floodplain and river channels. The data was later analyzed to determine the annual peak level per water year and these values formed the input to estimating the 200-year water levels using frequency analyses.

Results from the various runs are discussed under the vulnerability assessments presented in Section 5.

**Table 18. List of hydraulic model simulations.**

Run No.	Name	Year	SLR (m)	Precipitation	Landuse	Subsidence	Reporting
1	Design levels - 2010	2010	0	Historic	Existing	none	Flood extents and elevations, vulnerable infrastructure
2	Design levels - 2020	2020	0.11	Historic	Existing	none	Flood extents and elevations, vulnerable infrastructure
3	Design levels - 2040	2040	0.32	Historic	Future	none	Flood extents and elevations, vulnerable infrastructure
4	Design levels - 2070	2070	0.65	Historic	Future	none	Flood extents and elevations, vulnerable infrastructure
5	Design levels – 2100	2100	0.97	Historic	Future	none	Flood extents and elevations, vulnerable infrastructure
6	Sensitivity - Moderate Precipitation	2100	0.97	Moderate precipitation increase from climate change	Future	none	Flood extents and elevations.
7	Sensitivity - Severe Precipitation	2100	0.97	Severe precipitation increase from climate change	Future	none	Flood extents and elevations.
8	Sensitivity - Subsidence	2100	0.97 (RSLR=1.06)	Historic	Future	0.09 (1mm/yr)	Flood extents and elevations.
9	Sensitivity -Sea Level Rise	2200	1.97	Historic	Future	none	Flood extents and elevations.

#### **4.5.1 Run 1: Simulation of Present (2010) Conditions**

The model was first run to generate a time series of water levels representative of the historic 1964 to 2011 runoff and historic water levels in Mud Bay (without sea level rise).

The downstream water level boundaries in Mud Bay were specified as the reconstructed water level time series for the historic period from 1964 to 2011.

The upstream boundaries and inflows (point and distributed) were specified as the HSPF modelled inflow hydrographs from 1964 to 2011, reflective of existing land uses.

#### **4.5.2 Run 2, 3, and 4: Simulation of Intermediate Future (2020, 2040, and 2070) Conditions with Sea Level Rise**

To assist with phasing of infrastructure upgrades and to identify when certain improvements need to be implemented, the impacts of sea level rise under climate change were assessed for three intermediate years, 2020, 2040 and 2070.

Time series were generated for these intermediate years using simulated runoff values using historic precipitation records and existing land-use values for year 2020 and while future land-use values were used for year 2040 and 2070.

Intermediate allowances for sea level rise were added to the downstream water level boundaries in Mud Bay (0.11 m, 0.32 m, and 0.65 m).

#### **4.5.3 Run 5: Simulation of Projected Future (2100) Conditions with Sea Level Rise**

The model was then used to generate a time series of water levels representative of conditions anticipated in year 2100.

Historic precipitation and future land-use values were used to generate runoff time series for year 2100.

An allowance for sea level rise (0.97 m) was added to the downstream water level boundaries in Mud Bay. This is based on the underlying assumption of 1 m of sea level rise from 2000 to 2100 and an observed rise of 0.03 m between 2000 and 2010, the adopted base year for the assessments.

#### **4.5.4 Run 6 and 7: Simulation of Projected Future (2100) Conditions with Changes in Precipitation**

To provide an indication of the sensitivity of flood levels to variations in future rainfall amounts, simulations 6 and 7 generated time series of future water levels for year 2100 by imposing estimates of future rainfall under moderate and severe climate change regimes.

The same allowance for sea level rise (0.97 m) for year 2100 was added to the downstream water level boundaries in Mud Bay.

Additional details on the moderate and severe future precipitation regimes for year 2100 are included in Section 3.

#### **4.5.5 Run 8: Simulation of Projected Future (2100) Conditions with Subsidence**

Simulation 8 provides an indication of the sensitivity of flood levels for year 2100 to floodplain subsidence.

An average subsidence value of 1 mm/year was estimated by TEL and results in a total subsidence of 0.09 m from 2010 to 2100. Subsidence was modelled using a relative sea level rise approach which consists of adding the subsidence to the sea level rise (no changes to model geometry). Therefore, a relative sea level rise of 1.06 m for year 2100 was added to the downstream water level boundaries in Mud Bay.

Historic precipitation and future land-use values were used to generate runoff for year 2100.

#### **4.5.6 Run 9: Simulation of Projected Future (2200) Conditions with Sea Level Rise**

Finally, simulation 9 generated a time series of estimated water levels for year 2200.

Historic precipitation and future land-use values were used to generate runoff for year 2200 (same landuse as for year 2100, with no increase in precipitation from 2010 conditions).

An allowance for sea level rise (1.97 m) was added to the downstream water level boundaries in Mud Bay.

Whereas projecting flood levels to year 2200 is useful for long term planning, it needs to be recognized that such estimates are surrounded by significant uncertainty.

### **4.6 Model Limitations**

It is important to note that any inaccuracies in the ocean level boundary conditions or deviations between actual and modelled runoff will affect the hydraulic model results and the effects of any discrepancies could even be amplified in the hydraulic model. As per provincial guidelines, a linear increase in sea level rise was assumed, although median values of estimated rise suggest lesser increases until roughly year 2130 (Ausenco Sandwell 2011).

In a few locations, the model appears to neglect some components of the hydraulic system or comparisons between the simulated and observed levels are invalid because the observed water levels apply to specific localized areas rather than the average of the overall storage cell. The hydraulic model accuracy can likely be further improved by fine-tuning the structures incorporated in the model, optimizing the locations where observed and simulated levels are compared and by modelling the storage cells in two dimensions in order to capture the time lag needed for runoff to travel across the floodplain cells before reaching a pump station or floodbox.



The observed water levels in several of the lower floodplain cells were tidally affected. Some of these tidally-caused water level fluctuations were better simulated after additional floodboxes were included in the model. Perfect agreement was not expected and the main goal of the HEC-RAS model was to represent general flow trends during a flood event and obtain the best match to peak water levels. The limitations of the hydraulic model need to be recognized and caution must be applied when interpreting the model results.

It is recommended that further improvements be made as part of future phases of work. However, in terms of evaluating the relative impacts of climate change on flood levels in the Serpentine and Nicomekl basins, the HEC-RAS model is a useful tool.

## 5 VULNERABILITY ASSESSMENT

To assist with phasing of infrastructure upgrades and to identify when certain improvements need to be implemented, the City requested that the impacts of climate change be assessed for three intermediate years between 2010 and 2100. The 200-year flood levels were estimated for each of the intermittent years and compared to pertinent infrastructure elevations. Separate vulnerability assessments were completed for inland areas and the coastal diking. (See Section 3 for the coastal diking vulnerability.)

The inland vulnerability assessment includes:

- Evaluating changes in floodplain extents and flood levels.
- Identifying vulnerable infrastructure at the 200-year flood levels and comparing design dike crests, road / rail elevations and bridge low / high chord elevations with design levels.
- Evaluating the system capacity upstream of the sea dams.

### 5.1 200-year Flood Levels

#### 5.1.1 Inputs to Frequency Analyses

Annual maximum flood levels for the nine time series generated in Section 4.5 were analyzed in frequency analyses to estimate the 200-year return period flood levels at the key locations shown in Figure 18. NHC's in-house frequency analysis package 'DASH' was applied since this software conveniently uses the HEC-RAS DSS output file as input.

Annual peak water levels were determined based on water years (1 September to 31 August). The results demonstrate that peak water levels (comparing between events) can occur at different locations along the river channels for different tide and precipitation conditions. It also shows that the Nicomekl and Serpentine systems react differently to some events. Generally, flooding is caused by one of:

- High tides (Dec 82)
- Several days with the tide levels above the mean tide level combined with moderate precipitation (Dec 07, Nov 83)
- Large volumes of precipitation (Oct 03, Jan 09)
- High intensity of precipitation (May 97, Jan 05)

Plots of hourly precipitation and ocean levels for select flood events are included in Appendix E.

HEC-RAS Stream Network

Storage Cell  
(with cell number)

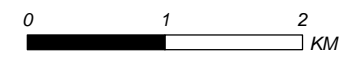
Key Output Locations

In-River  
(with chainage)

Storage Cell



SCALE - 1:55,000



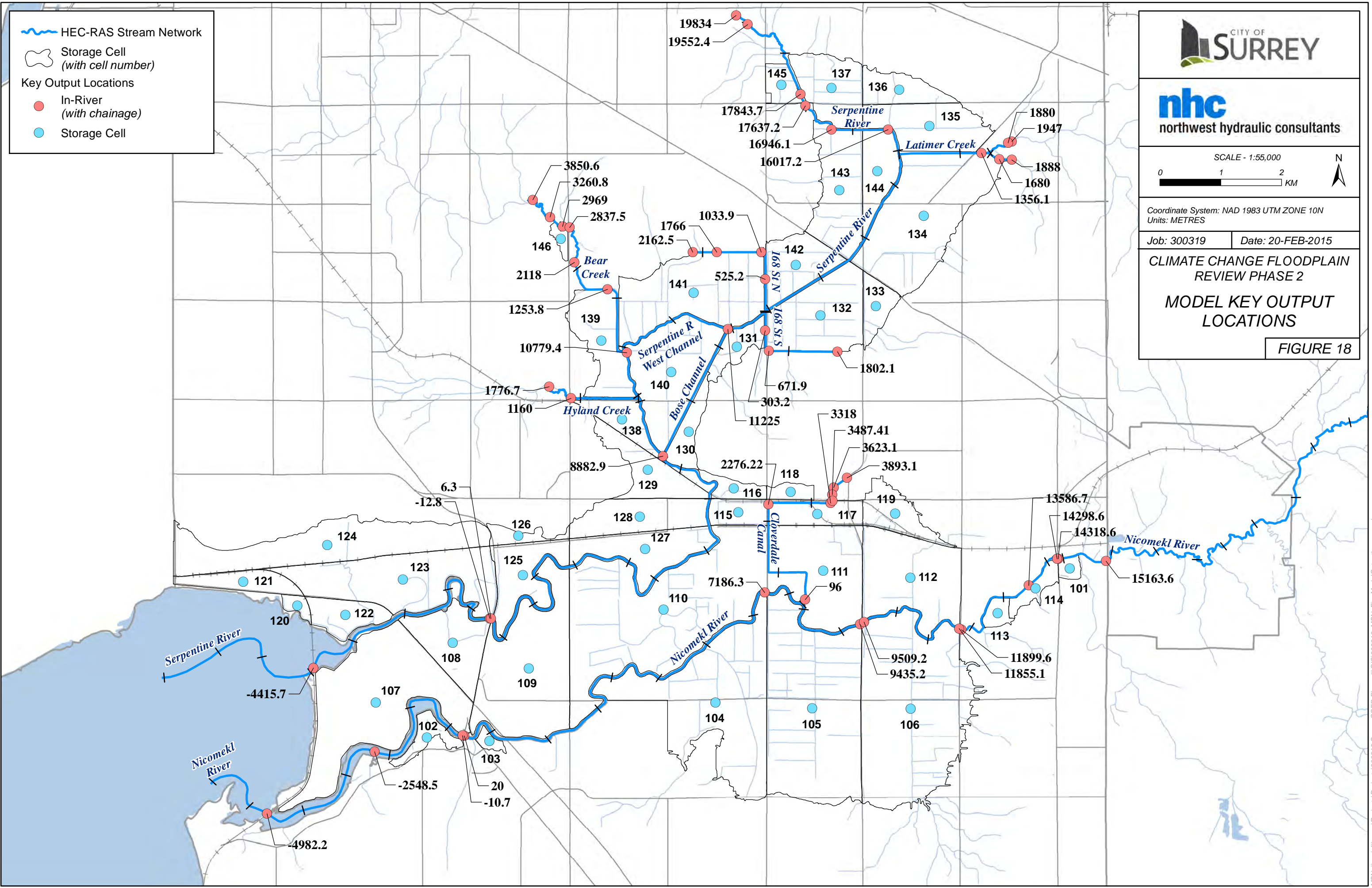
Coordinate System: NAD 1983 UTM ZONE 10N  
Units: METRES

Job: 300319 | Date: 20-FEB-2015

CLIMATE CHANGE FLOODPLAIN  
REVIEW PHASE 2

MODEL KEY OUTPUT  
LOCATIONS

FIGURE 18



MSN: \\mainfile-van\Projects\Projects\300319 Surrey CCFR Phase II\GIS\300319\_MSN\_Fig\_ModelOutputLocns.mxd

Longitudinal profiles plotted for the Serpentine River in Figure 19 show how different events result in peak water levels in different areas. Events with high intensity precipitation and high volume rainfall events result in peak water levels in the upper reaches and floodplain cells. In the Serpentine and Nicomekl Rivers upstream of the sea dams, it is a combination ocean/rainfall events that generate the peak water levels. In the majority of the storage cells and intermediate reaches of the rivers, events with the largest volume of precipitation generate the peak water levels. Figure 20 shows the spatial distribution of the highest ranked historic annual peak water levels for the various reaches or locations in the floodplain (Run1, year 2010).

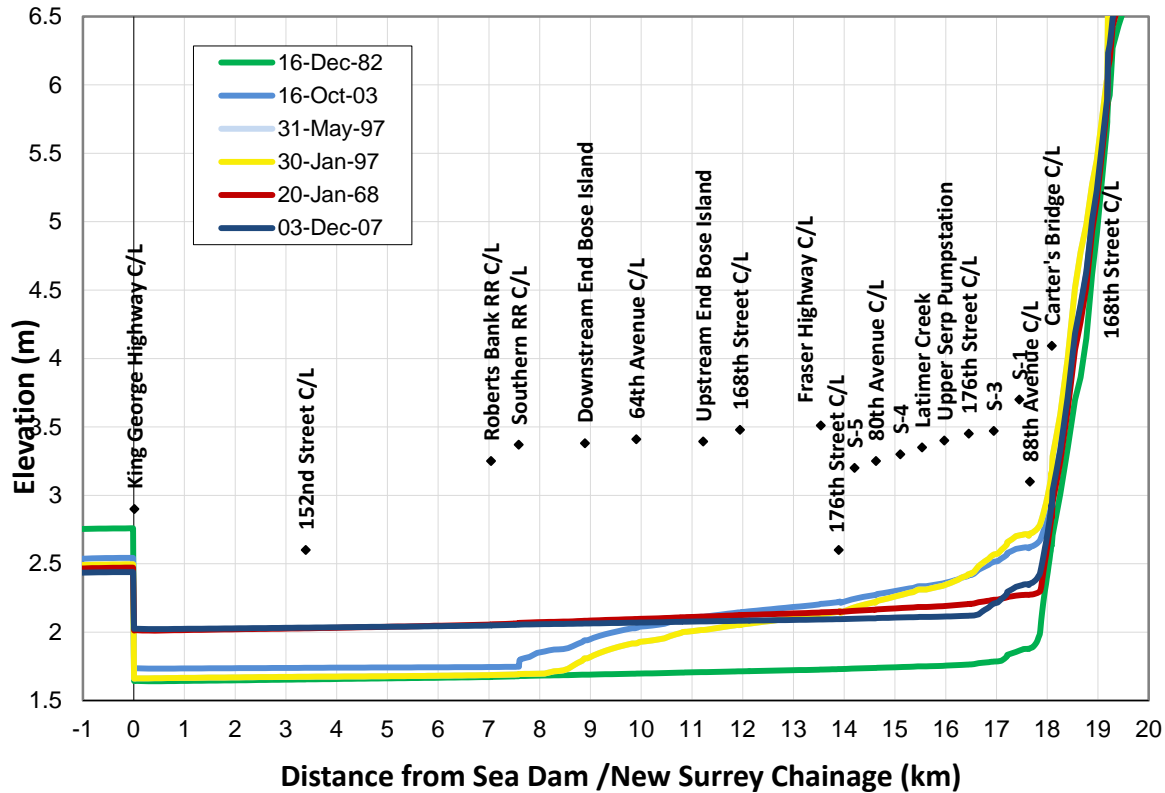
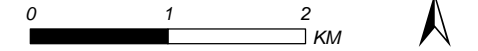


Figure 19. Serpentine River (sea dams = 0 km), longitudinal profiles of peak water levels from various types of events for Run1, year 2010.

SCALE - 1:55,000



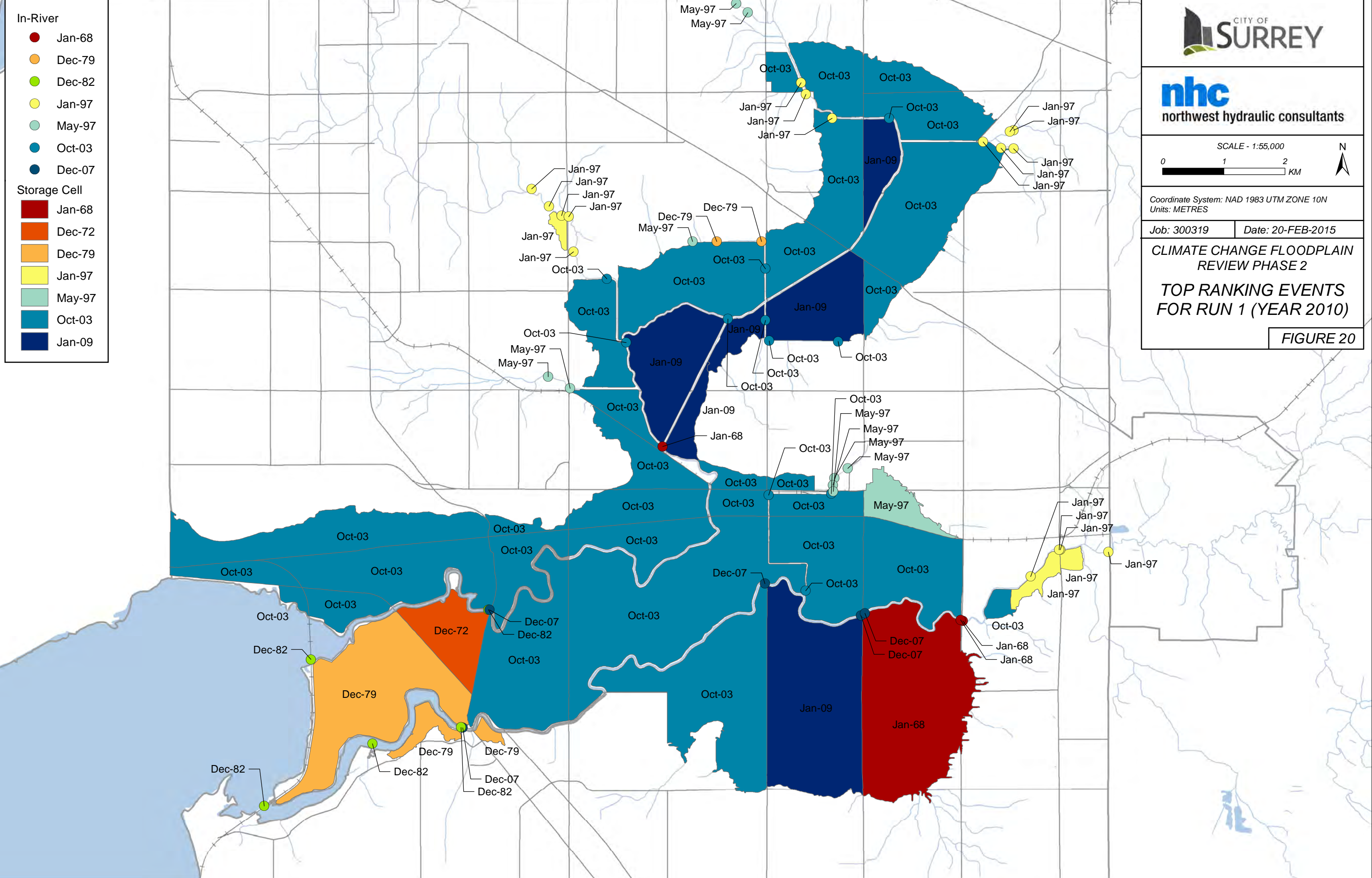
Coordinate System: NAD 1983 UTM ZONE 10N  
Units: METRES

Job: 300319 Date: 20-FEB-2015

**CLIMATE CHANGE FLOODPLAIN  
REVIEW PHASE 2**

**TOP RANKING EVENTS  
FOR RUN 1 (YEAR 2010)**

**FIGURE 20**



### 5.1.2 Frequency Analysis Results

#### Year 2010 to 2100 (Run 1 to Run 5)

Conventional flood frequency analysis in which a formal probability distribution (e.g. Generalized Extreme Value distribution) is fit to a record of annual peak flows or water levels was found to produce inconsistent and highly variable estimates of flood quantiles. To improve consistency of results amongst scenarios and between locations within the Serpentine and Nicomekl floodplain, a graphical approach to frequency analysis was adopted in which a moving average fit was applied to the simulated records of annual peak water levels.

At each of the 97 selected locations, a 3-point moving average fit was applied to the annual peak water levels to extrapolate the data to an annual exceedance probability (AEP) of 0.5% (return period of 200-years). The frequency distribution plots are included in Appendix E (note that these water levels do not include freeboard). For each location, frequency distributions for Runs 1 to 5 are plotted on one figure for comparison.

Typically, frequency analysis results are sensitive to the curve fitting method applied. For assessing the relative change from all scenarios, the 3-point moving average method was considered representative due to the shape of the distributions. Other distributions, for example the GEV method which was used for the coastal analysis, gave somewhat different, generally more conservative results. Also, in contrast to the ocean level analysis - based on partial duration series above a threshold value - the frequency analysis of internal flood levels used a data set of annual maxima. The choice of data series was found to have little effect on the results. The water levels from the coastal analysis were applied to the Nicomekl and Serpentine reaches downstream of the sea dams.

For modelling future flood levels, all dikes were assumed to be raised to prevent flow from spilling from the river channels to the floodplain storage areas. However, spillway elevations were not raised and were set according to 'build-out' configurations.

Longitudinal profiles of 200-year water levels for year 2010, 2020, 2040, 2070, and 2100 (Run 1 to Run 5) are plotted in Figure 21 and Figure 22 for the Serpentine and Nicomekl Rivers.

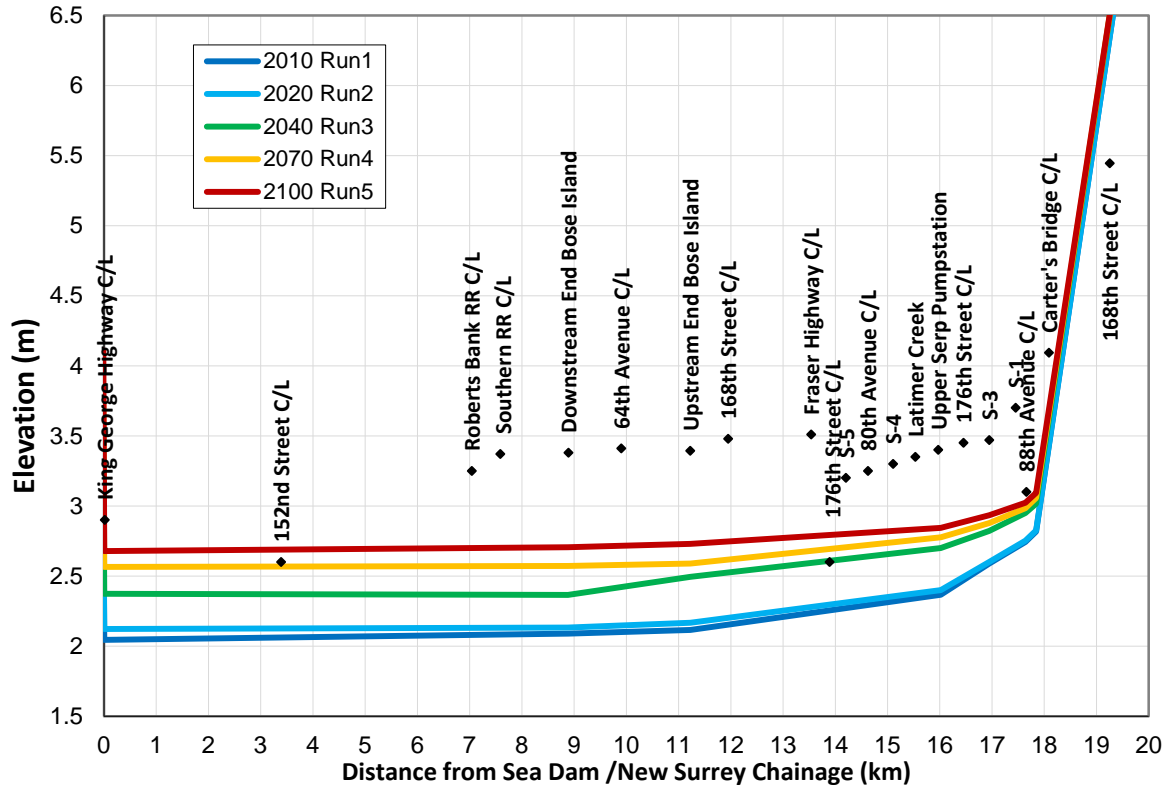
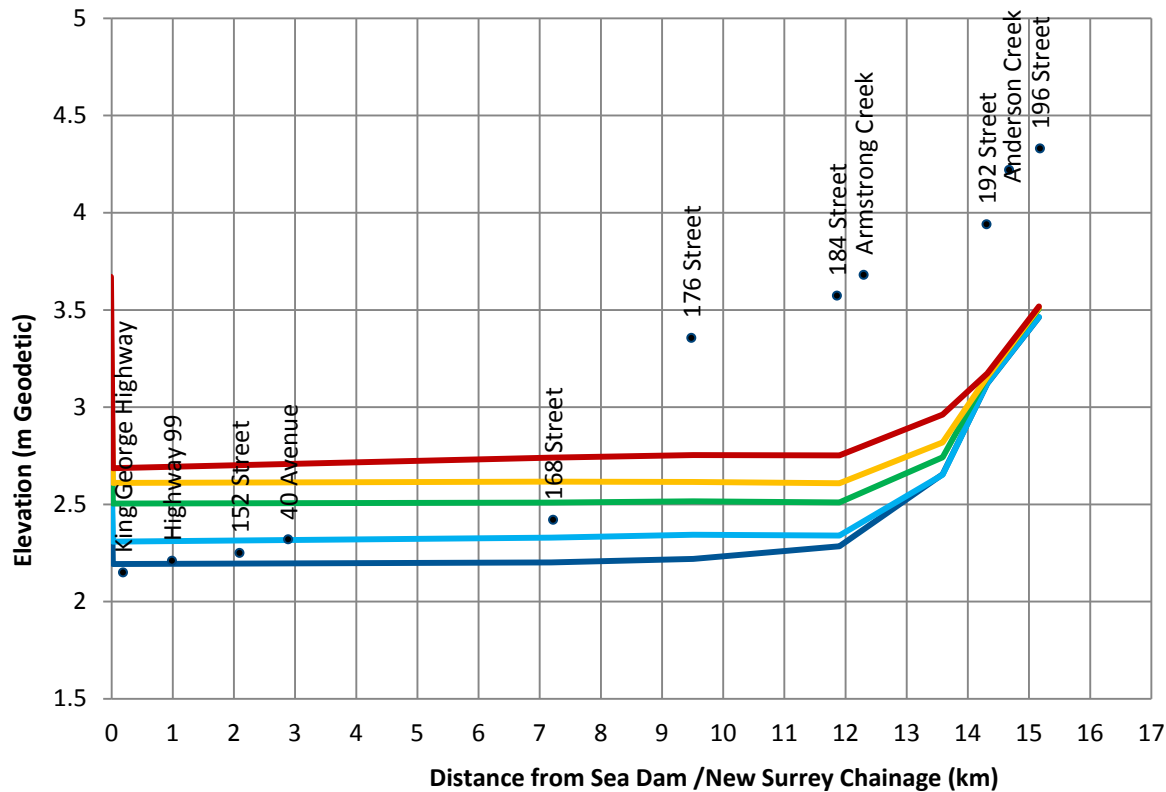


Figure 21. Longitudinal profiles of 200-year water levels for Serpentine River for years 2010 to 2100.



**Figure 22. Longitudinal profiles of 200-year water levels for Nicomekl River for years 2010 to 2100.**

The estimated increases (from 2010 to 2100) to the 200-year flood levels were relatively small for most of the **floodplain**, with values in most cells ranging from 0.1 m to 0.4 m. (Recall that dikes were assumed raised to contain river flows.) A few cells (seven) experienced increases between 0.4 and 0.9 m while three cells experienced increases of up to 1.3 m. The cells experiencing the greatest increases in 200-year water levels from 2010 to 2100 are connected to spillways that transfer more water to the floodplain in 2100.

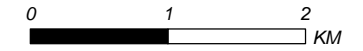
Within the river **channels**, flood levels will be higher as a result of sea level rise. The greatest increases occur downstream of the sea dams. Just upstream of the Nicomekl sea dam, the 200-year flood level is expected to increase by 0.5 m to 0.6 m compared to the present level. This raised flood level remains nearly horizontal for a distance of about 12 km. As the channel gradient begins to steepen, the increase in the flood level diminishes and over an additional distance of about 5 km the 2010 and 2100 200-year flood level are within 0.1 m (assuming no changes in precipitation).

Upstream of the Serpentine sea dam the 200-year flood level is expected to increase by 0.6 m, the flood profile remaining nearly horizontal for 16 km. Similar to the Nicomekl, the existing and future profiles nearly merge over a few kilometres in the upper basin due to the steep gradient.

At the upstream end of the floodplain where ocean levels have minimal influence on the 200-year water levels, the influence of future landuse changes on runoff (implemented in 2040) is noticeable.



SCALE - 1:55,000



Coordinate System: NAD 1983 UTM ZONE 10N  
Units: METRES

Job: 300319

Date: 20-FEB-2015

**CLIMATE CHANGE FLOODPLAIN  
REVIEW PHASE 2**  
**INCREASE IN 200 YEAR  
FLOODPLAIN WATER LEVELS  
FROM 2010 TO 2100 (Run 5 - Run 1)**

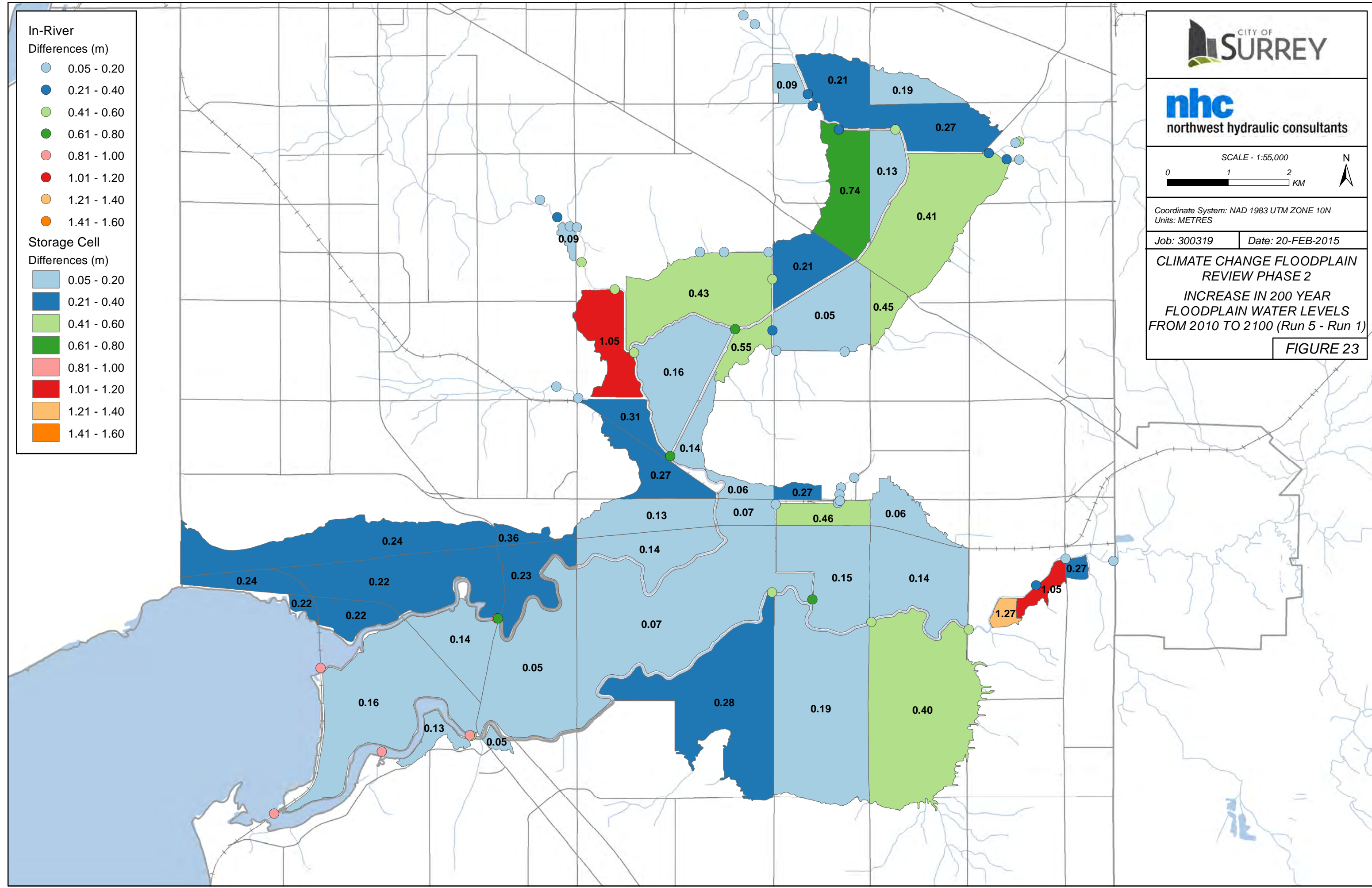
**FIGURE 23**

**In-River**  
Differences (m)

- 0.05 - 0.20
- 0.21 - 0.40
- 0.41 - 0.60
- 0.61 - 0.80
- 0.81 - 1.00
- 1.01 - 1.20
- 1.21 - 1.40
- 1.41 - 1.60

**Storage Cell**  
Differences (m)

- 0.05 - 0.20
- 0.21 - 0.40
- 0.41 - 0.60
- 0.61 - 0.80
- 0.81 - 1.00
- 1.01 - 1.20
- 1.21 - 1.40
- 1.41 - 1.60



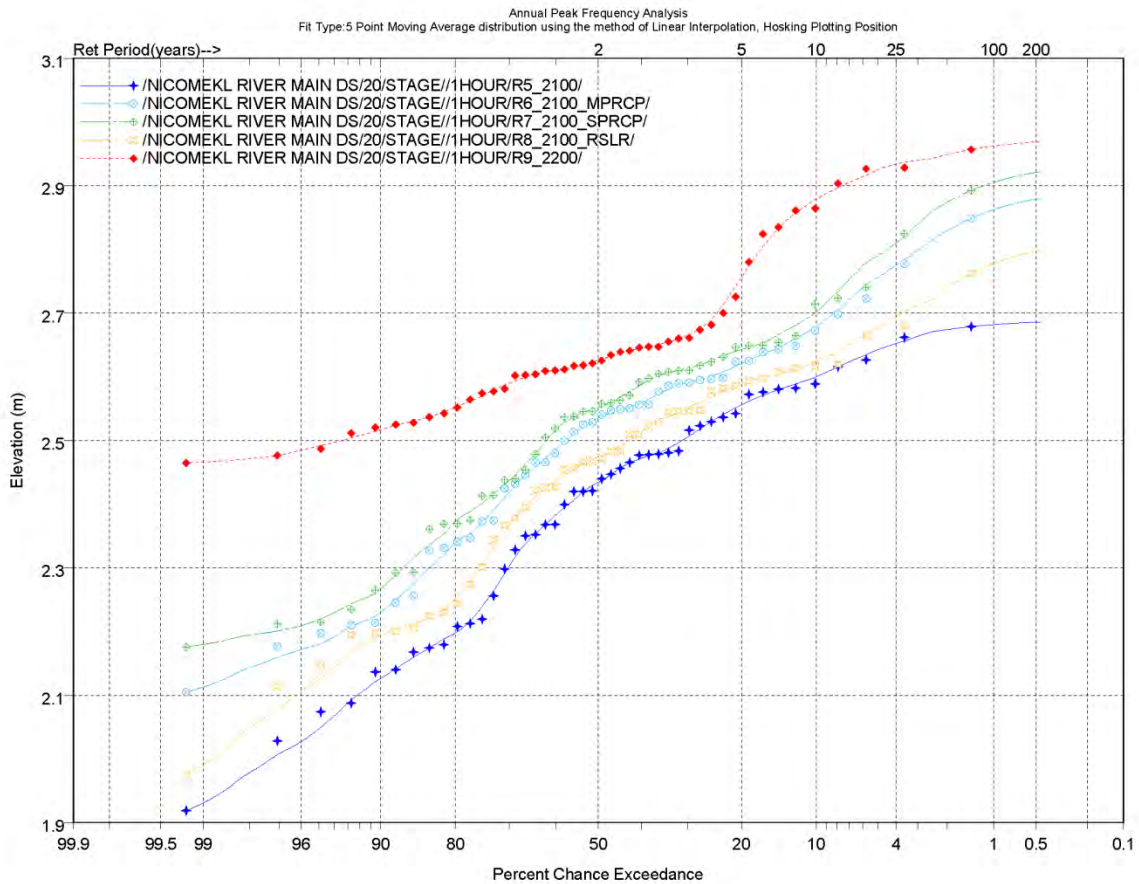
**Year 2100 to 2200 (Run 5 to Run 9)**

The system's sensitivity (year 2100) to future increases in sea levels, and sea level including a subsidence allowance, relative to increases in precipitation can be interpreted from the frequency distributions in Appendix E.

To illustrate the system's behaviour, three representative frequency distribution plots have been selected for discussion. The return period in years is provided along the top x-axis. Each plot shows the distributions for five runs at one selected location:

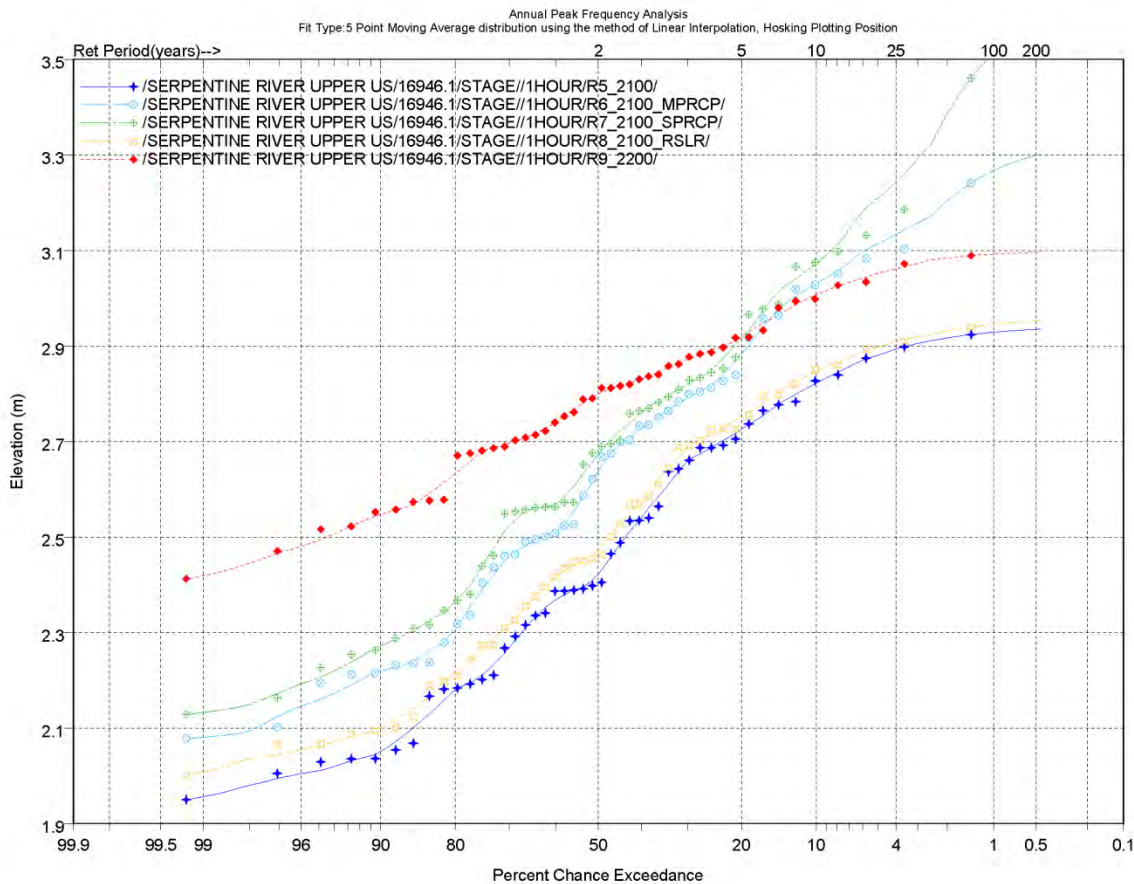
- Run 5 (Year 2100 with SLR)
- Run 6 (Year 2100 with moderate precipitation increase)
- Run 7 (Year 2100 with severe precipitation increase)
- Run 8 (Year 2100 with RSLR (including subsidence))
- Run 9 (Year 2200 with SLR; no precipitation increase)

Figure 24 shows frequency distribution curves at the Nicomekl River immediately upstream of the sea dams for the five runs. As expected, the plot shows that the sea level increase of 1m from 2100 to 2200 (or 2 m from 2010 to 2200) results in maximum water levels over the full range of estimated return periods. Interestingly, the largest variation occurs at frequent events.



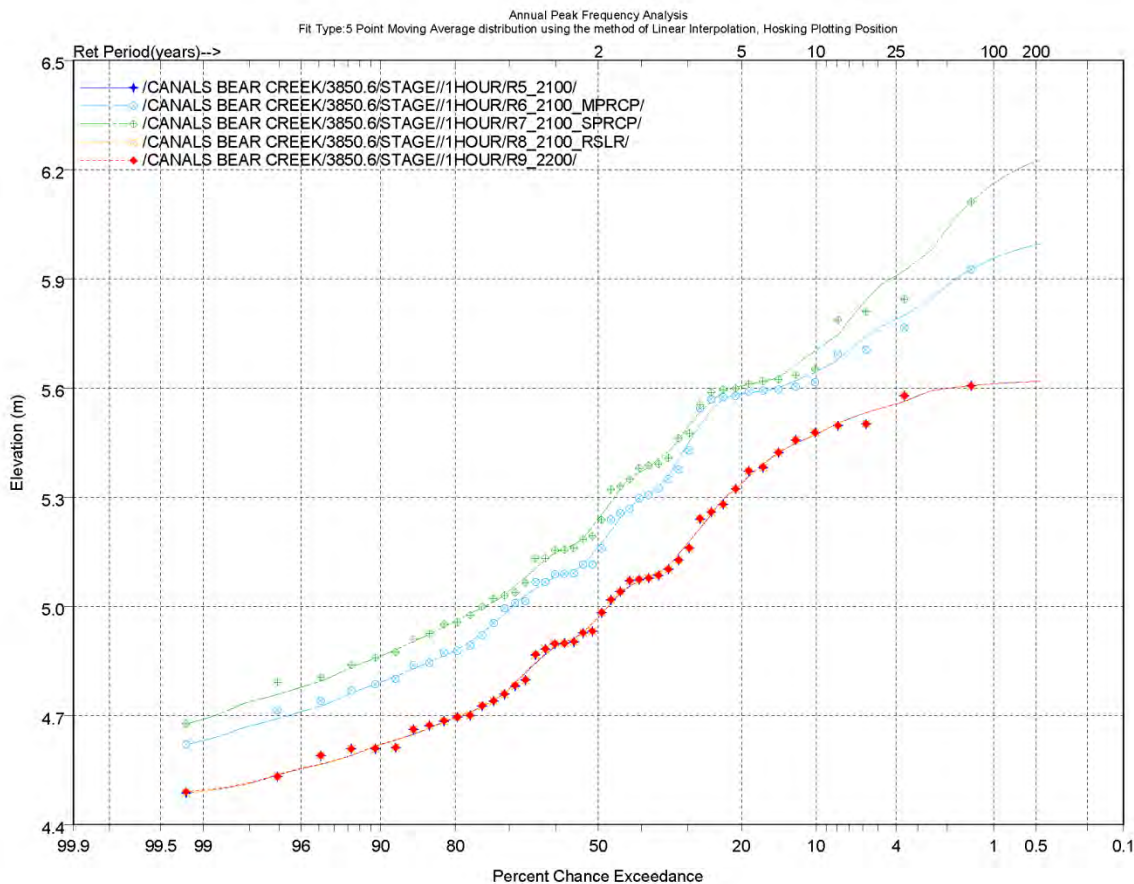
**Figure 24. Frequency distributions (Runs 5 to 9) for Nicomekl River immediately upstream of sea dam.**

Figure 25 shows the frequency distribution curves for the Serpentine River at a distance of 17 km upstream of the sea dam for the same five runs (Run 5 to 9). The plot shows that during events occurring frequently, an increase of 1 m in sea level (Run 9) would result in the highest water levels. However, peak water levels with return periods greater than 5 years would be governed by increases in precipitation (Run 6 and Run 7) rather than increases in ocean levels (Run 9).



**Figure 25. Frequency distributions (Run 5 to 9) for Serpentine River 17 km upstream of sea dam.**

Figure 26 shows frequency distribution curves for Bear Creek at a distance of roughly 4 km upstream of the confluence with the Serpentine River. All five runs were performed but it should be noted that Run 5 (2100 with SLR), Run 8 (2100 with RSLR) and Run 9 (2200 with SLR) plot in the same location, since this location is insensitive to increases in ocean levels. Furthermore, the distributions show that the severe climate change scenario (Run 7) results in only slightly higher peak water levels than the moderate scenario (Run 6) for relatively frequent events and that the relative difference between the two runs increases at return periods greater than about 10 years. This is because future increases in precipitation are expected to be higher at extreme events.



**Figure 26. Frequency distributions (Run 5 to 9) for Bear Creek at a distance of 3850 m upstream from East Newton pump station.**

Longitudinal profiles of peak water levels for Run 5 to Run 9 are included for the Serpentine and Nicomekl Rivers in Figure 27 and Figure 28. They illustrate the sensitivity of 200-year water levels in the lower reaches to increases in sea level and the sensitivity of 200-year water levels in the upper reaches to increases in precipitation.

The impacts of subsidence on water levels (analysed with Run 8) is minor compared to overall changes in sea level or precipitation - the total subsidence to year 2100 being estimated at only 0.09 m which is within the uncertainty of the hydraulic model.

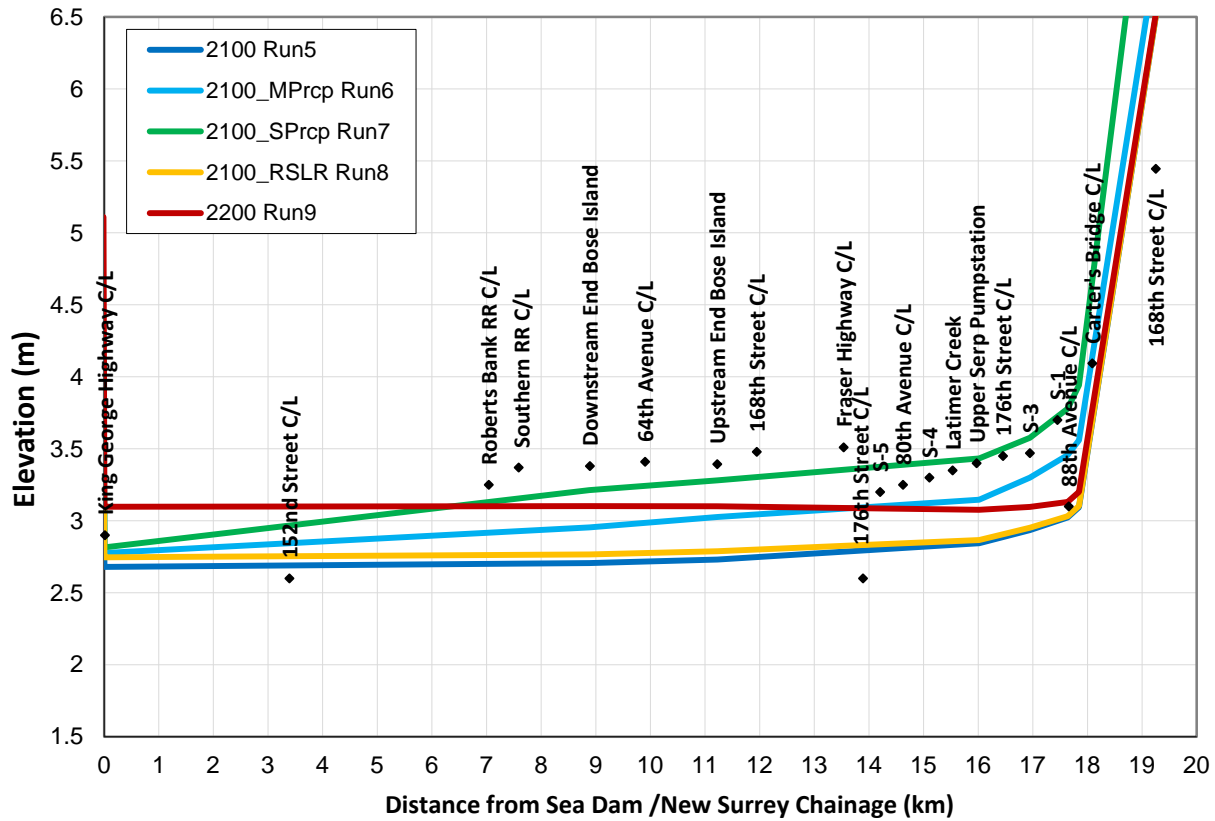
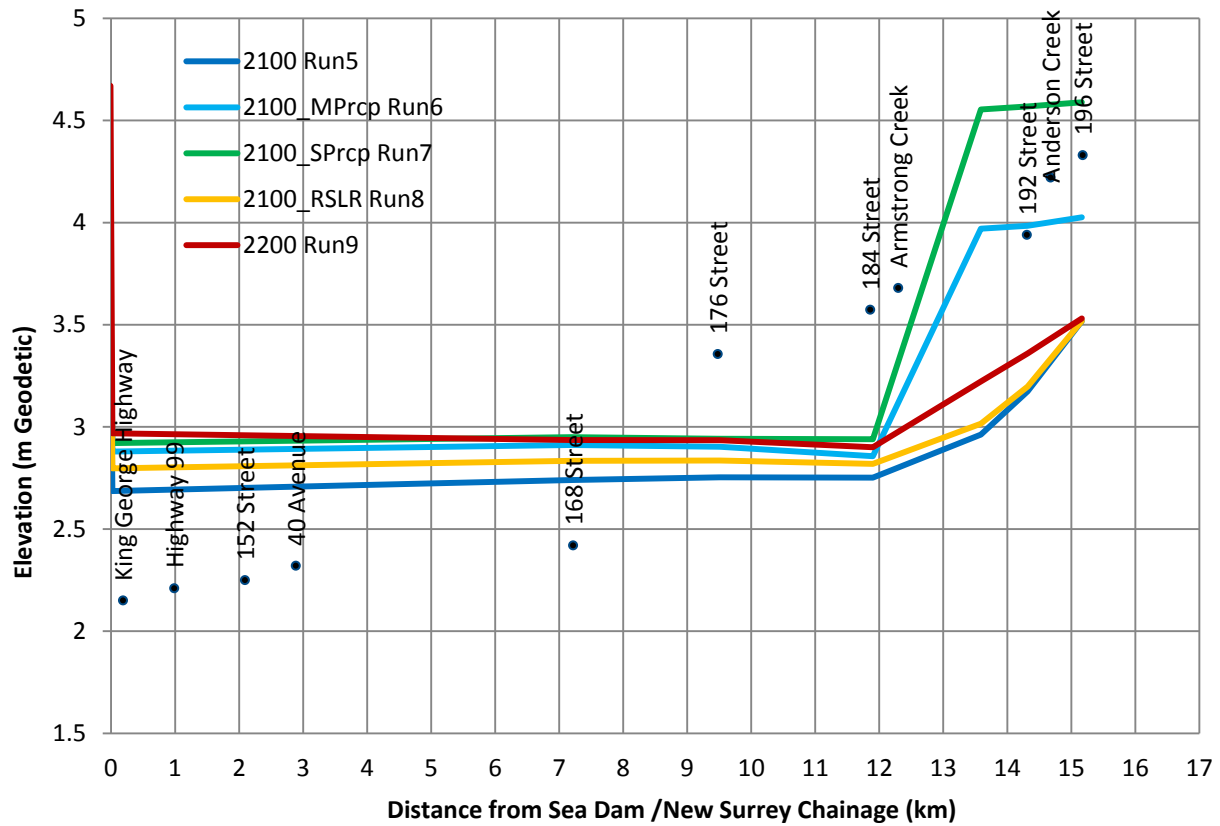


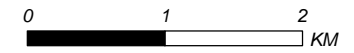
Figure 27. Longitudinal profiles of 200-year water levels for Serpentine River for year 2100 (Run5 to Run 9).



**Figure 28. Longitudinal profiles of 200-year water levels for Nicomekl River for year 2100 (Run5 to Run 9).**

Figure 29 summarises the impacts of changes in precipitation from a severe global climate model scenario by plotting differences in 200-year water levels from Run 7 and Run 5.

SCALE - 1:55,000



Coordinate System: NAD 1983 UTM ZONE 10N  
Units: METRES

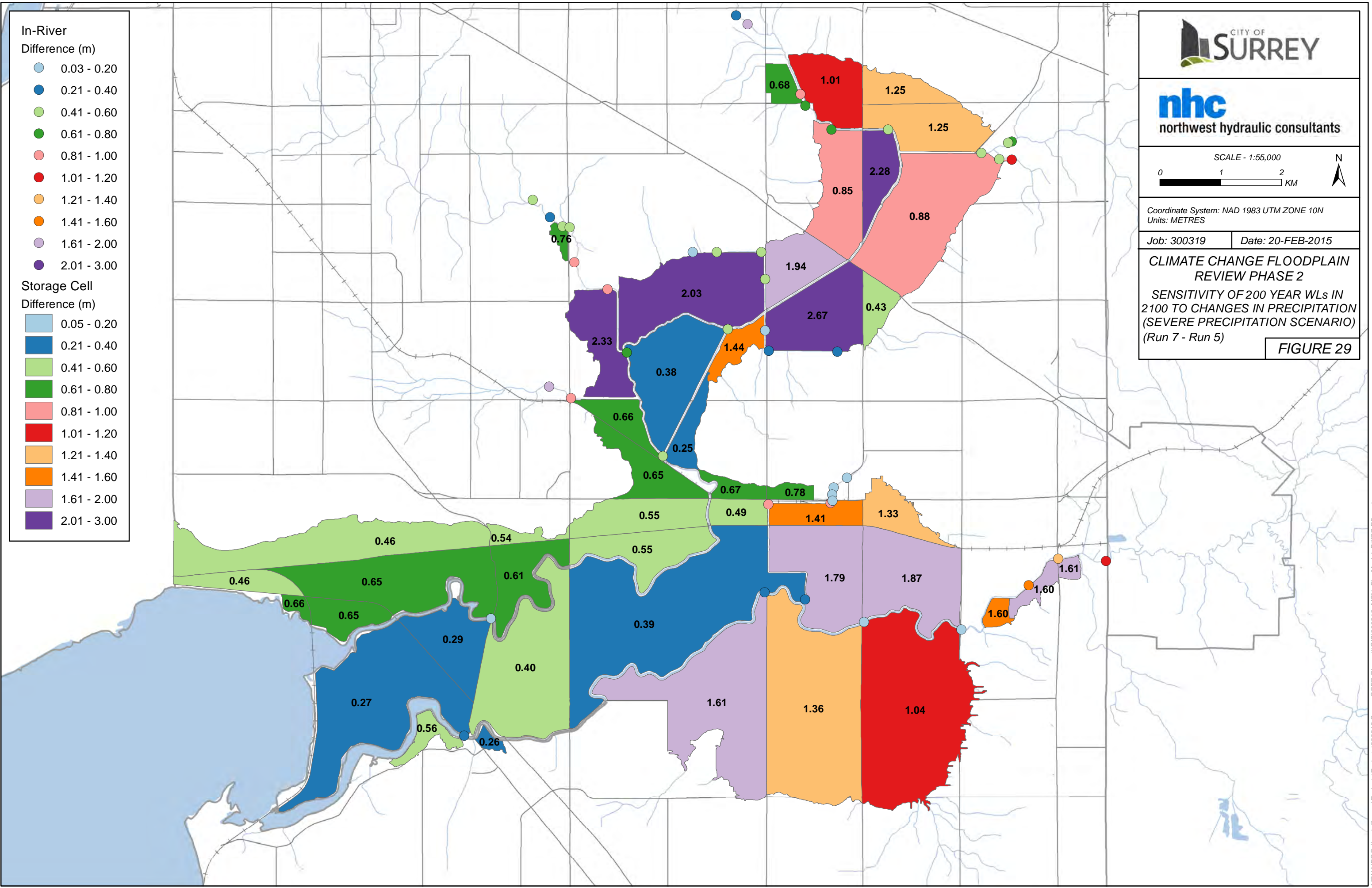
Job: 300319

Date: 20-FEB-2015

**CLIMATE CHANGE FLOODPLAIN  
REVIEW PHASE 2**

SENSITIVITY OF 200 YEAR WLs IN  
2100 TO CHANGES IN PRECIPITATION  
(SEVERE PRECIPITATION SCENARIO)  
(Run 7 - Run 5)

**FIGURE 29**





## 5.2 Flood Construction Levels

The estimated 200-year flood levels should not be adopted as accurate flood construction levels without further review. To improve the accuracy of the hydraulic model, refinements to hydraulic structures, representation of travel time within storage cells, improvements to boundary conditions, and more detailed calibration data for larger flood events (particularly for storage cells), would be needed before the results can be used for setting Flood Construction Levels.

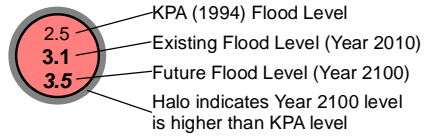
The estimated 200-year present (2010, Run 1) and future (2100, Run 5) flood levels are shown in Figure 30. The flood extents shown are based on MOE floodplain mapping from the 1990's. The City's current flood construction levels (FCLs) are based on design water levels computed by KPA (1994). Where available, the KPA levels were included in Figure 30 for comparison. Locations where year 2100 water levels are higher than KPA levels are identified with grey halos. In general, KPA levels are higher on the floodplain since they were established through simulations of dike breach scenarios. When comparing flood levels, it is helpful to recall some of the main differences between the KPA and NHC analyses.

- 1) The physical features and infrastructure included in the 1991 system modelled by KPA are significantly different from the design/build-out features and infrastructure included in the Phase 2 model. These major changes to infrastructure (i.e. pump stations upgrades and new installations, new and raised dikes, construction of all spillways, changes to roads, floodboxes, bridges, and culverts) would impact peak flood levels.
- 2) Different assumptions were made regarding coinciding ocean flood levels and peak flows. KPA combined the 200-year inflows with a historic tide from 1968 to establish peak water levels from runoff. Peak water levels from extreme tides were determined in a separate set of simulations. The extreme tide simulations were combined with a series of coastal and inland dike breach scenarios selected to maximize the peak flood levels in all floodplain cells.
- 3) In the KPA modelling, dikes were not raised to contain the instream flow thereby allowing uncontrolled overtopping and spilling to floodplain cells (the 1991 system did not include any spillways).
- 4) The 200-year runoff simulations done by KPA assumed that two of the seadam barrels were completely blocked by ice (sensitivity runs by KPA showed this had no significant impact on peak upstream water levels).

The estimated 200-year future (2200, Run 9) flood levels are shown in Figure 31 with the KPA levels. Again, the KPA levels are higher on the floodplain, since they were based on dike breaches.

Dike breach simulations conducted as part of the Phase 2 work is discussed in Section 6. Flood levels resulting from a breach in year 2100 are compared to KPA levels in Figure 49. It is important to stress that computed flood levels are sensitive to selected breach parameters and that those presented for year 2100 could be exceeded by selecting different breach parameters. Further investigations into the sensitivity of flood levels to various breach parameters is recommended prior to updating FCLs.

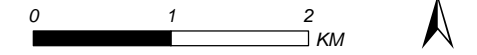
-  Floodplain Extents
-  River Levels
-  Storage Cell
-  Storage Cell Levels



KPA (1994) flood levels are based on values reported in the KPA report and floodplain maps, and include freeboard (KPA 1994, pp. 82-84). KPA added 0.3 metres freeboard, except along the Nicomekl River upstream of Anderson Creek, where 0.5 metres freeboard was added. NHC's modelled current and future flood levels include 0.6 metres freeboard.

**Note! Updated flood levels shown in bold are not to be used for official Flood Construction Levels.**

SCALE - 1:55,000



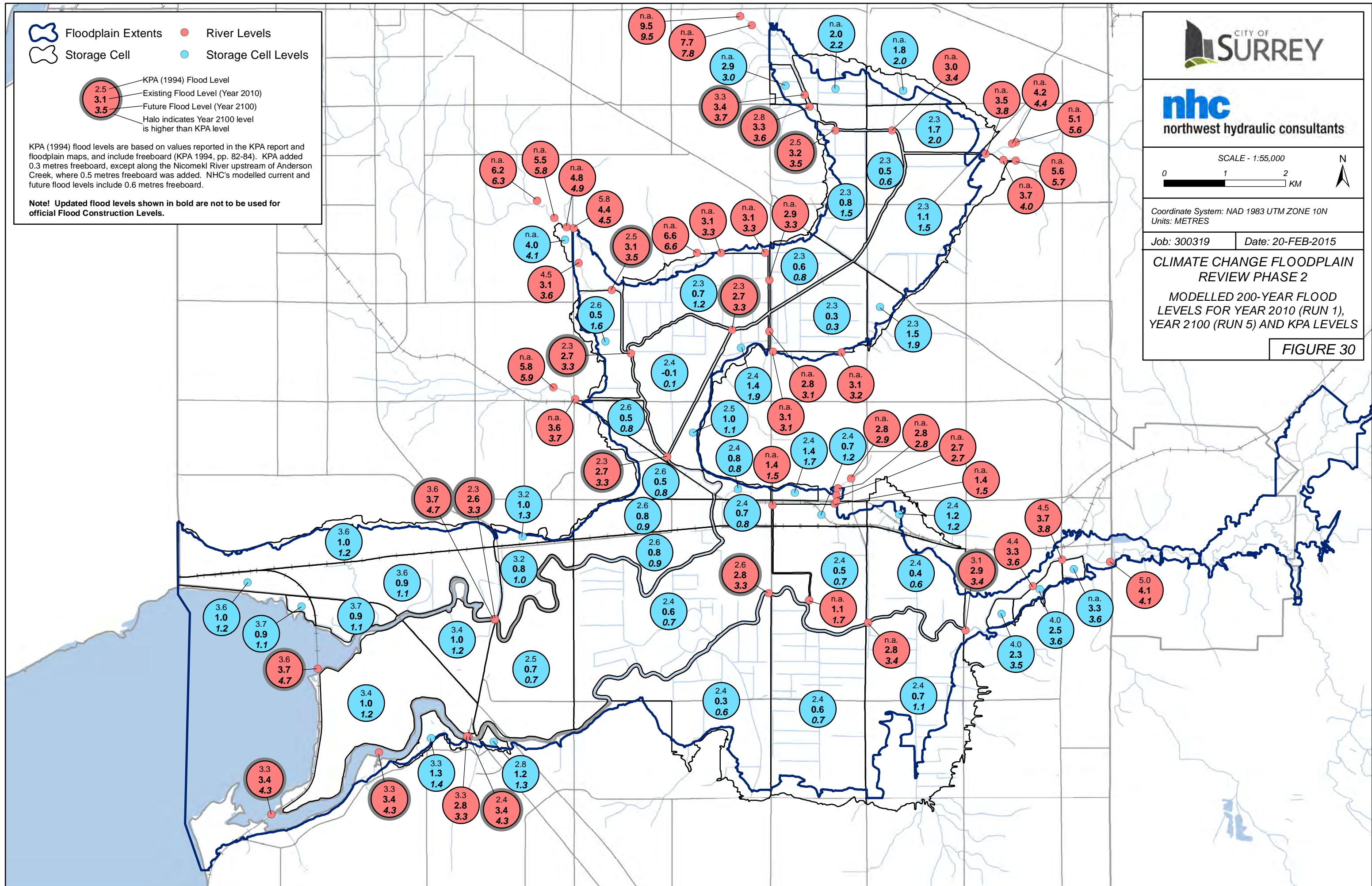
Coordinate System: NAD 1983 UTM ZONE 10N  
Units: METRES

Job: 300319 Date: 20-FEB-2015



CLIMATE CHANGE FLOODPLAIN REVIEW PHASE 2

MODELLED 200-YEAR FLOOD LEVELS FOR YEAR 2010 (RUN 1), YEAR 2100 (RUN 5) AND KPA LEVELS

FIGURE 30



-  Floodplain Extents
-  River Levels
-  Storage Cell
-  Storage Cell Levels

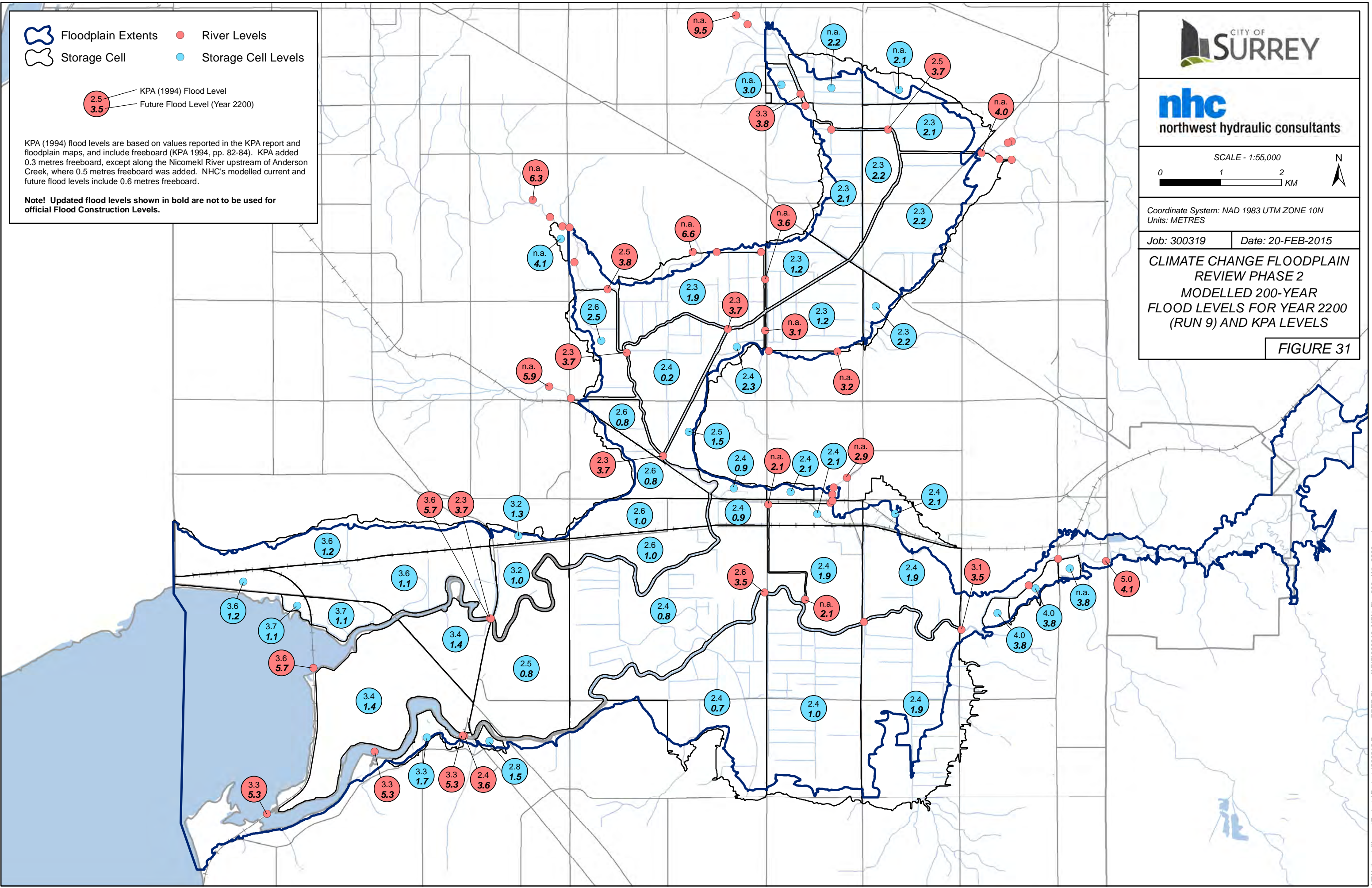
 KPA (1994) Flood Level  
 Future Flood Level (Year 2200)

KPA (1994) flood levels are based on values reported in the KPA report and floodplain maps, and include freeboard (KPA 1994, pp. 82-84). KPA added 0.3 metres freeboard, except along the Nicomekl River upstream of Anderson Creek, where 0.5 metres freeboard was added. NHC's modelled current and future flood levels include 0.6 metres freeboard.

**Note! Updated flood levels shown in bold are not to be used for official Flood Construction Levels.**

**CLIMATE CHANGE FLOODPLAIN  
REVIEW PHASE 2  
MODELLED 200-YEAR  
FLOOD LEVELS FOR YEAR 2200  
(RUN 9) AND KPA LEVELS**

**FIGURE 31**



### 5.3 Floodplain Extents

The intent of this work is not to produce detailed floodplain mapping but rather to show approximate flood extents (inundation boundaries) delineated in GIS and overlain on ortho-photography. Considering the rapid rise in topography around the nearly horizontal floodplain, inundation boundaries from 2010 to 2100 show only minor spatial variation (8% difference in flooded area) and the intermittent years even less so. However, upland/lowland interfaces that fall outside the flood boundaries established by KPA are of particular interest to the City.

Floodplain extents maps were generated for 200-year water levels (including 0.6m freeboard) for the following years:

- Map 2 – Year 2010 Design Levels (Run 1)
- Map 3 – Year 2100 Design Levels (Run 5)
- Map 4 – Year 2100 Design Levels with severe scenario (Run 7)
- Map 5 – Year 2200 Design Levels (Run 9)

Total 200-year flood extent areas were derived in GIS and are included in Table 19. The greatest incremental change in flooded area from years 2010 to 2100 (Run 1 to Run 5) occurs between year 2020 and 2040 and corresponds to a 4% increase. The increases in flood extent areas are due to increases in sea level and vary depending on the floodplain topography. The larger increase between 2020 and 2040 can be partly attributed to the change in landuse input values in the HSPF model from existing landuse values (2020) to anticipated future landuse values (2040).

When considering only the impacts of sea level rise, the total flood extents area appears to be slightly more sensitive (8% increase) to the first 1m increase in sea level from 2010 to 2100 (Run 1 to Run 5) compared to a 6% increase from a second 1 m increase in sea level from 2100 to 2200 (Run 5 to Run 9).

The effects of increases in precipitation on the total flood extents can be seen by comparing the areas from Run 5, 6 and 7. The changes in precipitation from the moderate global climate model results in an 11% increase in 2100 flooded area while the severe model yields a 16% increase in flood extents. In the majority of floodplain cells, the design water levels are more sensitive to increases in precipitation compared to increases in sea level.

The year 2100 flood extents show only a minor increase in area (1%) due to anticipated floodplain subsidence.

**Table 19. 200 year flood extents area.**

<b>Run #</b>	<b>Run Name</b>	<b>Area (sq.km)</b>
1	2010 Design levels	50.1
2	2020 Design levels	50.3
3	2040 Design levels	52.5
4	2070 Design levels	53.1
5	2100 Design levels	54.1
6	2100 Sensitivity: Moderate Precipitation	59.9
7	2100 Sensitivity: Severe Precipitation	62.6
8	2100 Sensitivity: Subsidence	54.4
9	2200 Design levels	57.6

In general, the 2010 flood extents fall within the 1997 floodplain extents delineated on the MOE floodplain maps. Exceptions occur where the model was extended in the fringe areas (Hyland, Cloverdale, Bear, Latimer, and upper Serpentine).

In Figure 32, the year 2010 200-year floodplain is shown along with the 1997 floodplain extents. Potential increases in floodplain extents due to climate change impacts in year 2100 and 2200 are shown in orange.

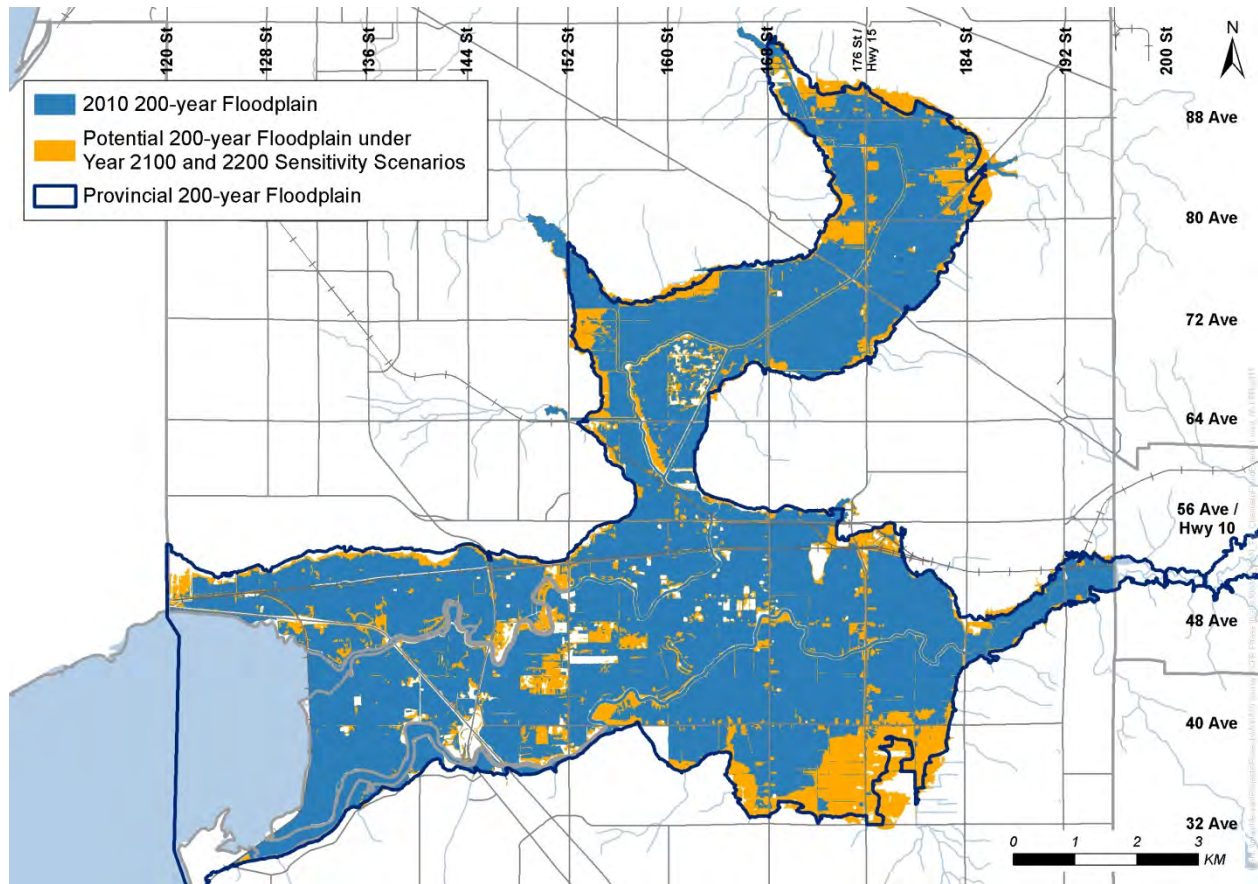
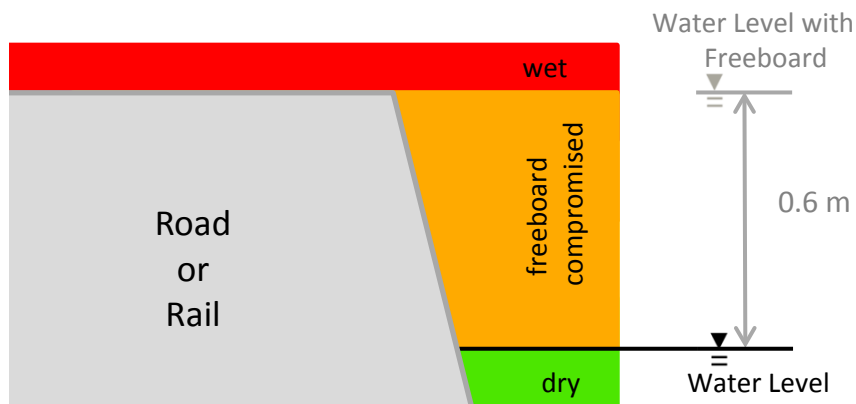
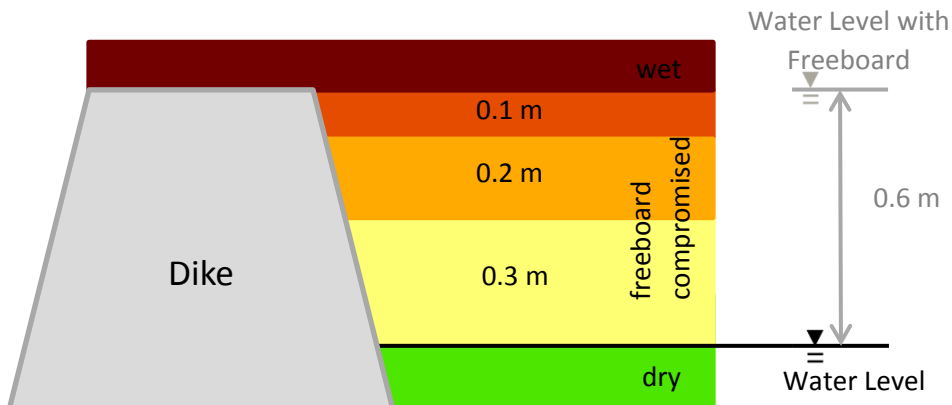


**Figure 32. Areas where floodplain extents change due to climate change**

## 5.4 Vulnerable Infrastructure

To assist with phasing of infrastructure upgrades and to identify when certain improvements need to be implemented, 200-year flood levels for years 2010, 2020, 2040, 2070 and 2100 were compared with infrastructure elevations. The vulnerability assessment focused on key components such as dikes, sea dams, bridges and main roads and rail.

The following sketches depict the classification schemes used to identify the vulnerable infrastructure:



At the sea dams, the 200-year water levels were compared with the elevation of the top of the structure (deck). At the bridges, the 200-year water levels were compared with the elevation of the high chord and the low chord. The road and rail classification scheme was applied to the sea dams and bridges.

Figure 33 to Figure 37 show example figures with the vulnerability of inland dikes to 200-year water levels in 2010 to 2100. All other figures with the results from the vulnerability assessment are included in Appendix F.

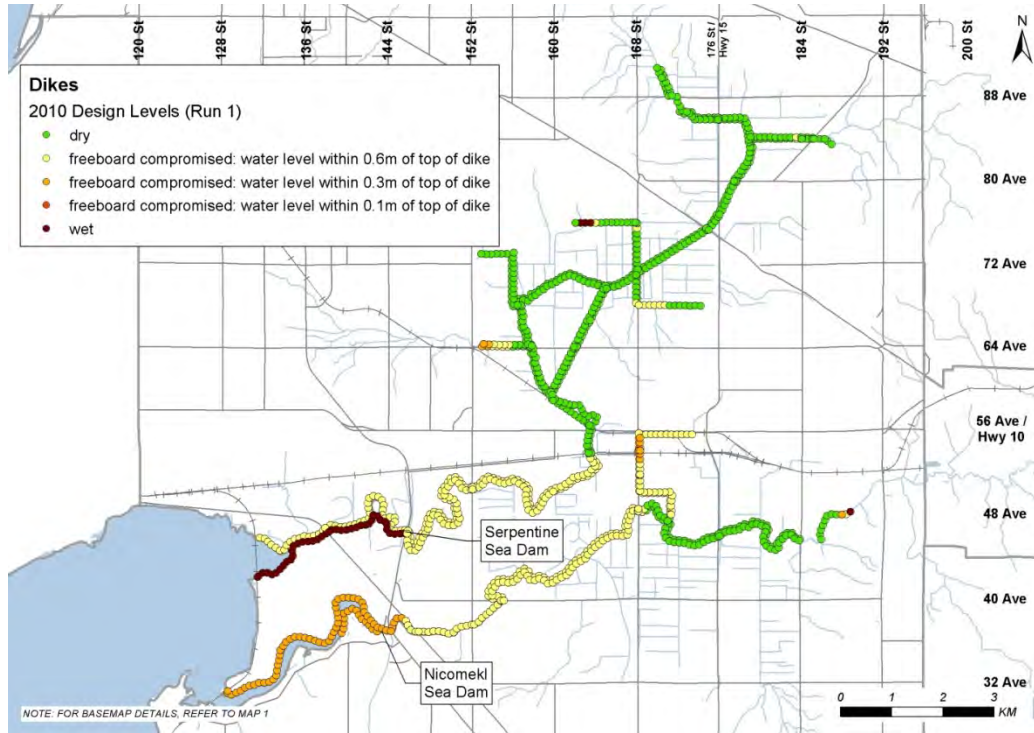


Figure 33. Vulnerability of dikes (current dike design elevations) to 2010 200-year water levels.

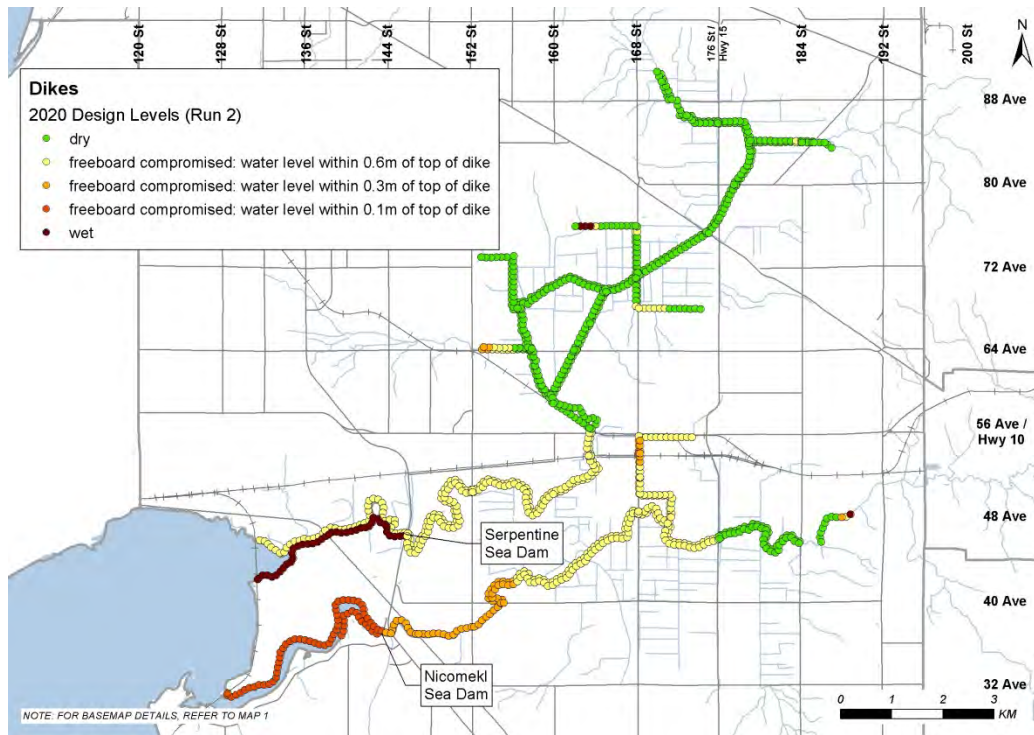


Figure 34. Vulnerability of dikes (current dike design elevations) to 2020 200-year water levels.



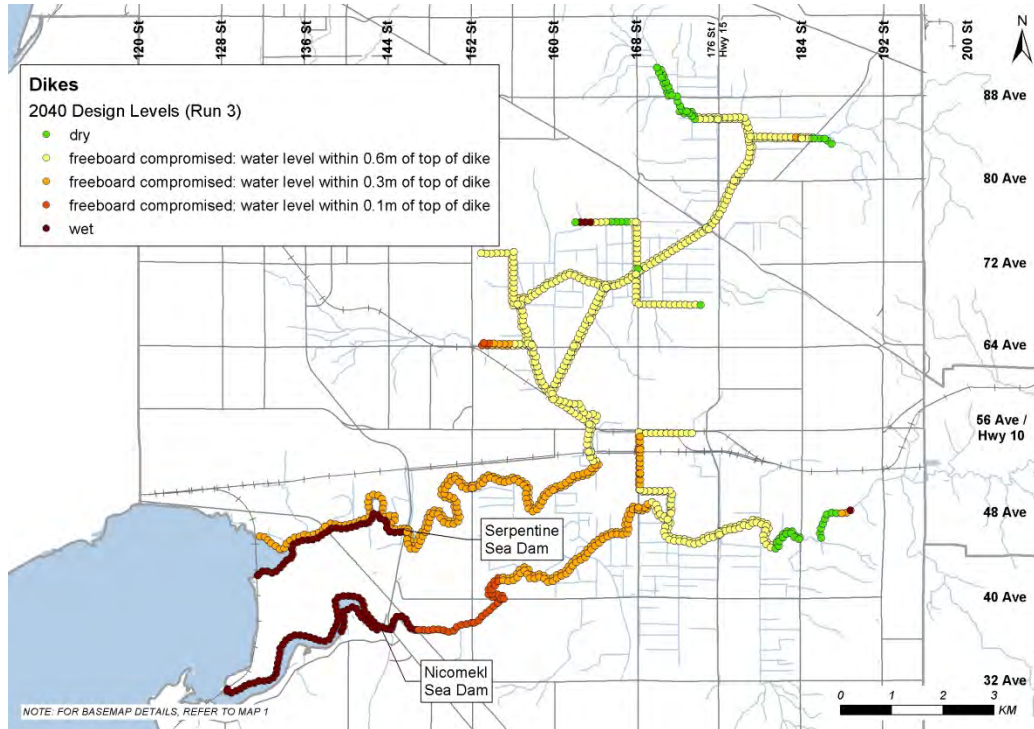


Figure 35. Vulnerability of dikes (current dike design elevations) to 2040 200-year water levels.

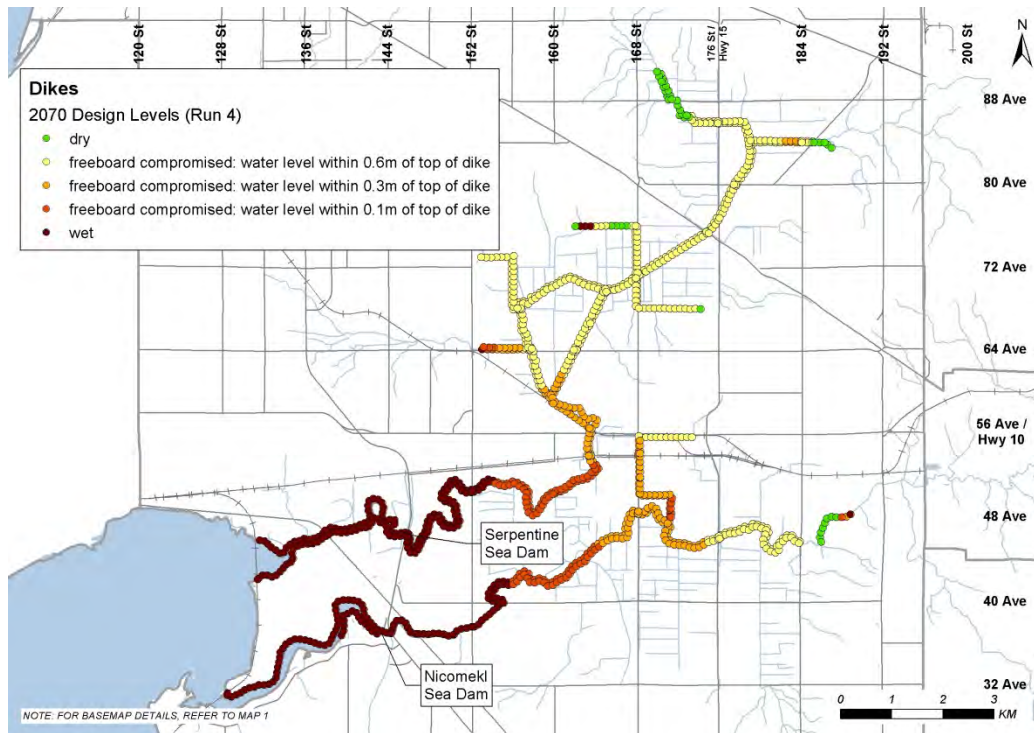
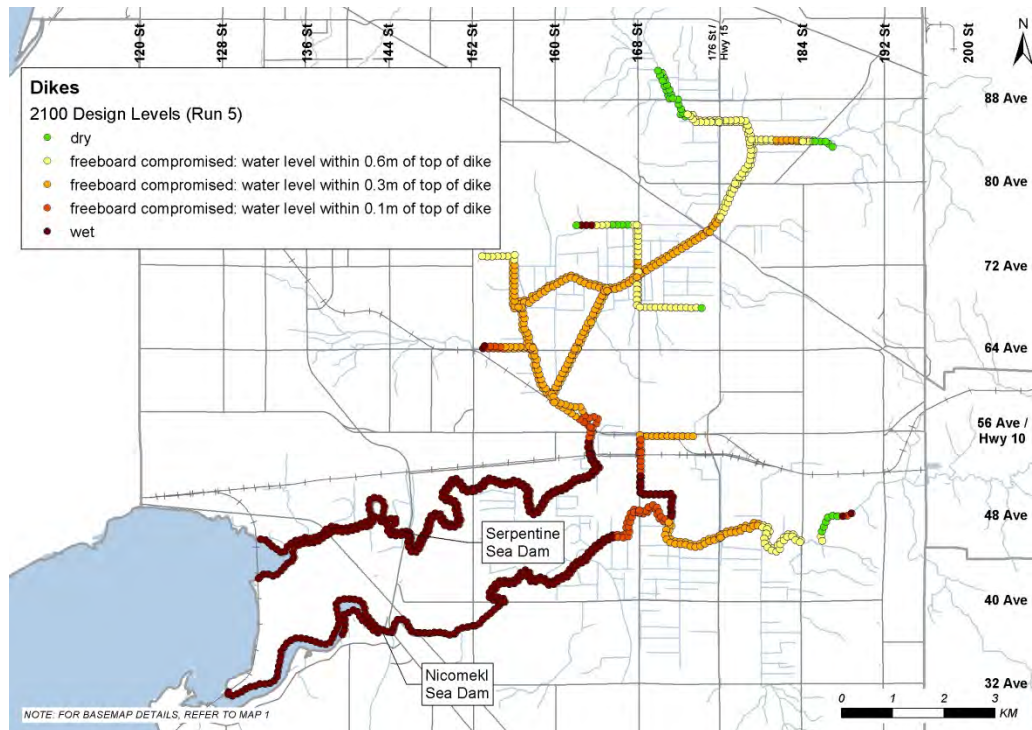


Figure 36. Vulnerability of dikes (current dike design elevations) to 2070 200-year water levels.



**Figure 37. Vulnerability of dikes (current dike design elevations) to 2100 200-year water levels.**

It is evident from the figures that key infrastructure will be compromised or wet at 200-year flood levels corresponding to year 2010 and that the situation will worsen by year 2100. Further investigation of the implications of climate change on vulnerable infrastructure is planned during future work.

## 5.5 System Capacity

The capacity of the inland diking system was analysed by comparing the dike design elevations with 2010 water levels. Return periods associated with the most vulnerable point along each river and reach was estimated using the frequency distribution curves for year 2010 (Run 1). Results are summarised in Table 20.

**Table 20. Summary of system capacity for year 2010.**

River/Reach	At Dike Design Crest Elevation (dike wet)		At Elevation when Freeboard Compromised	
	Water Level (m)	Return Period (years)	Water Level (m)	Return Period (years)
Canals 168 St North	3.03	> 200	2.43	~ 10
Canals 168 St South	2.97	> 200	2.37	> 15
Canals Cloverdale	1.00	> 200	0.40	10
Canals Hyland	3.01	> 200	2.41	5
Canals Latimer Creek	3.32	> 200	2.72	50
Nicomekl River Main DS	3.00	Refer to Section 3	2.40	Refer to Section 3
Nicomekl River Main US	2.53	8	1.93	<2
Serpentine River Main	3.00	Refer to Section 3	2.40	Refer to Section 3

**Note: Water levels listed in Table 20 do not include freeboard.**

**Return periods associated with the water levels are approximate.**

The dike vulnerabilities indicate that only two dike locations are overtopped at 2010 200-year water levels while the freeboard is compromised at several locations (refer to Figure 33). At the first location on the upper portion of 168<sup>th</sup> Street Canal North, results indicate that the dike would be overtopped during a 25-year flood. However, the slope of the water surface and inflows to the canal should be investigated prior to planning any dike upgrades. Results in Table 20 for that dike correspond to the low point near the 90 degree bend in the canal/ditch. At the upstream end of the Nicomekl River dike, the dike design elevation of 2.53 m would be overtopped during an event with return period of approximately 8 years.

Spillways corresponding to build-out geometry and invert elevations were included in the model when examining the system capacity for year 2010. Adding or lowering spillways would, depending on location, act to increase the system capacity by allowing additional controlled spilling of flow to the

floodplain. With future impacts of sea level rise and changes in precipitation, the spillways are expected to be used more frequently.

## 6 DIKE BREACH MODELLING

To develop an understanding of the impact of localized failures in the flood control infrastructure on surrounding lands, dike breach and dike failure scenarios were modelled. Conceivably, a near infinite combination of dike failures could occur and to reduce the modelling effort, specific types of breach scenarios were investigated and multiple independent events combined into single scenarios. The modelled scenarios were selected based on the most likely types of failures and provide an overview of moderate and severe scenarios.

### 6.1 Breach Mechanisms

Earth embankments have different possible modes of failure with overtopping and piping/seepage being the two most common. For an overtopping failure, the process is generally initiated by a headcutting erosion process on the downstream side of the embankment as a shallow stream of water flows over the dike crest. As the depth of flow increases above the dike crest, the surface vegetation is generally removed and the embankment starts to erode very rapidly. Once water levels on both sides of the embankment equalize or the breach invert reaches the elevation of the floodplain, the rate of erosion slows down or stops. During a falling tide, flow moves through the breach in the opposite direction draining water from the floodplain.

For an overtopping failure of the coastal dikes, TEL recommended adopting a final breach bottom width of 100 m at the elevation of the floodplain and an estimated breach formation time of less than one hour.

For a seismic breach, TEL predicted an instantaneous failure and anticipated that upon failure, the dike material would fill in the river channel. The City indicated that river reaches that have been straightened (i.e. Bose Canal) were more susceptible to subside or fail during a seismic event.

### 6.2 Model Selection

Dike breach scenarios were modelled using HEC-RAS2D 5.0 (beta) released by the USACE on October 1, 2014. HEC-RAS2D has the ability to perform two-dimensional hydrodynamic flow routing by coupling 2D floodplain flow area elements to 1D model elements. The model solves either the full 2D Saint-Venant equations or the 2D diffusive wave equations. Unlike standard 2D models, the 2D computational cells used in HEC-RAS2D do not have a single averaged elevation. Instead, each cell and cell face of the computation mesh is pre-processed in order to develop detailed hydraulic property tables based on the underlying terrain. This allows a large cell (i.e. 30 x 30 m) to be partially wet with the correct water volume based on the modelled water surface elevation and the DEM resolution (i.e. 1 m x 1 m).

### 6.3 Model Development

The dikes were modelled using the current dike crest design elevations and were allowed to overtop. The spillways were represented using the ultimate spillway locations and geometry. The dike breach scenarios were first modelled in the HEC-RAS (1D) model. Based on those results, selected 1D storage

areas were converted to 2D areas prior to running the breach scenarios using HEC-RAS2D. Note that the 1D model does not account for the travel time or any losses as water flows across the floodplain and generally results in more conservative water level estimates.

The floodplain topography was based on a DEM developed by the City based on LiDAR collected on April 3 and 11, 2013. The original 1 m cell DEM was resampled to 3 m for use in the 2D model. All structures that could impound or direct flow such as major roads, river dikes and spillways that were included in the 1D model were also included in the 2D model. The 2D model includes an accurate representation of the floodplain, roads, dikes, and spillways and is able to simulate the spread of flood water on the floodplain resulting from dike breaching or dike overtopping. The 2D model also includes flood infrastructure such as pump stations, floodboxes, culverts and the river channels and is therefore able to simulate all potential flow interactions between floodplain cells and the river channel over several tide cycles.

## 6.4 Model Calibration and Validation

It is not possible to calibrate the 2D model, as no observed data for breach events are available. Standard hydraulic coefficients for the breach parameters and floodplain roughness were used; NHC has considerable experience developing floodplain roughness coefficients for 2D models in agricultural areas in the lower mainland and elsewhere in the world. A uniform roughness value ( $n=0.06$ ) was used for these preliminary simulations. Detailed sensitivity analyses of breach and hydraulic parameters were not conducted during this phase of the project. Future sensitivity modelling for various scenarios is strongly recommended.

## 6.5 2D Model Runs

The 2D modelling for the Serpentine/Nicomekl floodplains investigated:

- Storm event failure of coastal dikes under current conditions
- Future storm event coastal dike breaches under sea level rise
- Current sunny day (seismic) failures of Inland dike (in the upper reaches)
- Conditions post-seadam failure over a 2-year duration (with overtopping of dikes)

Details of the breach scenarios and breach parameters are summarized in Table 21 and Table 22.

**Table 21. Summary of breach scenarios**

Details	Run 10	Run 11	Run 12	Run 13
Description	Coastal Dike Breaching	Coastal Dike Breaching	Seismic Failure - Breaching Inland Dike	Post-seadam Failure - Overtopping Inland Dike Lower Reach
Year	2010	2100	2100	2010
Simulation Conditions	WL with 10yr JP at Colebrook Dike	WL with 200yr JP at Colebrook Dike	Typical winter	2yr near seadam end of life
Peak Tide (m)	2.56	3.94	-	-
Selected Period from Historic Record	06DEC70 to 11DEC70	15DEC82 to 21DEC82	06NOV89 to 12 NOV89	01SEP08 to 01SEP10
SLR (m)	0	0.97	0.97	0
Precipitation	Historic	Historic	Historic	Historic
Landuse	Existing	Future	Future	Existing
Breach Locations	Mud Bay and Colebrook Dikes	Mud Bay and Colebrook Dikes	Coast Meridian Dike	Overtopping of dikes in lower reach

Note: JP = Joint Probability

**Table 22. Summary of breach parameters**

Breach/Failure Location	Mud Bay Dike	Colebrook Dike	Coast Meridian Dike
Final Bottom Width (m)	100	100	1500
Final Bottom Elevation (m)	0.5	0.5	0
Side Slopes	1:1	1:1	1:1
Breach Formation Time	1 hr	1 hr	20 min
Run 10 Trigger WL (m)	2.44	2.44	-
Run 11 Trigger WL (m)	3.84	3.84	-
Run 12 Trigger Time	-	-	06NOV89 15:00

### 6.5.1 Coastal Dike Breach, 2010 (Run 10)

For the coastal dike failures, two breaches were modelled at the sea dike, one on the Colebrook Dike north of the mouth of the Serpentine River and one on the Mud Bay Dike between the mouths of the Serpentine and Nicomekl Rivers. The modelling was performed with tidal boundary conditions for a storm with a peak water level corresponding to a 10-year joint probability value. The 2D hydrodynamic model simulated the spill of water through the breaches and subsequent inundation across the floodplain over several tidal cycles.

Figures included in Appendix G show water flowing across the floodplain as a result of the breach modelled in run 10 at 15 minute intervals for 2 hours, to a maximum of 23 hours. (Blue depth shading corresponds to same range as shown in Figures 37 to 39.)

From the Colebrook Dike breach (Cell 120 – Map 1), an initial pulse of water is shown flowing through the breach and along the railway under Highway 99. The water eventually spreads to adjacent areas (Cell 121, 122, 123) mostly by flowing through culverts. During the falling tide, water recedes through the breach and is evacuated from the floodplain by floodboxes in the Colebrook Dike. Some water does remain upstream of Highway 99 (Cell 121 and 123).

From the Mud Bay Dike breach (Cell 107), water spreads radially across the floodplain until it reaches Highway 99 and the Nicomekl Dike, roughly 1.5 hours after the breach initiation. The floodplain water level (Cell 107) is below the elevation of Highway 99 but some water is transferred upstream (Cell 108) through culverts under Highway 99. During the falling tide, water recedes through the breach and floodboxes but some water remains on the floodplain (Cell 107).

Maximum flood depths, water levels and flow velocities computed over the entire simulation period are shown in Figure 38 to Figure 40. Maximum velocities of 4 to 5 m/s were computed at the breach with peak velocities on the floodplain reaching approx. 1.5 m/s. No roads were overtopped during this breach scenario but velocities in the 0.9 to 1.8 m/s range were computed near the railway under the Highway 99 overpass (Cells 122 to 120, Cells 121 to 120).



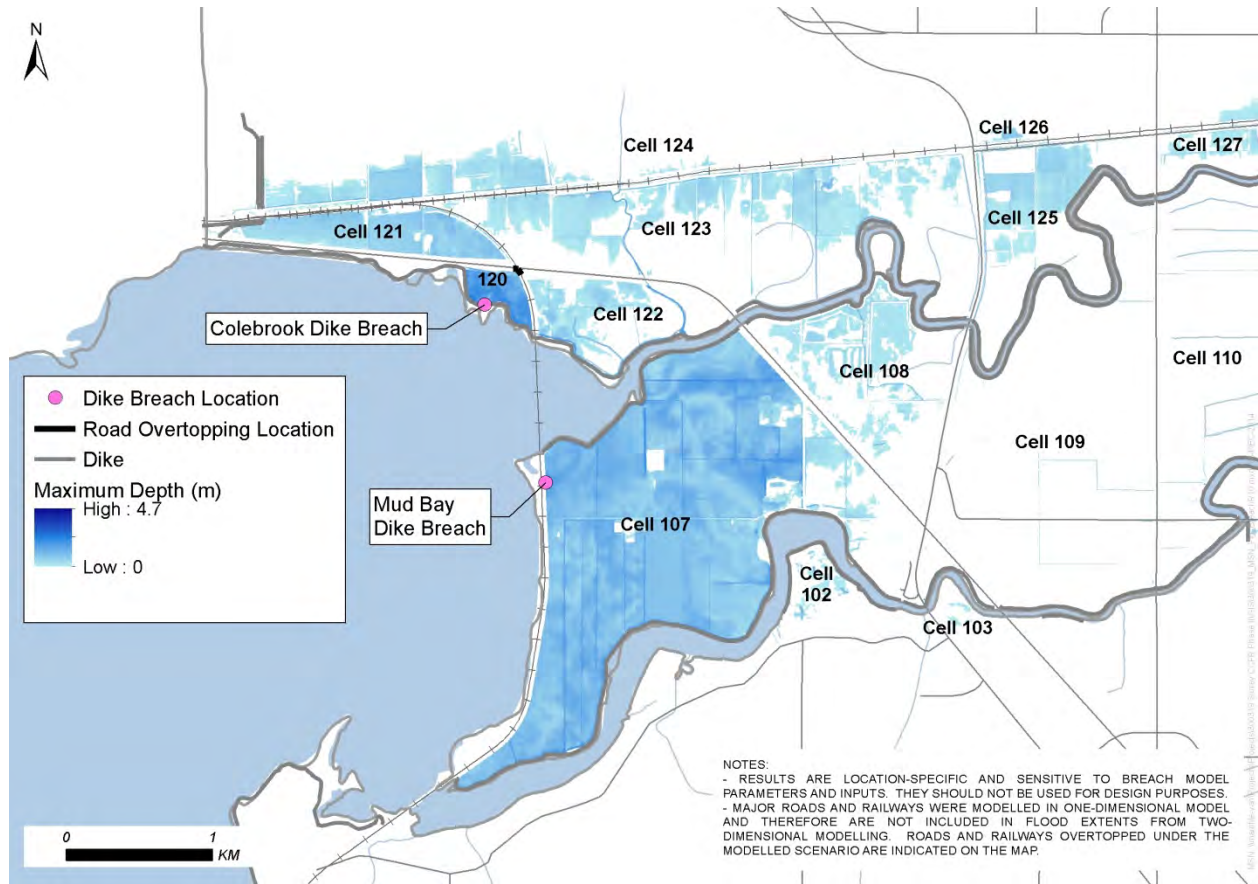


Figure 38. Maximum modelled flood depths from coastal dike breaches (Run 10).

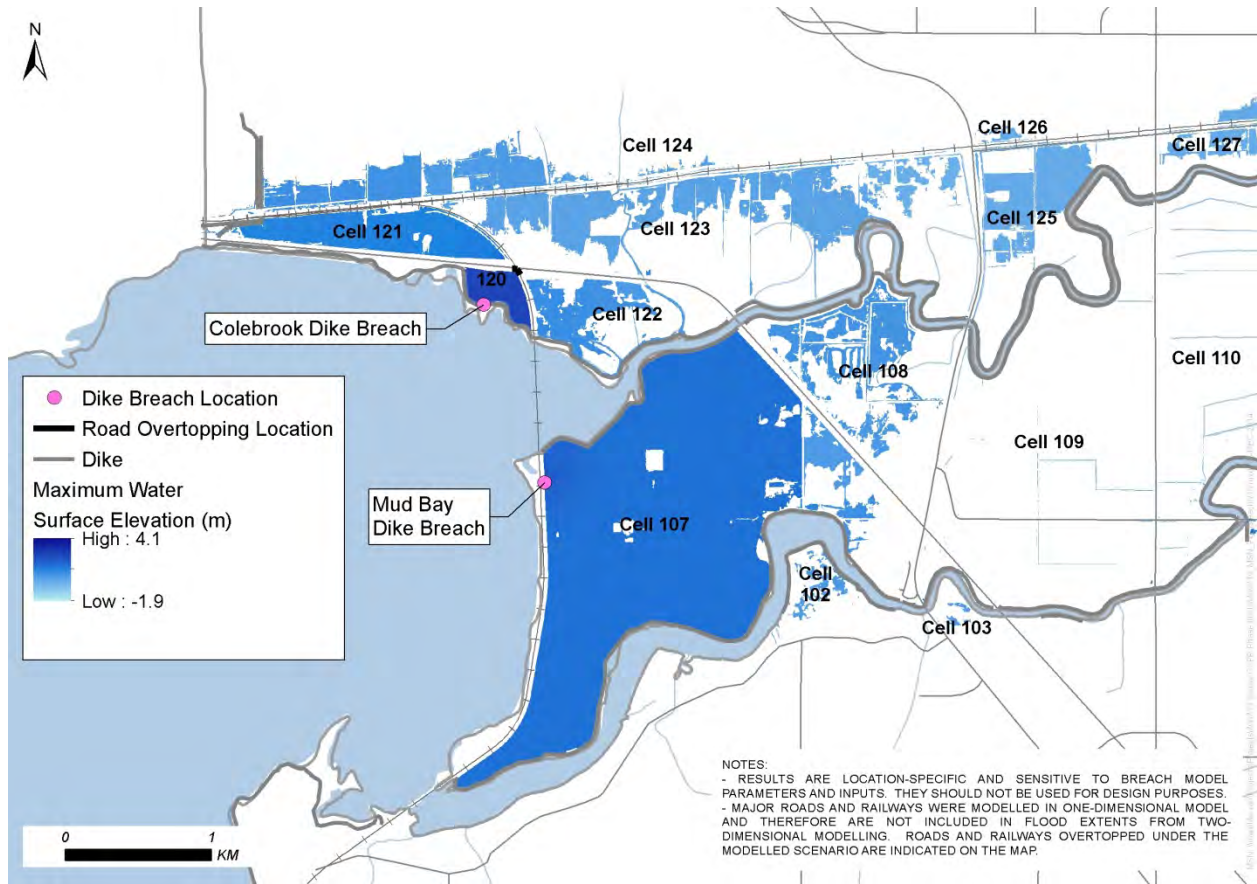
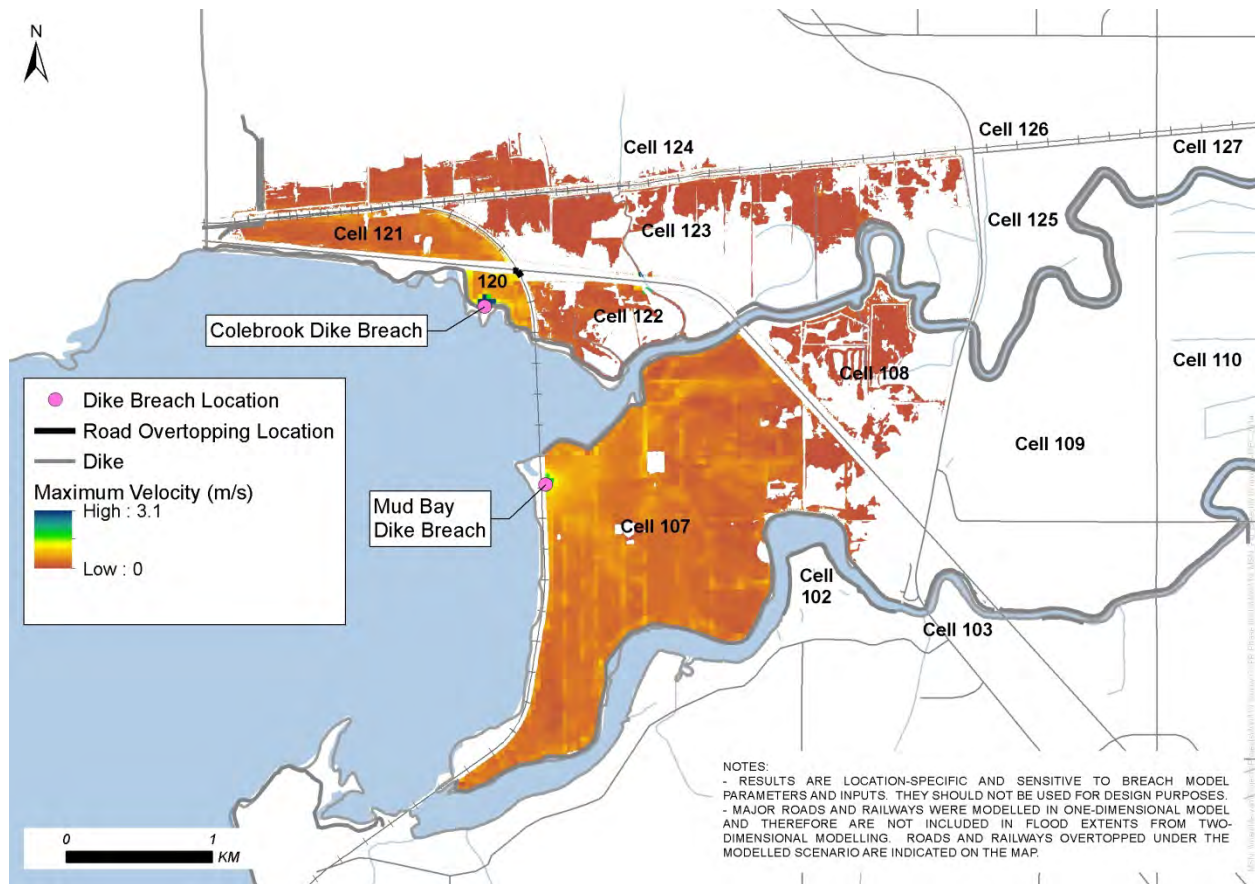


Figure 39. Maximum modelled water levels from coastal dike breaches (Run 10).



**Figure 40. Maximum modelled flow velocities from coastal dike breaches (Run 10).**

### 6.5.2 Coastal Dike Breach, 2100 (Run 11)

Figures included in Appendix G show a series of frames of water travelling across the floodplain as a result of the breach modelled in Run 11. With a 200-year tidal water level in year 2100 (includes approx. 1 m of sea level rise), the breaching of the Colebrook and Mud Bay Dikes is a more catastrophic event.

Within 30 minutes of breach initiation, sufficient water has flowed onto the floodplain (Cell 120) through the Colebrook Dike breach to start spilling to adjacent cells. Initially, water is transferred to adjacent areas (Cells 121, 122, 123) through culverts and under the overpass at Highway 99 but water levels in areas closest to the ocean eventually exceed the road elevations resulting in larger spills. Despite some water receding through the breach during the falling tide, each subsequent high tide brings in more water to the floodplain. King George Blvd acts as an obstruction, temporarily preventing water from flowing east (from Cell 123 to Cell 125). However, water eventually makes it way (flow from Cell 124 to Cell 126 to Cell 125 to Cell 127 to Cell 128) as far upstream as 56th Avenue (in 48 hours).

From the Mud Bay Dike breach (Cell 107), water spreads radially across the floodplain until it reaches Highway 99 and the Nicomekl Dike roughly 1.5 hours after the breach initiation. After 3 hours, the floodplain water level (Cell 107) has exceeded the elevation of Highway 99 and completely inundated

the area (Cell 108) downstream of King George Blvd. Water continues migrating eastward (Cells 109 and 110) by first moving through culverts and then flowing over King George Blvd and 152nd St. Once it arrives near Cloverdale Canal, water flows north through culverts under Colebrook Rd (to Cell 115). The water eventually overtops the Cloverdale Canal dikes and spreads east (Cell 117 and 111) primarily through the three spillways on the east Cloverdale Canal dike. During the falling tide, water recedes through the breach but significant amounts of water remain on the floodplain. With each subsequent high tide, more water fills in the lower cells and then flows east. At the end of the simulation, water has extended as far east as 184th St.

The in-channel water levels throughout the system also increase as a result of the breach as large amounts of water on the floodplain drain to the Serpentine and Nicomekl Rivers.

Maximum flood depths, water levels, and flow velocities computed on the floodplain over the entire simulation period are shown in Figure 41 to Figure 43.

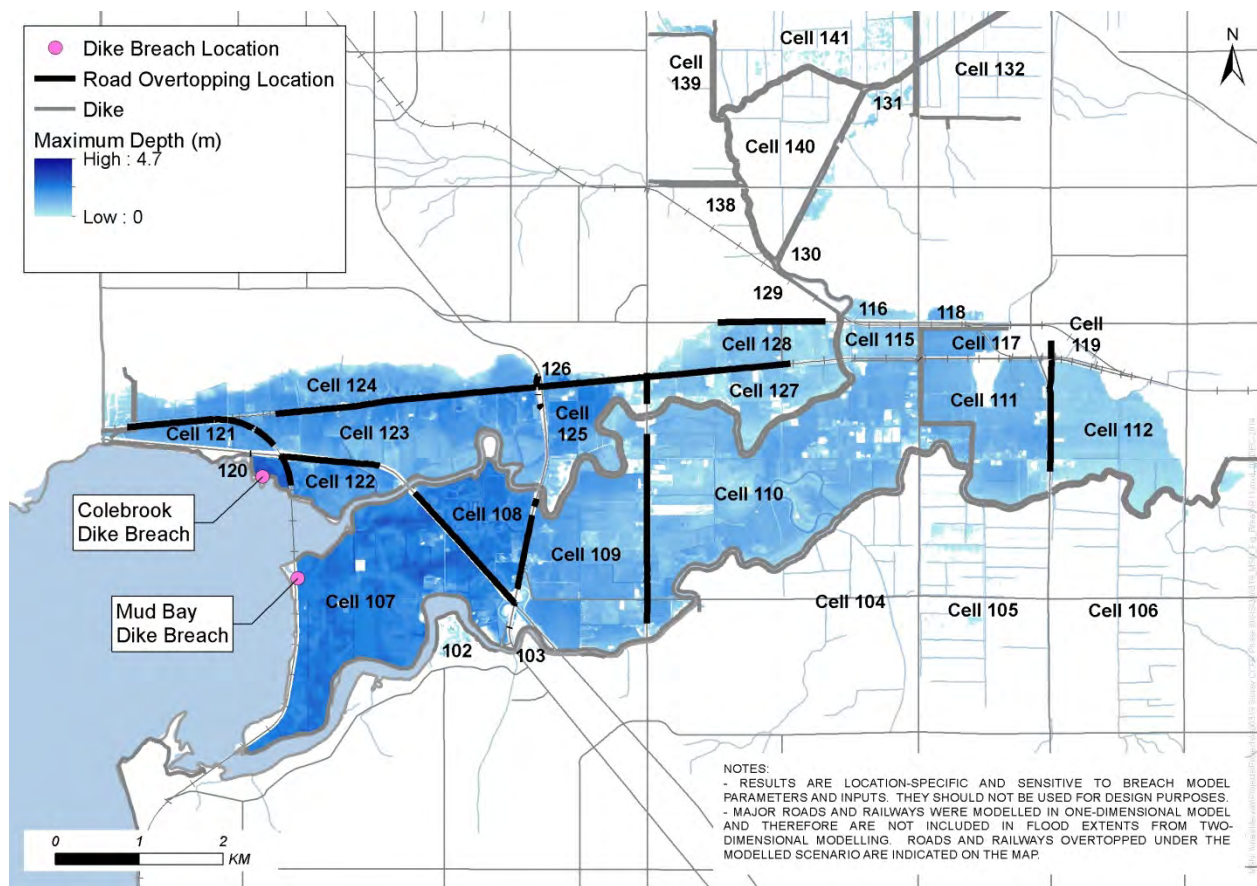


**Figure 41. Maximum modelled flood depths from coastal dike breaches (Run 11).**

Maximum velocities of 4 to 5 m/s were computed at the breach with peak velocities on the floodplain reaching up to 2.5 m/s. The highest velocities on the floodplain occur along ditches and at culvert entrances or outlets. Many roads were overtopped during this scenario with velocities in the 2.5 m/s

range computed under Highway 99 (Cell 120 to 121) and velocities of roughly 1.5 m/s over Highway 99 (Cell 120 to 122).

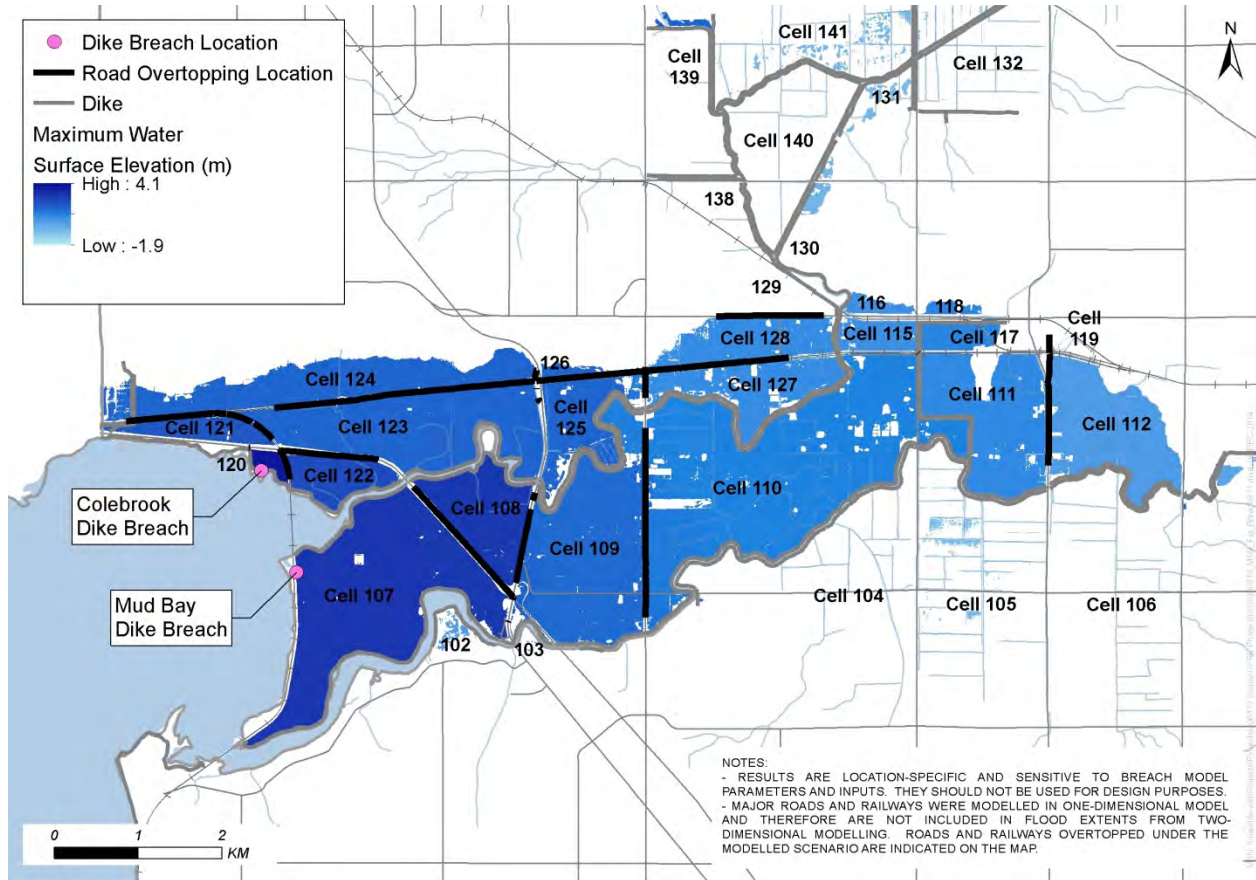


**Figure 42. Maximum modelled water levels from coastal dike breaches (Run 11).**

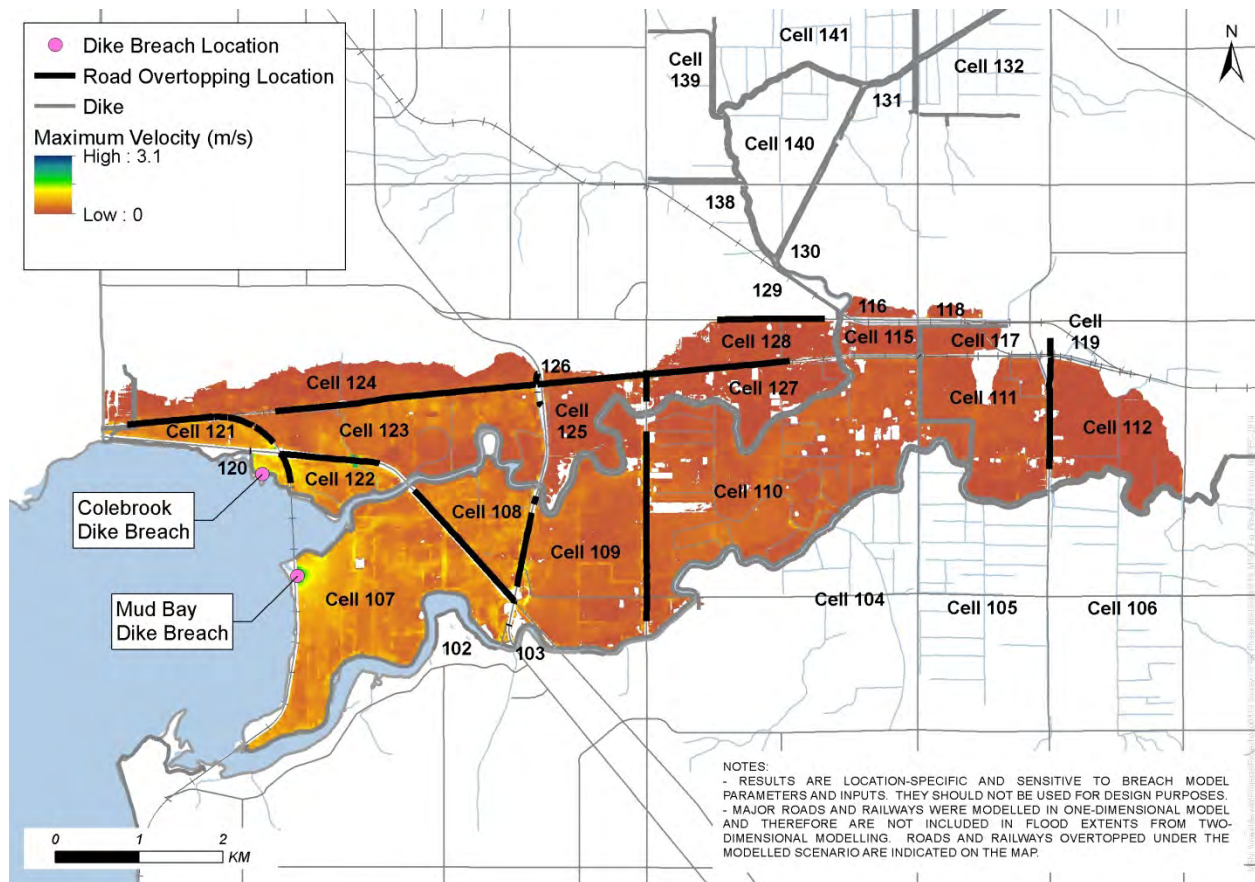


**Figure 43. Maximum modelled flow velocities from coastal dike breaches (Run 11).**

### 6.5.3 Seismic Inland Dike Failure (Run 12)

For the seismic inland dike failure, a location was selected with assistance from the City. Mean winter water levels were assumed during a seismic failure of the entire Coast Meridian dike along the left bank of the Serpentine River between 168th Street South Canal and Fraser Highway. This straightened reach of the Serpentine River was identified as being most susceptible to a dike failure during a seismic event. The dike is assumed to fail instantaneously but was modelled as a 20 minute failure due to model stability constraints. As the dike fails, it will likely slump into the channel, blocking all channel conveyance of flow from upstream. Since the model has a fixed bed, this blockage could not be accurately simulated nor could any potential floodplain erosion.

Appendix G includes a series of frames depicting water travelling across the floodplain as a result of the breach modelled in Run 12. Under mean winter conditions, the failure of the Coastal Meridian Dike results in an initial lowering of water levels in the Serpentine River and adjacent reaches as water stored in the river channel prior to the breach flows onto the floodplain.

Within less than one hour of breach initiation, water levels on the floodplain (Cell 132) increase from an initial elevation of -0.5 m to an elevation of -0.3 m. Water spreads across the floodplain but levels are

too low to overtop into adjacent floodplain cells. Since water levels in the river are relatively low at the time of the failure (roughly 0.5 m above the bottom of the breach elevation), the depth of water on the floodplain and flow velocities after breach initiation are relatively low. Over the course of the next few tide cycles, the water levels on the floodplain steadily increase to an elevation of 0.5 m. Under different conditions, a seismic failure of the Coast Meridian Dike could be more devastating.

Maximum flood depths, water elevations, and flow velocities computed on the floodplain over the entire simulation period are shown in Figure 44 to Figure 46. Maximum velocities of 0.6 m/s were computed at the breach with peak velocities on the floodplain reaching up to 0.4 m/s. The highest velocities on the floodplain occur along ditches. No roads are overtopped during this scenario.

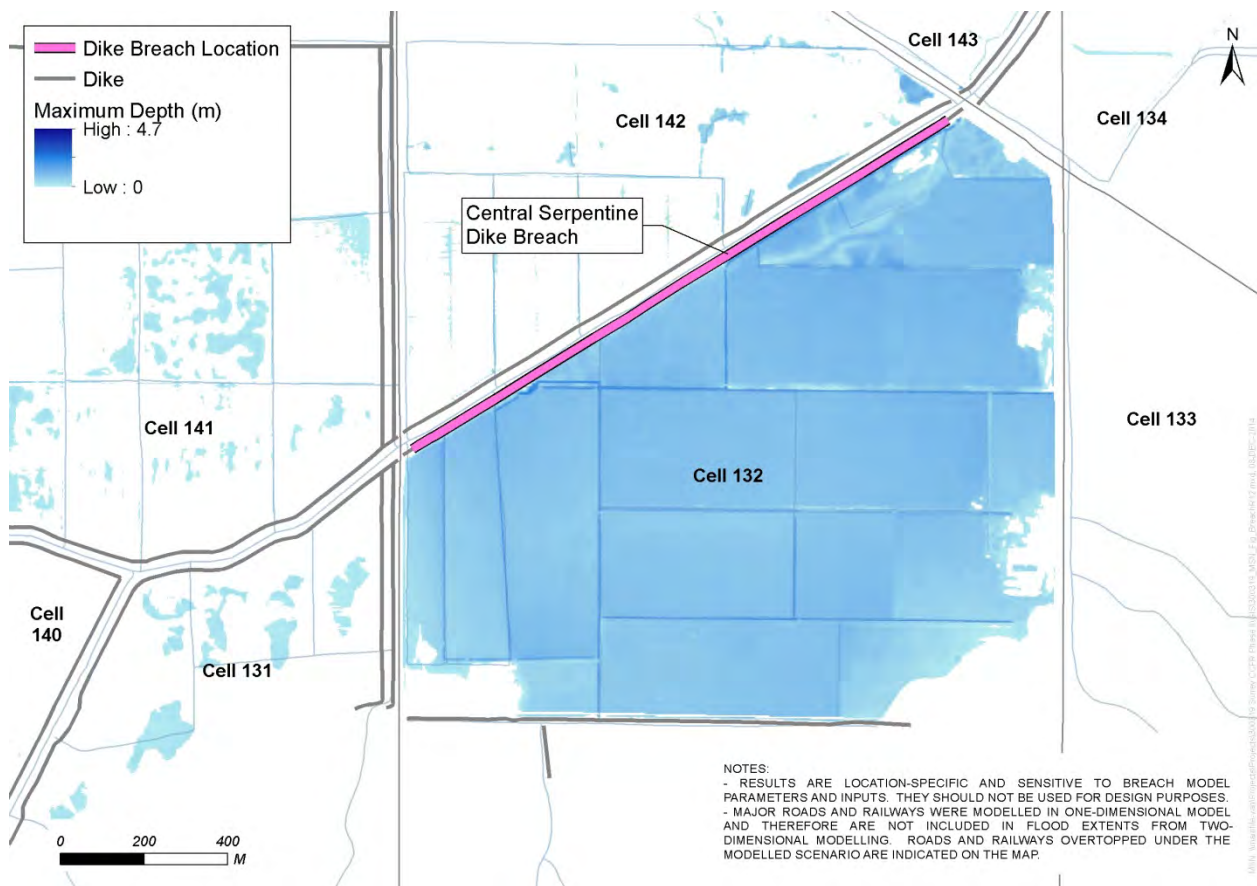


**Figure 44. Maximum modelled flood depths from coastal dike breaches (Run 12).**

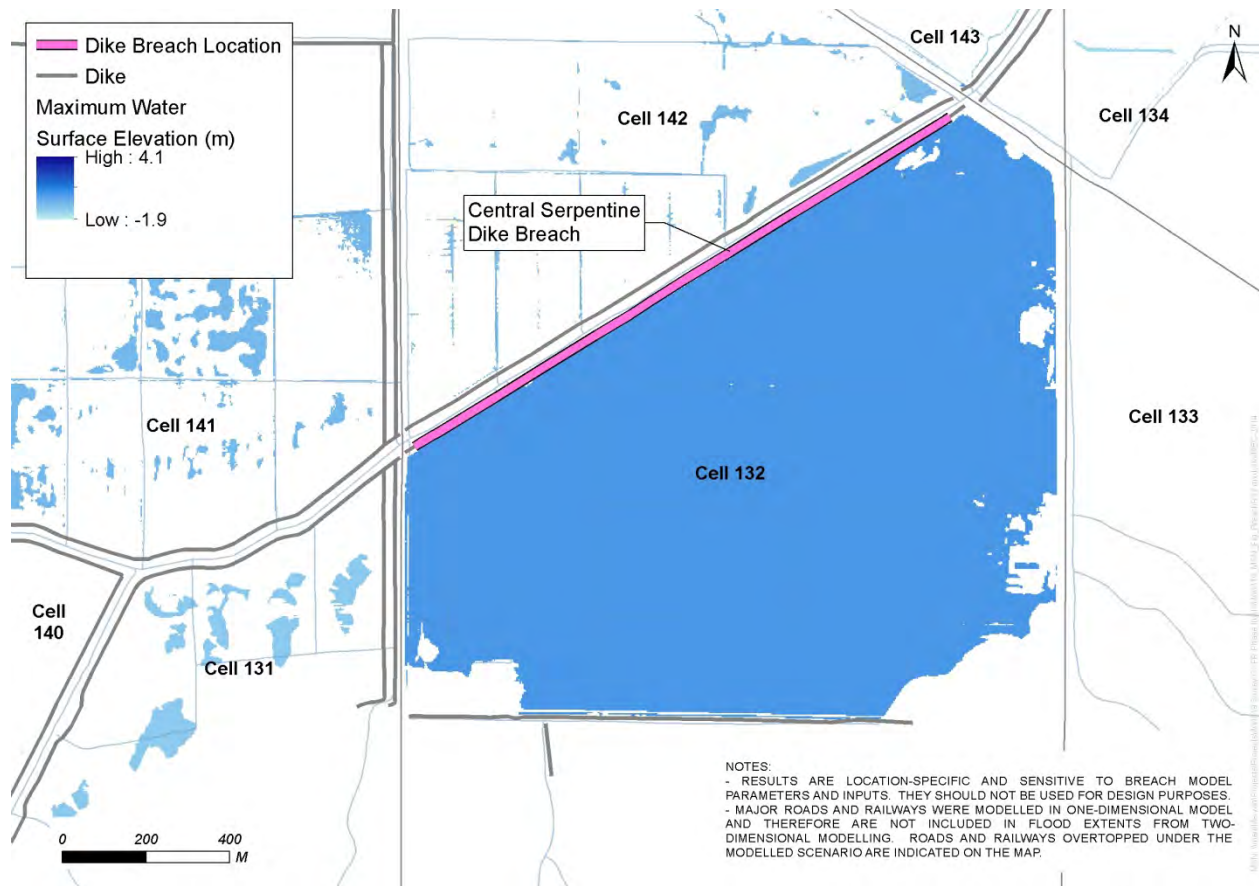
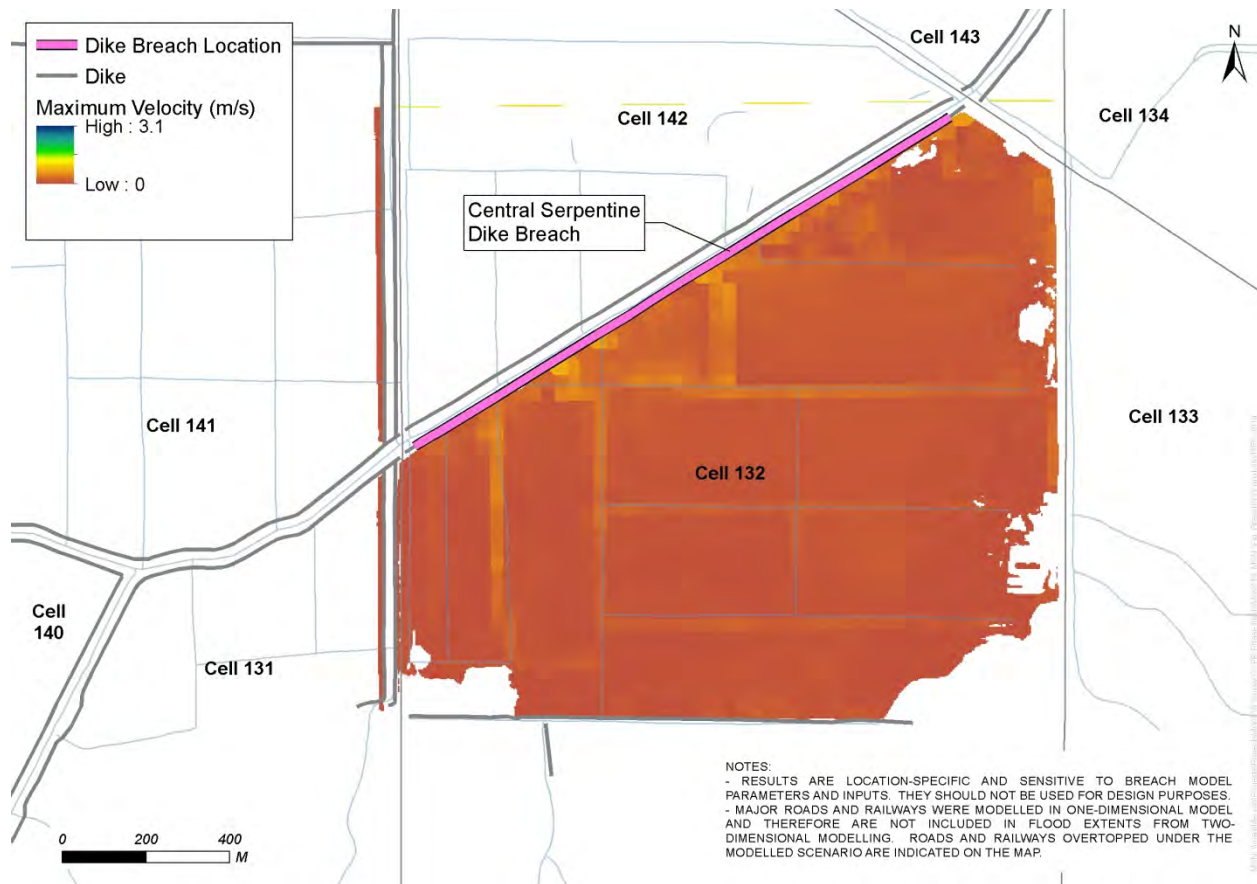


Figure 45. Maximum modelled water levels from coastal dike breaches (Run 12).





**Figure 46. Maximum modelled flow velocities from coastal dike breaches (Run 12).**

#### 6.5.4 Post Sea Dam Failure (Run 13)

A model run was done to investigate the effects on water levels and flow velocities during a two year period after the hypothetical failure of the Nicomekl and Serpentine River sea dams. The sea dams were removed from the model prior to the start of the simulation which covered a period similar to that from September 2008 to September 2010 (assumed conditions in 2010). This two year period was selected near the end of the design life of the structures and included the larger January 2009 flood event but no very large tides.

During the two year period simulated without sea dams, the dikes modelled using the current design dike crest elevations are not overtopped but spillways (S-12 and S-19) are activated (January 2009, January 2010, and November 2009). However, along a distance of 9 km upstream of the Nicomekl sea dam, the dike freeboard is compromised. At the most vulnerable location along that reach, peak water levels reach an elevation of 2.35 m where the design dike crest elevation is set at 2.46 m. It should be noted that the 2013 LiDAR shows the dike crest at elevations ranging between 2.7 and 3.0 m.

For a distance of 12 km upstream of the Serpentine sea dams, the dike freeboard is compromised at the peak water levels (2.5 m). At the most vulnerable location (immediately upstream of the sea dam), the

results indicate only a few centimeters of freeboard. However, the 2013 LiDAR shows that the dike crest elevations at that location range between 2.7 and 3.0 m.

The impacts of the absence of sea dams at bridges were investigated. Values summarised in Table 23 include the maximum modelled water levels and velocities at each of the bridges along the Nicomekl and Serpentine Rivers. The table also identifies any bridge deck low or high chords that were submerged during the simulated two year period.

**Table 23. Maximum modelled water levels and velocities at Nicomekl and Serpentine bridges.**

Bridge Name	River	Chainage m	Max Water Level (m GD)	Max Velocity (m/s)	Deck Low Chord Elev. (m GD)	Deck High Chord Elev. (m GD)
RR Bridge	Nicomekl	-4972				
King George Blvd	Nicomekl	209	2.35	1.11	1.9	2.62
Hwy 99	Nicomekl	1010	2.35	0.92	2.4	4.95
152 St	Nicomekl	2101	2.35	0.73	13.85	9.219
40 Ave	Nicomekl	2891	2.35	0.73	1.88	2.55
168 St	Nicomekl	7216	2.35	1.14	2.28	2.49
176 St	Nicomekl	9486	2.35	1.28	3.34	5
184 St	Nicomekl	11871	2.33	0.72	3.26	4.08
192 St	Nicomekl	14318	2.77	0.67	4.08	5.21
small unnamed crossing	Nicomekl	15179	3.09	0.54	1.88	2.65
200 St	Nicomekl	16419.3	3.69	1.17	5.33	5.9
203 St	Nicomekl	17281	3.83	0.5	5.403	6.153
51B Ave	Nicomekl	18506.7	5.29	0.27	6.3	8.7
RR Bridge	Serpentine	-4416.6				
Hwy 99	Serpentine	-2651	2.5	0.95	3.62	4.43
King George Blvd	Serpentine	20	2.46	0.83	2.69	4.44
152 St	Serpentine	3405	2.39	0.87	2.65	4.16
160 St	Serpentine	5791				
BCR	Serpentine	7045	2.32	1.04	2.04	5.44
56 Ave/Hwy 10	Serpentine	7503	2.32	1.21	2.91	3.78
SRY	Serpentine	7593	2.32	0.91	1.64	2.94
64 Ave (Canal)	Serpentine	9917	2.35	0.6	2.00	3.69
64 Ave (River)	Serpentine	9929	2.36	0.52	2.05	3.74
Northview Golf	Serpentine	10771				
168 St Pedestrian	Serpentine	11932	2.38	0.54	2.8	3.03
168 St	Serpentine	11960	2.38	0.52	3.02	3.82
Fraser Hwy (South)	Serpentine	13551	2.39	0.34	3	3.93
176 St	Serpentine	13912	2.39	0.3	3.94	5.19
80 Ave	Serpentine	14622	2.4	0.48	2.94	5.19

Fraser Hwy (North)	Serpentine	16469	2.41	0.35	1.88	3.09
88 Ave	Serpentine	17688	2.42	0.31	3.34	4.84
cattle bridge	Serpentine	18091	2.78	0.93	3.03	4.14

1. Model was not calibrated to observed velocity data so modelled velocities should be used with caution.
2. Modelled velocities correspond to cross-section averaged velocities. Higher local velocities are to be expected.
3. Blue shading indicates modelled water levels above the bridge deck low chord elevation.

The greatest impact of the sea dam failure will be the upstream migration of salt water which will impact the ability to irrigate agricultural lands. Spillways may also be activated more frequently as high tides migrate upstream, potentially damaging crops with brackish water. It is anticipated that impacts would have been more severe under higher tide conditions than those experienced from September 2008 to 2010.

## 6.6 Breach Flood Levels

The City's current flood construction levels (FCLs) are based on design water levels computed by KPA (1994). The KPA levels on the floodplain were computed through simulations of various dike breach scenarios. Where available, the KPA levels were included in Figure 47 for comparison with peak levels from the coastal dike breach in year 2100 (Run 11). Locations where year 2100 water levels are higher than KPA are identified with grey halos.

It is important to stress that computed flood levels are sensitive to selected breach parameters and that those presented here for year 2100 could be exceeded by selecting different breach parameters. Further investigations into the sensitivity of flood levels to various breach parameters is recommended prior to updating FCLs.



## 6.7 Breach Flood Hazard

Standard hazard ratings for dam or dike breach failures used around the world are based on a combination of water depth and velocity. However, when considering risk ratings, especially those pertaining to loss-of-life, the time to peak flooding and rise-rates of the water become crucial. The calculation of any of these hazard or risk inputs can be completed with spatial 2D information. The hazards resulting from the failure of the coastal and inland dikes under the three modelled scenarios described above are shown in Figure 48 to Figure 50. Hazard ratings were based on the ratings from the UK shown in Table 24.

**Table 24. Flood hazard ratings (source: UK DEFRA/EA 2006)**

Hazard Rating depth * (velocity + 0.5) (m·m/s)	Degree of Flood Hazard	Description
< 0.75	Low	<b>Caution</b> “Flood zone with shallow flowing water or deep standing water”
0.75 to 1.25	Moderate	<b>Dangerous for some</b> (i.e. children) “Danger: flood zone with deep or fast flowing water”
1.25 to 2.5	Significant	<b>Dangerous for most people</b> “Danger: flood zone with deep fast flowing water”
> 2.5	Extreme	<b>Dangerous for all</b> “Extreme danger: flood zone with deep fast flowing water”

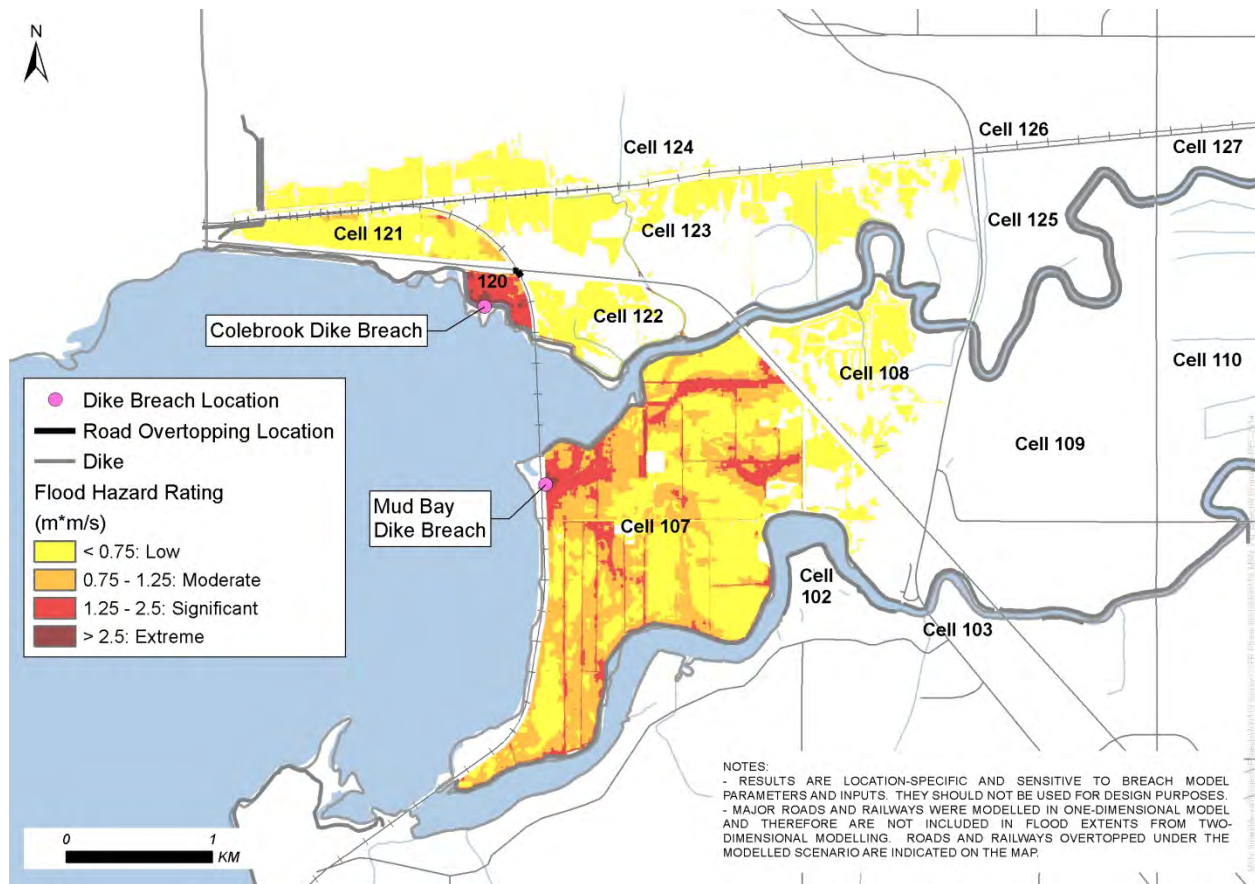


**Figure 48. Flood hazard mapping for coastal dike breaches (Run 10).**

In summary, a breach in the Colebrook and Mud Bay dikes at a 10-year return period ocean level under present conditions, would result in extreme hazards in the immediate vicinity of the breaches. Flood depths and velocities within the flow paths of the flood waves would cause significant hazards, reducing to “moderate” and “low” away from the areas of immediate impact. Major transportation corridors would generally not be affected. Based on the breach parameters selected, inundation would be limited to the area west of King George Highway.

Depending on the time of day, loss of life could occur. Economic losses would primarily result from flooded or damaged homes and farm buildings, saltwater intrusion of agricultural lands, wash-out of local roads and extensive clean-up costs. Spillage of sewage or chemicals would have environmental impact.

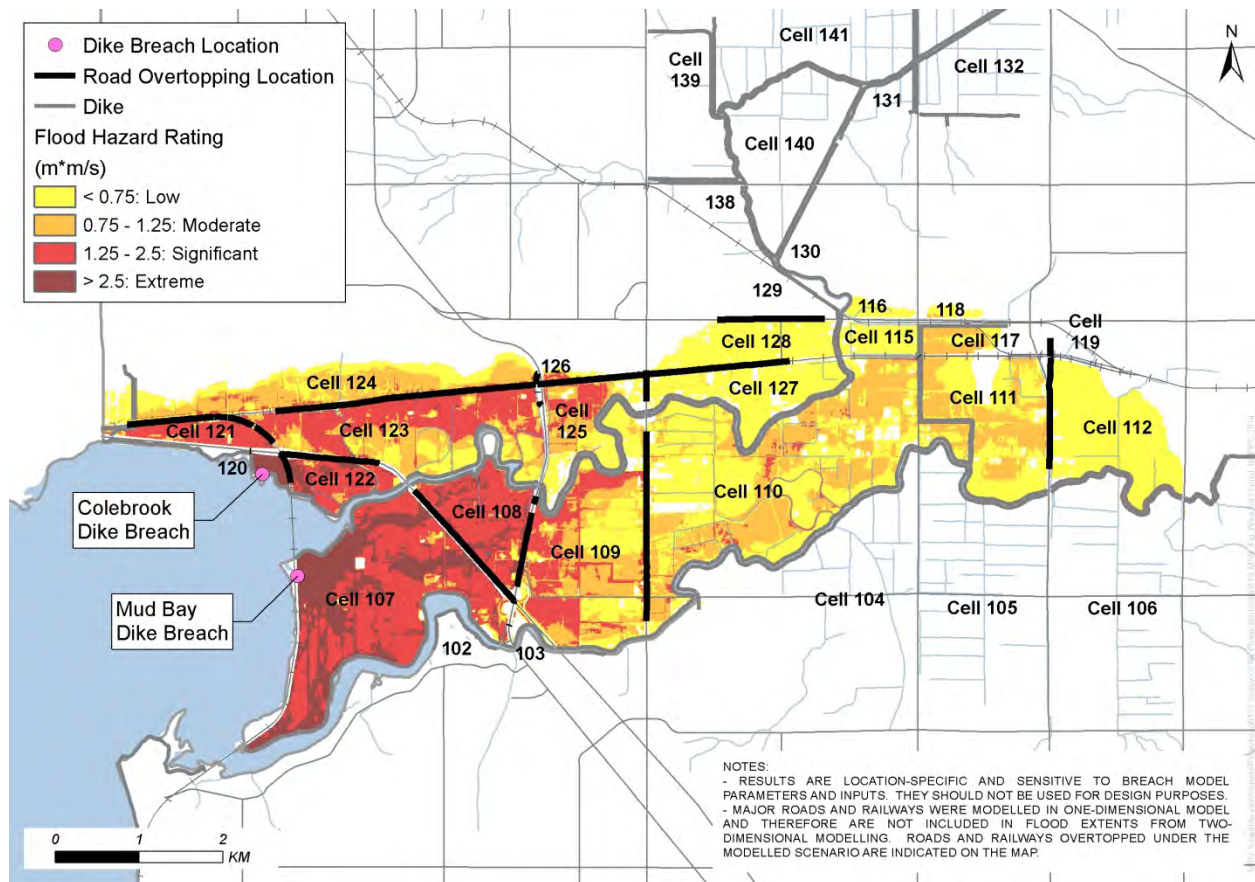


**Figure 49. Flood hazard mapping for coastal dike breaches (Run 11).**

The coastal dike breaches modelled in Run 11 (200-year ocean levels for year 2100) would have catastrophic consequences, essentially dividing the city into two parts. The flood hazard rating would be extreme for well over 1 km from the breach, with significant hazards extending to 152<sup>nd</sup> Street. Inundation would be experienced all the way to 148<sup>th</sup> Street or potentially farther, depending on the breach parameters selected.

The risk of loss of life would be high. All major roads and railroads in the area would be overtopped, severing transportation routes, resulting in extensive direct and indirect economic losses. Residential, commercial, industrial and agricultural development would incur extensive damage.

The scenario is hypothetical in the sense that the present diking would not withstand a year 2100, 200-year ocean event; all dikes overtopping by year 2040 for ocean levels with return periods of less than 10 years (Section 2).

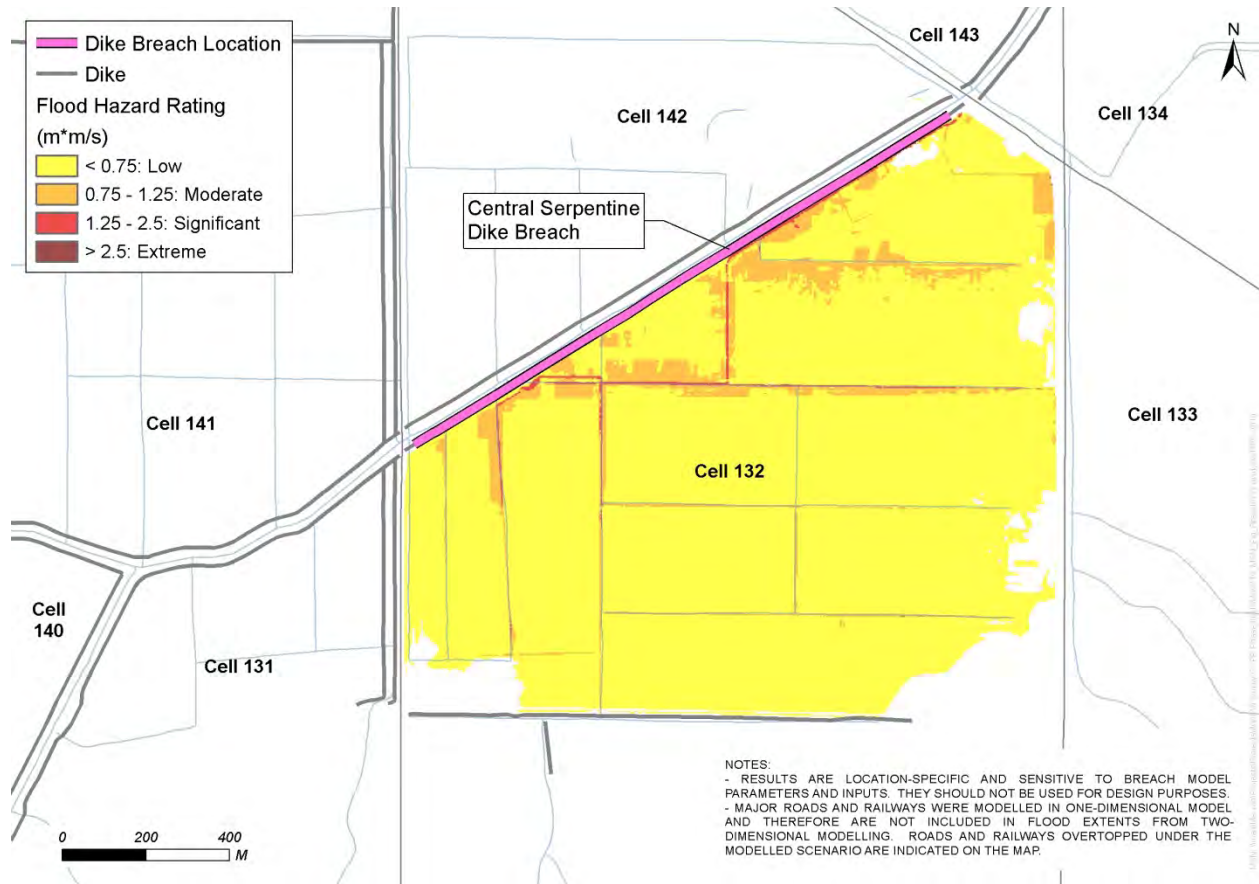


**Figure 50. Flood hazard mapping for inland seismic dike failure (Run 12).**

Compared to the ocean dike breaches, the seismically induced inland dike breach modelled in Run 12 resulted in relatively low hazard ratings. Damage is highly location sensitive and for a better understanding of inland failures, it is recommended that several different types of failures be modelled and in various locations.

Hazard mapping was not prepared for Run 13 as flow was largely confined to the river channels and fields next to spillways. Only fairly moderate tidal levels were simulated and it is recommended that more extensive modelling without the sea dams in place be completed to better understand their present and future value in terms of reducing flood losses.



## 7 SUMMARY AND CONCLUSIONS

### 7.1 Coastal Flooding

**Most of the City's coastal dikes offer inadequate protection against flooding and immediate attention is required to reduce the risk of overtopping and breaching. Provincial guidelines assume sea level will rise linearly by 1 m between year 2010 and 2100 and with sea level rise, conditions are expected to continuously worsen.**

Required coastal dike design crest elevations were calculated at nine locations for years 2010, 2020, 2040, 2070, 2100 and 2200. Unlike CCFR Phase 1, which assumed that all dikes would be raised by 1.5 m to prevent overtopping, the Phase 2 computations allowed for inundation of dike crests. Existing coastal dike crest elevations range from 2.3 m to 3.3 m (GSC) and are up to 0.9 m below 200-year design crest elevations for present ocean conditions and 1.9 m below projected 2100 conditions.

The estimated return period ocean event that each dike is able to withstand will decrease with time due to sea level rise. For 2010 conditions, the return period ranges from 2 to 350 years, with only two of the dikes meeting 200-year ocean level standards. Assuming the linear increase in sea level recommended by provincial guidelines, by year 2020, none of the dikes will meet the 200-year standard; by 2040, the return period event the dikes can withstand without overtopping will be less than 10 years; and, by 2070, it is expected that all dikes will be inundated multiple times per year. The dikes are not designed for overtopping and would likely fail if ocean waters washed over the crests or, potentially as the dike freeboard is compromised.

### 7.2 Precipitation, Runoff and Climate Change Impacts

**The precipitation projections presented reflect plausible representations of the future, given the best current scientific information, but do not represent specific predictions. As climate science improves, the estimates will need refinement.**

The Phase 2 hydrologic model reproduced observed calibration storm volumes within about 5% and event peaks within 10%. Some uncertainty continues to surround reported flows at WSC Station 08MH155, Nicomekl at 203<sup>rd</sup> Street.

Climate change is expected to affect precipitation, with winters generally becoming wetter but the number of wet days becoming fewer. A unique approach was developed to assess climate change impacts on future precipitation. Two alternative synthetic time series of hourly precipitation were developed to reflect a moderate and a severe climate change scenario based on downscaled results from Global Climate Models. The analyses suggest that at the 200-year return period level the moderate scenario may increase daily precipitation by roughly 33% and the severe scenario by 50%. Long-term hydrologic simulations were carried out using the synthetic moderate and severe precipitation records to develop corresponding hydraulic model inflow timeseries.

## 7.3 Inland Flooding

The current work focussed on year 2010 and 2100 flood conditions. Tentative projections were made for year 2200 flood conditions; however, the associated climate change projections are highly uncertain. Coastal dikes appear to be in the most critical condition, with inland dikes generally having some degree of freeboard at present 200-year flood conditions. By year 2100, the region's sea dams, dikes, bridges, roads and railroads will be extensively vulnerable to flooding. An initial assessment of dike failures indicated high hazard ratings for present conditions, with potential loss of life in the vicinity of the breaches. Similar breach scenarios in 2100 would have catastrophic consequences, likely with significant loss of life. Considering the topography of the floodplain, relatively minor increases to the inundation area are expected by year 2100. A comparison of present model results and FCLs in effect since the 1990's indicates a need to update the FCLs. However, presently estimated 200-year flood levels plus freeboard should not be adopted as accurate FCLs without further review.

### 7.3.1 Hydraulic Modelling

Phase 2 enhanced the HEC-RAS hydraulic model developed in Phase 1 and the model validations to the January 2014 and January 2013 flood events showed good agreement at most locations. Observed discrepancies are likely due to some water levels being recorded in ditches and not being representative of the floodplain. The model was run for years 2010, 2020, 2040, 2070, 2100 and 2200, each run accounting for projected sea level rise; for year 2100 incorporating moderate and severe climate change impacts on precipitation in addition to sea level rise; and finally, for year 2100 also incorporating a 1 mm/year subsidence allowance. Flood levels were output at 97 locations for the near 50 year simulation time period and annual peak levels were extracted for frequency analyses to estimate the 200-year flood level at each location.

The lower river reaches are more susceptible to flooding caused by increases in sea level than the upper reaches. The floodplain cells experiencing the largest increases in peak 200-year water levels from 2010 to 2100 (about 0.5 m to 1 m) are those connected to the river channels with spillways. The upper reaches are most sensitive to increases in runoff and the 200-year water levels showed a noticeable change from 2020 to 2040, coinciding with the adopted change from existing to future landuse. This was further confirmed by the model runs incorporating precipitation increases due to climate change. Impacts of revised subsidence rates appear to fall within the accuracy of modelling.

### 7.3.2 Frequency Analyses

In the lower floodplain (above the sea dams) the present 200-year flood level will have a return period of less than 2 years by year 2100. In the upper Nicomekl and upper Serpentine reaches, the present 200-year flood level will have a return period of roughly 75 years in year 2100, assuming no changes in precipitation. With the estimated precipitation increases corresponding to a moderate or severe climate change scenario, the present 200-year water level would occur on average every 5 to 10 years.

### 7.3.3 Vulnerabilities

The vulnerability assessment of the sea dams, dikes, bridges, roads and railroads indicated that at the present 200-year flood condition, freeboard would be compromised at the Serpentine Sea Dam; the Serpentine left bank dike downstream of the sea dam would be inundated and freeboard would be compromised at all of the lowland dikes; bridge decks would be inundated at three of the bridges and the low chords submerged at nine other bridges; a portion of Highway 99 would be inundated and freeboard compromised at Colebrook Road, with a few sections of railroad having compromised freeboard as well. Infrastructure upgrades are required for current conditions.

In 2100 at the 200-year flood, ignoring potential precipitation increases, both the Serpentine and Nicomekl Sea Dams would be inundated; the lowland dikes upstream and downstream of the sea dams would also be inundated and nearly all other dikes would have compromised freeboard; the bridge decks would be inundated at seven bridges and the low chords submerged at 10 other bridges; major roads and railroads would have either compromised freeboard or some inundation.

### 7.3.4 Dike Breaches

The US Corps' RAS2D software was used for an initial assessment of flood depths and velocities following a dike breach. The impacts of breaches were last modelled 30 years ago and did not include any SLR projections. Results are sensitive to the selected breach locations, adopted parameters and river or ocean water levels, prior to and following a breach. The breach modelling simulated: 1) a storm induced failure of coastal dikes under existing (2010) and future (2100) conditions; 2) a future seismic failure of an inland dike; and, 3) conditions following failure of the sea-dams. Sea dike failures had flow velocities in the order of 4-5 m/s at the breach, dropping to 1.5 – 2.5 m/s on the floodplain. At present conditions, the breaches modelled could potentially result in some loss of life and extensive damage, whereas future breaches would be catastrophic with water depths reaching over 3 m. Based on the particular inland seismic breach modelled during typical winter conditions (the Coast Meridian dike) inundation depths and velocities were moderate. However, impacts of a seismic breach occurring during a period with high river level are anticipated to be severe. The post sea-dam scenario modelled, reflecting moderate tidal conditions in 2008 to 2010, did not result in dike overtopping but freeboard was compromised in several locations. It is anticipated that impacts would have been more severe under higher tide conditions. The greatest impact of the sea dam failure will be the upstream migration of salt water which will impact the ability to irrigate agricultural lands. Further breach modelling is required to better understand the impacts to the City's many valuable assets in the at risk areas.

### 7.3.5 Flood Extents and FCLs

With the steep rise in topography bordering the near horizontal floodplain, inundation extents for the different model scenarios showed relatively minor variation. Year 2100, in combination with a severe precipitation scenario, had the largest increase in floodplain compared to present conditions, showing a total area increase of 25% (with main expansions in floodplain south of the Erickson and Burrows pump stations and by the Latimer and Bear Creek tributaries).

The City's current flood construction levels (FCLs) are based on design water levels computed by KPA (1994). Considering the different approaches adopted for the present modelling, simulated 200-year flood levels plus freeboard were expected to vary from the FCLs. In general, the CCFR Phase 2 flood levels for both 2010 and 2100 are lower than KPA levels in the floodplain storage cells but higher where flood levels are directly influenced by the ocean and in some of the upper river reaches. There is a need for updating the FCLs but further refinement of the modelling is necessary before developing official floodplain maps and setting FCLs.

## 8 RECOMMENDATIONS

The CCFR Phase 2 findings led to several recommendations, here divided into recommendations pertaining to developing a flood management plan (Section 8.1) and to improving the modelling (Section 8.2).

### 8.1 Recommendations for Developing a Flood Management Plan

For clarity, coastal and inland flooding are discussed separately but it should be recognized that the two flood hazards are interrelated and that an overall flood management strategy is needed that takes both types of flooding into account.

#### 8.1.1 Coastal Flooding

1. Develop an emergency response plan for coastal flooding outlining temporary protection measures, the evacuation of people/livestock and procedures for repairing dikes. Develop flood preparedness guidelines to minimize property and environmental damage associated with a dike breach.
2. As feasible, take action to improve the degree of protection provided by the Crescent Beach North; BNSF Railway; and, 8th Avenue – Campbell dikes. In the near term, improvements are also required to the Colebrook – Serpentine; Mud Bay – Serpentine; and, Colebrook (Highway 99) dikes. The Mud Bay – Nicomekl; Crescent Beach East; and, Crescent Beach South dikes appear to be less prone to overtopping but areas behind the dikes may flood from other sources or from other types of dike failures than overtopping. These interim measures would be incorporated into a comprehensive long-term flood management plan for mitigating coastal flooding.
3. Assess geotechnical, seismic, structural and erosion characteristics of the existing dikes.
4. Undertake studies to develop a long term coastal flood management plan. Assess the feasibility, costs and benefits of various coastal protection options such as: 1) improved diking; 2) coastal protection (jetties, breakwaters, beach nourishment and different edge treatments such as riprap and sheet piling); 3) introduction of adaptation measures to increase the resilience of affected areas; 4) introduction of landuse change; or, 5) a combination of the options mentioned. Coastal flood management is both location specific and time dependent and strategies will need to be developed for particular locations and fine-tuned over time.
5. Assess the potential impacts of a tsunami generated flood waves.

#### 8.1.2 Precipitation, Run-off and Climate Change Impacts

1. Recognize present climate science limitations. As more information becomes available, review and update the synthetic precipitation time series developed as part of Phase 2.

### 8.1.3 Inland Flooding

It is recommended that a long-term flood management plan be developed for the Nicomekl/ Serpentine watersheds that the City can gradually implement over time. The strategy must be flexible and allow for adjustment based on the observations of actual changes to sea levels, runoff, subsidence and land use. Development of the strategy will involve assessing the status of the existing flood protection and developing potential improvements, identifying flood hazards in more detail, and prioritizing upgrades based on sustainability, socio-economic and cost/benefit perspectives.

**To assess the present status of flood protection and develop potential improvements the following is recommended:**

1. Use the Phase 2 vulnerability assessment results to highlight deficiencies and the point in time when structures become functionally inadequate. The comparisons can be performed graphically and summarized in table format.
2. Complete structural and geotechnical assessments of existing flood protection measures.
3. Carry out a preliminary assessment of the different protection measures and their relative importance to identify the weakest 'links' in the mitigation measures that, if upgraded, would likely provide the greatest benefit.
4. Develop a better understanding of potential flood mitigation options by investigating the interrelationship and trade-offs between modifications to outfall pumping capacities and spillway ratings. Assess the system response in terms of hydraulic gradients within the rivers and water levels on the floodplain for short (2040) and long-term (2100) time horizons. Short list scenarios for further study based on equitable flood depths and durations, frequency of spillway activation, dike overtopping, additional pumping capacity and run-time requirements, and the flexibility of implementation phasing.
5. Review what non-structural flood protection measures are in place, including flood bylaws.

**To assess flood hazards in more detail the following is recommended:**

6. Develop detailed floodplain maps and revise the City's FCLs. (Coordinate with provincial and federal governments in the event that a national floodplain mapping program is announced). For detailed floodplain mapping, the results from the Phase 2 modelling should be reviewed, the HEC-RAS model further refined as described in Section 8.1 and inundation boundaries checked in the field. Inundation boundaries corresponding to return periods other than 200-year conditions may also be relevant. Expand and refine the Phase 2 flood depth and vulnerability maps as required.
7. Identify in more detail how flood hazards will change over time (assuming present infrastructure in place). Prepare floodplain maps that illustrate how flood extent and depth could change over

time to inform planners and the public about potential changes that may occur due to climate change.

8. Carry out hydrologic and hydraulic modelling for the Campbell River.
9. Estimate the impact of groundwater flow and dike seepage on floodplain water levels.

**To prioritize upgrades based on sustainability, socio-economic and cost/benefit perspectives the following is recommended:**

10. Develop economic loss estimates using the updated floodplain maps and available asset inventories. Using the Canadian HAZUS-MH software, estimate the direct economic losses to residential, commercial and agricultural sectors for present and future flood conditions. Indirect losses are more difficult to assess but should be approximated based on disruption to critical infrastructure and related cascade effects. Evaluate the relative vulnerability of different parts of the floodplain as well as the overall vulnerability based on present and future flood hazards and present and projected future development and densification.
11. Traditionally, risk assessments tend to ignore social, cultural, environmental and personal losses but it is recommended that some subjective evaluation of these be included. The loss of life also falls outside a standard risk assessment and it is recommended that the potential for loss of life from a sudden dike /sea dam failure be assessed, if even in a cursory manner.
12. In consultation with the City, develop flood mitigation improvements meeting the City’s long range objectives. In addition to construction and maintenance costs and direct benefits, consider socio-economic and sustainability aspects. It is expected that several types of solutions will need to be developed and assessed in an iterative process of evaluating associated flood hazard reductions, reduced consequences and losses, including loss of life, and direct/indirect benefits. In order to increase the efficiency of assessing different solutions, it may be possible to classify the floodplain into typical areas, where the inundation problems are similar and similar solutions may be effective.
13. Prioritize improvement projects by area (HEC-RAS storage cells) and by region. Determine in what order the preferred flood protection measures should be implemented and at what point in time. To minimize losses from flood damage, the time frame for introducing protection measures becomes critical. There are likely to be severe damages associated with a “do nothing” approach. Based on the prioritisation process, develop a time line for implementing improvements and set appropriate standards for the flood reduction projects. Summarize results in a long-term flood management strategy for the Nicomekl/Serpentine watersheds.

## **8.2 Recommendations for Modelling**

1. The Serpentine and Nicomekl channel cross-sections (surveyed prior to 2003) may now be outdated and it is recommended that the rivers be resurveyed. A comparison of the previous and

updated cross-sections should be carried out to better understand the geomorphology of the rivers and any trends of aggradation/degradation and lateral shifting.

2. Both the hydrologic and hydraulic models are highly complex and should preferably be further fine-tuned by collecting additional calibration data and improving the accuracy of the input data. The following data collection tasks are recommended:
  - a. Collect high quality flow data, stage data and high water mark information during flood events with return periods greater than about 2 years. Maintain and improve reliability of stage-discharge ratings at existing gauge stations. Collect additional stage data at various points in the floodplain (not only at pump stations). Other information such as photos, condition of pump stations (on/off set levels, pump failures, changes in pump capacity), duration of spilling at spillways, road closures, etc., should continue to be documented.
  - b. Conduct a field program to inspect infrastructure and to verify and further update the City's GIS database. Maintain the database and revise the model as necessary.
  - c. Coordinate with other jurisdictions to improve rainfall monitoring in the eastern parts of the Nickomekl and Serpentine watersheds.
  
3. The following model improvements are recommended:
  - a. Further improve the hydrologic and hydraulic models based on the additional data collected.
  - b. Expand the breach modelling to consider other areas and time frames than those evaluated in Phase 2. Simulations of dike breaches are very sensitive to breach location and breach parameters. Further work should be done to investigate the system's sensitivity to various breach scenarios. As newer versions of the RAS2D software become available, these should be used.
  
4. Consideration should be given to expanding the evaluation of the impacts of climate change on rainfall regime by analysing outputs from additional GCMs. Results from the two GCMs analysed in Phase 2 showed large differences in projected future extreme rainfall amounts. Analysis of outputs from additional GCMs would help to better understand the uncertainty in projections of future rainfall regimes.
  
5. Update the ocean analysis as new information or SLR projections become available.

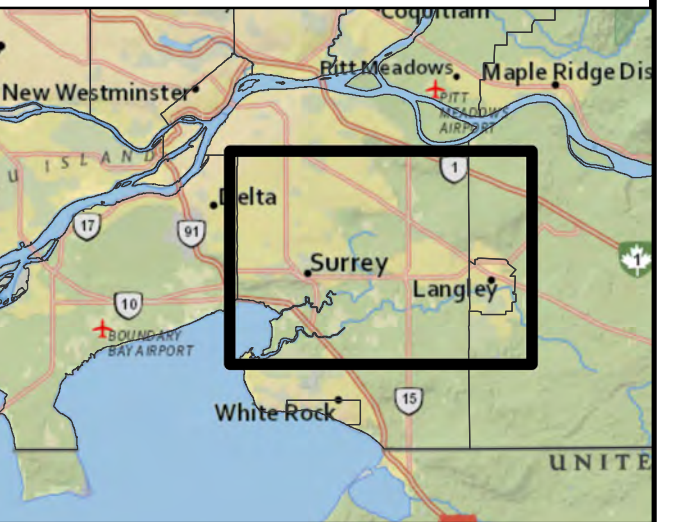


## 9 REFERENCES

- Ausenco Sandwell, 2011. Sea Dike Guidelines. Technical report, BC Ministry of Environment.
- Baron, 2011. Challenge of Sea Level Rise for the City of Surrey. Presentation at Sea level rise workshop 2011.
- Booij, N.; Ris, R. & Holthuijsen, L. 1999. A third-generation wave model for coastal regions. 1. Model description and validation. *Journal of Geophysical Research* 104(C4), 7649--66.
- City of Surrey Engineering Department, 2004. Design Criteria Manual. Version, May 2004. 245 pp.
- City of Surrey, 2009. City Flood Protection/Dyke Initiatives and Related Funding Needs. Corporate Report No: R005 for Council date of 19 January 2009. Report prepared for Mayor and Council by General Manager of Engineering, January 15, 2009, 7 pp.
- Clague, J. 1998: Geological Setting of the Fraser River Delta, pg. 7-16, in "Geology and Natural Hazards of the Fraser River Delta, British Columbia", edited by Clague, J., Luternauer, J. and D.C. Mosher, Geological Survey of Canada, Bulletin 525 1998, Natural Resources Canada.
- Dillon Consulting Ltd. (2013). Rainfall Trending Analysis for the City of Surrey. Draft report prepared for the City of Surrey, May 2013.
- Dinicola, R.S., 1990. Characterization and Simulation of Rainfall-Runoff Relations for Headwater Basins in Western King and Snohomish Counties, Washington. U.S. Geological Survey Water-Resources Investigations Report 89-4052.
- Hawkins E, Sutton R (2010). The potential to narrow uncertainty in projections of regional precipitation change. *Climate Dynamics* 37:407–418. DOI: 10.1007/s00382-010-0810-6.
- Kellerhals, P. and Murray, J., 1969. Tidal flats at Boundary Bay, Fraser River Delta, British Columbia, *Bulletin of Canadian Petroleum Geology*, Vol. 17, No. 1, pg. 67-91.
- KPA Engineering Ltd. (1993) 1994. Floodplain Mapping Program Serpentine and Nicomekl Rivers. Design Brief. Report prepared for BC Environment Water Management Division.
- Kundewicz AW, Kanae S, Seneviratne SI, Handmer J, Nicholls N, Peduzzi P, Mechler R, Bouwer LM, Arnell N, Mach K, Muir-Wood R, Brakenridge GR, Kron W, Benito G, Honda Y, Takahashi K, Sherstyukov B (2013). Flood risk and climate change: global and regional perspectives. *Hydrological Sciences Journal - Journal des Sciences Hydrologiques* 59(1): 1-28. DOI: 10.1080/02626667.2013.857411.
- NHC & Triton 2006. Final Report. Lower Fraser River Hydraulic Model. Report prepared for Fraser Basin Council.
- Mantua NH, Hare SR, Zhang Y, Wallace JM, Francis RC (1997). A Pacific interdecadal climate oscillation with impacts on salmon production. *Bulletin of the American Meteorological Society* 78: 1069-1079.
- Mazzotti, S.; Jones, C. & Thomson, R. E., 2008. Relative and absolute sea level rise in western Canada and northwestern United States from a combined tide gauge-GPS analysis. *J. Geophys. Res.* 113(C11), C11019--.

- McElhanney Consulting Services Ltd., 2002. Review of Runoff Coefficients. Report prepared for City of Surrey, January 25, 2002. 48 pp.
- Pawlowicz, R.; Beardsley, B. & Lentz, S., 2002. Classical tidal harmonic analysis including error estimates in MATLAB using T-TIDE. *Computers & Geosciences* 28(8), 929--37.
- Pullen, T. & fur Forschung im Kusteningenieurwesen., K., 2007. Eurotop.; Wave overtopping of sea defences and related structures : assessment manual, Boyens, Heide i. Holstein.
- Rodenhuis, D, Bennett, K.E., Werner, A., Murdock, T.Q., Bronaugh, D. 2007. Hydroclimatology and future climate impacts in British Columbia. Pacific Climate Impacts Consortium.
- Septre, 2000. Flood Damage Southern British Columbia 1850-2000
- Thompson, R. O. R. Y., 1983. Low-Pass Filters to Suppress Inertial and Tidal Frequencies. *J. Phys. Oceanogr.* 13(6), 1077--1083.
- Thomson, R. E., Bornhold, B., Mazzotti, S., 2008. An Examination of the factors affecting relative and absolute sea level in coastal British Columbia. Canadian Technical Report of Hydrography and Ocean Sciences 260, Fisheries and Oceans Canada, 49 pp.
- TEL, 2014. Surrey Flood Plain Subsidence Statistical Characterization and Geotechnical Review. Report prepared for City of Surrey. 74 pp.
- TRE Canada Inc., 2011. Final Report on Ground Movement within the City of Surrey using SqueeSAR. Report prepared for City of Surrey, December 23, 2011. 42 pp.
- UK DEFRA/Environment Agency 2006. *R&D Outputs: Flood Risks to People, Phase 2*. FD2321/TR2 Guidance Document
- UMA, 2001. Conversion of the Serpentine-Nicomekl Lowlands Model from ONE-D to MIKE11. Report prepared for City of Surrey.
- Zhang U, Wallace JM, Battisti DS (1997). ENSO-like interdecadal variability: 1900-93. *J Climate* 10: 1004-1020.

**MAPS**



- Water Level Gauge (WSC)
- Water Level Gauge (COS)
- ★ Sea Dam
- Pump Station - River Level = No
- Pump Station - River Level = Yes
- ▲ Flood Box
- ◆ Bridge
- In-line Culvert
- Floodplain Culvert
- ◆ Spillway
- Lateral Structure
- ▲ Lateral Inflow
- Point Source Inflow
- Storage Cell
- Area Modelled with Extended Cross Sections
- Drainage Area
- HEC-RAS Stream Network (with chainage)
- Watercourse
- Railway
- Road

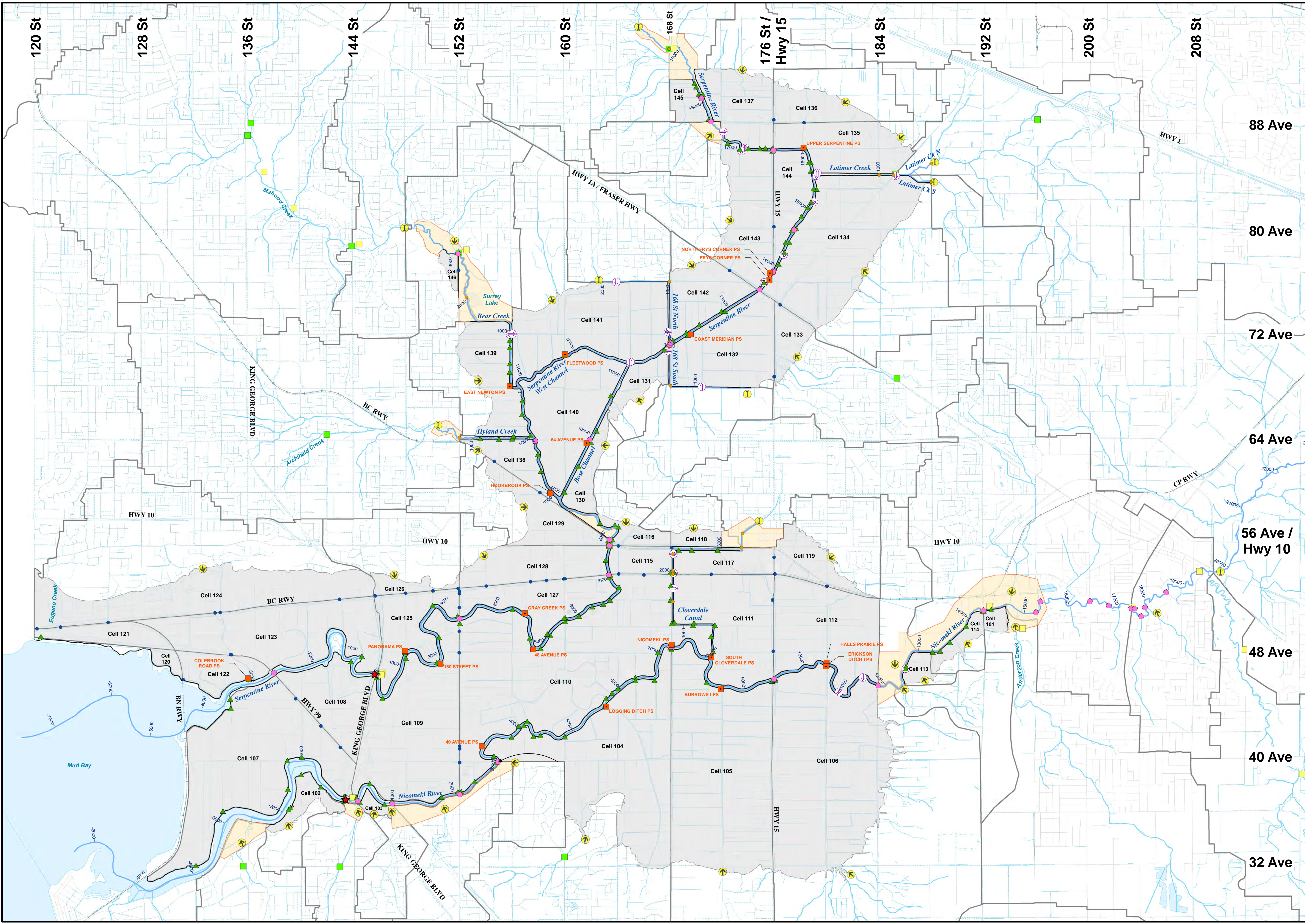
Data Sources:  
1. Drainage network, road and rail supplied by City of Surrey, City of Langley and Township of Langley. No drainage network available for City of Langley.  
2. BC Freshwater Atlas (FWA) stream network is shown for reference.  
3. Index basemap from National Geographic and Esri.

SCALE - 1:25,000  
0 0.5 1 1.5 KM

Coordinate System: NAD 1983 UTM ZONE 10N  
Units: METRES

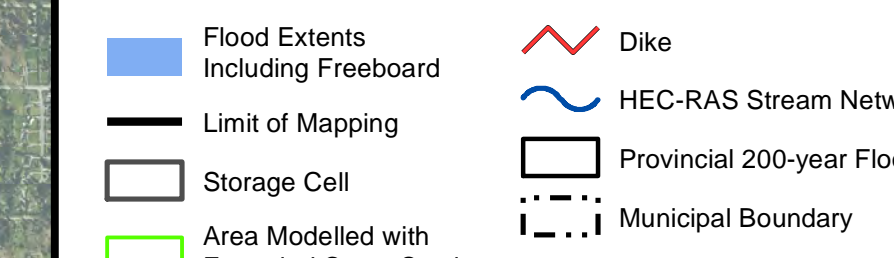
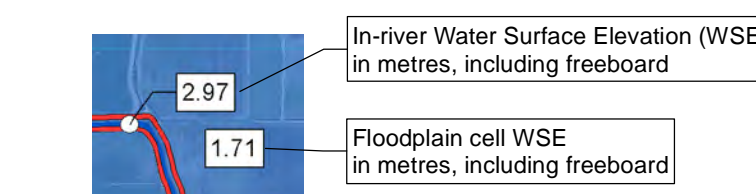
Engineer	GIS	MSN	Reviewer
VFOC		MSN	n/a
Job Number	Date		
300319	26-FEB-2015		

**CLIMATE CHANGE  
FLOODPLAIN REVIEW  
PHASE 2  
HYDRAULIC MODEL  
OVERVIEW MAP**



120 St  
128 St  
136 St  
144 St  
152 St  
160 St  
168 St  
176 St / Hwy 15  
184 St  
192 St  
200 St  
208 St

88 Ave  
80 Ave  
72 Ave  
64 Ave  
56 Ave / Hwy 10  
48 Ave  
40 Ave  
32 Ave

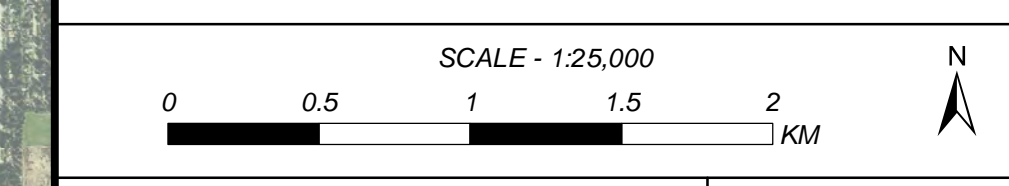


- Notes:**
- Flood levels were developed for nine coastal flood scenarios as described in NHC et al. (2014).
  - This map delineates the Serpentine and Nicomekl Rivers approximate flood potential under present (Year 2010) conditions for a current 200-year return period flood event, including freeboard. A 200-year return period flood means that, on average, the flood will occur once in 200 years and that there is a one-in-200 chance that the flood levels mapped could be equalled or exceeded in any one year. Flood levels shown are not to be used for Official Flood Construction Levels.
  - The adopted value for SLR is based on guidelines from Ausenco-Sandwell (2011).
  - A freeboard allowance (safety factor) of 0.6 m is included in the flood levels and extents shown.
  - The flood levels are based on water surface profiles simulated using a one-dimensional hydrodynamic model developed by NHC (NHC, 2014). Water levels shown on the river and for areas of the floodplain were estimated using the model. The model geometry was kept constant at all flows although variations (scour and erosion) may occur during a flood. In the model, some dikes and roadways were raised to confine the flow. The one-dimensional model did not simulate water level variations perpendicular to flow. Channel avulsions or blockages were assumed to be absent. The accuracy of the simulated flood levels is limited by the reliability and magnitude of the flow and water level data used for calibrating the model.
  - LIDAR data surveyed in 2013 was used to create a Digital Elevation Model (DEM) for the City of Surrey; the DEM surface was edited to remove buildings. The maps depict flood levels based on ground conditions at the time of the surveys. The accuracy of the location of a floodplain boundary is limited by the accuracy of the DEM. Changes to the channel, floodplain, and river basin runoff will affect the flood levels and render site-specific information obsolete. Local features such as roads, railways or dikes can restrict flow and locally affect flood levels. Channel obstructions, local storm water, groundwater or tributary streams may also affect flood levels. The flood mapping does not take local features into account. A Qualified Professional must be consulted for site-specific engineering analysis. Flooding from other sources, such as tsunamis or landslide generated waves, should be confirmed with appropriate maps and resources.
  - Industry best practices were followed to generate the flood maps. However, actual flood levels and extents may vary from those shown and Northwest Hydraulic Consultants Ltd. (NHC) does not assume any liability for such variations.

- Data Sources:**
- Provincial 200-year floodplain boundary from DataBC.
  - 2013 orthophoto supplied by City of Surrey.
  - Index basemap from National Geographic and Esri.

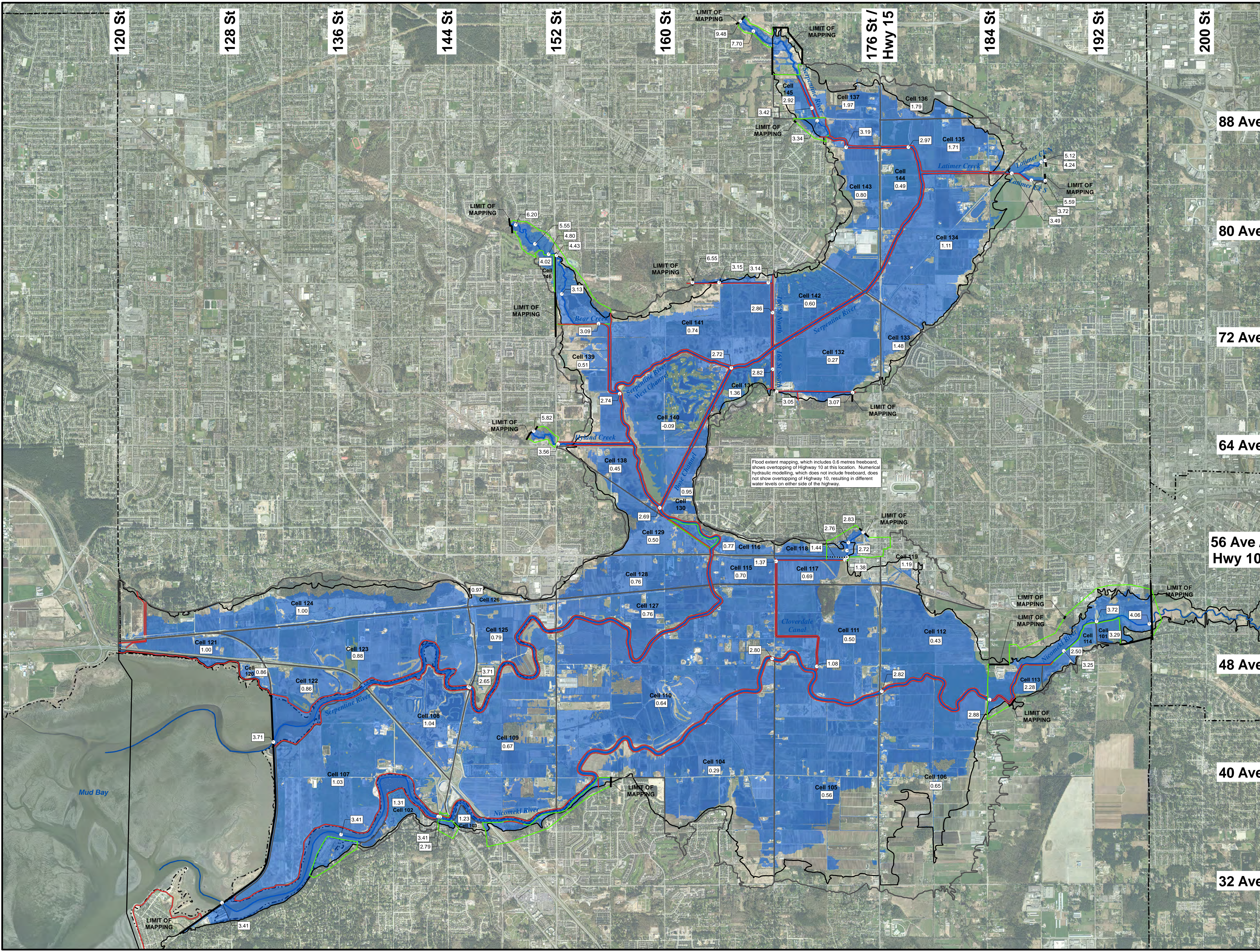
- References:**
- NHC (2014). Serpentine and Nicomekl Rivers Climate Change Floodplain Review Phase 2 (Final Report). Report prepared for the City of Surrey.
  - NHC (2012). Serpentine, Nicomekl and Campbell Rivers Climate Change Floodplain Review (Final Report). Report prepared for City of Surrey.
  - Ausenco-Sandwell (2011). Climate Change Adaptation Guidelines for Sea Dikes and Coastal Flood Hazard Land Use: Guidelines for Management of Coastal Flood Hazard Land Use. Prepared by Ausenco-Sandwell for BC Ministry of Environment.

**Disclaimer:**  
This document has been prepared by Northwest Hydraulic Consultants Ltd. in accordance with generally accepted engineering and geoscience practices and is intended for the exclusive use and benefit of the City of Surrey and their authorized representatives for specific application to the Climate Change Floodplain Review Phase II Project for the City of Surrey Serpentine River and Nicomekl River floodplains. The contents of this document are not to be relied upon or used, in whole or in part, by or for the benefit of others without specific written authorization from Northwest Hydraulic Consultants Ltd. No other warranty, expressed or implied, is made.  
Northwest Hydraulic Consultants Ltd. and its officers, directors, employees, and agents assume no responsibility for the reliance upon this document or any of its contents by any parties other than the City of Surrey.

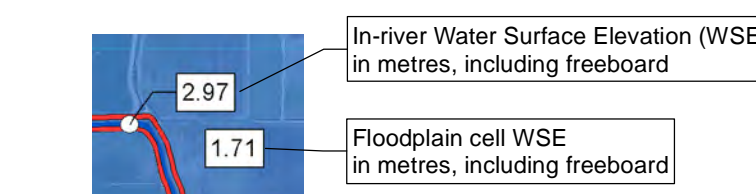


Coordinate System: NAD 1983 UTM ZONE 10N	Date: 20-JAN-2015		
Units: METRES			
Engineer: VFOC	GIS: MSN	Reviewer: n/a	Job Number: 300319

**CLIMATE CHANGE FLOODPLAIN REVIEW PHASE 2  
SERPENTINE AND NICOMEKL RIVERS  
FLOOD EXTENTS INCLUDING FREEBOARD  
YEAR 2010 DESIGN LEVELS  
(RUN 1)**



Flood extent mapping, which includes 0.6 metres freeboard, shows overtopping of Highway 10 at this location. Numerical hydraulic modelling, which does not include freeboard, does not show overtopping of Highway 10, resulting in different water levels on either side of the highway.



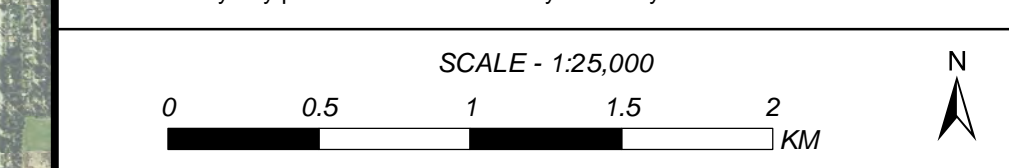
- Flood Extents Including Freeboard
- Dike
- HEC-RAS Stream Network
- Limit of Mapping
- Storage Cell
- Provincial 200-year Floodplain
- Area Modelled with Extended Cross Sections
- Municipal Boundary

- Notes:**
- Flood levels were developed for nine coastal flood scenarios as described in NHC et al. (2014).
  - This map delineates the Serpentine and Nicomekl Rivers approximate flood potential under Year 2100 conditions, assuming a 0.97 m sea level rise (SLR) and a current 200-year return period flood event, including freeboard. A 200-year return period flood means that, on average, the flood will occur once in 200 years and that there is a one-in-200 chance that the flood levels mapped could be equalled or exceeded in any one year. Flood levels shown are not to be used for Official Flood Construction Levels.
  - The adopted value for SLR is based on guidelines from Ausenco-Sandwell (2011).
  - A freeboard allowance (safety factor) of 0.6 m is included in the flood levels and extents shown.
  - The flood levels are based on water surface profiles simulated using a one-dimensional hydrodynamic model developed by NHC (NHC, 2014). Water levels shown on the river and for areas of the floodplain were estimated using the model. The model geometry was kept constant at all flows although variations (scour and erosion) may occur during a flood. In the model, some dikes and roadways were raised to confine the flow. The one-dimensional model did not simulate water level variations perpendicular to flow. Channel avulsions or blockages were assumed to be absent. The accuracy of the simulated flood levels is limited by the reliability and magnitude of the flow and water level data used for calibrating the model.
  - LIDAR data surveyed in 2013 was used to create a Digital Elevation Model (DEM) for the City of Surrey; the DEM surface was edited to remove buildings. The maps depict flood levels based on ground conditions at the time of the surveys. The accuracy of the location of a floodplain boundary is limited by the accuracy of the DEM. Changes to the channel, floodplain, and river basin runoff will affect the flood levels and render site-specific information obsolete. Local features such as roads, railways or dikes can restrict flow and locally affect flood levels. Channel obstructions, local storm water, groundwater or tributary streams may also affect flood levels. The flood mapping does not take local features into account. A Qualified Professional must be consulted for site-specific engineering analysis. Flooding from other sources, such as tsunamis or landslide generated waves, should be confirmed with appropriate maps and resources.
  - Industry best practices were followed to generate the flood maps. However, actual flood levels and extents may vary from those shown and Northwest Hydraulic Consultants Ltd. (NHC) does not assume any liability for such variations.

- Data Sources:**
- Provincial 200-year floodplain boundary from DataBC.
  - 2013 orthophoto supplied by City of Surrey.
  - Index base map from National Geographic and Esri.

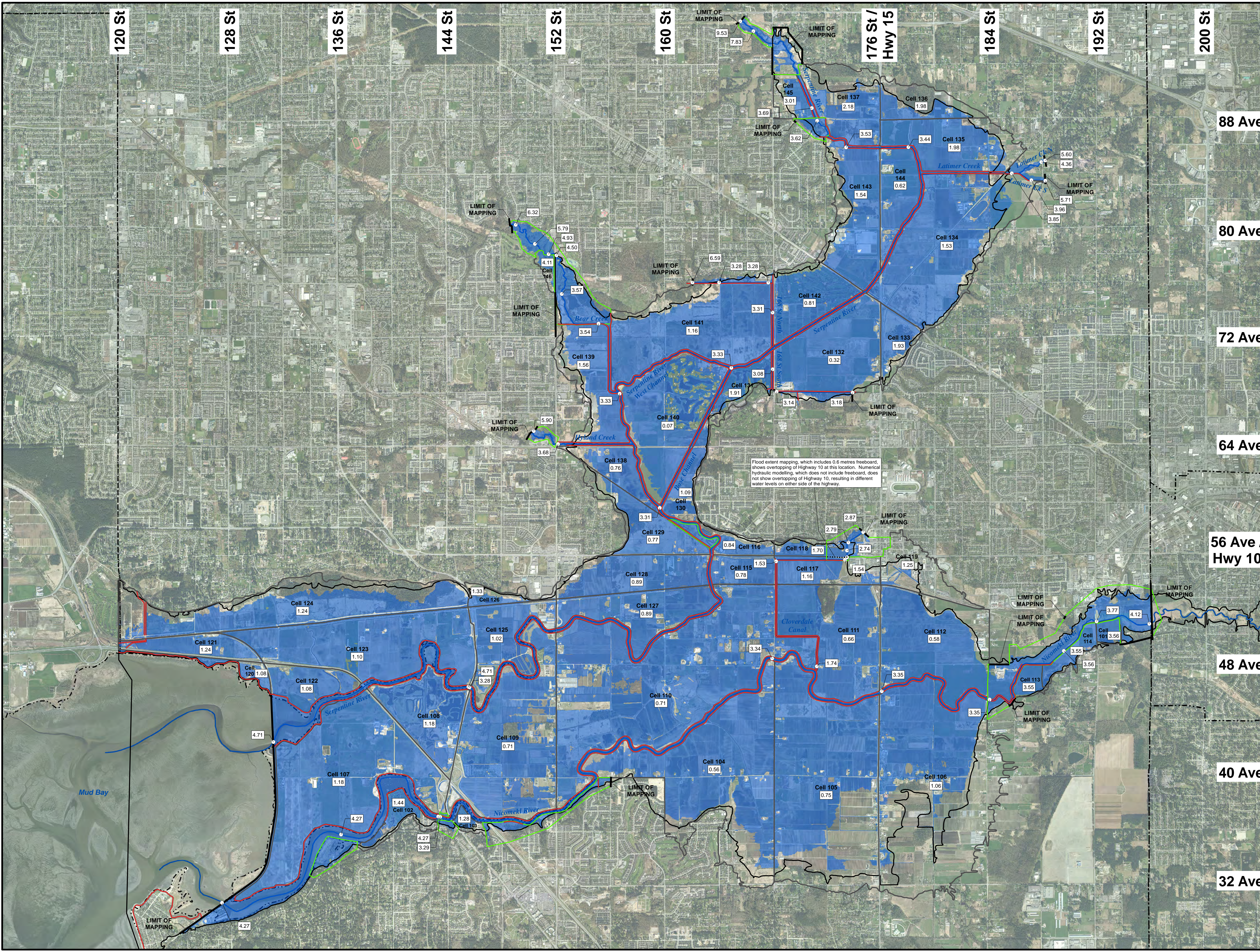
- References:**
- NHC (2014). Serpentine and Nicomekl Rivers Climate Change Floodplain Review Phase 2 (Final Report). Report prepared for the City of Surrey.
  - NHC (2012). Serpentine, Nicomekl and Campbell Rivers Climate Change Floodplain Review (Final Report). Report prepared for City of Surrey.
  - Ausenco-Sandwell (2011). Climate Change Adaptation Guidelines for Sea Dikes and Coastal Flood Hazard Land Use: Guidelines for Management of Coastal Flood Hazard Land Use. Prepared by Ausenco-Sandwell for BC Ministry of Environment.

**Disclaimer:**  
This document has been prepared by Northwest Hydraulic Consultants Ltd. in accordance with generally accepted engineering and geoscience practices and is intended for the exclusive use and benefit of the City of Surrey and their authorized representatives for specific application to the Climate Change Floodplain Review Phase II Project for the City of Surrey Serpentine River and Nicomekl River floodplains. The contents of this document are not to be relied upon or used, in whole or in part, by or for the benefit of others without specific written authorization from Northwest Hydraulic Consultants Ltd. No other warranty, expressed or implied, is made.  
Northwest Hydraulic Consultants Ltd. and its officers, directors, employees, and agents assume no responsibility for the reliance upon this document or any of its contents by any parties other than the City of Surrey.

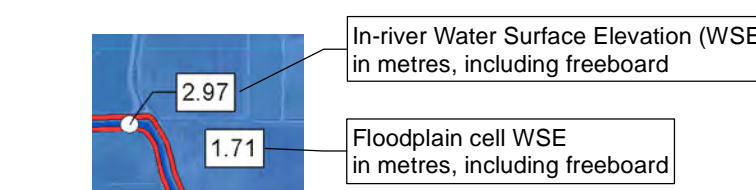
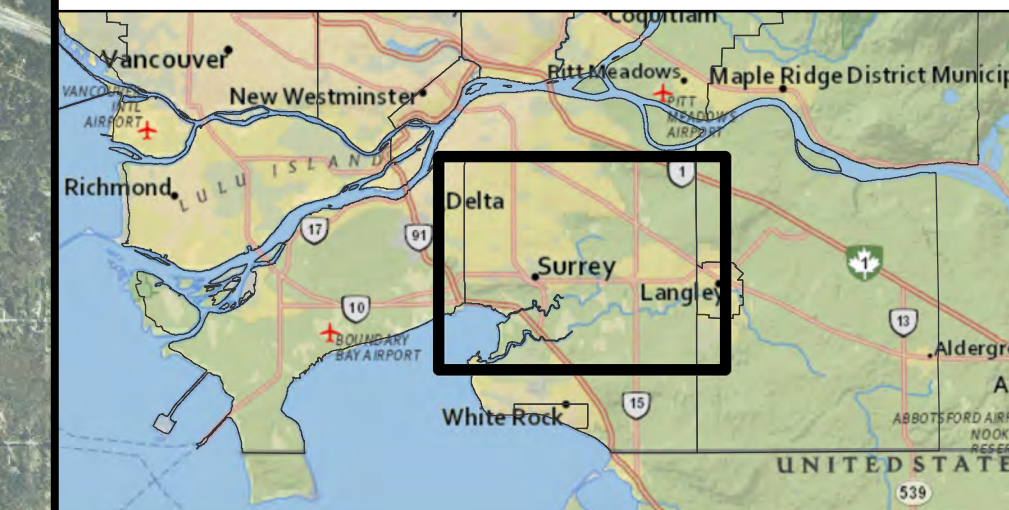


Coordinate System: NAD 1983 UTM ZONE 10N	Date: 20-JAN-2015		
Units: METRES			
Engineer: VFOC	GIS: MSN	Reviewer: n/a	Job Number: 300319

**CLIMATE CHANGE FLOODPLAIN REVIEW PHASE 2  
SERPENTINE AND NICOMEKL RIVERS  
FLOOD EXTENTS INCLUDING FREEBOARD  
YEAR 2100 DESIGN LEVELS,  
SLR 0.97 M (RUN 5)**



Flood extent mapping, which includes 0.6 metres freeboard, shows overtopping of Highway 10 at this location. Numerical hydraulic modelling, which does not include freeboard, does not show overtopping of Highway 10, resulting in different water levels on either side of the highway.



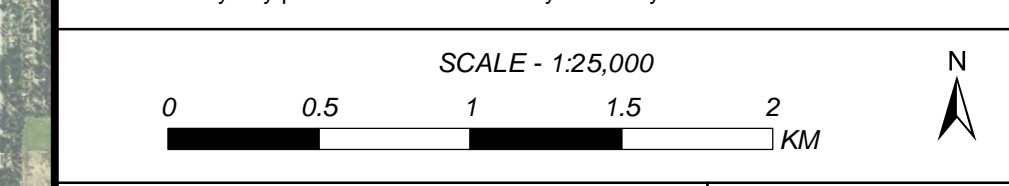
- Flood Extents Including Freeboard
- Dike
- HEC-RAS Stream Network
- Limit of Mapping
- Storage Cell
- Provincial 200-year Floodplain
- Municipal Boundary
- Area Modelled with Extended Cross Sections

- Notes:**
- Flood levels were developed for nine coastal flood scenarios as described in NHC et al. (2014).
  - This map delineates the Serpentine and Nicomekl Rivers approximate flood potential under Year 2100 conditions, assuming a 0.97 m sea level rise (SLR), a severe precipitation climate change scenario and a current 200-year return period flood event, including freeboard. A 200-year return period flood means that, on average, the flood will occur once in 200 years and that there is a one-in-200 chance that the flood levels mapped could be equalled or exceeded in any one year. Flood levels shown are not to be used for Official Flood Construction Levels.
  - The adopted value for SLR is based on guidelines from Ausenco-Sandwell (2011).
  - A freeboard allowance (safety factor) of 0.6 m is included in the flood levels and extents shown.
  - The flood levels are based on water surface profiles simulated using a one-dimensional hydrodynamic model developed by NHC (NHC, 2014). Water levels shown on the river and for areas of the floodplain were estimated using the model. The model geometry was kept constant at all flows although variations (scour and erosion) may occur during a flood. In the model, some dikes and roadways were raised to confine the flow. The one-dimensional model did not simulate water level variations perpendicular to flow. Channel avulsions or blockages were assumed to be absent. The accuracy of the simulated flood levels is limited by the reliability and magnitude of the flow and water level data used for calibrating the model.
  - LIDAR data surveyed in 2013 was used to create a Digital Elevation Model (DEM) for the City of Surrey; the DEM surface was edited to remove buildings. The maps depict flood levels based on ground conditions at the time of the surveys. The accuracy of the location of a floodplain boundary is limited by the accuracy of the DEM. Changes to the channel, floodplain, and river basin runoff will affect the flood levels and render site-specific information obsolete. Local features such as roads, railways or dikes can restrict flow and locally affect flood levels. Channel obstructions, local storm water, groundwater or tributary streams may also affect flood levels. The flood mapping does not take local features into account. A Qualified Professional must be consulted for site-specific engineering analysis. Flooding from other sources, such as tsunamis or landslide generated waves, should be confirmed with appropriate maps and resources.
  - Industry best practices were followed to generate the flood maps. However, actual flood levels and extents may vary from those shown and Northwest Hydraulic Consultants Ltd. (NHC) does not assume any liability for such variations.

- Data Sources:**
- Provincial 200-year floodplain boundary from DataBC.
  - 2013 orthophoto supplied by City of Surrey.
  - Index base map from National Geographic and Esri.

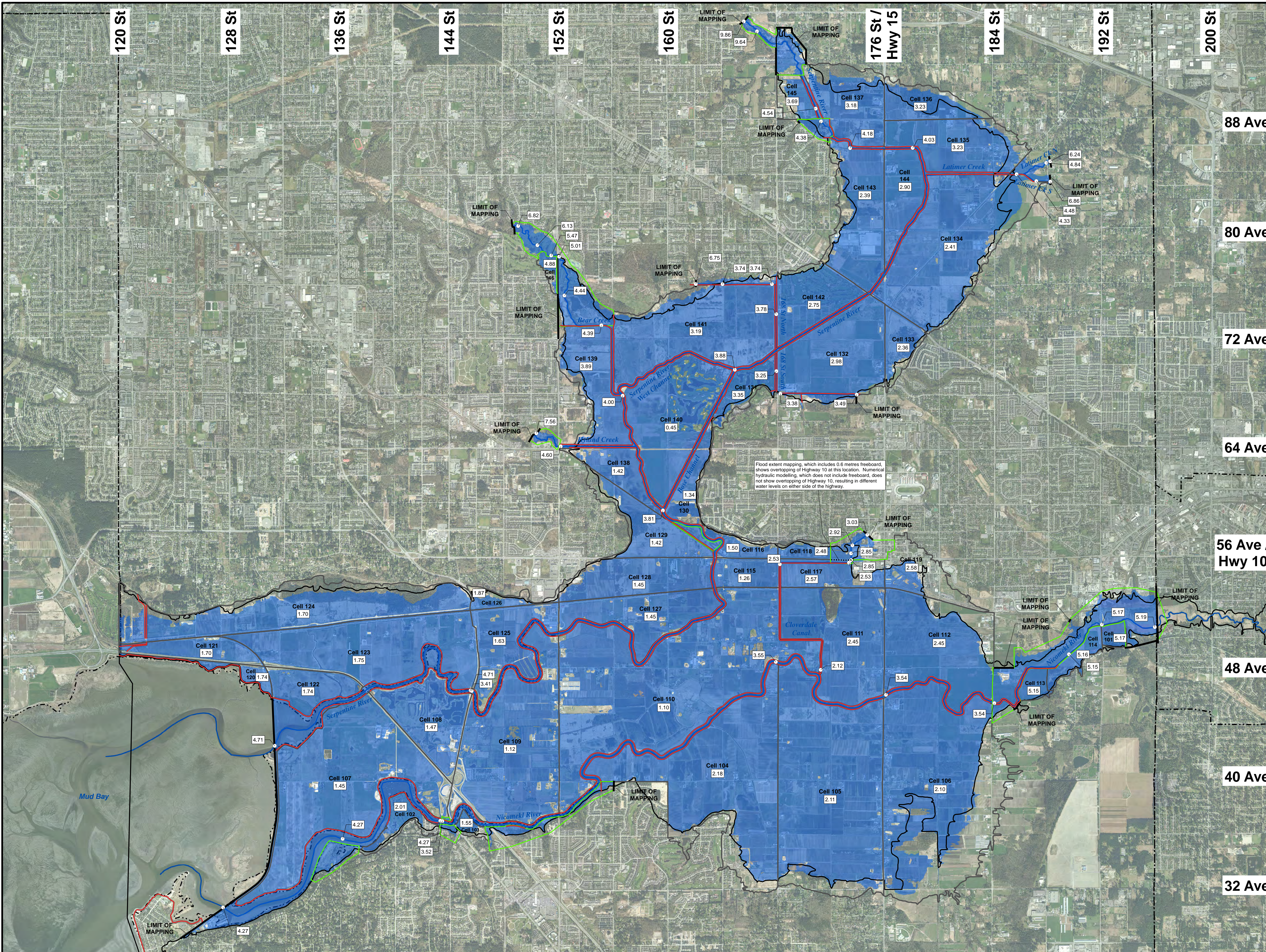
- References:**
- NHC (2014). Serpentine and Nicomekl Rivers Climate Change Floodplain Review Phase 2 (Final Report). Report prepared for the City of Surrey.
  - NHC (2012). Serpentine, Nicomekl and Campbell Rivers Climate Change Floodplain Review (Final Report). Report prepared for City of Surrey.
  - Ausenco-Sandwell (2011). Climate Change Adaptation Guidelines for Sea Dikes and Coastal Flood Hazard Land Use: Guidelines for Management of Coastal Flood Hazard Land Use. Prepared by Ausenco-Sandwell for BC Ministry of Environment.

**Disclaimer:**  
This document has been prepared by Northwest Hydraulic Consultants Ltd. in accordance with generally accepted engineering and geoscience practices and is intended for the exclusive use and benefit of the City of Surrey and their authorized representatives for specific application to the Climate Change Floodplain Review Phase II Project for the City of Surrey Serpentine River and Nicomekl River floodplains. The contents of this document are not to be relied upon or used, in whole or in part, by or for the benefit of others without specific written authorization from Northwest Hydraulic Consultants Ltd. No other warranty, expressed or implied, is made.  
Northwest Hydraulic Consultants Ltd. and its officers, directors, employees, and agents assume no responsibility for the reliance upon this document or any of its contents by any parties other than the City of Surrey.

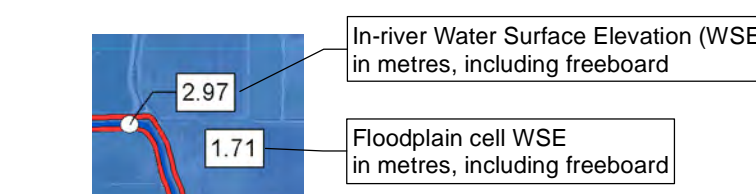


Coordinate System: NAD 1983 UTM ZONE 10N	Date: 20-JAN-2015		
Units: METRES			
Engineer: VFOC	GIS: MSN	Reviewer: n/a	Job Number: 300319

**CLIMATE CHANGE FLOODPLAIN REVIEW PHASE 2  
SERPENTINE AND NICOMEKL RIVERS  
FLOOD EXTENTS INCLUDING FREEBOARD  
YEAR 2100 SEVERE PRECIPITATION,  
SLR 0.97 M (RUN 7)**



Flood extent mapping, which includes 0.6 metres freeboard, shows overtopping of Highway 10 at this location. Numerical hydraulic modelling, which does not include freeboard, does not show overtopping of Highway 10, resulting in different water levels on either side of the highway.



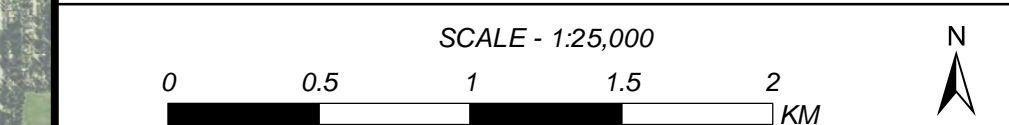
- Flood Extents Including Freeboard
- Dike
- HEC-RAS Stream Network
- Limit of Mapping
- Storage Cell
- Provincial 200-year Floodplain
- Municipal Boundary
- Area Modelled with Extended Cross Sections

- Notes:**
- Flood levels were developed for nine coastal flood scenarios as described in NHC et al. (2014).
  - This map delineates the Serpentine and Nicomekl Rivers approximate flood potential under Year 2200 conditions, assuming a 1.97 m sea level rise (SLR) and a current 200-year return period flood event, including freeboard. A 200-year return period flood means that, on average, the flood will occur once in 200 years and that there is a one-in-200 chance that the flood levels mapped could be equalled or exceeded in any one year. Flood levels shown are not to be used for Official Flood Construction Levels.
  - The adopted value for SLR is based on guidelines from Ausenco-Sandwell (2011).
  - A freeboard allowance (safety factor) of 0.6 m is included in the flood levels and extents shown.
  - The flood levels are based on water surface profiles simulated using a one-dimensional hydrodynamic model developed by NHC (NHC, 2014). Water levels shown on the river and for areas of the floodplain were estimated using the model. The model geometry was kept constant at all flows although variations (scour and erosion) may occur during a flood. In the model, some dikes and roadways were raised to confine the flow. The one-dimensional model did not simulate water level variations perpendicular to flow. Channel avulsions or blockages were assumed to be absent. The accuracy of the simulated flood levels is limited by the reliability and magnitude of the flow and water level data used for calibrating the model.
  - LIDAR data surveyed in 2013 was used to create a Digital Elevation Model (DEM) for the City of Surrey; the DEM surface was edited to remove buildings. The maps depict flood levels based on ground conditions at the time of the surveys. The accuracy of the location of a floodplain boundary is limited by the accuracy of the DEM. Changes to the channel, floodplain, and river basin runoff will affect the flood levels and render site-specific information obsolete. Local features such as roads, railways or dikes can restrict flow and locally affect flood levels. Channel obstructions, local storm water, groundwater or tributary streams may also affect flood levels. The flood mapping does not take local features into account. A Qualified Professional must be consulted for site-specific engineering analysis. Flooding from other sources, such as tsunamis or landslide generated waves, should be confirmed with appropriate maps and resources.
  - Industry best practices were followed to generate the flood maps. However, actual flood levels and extents may vary from those shown and Northwest Hydraulic Consultants Ltd. (NHC) does not assume any liability for such variations.

- Data Sources:**
- Provincial 200-year floodplain boundary from DataBC.
  - 2013 orthophoto supplied by City of Surrey.
  - Index base map from National Geographic and Esri.

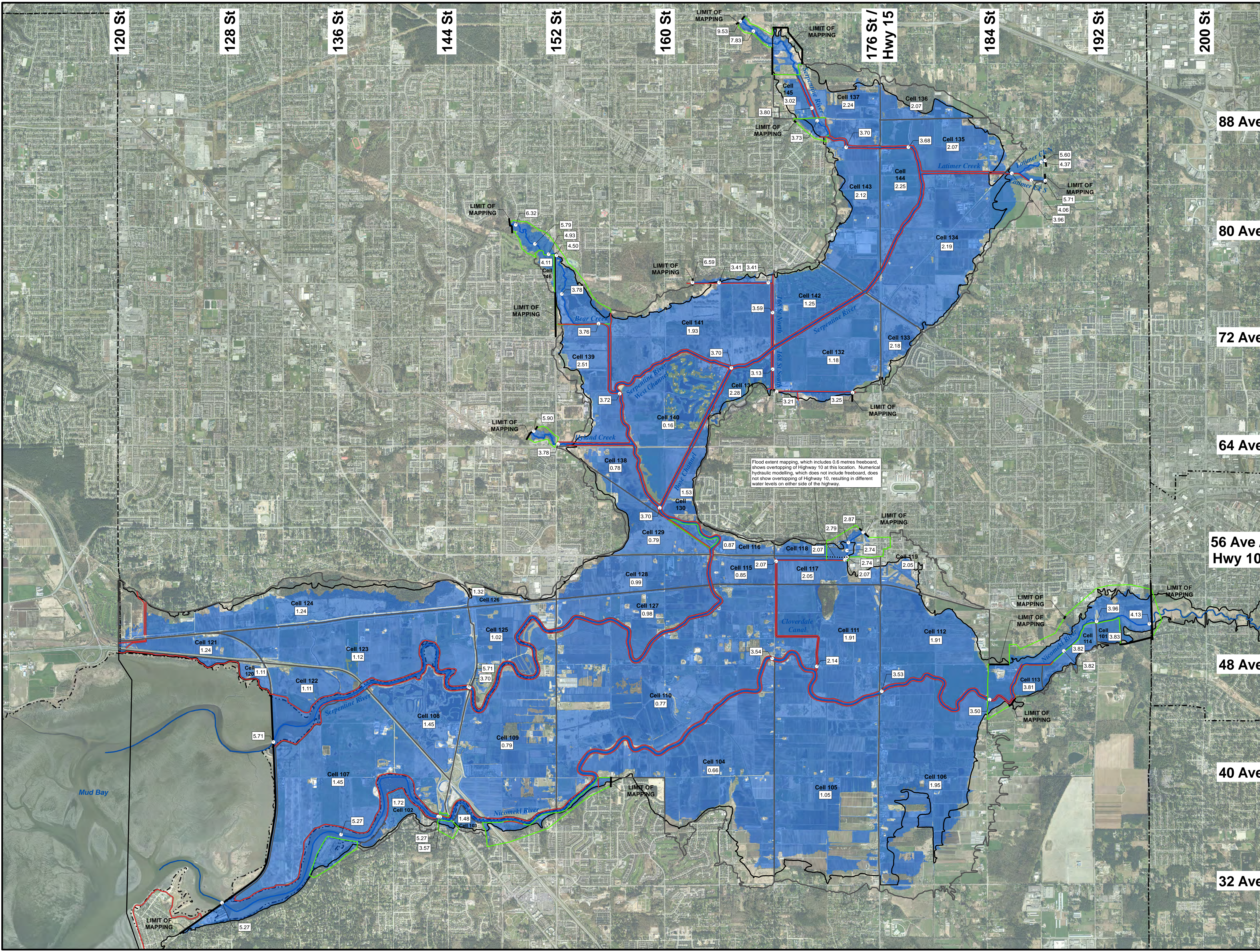
- References:**
- NHC (2014). Serpentine and Nicomekl Rivers Climate Change Floodplain Review Phase 2 (Final Report). Report prepared for the City of Surrey.
  - NHC (2012). Serpentine, Nicomekl and Campbell Rivers Climate Change Floodplain Review (Final Report). Report prepared for City of Surrey.
  - Ausenco-Sandwell (2011). Climate Change Adaptation Guidelines for Sea Dikes and Coastal Flood Hazard Land Use: Guidelines for Management of Coastal Flood Hazard Land Use. Prepared by Ausenco-Sandwell for BC Ministry of Environment.

**Disclaimer:**  
This document has been prepared by Northwest Hydraulic Consultants Ltd. in accordance with generally accepted engineering and geoscience practices and is intended for the exclusive use and benefit of the City of Surrey and their authorized representatives for specific application to the Climate Change Floodplain Review Phase II Project for the City of Surrey Serpentine River and Nicomekl River floodplains. The contents of this document are not to be relied upon or used, in whole or in part, by or for the benefit of others without specific written authorization from Northwest Hydraulic Consultants Ltd. No other warranty, expressed or implied, is made.  
Northwest Hydraulic Consultants Ltd. and its officers, directors, employees, and agents assume no responsibility for the reliance upon this document or any of its contents by any parties other than the City of Surrey.



Coordinate System: NAD 1983 UTM ZONE 10N	Date: 26-FEB-2015		
Units: METRES			
Engineer: VFOC	GIS: MSN	Reviewer: n/a	Job Number: 300319

**CLIMATE CHANGE FLOODPLAIN REVIEW PHASE 2  
SERPENTINE AND NICOMEKL RIVERS  
FLOOD EXTENTS INCLUDING FREEBOARD  
YEAR 2200 DESIGN LEVELS,  
SLR 1.97 M (RUN 9)**



Flood extent mapping, which includes 0.6 metres freeboard, shows overtopping of Highway 10 at this location. Numerical hydraulic modelling, which does not include freeboard, does not show overtopping of Highway 10, resulting in different water levels on either side of the highway.



## **APPENDIX A**

Background Information

300319 - City of Surrey Climate Change Floodplain Review Phase 2

List of GIS Data Produced for this Project and Delivered to City of Surrey

Last updated: MSN, 21-Jan-2015

Category	Title	Description	Key Attribute Description	Folder	File
Hydrology	Drainage areas	Drainage areas defined by NHC for Phase 2 hydrologic modelling. Based on CoS drainage areas, hydrography, topography, and floodplain storage cells. Polygon shapefile.	DA_Name = drainage area name; DA_Short = unique four letter code; Old_Short = four letter code from Phase 1 modelling; FP_Cell = corresponding floodplain storage cell; Inflow = location of inflow to 1D model.	GIS\Hydrology\	NHC_DrainageAreas8.shp
Subsidence	Approximate Subsidence Isolines	Isolines showing approximate rate of subsidence in mm/year. Digitized by NHC based on sketch by Thurber Engineering Limited. Polyline shapefile.	Rate = approximate subsidence rate (mm/year).	GIS\Subsidence\	SubsidenceRateCtrs1.shp
Flood Model Inputs	Water level gauges (COS)	City of Surrey hydrometric stations. Point shapefile.	DESC_ = description of station location.	GIS\HydrometricStns\	Streamflow_Stations.shp
Flood Model Inputs	Water level gauges (WSC)	Water Survey of Canada hydrometric stations. Point shapefile.	STATION_NO = WSC station ID; STATN_NAME = WSC station name.	GIS\HydrometricStns\	ENVCAN_HYD_sel1.shp
Flood Model Inputs	Stream network	Stream network as defined in the HEC-RAS 1D model. Polyline shapefile. Lines are calibrated with reach stationing; station values are embedded in the polyline m-values.	Riv_Rch = River and reach name from the Phase 2 HEC-RAS 1D model; RivRch_RAS, Riv_Rch2 = modified formats of Riv_Rch.	GIS\Modelling\Network\	Nwk_lines_chRAS6.shp
Flood Model Inputs	Cross sections	Cross section point locations from the HEC-RAS 1D model. Point shapefile.	Riv_Rch = River and reach name from the Phase 2 HEC-RAS 1D model; RivStn = station (chainage) location of the section on the reach; XSType = indicates whether the section is a surveyed ("measured") section, or interpolated in the model.	GIS\Modelling\CrossSections	XS_frRAS20140814_XSPts1.shp
Flood Model Inputs	Floodplain storage cells	Floodplain storage cells defined by NHC for Phase 2 hydraulic modelling. Based on CoS drainage areas, hydrography, and topography. Polygon shapefile.	NHCName2 = storage cell name for Phase 2 modelling; NHCNum2 = storage cell number; NHC_oldNo = storage cell number from Phase 1 modelling; NHCNameLng = descriptive name.	GIS\Modelling\StorageCells\	NHC_StorageCells6.shp
Flood Model Inputs	Lateral and point source inflow points	Lateral inflow and point source inflow locations. Point shapefile. (Layer file also included, with symbology defined.)	Type = Lateral Inflow or Point Source Inflow; Angle = direction of lateral inflow (for cartographic purposes); FlowTo = floodplain cell or stream reach that flow goes to; FlowFrom = drainage area that flow comes from.	GIS\Modelling\Inflow\	NHC_InflowPts3.shp, NHC_InflowPts3.lyr
Flood Model Inputs	Extended cross section areas	Areas modelled with extended cross sections. For cartographic purposes. Polygon shapefile.	Descrip = description of location	GIS\Modelling\CrossSections	ExtendedXSArea3.shp
Flood Model Inputs - Infrastructure	Sea dams	Sea dam locations. Based on CoS infrastructure data. Point shapefile.	Name = sea dam name.	GIS\Infrastructure\SeaDams\	SeaDamPts1.shp
Flood Model Inputs - Infrastructure	Pump stations	Pump station locations. Based on CoS drainage infrastructure data. Point shapefile.	Model = indicates whether PS is included in HEC-RAS model; Name = name of PS; StorCell = name of associated floodplain storage cell.	GIS\Infrastructure\PumpStations\	COS_DrainagePumpStation.shp

Category	Title	Description	Key Attribute Description	Folder	File
Flood Model Inputs - Infrastructure	Floodboxes	Floodbox locations. Based on information from: the MIKE11 model, CoS drainage infrastructure, CoS communications, and Stantec 2012. Point shapefile. Note: RAS is limited to 10 floodboxes per lateral structure. Some individual floodboxes have been combined into a single feature with multiple barrels in RAS to accomodate this limitation.	StorCell = name of associated floodplain storage cell; fbID = floodbox unique ID; FeatSource, AttrSource = source information for GIS feature and for attributes; Name = floodbox name; FBShape = shape, 1 = circular, 2 = box; Size = culvert size (m), for box culvert size is rise (height); Span = box culvert span (width) (m), value 0 for circular culvert; FBLength = culvert length (m); nTop, nBotm = Mannings' n value for top and bottom of floodbox; EntrLoss, ExitLoss = default values of 0.9 and 1.0, respectively; ChartNum, ScaleNum = default values of 2 and 3, respectively; USInv, DSInv = upstream and downstream invert elevation (m CVD28GVRD), upstream is on river side of dike; NumBarrels = number of identical barrels; InRAS = indicates whether feature is included in HEC-RAS model; RivRch_RAS = river and reach name; LS_ID = associated lateral structure ID; LSCh = lateral structure chainage; USSt, DSSt = stationing of floodbox along lateral structure. Note: Other attributes come from previous MIKE11 model data or from CoS data.	GIS\Infrastructure\Floodboxes\	NHC_FloodBoxes.shp
Flood Model Inputs - Infrastructure	Bridges	Bridge locations as represented in HEC-RAS model. Point shapefile.	InRAS = indicates if feature was included in HEC-RAS model; BridgeName = bridge name; Riv_Rch = river and reach name; RAS_Chain = chainage from RAS model; Wd_Strm = width (along stream) in m; US_LowChEl = low chord elevation (m) for upstream face; US_HiChEl = high chord elevation (m) for upstream face; US_Const = are values constant across upstream face?; US_WdAbut = opening width between abutments at upstream face; DS_LowChEl = low chord elevation (m) for downstream face; DS_HiChEl = high chord elevation (m) for downstream face; DS_Const = are values constant across downstream face?; DS_WdAbut = opening width between abutments at downstream face; Piers_Num = number of piers; Piers_Size = pier size, width or diameter (m); DataQuality = comment on quality of data entered in RAS; DatumAdj = vertical datum adjustment applied; ChangeNote = notes major changes between 2005, 2009 and build out (2010). Note: Other attributes come from previous MIKE11 model or CoS data.	GIS\Infrastructure\Bridges\	StreamCrossings_Bridges1.shp

Category	Title	Description	Key Attribute Description	Folder	File
Flood Model Inputs - Infrastructure	In-line culverts	In stream culvert locations as represented in HEC-RAS model. Point shapefile.	InRAS = indicates if feature is included in HEC-RAS model; CulvertNam = culvert name; Riv_Rch = river and reach name; RAS_Chain = chainage from RAS model; ChangeNote = notes major changes between 2005, 2009 and build out (2010); Comments = additional comments. Note: Other attributes come from previous MIKE11 model or CoS data.	GIS\Infrastructure\Bridges\	StreamCrossings_Culverts1.shp
Flood Model Inputs - Infrastructure	Floodplain culverts	Polyline shapefile. (Point shapefile developed for cartographic purposes only.)	FeatSource, AttrSource = source information for GIS feature and for attributes; Name = culvert name; Conection = name of floodplain cells connected by culvert; CulvShape = culvert shape, 1 = circular, 2 = box; Size = culvert size (m); for box culvert size is rise (height); Span = box culvert span (width) (m), value 0 for circular culvert; Length = culvert length (m); nTop, nBotm = Mannings' n value for top and bottom of culvert; EntrLoss, ExitLoss = default values of 0.9 and 1.0, respectively; ChartNum, ScaleNum = default values of 2 and 3, respectively; USInv, DSInv = upstream and downstream invert elevation (m CVD28GVRD), upstream is on left side of road; NumBarrels = number of identical barrels; RdLineName = ID from RoadProfileLn1; USSt, DSSt = station of culvert centreline along road; CulvID = unique ID; InRAS = indicates whether feature is included in HEC-RAS model. Note: Other attributes come from previous MIKE11 model or CoS data.	GIS\Infrastructure\Culverts\	Culverts1.shp, Culverts1_pts.shp

Category	Title	Description	Key Attribute Description	Folder	File
Flood Model Inputs - Infrastructure	Spillways	Spillway locations. Point shapefile.	<p>GIS_ID = point unique ID;</p> <p>Directn = direction of spill, clockwise angle in degrees referenced from North = 0;</p> <p>Locn = description of accuracy of location in GIS file;</p> <p>Reach = river and reach name;</p> <p>Y2011_ID = interim spillway ID, as of 2011-2013;</p> <p>Y2013_W = interim spillway width (m), approximate based on 2013 Lidar, value 0 indicates spillway not yet built in 2013 or already decommissioned;</p> <p>Y2013_Inv = interim spillway elevation (m, new MV datum) based on 2013 Lidar, value 0 indicates spillway not yet built in 2013;</p> <p>Ultim_ID = ultimate spillway ID;</p> <p>Ultim_W = ultimate spillway width (m), value 0 indicates spillway will be decommissioned;</p> <p>Ultim_Inv = ultimate spillway elevation (m, new MV datum);</p> <p>Status = description of spillway status;</p> <p>InRAS = indicates if spillway is included in HEC-RAS model;</p> <p>LS_ID = lateral structure ID;</p> <p>LS_Stn = station location of spillway along lateral structure.</p>	GIS\Infrastructure\Spillways	COS_Spillways5.shp
Flood Model Inputs - Infrastructure	Dikes	Dike locations. Based on CoS dike mapping. Polyline shapefile.	<p>NAME = name of dike;</p> <p>LOCATION = description of dike location.</p>	GIS\Infrastructure\Dikes	Dikes2.shp
Flood Model Inputs - Infrastructure	Lateral structures for model, calibrated with RAS lengths	<p>Lateral structures used in the HEC-RAS model. These are primarily dikes (with some modifications made from the City's original GIS file), with the addition of some unofficial dikes (e.g., embankments) and roads. Polyline shapefile. Lines are calibrated based on length as defined in the HEC-RAS model (which may be different from the GIS length); station values are embedded in the polyline m-values.</p> <p>Main areas where NHC added features not mapped by City: Cloverdale Canal, Upper Nicomekl (upstream portion), Nicomekl (near Riverside Golf Centre upstream of King George Blvd; downstream of Nico-Wynd Golf Course), Bear Creek, Latimer Creek South, Upper Serpentine (upstream portion). See also the "LSType" attribute.</p>	<p>LS_ID = lateral structure unique ID;</p> <p>Length = structure length based on GIS measurement (m);</p> <p>RivRch_RAS = river and reach name;</p> <p>LSCh = lateral structure chainage, based on model reach and cross section chainages;</p> <p>LSName = lateral structure name, incorporating spillway name if any;</p> <p>Pos = position, 0 for left overbank, 3 for right overbank;</p> <p>Cell = floodplain cell;</p> <p>DistUSXS = distance to upstream cross section;</p> <p>USXS = change of upstream cross section;</p> <p>DSXS = chainage of downstream cross section;</p> <p>Width = dike width perpendicular to flow;</p> <p>SpillwayID = spillway ID number;</p> <p>LenCalib = structure length based on model cross sections (m);</p> <p>InRAS = indicates whether feature was included in HEC-RAS model;</p> <p>LSType = description of lateral structure type;</p> <p>Raise = indicates if lateral structure will be raised to new design elevation or not (e.g., for a road or unofficial dike).</p>	GIS\Infrastructure\Dikes	LatStructures1.shp
Flood Model Inputs - Infrastructure	Extra lateral structure features	Lateral structures not included in the HEC-RAS model. These are typically proposed dikes. Polyline shapefile.	<p>RivRch_RAS = river and reach name;</p> <p>Comment = description of proposed structure.</p>	GIS\Infrastructure\Dikes	LatStructuresExtra1.shp

Category	Title	Description	Key Attribute Description	Folder	File
Flood Model Inputs - Infrastructure	Dike (Lateral structure) design elevation calibration points	Points used to calibrate lateral structures with design elevations. Includes data source information. Point shapefile. Note: For 168 St North Canal, design elevations upstream of chainage 1105 are estimated, as values were not available from other sources.	LS_ID = lateral structure ID; RivReach = river and reach name; RASChngs = reach station location of point; F15yWPkWL = 15 year flood design elevation from KWL data; F200yWPkWL = 200 year flood design elevation from KWL data; DikeDsnLvl = dike design elevation; Source = description of data source.	GIS\Infrastructure\Dikes\	LatStructures1_DesignElevPts1.shp
Flood Model Inputs - Infrastructure	Lateral structures for model, calibrated with design elevations.	Lateral structure lines (LatStructures1.shp) calibrated with dike design elevations (LatStructures1_DesignElevPts1.shp); design elevations are embedded in the polyline m-values. Polyline shapefile.	LS_ID = lateral structure ID.	GIS\Infrastructure\Dikes\	LatStructures1_DesignElevLns1.shp
Flood Model Inputs - Infrastructure	Dike (Lateral structure) points	Points used to represent lateral structures and spillways in the model. Separate files for spillway points and for other points on each lateral structure. Eight points per lateral structure. Point shapefiles.	LS_RIS = lateral structure ID; STN = station position of point along lateral structure; ElevCbrn/CBRNEL = elevation for model calibration runs; ElevDsgn/DSGNEL = elevation for model design runs; ElevBrch/BRCHEL = elevation for model breach runs.	GIS\Infrastructure\Dikes\	LS_GeneralPts2.shp, LS_SpillwayPts2.shp
Flood Model Inputs - Infrastructure	Road profile lines	Road profile lines used as storage cell connections in 1D hydraulic model. Profile elevations typically based on 2013 Lidar DEM. Polyline shapefile.	FPCell_L = floodplain cell to left of line; FPCell_R = floodplain cell to right of line; LineName = unique name for each line, based on FPCell_L and FPCell_R.	GIS\Infrastructure\Dikes\	RoadProfileLn1.shp
Flood Mapping Results	Floodplain cell water surface elevations - including freeboard	Water surface elevation values from the 1D hydraulic model results (plus 0.6 metres freeboard). A single point value within each floodplain cell. Point shapefile.	NHCName2 = storage cell name for Phase 2 modelling (see also field descriptions for "Floodplain storage cells"); WSE_R? = water surface elevation (m) based on the 1D model run specified; WSEfb_R? = water surface elevation (m) based on the 1D model run specified, including freeboard.	GIS\Modelling\RASResults\	FPCellCentroids2.shp
Flood Mapping Results	In-river water surface elevations - including freeboard	Water surface elevation values from the 1D hydraulic model results (plus 0.6 metres freeboard). Point values along the river channel. Point shapefile and dBase table (join RivRch from table to RivRch_Stn from shapefile).	RivRch_Stn = river reach and station location of each point; Duplicate = "original" for point based directly on RAS results, "duplicate" for extra point created to ensure results map properly; ShowOnMap = points to show on flood extent maps; WSE_R? = water surface elevation (m) based on the 1D model run specified; WSEfb_R? = water surface elevation (m) based on the 1D model run specified, including freeboard.	GIS\Modelling\RASResults\	RivNwkKeyPts4.shp, ReachPtWLS_20141124 Final
Flood Mapping Results	Flood extent polygons - including freeboard	Flood extent polygons mapped based on 1D hydraulic model results (plus 0.6 metres freeboard) and the 2013 Lidar DEM. 1D model results for floodplain cells and the river channel have been combined to create a single flood extent layer. One shapefile per modelling run. Polygon shapefiles.	Area = area in square metres; Descrip = model run description.	GIS\FloodMapping\FloodExtents\	floodpoly_R?.shp
Flood Mapping Results	Mapping limits	Spatial limits of flood extent 1D modelling and mapping. Polyline shapefile.	Descrip = brief description of extent.	GIS\FloodMapping\	MappingLimits1.shp
Flood Mapping Results - Vulnerable Infrastructure	Road vulnerabilities	Points mapped at 100 metre intervals along key roads, attributed with road elevation from 2013 Lidar and classified, for each 1D model run, according to whether the flood water overtops the feature. Classification is: "wet" if the the flood water level (WL) is greater than the road elevation plus 0.6 m freeboard; "freeboard compromised" if the WL is up to 0.6 m greater than the road elevation; "dry" if the WL is less than the road elevation. Point shapefile.	ROAD_NAME = road name from CoS dataset; LidarZ = point elevation (m) based on 2013 Lidar DEM; WL_R? = water level (m) based on the 1D model run specified, including freeboard; Vuln_R? = vulnerability classification, based on comparison of LidarZ to WL_R?.	GIS\FloodMapping\VulnerableInfrastructure\	Roads_Pts100m1.shp

Category	Title	Description	Key Attribute Description	Folder	File
Flood Mapping Results - Vulnerable Infrastructure	Railway vulnerabilities	Points mapped at 100 metre intervals along key rail lines, attributed with with rail elevation from 2013 Lidar and classified, for each 1D model run, according to whether the flood water overtops the feature. Classification is: "wet" if the the flood water level (WL) is greater than the rail elevation plus 0.6 m freeboard; "freeboard compromised" if the WL is up to 0.6 m greater than the rail elevation; "dry" if the WL is less than the rail elevation. Point shapefile.	LidarZ = point elevation (m) based on 2013 Lidar DEM; WL_R? = water level (m) based on the 1D model run specified, including freeboard; Vuln_R? = vulnerability classification, based on comparison of LidarZ to WL_R?.	GIS\FloodMapping\VulnerableInfrastructure\	Rail_Pts100m1.shp
Flood Mapping Results - Vulnerable Infrastructure	Sea dam vulnerabilities	Points mapped at locations of sea dams, attributed with sea dam elevation from 2013 full feature Lidar and classified, for each 1D model run, according to whether the flood water overtops the feature. Classification is: "wet" if the the flood water level (WL) is greater than the road elevation plus 0.6 m freeboard; "freeboard compromised" if the WL is up to 0.6 m greater than the road elevation; "dry" if the WL is less than the road elevation. Point shapefile.	DeckEI = point elevation (m) based on 2013 Lidar DEM; WL_R? = water level (m) based on the 1D model run specified, including freeboard; Vuln_R? = vulnerability classification, based on comparison of DeckEI to WL_R?.	GIS\FloodMapping\VulnerableInfrastructure\	SeaDams_VulnPts1.shp
Flood Mapping Results - Vulnerable Infrastructure	Bridge vulnerabilities	Points mapped at bridge locations, attributed with minimum high chord elevation and minimum low chord elevation. Points are classified, for each 1D model run, according to whether the flood water overtops the feature. Classification is: "wet" if the the flood water level (WL) is greater than the bridge chord elevation plus 0.6 m freeboard; "freeboard compromised" if the WL is up to 0.6 m greater than the bridge chord elevation; "dry" if the WL is less than the bridge chord elevation. Point shapefile.	BridgeName = bridge name from bridges data layer; BridgeID = bridge ID number from bridges data layer; LowChEImin = minimum low chord elevation (m); HiChEImin = minimum high chro elevation (m); WL_R? = water level (m) based on the 1D model run specified, including freeboard; VulnHi_R? = vulnerability classification for the bridge high chord, based on comparison of HiChEImin to WL_R?; VulnLo_R? = vulnerability classification for the bridge low chord, based on comparison of LowChEImin to WL_R?.	GIS\FloodMapping\VulnerableInfrastructure\	StreamCrossings_Bridges1_Pts1.shp
Flood Mapping Results - Vulnerable Infrastructure	Dike vulnerabilities	Points mapped at 100 metre intervals along dikes, attributed with dike design elevations. Points are classified, for each 1D model run, according to whether the flood water overtops the feature. Classification is: "wet" if the the flood water level (WL) is greater than the design elevation plus 0.6 m freeboard; "freeboard compromised, WL within 0.1 m of top of dike"; "freeboard compromised, WL within 0.3 m of top of dike"; "freeboard compromised, WL within 0.6 m of top of dike"; "dry" if the WL is less than the design elevation. Point shapefile.	LS_ID = lateral structure ID from the lateral structures data layer; DsgnElev = dike design elevation (m); WL_R? = water level (m) based on the 1D model run specified, including freeboard; Vuln_R? = vulnerability classification, based on comparison of DsgnElev to WL_R?.	GIS\FloodMapping\VulnerableInfrastructure\	LatStructures1_Pts100m1.shp
Base Mapping	Surrey Lake	Surrey Lake digitized based on CoS as-constructed drawings. Polygon shapefile.	n.a.	GIS\Hydrography\	SurreyLake.shp
Base Mapping	Municipal boundaries	Metro Vancouver municipal boundaries. Polygon shapefile.	n.a.	GIS\AdminBnds\	gvrd.shp
Base Mapping	Provincial floodplain boundary	Provincial 200-year floodplain boundary. Data downloaded from DataBC. See DataBC metadata file (CWBFP_SVW_metadata.html) for details. Polygon shapefile.	FP_NAME = floodplain name	GIS\HistoricFP\	CWBFP_SVW_SerpentineNicomekl.shp
Cartography	Hydraulic model inputs map	ArcGIS Map Document for the Hydraulic Model Overview map. One map sheet at 1:25,000 scale. ArcGIS 10.0 MXD file. Note: This MXD references several hydrography and transportation base layers, which are not included in the NHC GIS data deliverables.	n.a.	GIS\	300319_Map_HydraulicModelArea2_Arc10_0.mxd
Cartography	Flood extent maps	ArcGIS Map Document for production of the flood extent maps. One map sheet at 1:25,000 scale, Runs 1, 5, 7 and 9. See notes in Layout View for detailed map production instructions. ArcGIS 10.0 MXD file. Note: This MXD references CoS 2013 orthoimagery, which is not included in the NHC GIS data deliverables.	n.a.	GIS\	300319_Map_FloodExtents_Arc10_0.mxd

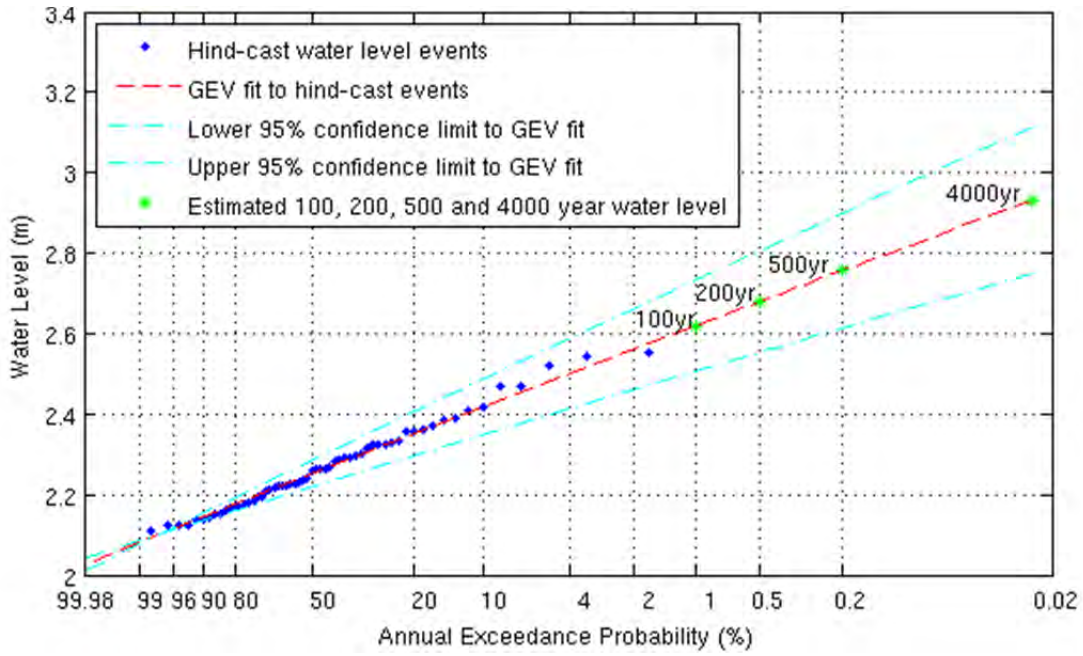
Category	Title	Description	Key Attribute Description	Folder	File
Cartography	Vulnerable infrastructure	Map legends developed for the vulnerable infrastructure figures. ArcGIS version 10.0 Layer File.	n.a.	GIS\FloodMapping\VulnerableInfrastructure\	Vulnerability Assessment Results_Arc10_0.lyr
Cartography	Cartographic dummy features	Features created for cartographic purposes only. Polygon, polyline shapefiles.	n.a.	GIS\Carto\	dummyPolygon.shp, dummyLine.shp



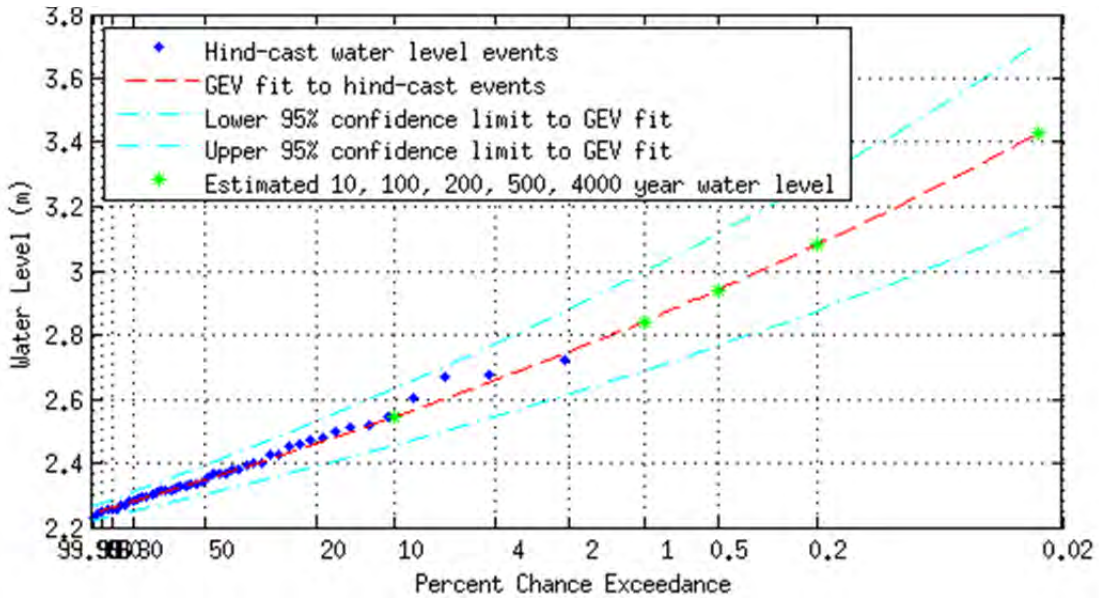
## **APPENDIX B**

Ocean Analysis

GEV Distribution Plot – Nicomekl River



GEV Distribution Plot – Serpentine River



**APPENDIX C**

Hydrologic Analysis

# Two 21<sup>st</sup> Century scenarios of hourly precipitation for the City of Surrey, B.C.

---

## Table of Contents

Summary .....	3
1. Analysis of PCIC’s twelve downscaled GCM projections .....	3
1.1 Uncertainty associated with the GCM projections .....	4
1.2 Interpreting the differences between the historical period and future periods in the downscaled GCM grid cell data.....	7
2. Selecting two GCMs for this project .....	24
2.1 Selection of the “severe scenario” GCM.....	24
2.2 Selection of the “moderately high scenario” GCM.....	24
2.3 Summary of the two scenarios selected.....	26
3. Creating 21 <sup>st</sup> Century hourly precipitation time series.....	27
3.1 Methodology description.....	27
3.2 Step 1: Remove wet days from the observed precipitation time series.....	28
3.3 Step 2: Modify each day’s precipitation total (and scale the hourly values accordingly) .....	30
Detailed description of Step 2.....	35
Case Example .....	36
3.4 Return periods of daily precipitation in the future scenarios.....	37
Case Example .....	39
4. Evaluation of the GCM-based scenarios and choice of final scenarios .....	40
5. References .....	42

## Summary

This appendix describes the development of two synthetic series of hourly precipitation, covering the 21<sup>st</sup> Century, for the City of Surrey, British Columbia. These time series will be used as input to the HSPF hydrologic model that simulates runoff for use in analysis of flooding and inundation conditions in the Serpentine and Nicomekl watersheds. Each time series should be consistent, in a statistical sense, with the projections of a particular global climate model (GCM) run selected from the most recent runs that served as the basis for the recent IPCC Fifth Assessment Report, i.e., the CMIP5 climate projections.

We use GCM precipitation projections downscaled by the Pacific Climate Impacts Consortium (PCIC). Data from twelve GCMs are available from PCIC, and our first step is to analyze their downscaled results (section 1). The second step of our work (section 2) consists in selecting two appropriate GCM runs. It is desired to identify which GCM runs represent, in the context of all PCIC projections, a “severe scenario” and a “moderately high scenario” in terms of flooding risk. The third step (section 3) consists in altering the observed historical time series of hourly precipitation at the Surrey Municipal Hall gauge, so as to create two new hourly time series, representative of projected precipitation regimes toward the end of the 21<sup>st</sup> Century, one of which is statistically consistent with the “moderately high” GCM run, and the other representing a “very high scenario” situated between the “moderately high” and “severe” GCM runs.

### 1. Analysis of PCIC’s twelve downscaled GCM projections

In this project, we use GCM projections downscaled by the Pacific Climate Impacts Consortium and downloaded from their data portal. We have not evaluated the quality of these data (other than the basic comparison shown in Figure 1), as this is outside the scope of this project.

Here we describe our reasoning and methodology for selection of two GCM runs for this project. The representative pathway of greenhouse gas concentrations known as RCP8.5<sup>1</sup> was chosen first, representing not an optimistic view of future emissions, but which is provoked by the consistent failure thus far in significantly curtailing global greenhouse gas emissions. We felt that a scenario with a lower future greenhouse gas concentration, such as RCP 4.5, might be overly optimistic with regards to future success in limiting emissions.

For RCP8.5 (as well as for RCP4.5 and RCP2.6), the Pacific Climate Impacts Consortium (PCIC) has used the BCCAQ (Bias Correction/Constructed Analog Quantile Mapping) methodology of statistical downscaling to produce daily values of precipitation for the 21<sup>st</sup> Century at a spatial resolution of 1/12 of a degree of latitude and longitude (5 arc-minutes), i.e., for grid cells of roughly 50 km<sup>2</sup> in area. PCIC has also used the BCSD (Bias Correction/Statistical Downscaling) methodology of statistical downscaling, however PCIC has recommended the BCCAQ methodology for studies focused on climatic extremes, as BCCAQ is considered more reliable for downscaling of extreme values. The reader is referred to the

---

<sup>1</sup> RCP 8.5 (Representative Concentration Pathway with radiative forcing of 8.5 watts/m<sup>2</sup>) represents the greatest future greenhouse gas concentration among the RCP scenarios available.

documentation provided in the PCIC internet site<sup>2</sup> for further information and references on these techniques.

Surrey Municipal Hall's geographical co-ordinates were estimated using GoogleEarth, as {49.104°N, -122.828°E}. The data was downloaded for the grid cell centered at latitude 49.20833°N and longitude -122.7917°E, within which the precipitation gauge of Surrey Municipal Hall is located. We downloaded (on 6/13/2014) and analyzed the downscaled daily precipitation data for this grid cell for all 12 GCMs available on the PCIC data portal<sup>3</sup> for BCCAQ-CMIP5-RCP8.5.

## 1.1 Uncertainty associated with the GCM projections

While there is a need to provide quantitative information for water resources planning and flood risk management planning, the underlying projections of climate change are subject to large and unquantifiable uncertainty. The main sources of uncertainty are unknown future emissions of greenhouse gases, uncertain response of the global climate system to increases in greenhouse gas concentrations, and incomplete understanding of regional manifestations that will result from global changes (e.g., Hawkins and Sutton 2010). Additionally, precipitation processes are very complex and difficult to simulate accurately in models.

The downscaling, in space and time, of GCM-projected climate variables, and the extrapolation of frequency analyses to extreme return periods, represent additional sources of uncertainty. The precipitation projections developed in this work should therefore be considered to be plausible representations of the future, given the best current scientific information, and do not represent specific predictions. The actual future realizations of precipitation at Surrey will differ from any of these scenarios, and their difference compared to historical precipitation may be greater or smaller than the differences projected in this work. To gain a wider perspective on issues related to uncertainty associated with extreme streamflow projections, the reader is referred to the analysis by Kundewicz et al. (2013) which is based on a vast body of literature, including the IPCC SREX report (IPCC, 2012) on climate extremes. The analysis by Kundewicz et al. (2013) concludes that *"...presently we have only low confidence in numerical projections of changes in flood magnitude or frequency resulting from climate change"*.

With respect to the downscaled GCM-simulated precipitation values used here, the issue of spatial scale is important to consider. The downscaled simulations of the GCMs are grid cell values, not point values. The precipitation gauge values may be conceptualized as point values. Grid cells are defined by geographical coordinates, which in the present case have a spacing of 5 arc minutes (1/12°) along parallels (longitude) and meridians (latitude). At the latitude of Surrey, grid cells have a surface area of roughly 50 km<sup>2</sup>. The process of BCCAQ downscaling<sup>4</sup> of GCM hindcasts (i.e., the GCM simulations for the historical period for which gauge records are available) improves the agreement between the grid cell values and gauge records, as it uses quantile mapping to bring the simulated distribution into agreement

---

<sup>2</sup> <http://www.pacificclimate.org/data/statistically-downscaled-climate-scenarios>

<sup>3</sup> [http://tools.pacificclimate.org/dataportal/downscaled\\_gcms/map/](http://tools.pacificclimate.org/dataportal/downscaled_gcms/map/)

<sup>4</sup> See <http://www.pacificclimate.org/data/statistically-downscaled-climate-scenarios>

with the statistical distribution derived from nearby gauge observations. Nevertheless, we should not expect to find too close an agreement between the downscaled GCM hindcasts and any particular gauge of interest.

In the present case, the Municipal Hall's daily precipitation values were obtained by adding the original hourly record from midnight to the subsequent midnight, and the smallest non-zero daily value is 0.1 mm/day. In the case of the downscaled GCM data, the smallest non-zero daily value downloaded is 0.03125 mm/day. This very small value inflates the number of GCM wet days and results in low values of mean daily precipitation intensity, but this is inconsequential to this project because, as we will see later, we will be comparing like to like, i.e., future versus historical GCM run results.

The comparison shown in Figure 1 is interpreted in light of the above considerations. Mean annual precipitation (which can be considered in Figure 1 as the product of mean daily precipitation intensity and number of wet days per year) over the grid cell of interest (1,380 mm/year, in the average of the 12 downscaled GCM runs for the historical period 1950-2009) is 9% higher than the corresponding value for the Municipal Hall gauge (1,265 mm/year for water years 1963-2009). The 9% difference is considered small and is not a reason for concern in this study.

Figure 2 shows the observed and GCM-simulated (for the MPI-ESM-LR GCM) historical distributions of daily precipitation, showing good overall agreement. The upper portions of these distributions, not discernible from Figure 2, will be the focus of a later section of this document.



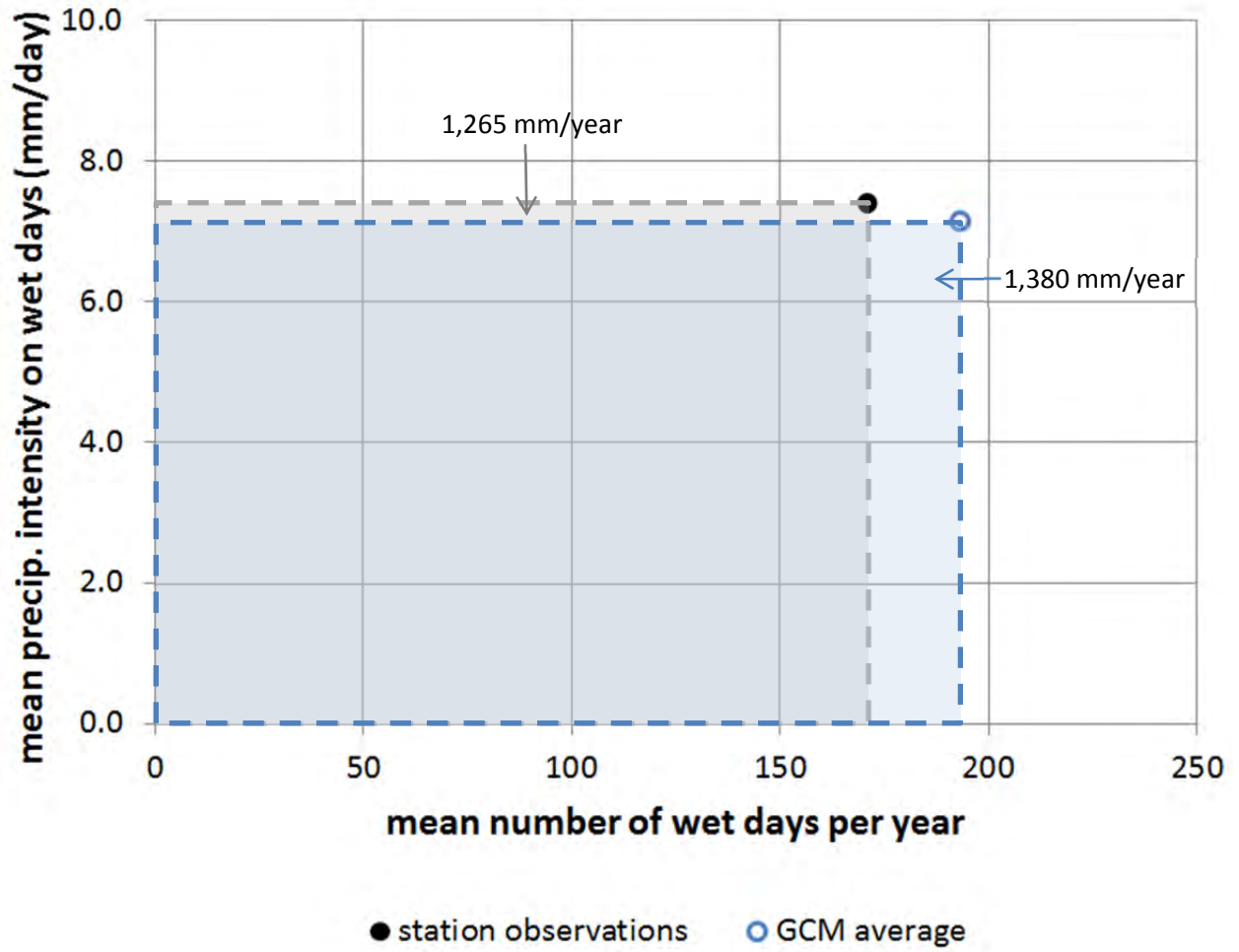


Figure 1. Comparison of two statistics between the downscaled GCM historical runs (hindcasts) and the precipitation gauge records at Surrey Municipal Hall.

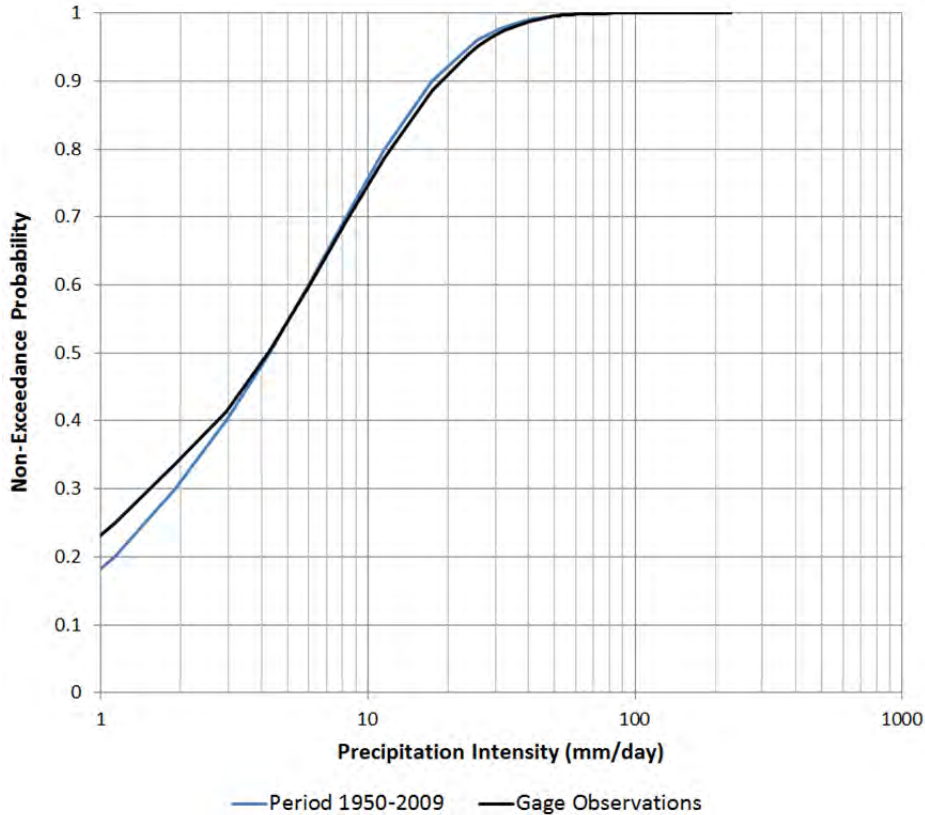


Figure 2. Distributions of the observed time series (WY 1963-2009) and historical simulated (MPI-ESM-LR) (1950-2009) of daily precipitation. Empirical plotting positions are used, except for the upper end (rare events), where a fitted extreme-value distribution is used, as described in a later section of this document.

## 1.2 Interpreting the differences between the historical period and future periods in the downscaled GCM grid cell data

We now look at the evolution over time, throughout the 21<sup>st</sup> Century, of the downscaled GCM simulations. This evolution is depicted in Figure 3 for all 12 GMC runs (divided into groups of 3, to make each figure panel less busy). Take for example the blue line in the first panel (top left) of Figure 3. That blue line represents the results from the ACCESS1-0 model run. The line starts on the right, at the open blue circle, which represents the average values simulated by this GCM in the historical period (1950-2009), after downscaling. These values are an average of 193 wet days per year with average precipitation intensity of 7.4 mm/day. The blue line then advances to the closed blue circle, which represents the period 2010-2039; then to the blue square, which represents the period 2040-2069; and at last to the blue triangle, which represents the period 2070-2100. In this end-of-century period, the average number of wet days per year is 173 (i.e., 20 fewer wet days per year than the historical average, a decline by 10.4%) and the mean precipitation intensity on wet days is 8.9 mm/day (an increase of about 20% relative to the historical average).

All GCMs indicate a future increase in mean precipitation intensity, obtained by dividing total precipitation by the number of wet days (in Figure 3). Most GCMs indicate a future decline in the mean annual number of wet days. The increase in intensity wins over the decline in wet days, and all GCMs but one indicate a future increase in mean annual precipitation (Figure 4). The exception is CCSM4 which obtained a lower value for the period 2010-2039. Three GCMs (MIROC5, GFDL-ESM2G and MPI-ESM-LR) have the largest increases in mean annual precipitation in all future time horizons, reaching 17%-18% at end of century (2070-2100) compared to historical (1950-2009).

For each GCM, we compare the statistical distribution of its downscaled historical simulations against its downscaled future simulations. This comparison is made through quantile-to-quantile plots (Figure 5 through Figure 16), where the precipitation quantiles are computed using the rank of each value (*rank*), the number of wet days (*n*) and the simple formula for empirical non-exceedance probability ( $p_c$ ),  $p_c = \frac{rank}{(n+1)} \cdot 100\%$ . The maximum of all downscaled daily values is also compared in these figures (red dots). All quantile-to-quantile plots are approximately linear, and the coefficient obtained by linear regression is shown in each figure panel (Figure 5 through Figure 16). These linear coefficients are summarized in Figure 17. The highest values of the linear coefficients for the end of century period (2070-2100) are reached by MPI-ESM-LR (1.2357, indicating an increase by over 23%), CSIRO-Mk3-6-0 (1.2303), and HadGEM2-CC (1.2260). Because of the projected decline in the mean number of wet days, the projected increases in mean annual precipitation are below 20%, as we already saw in Figure 4.

Similar to Figure 17, we plot in Figure 18 the linear coefficients of the quantile-to-quantile relationships of the three-day precipitation distributions. The differences between Figure 17 and Figure 18 are modest and, for most GCMs the linear coefficients for the 3-day precipitation quantiles are a little lower than those for the 1-day precipitation, which is generally consistent with the projected future decline in the mean number of wet days. In the case of INMCM4, however, the coefficients in Figure 18 are higher than in Figure 17, for all future time periods, possibly indicating a future increased tendency for clustering of similarly-valued precipitation days. This possibility is not explored further here, because INMCM4 is not one of the two GCMs that we select for this study in the next section. Although an increase in future clustering of high precipitation days will in general increase flooding risk, nevertheless INMCM4 hardly qualifies as a severe scenario when compared with other GCMs which project stronger increases in 3-day precipitation as well as 1-day precipitation.

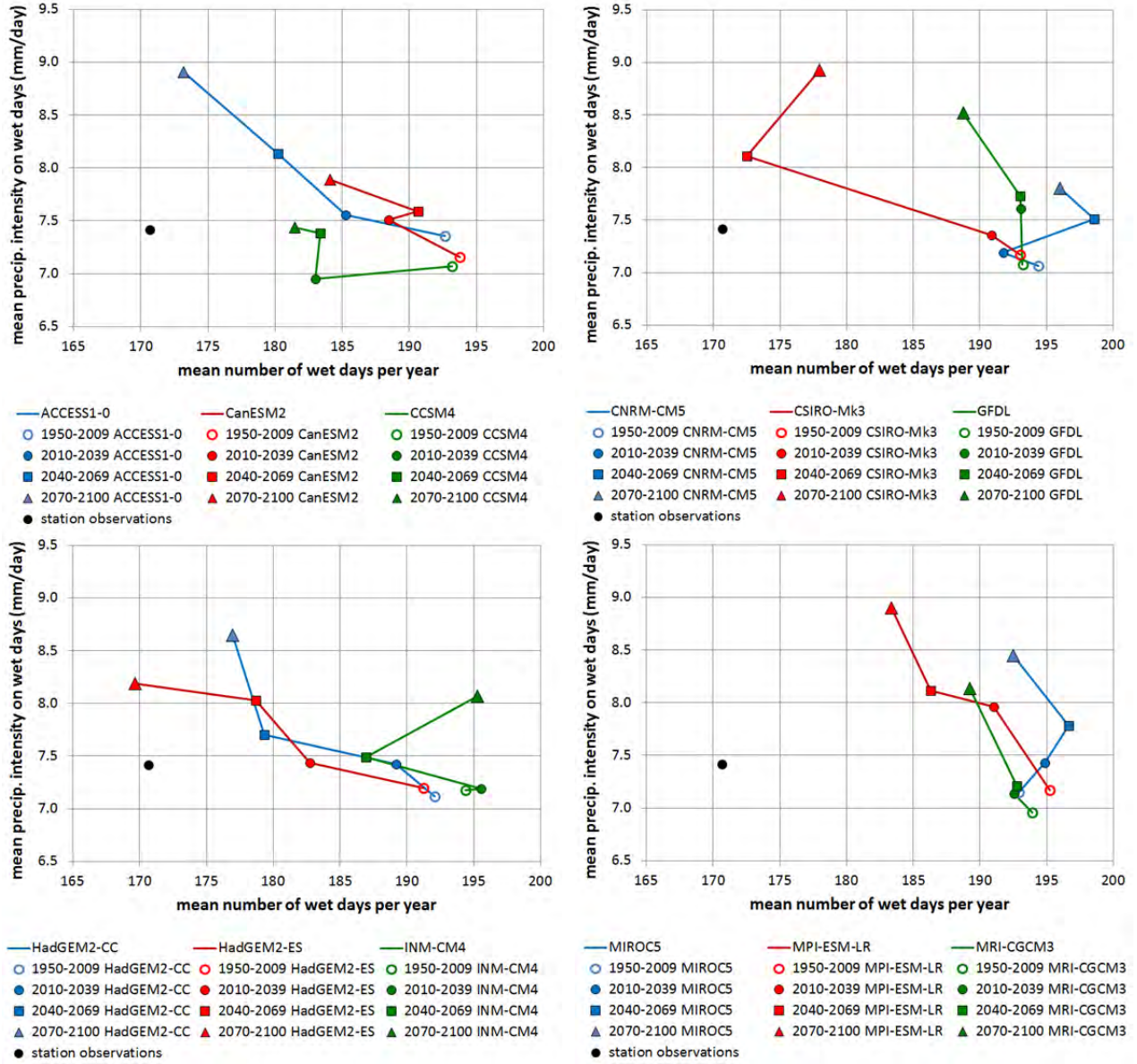


Figure 3. Trajectory over time of the future simulated mean number of wet days per year, and mean precipitation intensity on those days, for the 12 GCM runs analyzed. All GCM runs are for RCP8.5. Each figure panel displays 3 GCM runs, as labeled. The axes do not have their origin at zero; instead they cover a restricted range of values.

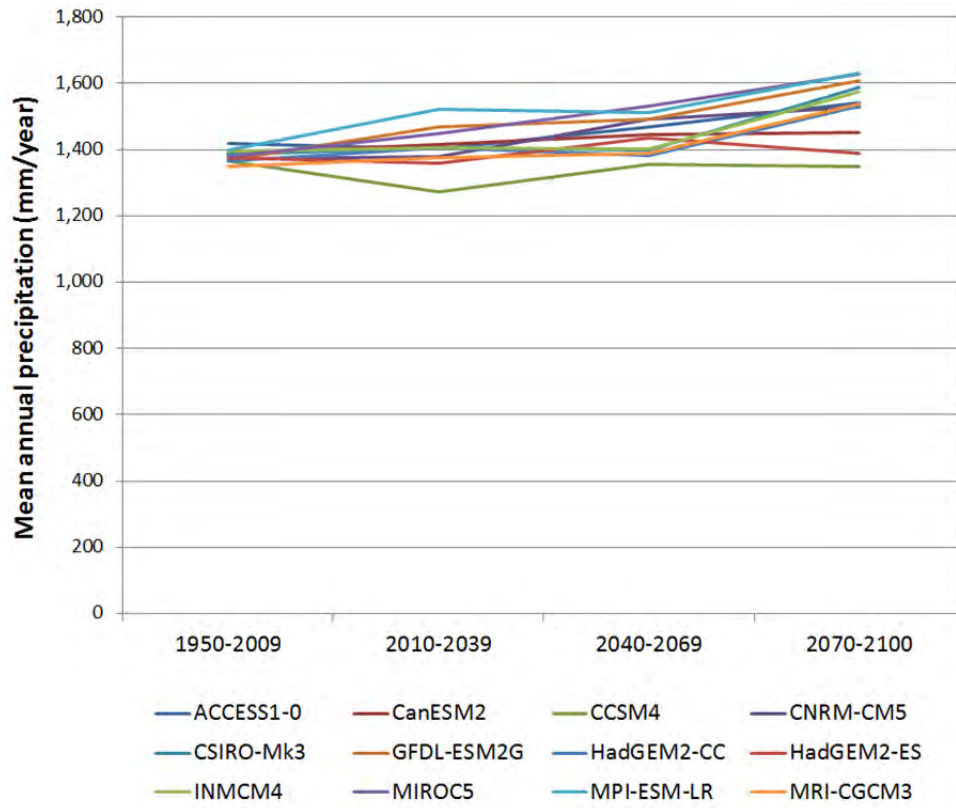


Figure 4. Projected mean annual precipitation for each GCM run. The average for multi-year periods is displayed.

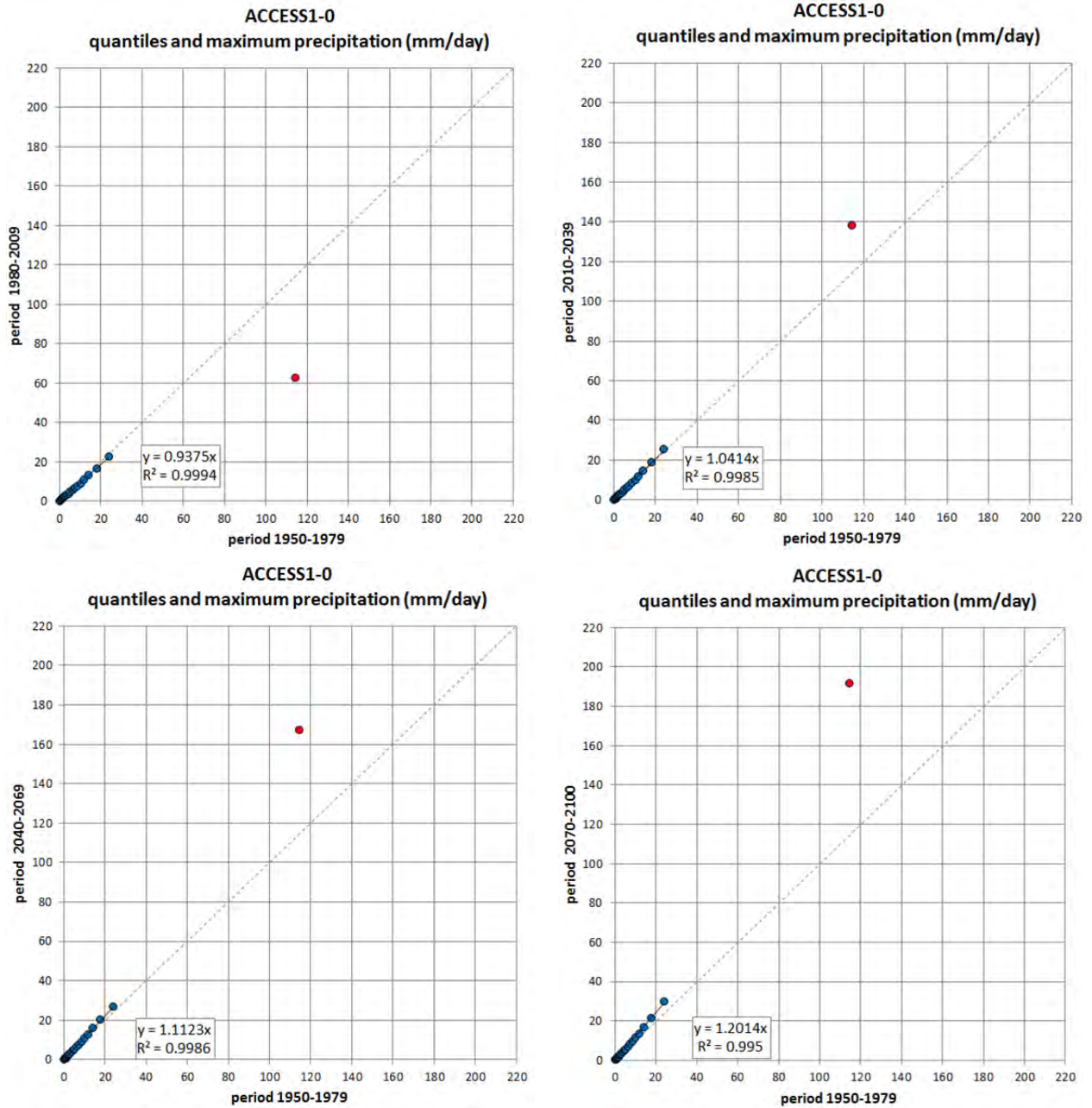


Figure 5. For ACCESS1-0, quantile-to-quantile plots for the 5<sup>th</sup>, 10<sup>th</sup>, 15<sup>th</sup>, ..., and 95<sup>th</sup> quantiles, for which the linear regression line is shown. The maximum value is also shown, in red. On each figure panel, a period of 30 years is compared against the first 30 years of simulation (1950-1979). The identity (1:1) line is dashed.

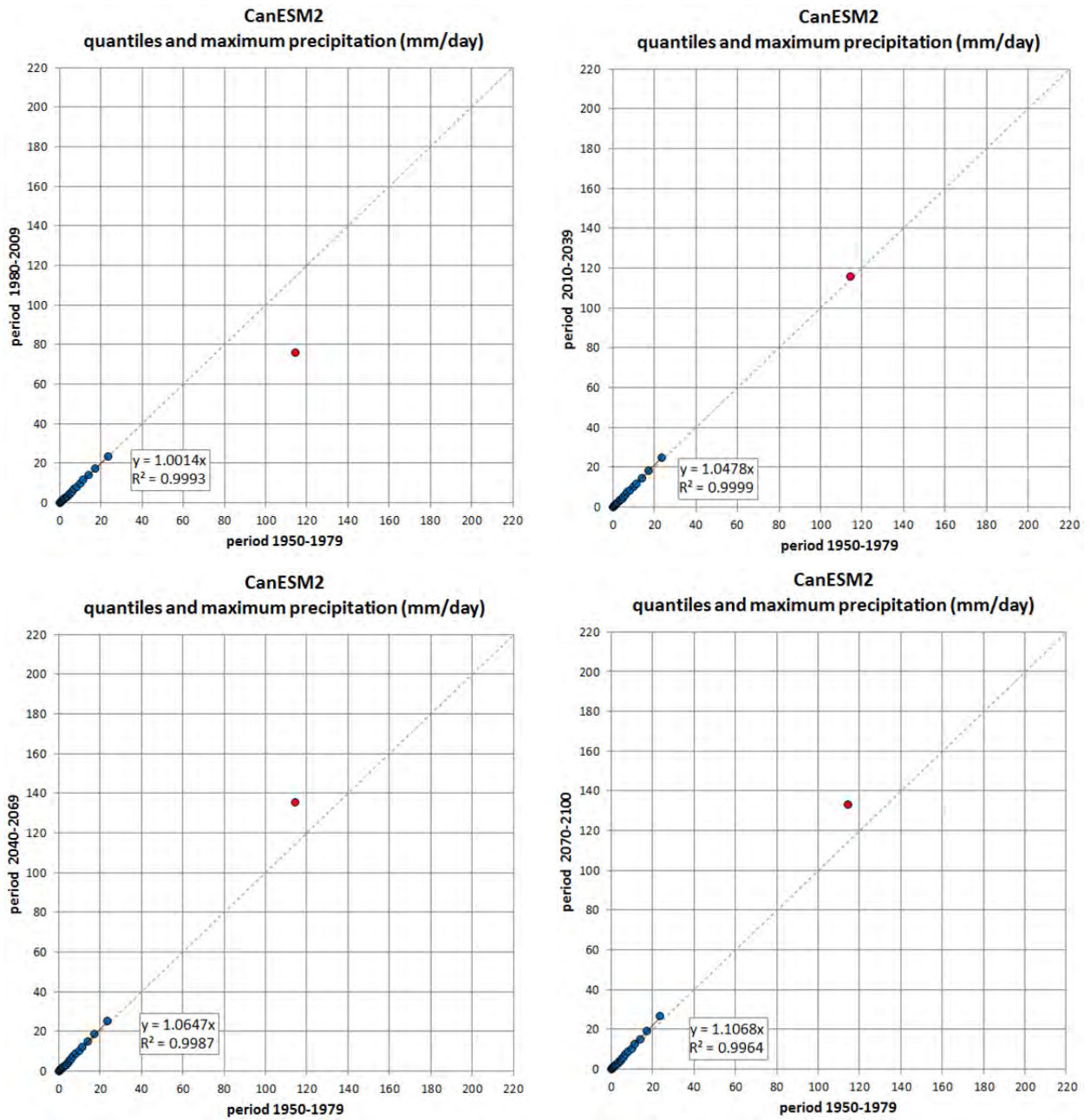


Figure 6. For CanESM2, quantile-to-quantile plots for the 5<sup>th</sup>, 10<sup>th</sup>, 15<sup>th</sup>, ..., and 95<sup>th</sup> quantiles, for which the linear regression line is shown. The maximum value is also shown, in red. The identity (1:1) line is dashed.

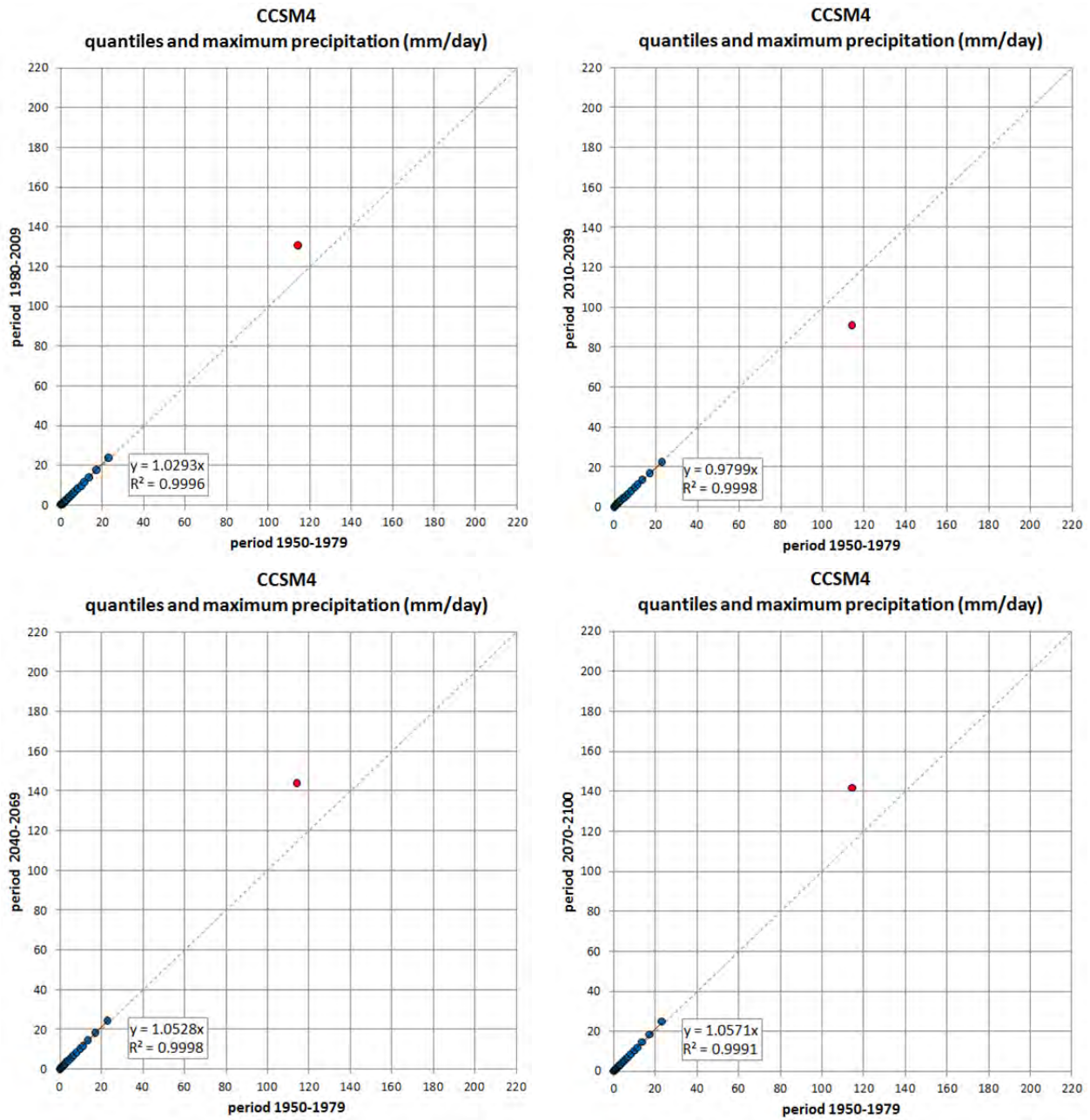


Figure 7. For CCSM4, quantile-to-quantile plots for the 5<sup>th</sup>, 10<sup>th</sup>, 15<sup>th</sup>, ..., and 95<sup>th</sup> quantiles, for which the linear regression line is shown. The maximum value is also shown, in red. The identity (1:1) line is dashed.



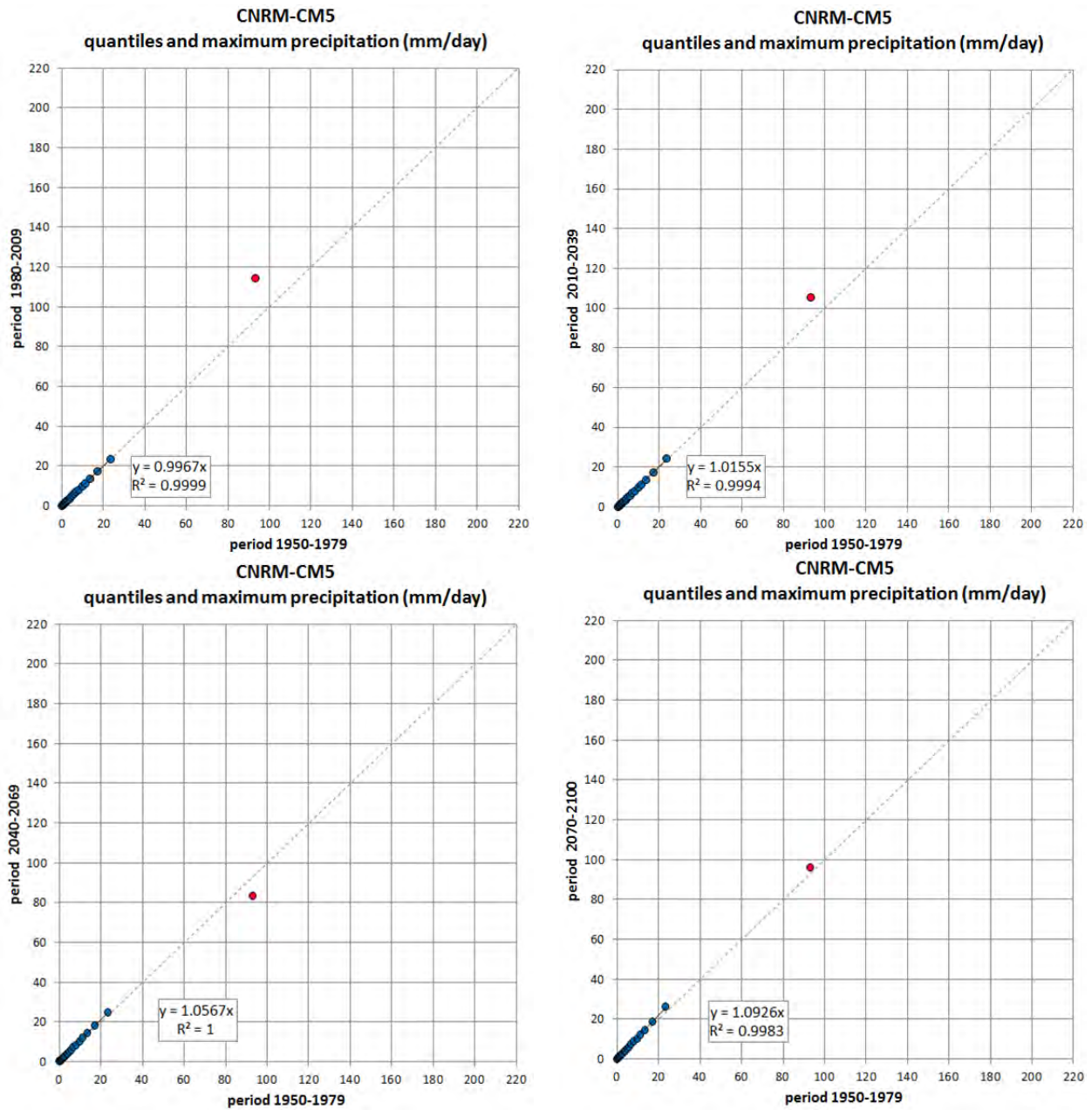


Figure 8. For CNRM-CM5, quantile-to-quantile plots for the 5<sup>th</sup>, 10<sup>th</sup>, 15<sup>th</sup>, ..., and 95<sup>th</sup> quantiles, for which the linear regression line is shown. The maximum value is also shown, in red. The identity (1:1) line is dashed.

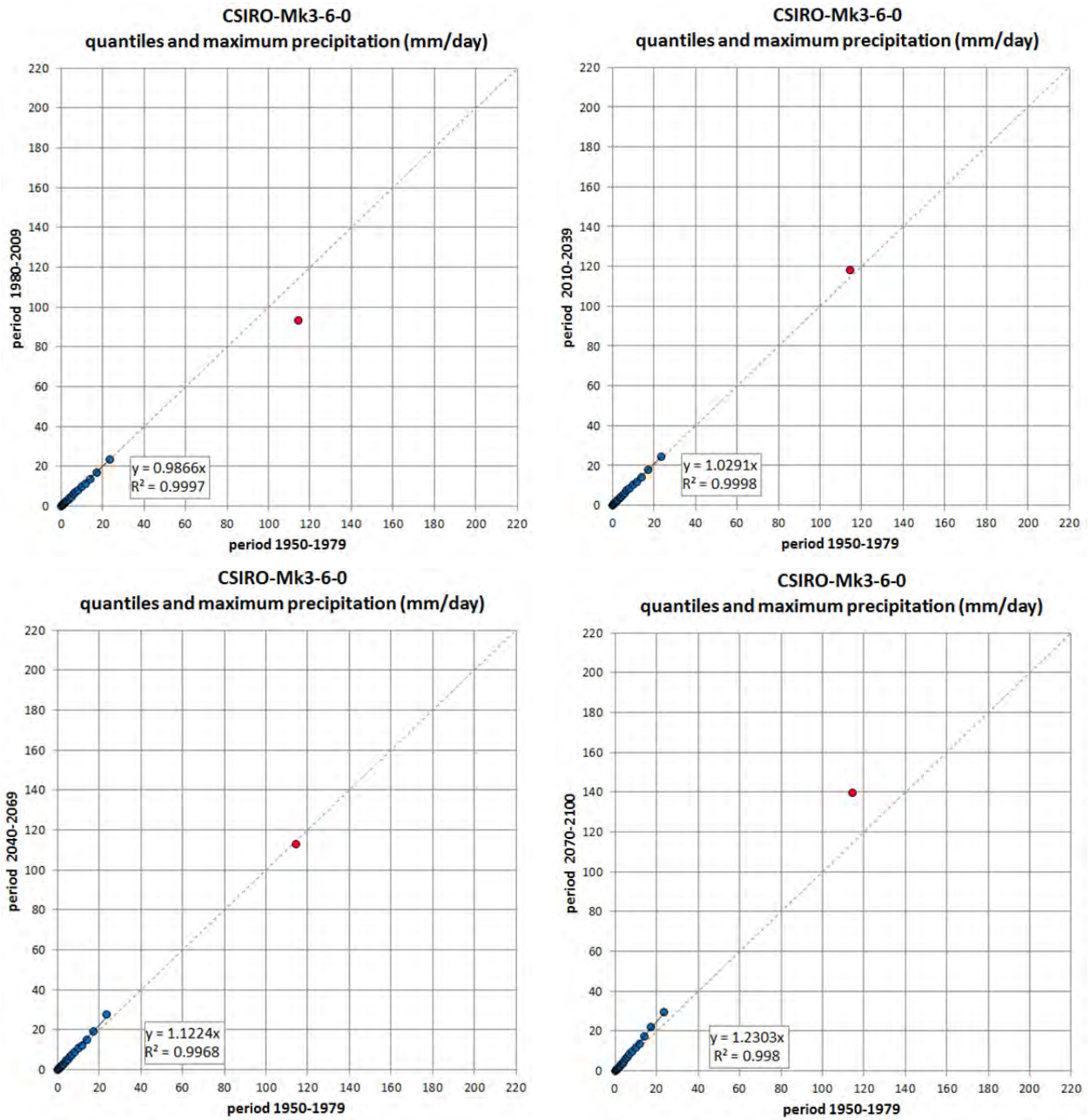


Figure 9. For CSIRO-Mk3-6-0, quantile-to-quantile plots for the 5<sup>th</sup>, 10<sup>th</sup>, 15<sup>th</sup>, ..., and 95<sup>th</sup> quantiles, for which the linear regression line is shown. The maximum value is also shown, in red. The identity (1:1) line is dashed.

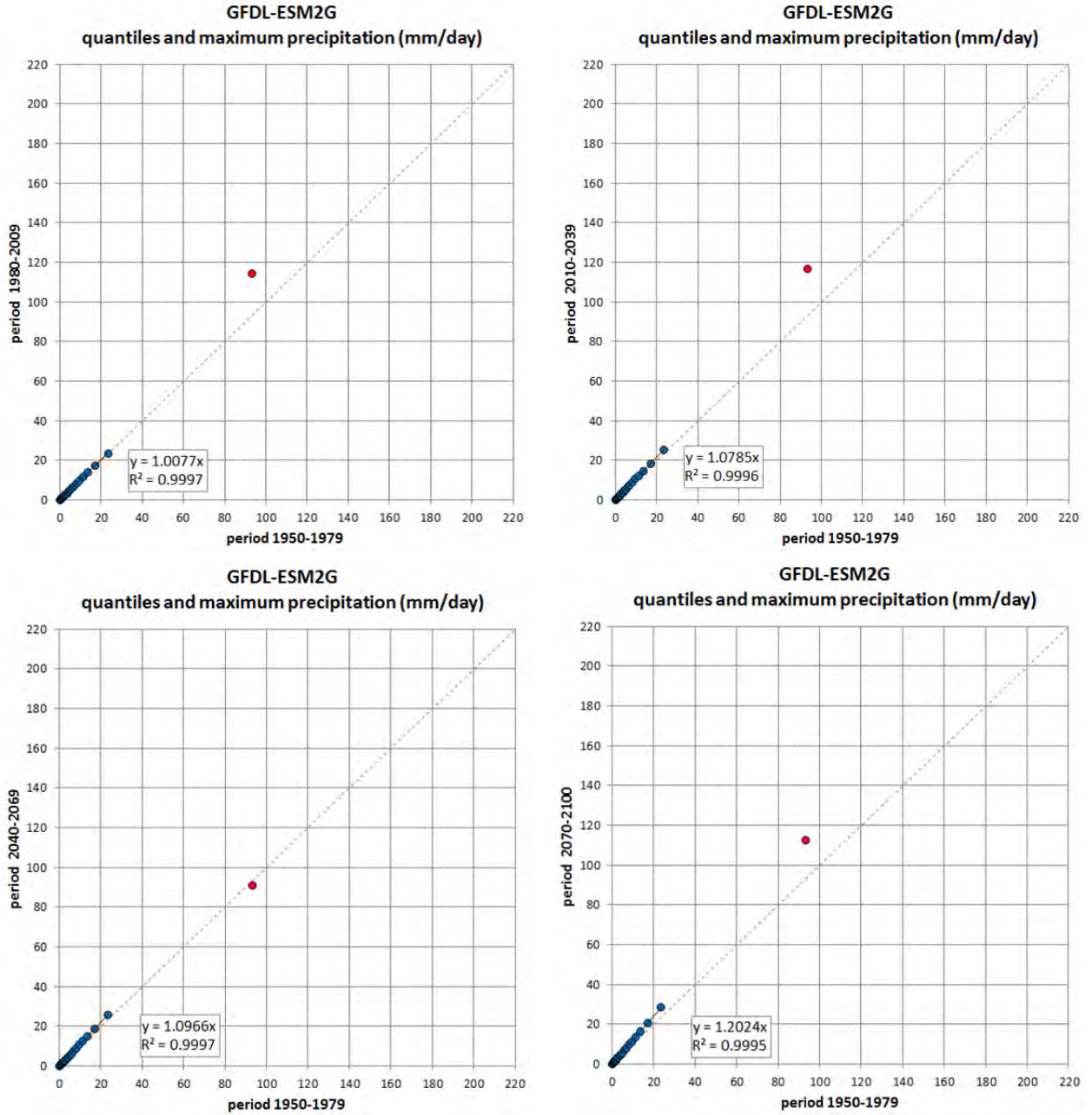


Figure 10. For GFDL-ESM2G, quantile-to-quantile plots for the 5<sup>th</sup>, 10<sup>th</sup>, 15<sup>th</sup>, ..., and 95<sup>th</sup> quantiles, for which the linear regression line is shown. The maximum value is also shown, in red. The identity (1:1) line is dashed.

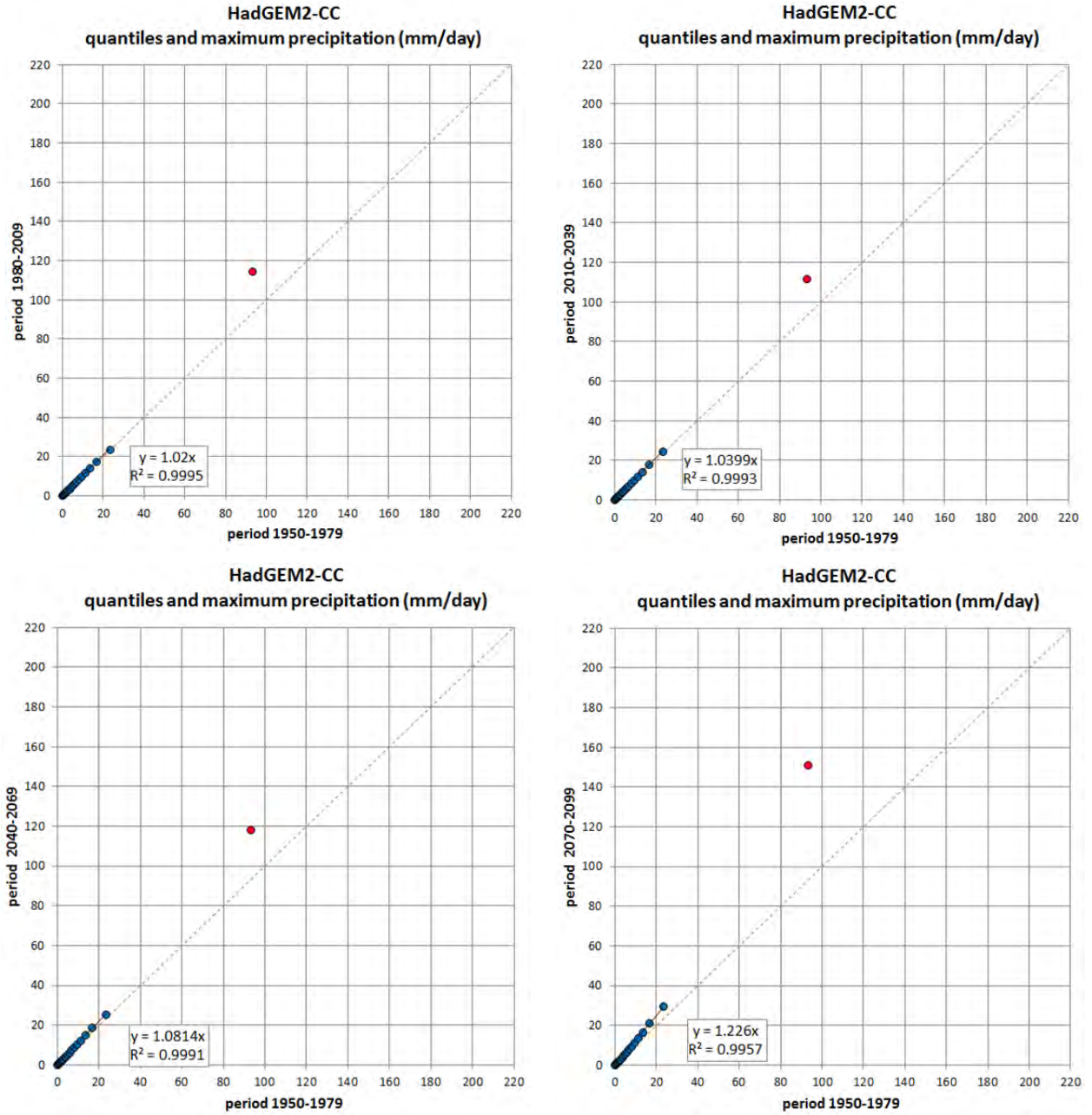


Figure 11. For HadGEM2-CC, quantile-to-quantile plots for the 5<sup>th</sup>, 10<sup>th</sup>, 15<sup>th</sup>, ..., and 95<sup>th</sup> quantiles, for which the linear regression line is shown. The maximum value is also shown, in red. The identity (1:1) line is dashed.

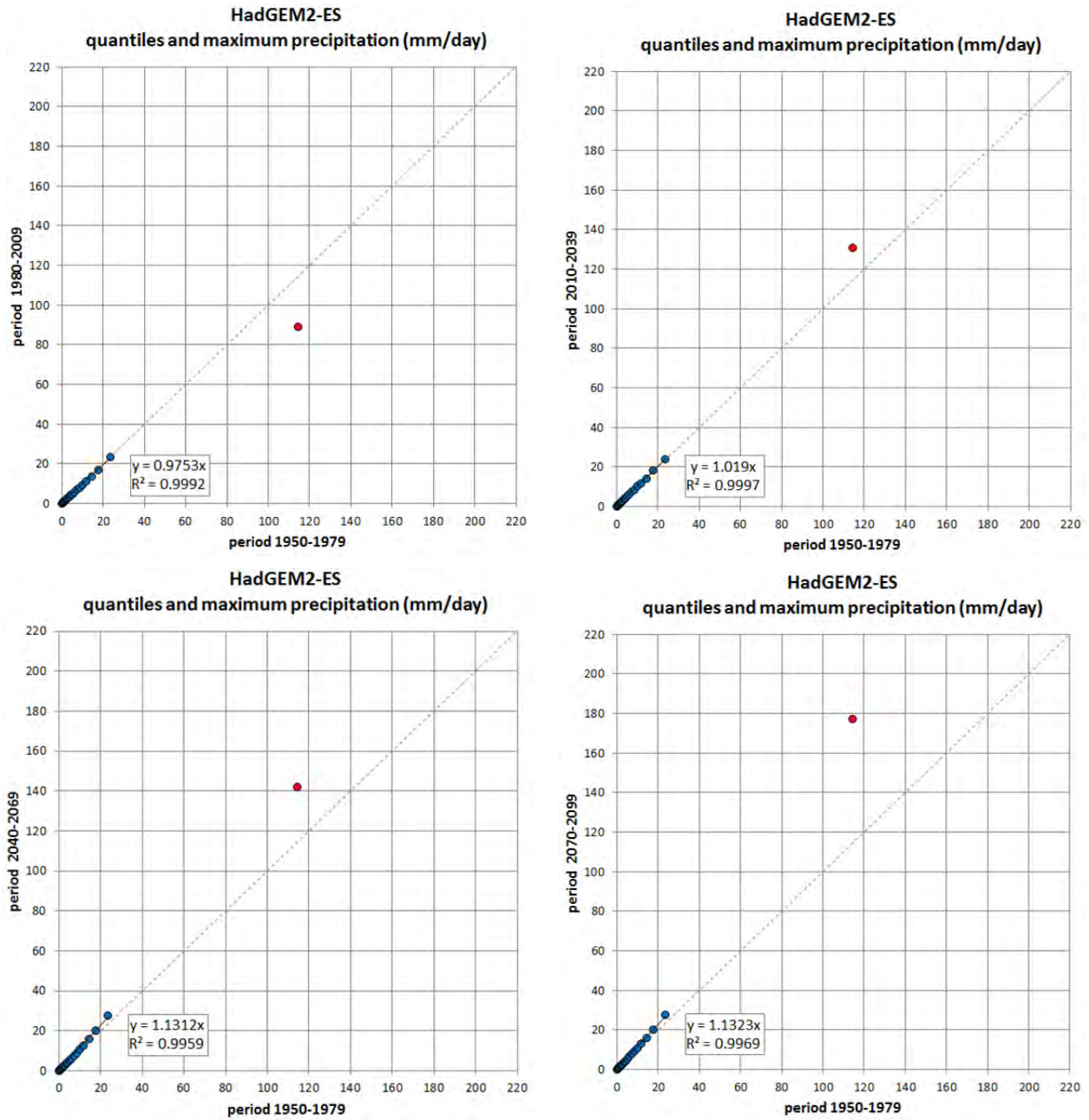


Figure 12. For HadGEM2-ES, quantile-to-quantile plots for the 5<sup>th</sup>, 10<sup>th</sup>, 15<sup>th</sup>, ..., and 95<sup>th</sup> quantiles, for which the linear regression line is shown. The maximum value is also shown, in red. The identity (1:1) line is dashed.

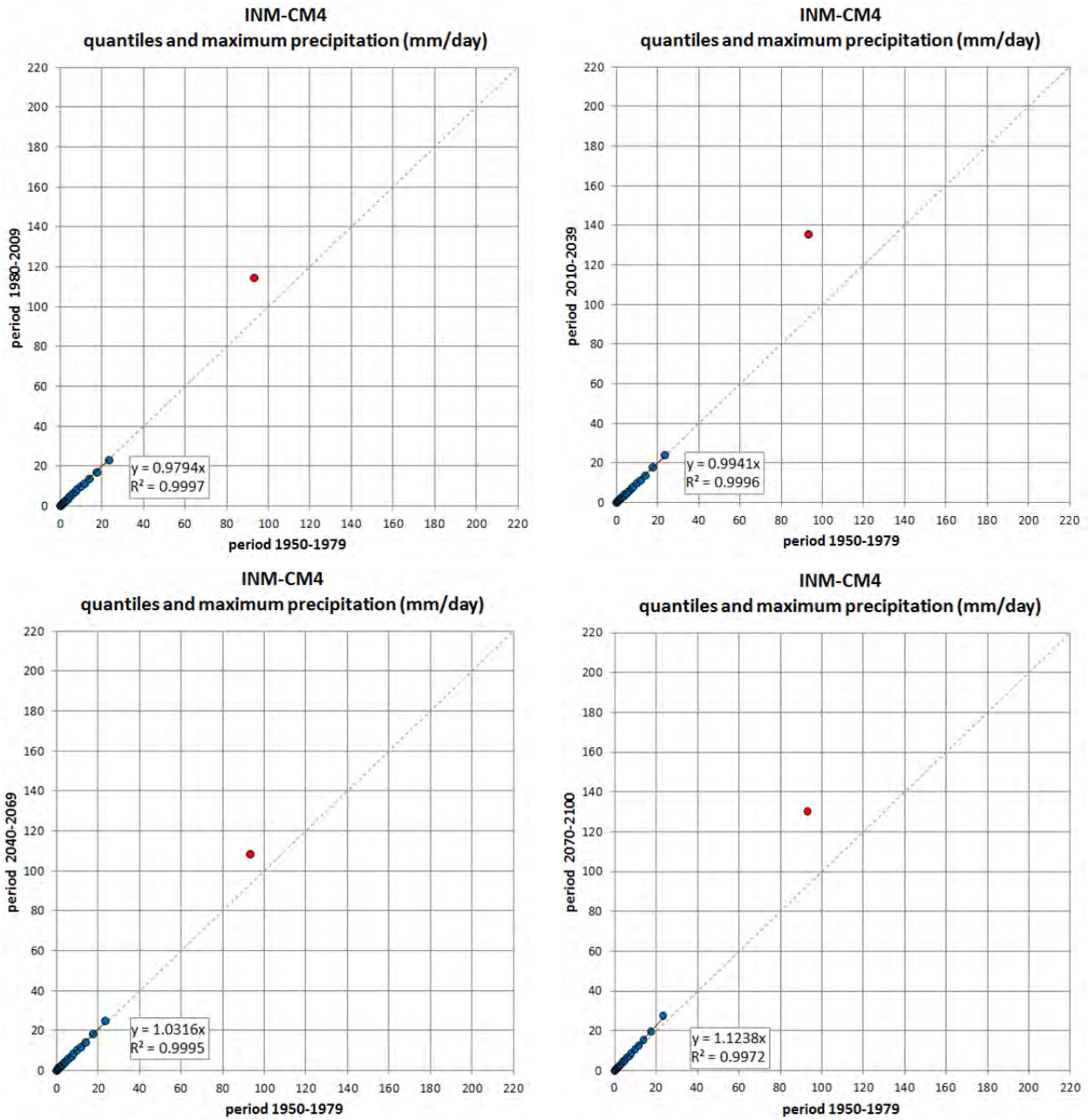


Figure 13. For INM-CM4, quantile-to-quantile plots for the 5<sup>th</sup>, 10<sup>th</sup>, 15<sup>th</sup>, ..., and 95<sup>th</sup> quantiles, for which the linear regression line is shown. The maximum value is also shown, in red. The identity (1:1) line is dashed.

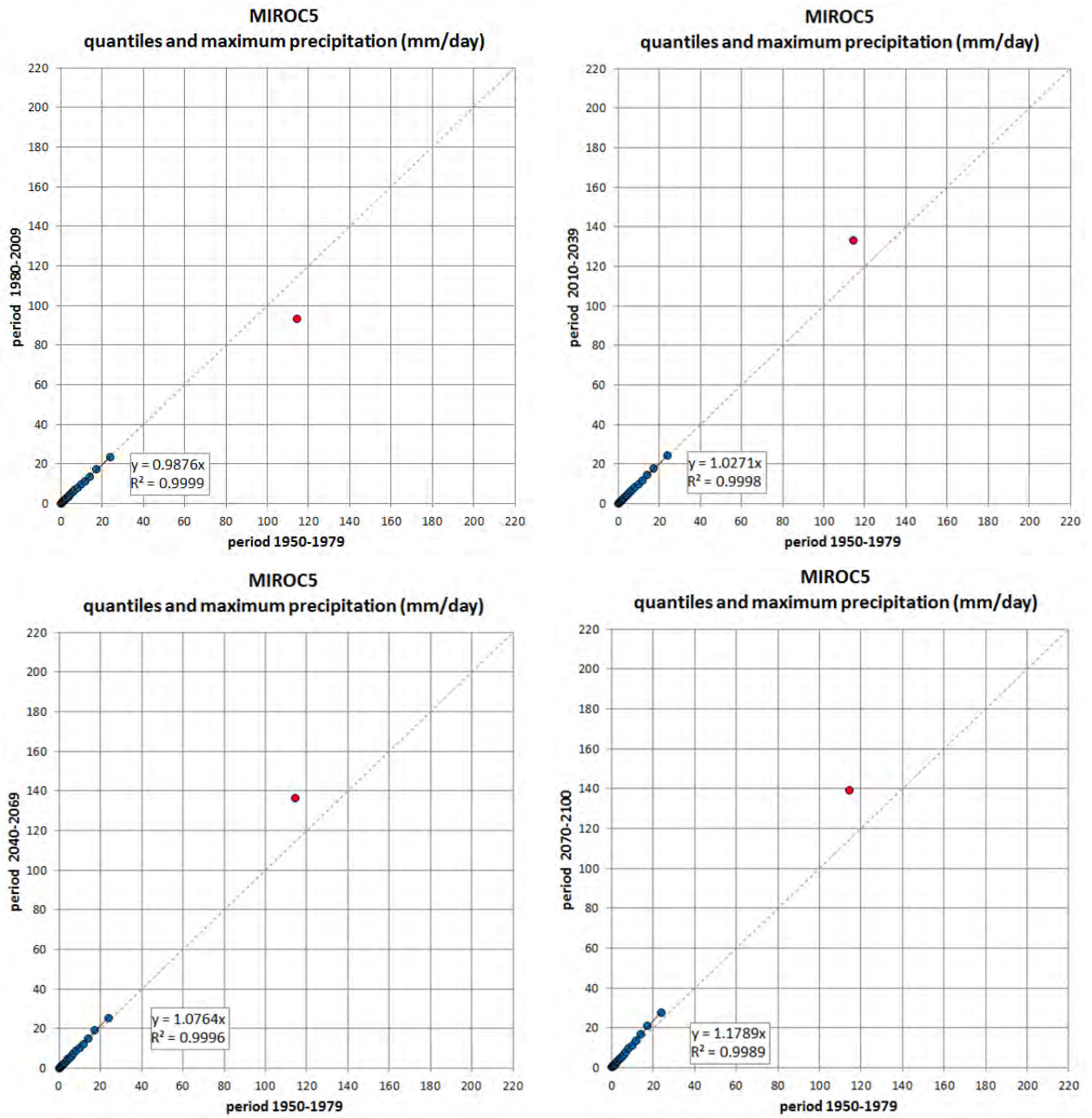


Figure 14. For MIROC5, quantile-to-quantile plots for the 5<sup>th</sup>, 10<sup>th</sup>, 15<sup>th</sup>, ..., and 95<sup>th</sup> quantiles, for which the linear regression line is shown. The maximum value is also shown, in red. The identity (1:1) line is dashed.

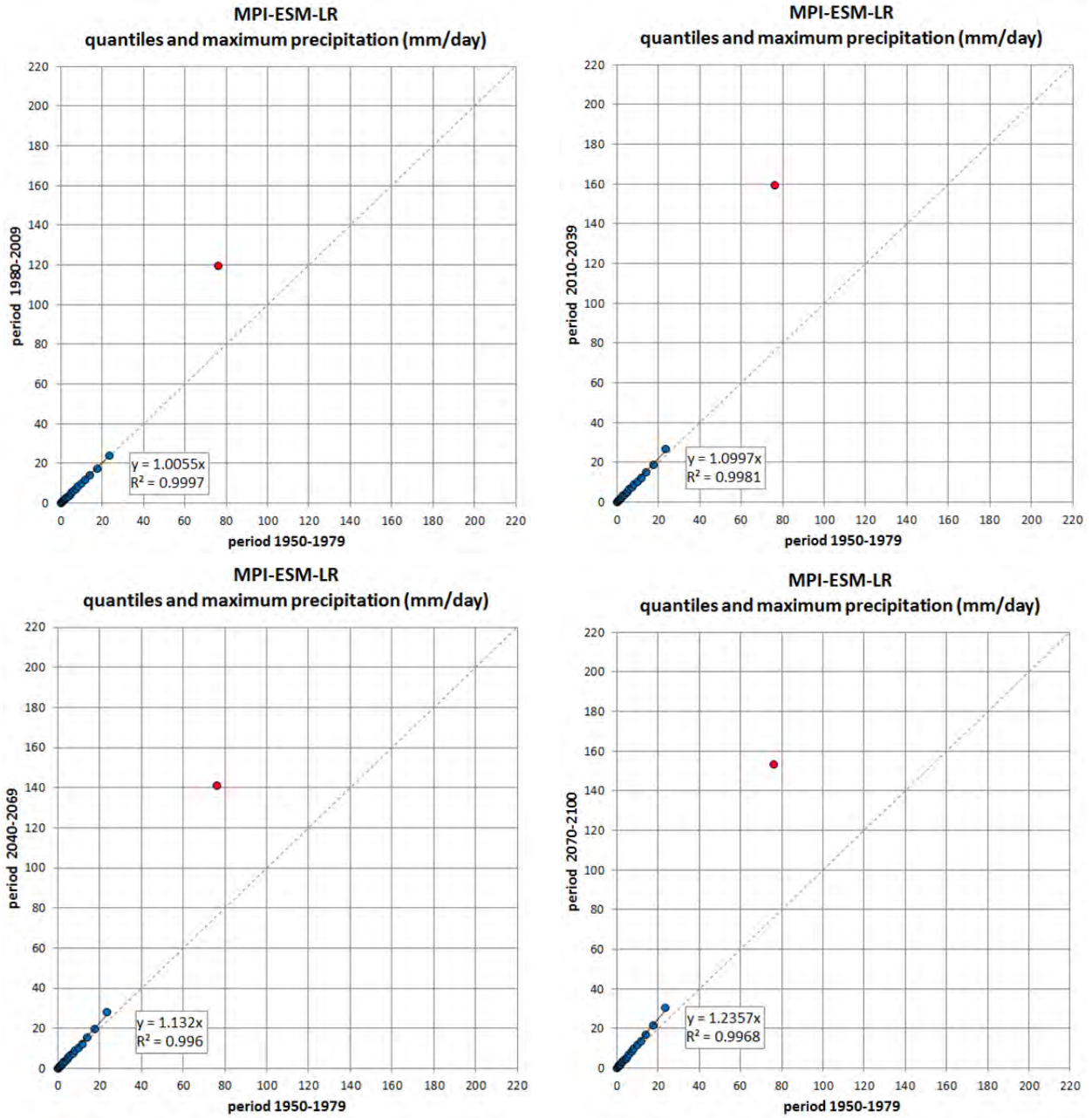


Figure 15. For MPI-ESM-LR, quantile-to-quantile plots for the 5<sup>th</sup>, 10<sup>th</sup>, 15<sup>th</sup>, ..., and 95<sup>th</sup> quantiles, for which the linear regression line is shown. The maximum value is also shown, in red. The identity (1:1) line is dashed.



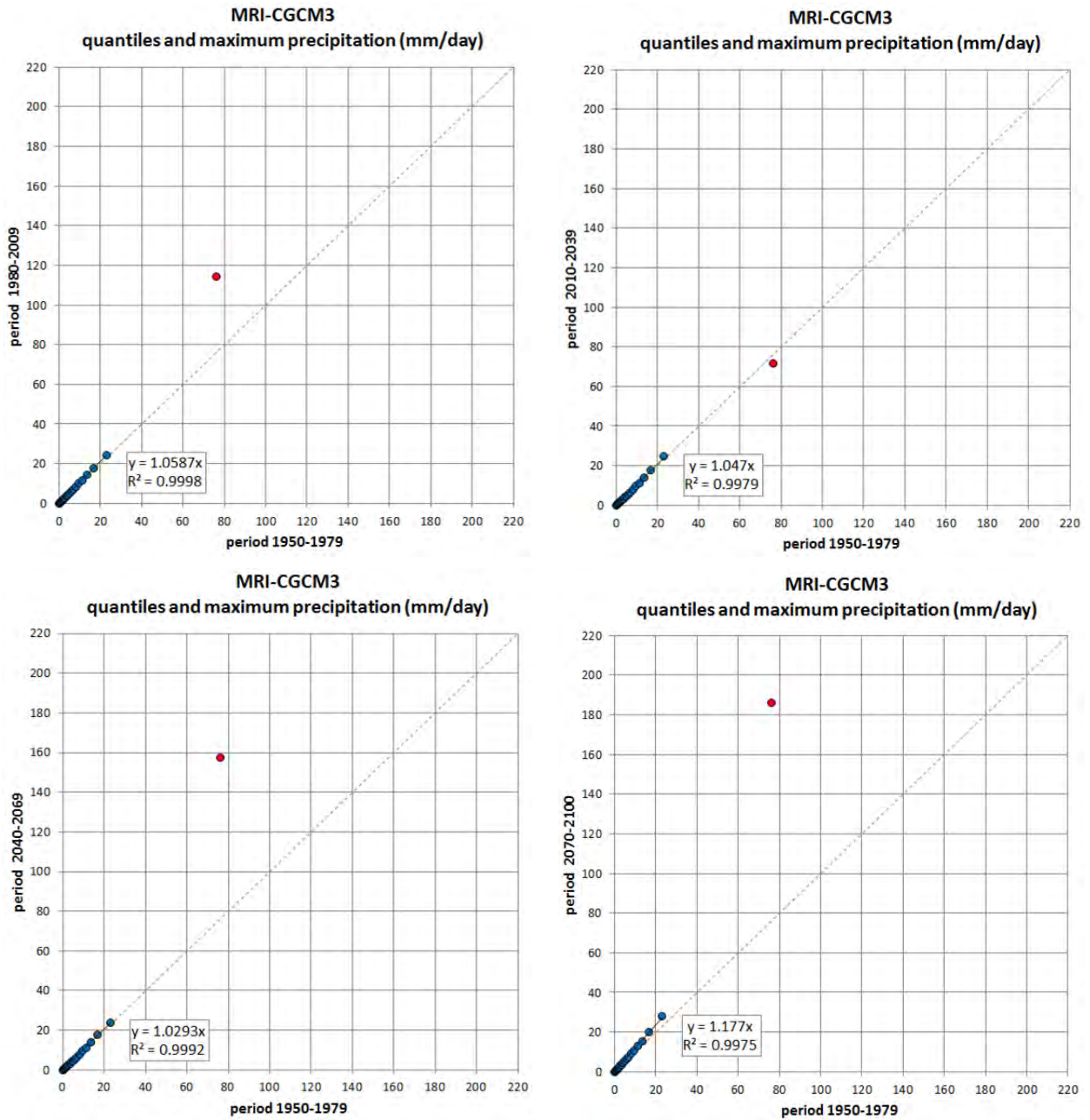


Figure 16. For MRI-CGCM3, quantile-to-quantile plots for the 5<sup>th</sup>, 10<sup>th</sup>, 15<sup>th</sup>, ..., and 95<sup>th</sup> quantiles, for which the linear regression line is shown. The maximum value is also shown, in red. The identity (1:1) line is dashed.

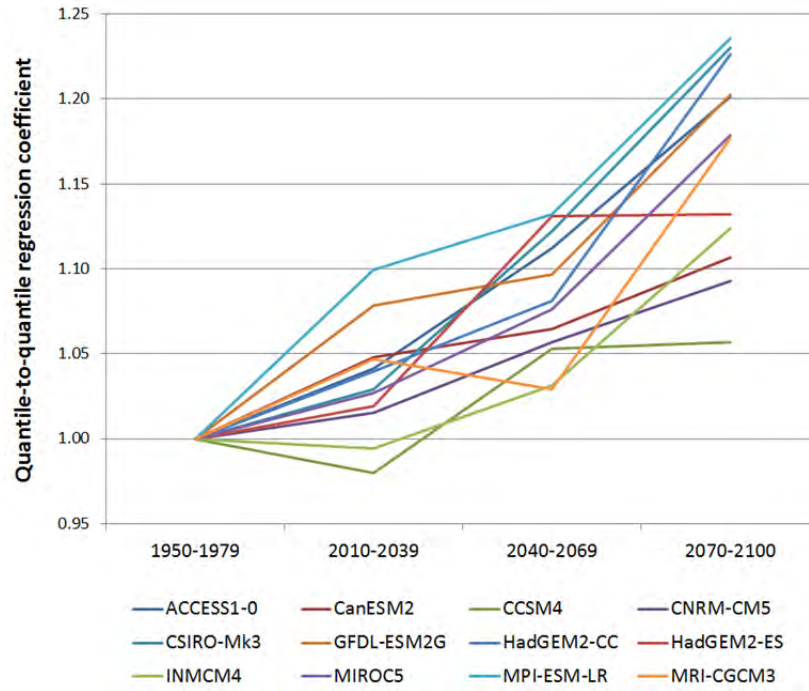


Figure 17. Linear regression coefficient of the quantile-to-quantile plots in Figure 5 through Figure 16.

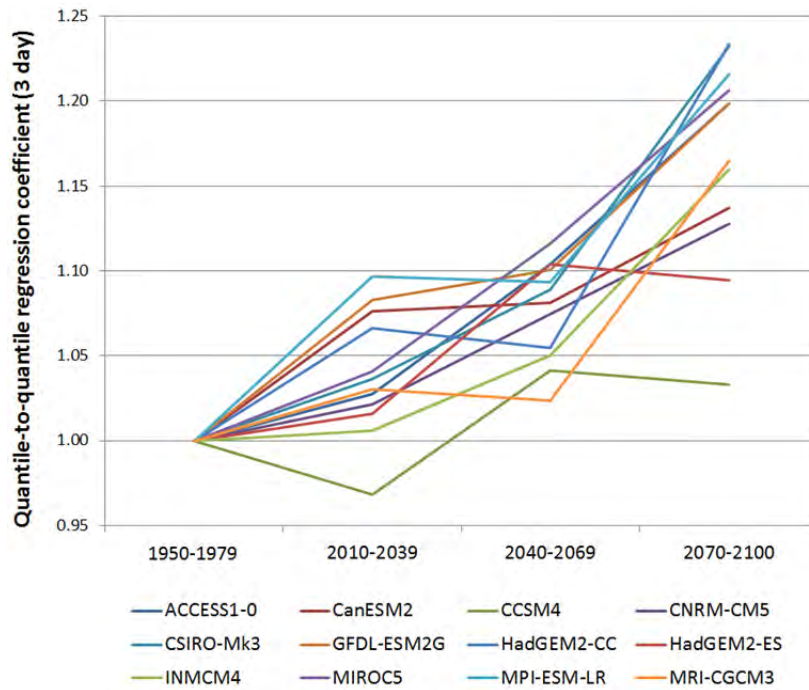


Figure 18. Linear regression coefficient of the quantile-to-quantile plots based on the three-day precipitation distribution.

## 2. Selecting two GCMs for this project

The selection of two GCMs for this project was done based on the characterization of downscaled GCM projections presented in the previous section.

### 2.1 Selection of the “severe scenario” GCM

We used the following criteria to estimate what might represent a severe scenario in terms of flood risk:

Criterion 1: The projected change in precipitation intensity, characterized by the values of the linear regression coefficients of the 1-day quantile-to-quantile plots, i.e., the values in Figure 17. We rely on the fact that the corresponding 3-day coefficients, from Figure 18, do not result in very different ranking of GCM runs.

Criterion 2: The projected change in the mean number of wet days per year.

In Table 1, we ranked the 12 GCM runs according to these two criteria, for the mid-century and end-of-century periods. We then used those rankings to assign an overall “severity score” to each GCM run, in Table 2. The formula we used to compute the severity score is the sum of the rank given to the GCM in each column of Table 1, to which 2 points are subtracted for each rank 1, and 1 point is subtracted for each rank 2. The lowest score, obtained by MPI-ESM-LR, corresponds to the most severe scenario. On this basis, MPI-ESM-LR is chosen to represent our “severe scenario”.

The formula used to compute a severity score is somewhat arbitrary, and a different formula could have led to choosing a different GCM. However, the choice of MPI-ESM-LR seems reasonable. It does have a considerable decline in the number of wet days, however its linear coefficient is the highest of all GCMs (see Table 1).

### 2.2 Selection of the “moderately high scenario” GCM

We used the following criterion to estimate what might represent a moderately high scenario in terms of flood risk: it should not rank among the top three or bottom three, and especially not the very top one or bottom one, of any of the categories in Table 1. Thus, we used a “moderation score” which adds 1 point to a GCM’s score for each entry in the third position from top or bottom in Table 1, adds 2 points for the second position from top or bottom, and adds 3 points for the top or bottom position.

The resulting “moderation score” awards both CanESM2 and GFDL-ESM2G with only 1 point, at the top of Table 3. We chose CanESM2 for the moderate scenario because it is less severe than GFDL-ESM2G according to the severity score in Table 2.

**Table 1.** Ranked list of GCM runs, according to four characteristics of the downscaled simulations. The GCM selected to represent the “severe scenario”, MPI-ESM-LR, is highlighted in yellow, and the GCM selected for the “moderately high scenario”, CanESM2, is highlighted in blue.

<b>Rank</b>	<b>Linear coeff. 2040-2069</b>	<b>Linear coeff. 2070-2100</b>	<b>Change in wet days 2040-2069</b>	<b>Change in wet days 2070-2099</b>
1	MPI-ESM-LR	MPI-ESM-LR	CNRM-CM5	CNRM-CM5
2	HadGEM2-ES	CSIRO-Mk3	MIROC5	INMCM4
3	CSIRO-Mk3	HadGEM2-CC	GFDL-ESM2G	MIROC5
4	ACCESS1-0	GFDL-ESM2G	MRI-CGCM3	GFDL-ESM2G
5	GFDL-ESM2G	ACCESS1-0	CanESM2	MRI-CGCM3
6	HadGEM2-CC	MIROC5	INMCM4	CanESM2
7	MIROC5	MRI-CGCM3	MPI-ESM-LR	CCSM4
8	CanESM2	HadGEM2-ES	CCSM4	MPI-ESM-LR
9	CNRM-CM5	INMCM4	ACCESS1-0	CSIRO-Mk3
10	CCSM4	CanESM2	HadGEM2-ES	HadGEM2-CC
11	INMCM4	CNRM-CM5	HadGEM2-CC	ACCESS1-0
12	MRI-CGCM3	CCSM4	CSIRO-Mk3	HadGEM2-ES

**Table 2.** Severity score for each GCM run, obtained from the rankings in Table 1, as described in the text.

<b>GCM</b>	<b>SEVERITY SCORE</b>
MPI-ESM-LR	13
GFDL-ESM2G	16
MIROC5	17
CNRM-CM5	20
CSIRO-Mk3	25
INMCM4	27
MRI-CGCM3	28
CanESM2	29
ACCESS1-0	29
HadGEM2-CC	30
HadGEM2-ES	31
CCSM4	37

Table 3. Moderation score for each GCM run, obtained from the rankings in Table 1, as described in the text.

GCM	MODERATION SCORE
CanESM2	1
GFDL-ESM2G	1
ACCESS1-0	2
MIROC5	3
MRI-CGCM3	3
HadGEM2-CC	4
CSIRO-Mk3	4
INMCM4	4
CCSM4	4
HadGEM2-ES	6
MPI-ESM-LR	6
CNRM-CM5	8

### 2.3 Summary of the two scenarios selected

The two scenarios selected above are summarized in Table 4.

Table 4. The two scenarios selected for this study.

Scenario	GCM	Representative greenhouse gas concentration pathway (RCP)	Model run	Institution developing the GCM
<b>Severe</b>	MPI-ESM-LR	8.5 Wm <sup>-2</sup>	Run 3	Max Planck Institut für Meteorologie, Germany
<b>Moderately High</b>	CanESM2	8.5 Wm <sup>-2</sup>	Run 1	Canadian Centre for Climate Modelling and Analysis, Canada

In the case of the MPI-ESM-LR scenario, there is a marked increase in mean precipitation intensity on wet days. Mean intensity increases progressively over time, reaching 8.9 mm/day in the late-century period (2070-2099). The average number of wet days in a year is projected to decline, from this run's simulated historical (1950-2009) of 195 days/year, reaching 183 days/year in the late-century period (2070-2099).

In the case of the CanESM2 scenario, the projected mean precipitation intensity on wet days also increases progressively over time, reaching 7.89 mm/day in the late-century period (2070-2099). The average number of wet days in a year is projected to decline, from this run's simulated historical (1950-2009) of 194 days/year, to 184 days/year in the late-century period (2070-2099).

The two scenarios are close in their simulated number of wet days in the historical period (1950-2009) and end of century time period (2070-2100), though they differ a bit in the periods 2010-2039 and 2040-2069 (Figure 3). The two scenarios differ substantially in their projected increase in mean precipitation intensity in wet days (Figure 3) and mean annual precipitation (Figure 19 and Figure 4). As we shall see in the next section, the two scenarios also differ substantially in their projected increase in extreme daily precipitation intensity, with MPI-ESM-LR having larger estimated parameter values for the fitted extreme value distribution, compared to CanESM2.

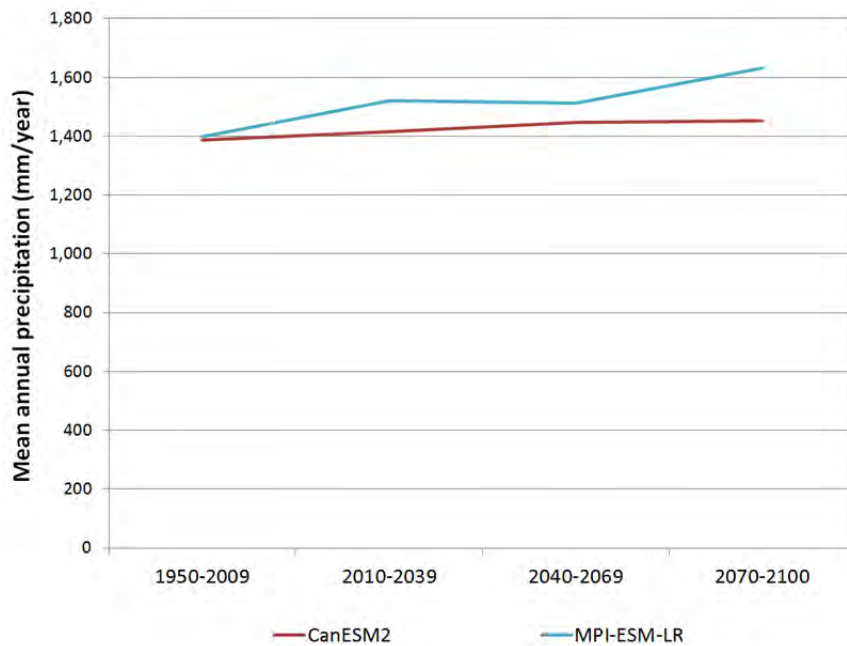


Figure 19. Increase of period-mean annual precipitation for the two selected GCMs.

### 3. Creating 21<sup>st</sup> Century hourly precipitation time series

In this section we describe our methodology for creating two synthetic hourly precipitation time series for the 21<sup>st</sup> Century (2010-2100) to represent a future “moderately high scenario” and a “very high scenario”. These time series will be used as input to the hydrologic model in this project, to evaluate future flood risk.

#### 3.1 Methodology description

The diagram in Figure 20 summarizes our methodology for creating the future synthetic time series of hourly precipitation. Given the differences seen (and which are to be expected) between the gauge daily values and the GCM-simulated downscaled daily grid-cell values, and given that the hydrologic model was calibrated and run using the (hourly) gauge values, our methodology uses the gauge observed time series as the basis for creating the future time series. This ensures that the future time series, and their associated hydraulic-model results, are fully comparable to the observed time series and its hydraulic-model results.

Step 1 of the methodology (Figure 20) ensures that the future precipitation time series are consistent with the GCM-simulated decline in mean number of wet days per year. Step 2 of the methodology (Figure 20) ensures consistency with the GCM-simulated increase in precipitation intensity and its distribution.

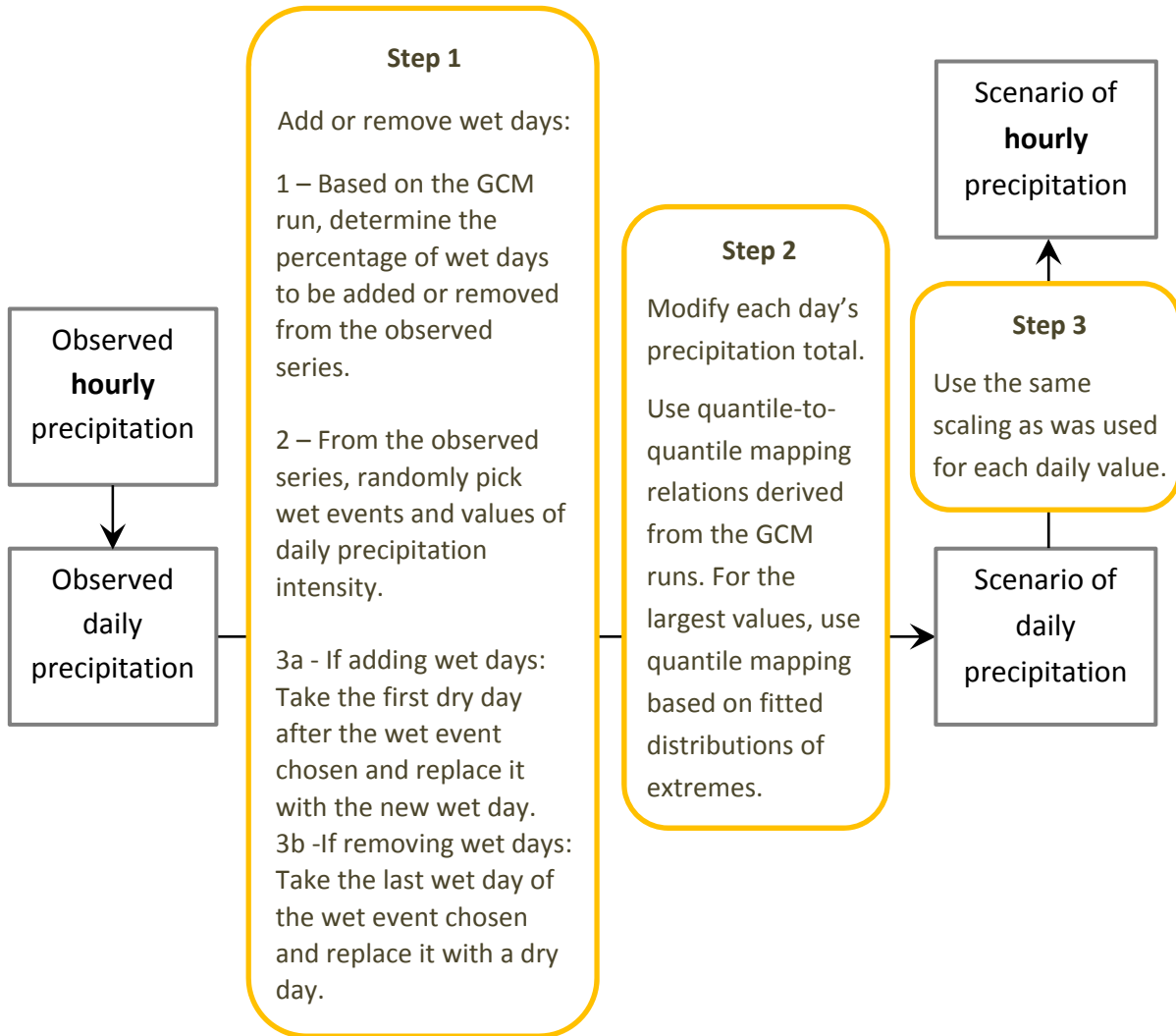


Figure 20. Methodology for generating a synthetic time series of future hourly precipitation by modification of an observed hourly record.

### 3.2 Step 1: Remove wet days from the observed precipitation time series

Both scenarios project similar declines in the mean number of wet days per year (Figure 3). The percentual declines sampled by the GCM runs are given in Table 5. Although small across the table, these changes have significant impact on the calculated return periods of precipitation intensity. While these changes may not be strongly significant statistically, for a sample size of 30 years per period and some (not analyzed) variability between years, when we consider the level of agreement among GCMs

with respect to a future decline in wet days by the end of this century (Figure 3), these sampled values do assume significance.

The number of observed wet days at the Municipal Hall gauge in the period of record (October 1962-September 2009, i.e. 47 water years) is 8,023 days. We use the percent changes in Table 5 to calculate the total number of wet days to be replaced by dry days, given in Table 6.

**Table 5. Projected changes in the mean number of wet days per year, in the two scenarios.**

Scenario	GCM	Percent change in mean number of wet days per year relative to the historical period (1950-2009)		
		Period 2010-2039	Period 2040-2069	Period 2070-2100
Severe	MPI-ESM-LR	-2.14%	-4.57%	-6.08%
Moderately High	CanESM2	-2.75%	-1.62%	-4.99%

**Table 6. Number of wet days in the observed precipitation record to be replaced by dry days, to represent each of the 3 future time horizons in each scenario.**

Scenario	GCM	Number of wet days to be removed from the observed gauge record		
		Period 2010-2039	Period 2040-2069	Period 2070-2100
Severe	MPI-ESM-LR	172	367	488
Moderately High	CanESM2	221	130	400

Removal of wet days was performed by randomly picking a corresponding number of precipitation *events* from the 47-year gauge record, and removing the last day in the event. A precipitation event is defined, for this purpose, as any group of consecutive wet days. An isolated wet day is also a precipitation event. The choice of the last day of the event, as opposed to just any day of the event, is somewhat arbitrary. This choice is motivated by not wanting to introduce dry days into an event and increase the number of events. However, it is recognized that the last day of an event may have a statistical tendency towards lower daily average (as only a fraction of this day may have received precipitation), which implies that there will be a tendency to remove lower-intensity precipitation days, altering the distribution of remaining wet days. However, given the small percentage of wet days to be removed, this effect is expected to be small.



### 3.3 Step 2: Modify each day’s precipitation total (and scale the hourly values accordingly)

The values of daily precipitation simulated by a GCM for a future time horizon (for example, 2040-2069) have a different statistical distribution than those simulated for the historical period, 1950-2009. Considering the most intense precipitation days, i.e., any daily precipitation value  $x$  exceeding a threshold value  $u$ , which in the historical period had non-exceedance probability  $F_s^h(x)$ , will in the future period have a different non-exceedance probability,  $F_s^f(x)$ . Subscript  $s$  stands for GCM-simulated distribution, and superscripts  $h$  and  $f$  stand for “historical period” and “future period”. Because both of our scenarios entail future intensification of precipitation, then we can expect to have a decline over time in the probability of any given value  $x$  not being exceeded, i.e.:

Equation 1

$$F_s^f(x) < F_s^h(x)$$

The probability of non-exceedance of high precipitation values, above an appropriately chosen high threshold value  $u$ , can be estimated by fitting an extreme value distribution to the time series. This is often done using the series of annual maxima, which in this case would be the 47 values that represent the wettest day in each of the 47 water years. Alternatively, it can be done using all the observed values above a chosen high threshold (several of which values may fall on the same year). We chose the latter method, known as “peaks over threshold” (or POT) analysis, as it makes use of a larger number of data points, reducing the uncertainty in parameter estimation. Uncertainty however remains high, as is always the case in extreme value analysis of precipitation time series covering only a few decades, and we do not quantify parameter uncertainty in this study.

To choose an appropriate threshold value  $u$ , and to fit the Generalized Pareto distribution to the exceedance values above  $u$ , we followed the methodology described in Coles (2001), using maximum likelihood for parameter estimation (Coles, 2001, Eqn. 4.10 and following ones). The CDF of the Generalized Pareto distribution is given by the following general expression, when  $\xi \neq 0$  (a different expression applies for  $\xi = 0$ , but is not given here):

Equation 2

$$p(x_i \leq x | x_i > u) = 1 - \left( 1 + \xi \cdot \left( \frac{x - u}{\sigma} \right) \right)^{-\frac{1}{\xi}}$$

for  $x, x_i > u$

In this equation,  $x$  is the daily precipitation total,  $u$  is the high threshold value,  $p(x_i \leq x | x_i > u)$  is the non-exceedance probability of  $x$ , conditioned on  $x_i$  surpassing the threshold  $u$ , and  $\sigma$  and  $\xi$  are the distribution’s parameters (designated the “scale” and “shape” parameters, respectively).

Equation 2 gives the non-exceedance probability conditional on  $x$  exceeding  $u$ . To obtain the unconditional non-exceedance probability of  $x$ ,  $F(x)$ , we must account for the non-exceedance probability of the threshold  $u$ ,  $F(u)$ , as follows:

Equation 3

$$F(x) = p(x_i \leq x | x_i > u) \cdot (1 - F(u)) + F(u)$$

*for  $x, x_i > u$*

Combining Equation 2 and Equation 3, we obtain:

Equation 4

$$F(x) = \left\{ 1 - \left( 1 + \xi \cdot \left( \frac{x - u}{\sigma} \right)^{\frac{1}{\xi}} \right) \right\} \cdot (1 - F(u)) + F(u)$$

*for  $x > u$*

The value of  $F(u)$  can be estimated empirically using the rank-based expression that we used for all non-extreme values of  $x$ , i.e., for all  $x < u$ :

Equation 5

$$F(x) = \frac{r(x)}{n + 1}$$

*for  $x \leq u$*

In Equation 5,  $r(x)$  represents the rank of  $x$  (when all values in the series are ranked from smallest to largest). Many other options could be used instead of Equation 5, but the specific choice is of little practical consequence to this study.

Solving Equation 4 for  $x$ , we obtain Equation 6:

Equation 6

$$x = \frac{\sigma}{\xi} \cdot \left[ \left( 1 - \frac{F(x) - F(u)}{1 - F(u)} \right)^{-\xi} - 1 \right] + u$$

*for  $x > u$*

Table 7 gives our estimated parameter values for the above equations, for the daily observed series and the simulated downscaled daily series for the GCM-based scenarios and different time horizons. The parameters for each GCM historical simulation series show reasonable agreement with the observed series.

Table 7. Parameter estimates for the generalized Pareto distribution (GPD) using the POT method and maximum likelihood, for the observations, and for the downscaled simulated precipitation by MPI-ESM-LR and CanESM2.

Time Period	Average number of wet days per year $n_w$	Threshold $u$ (mm) and $F(u)$		Number of exceedances	$\hat{\sigma}$	$\hat{\xi}$
<b>Gauge Observations</b>						
<b>WY 1963-2009</b>	170.7	47	0.99339	53	8.48	0.38
<b>MPI-ESM-LR</b>						
<b>1. 1950-2009</b>	195.2	49	0.99530	55	6.69	0.40
<b>2. 2010-2039</b>	191.0	46	0.98814	68	10.10	0.51
<b>3. 2040-2069</b>	186.3	45	0.98623	76	13.29	0.41
<b>4. 2070-2100</b>	183.4	49	0.98276	98	9.87	0.45
<b>CanESM2</b>						
<b>1. 1950-2009</b>	193.8	49	0.99520	51	7.09	0.29
<b>2. 2010-2039</b>	188.4	44	0.98992	57	7.82	0.30
<b>3. 2040-2069</b>	190.6	50	0.99248	42	6.08	0.37
<b>4. 2070-2100</b>	184.1	51	0.99071	53	8.16	0.27

Figure 21 and Figure 22 show the distributions that were fitted to the MPI-ESM-LR simulations for different time periods. Below the threshold  $u$  (Table 7), empirical plotting positions are used, while above  $u$  the Generalized Pareto distribution is used, using the parameters in Table 7.

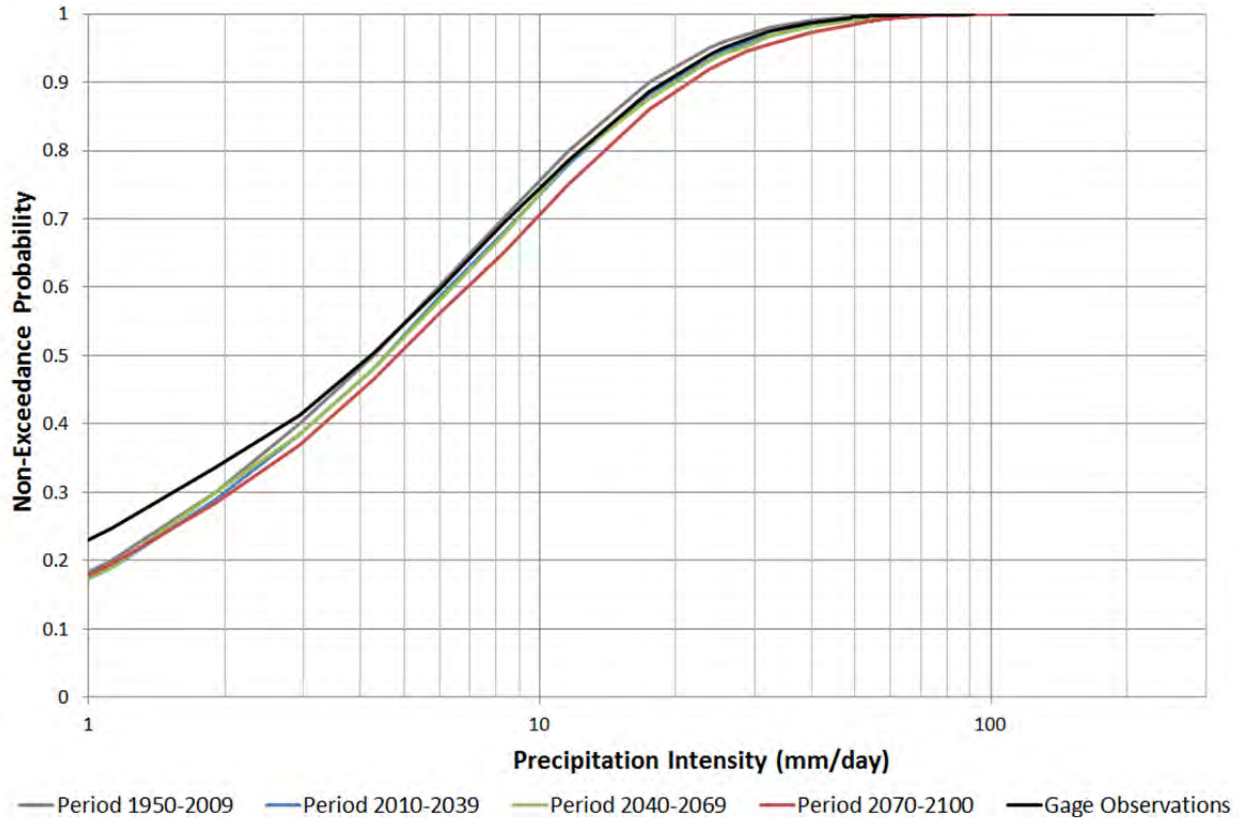


Figure 21. Fitted distribution of daily precipitation simulated for the historical period and future periods in the MPI-ESM-LR run, and gauge observations. For any fixed value of non-exceedance probability, the value for the future distribution (for any of the future time periods) is higher than for the historical distribution (period 1950-2009).

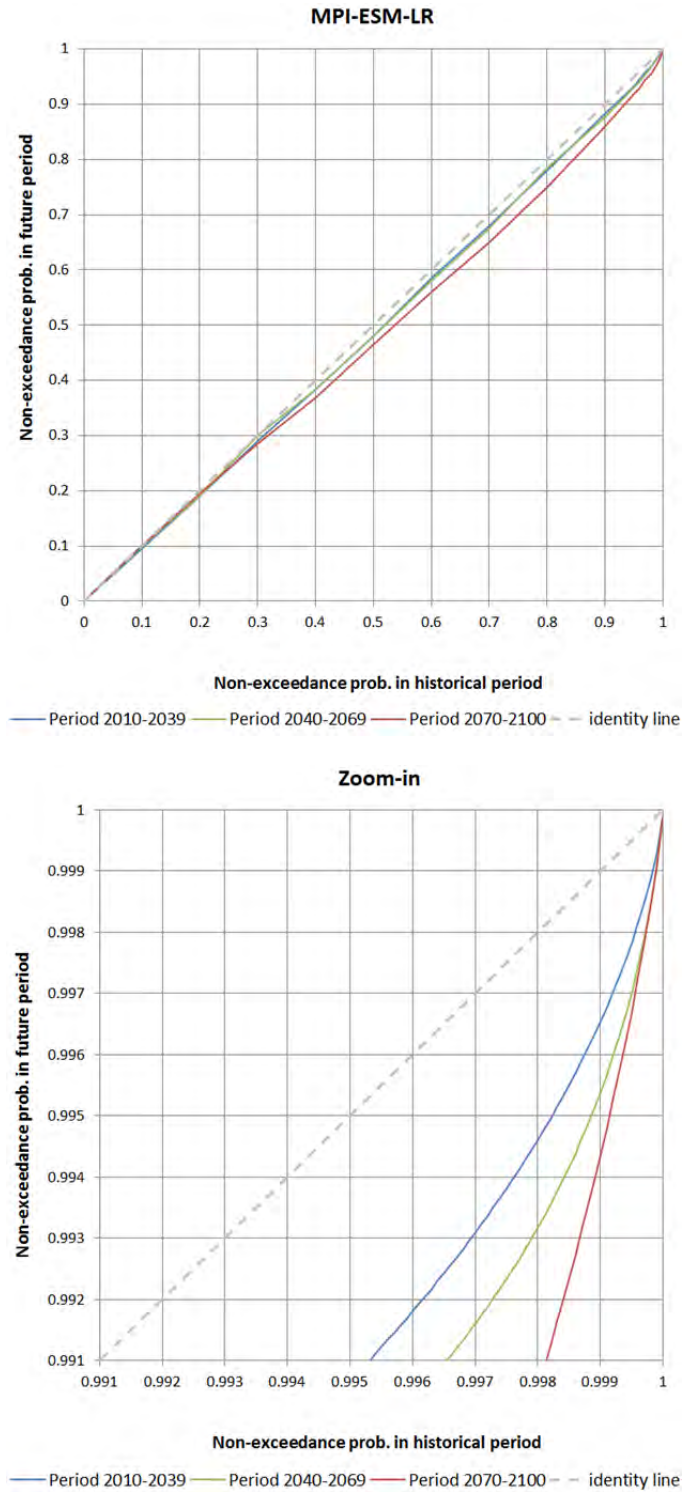


Figure 22. Probability-to-probability plots comparing the fitted distributions for future period simulations to the historical simulations, for the MPI-ESM-LR run. Any given value of daily precipitation has a lower probability of non-exceedance (i.e., a higher probability of being exceeded) in the future period compared to the historical period.

## Detailed description of Step 2

Consider we are performing Step 2 (in Figure 20) and that we will now perform this step for a high observed daily value,  $x$ , where  $x$  is above a high threshold  $u$ . We want to transform  $x$  into a new value ( $x'$ ) for the future time series based on the MPI-ESM-LR model run for 2070-2100 (for example). We do this through the following sub-steps:

- i. We take the observed value  $x$  and determine its non-exceedance probability,  $F(x)$ , using Equation 4, and the parameter values in Table 7, 1<sup>st</sup> row.
- ii. We determine what value has this same non-exceedance probability  $F(x)$  in the distribution corresponding to the MPI-ESM-LR simulations for 2070-2100. Call this value  $x_{MPI}^f$  (where the superscript  $f$  stands for “future period”).
- iii. Determine the original non-exceedance probability of value  $x_{MPI}^f$ , i.e., in the distribution corresponding to the MPI-ESM-LR simulations for the historical period, 1950-2009. Call this  $F_{MPI}^h(x_{MPI}^f)$ .
- iv. Determine the value  $x'$  for which the non-exceedance probability in the distribution of observed values equals the probability in (iii). We will have  $x' > x$ .
- v. Replace  $x$  with  $x'$ .

## Case Example

Suppose we are creating the daily precipitation time series that will represent the MPI-ESM-LR scenario for period 2070-2100. Consider the value of 70.3 mm, which was observed on 3 November 1971. In **sub-step (i)**, we take  $x=70.3$  mm and we use Equation 4, and the values in Table 7 to calculate:

Equation 7

$$\begin{aligned} F(70.3) &= p(x \leq 70.3 | x > 47) \cdot (1 - F(47)) + F(47) \\ &= \left\{ 1 - \left( 1 + 0.38 \cdot \left( \frac{70.3 - 47}{8.48} \right)^{-\frac{1}{0.38}} \right) \right\} \cdot (1 - 0.99339) + 0.99339 \\ &= 0.998993 \end{aligned}$$

In **sub-step (ii)**, we find the value which had this same non-exceedance probability in the historical simulations by MPI-ESM-LR. For this, we use Equation 6, set  $F(x) = 0.998993$ , and use the parameter values from Table 7 to calculate  $x_{MPI}^f$ :

Equation 8

$$\begin{aligned} x_{MPI}^f &= \frac{9.87}{0.45} \cdot \left[ \left( 1 - \frac{0.998993 - 0.98276}{1 - 0.98276} \right)^{-0.45} - 1 \right] + 49 \\ &= 105.8 \text{ mm} \end{aligned}$$

In **sub-step (iii)**, we determine the original non-exceedance probability of this value  $x_{MPI}^f = 105.8$  mm. Again using Equation 4, we obtain:

Equation 9

$$\begin{aligned} F_{MPI}^h(105.8) &= \left\{ 1 - \left( 1 + 0.4 \cdot \left( \frac{105.8 - 49}{6.69} \right)^{-\frac{1}{0.4}} \right) \right\} \cdot (1 - 0.9953) + 0.9953 \\ &= 0.999884 \end{aligned}$$

In **sub-step (iv)**, we determine the value  $x'$  for which the non-exceedance probability in the distribution of observed values equals the result of Equation 9, 0.999884. To do this, we apply Equation 6, setting  $F(x) = 0.999884$ :

Equation 10

$$\begin{aligned} x' &= \frac{8.48}{0.38} \cdot \left[ \left( 1 - \frac{0.999884 - 0.99339}{1 - 0.99339} \right)^{-0.38} - 1 \right] + 47 \\ &= 128.4 \text{ mm} \end{aligned}$$

In **the final sub-step (v)**, we replace the observed value 70.3 mm with this larger value 128.4 mm.

Figure 23 shows a graphical depiction of the above calculations.

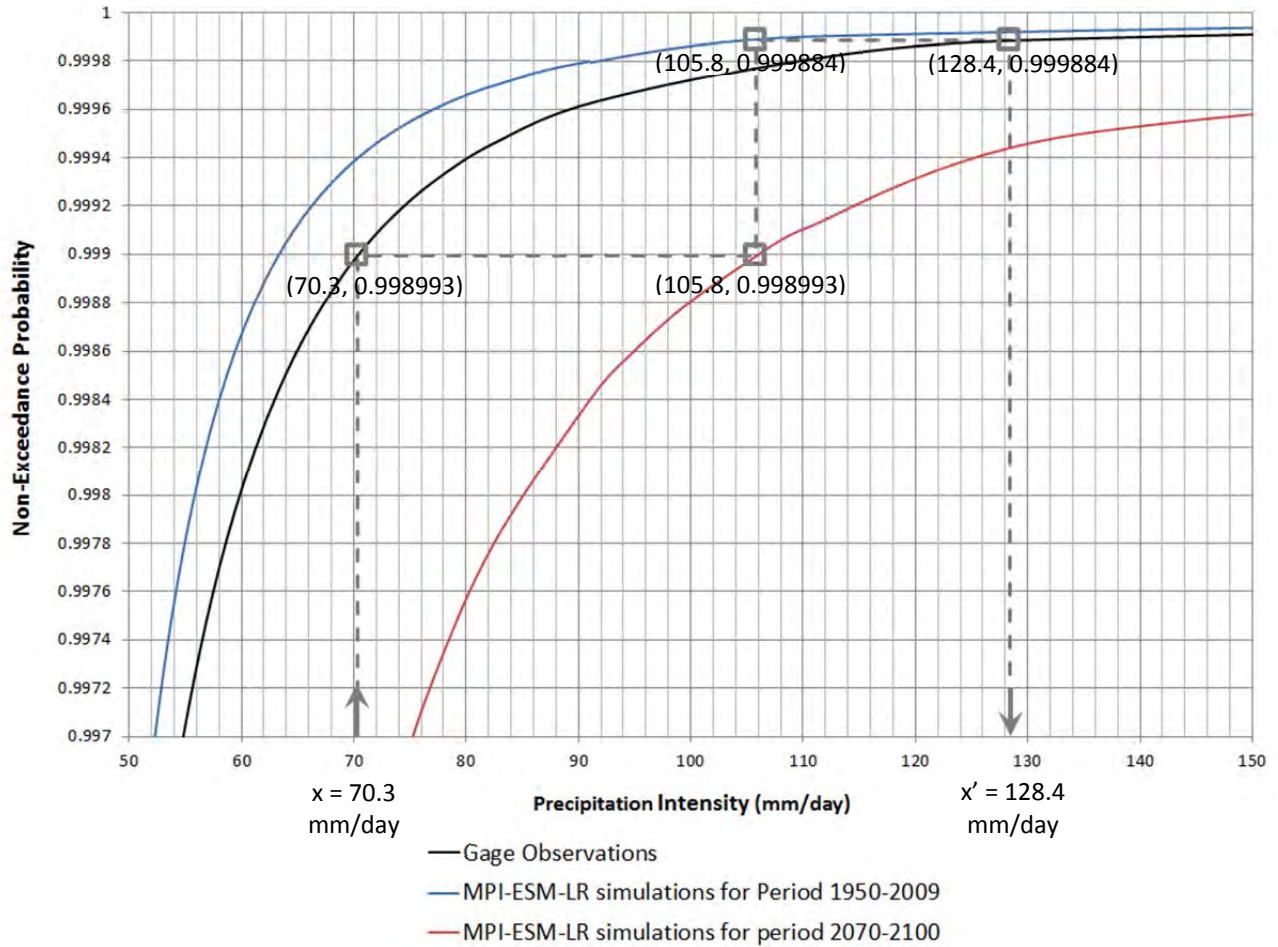


Figure 23. Graphical representation of the calculations in our case example. The lines show the fitted extreme-value distributions. The observed gauge value 70.3 mm/day is replaced with value 128.4 mm/day in the future time series that represents the MPI-ESM-LR scenario. The change in the non-exceedance probability in the observations-based distribution (from 0.998993 for 70.3 mm/day to 0.999884 for 128.4 mm/day) is the same as the change from the historical GCM simulation (blue line) to the future GCM simulation (red line).

### 3.4 Return periods of daily precipitation in the future scenarios

The return period of the few largest values observed at the gauge can in general not be estimated by means of an empirical equation simply on the basis of the sample size. Instead, an extreme value distribution is fitted to the highest values – as done in the previous section –, and this distribution is then used to estimate the return period of each of those values. Assuming, as an approximation, that the data are not serially correlated, then we can write for the return period,  $T(x)$ :

Equation 11

$$T(x) = \frac{1}{(1 - F(x)) \cdot n_w}$$



In Equation 11,  $T(x)$  is the return period given in years of the daily value  $x$ , and  $n_w$  is the mean number of wet days in a year. The decline in  $n_w$  projected in both scenarios selected for this study (and for most of the 12 original downscaled scenarios) results in an increase in what otherwise would be the return period of any given value of  $x$ . To create our future scenario time series, we took the value of  $n_w$  recorded at the gauge, and altered it for each scenario according to the percent change indicated by the downscaled global climate models results. The final  $n_w$  values are given in Table 8.

Using Equation 11, we find that the estimated return period for the maximum value observed at the gauge, 158.6 mm/day, has a return period of about 98 years.

Table 8 lists the daily precipitation totals for fixed return periods of 10, 100 and 200 years. The 100-year return period is close to the estimated return period of the largest daily value observed at the gauge (158.6 mm/day, with an estimated return period of 98 years), hence the maximum value in each time series will be close to the 100-year values shown in Table 8. A case example computation from Table 8 is provided next.

**Table 8. Daily precipitation values (in millimeters) for fixed return periods, for different scenarios and time horizons. The agreement between the values for each GCM’s historical period and the gauge observations results by construct of the algorithm described in the text.**

Time Period	$n_w$ (average no. wet days per year)	Daily Precipitation Values (mm/day) for Fixed Return Periods		
		10 Years	100 Years	200 Years
<b>Gauge Observations</b>				
<b>WY 1963-2009</b>	170.7	81	159(*)	200
<b>MPI-ESM-LR</b>				
<b>1950-2009</b>	170.7	81	159	200
<b>2010-2039</b>	167.0	143	404	558
<b>2040-2069</b>	162.9	159	392	514
<b>2070-2100</b>	160.3	154	382	507
<b>CanESM2</b>				
<b>1950-2009</b>	170.7	81	159	200
<b>2010-2039</b>	166.0	96	215	278
<b>2040-2069</b>	167.9	91	200	264
<b>2070-2100</b>	162.2	105	213	267

(\*) The maximum precipitation value recorded at the gauge in a day (defined from midnight to midnight) was 158.6 mm/day, which has an estimated return period of about 98 years.

## Case Example

The following is the calculation of the entry in Table 8 for MPI-ESM-LR, period 2070-2100, return period of 100 years.

Rearranging Equation 11 we write:

Equation 12

$$F(x) = 1 - \frac{1}{T(x) \cdot n_w}$$

For  $T(x) = 100$  years, and  $n_w = 160.3$  days/year (from Table 8), Equation 12 becomes:

Equation 13

$$\begin{aligned} F(x) &= 1 - \frac{1}{100 \cdot 160.3} \\ &= 0.9999376 \end{aligned}$$

We insert the result from Equation 13 into Equation 6 and use the distribution parameters from Table 7, to obtain:

Equation 14

$$\begin{aligned} x &= \frac{9.87}{0.45} \cdot \left[ \left( 1 - \frac{0.9999376 - 0.98276}{1 - 0.98276} \right)^{-0.45} - 1 \right] + 49 \\ &= 302.4 \text{ mm/day} \end{aligned}$$

We then apply Equation 4 with the parameters in Table 7:

Equation 15

$$\begin{aligned} F_{MPI}^h(302.4) &= \left\{ 1 - \left( 1 + 0.4 \cdot \left( \frac{302.4 - 49}{6.69} \right)^{\frac{1}{0.4}} \right) \right\} \cdot (1 - 0.9953) + 0.9953 \\ &= 0.99999551 \end{aligned}$$

And the result is given by Equation 9 with the parameters in Table 7:

Equation 16

$$\begin{aligned} x' &= \frac{8.48}{0.38} \cdot \left[ \left( 1 - \frac{0.99999551 - 0.99339}{1 - 0.99339} \right)^{-0.38} - 1 \right] + 47 \\ &= 381.6 \text{ mm} \end{aligned}$$

## 4. Evaluation of the GCM-based scenarios and choice of final scenarios

Review of Table 8 shows that the MPI-ESM-LR scenario is not only very extreme, but also indicates a large sudden change from historical conditions to the very first time horizon, 2010-2039. Its 100-year and 200-year return values for 2010-2039 are more than 2.5 times those for 1950-2009. Such a sudden change in climate appears unrealistic and may possibly be an artifact of the automated BCCAQ downscaling methodology when applied to the more extreme portion of the distribution.

Thus, we used the CanESM2 but not the MPI-ESM-LR as a scenario for running the HSPF hydrologic model. CanESM2 was used to represent our “moderately high” scenario for 2070-2100. We saw in Table 8 that the CanESM2 100-year and 200-year return values for 2070-2100 are about 34% higher than the corresponding historical values. This increase in projected extreme precipitation happened despite the fact that the projected value of parameter  $\xi$  was actually lower (0.27) than the CanESM2  $\xi$  value for the historical period ( $\xi = 0.29$ ), and is due to the projected rise in the scale parameter,  $\sigma$  (from 7.09 to 8.16) (Table 7). Parameter  $\xi$  describes the shape of the upper tail of the extreme-value distribution.

For our “extreme high” scenario, we again used the CanESM2 projected scale parameter,  $\sigma = 0.16$ , but we combined it with a more severe than projected  $\xi$  parameter value, by simply using the  $\xi$  value derived from the observations,  $\xi = 0.38$  (in place of the projected value  $\xi = 0.27$ ) (Table 9). The result is an “extreme high” scenario for which projected 100-year and 200-year precipitation values represent a 85% and 100% (respectively) increase over the corresponding historical estimates (Table 10).

The HSPF hydrologic model will be run under the two different future scenario hourly time series of rainfall summarized in Table 9 and Table 10. Each future scenario time series of hourly precipitation is 47 years in length, as a result of having been derived from the time series observed at the Municipal Hall gauge, which covered the 47 water years, 1963-2009. Despite the 47-year length, each future scenario time series represents the climate conditions of a future time horizon of 30 years. Thus, for each of the two selected global climate models (GCMs), there is a future scenario time series at hourly time step and which is 47 years in length, but which represents the time horizon 2070-2100. These time series will be used to drive the hydrologic model.

Each future scenario hourly time series is obtained from the corresponding daily time series, by disaggregating each daily value using the hourly pattern recorded by the gauge on that day. Thus, comparing future scenario hourly values to the original gauge records, the multiplying factor for each hourly value is determined by the ratio between the future and the observed daily values. As a consequence, the hourly values in days with very high precipitation totals receive the highest multiplication factors.

Table 9. Parameter values of the generalized Pareto distribution (GPD) used to create our two scenarios for HSPF. The parameters of the two scenarios are the same (obtained from the extreme-value analysis of the CanESM2 results), except that the extreme high scenario is created by altering the value of parameter  $\xi$ , from 0.27 to 0.29.

Time Period	Average number of wet days per year $n_w$	Threshold $u$ (mm) and $F(u)$	Number of exceedances	$\hat{\sigma}$	$\hat{\xi}$
<b>Gauge Observations</b>					
<b>WY 1963-2009</b>	170.7	47 0.99339	53	8.48	0.38
<b>Extreme high scenario (based on CanESM2 by altering <math>\xi</math>)</b>					
<b>2070-2100</b>	184.1	51 0.99071	53	8.16	0.38
<b>Moderately high scenario (based on CanESM2)</b>					
<b>2070-2100</b>	184.1	51 0.99071	53	8.16	0.27

Table 10. Daily precipitation values (in millimeters) for fixed return periods, for final selected scenarios for HSPF.

Time Period	$n_w$ (average no. wet days per year)	Daily Precipitation Values (mm/day) for Fixed Return Periods		
		10 Years	100 Years	200 Years
<b>Gauge Observations</b>				
<b>WY 1963-2009</b>	170.7	81	159(*)	200
<b>Extreme high scenario (based on CanESM2 by altering <math>\xi</math>)</b>				
<b>2070-2100</b>	162.2	106	294	402
<b>Moderately high scenario (based on CanESM2)</b>				
<b>2070-2100</b>	162.2	105	213	267

(\*) The maximum precipitation value recorded at the gauge in a day (defined from midnight to midnight) was 158.6 mm/day, which has an estimated return period of about 98 years.

## 5. References

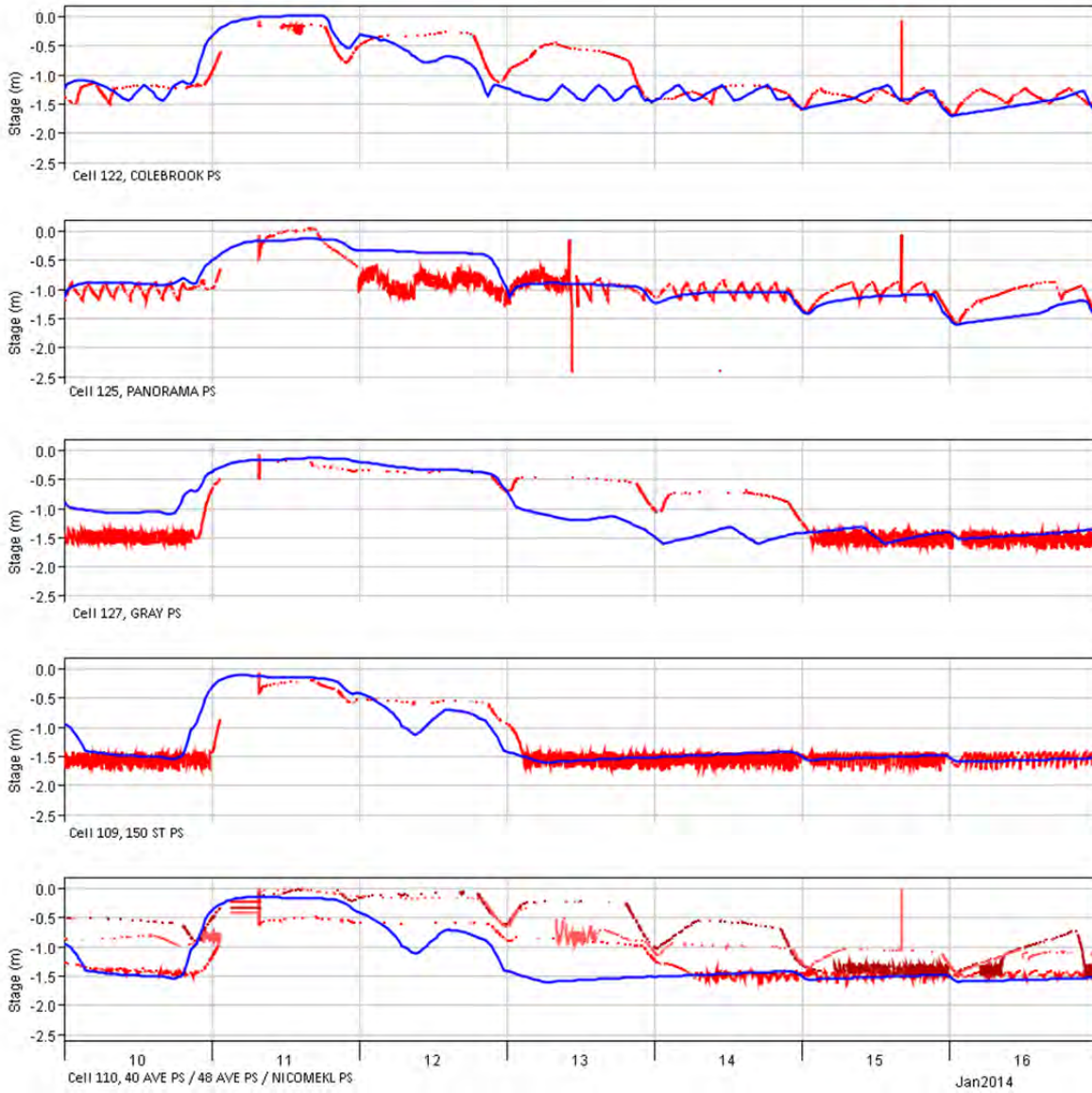
- Coles S. (2001) An introduction to statistical modeling of extreme values. Springer-Verlag, London, UK. 208 pp. WA273.6.C63 2001.
- Hawkins E., Sutton R. (2010) The potential to narrow uncertainty in projections of regional precipitation change. *Clim Dyn* 37:407–418. DOI:10.1007/s00382-010-0810-6.
- IPCC (Intergovernmental Panel on Climate Change) (2012) Managing the risks of disasters to advance climate change adaptation. In Field, C.B., et al. (Editors) A Special Report of Working Groups I and II of the Intergovernmental Panel on Climate Change. Cambridge University Press, Cambridge, UK, and New York, NY, USA, pp. 1-19.
- Kundewicz A.W., Kanae S., Seneviratne S.I., Handmer J., Nicholls N., Peduzzi P., Mechler R., Bouwer L.M., Arnell N., Mach K., Muir-Wood R., Brakenridge G. R., Kron W., Benito G., Honda Y., Takahashi K., Sherstyukov B. (2013) Flood risk and climate change: global and regional perspectives. *Hydrological Sciences Journal - Journal des Sciences Hydrologiques* 59(1): 1-28. DOI: 10.1080/02626667.2013.857411.

**APPENDIX D**

Hydraulic Analysis

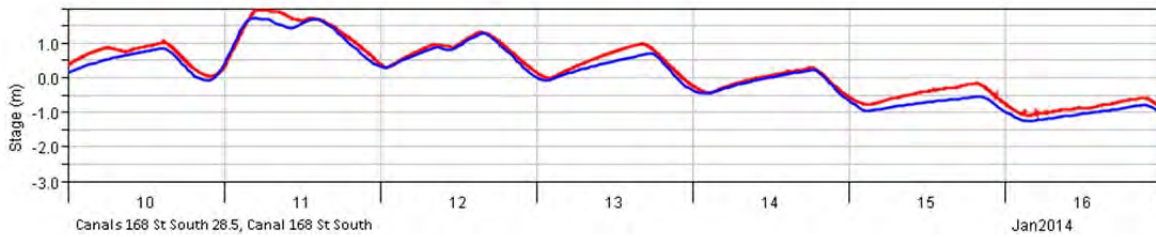
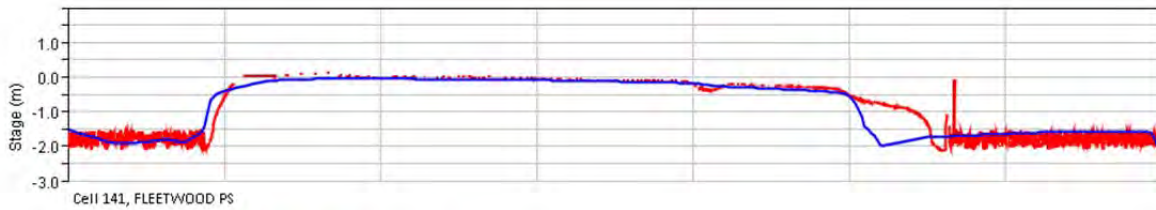
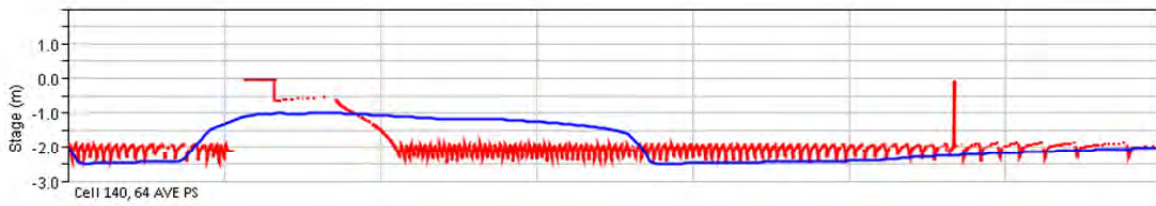
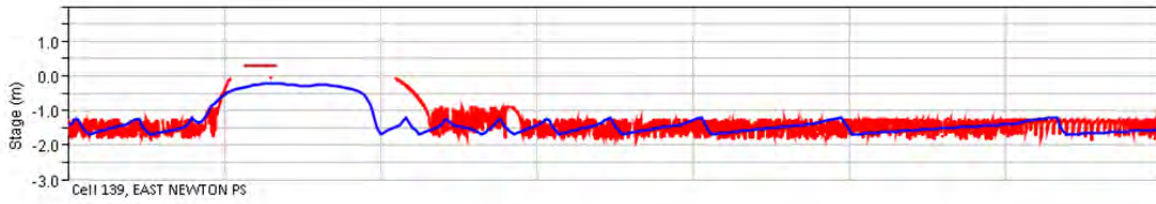
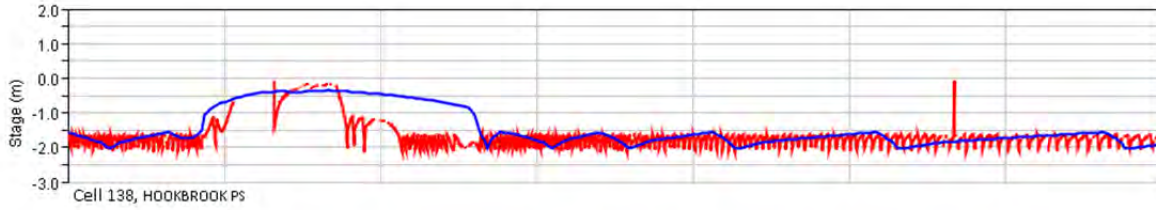
# January 2014

## Floodplain Cells



# January 2014

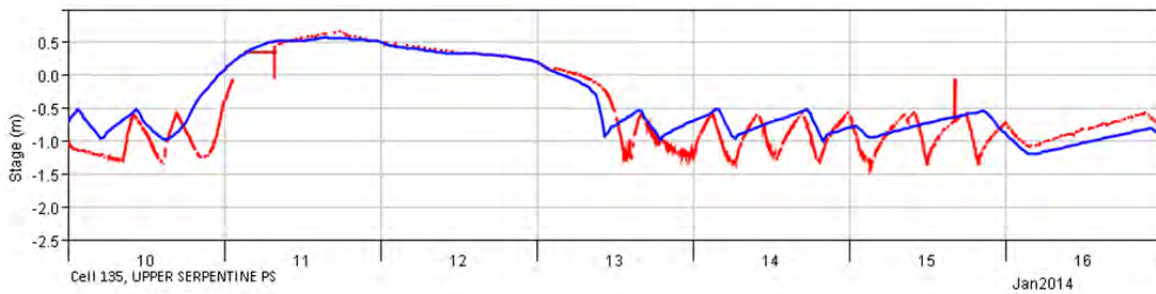
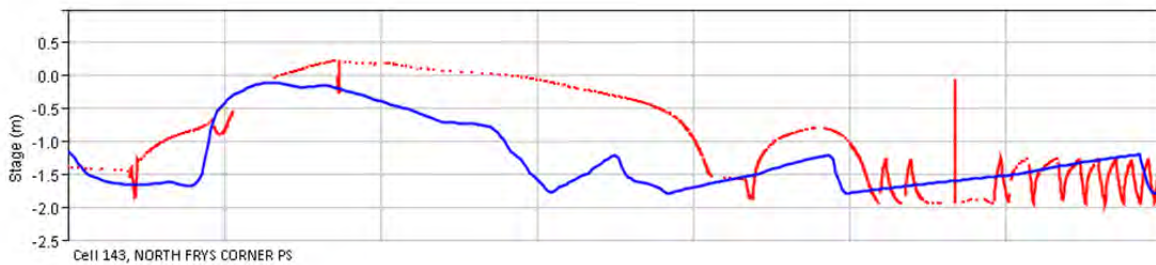
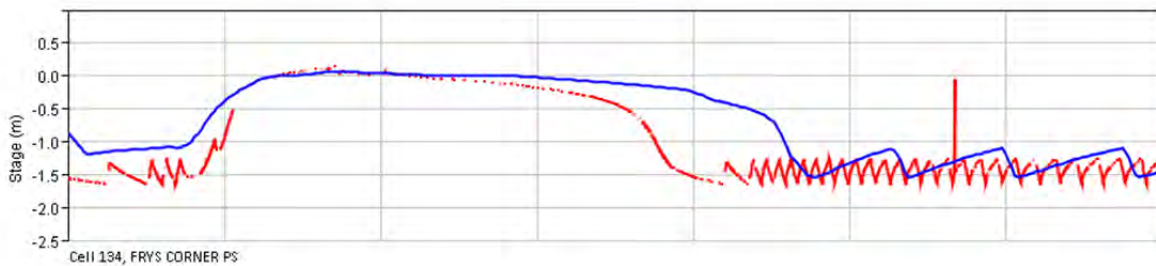
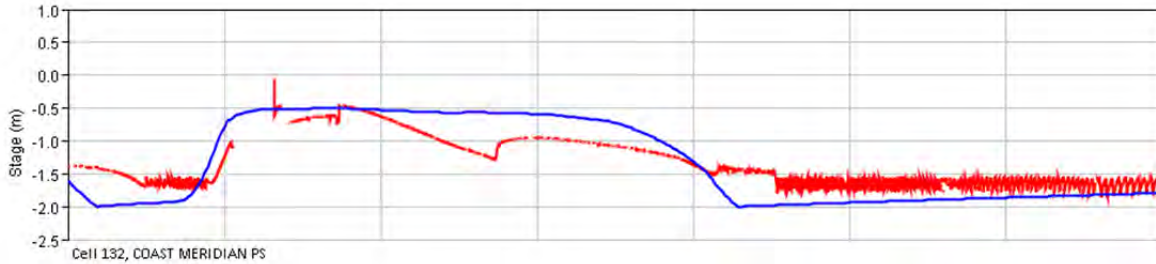
## Floodplain Cells





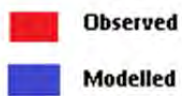
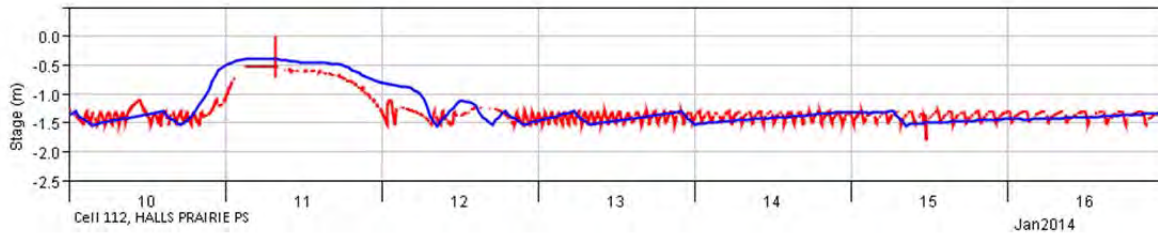
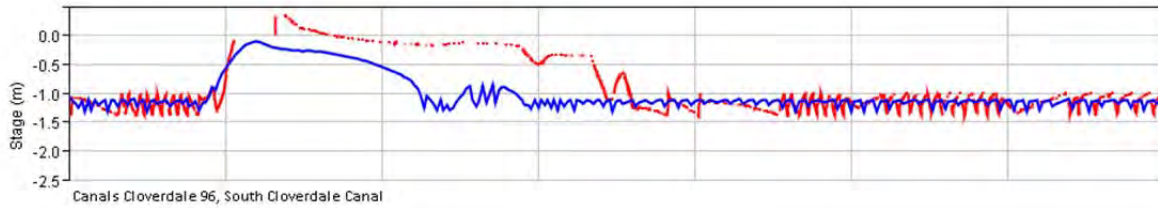
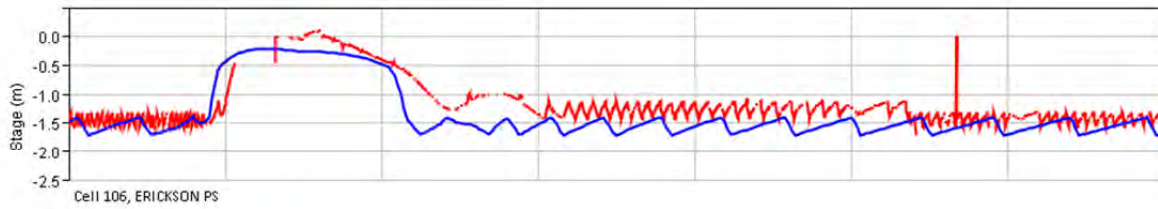
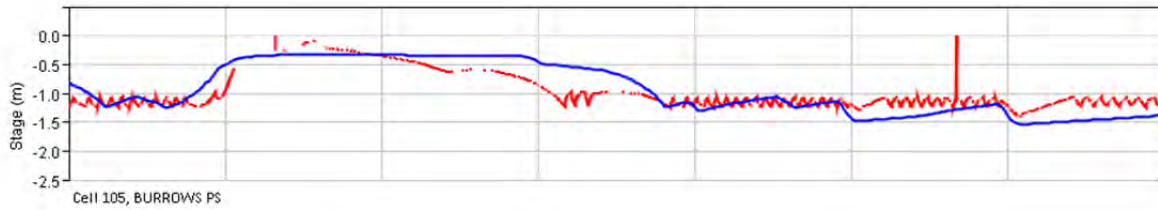
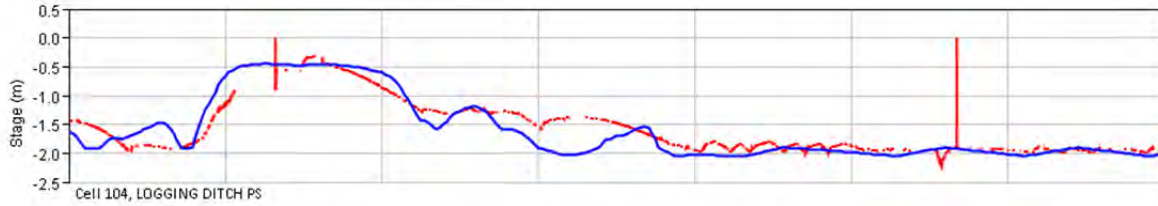
# January 2014

## Floodplain Cells



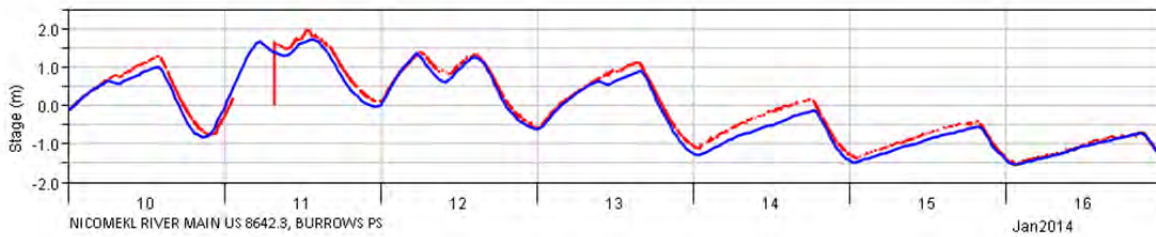
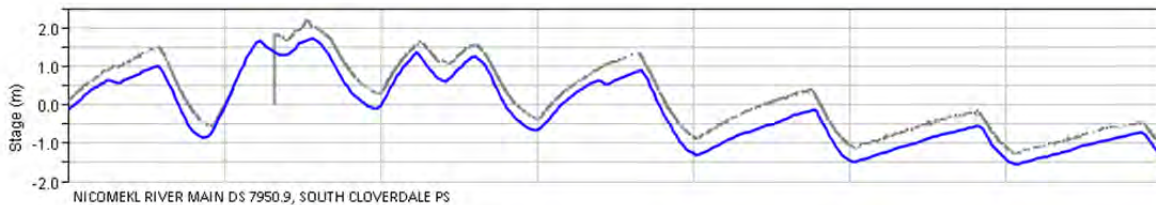
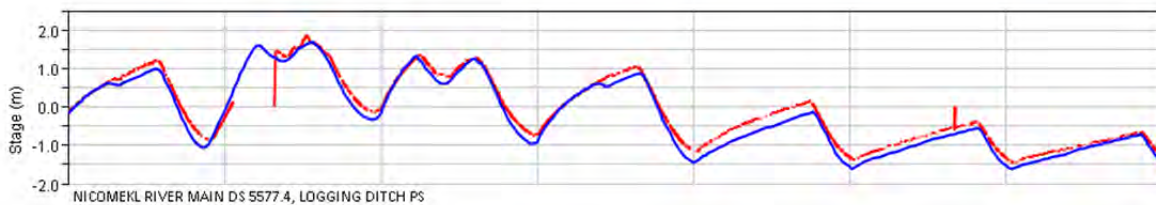
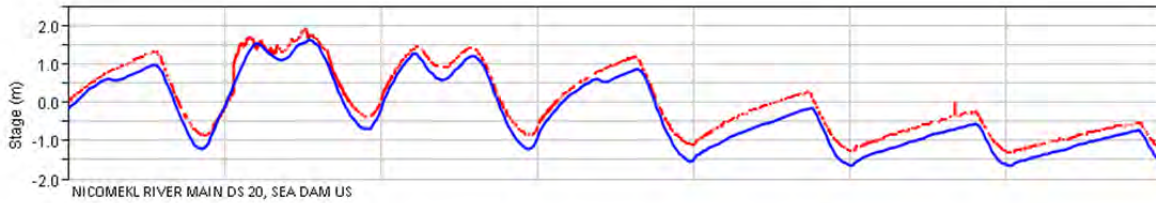
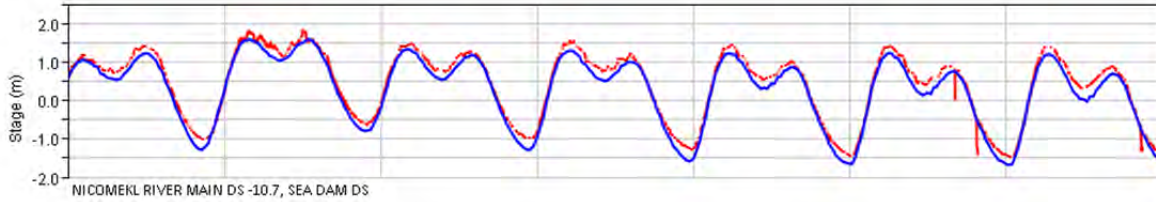
# January 2014

## Floodplain Cells



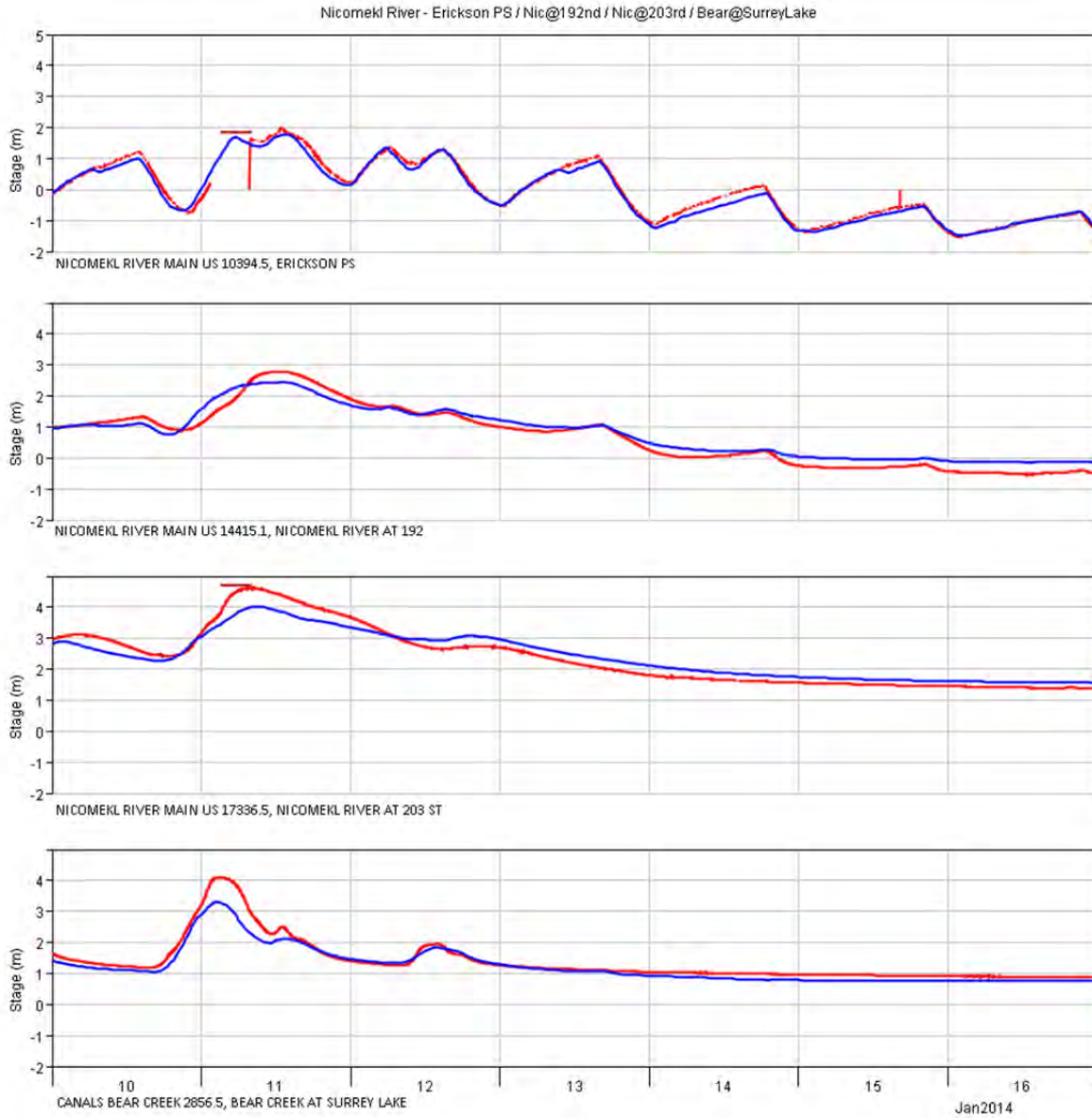
# January 2014

## Channel



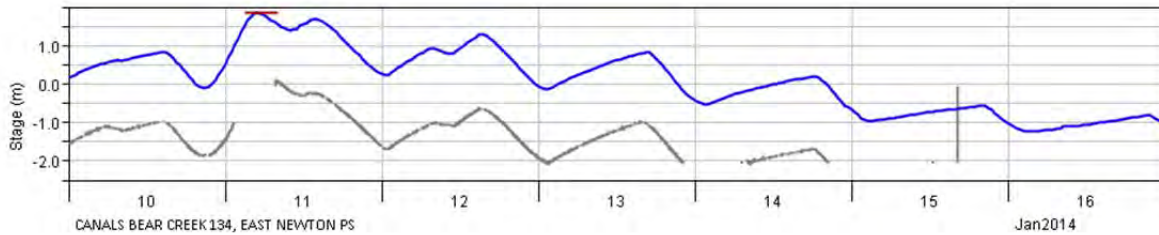
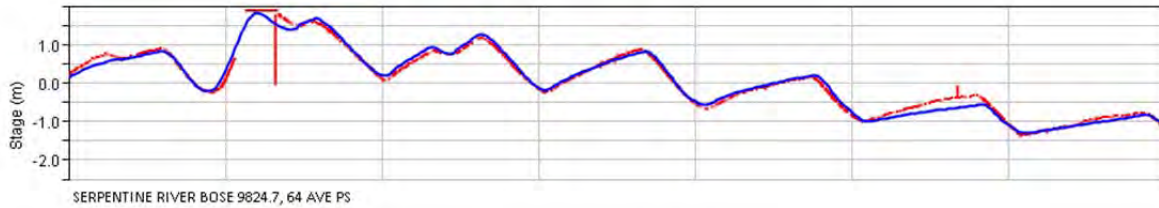
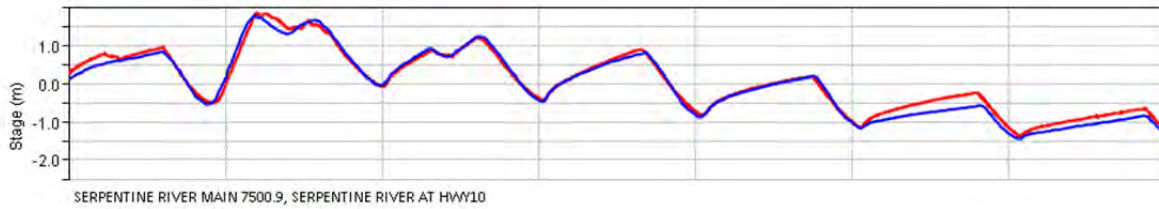
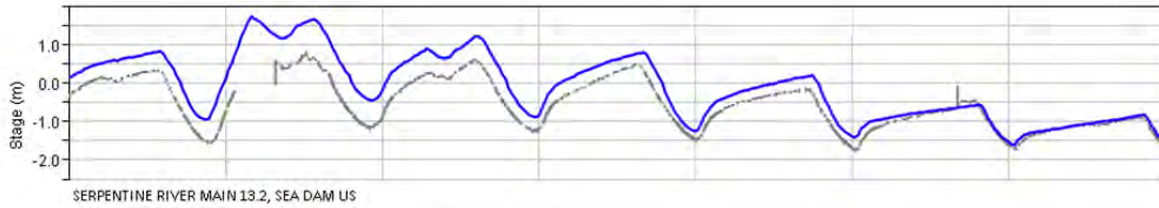
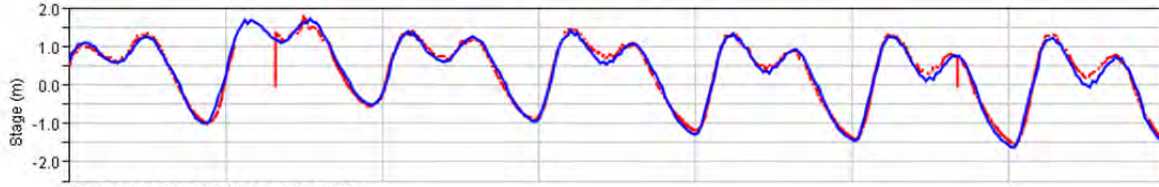
# January 2014


## Channel



# January 2014

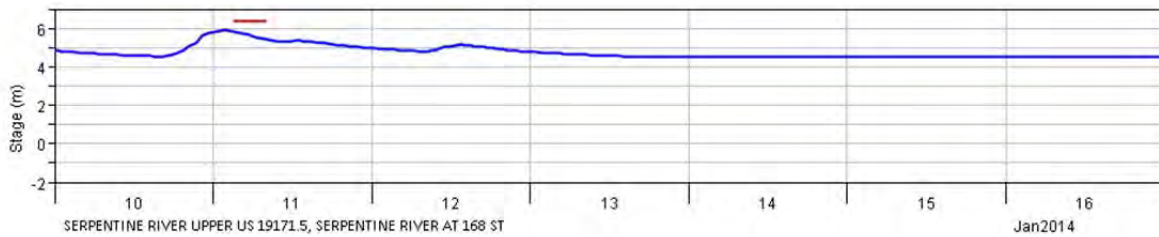
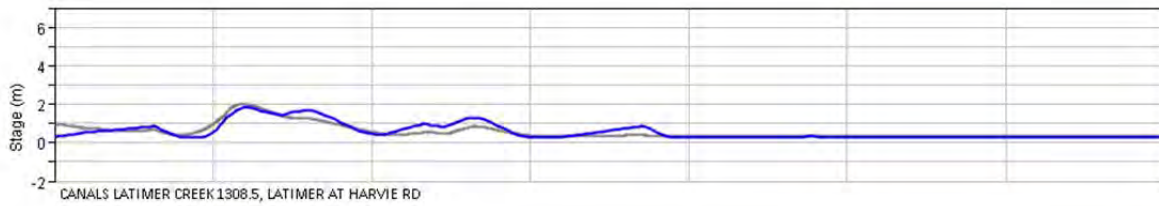
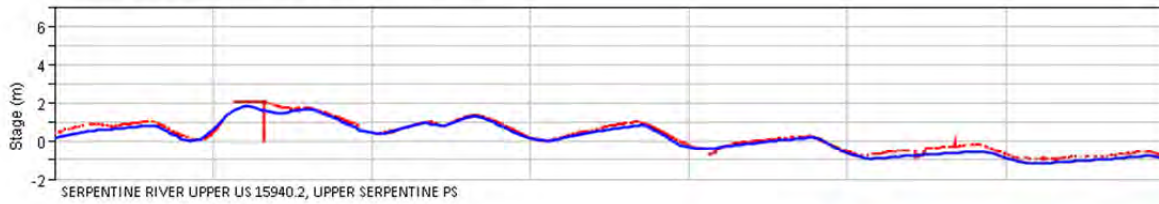
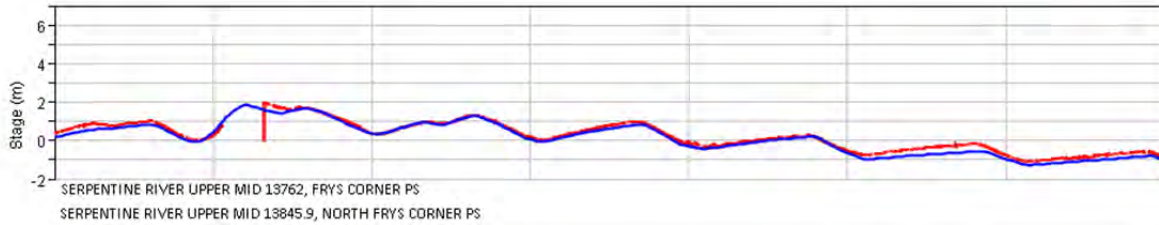
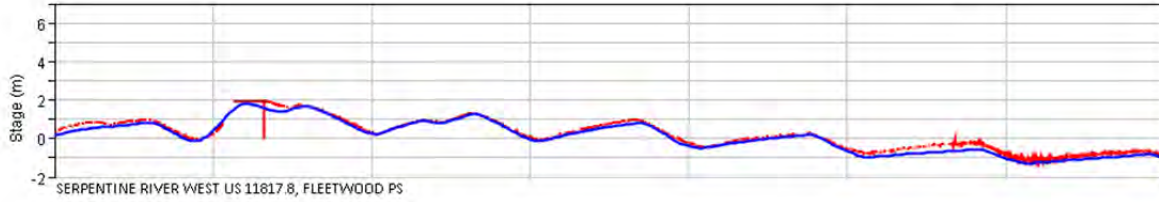
## Channel



 **Observed**  
 **Modelled**

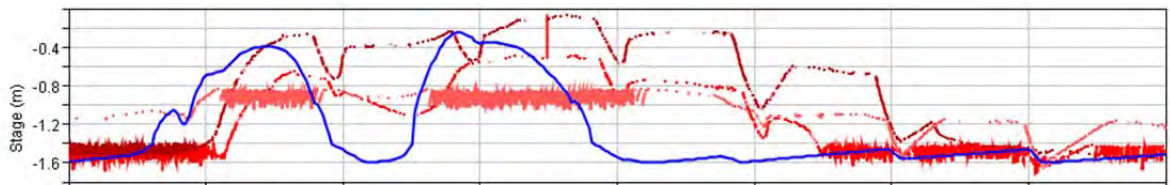
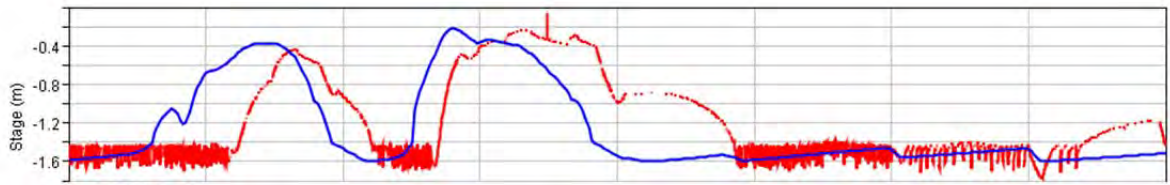
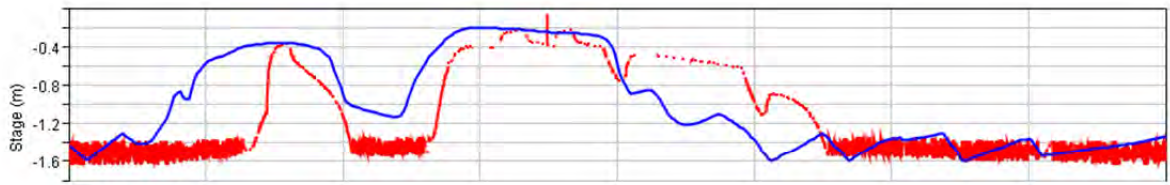
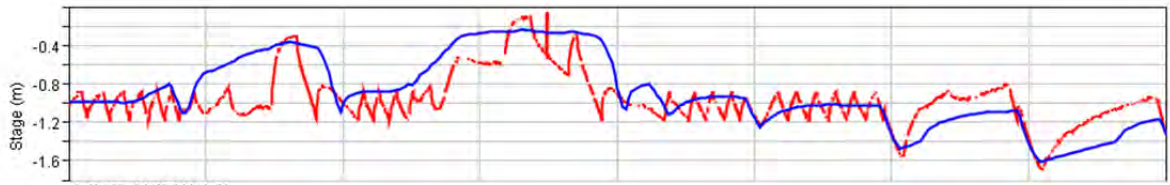
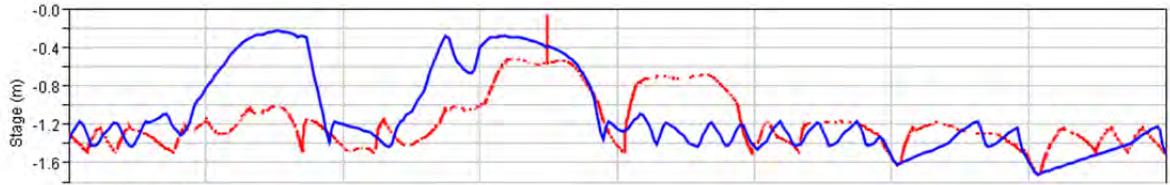
# January 2014

## Channel

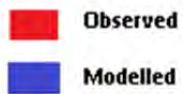


# January 2014

## Channel

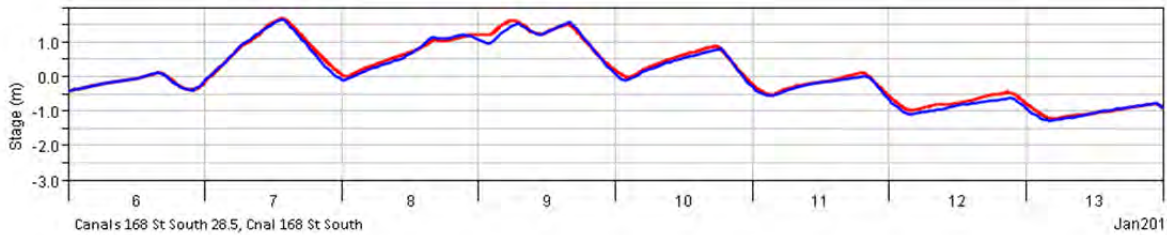
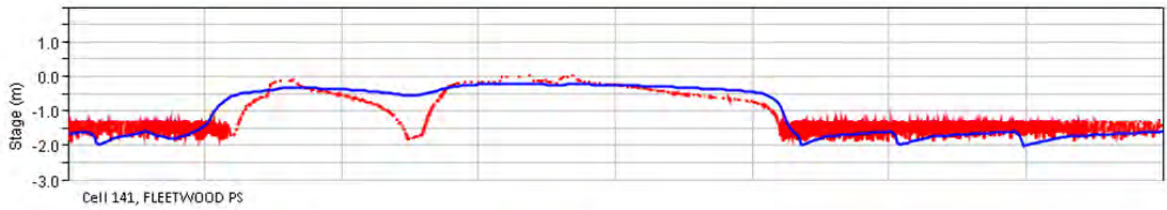
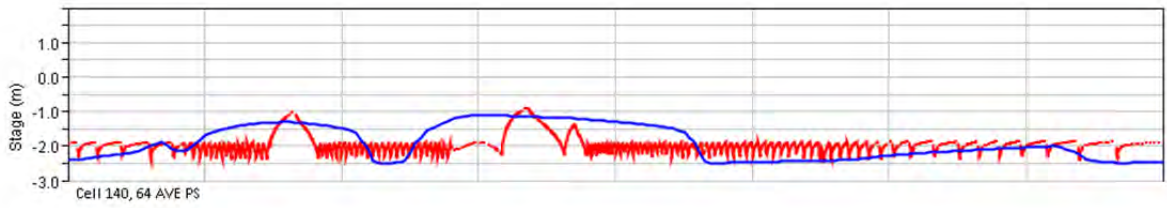
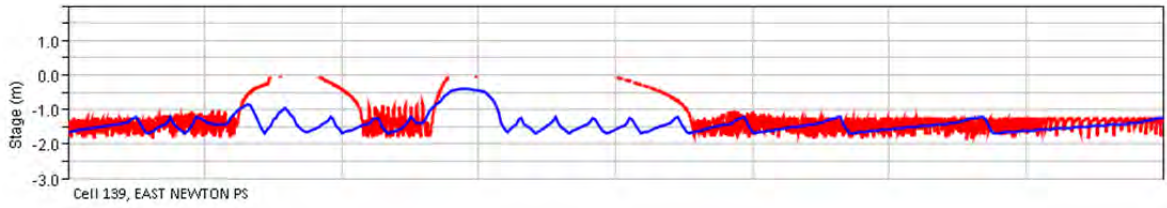
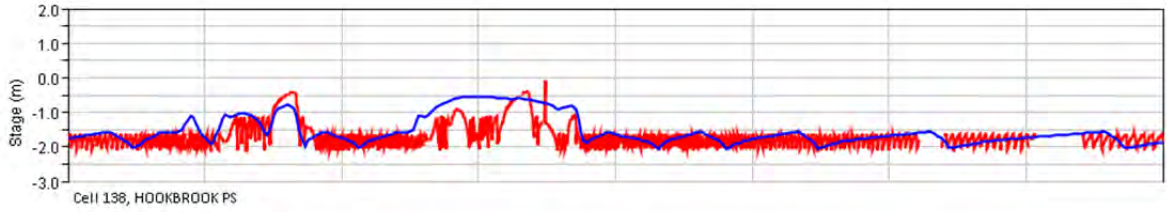


Jan2013



# January 2013

## Floodplain Cells



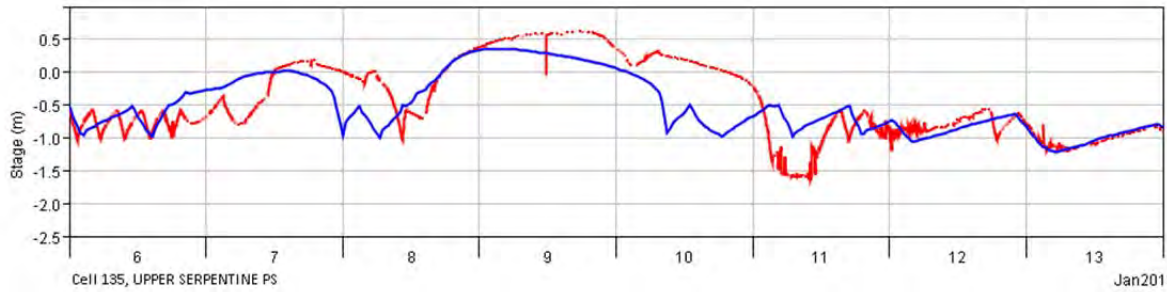
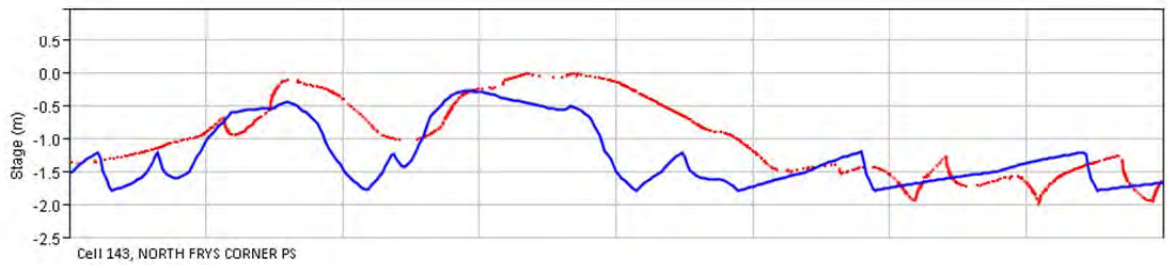
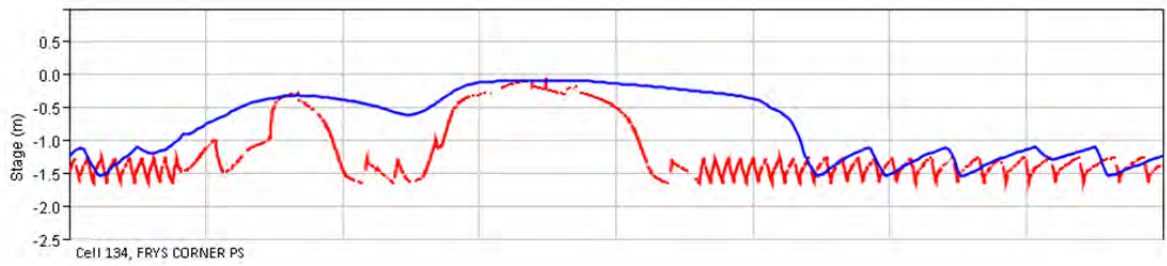
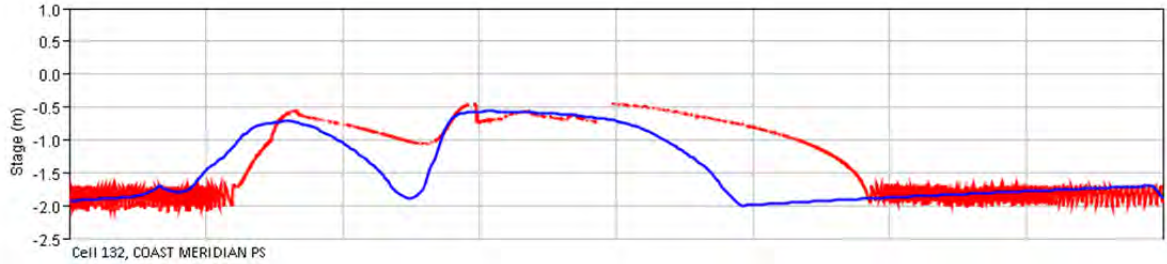
Jan2013





# January 2013

## Floodplain Cells

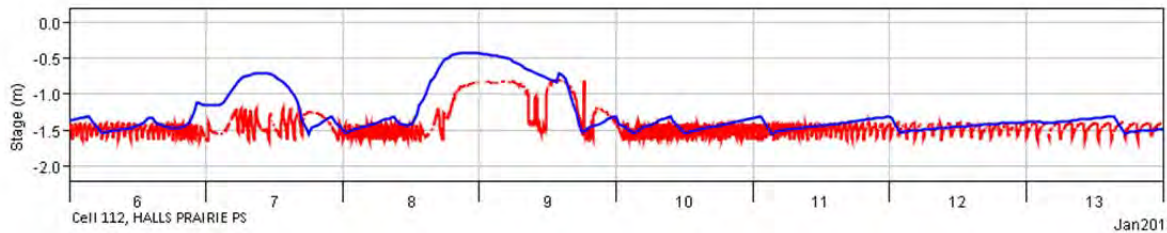
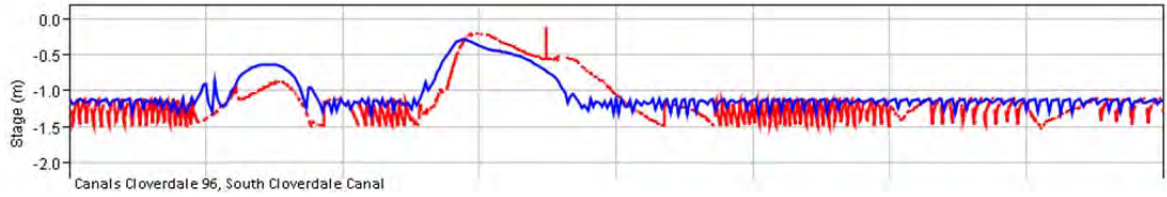
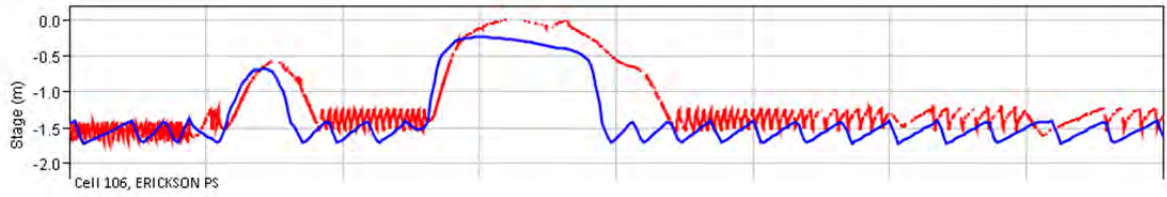
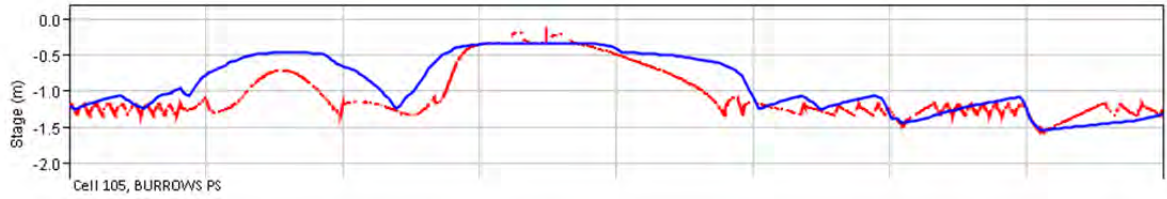
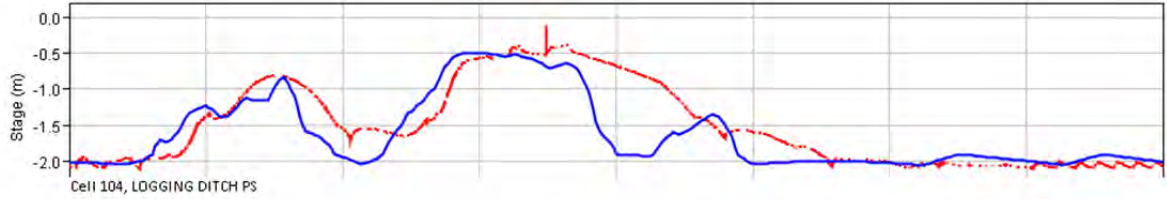


Jan2013



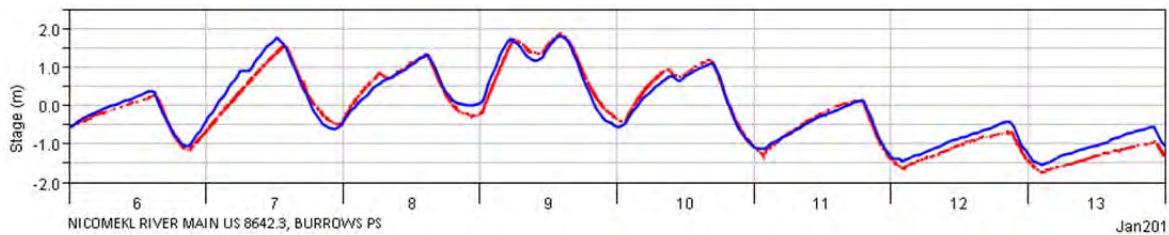
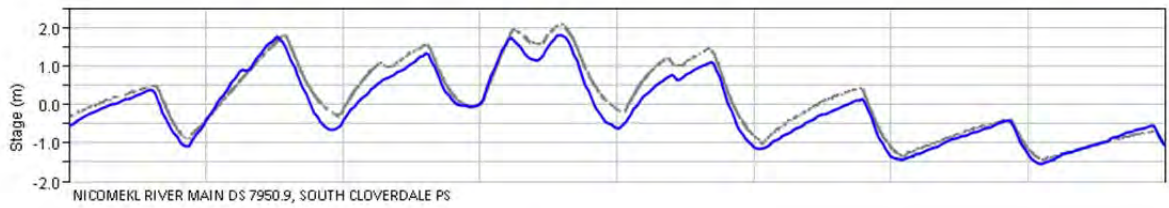
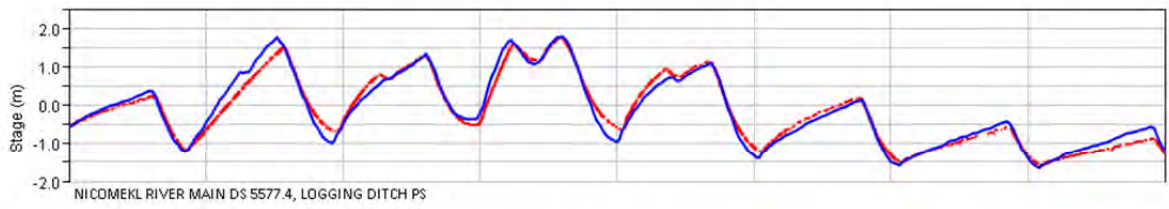
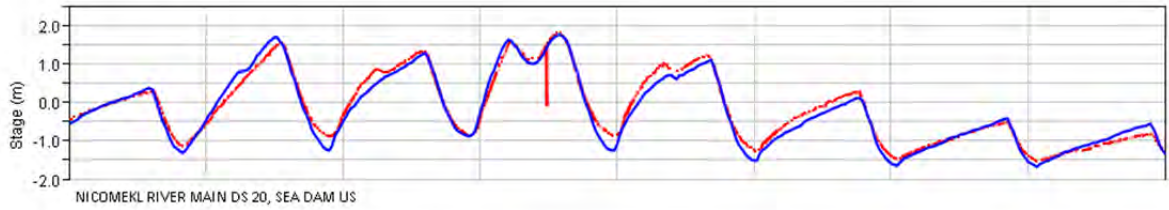
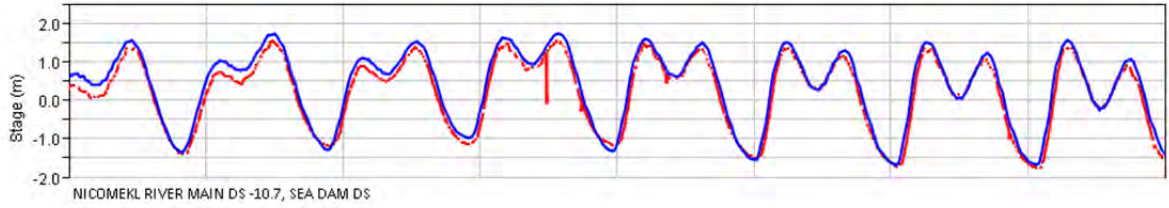
# January 2013

## Floodplain Cells

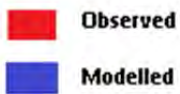


# January 2013

## Channel

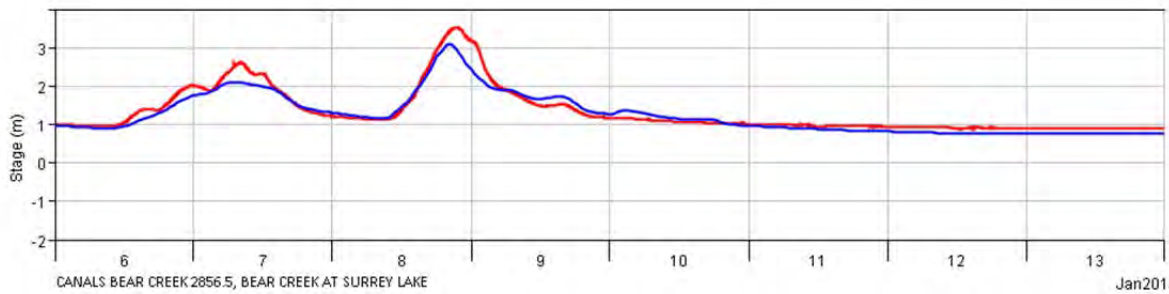
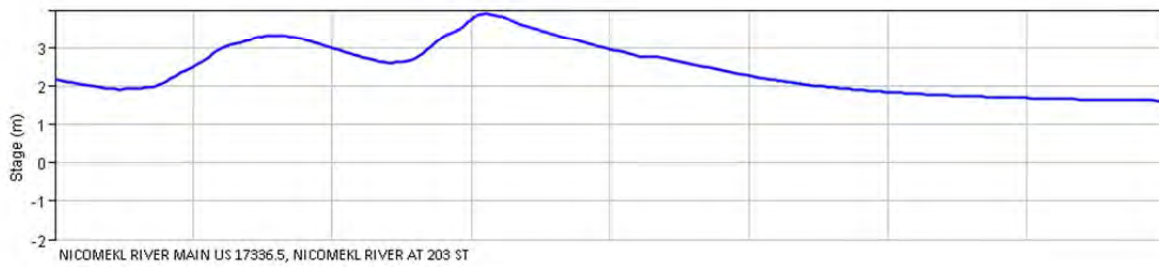
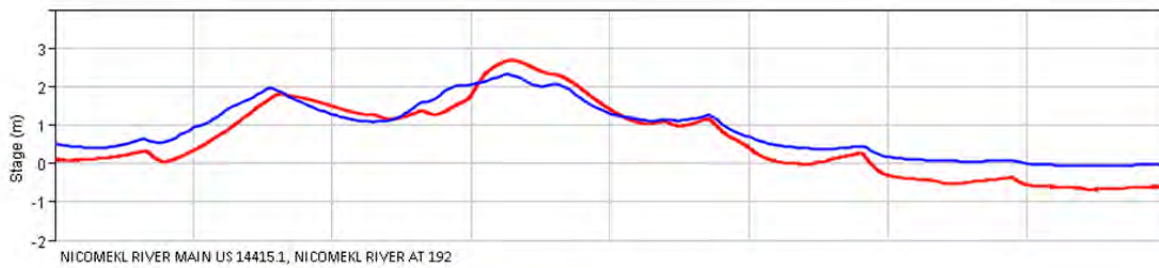
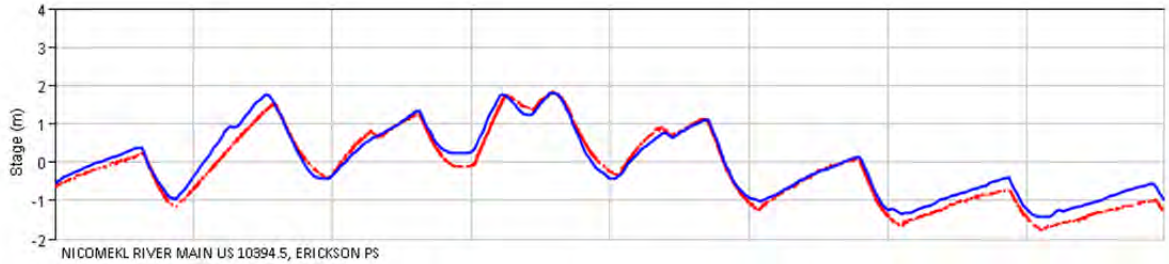


Jan2013



# January 2013

## Channel

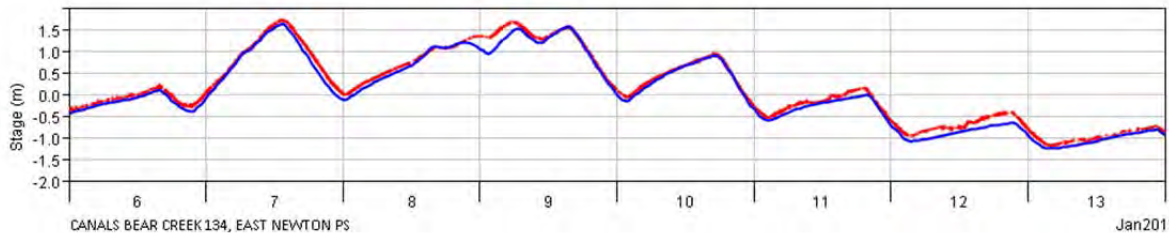
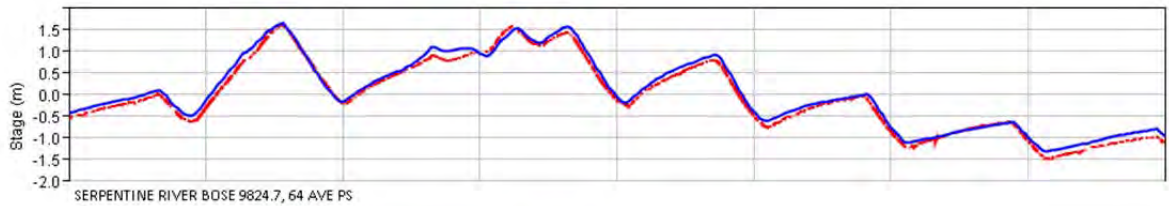
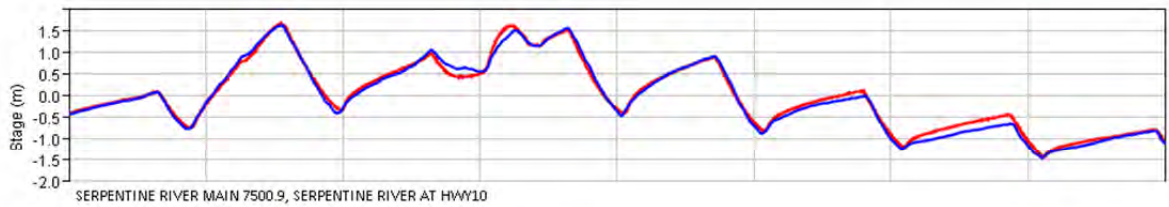
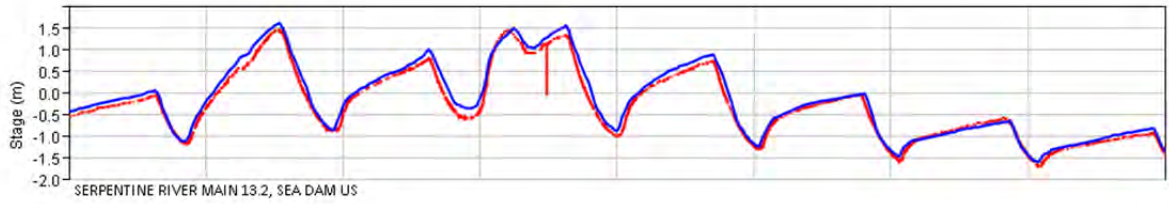
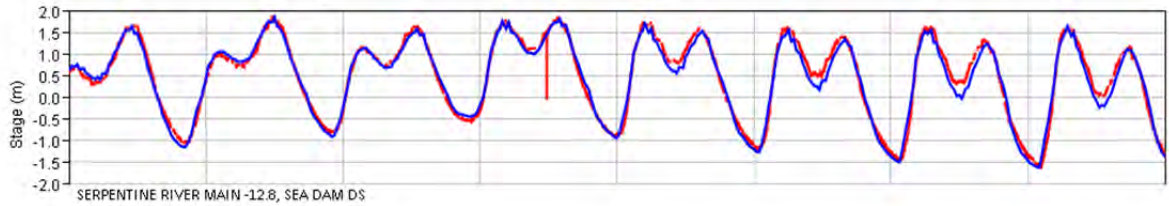


Jan2013

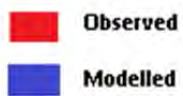
 **Observed**  
 **Modelled**

# January 2013

## Channel

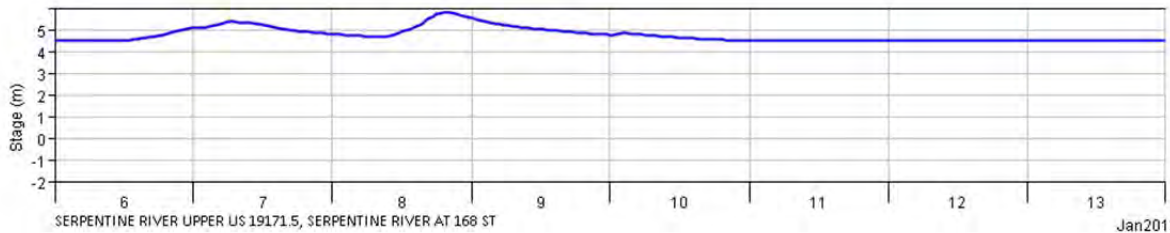
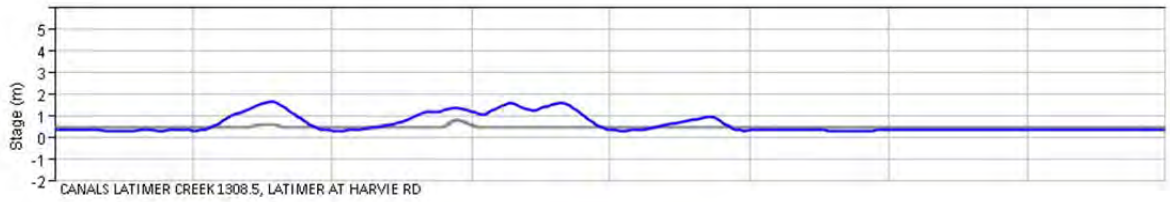
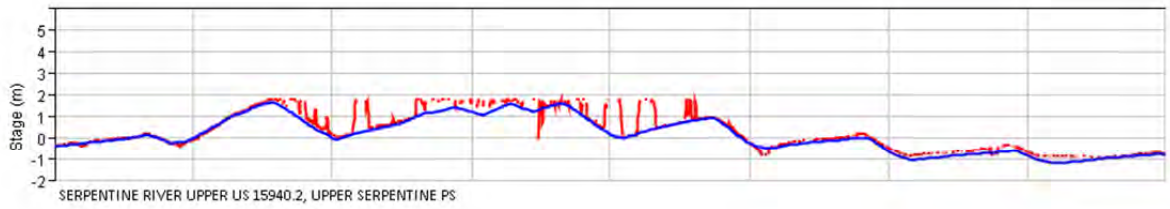
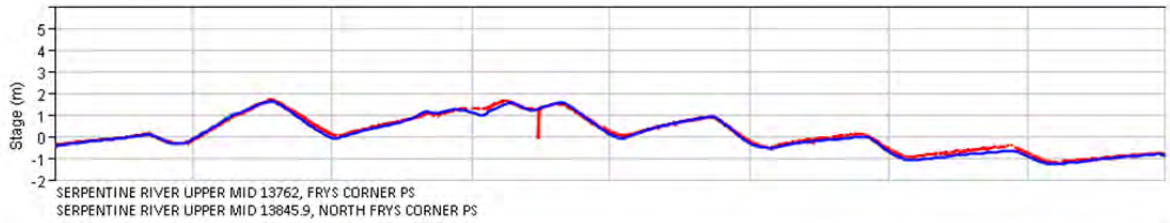
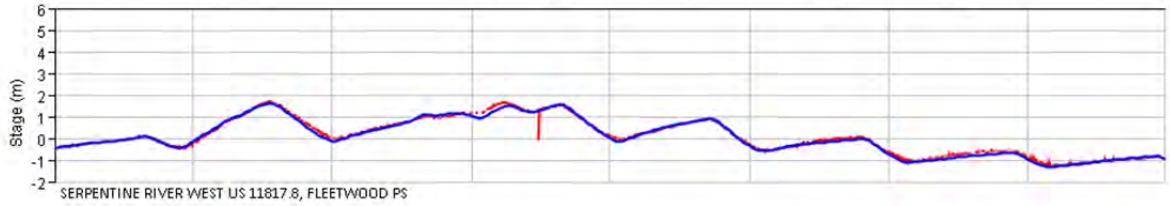


Jan2013





# January 2013

## Channel

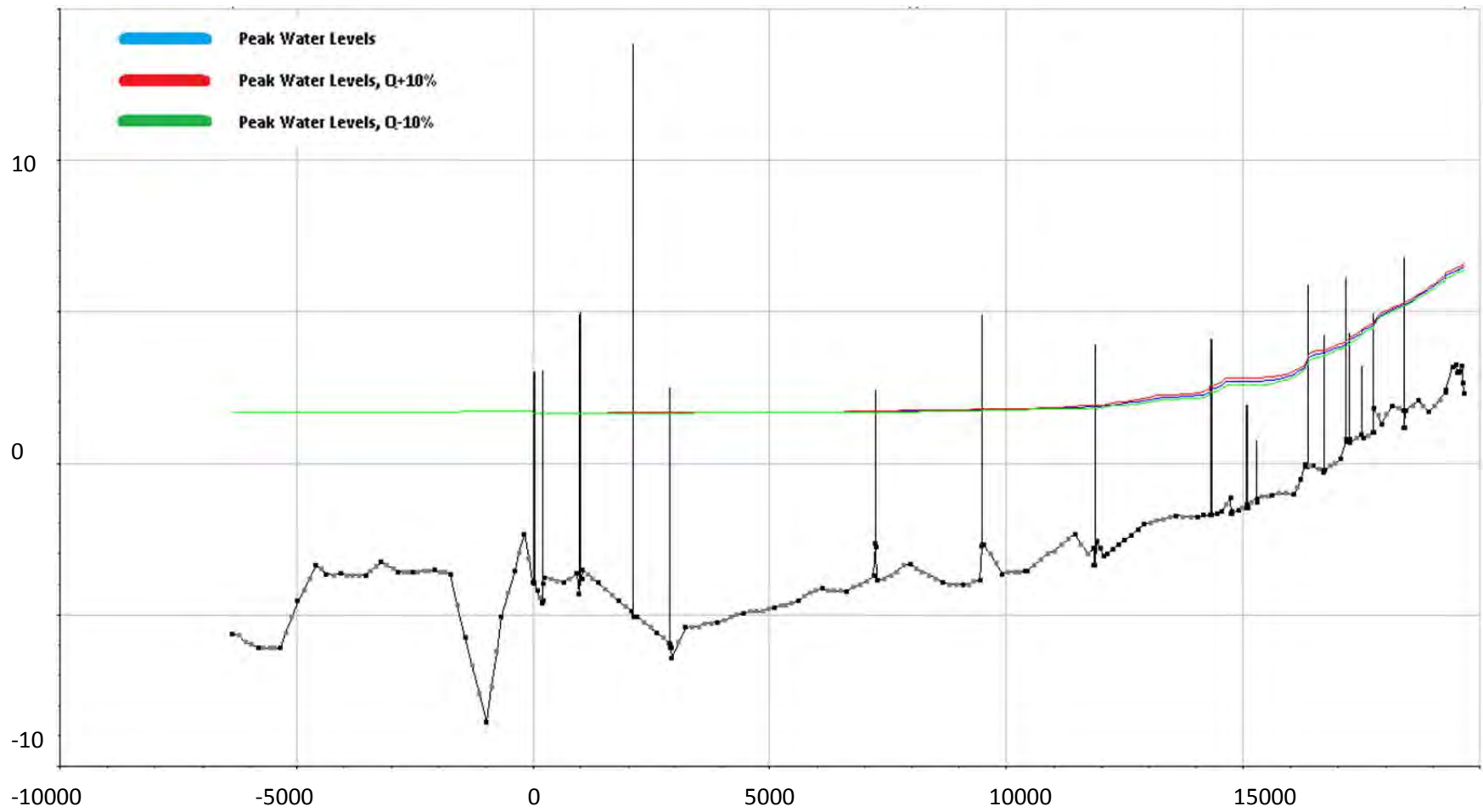


Jan2013

 **Observed**  
 **Modelled**

January 2014

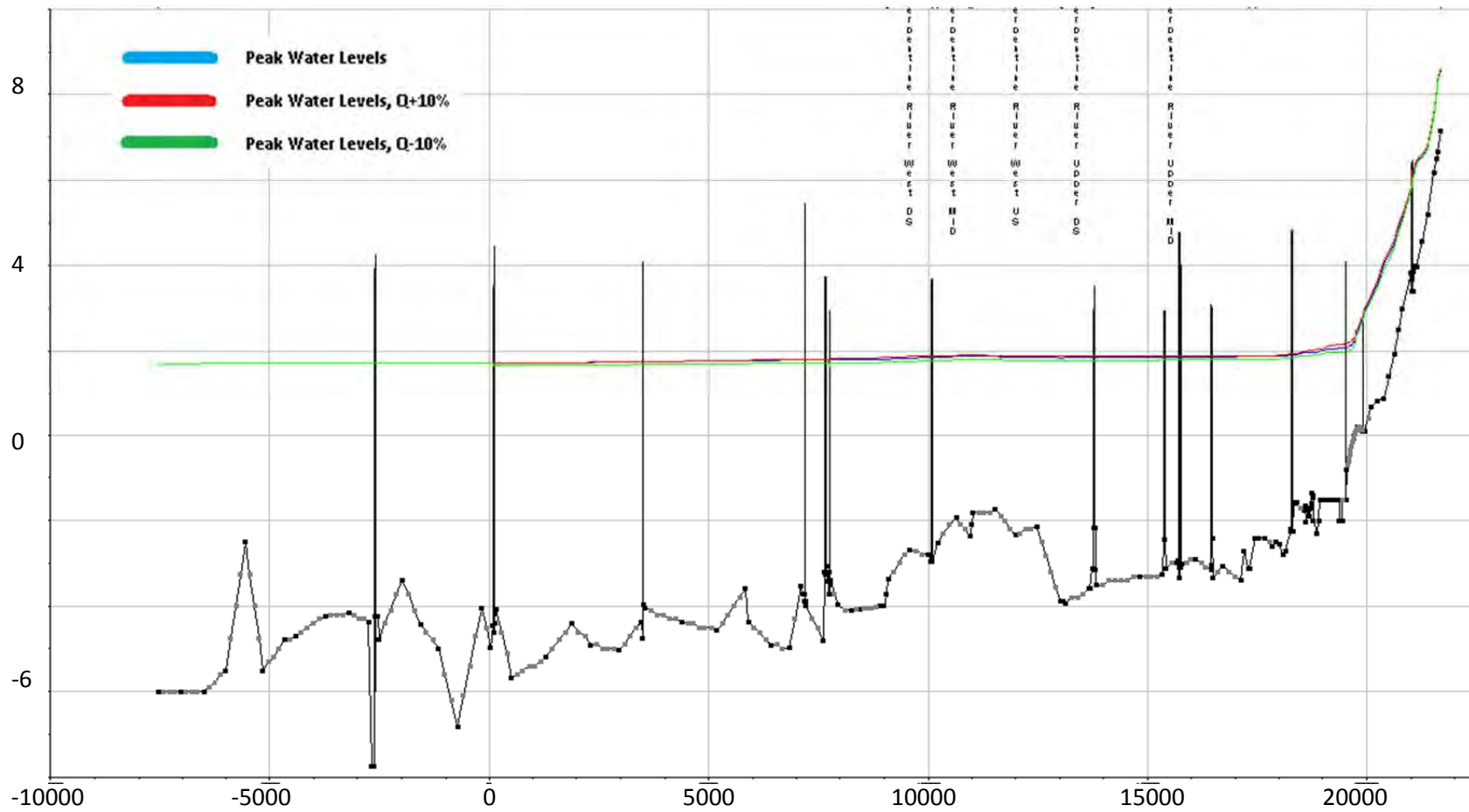
Sensitivity Analysis,  $Q \pm 10\%$



Nicomekl River longitudinal profile (Chainage 0 = sea dam)

January 2014

Sensitivity Analysis,  $Q \pm 10\%$

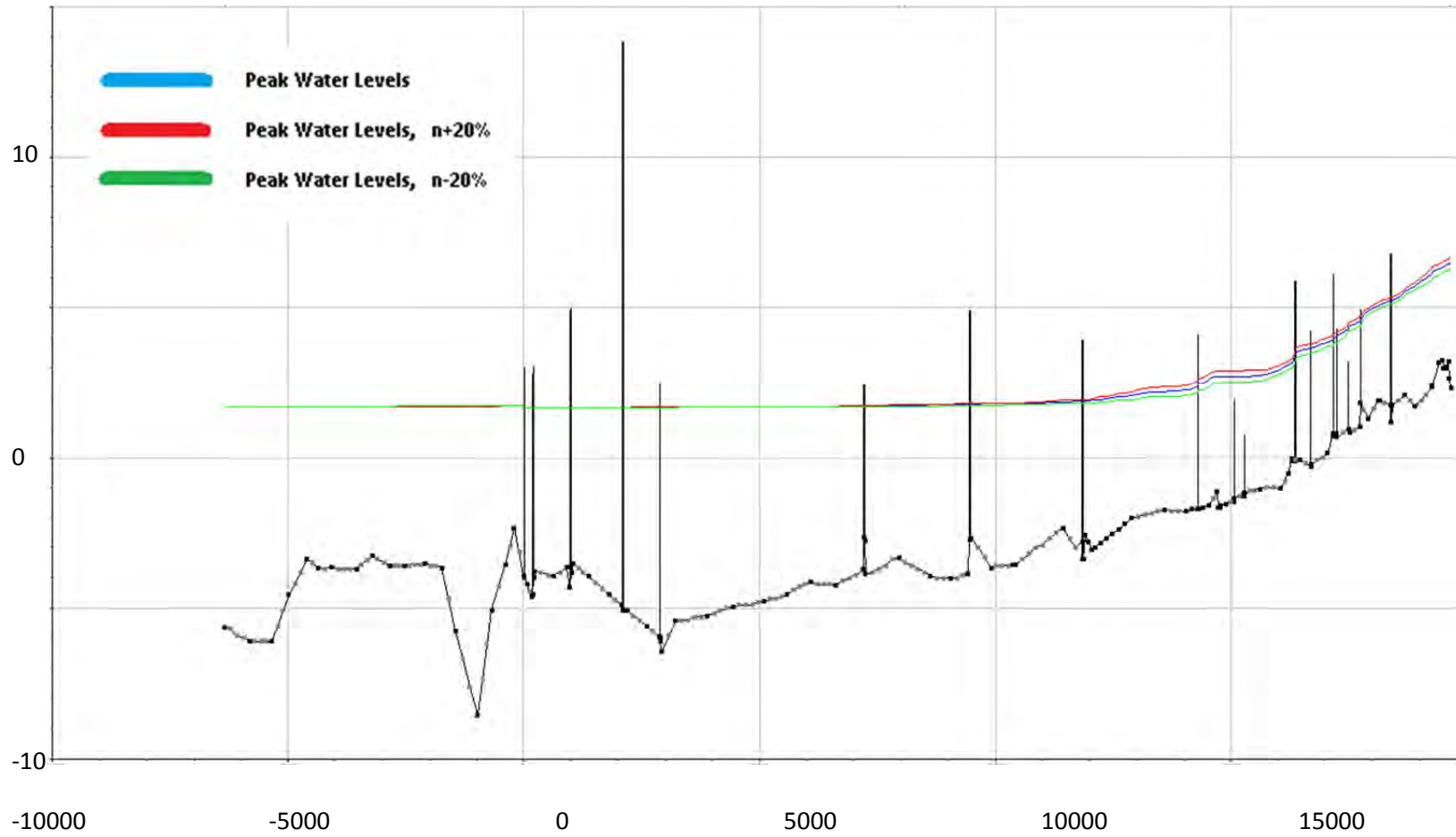


Serpentine River longitudinal profile (Chainage 0 = sea dam)



January 2014

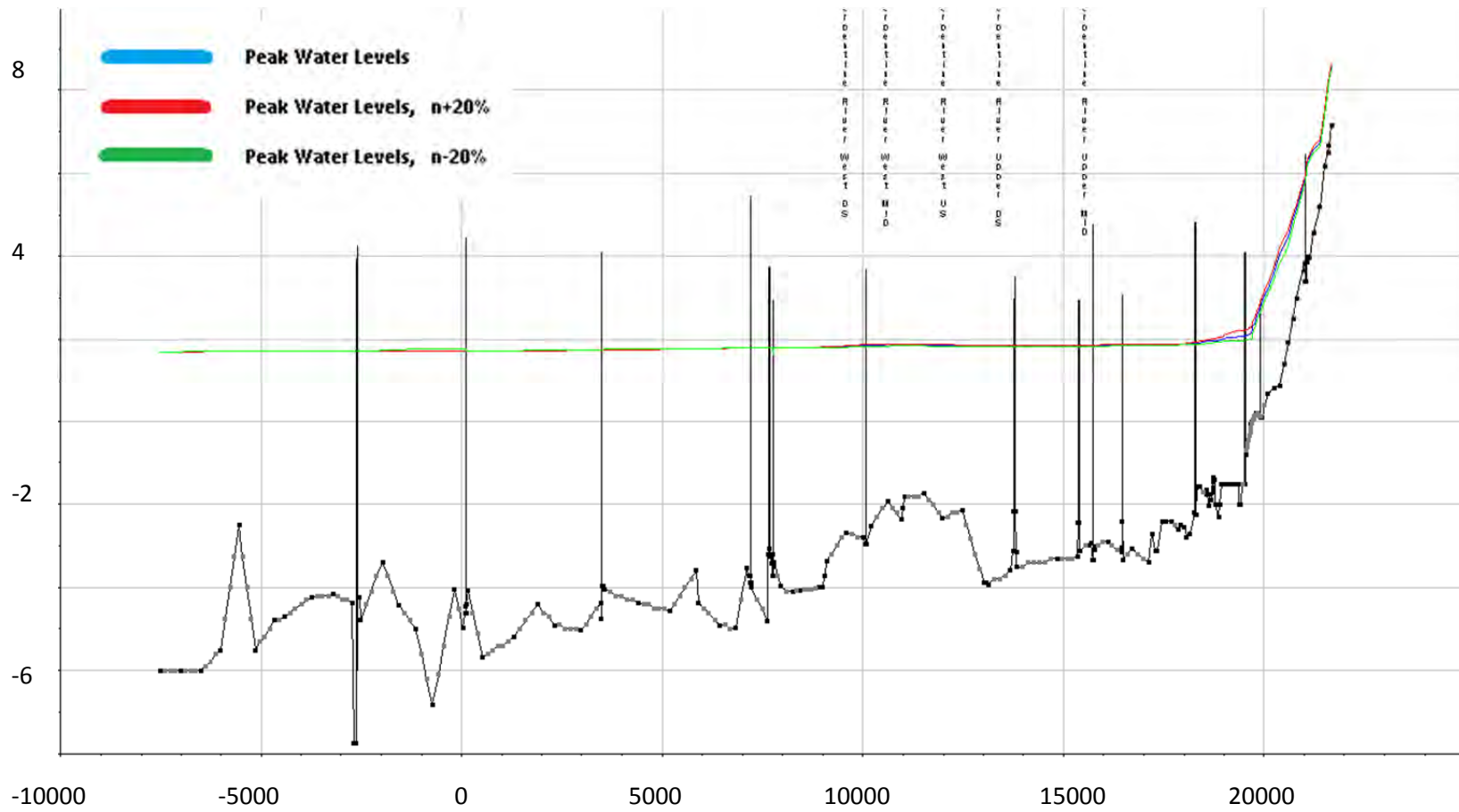
Sensitivity Analysis,  $n \pm 20\%$



Nicomekl River longitudinal profile (Chainage 0 = sea dam)

January 2014

Sensitivity Analysis,  $n \pm 20\%$



Serpentine River longitudinal profile (Chainage 0 = sea dam)

## **APPENDIX E**

Frequency Analysis

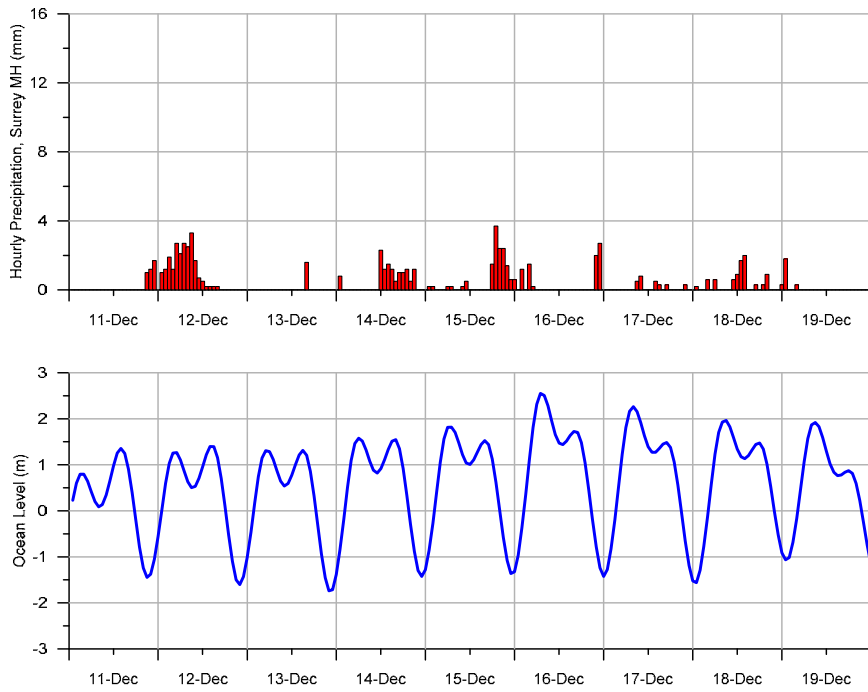


**Figure E.1: Ocean level and rainfall data, December 1982 (peak tide level 2.57m)**

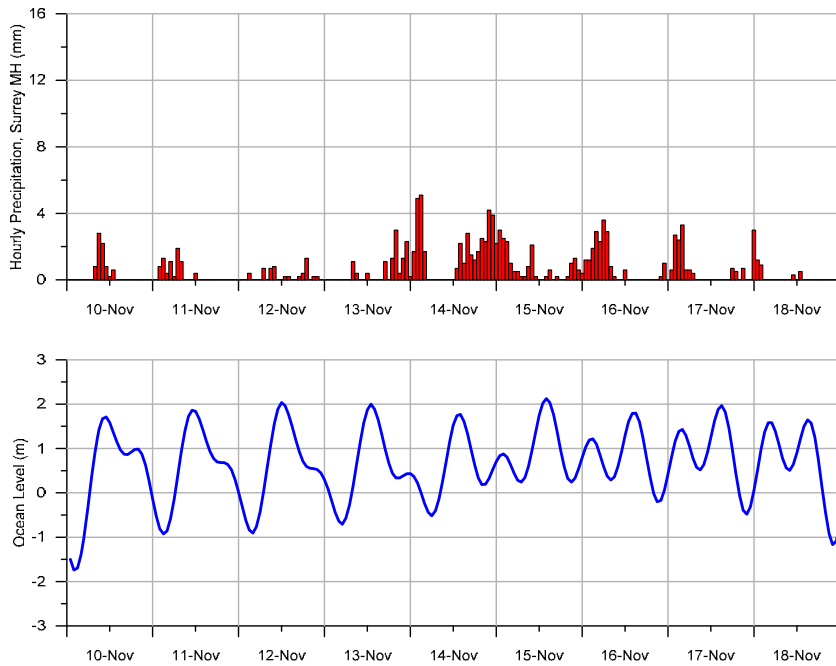


**Figure E.2: Ocean level and rainfall data, November 1983 (moderate precipitation combined with several days of ocean levels above 0 m).**

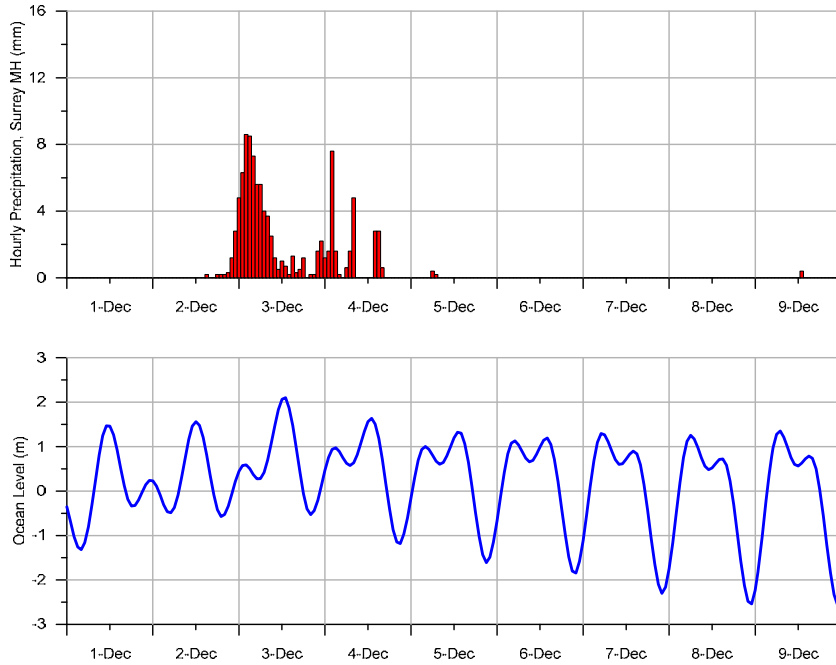


**Figure E.3: Ocean level and rainfall data, December 2007 (moderate precipitation combined with several days of ocean levels above -0.5 m).**

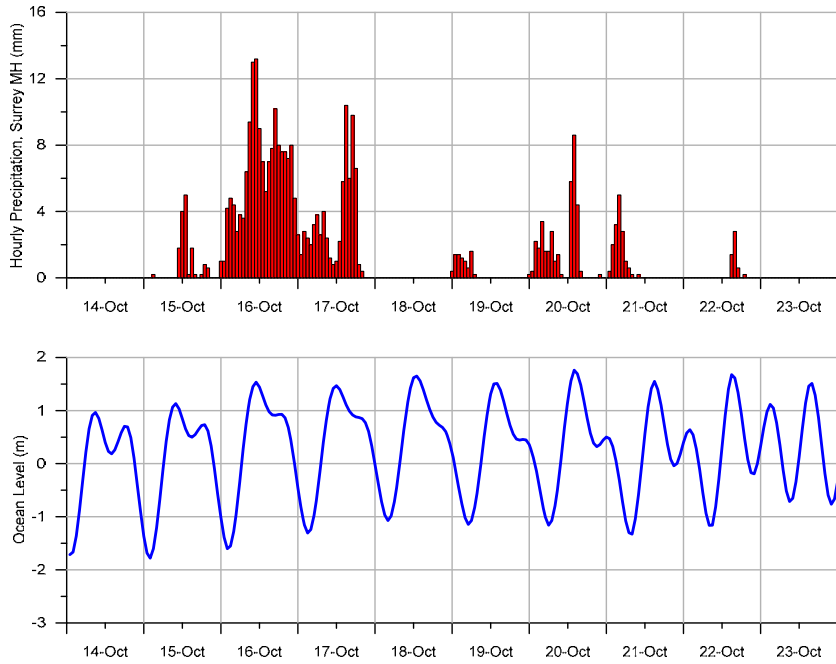


**Figure E.4: Ocean level and rainfall data, October 2003 (large volume of precipitation with tides above -1.0 m).**

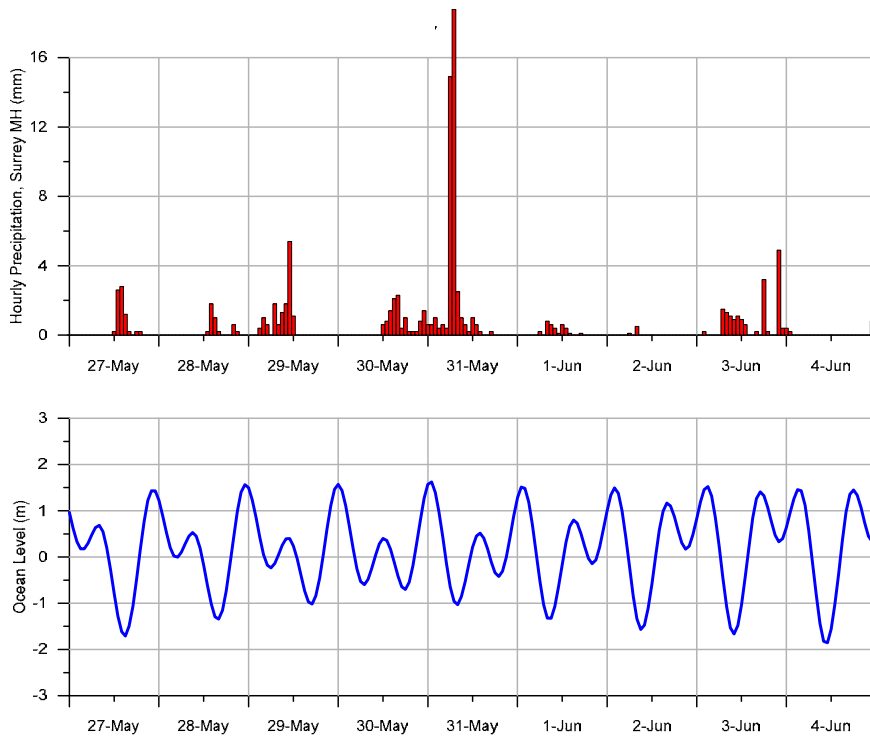


**Figure E.5: Ocean level and rainfall data, May 1997 (high intensity precipitation).**

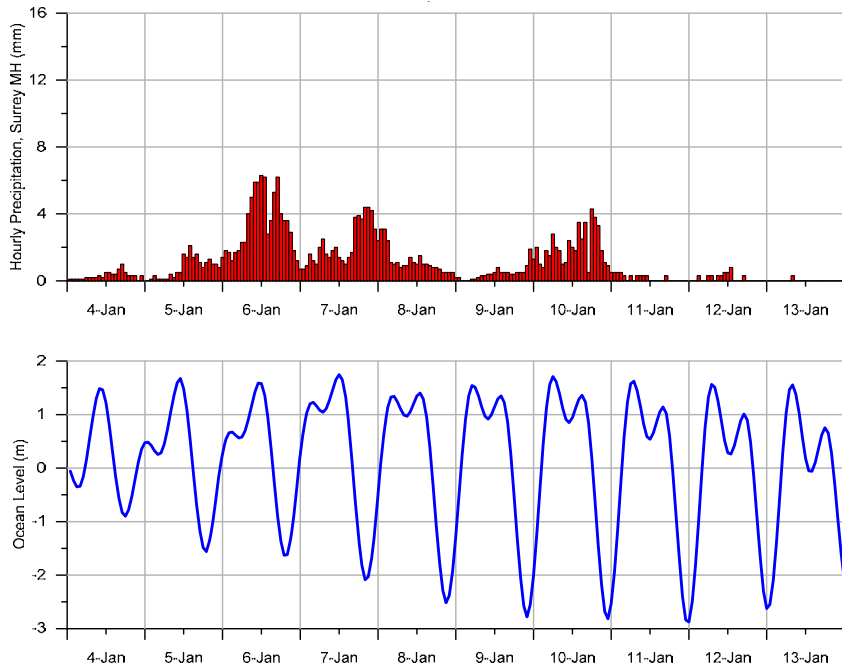


**Figure E.6: Ocean level and rainfall data, January 2009 (high volume rainfall, fairly high tides)**

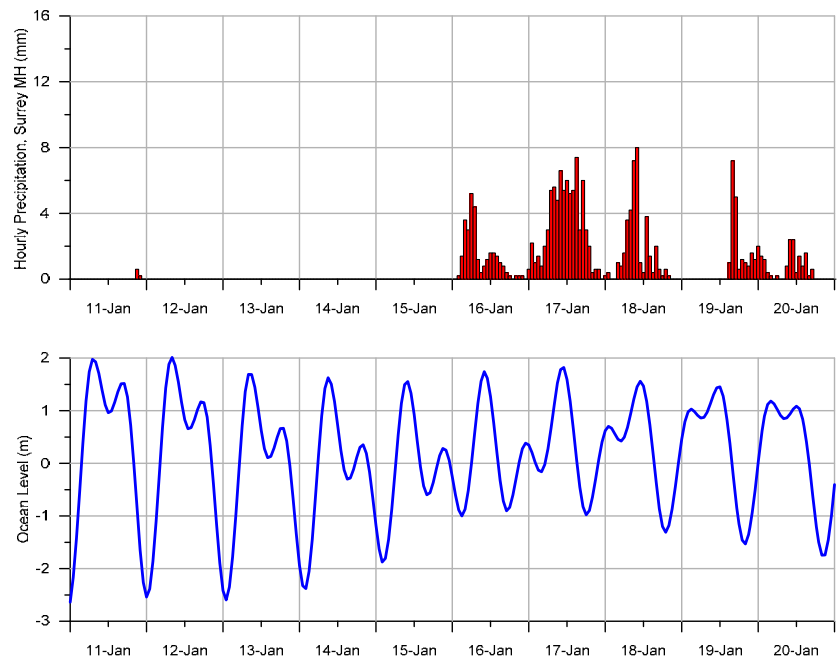


**Figure E.7: Ocean level and rainfall data, January 2005 (relatively high volume and intensity rainfall).**

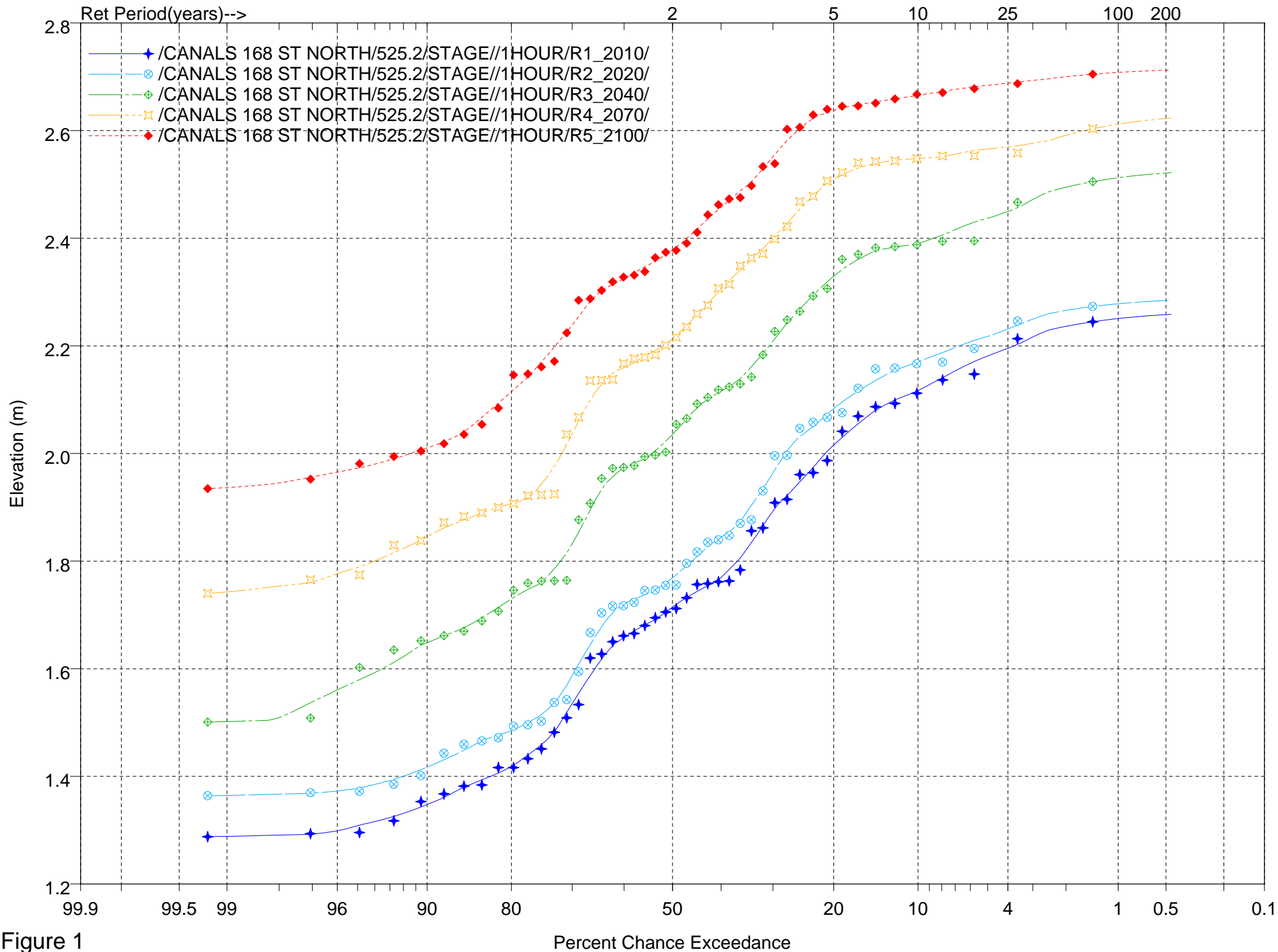


Figure 1



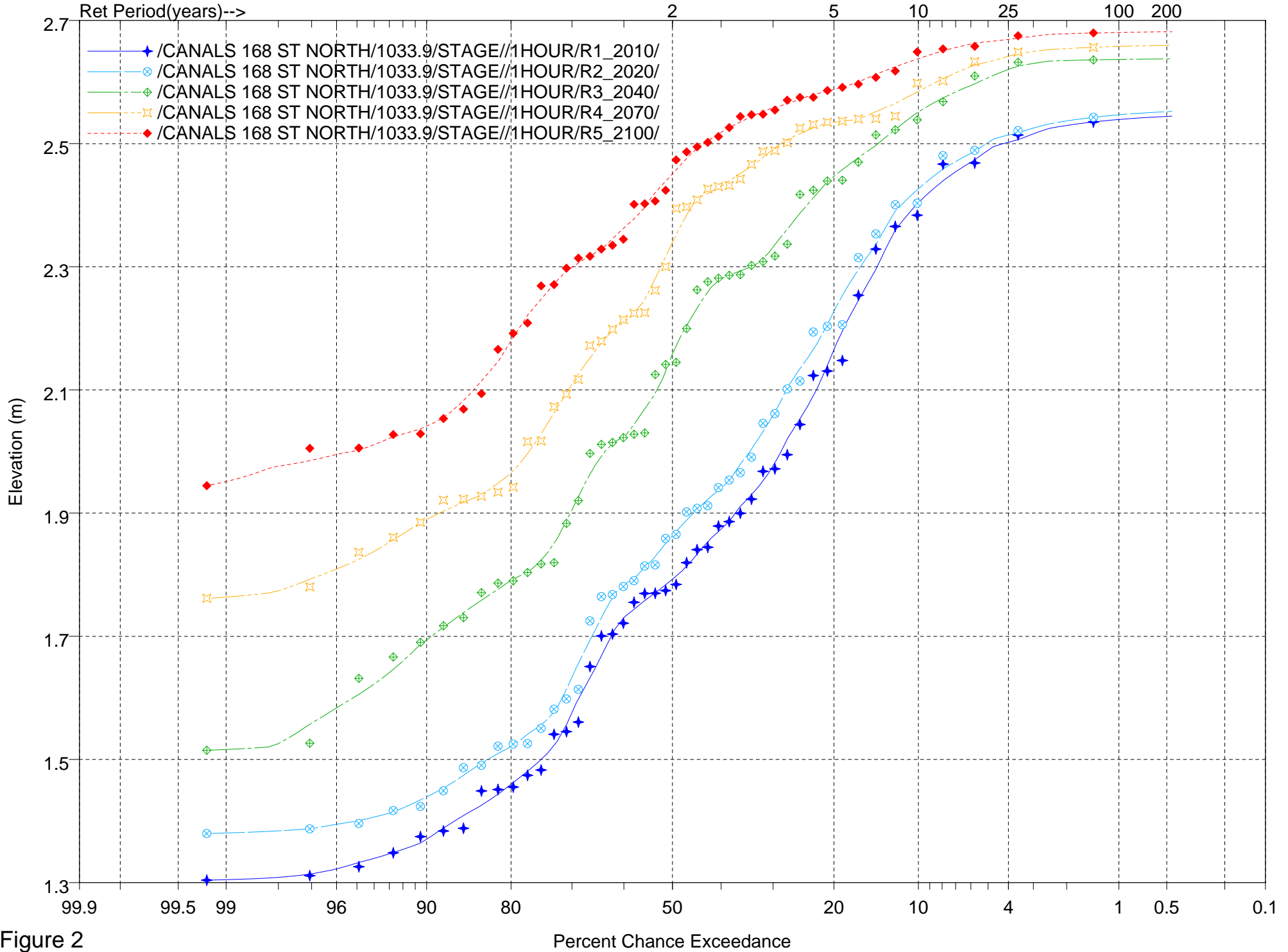


Figure 2

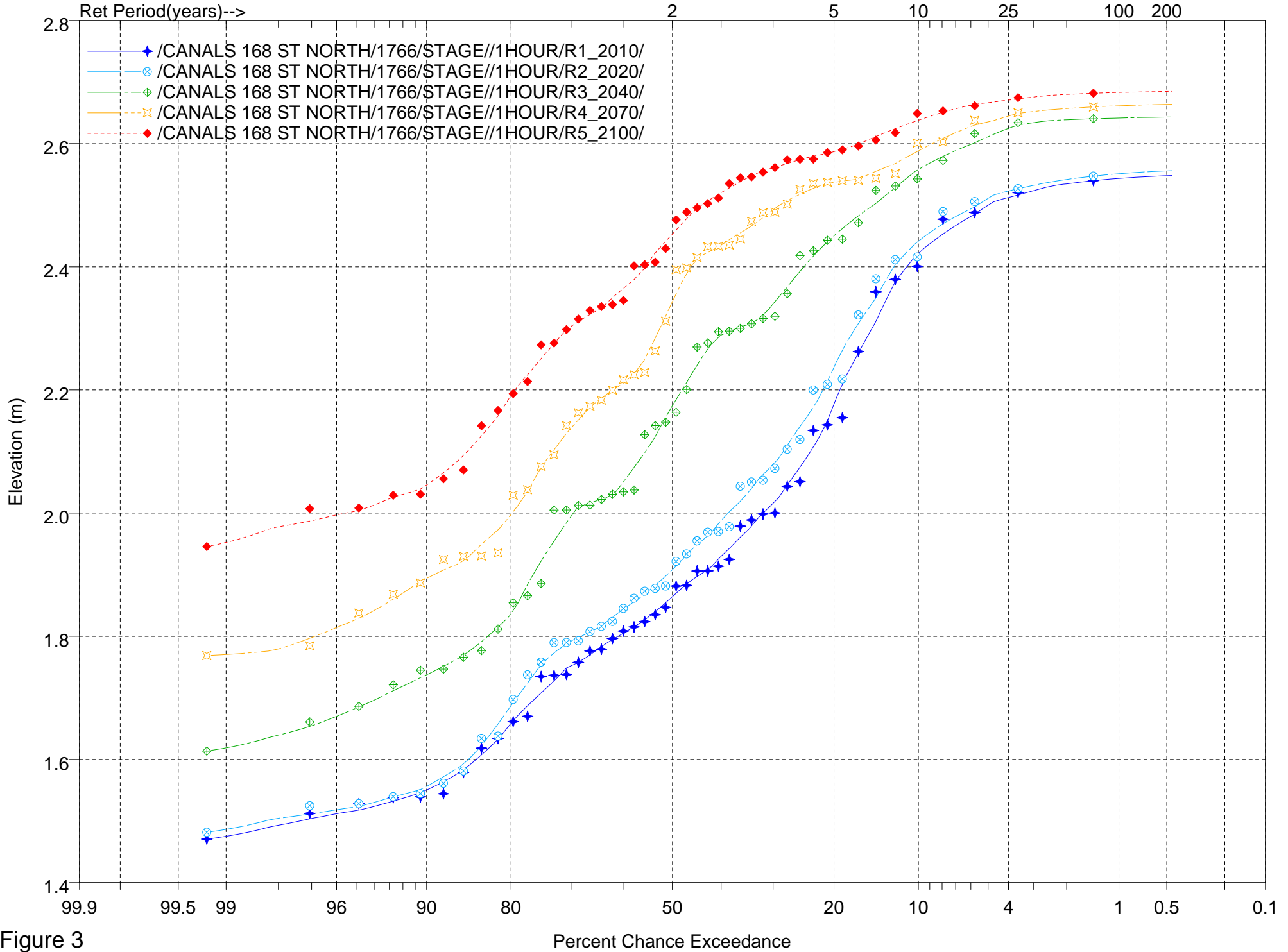


Figure 3

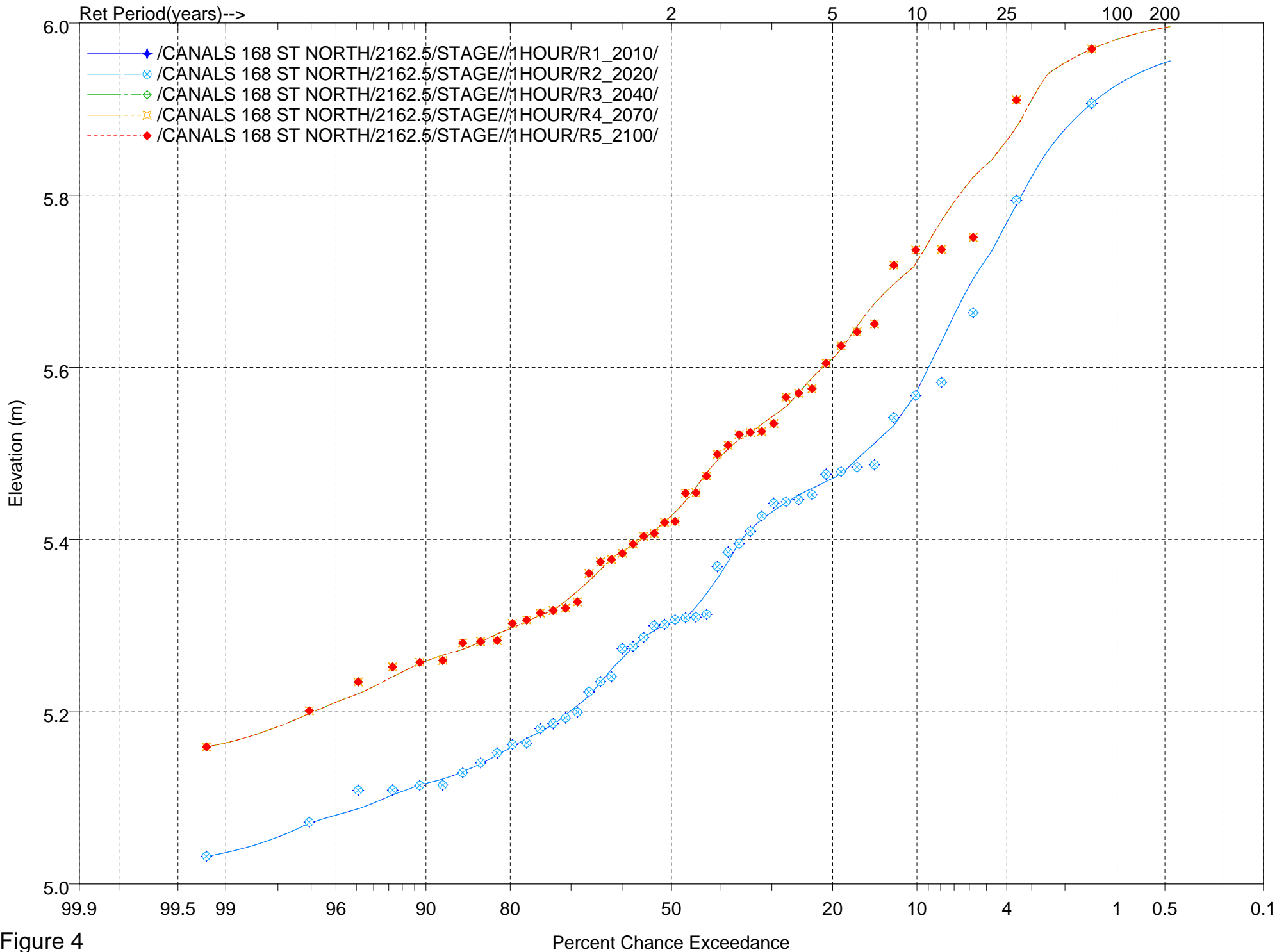


Figure 4

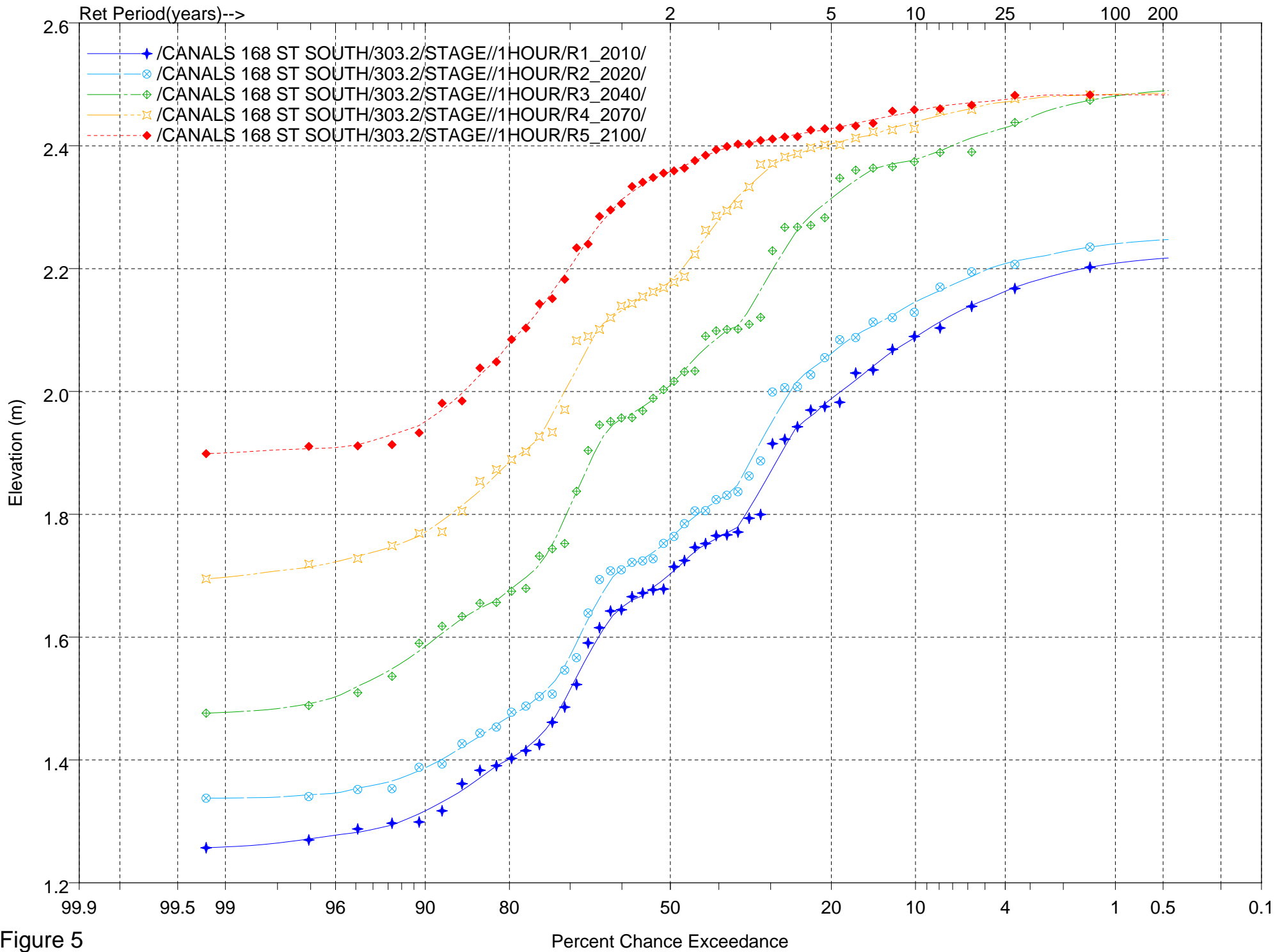


Figure 5

Annual Peak Frequency Analysis  
 Fit Type: 5 Point Moving Average distribution using the method of Linear Interpolation, Hosking Plotting Position

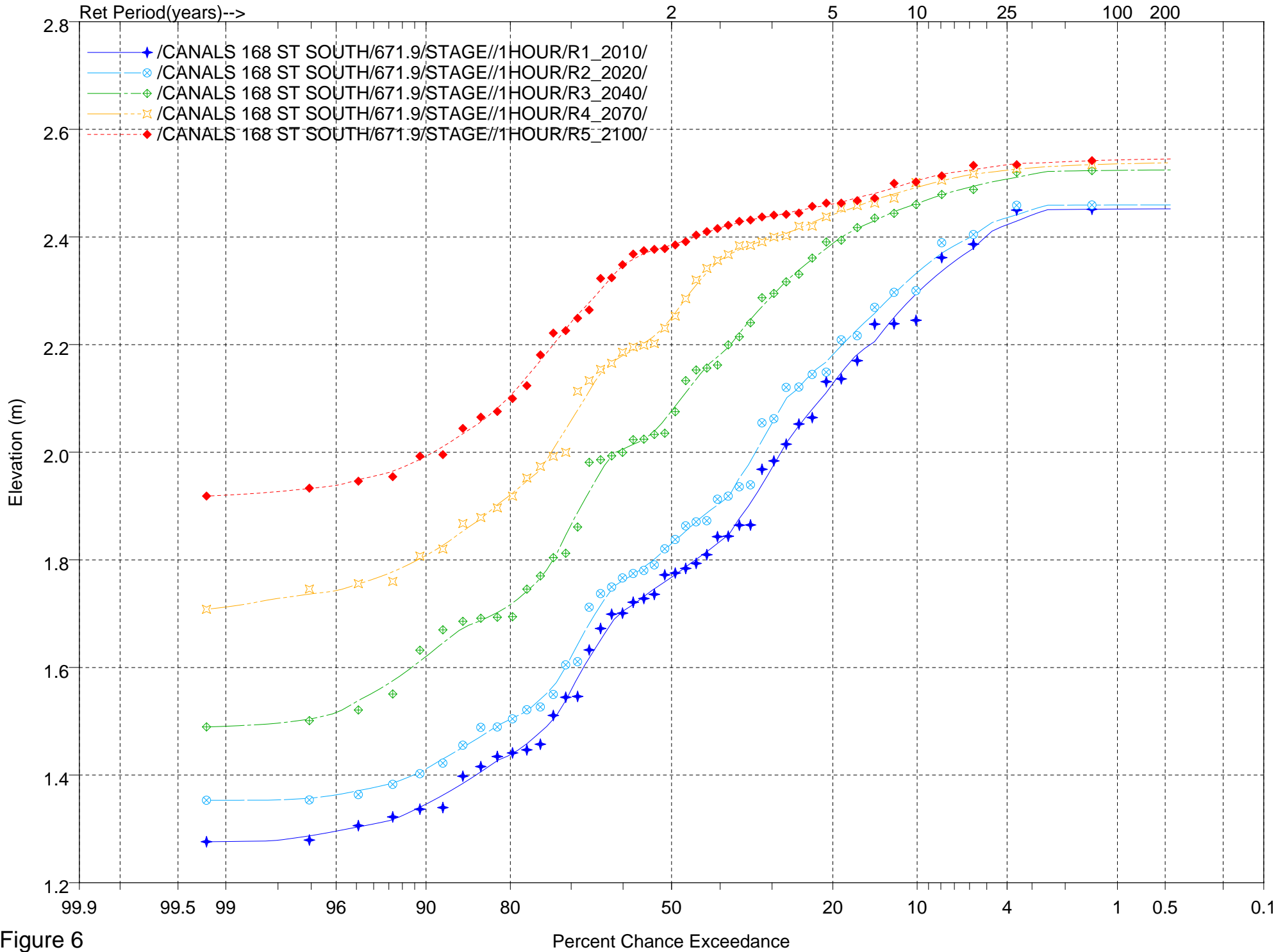


Figure 6

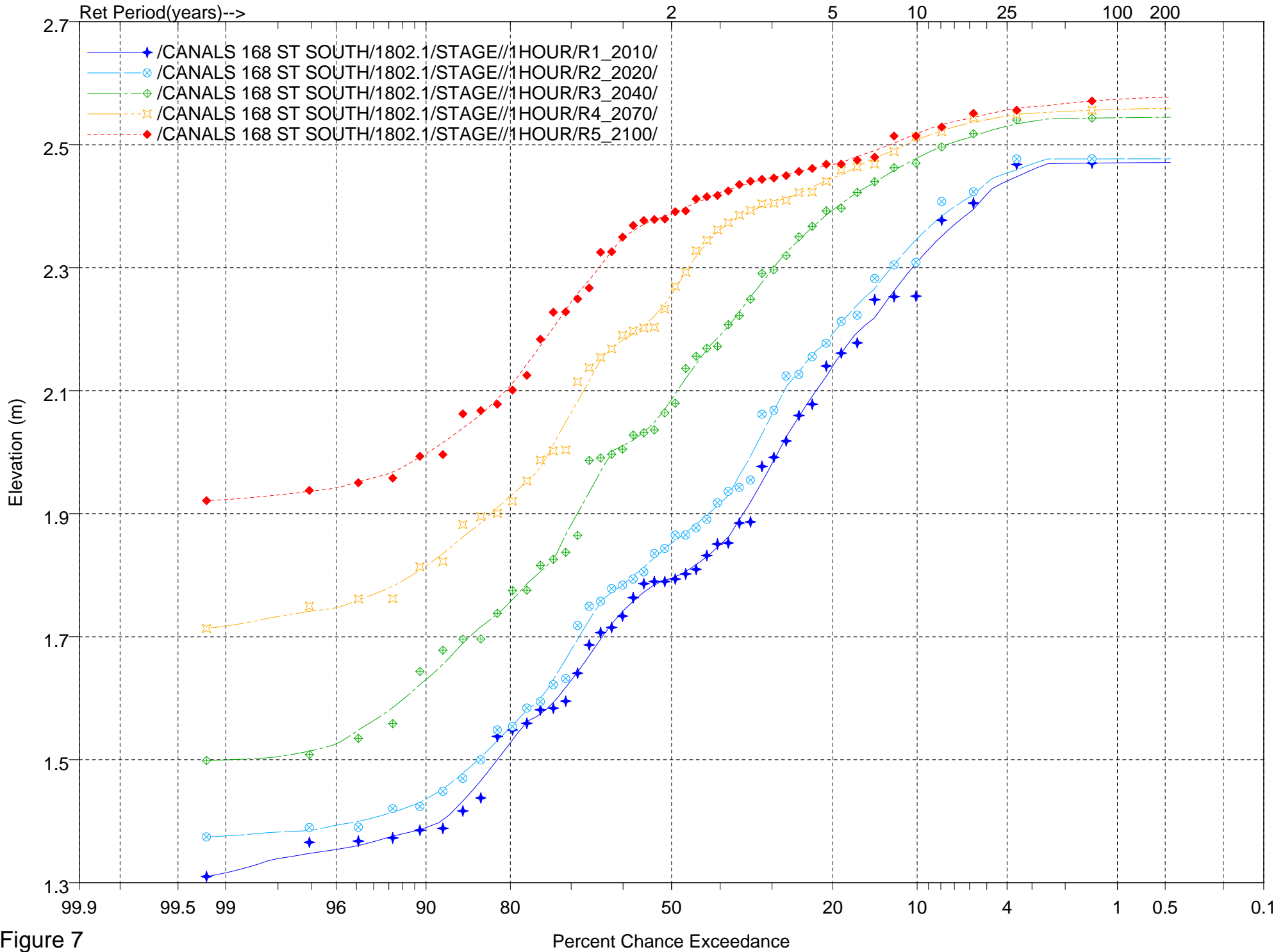


Figure 7

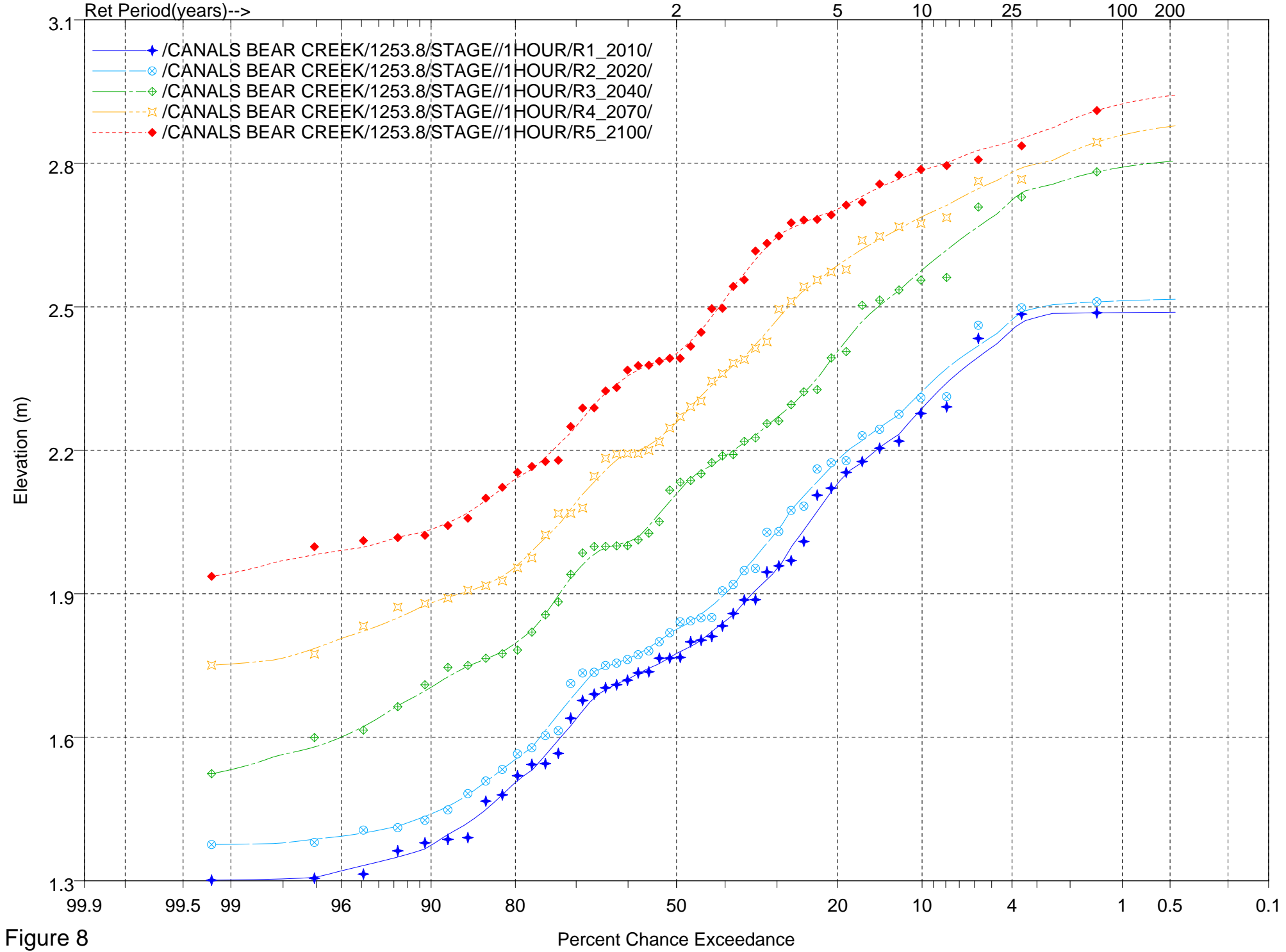


Figure 8

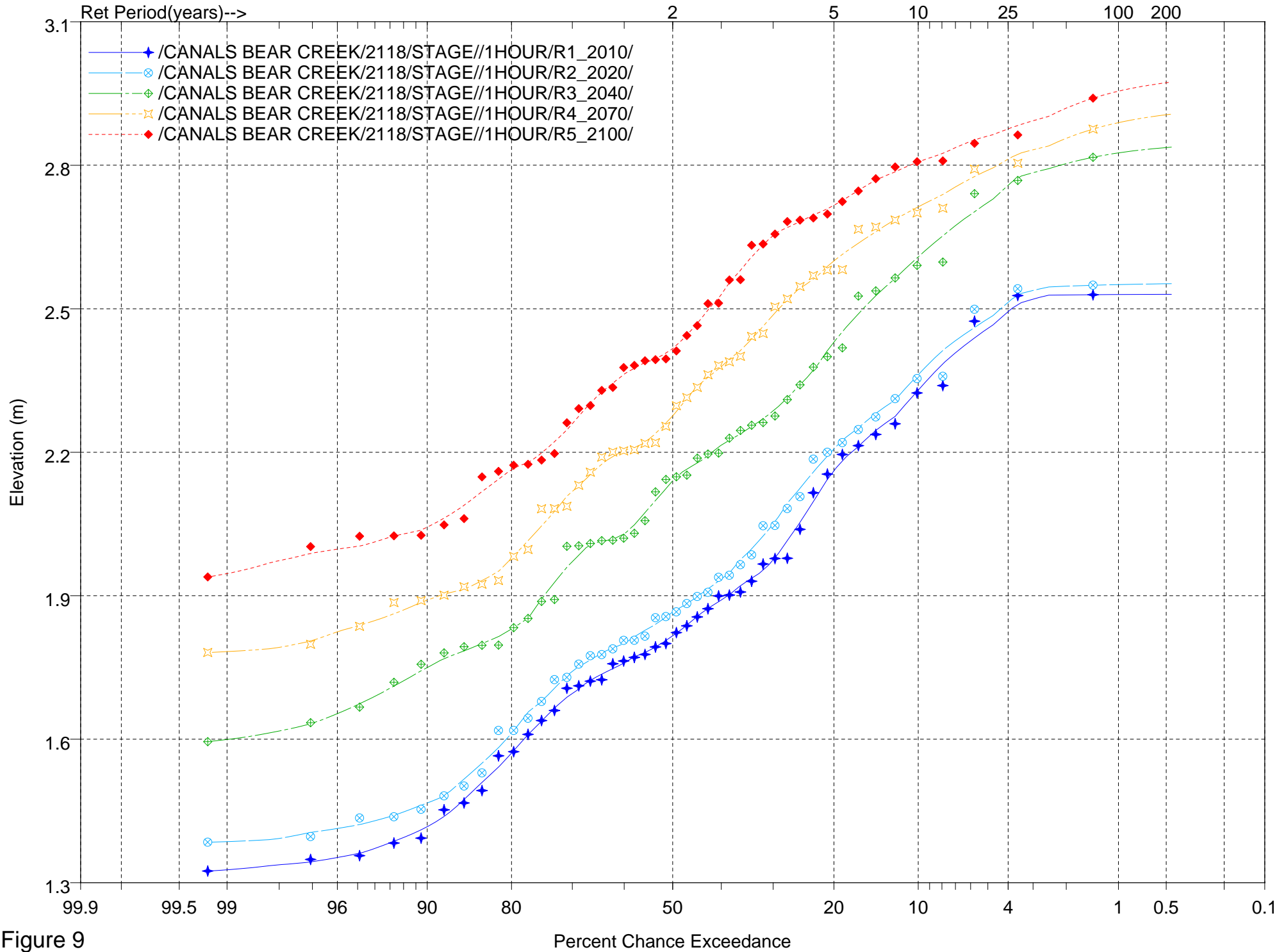


Figure 9



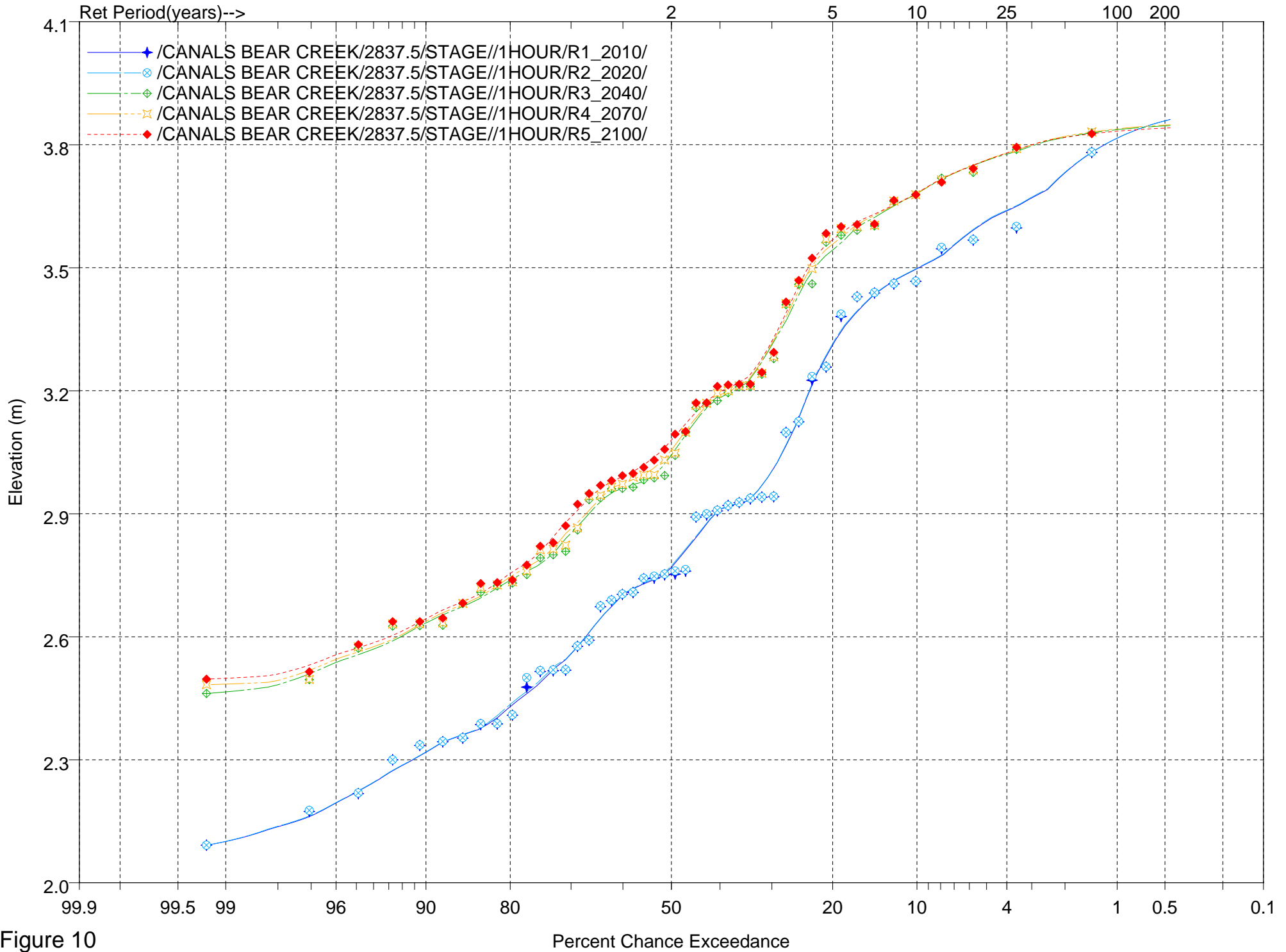


Figure 10

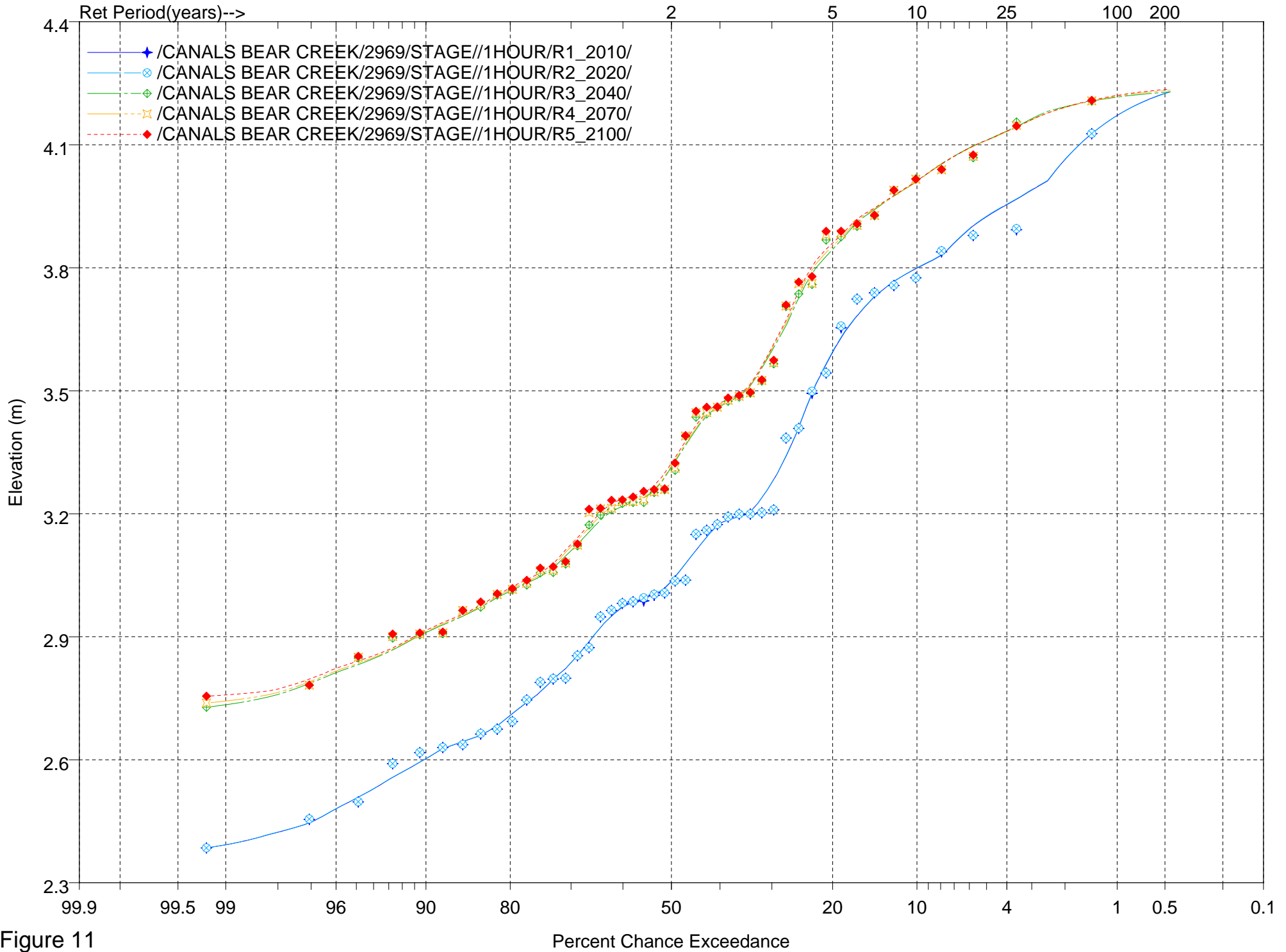


Figure 11

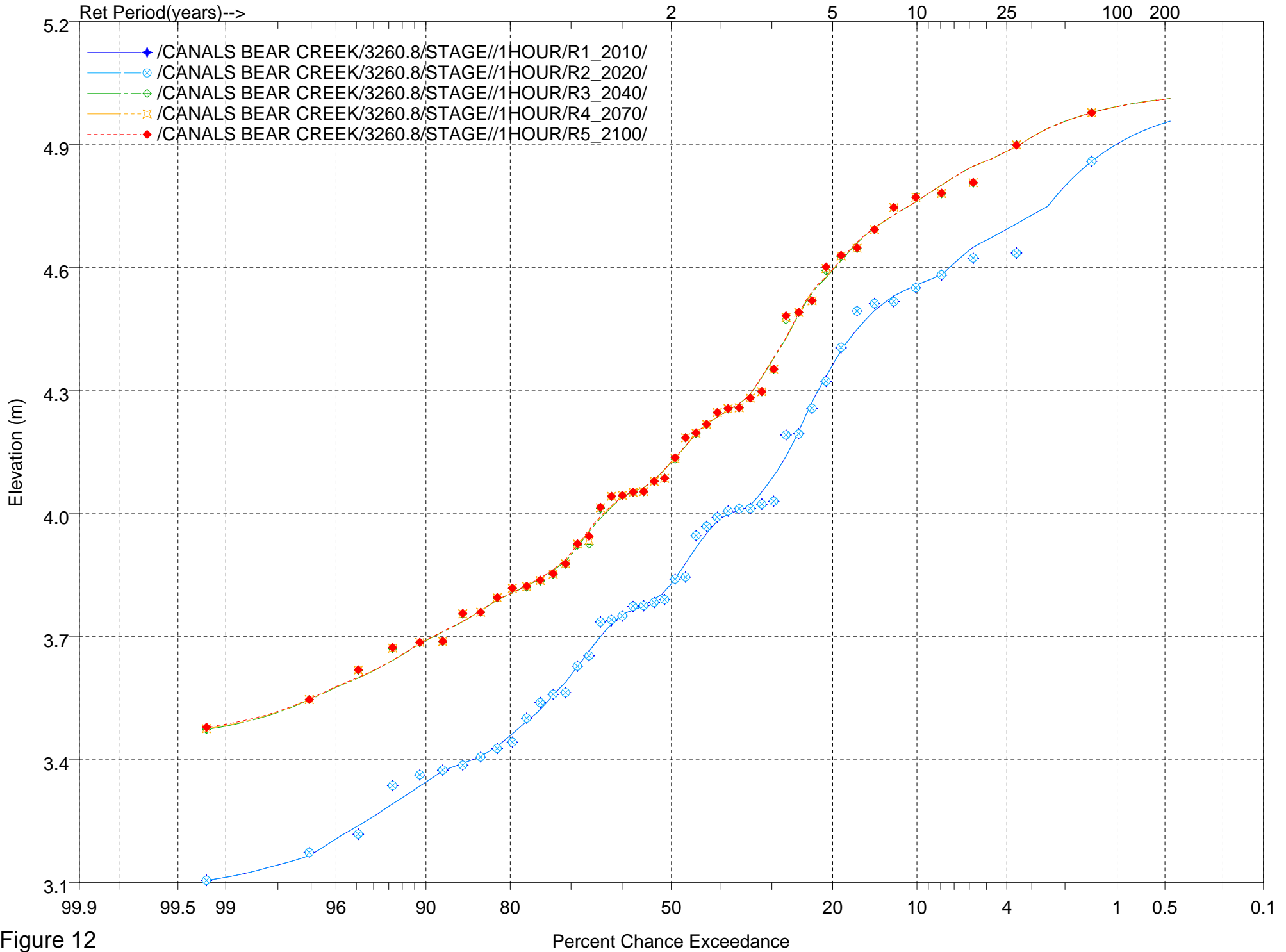


Figure 12

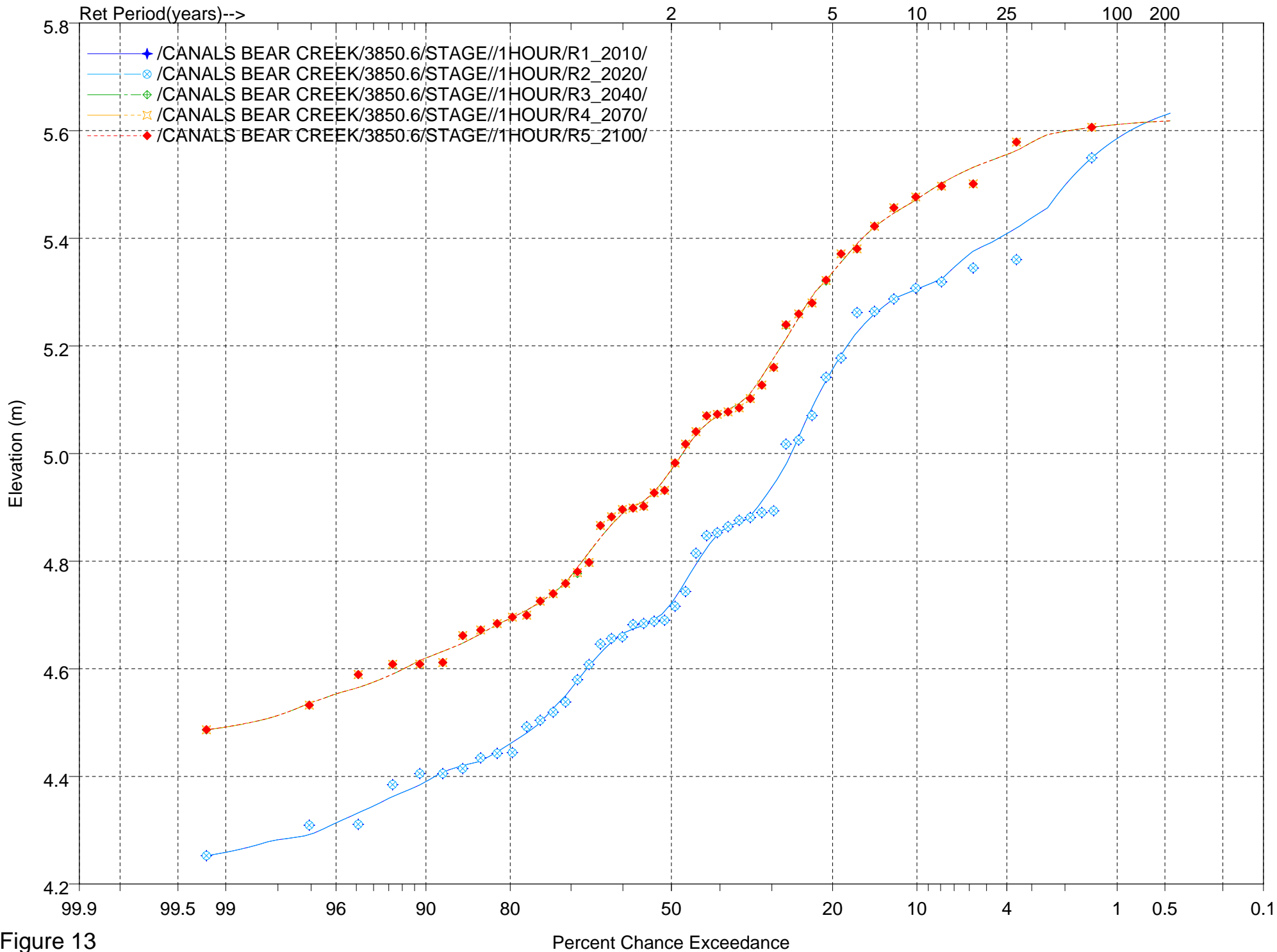


Figure 13

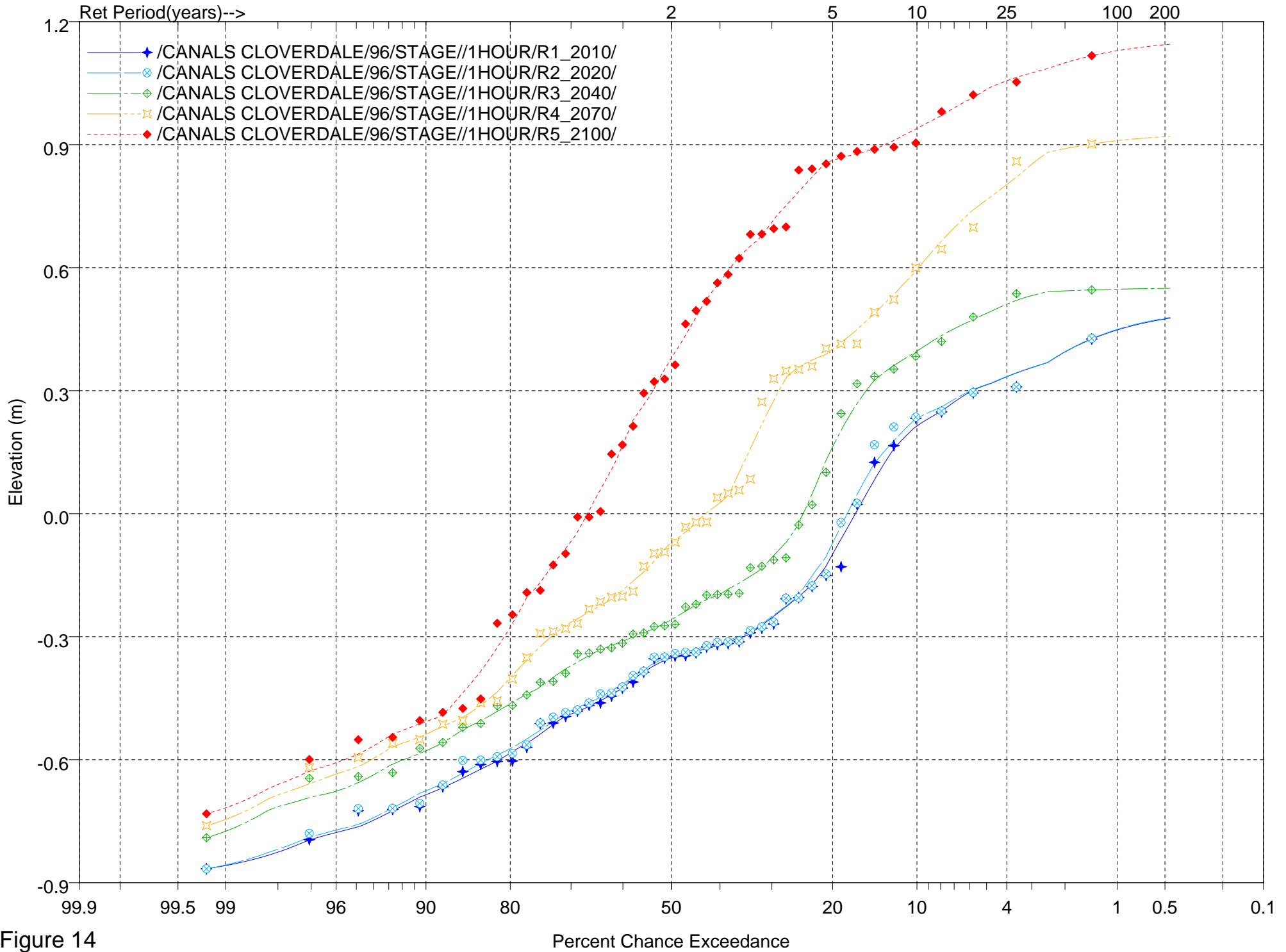


Figure 14

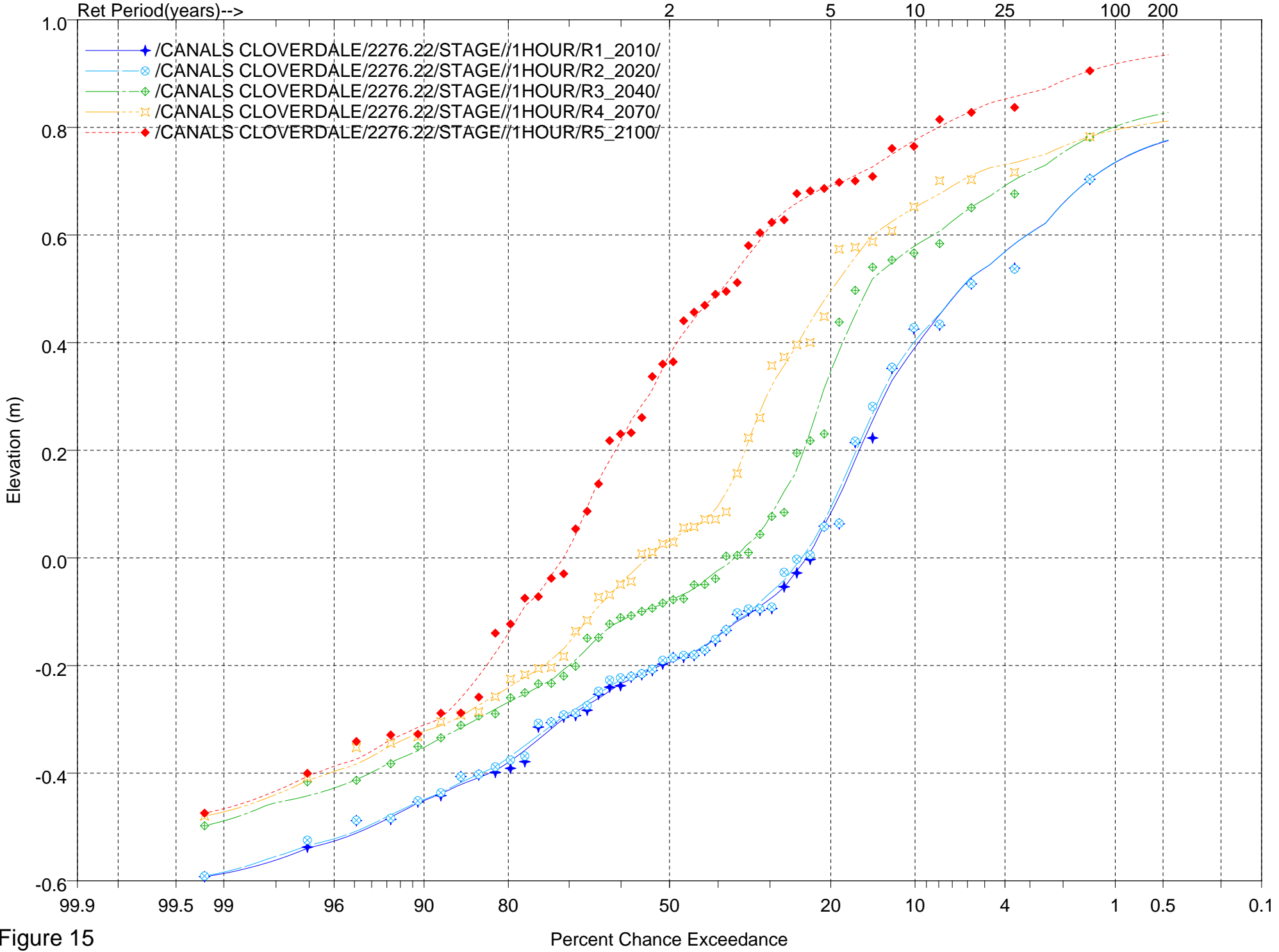


Figure 15

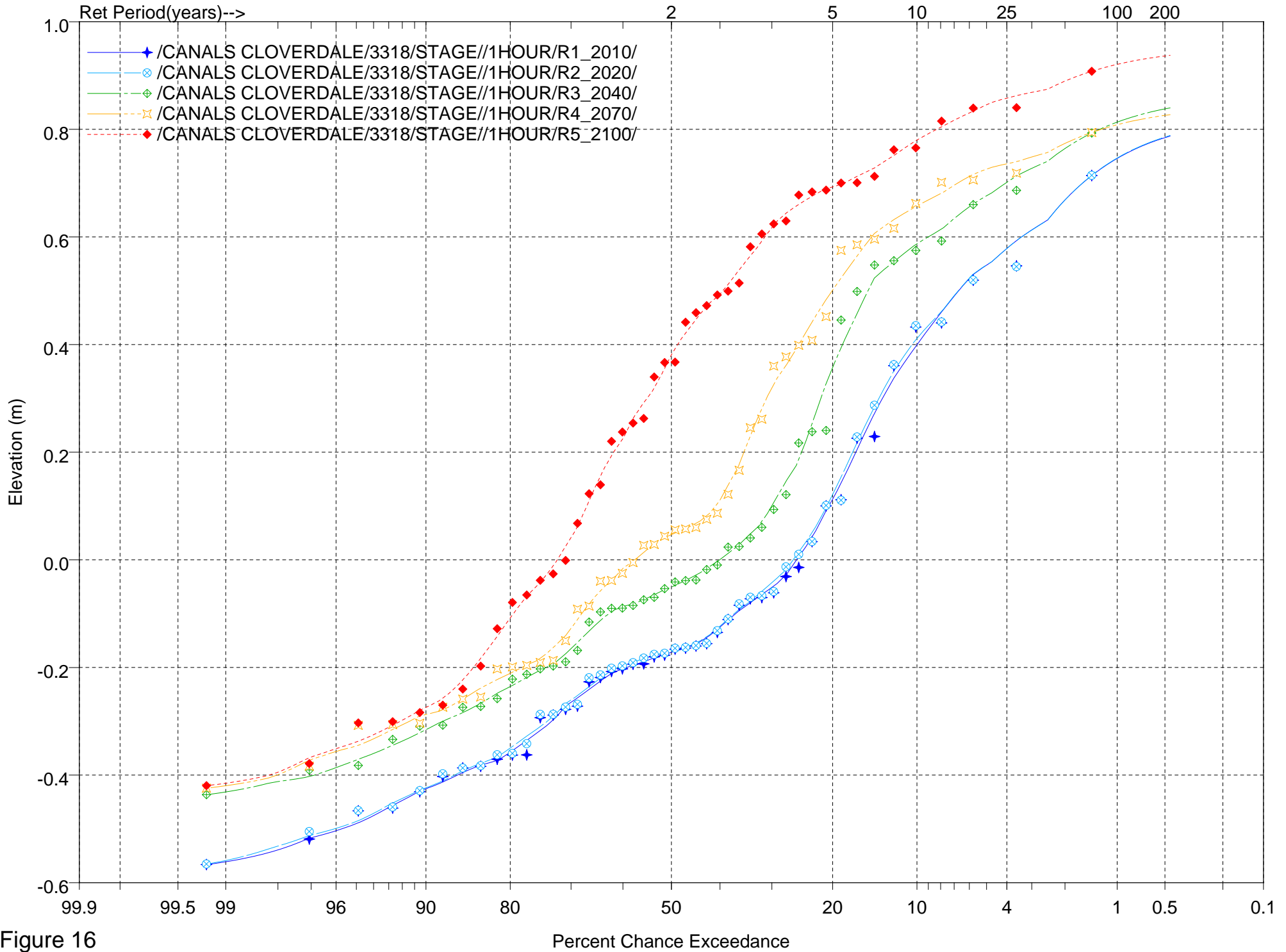


Figure 16

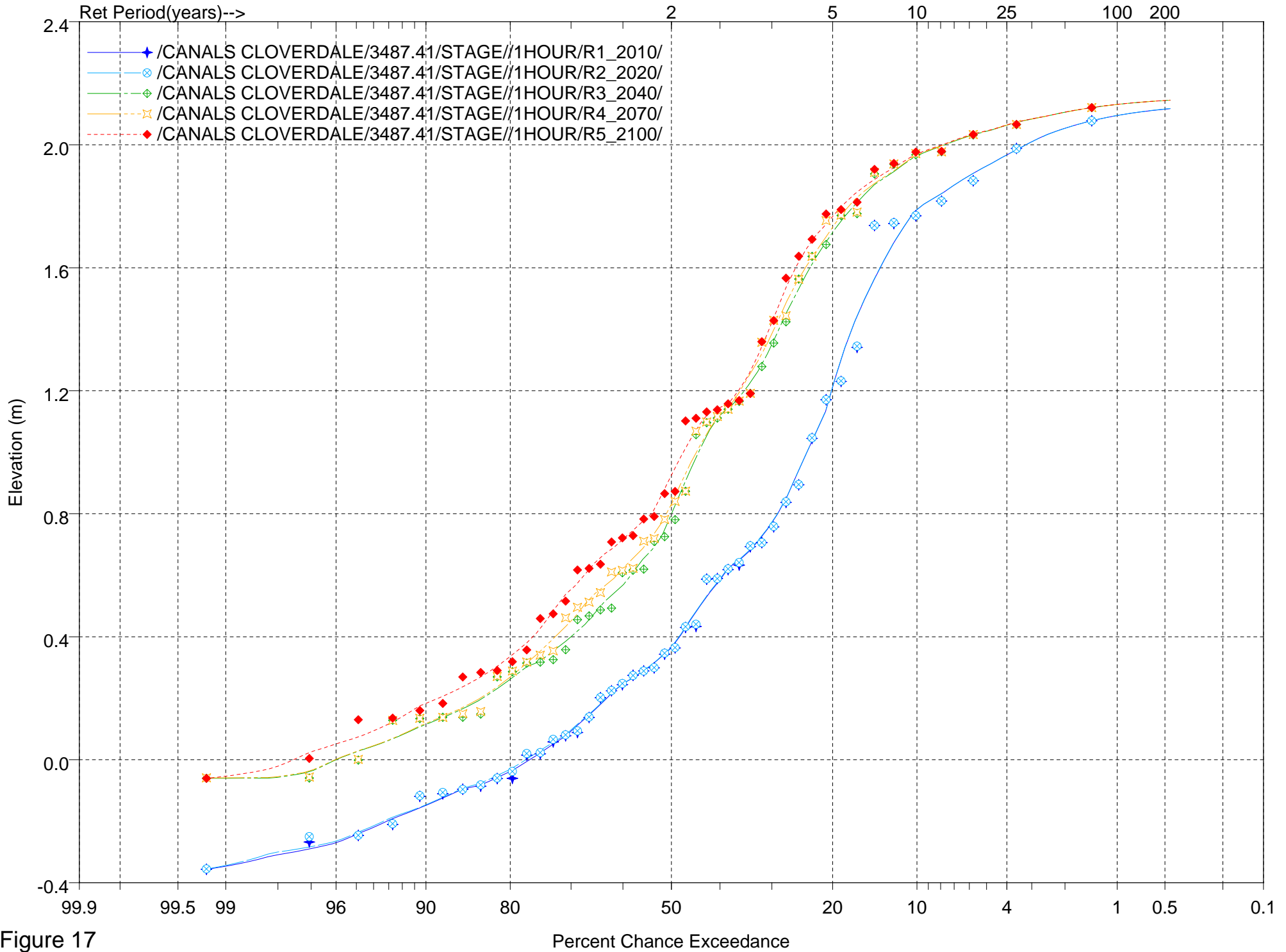


Figure 17



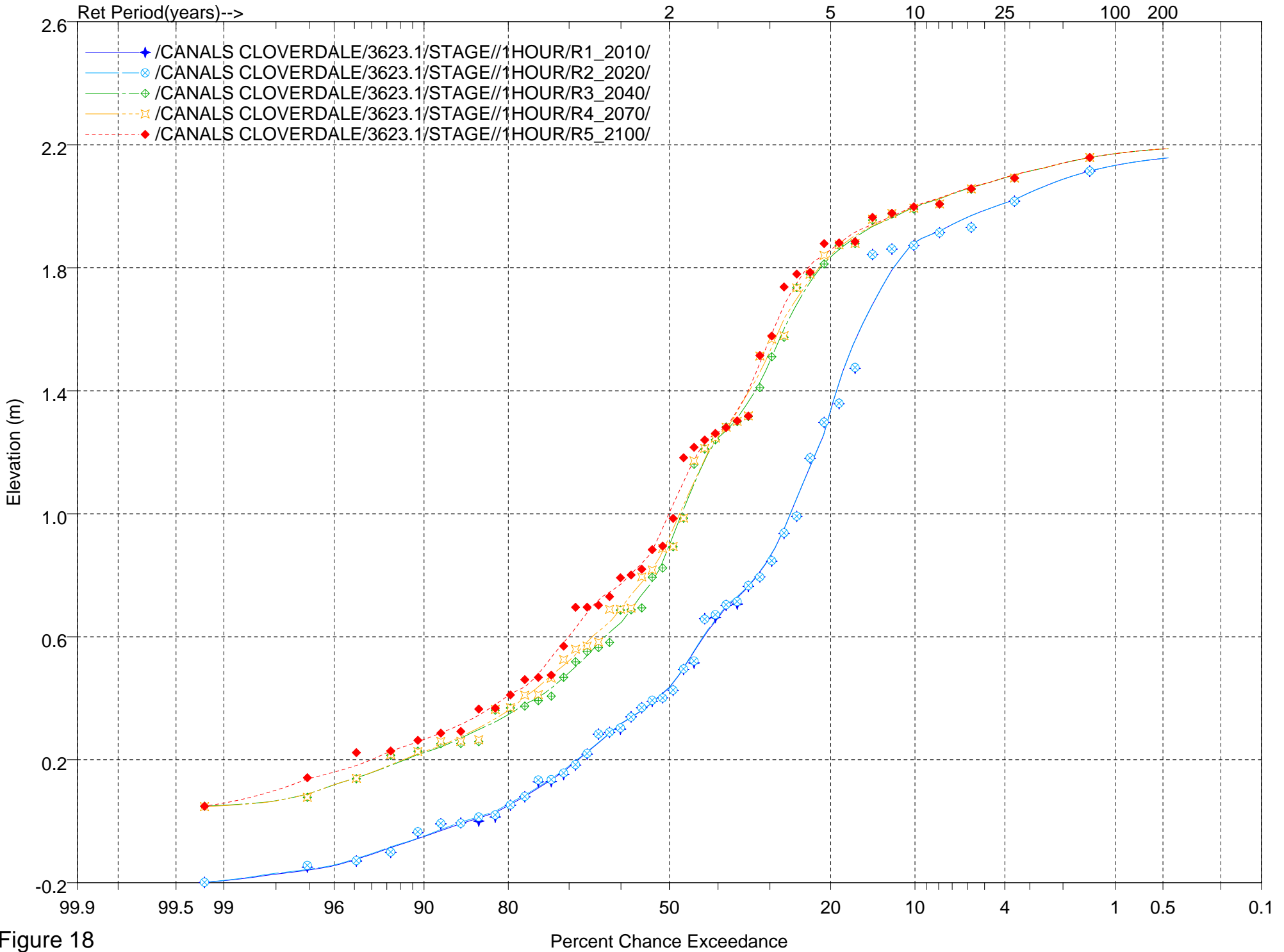


Figure 18

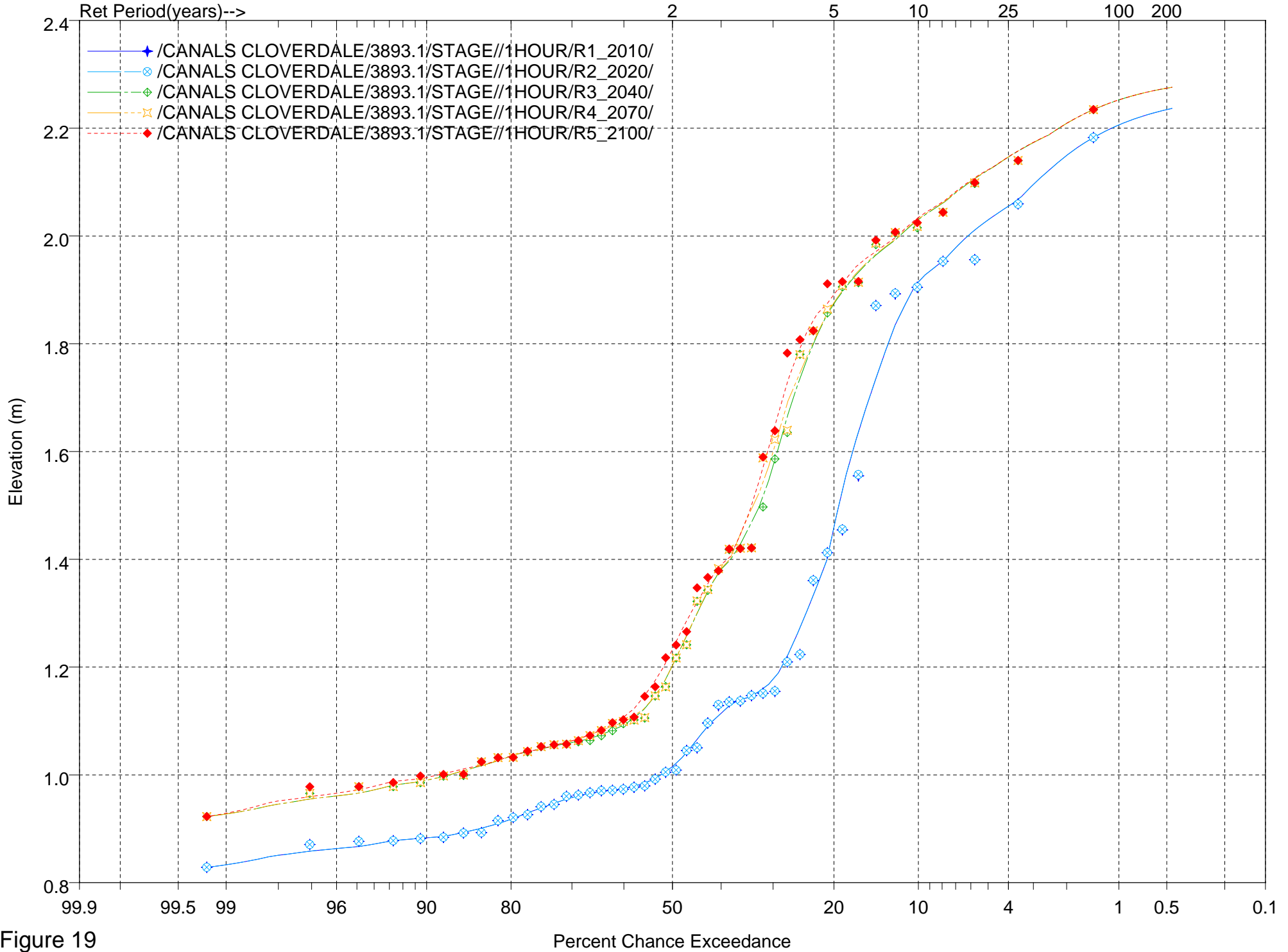


Figure 19

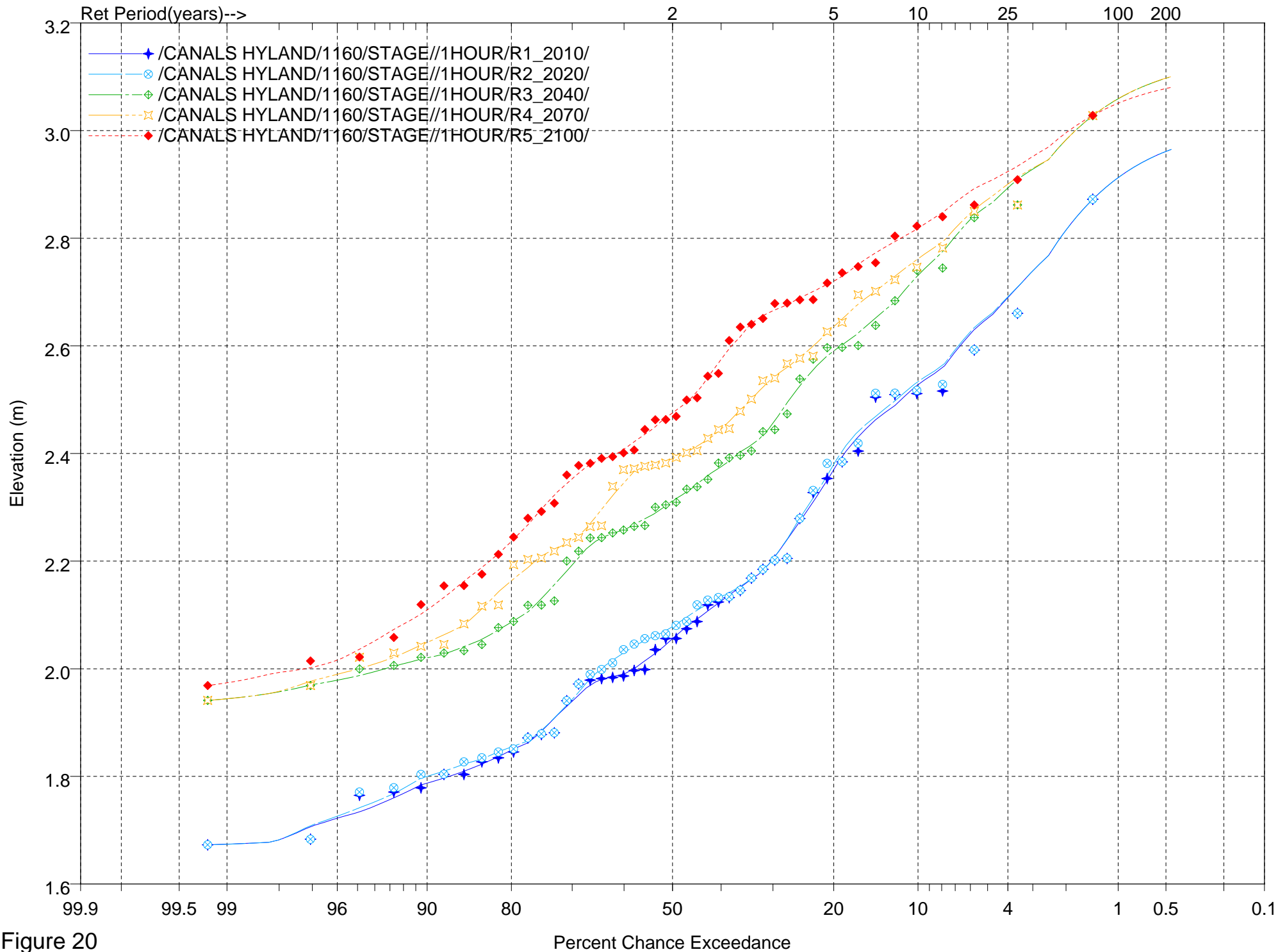


Figure 20

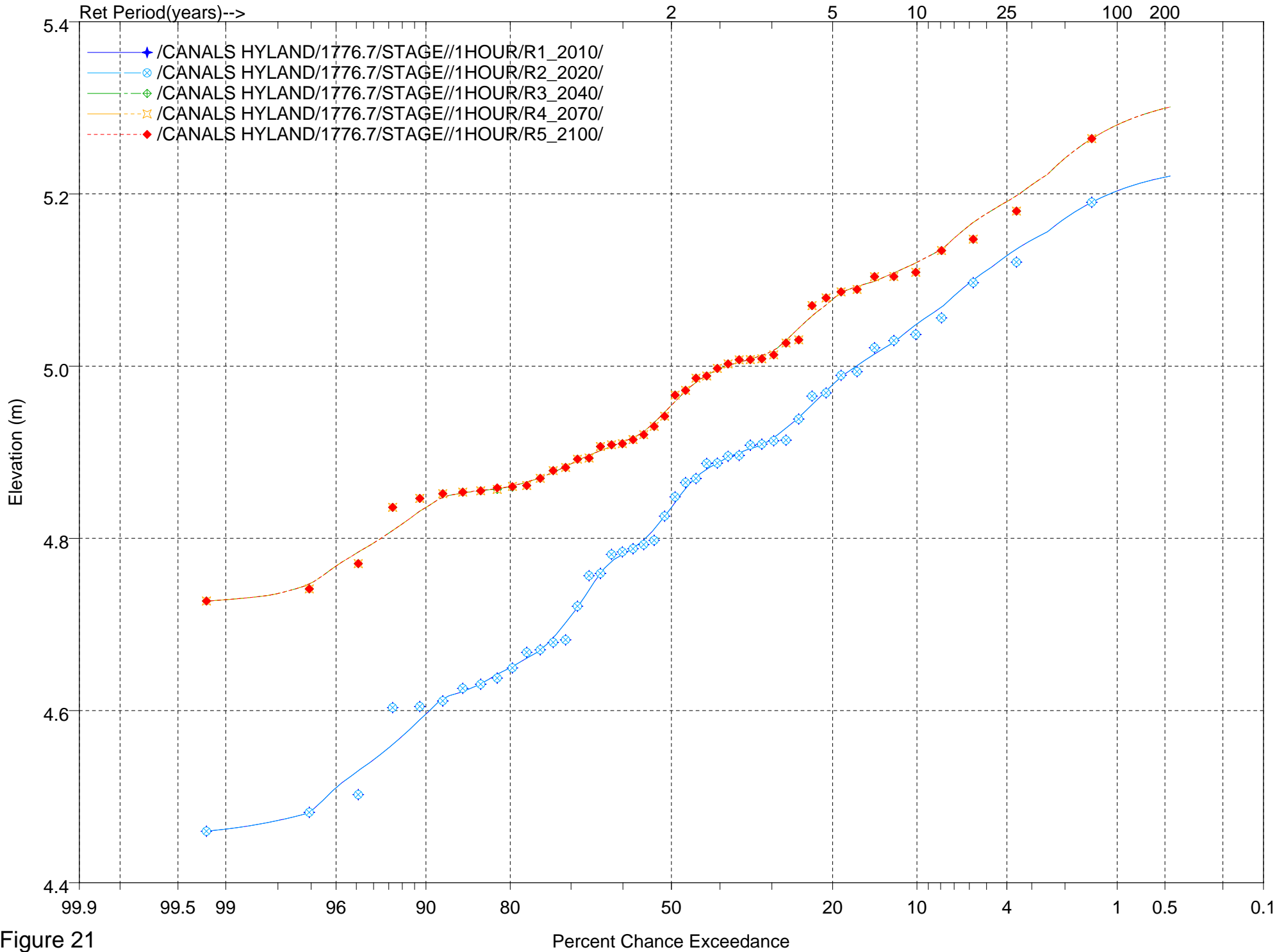


Figure 21

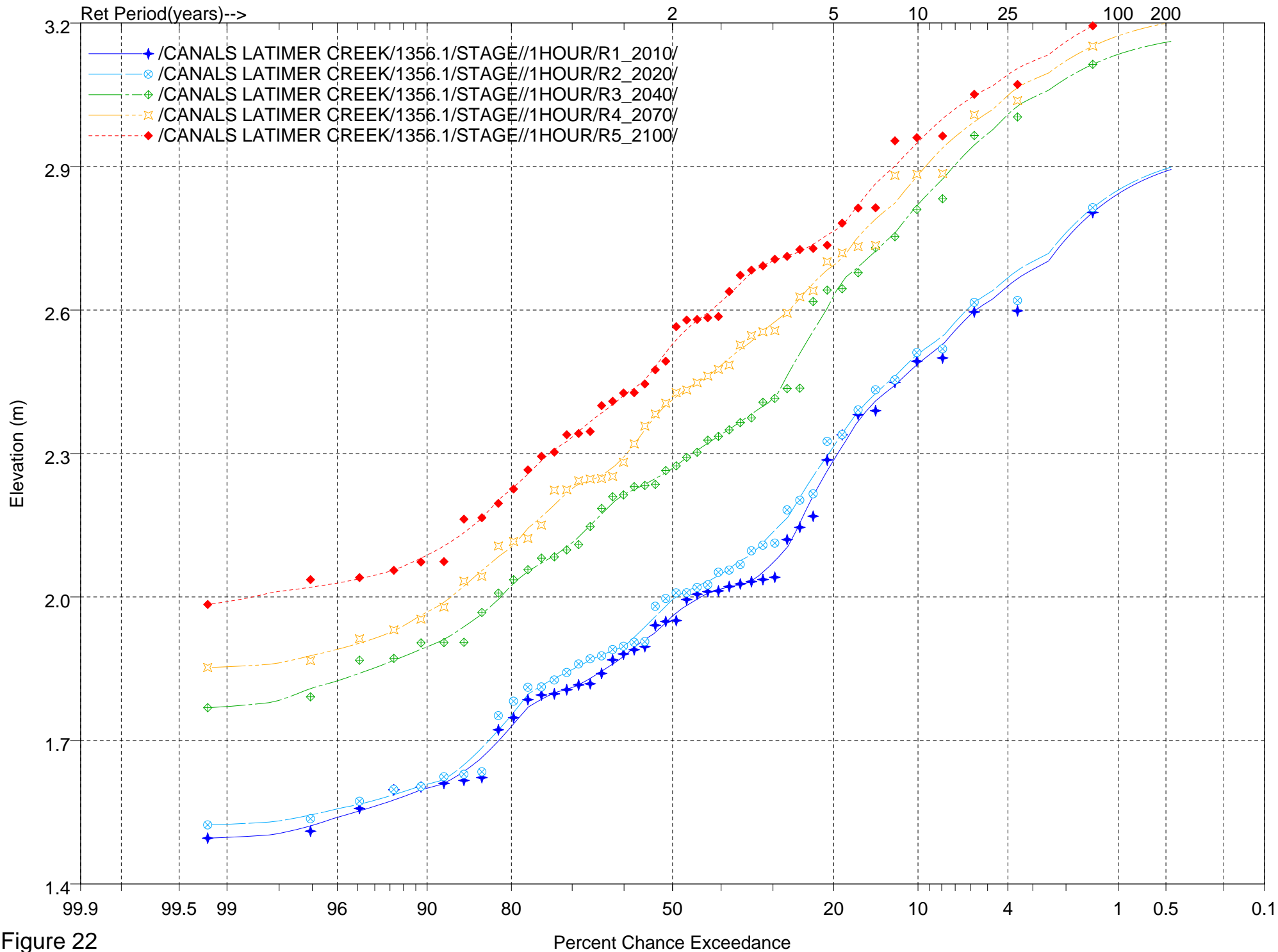


Figure 22

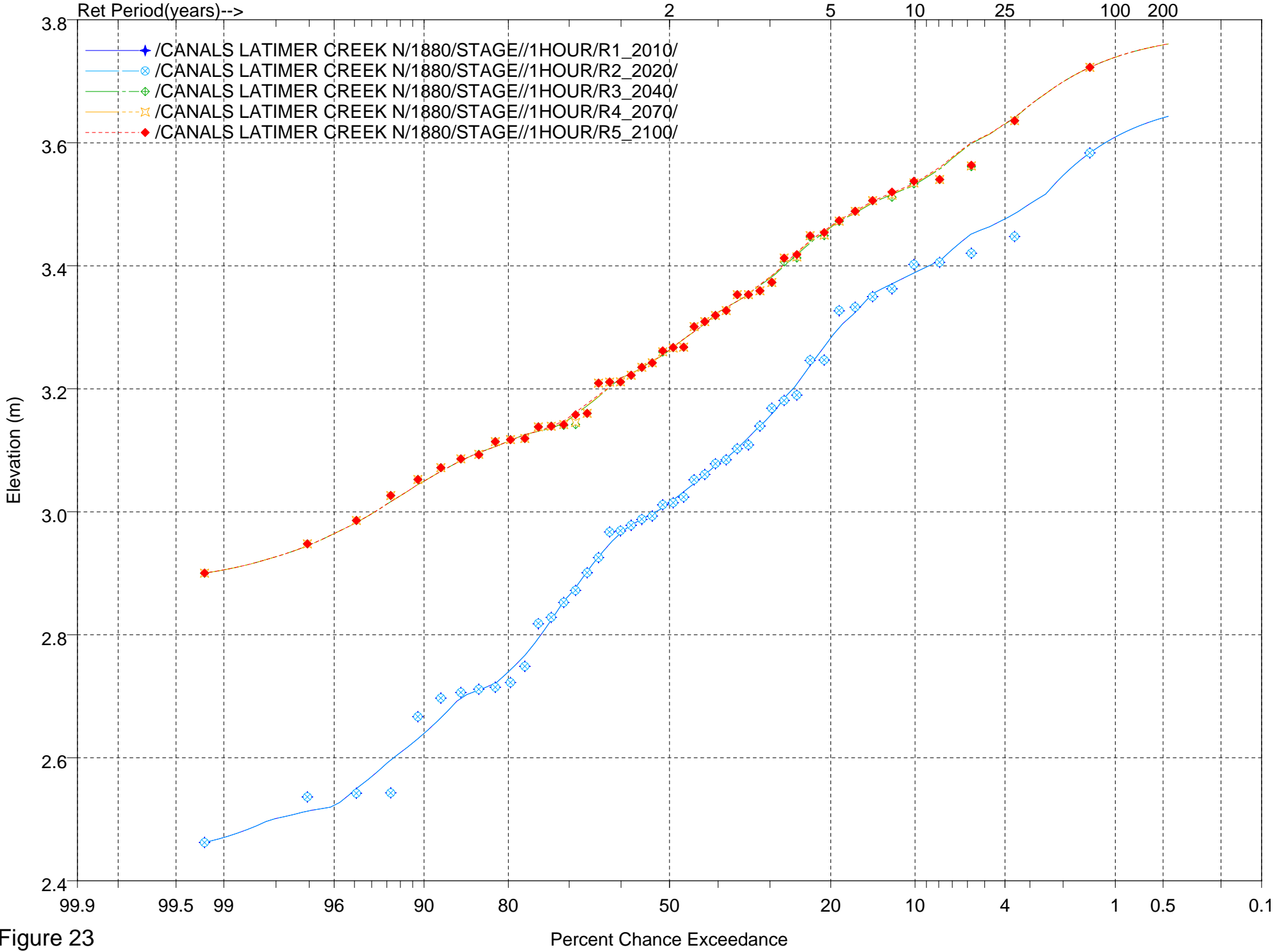


Figure 23

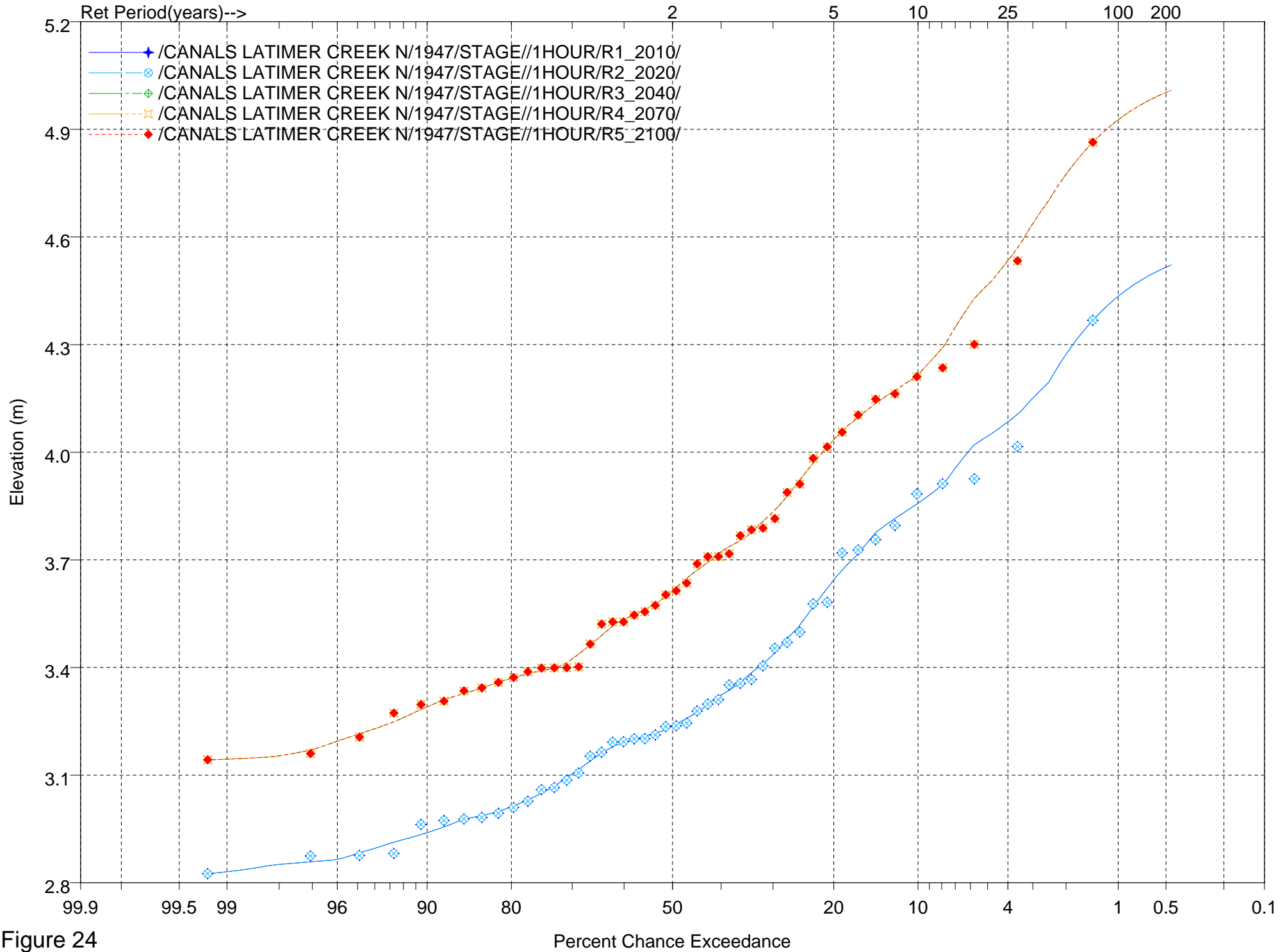


Figure 24

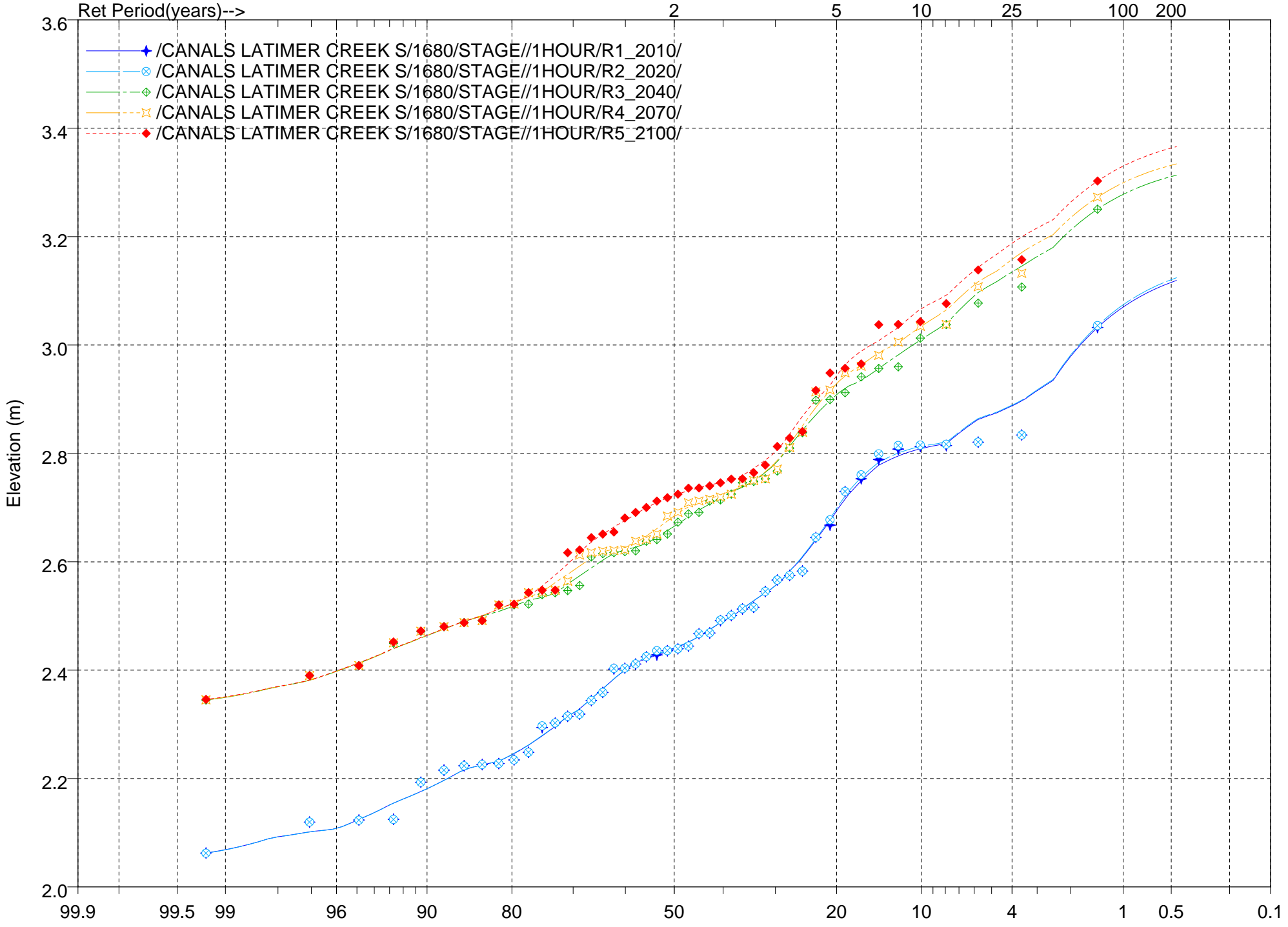


Figure 25

Percent Chance Exceedance



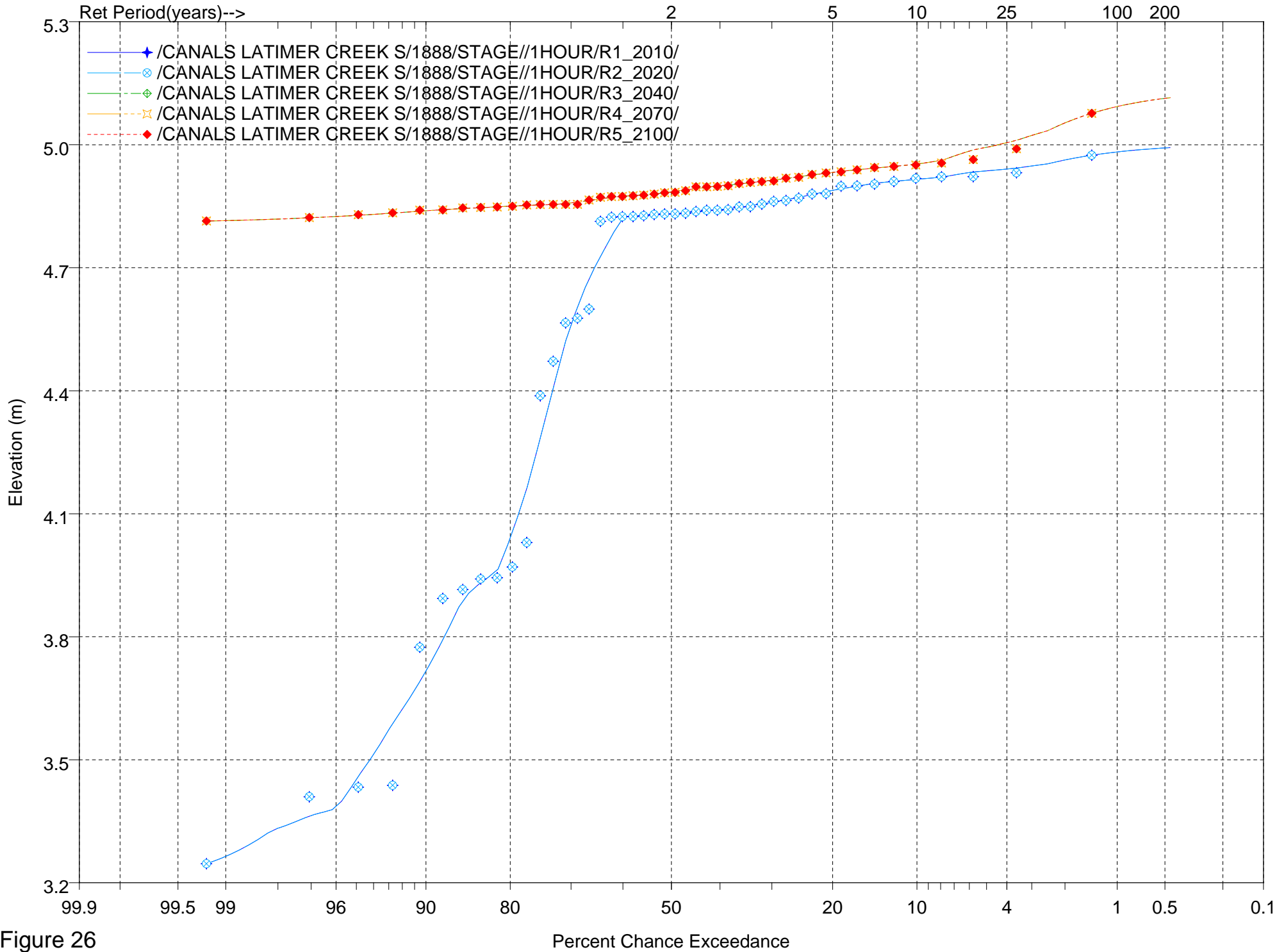


Figure 26

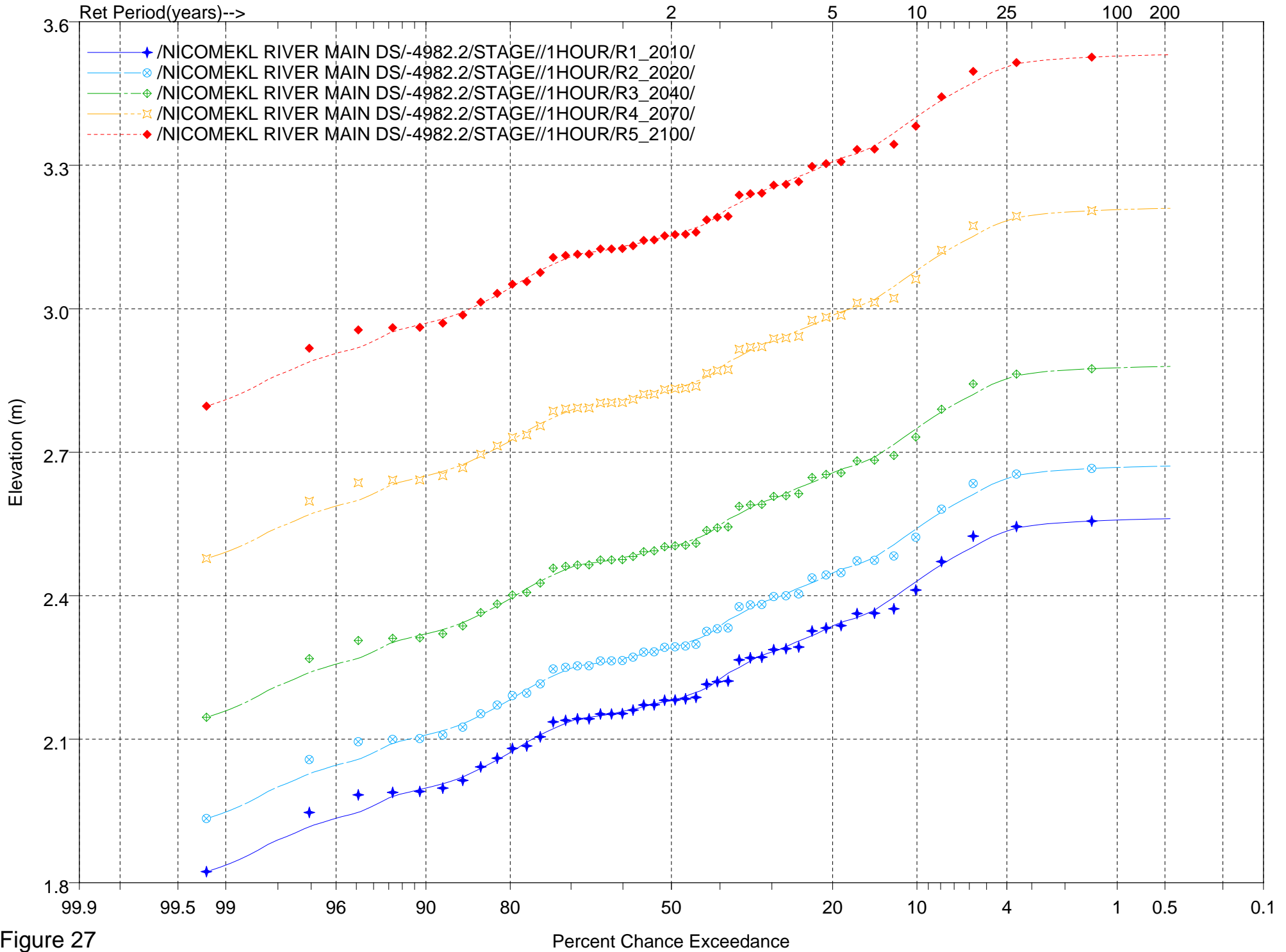


Figure 27

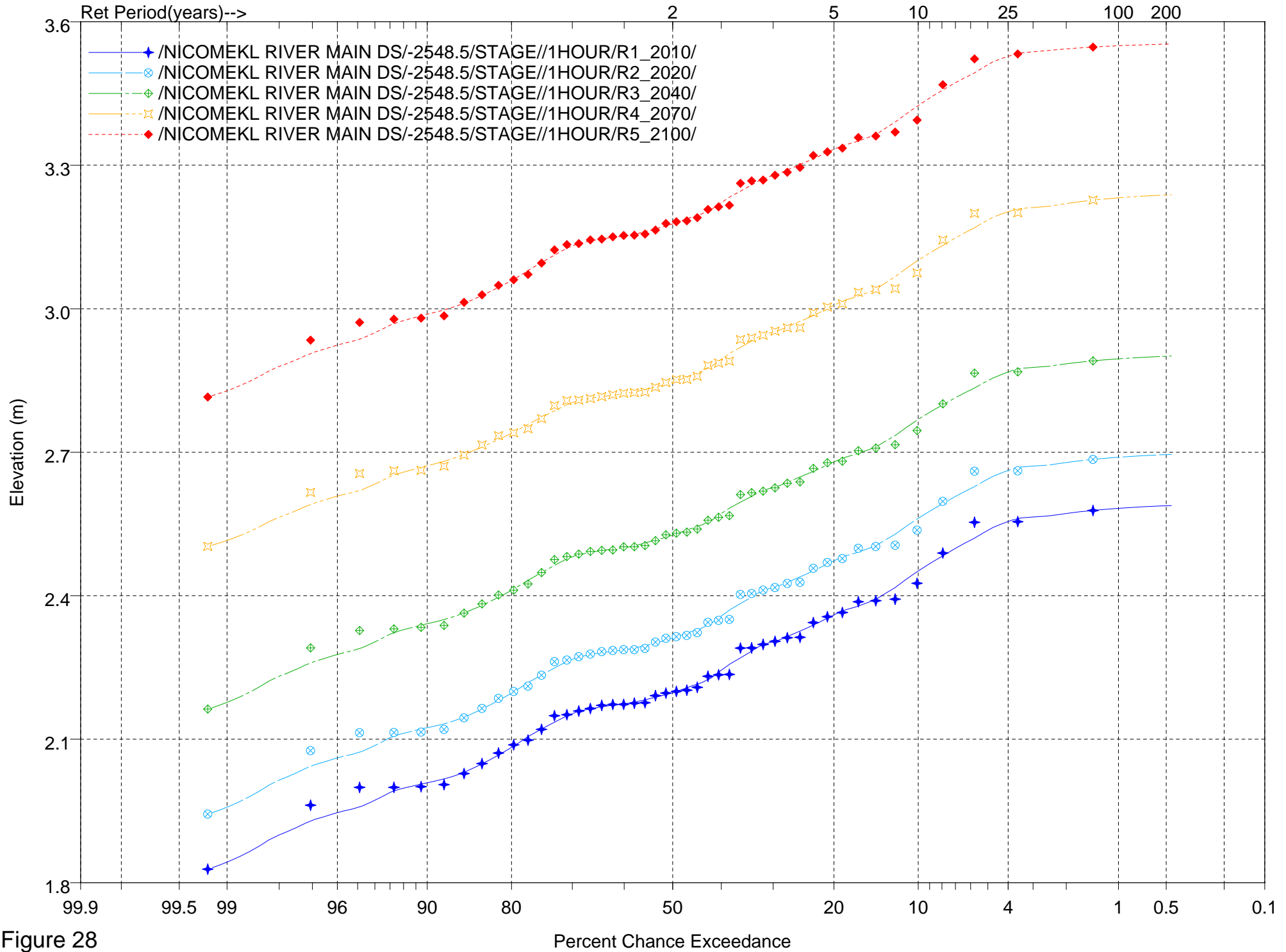


Figure 28

Annual Peak Frequency Analysis  
 Fit Type: 5 Point Moving Average distribution using the method of Linear Interpolation, Hosking Plotting Position

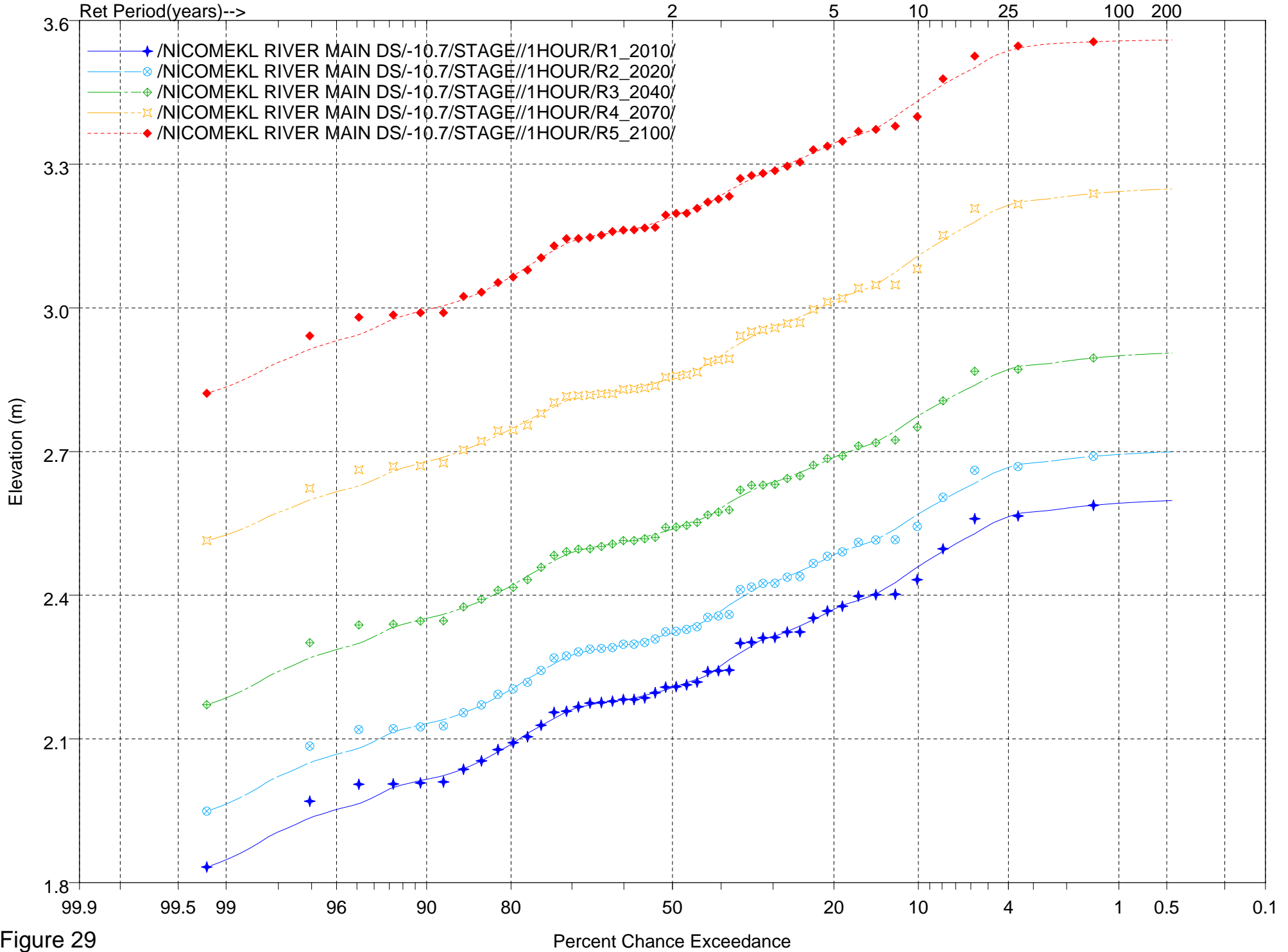


Figure 29

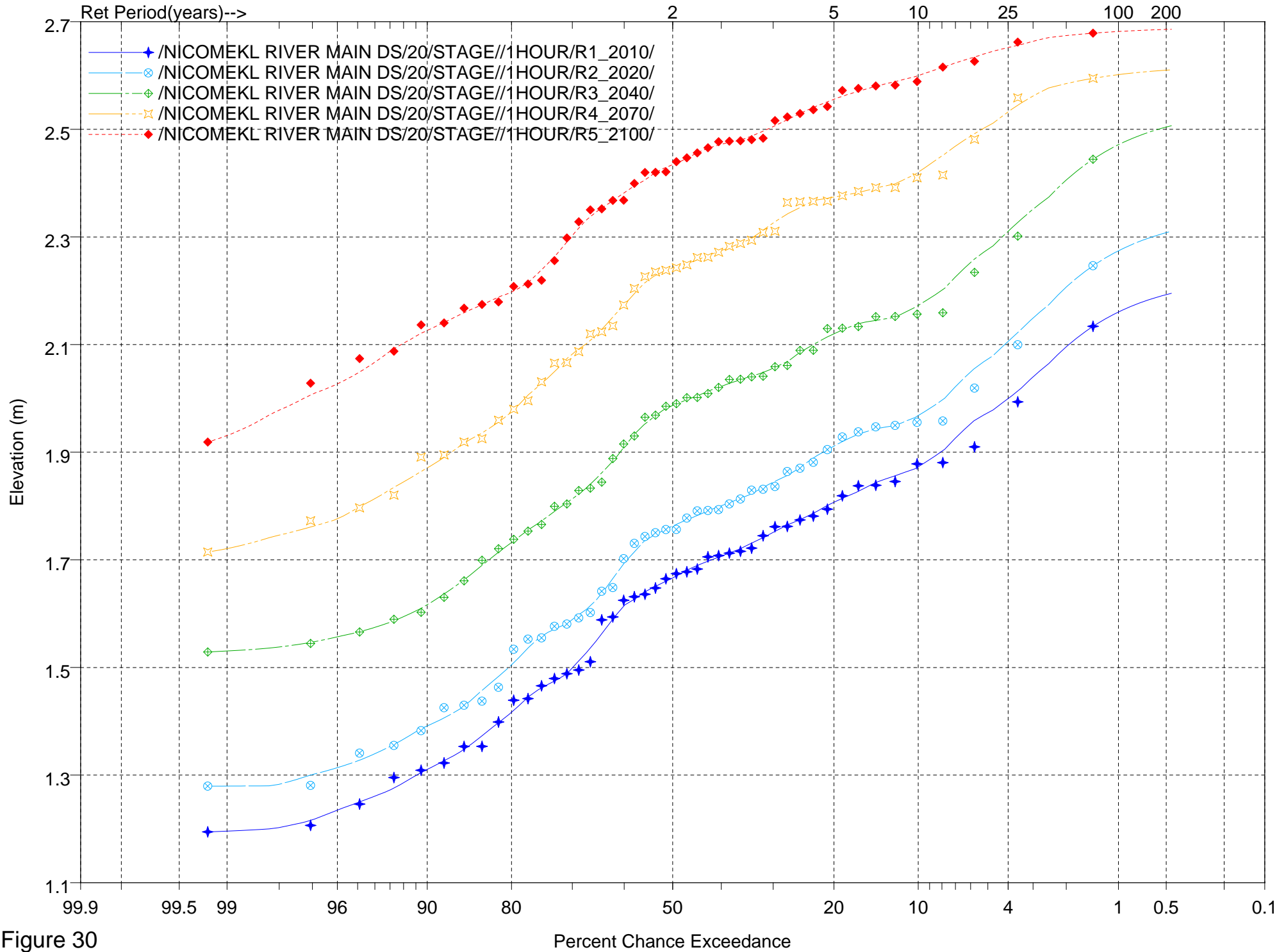


Figure 30

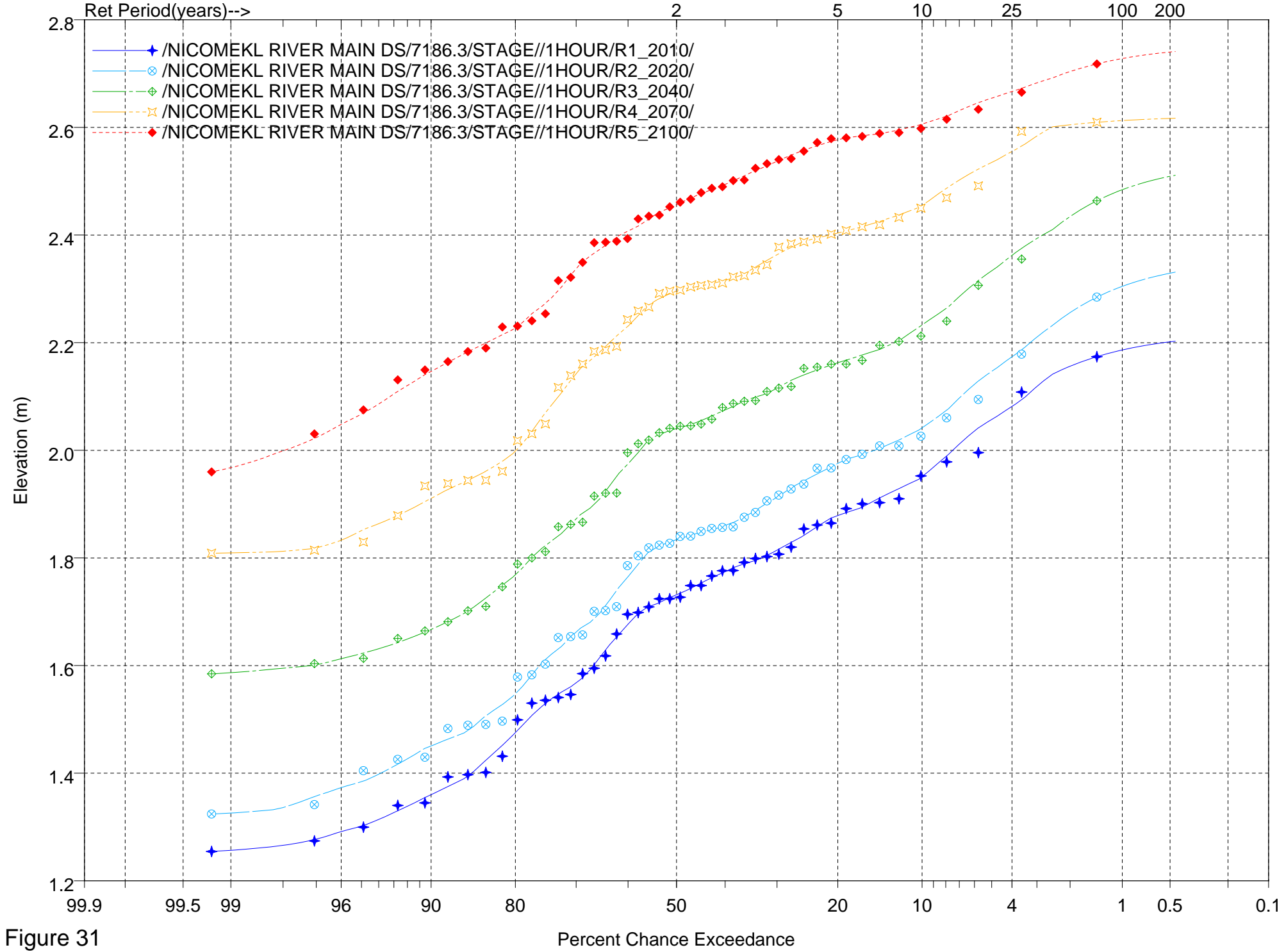


Figure 31

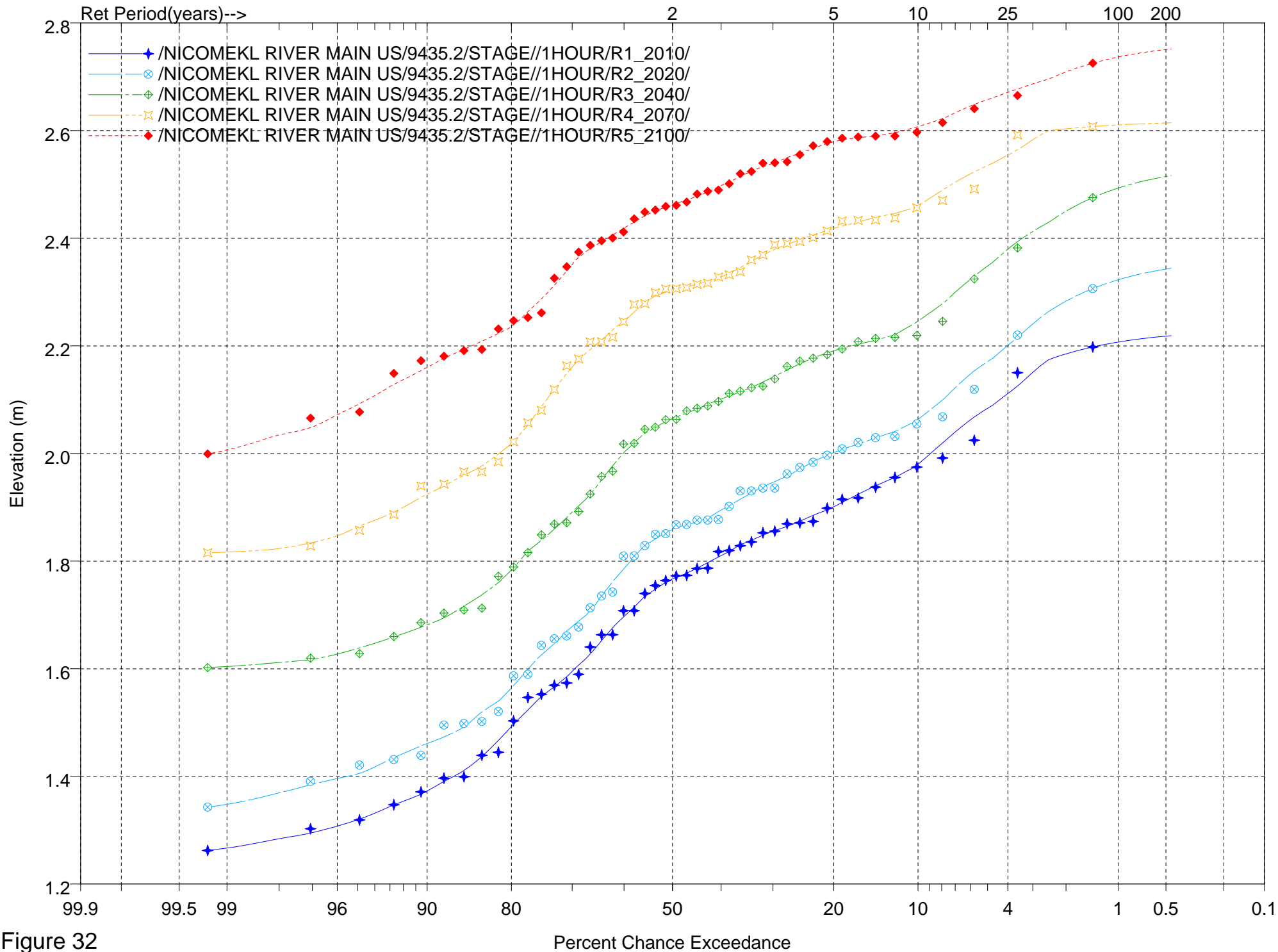


Figure 32

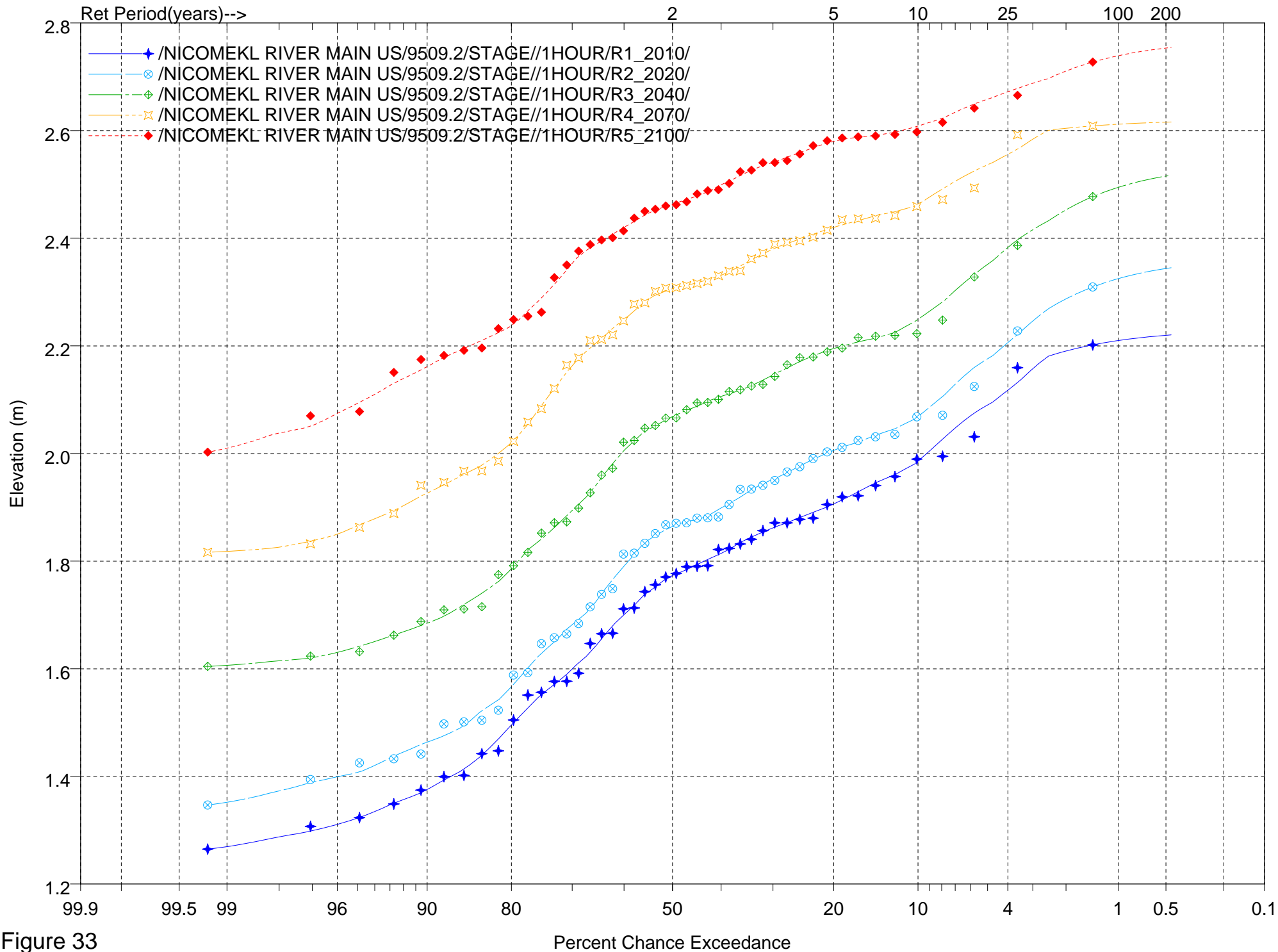


Figure 33



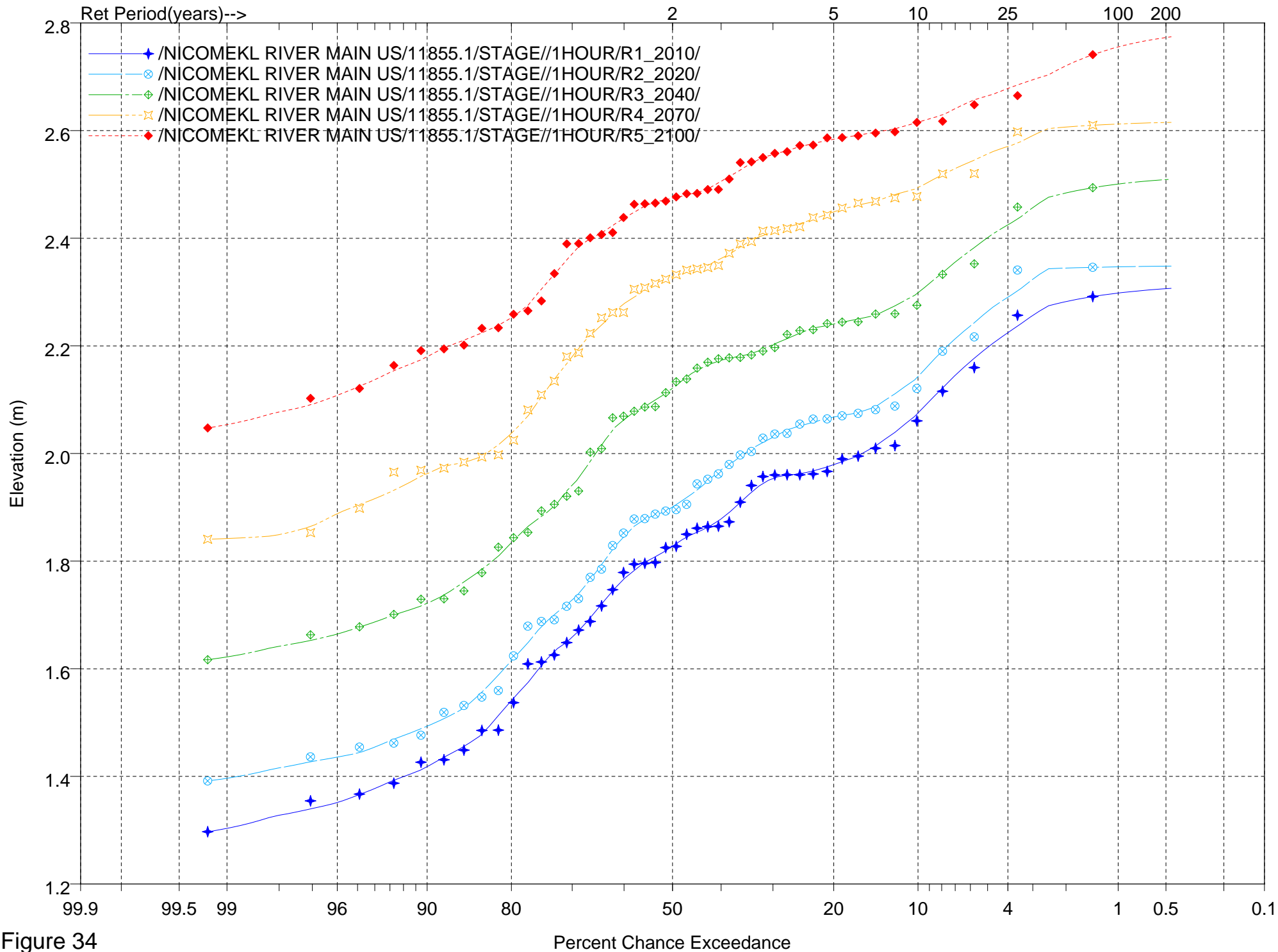


Figure 34

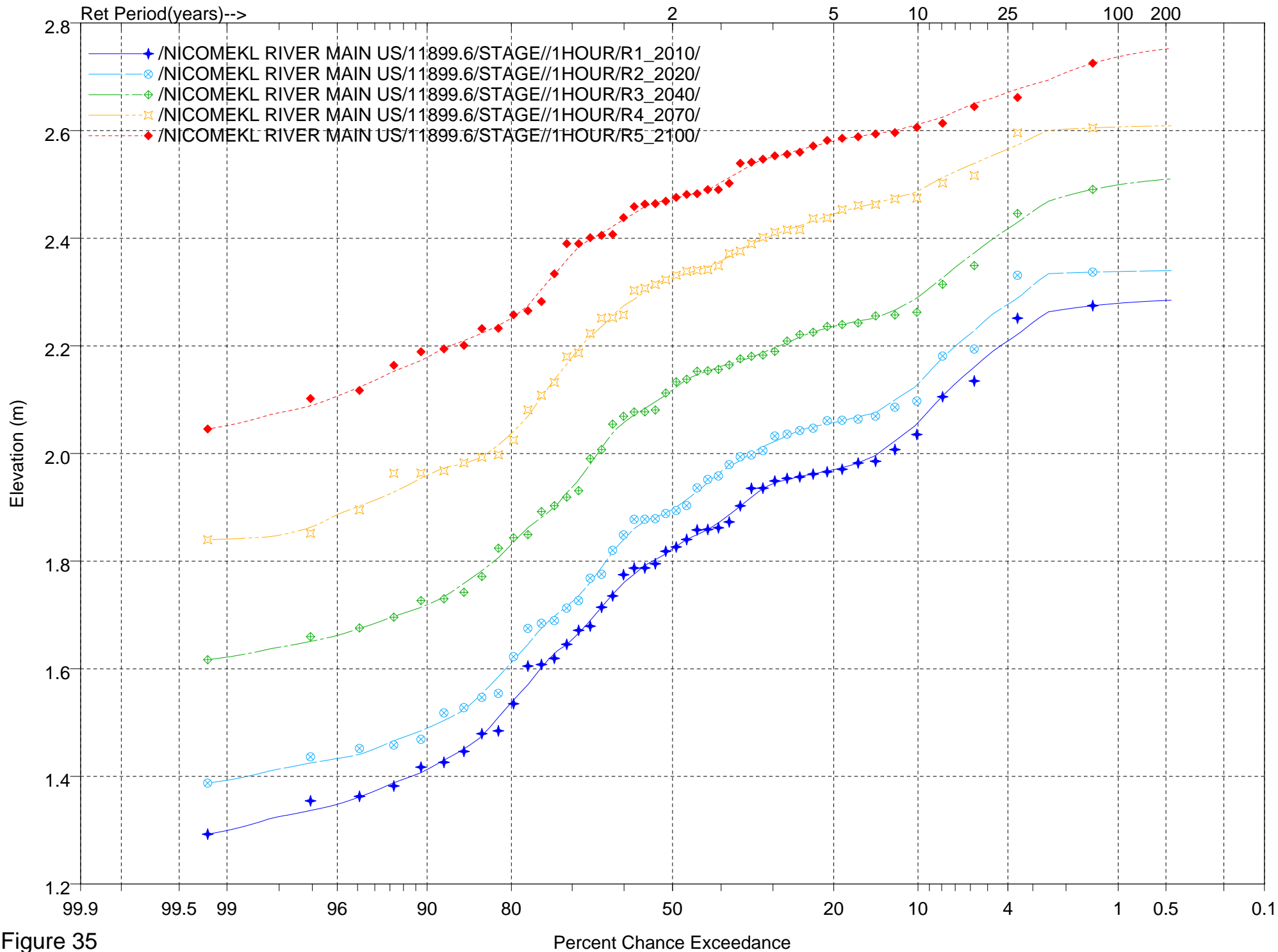


Figure 35

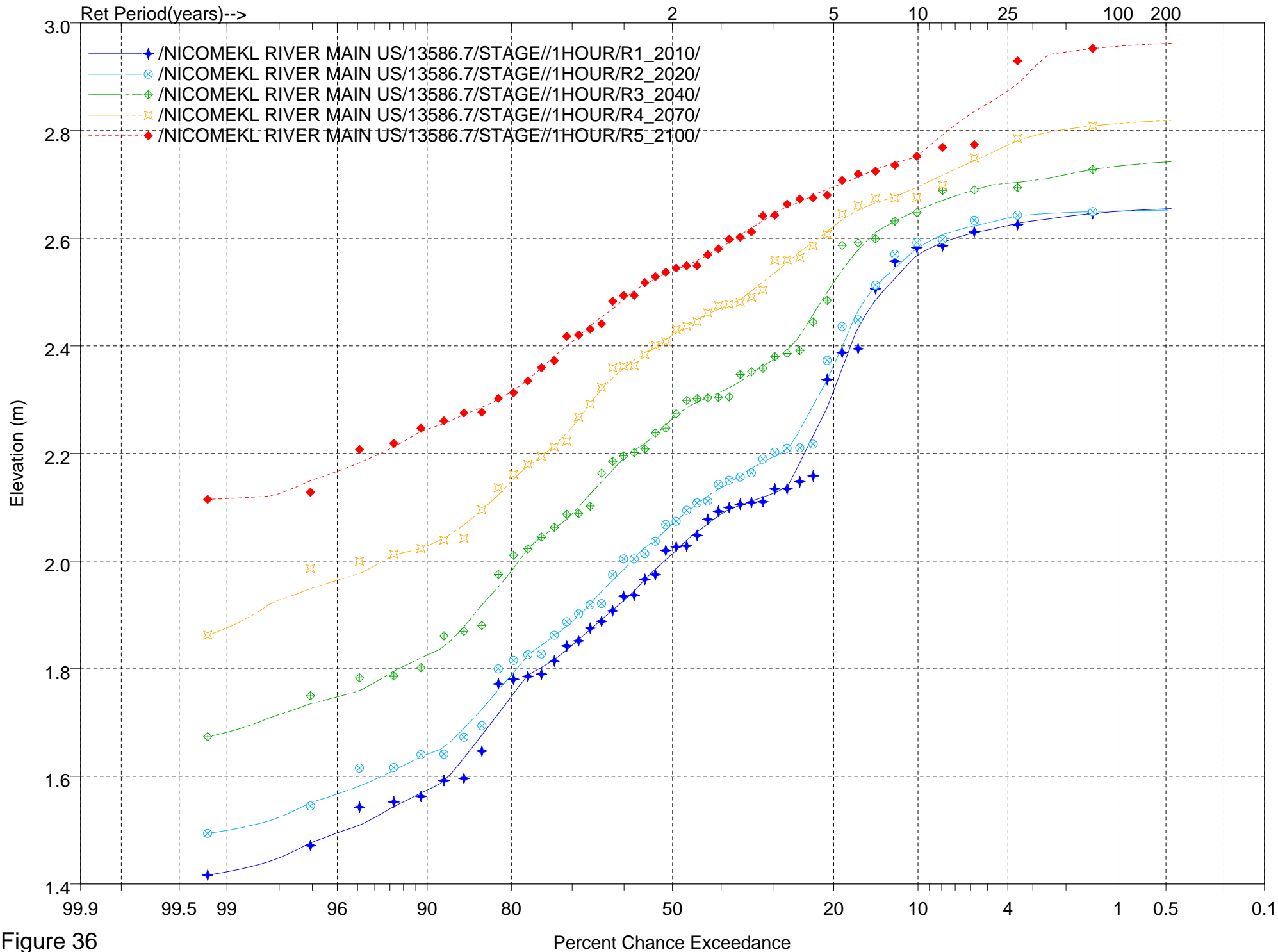


Figure 36

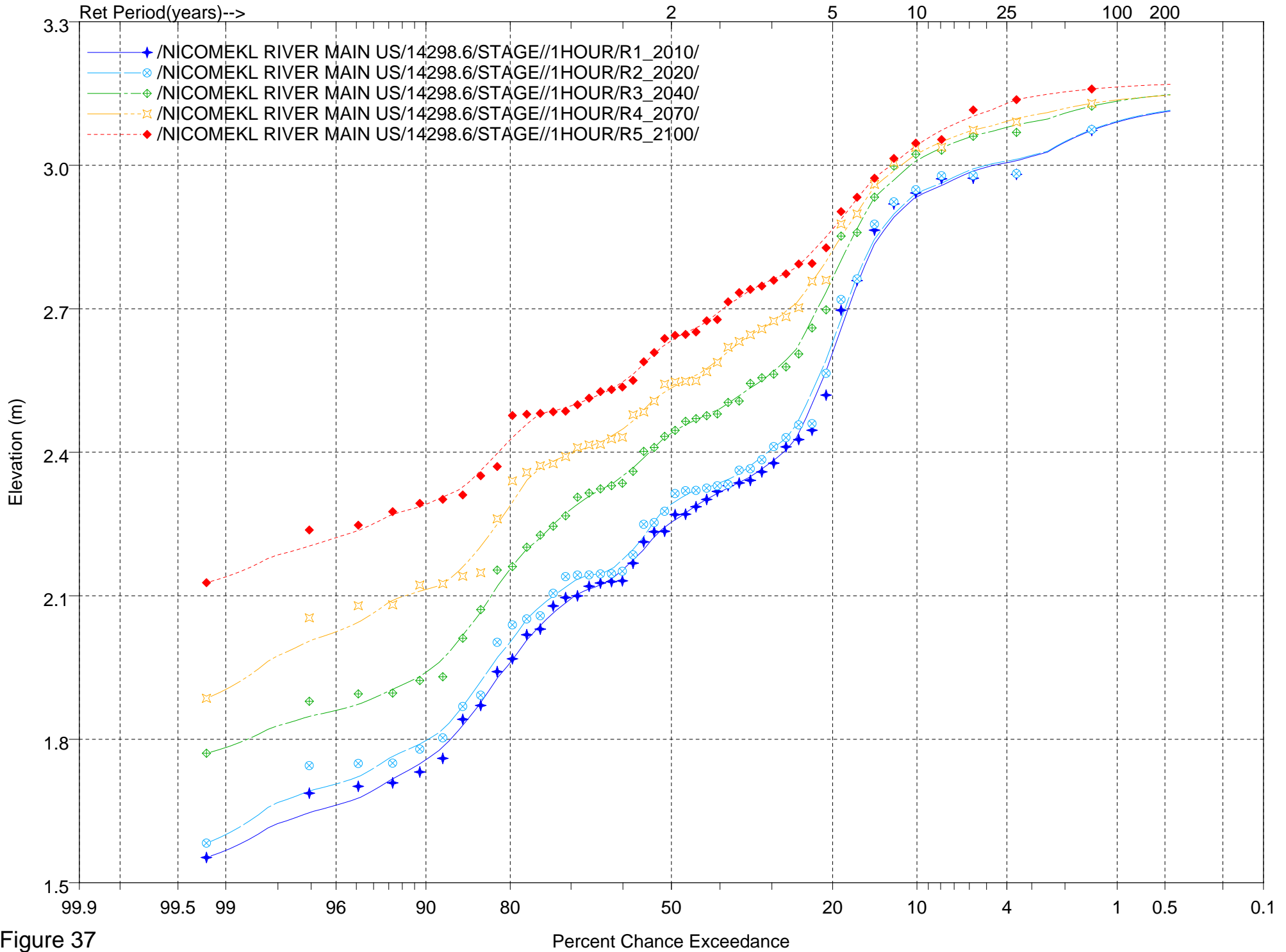


Figure 37

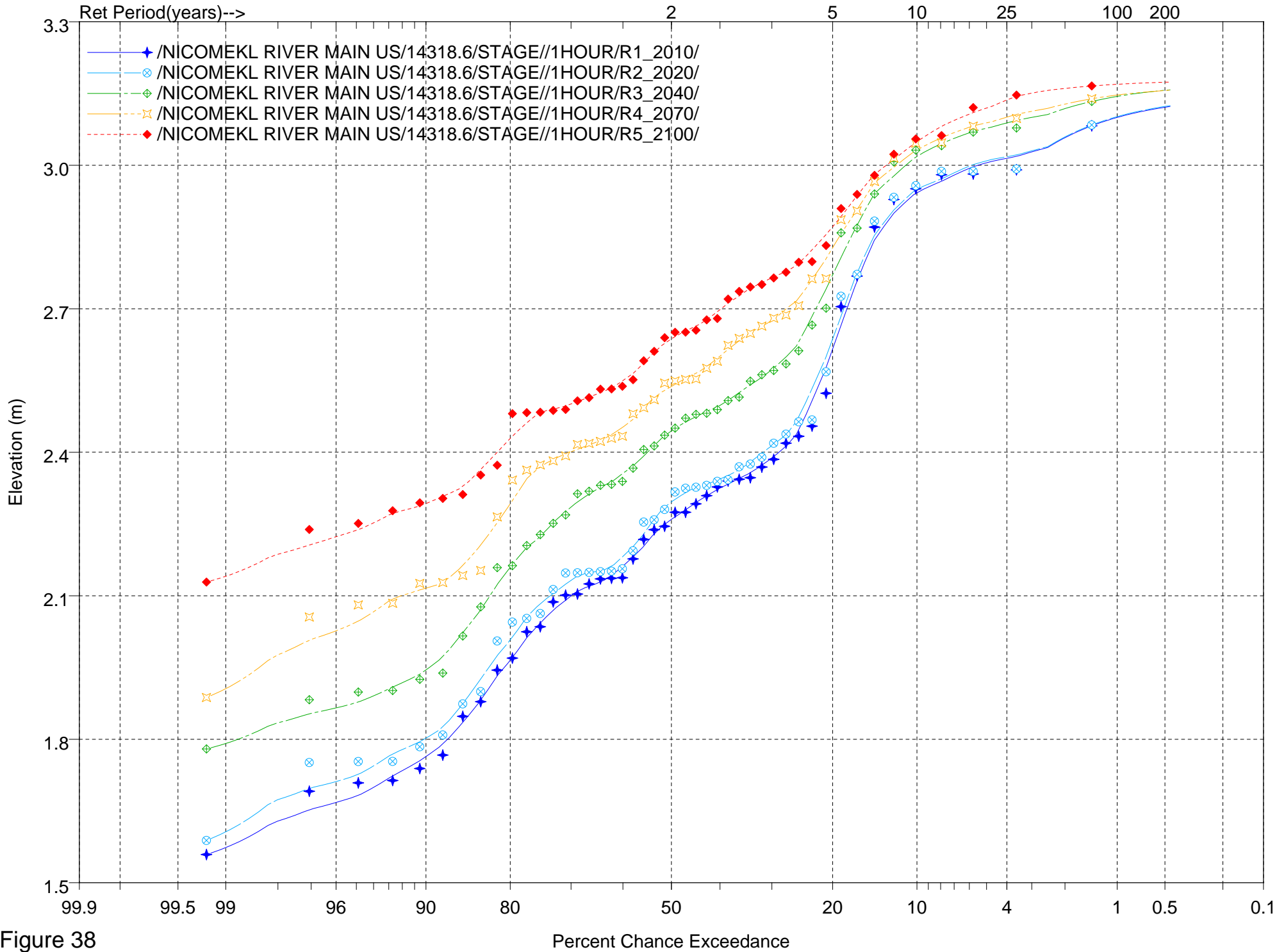


Figure 38

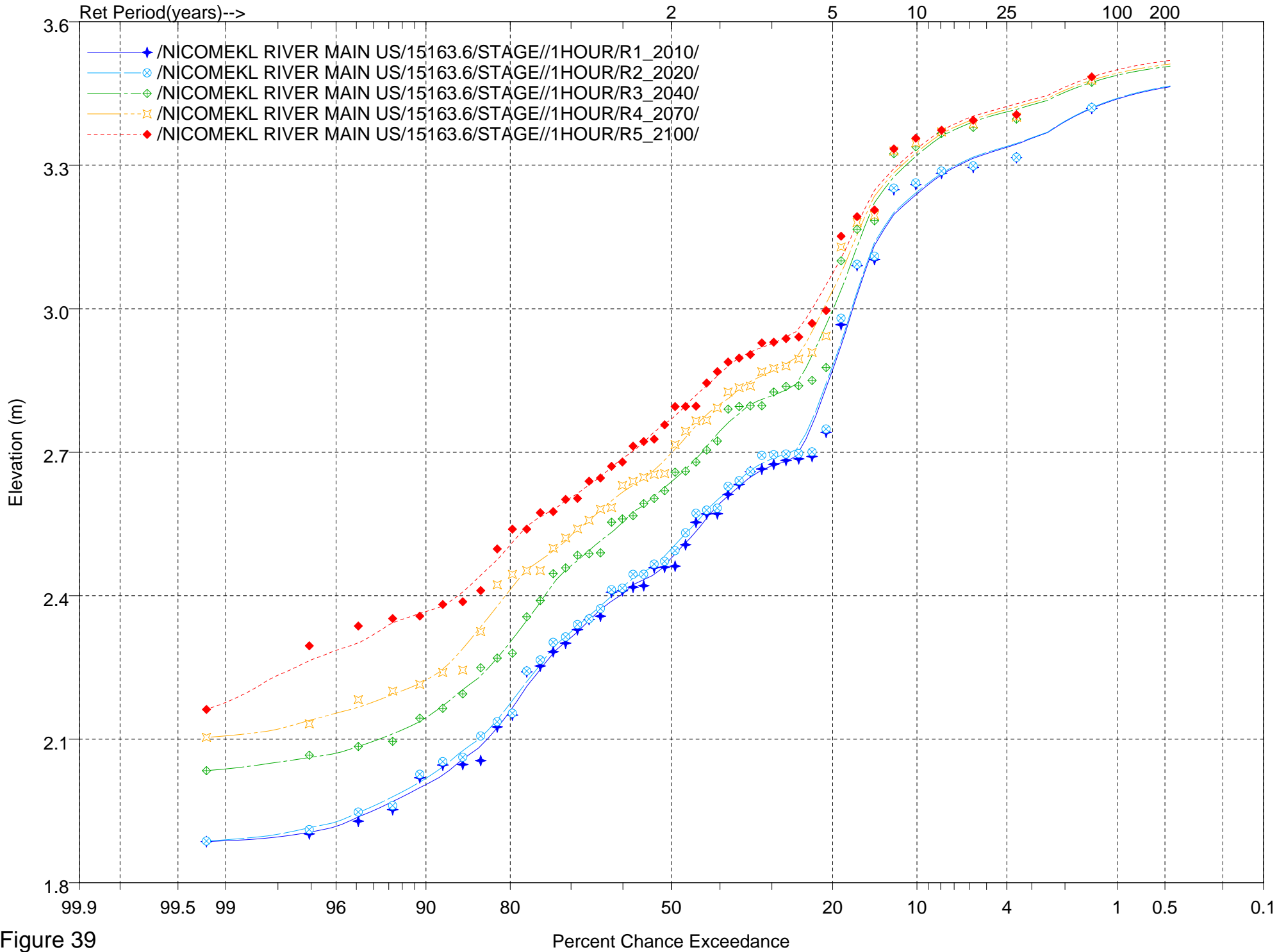


Figure 39

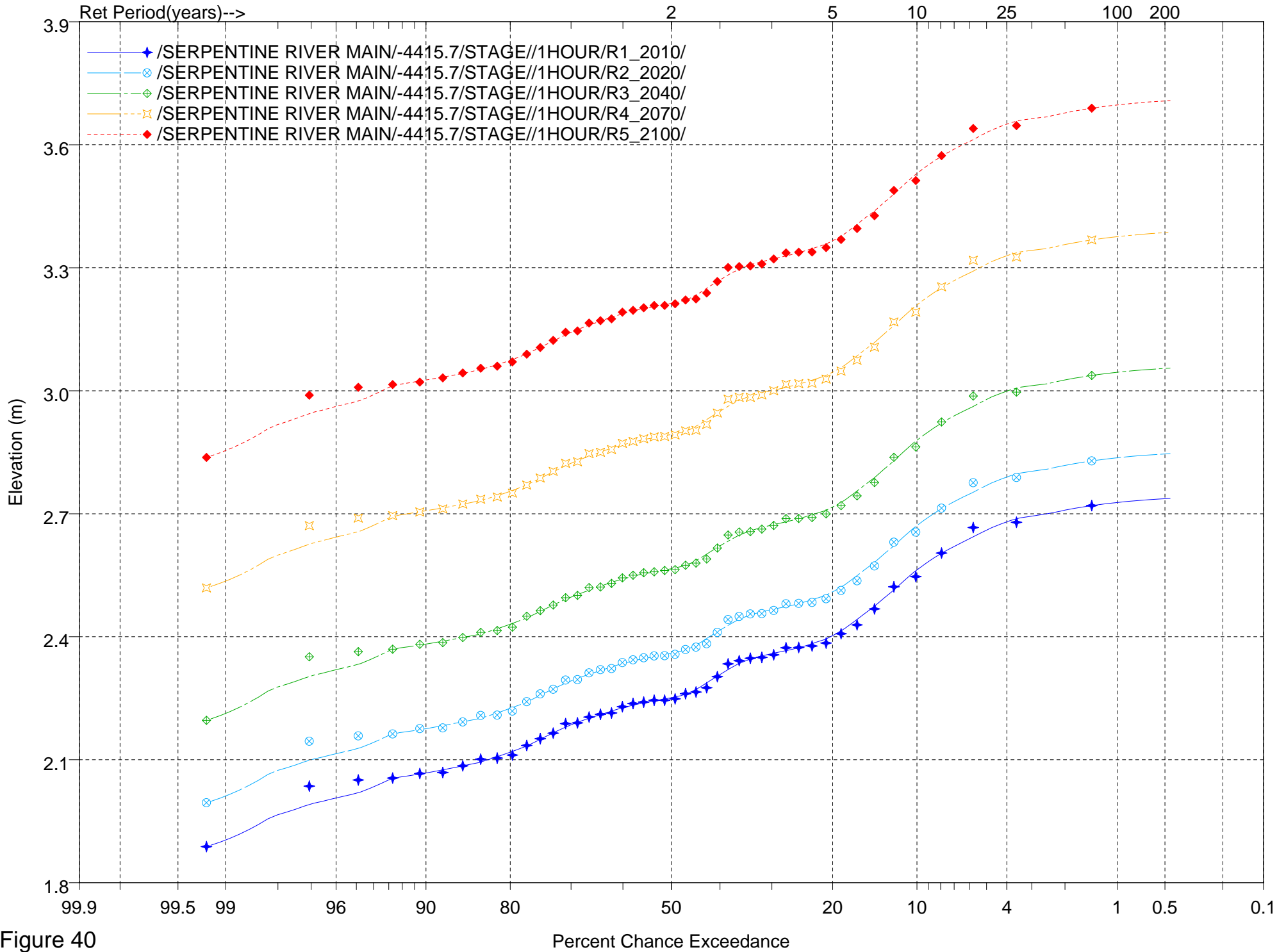


Figure 40

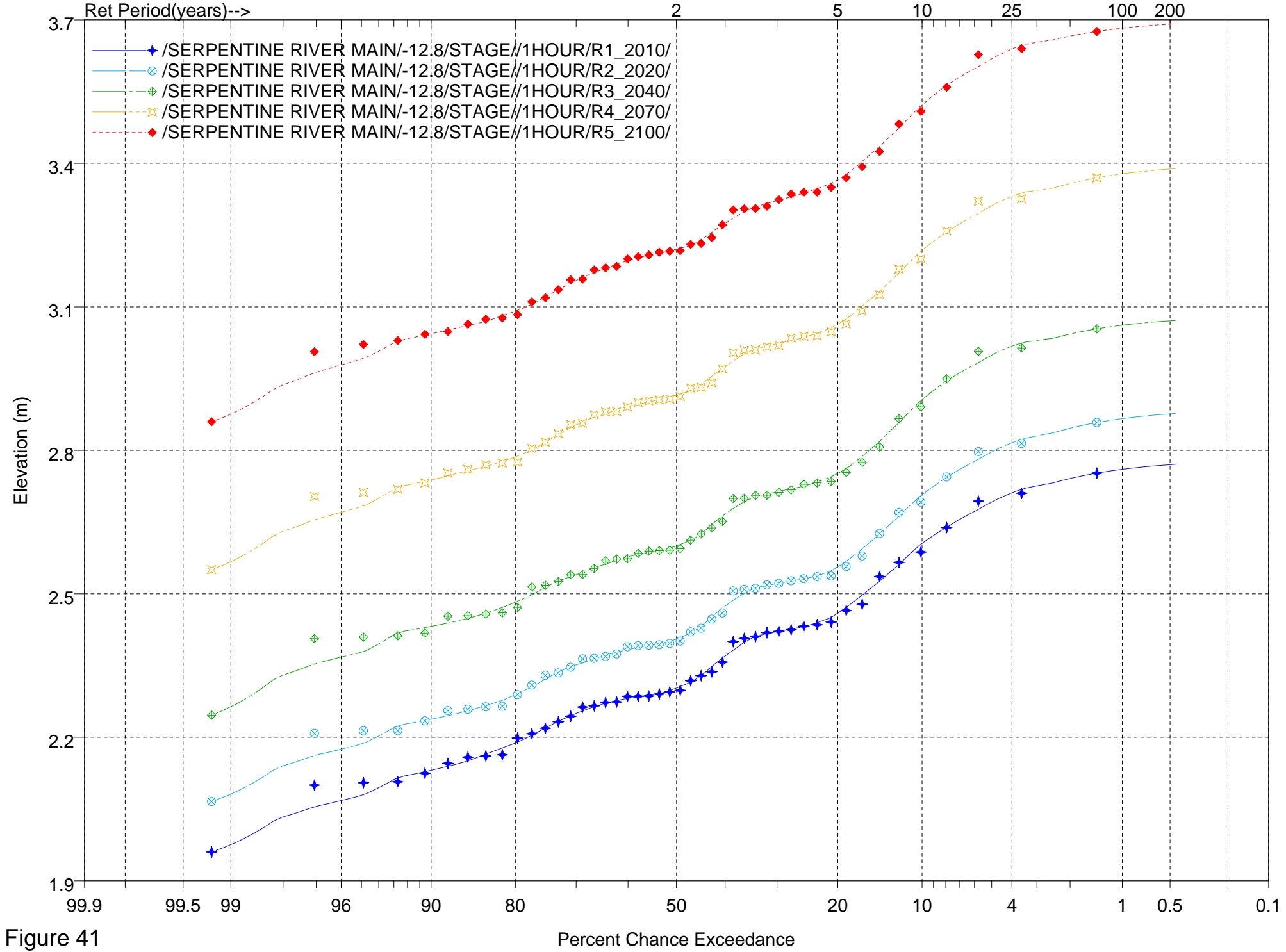


Figure 41



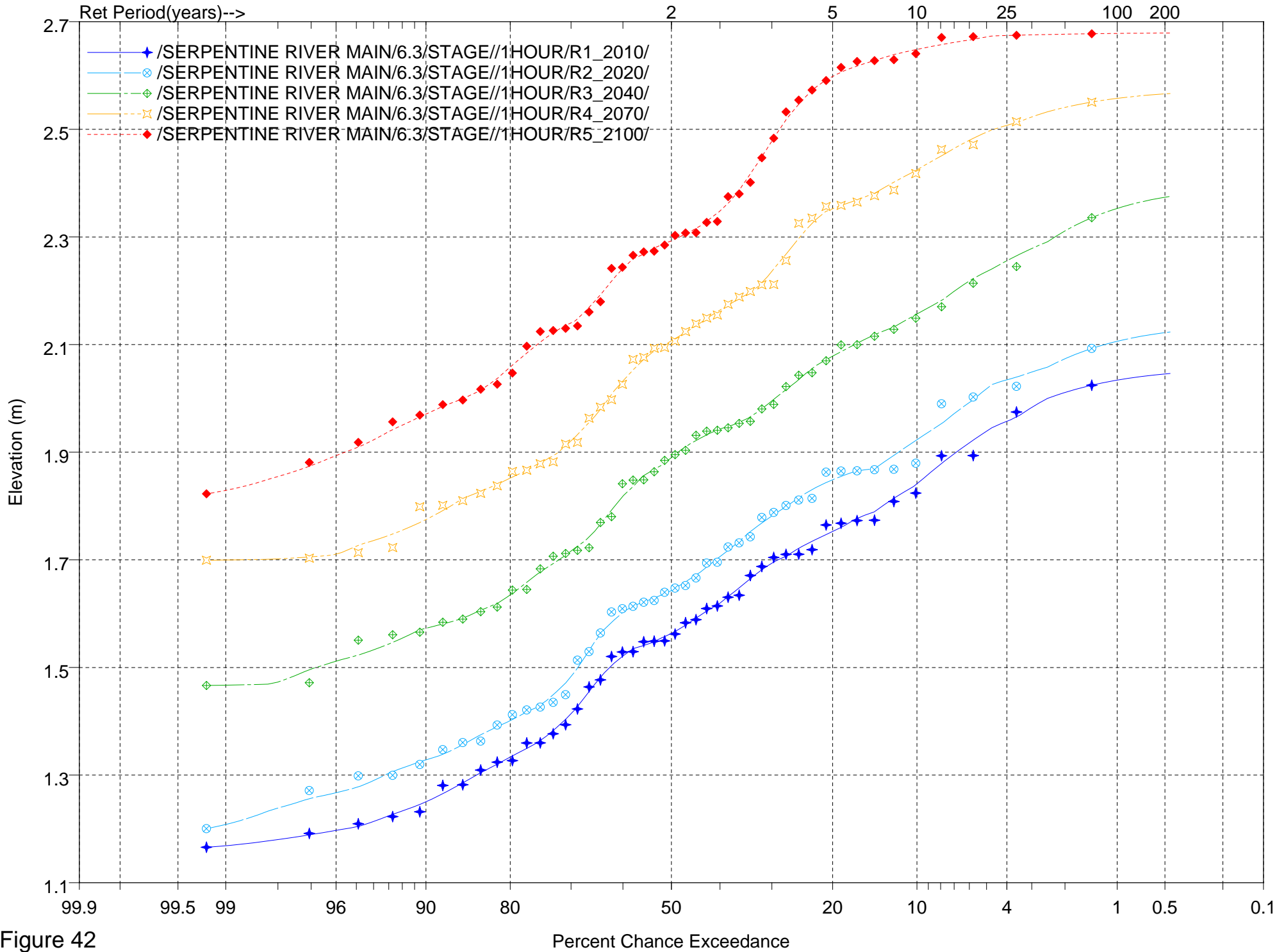


Figure 42

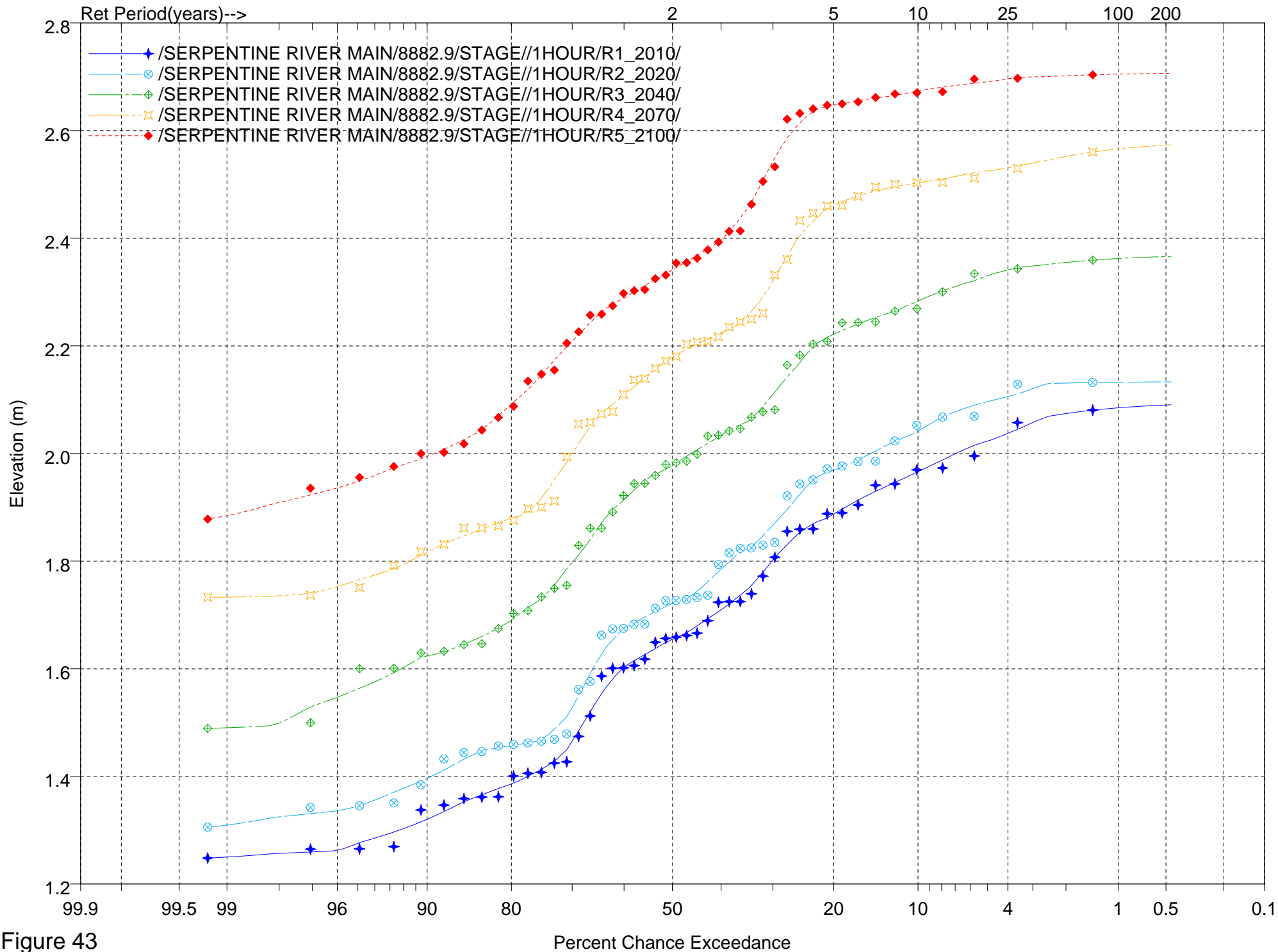


Figure 43

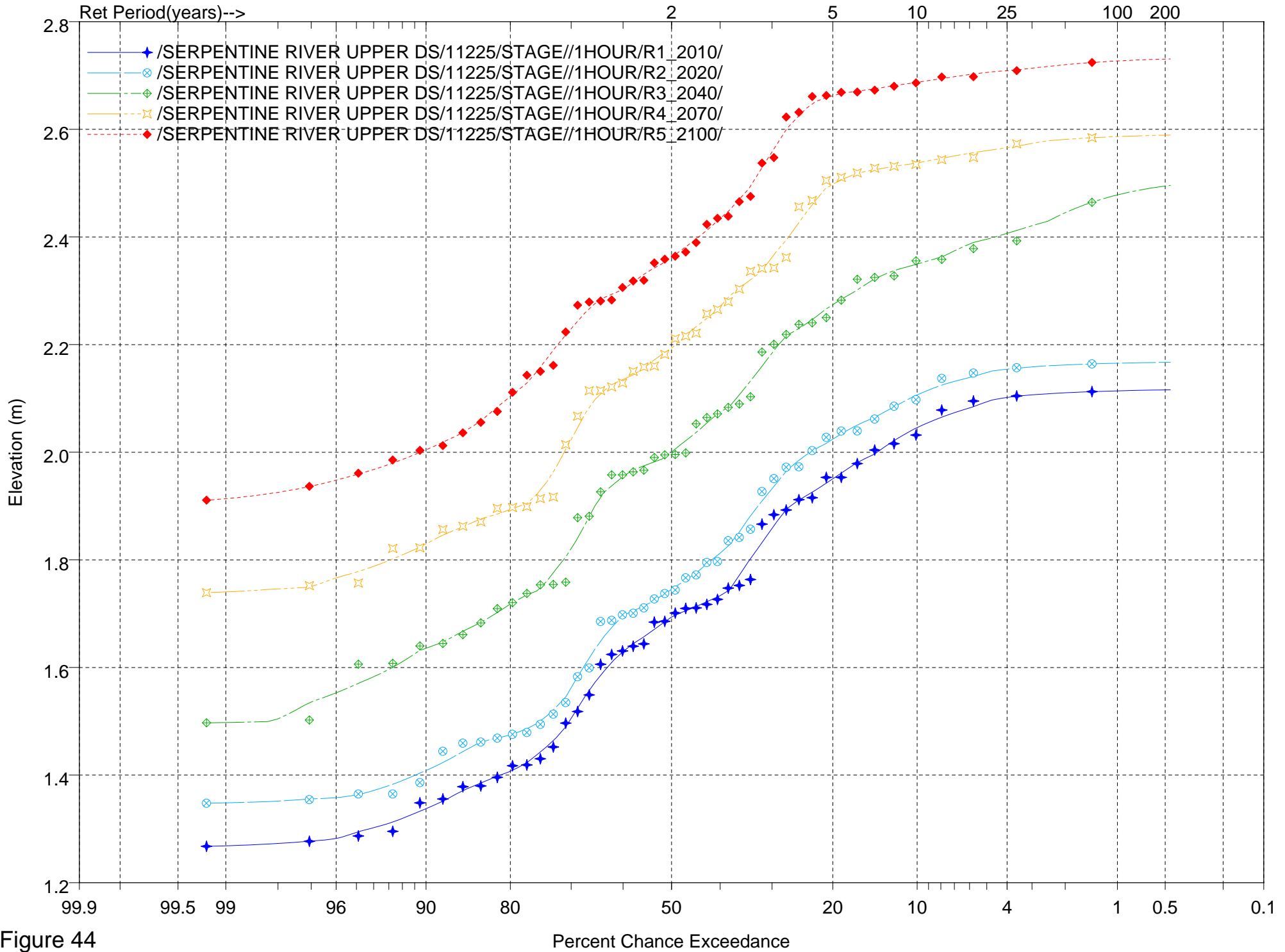


Figure 44

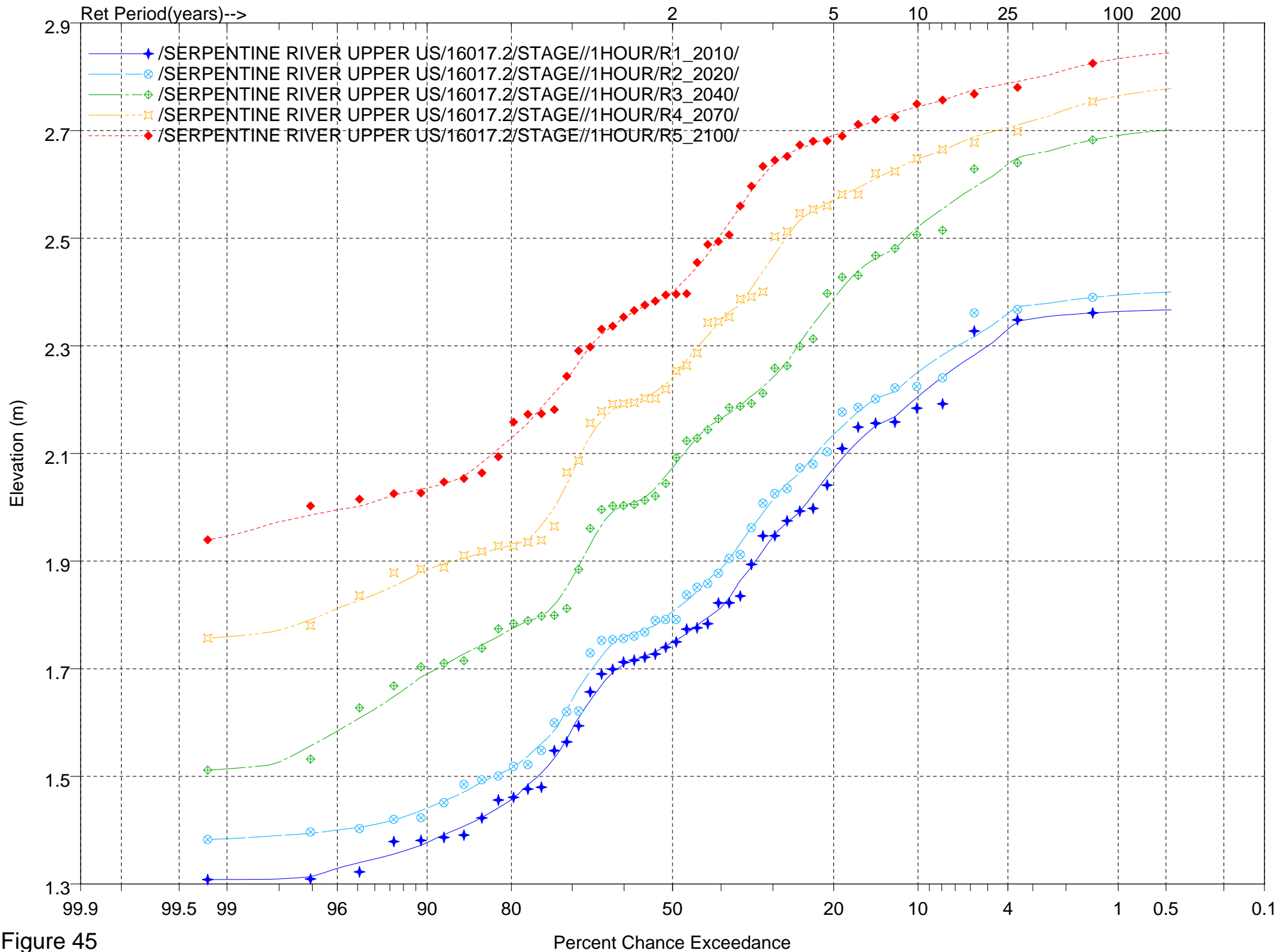


Figure 45

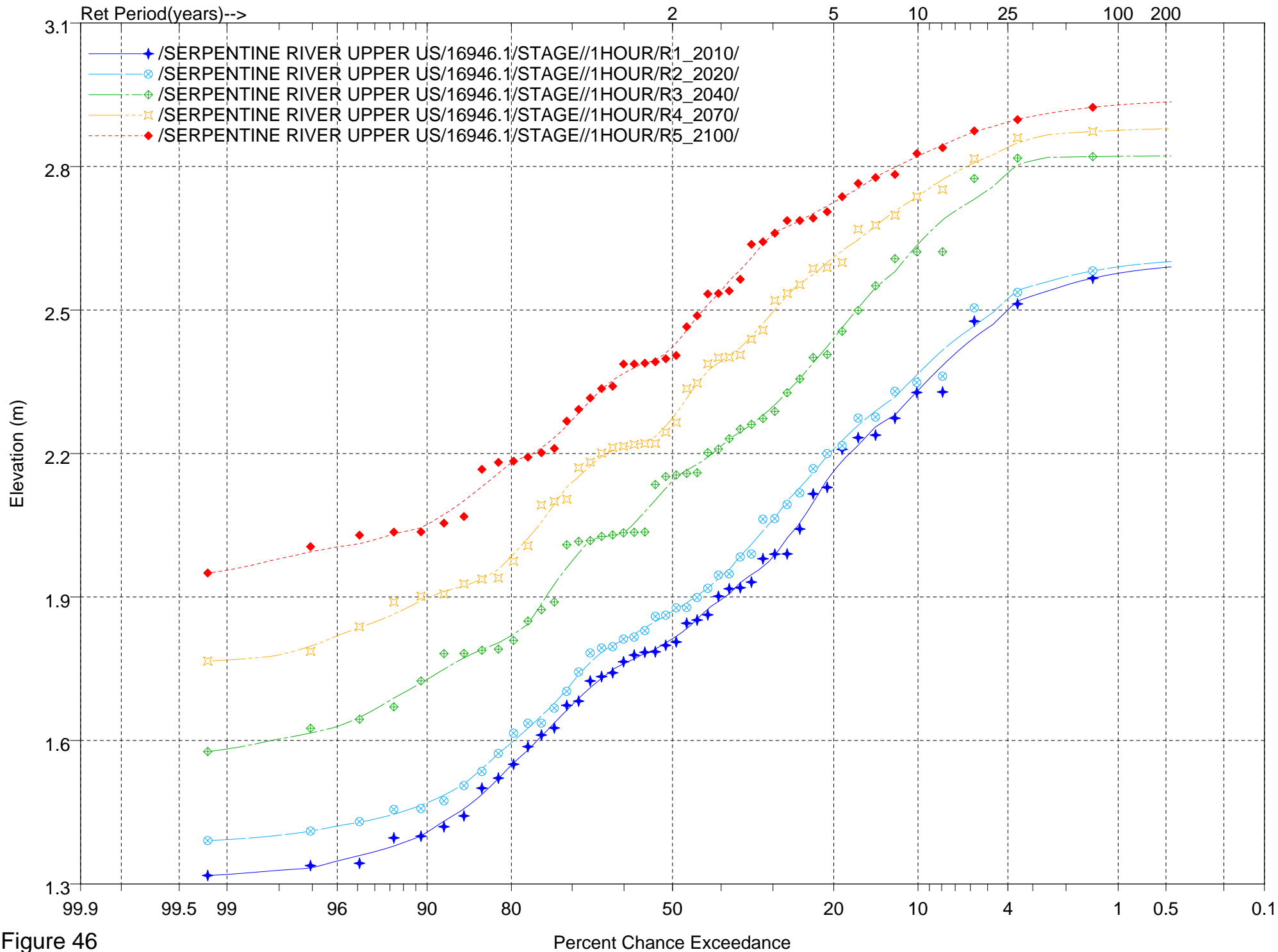


Figure 46

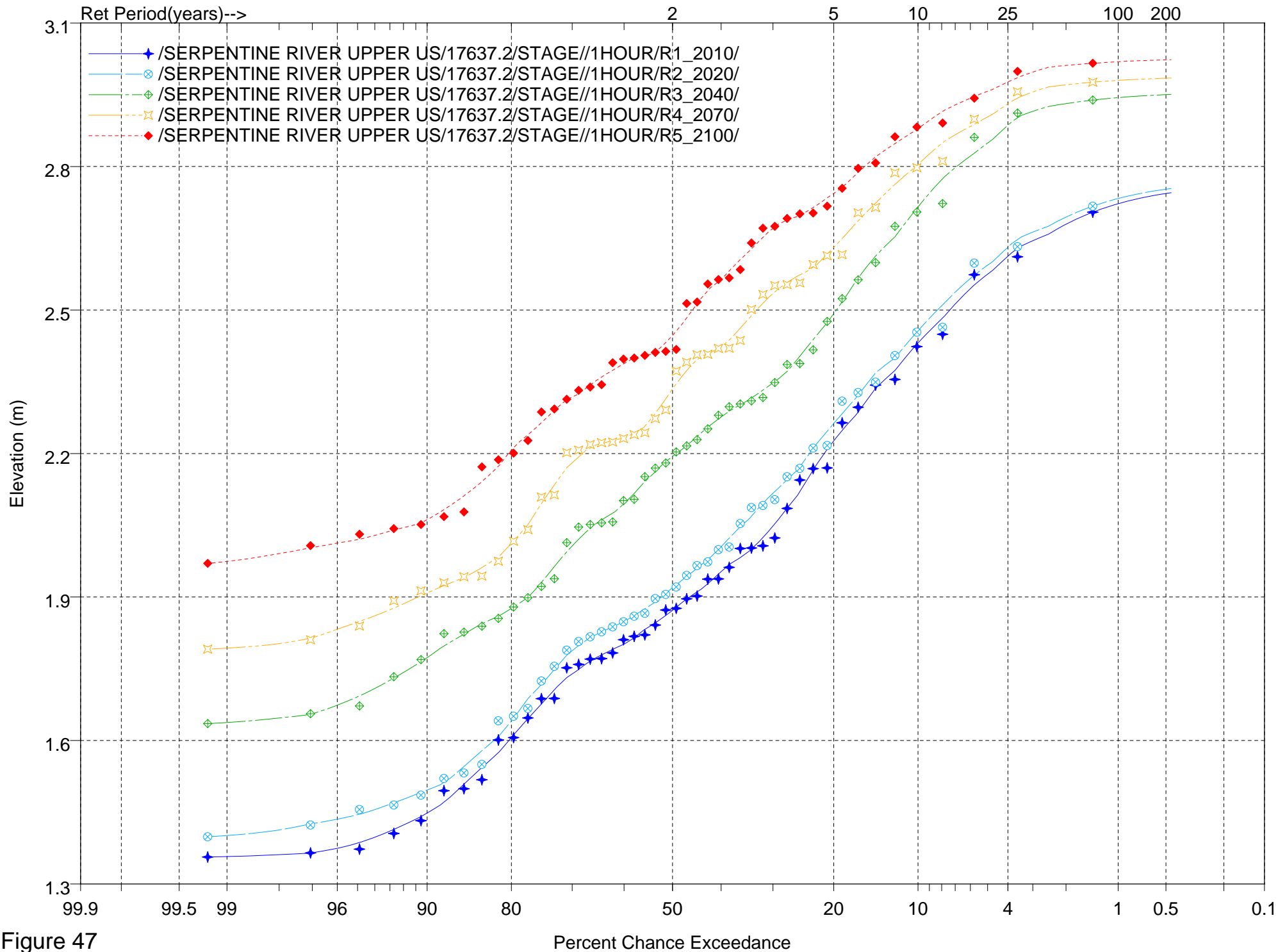


Figure 47

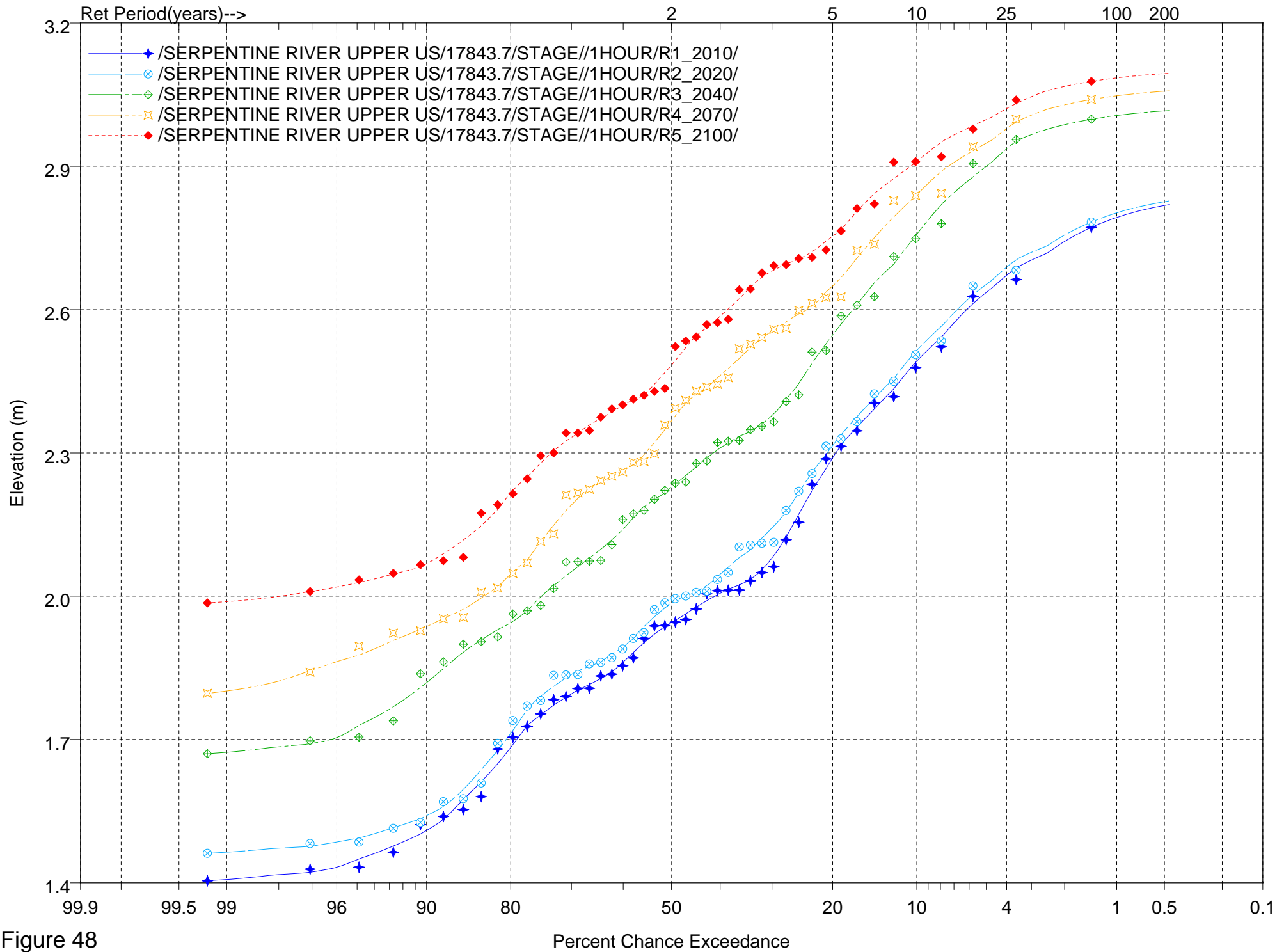


Figure 48

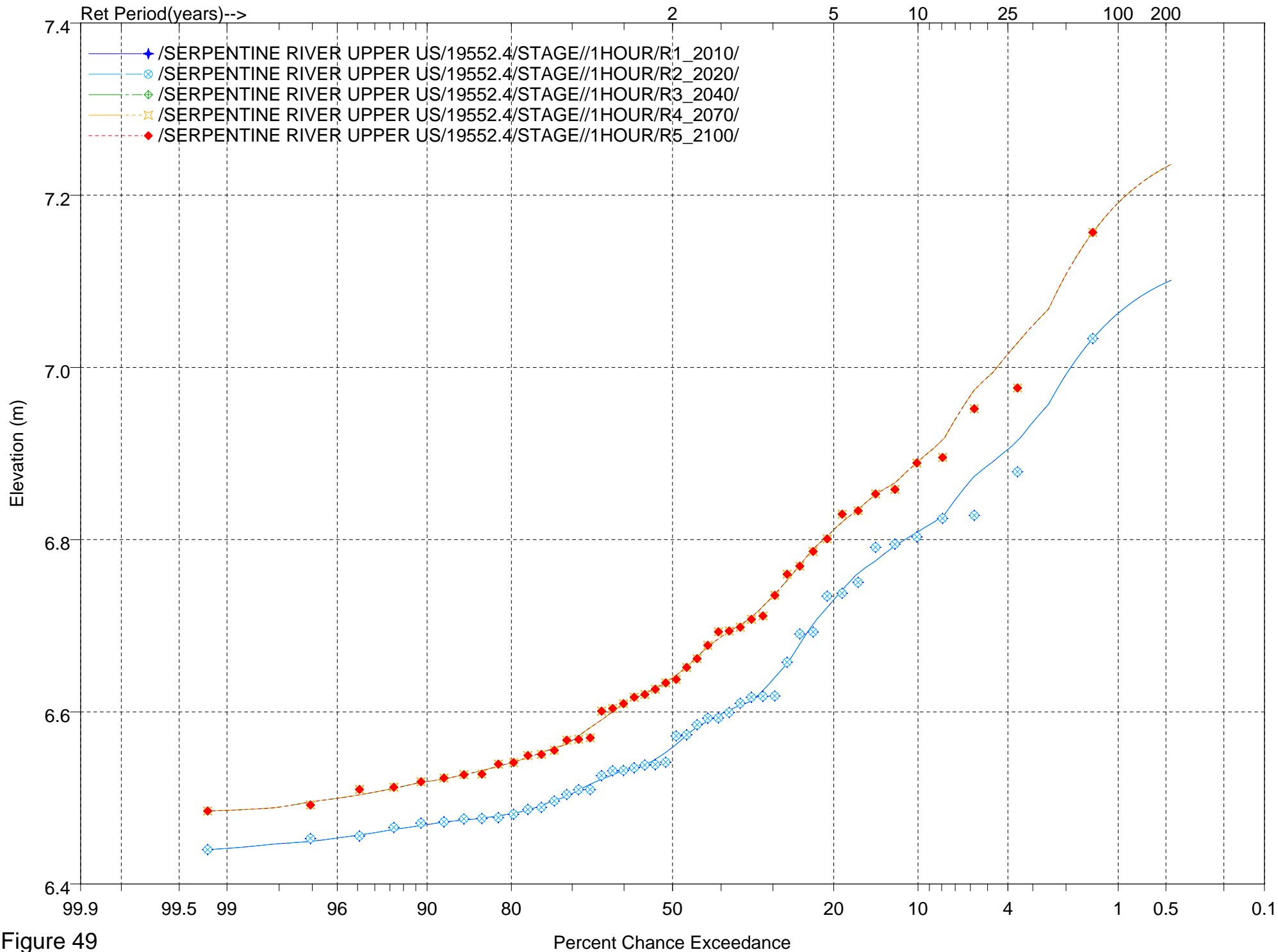


Figure 49



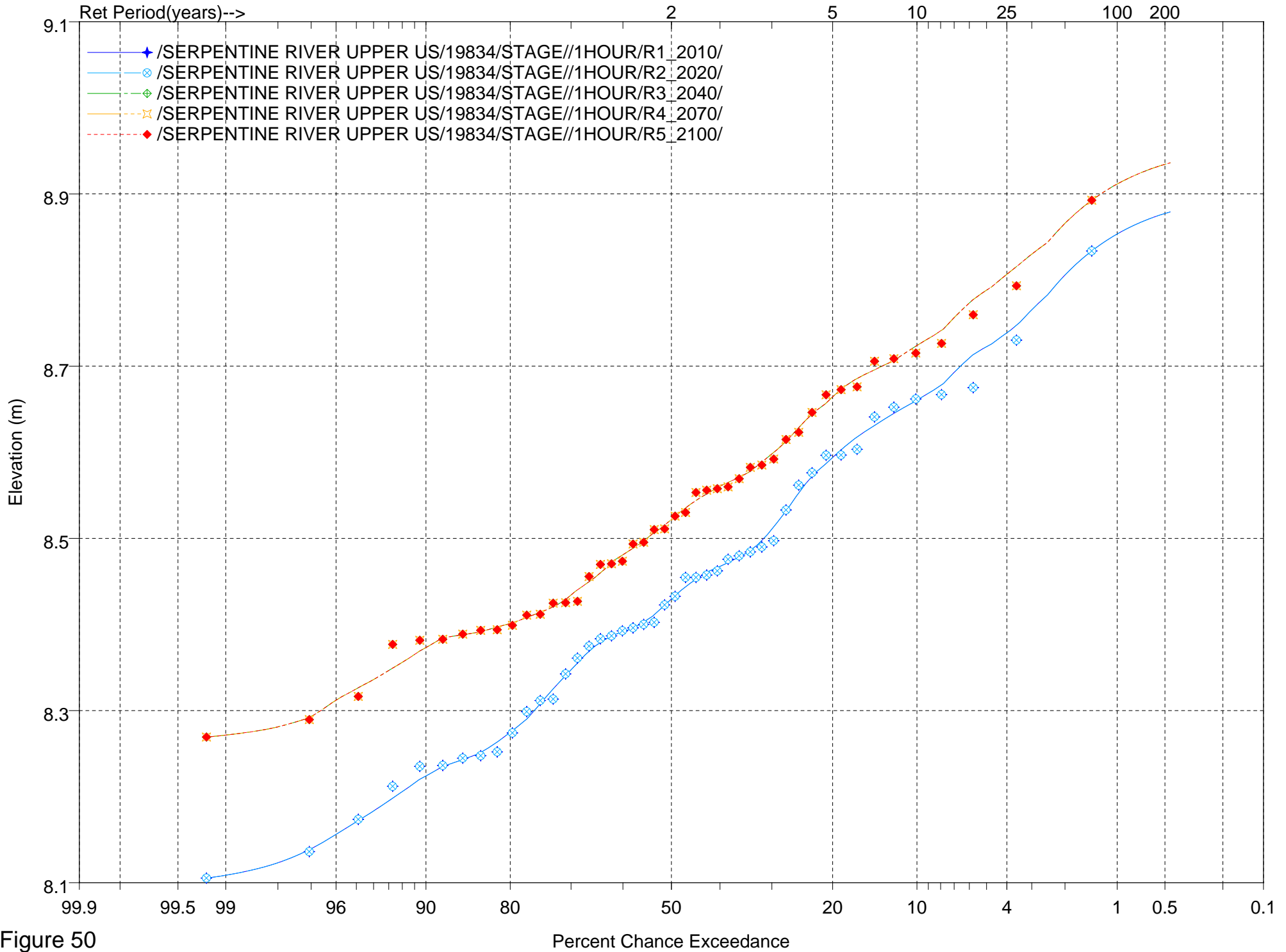


Figure 50

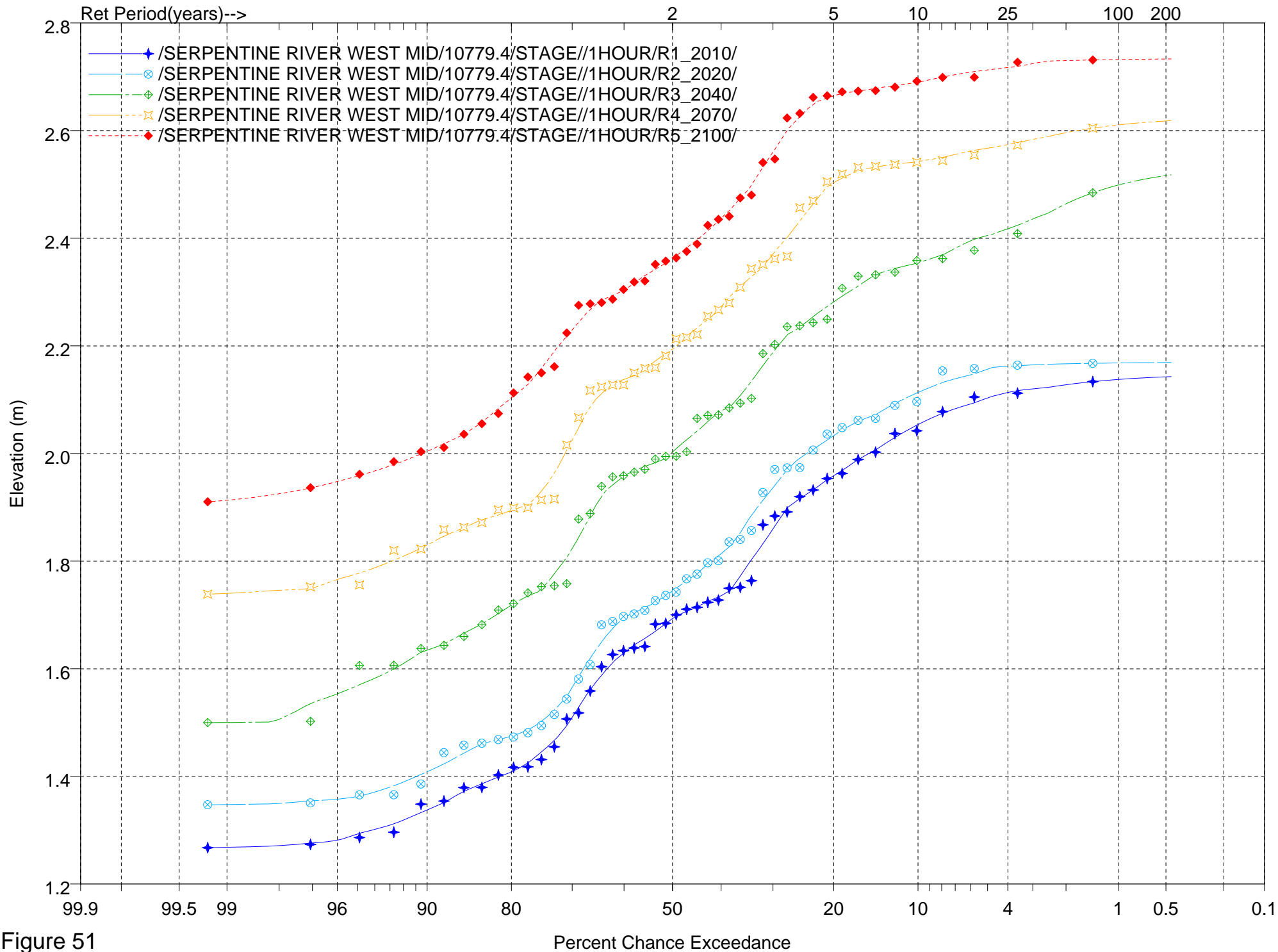


Figure 51

Percent Chance Exceedance

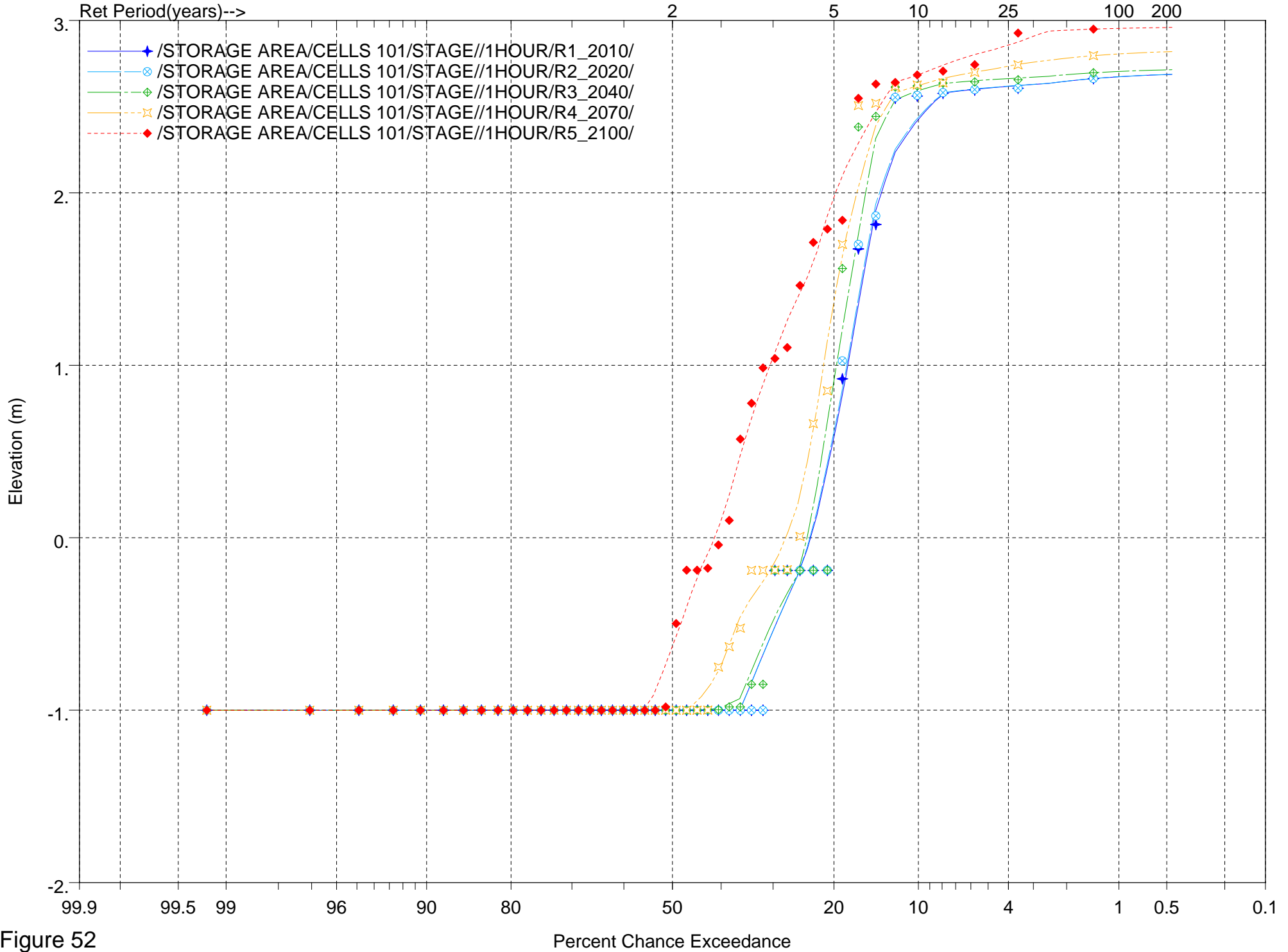


Figure 52

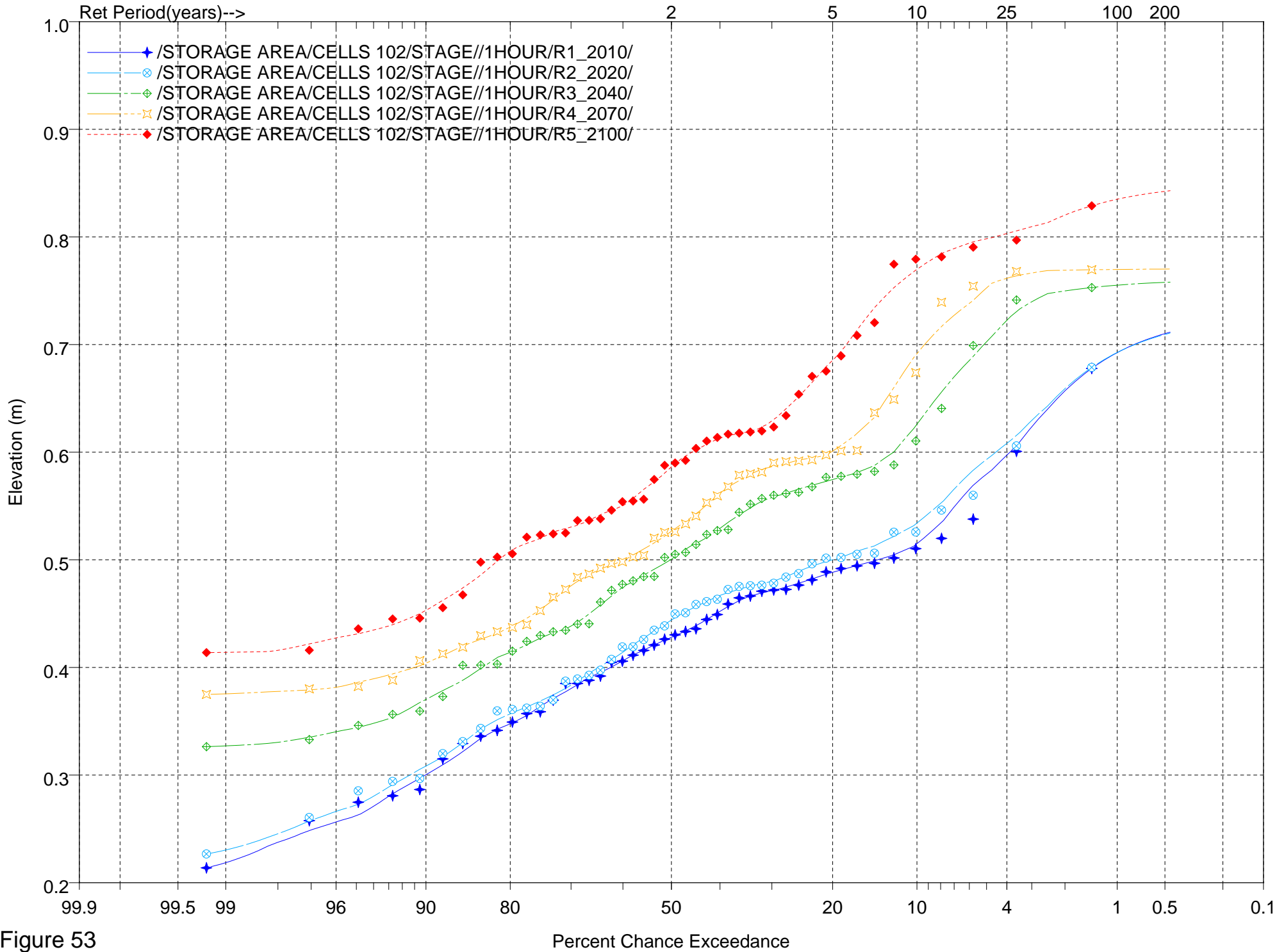


Figure 53

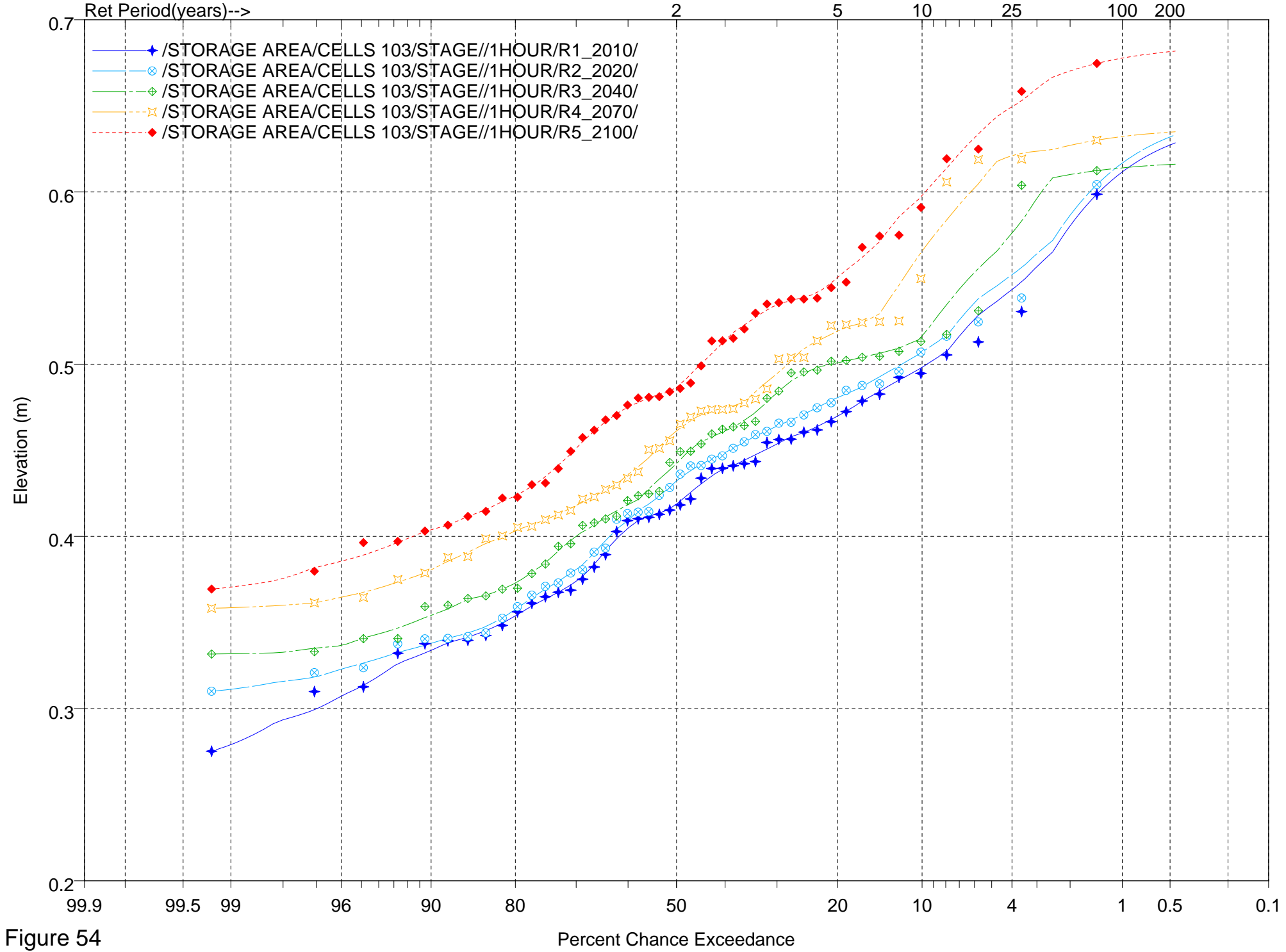


Figure 54

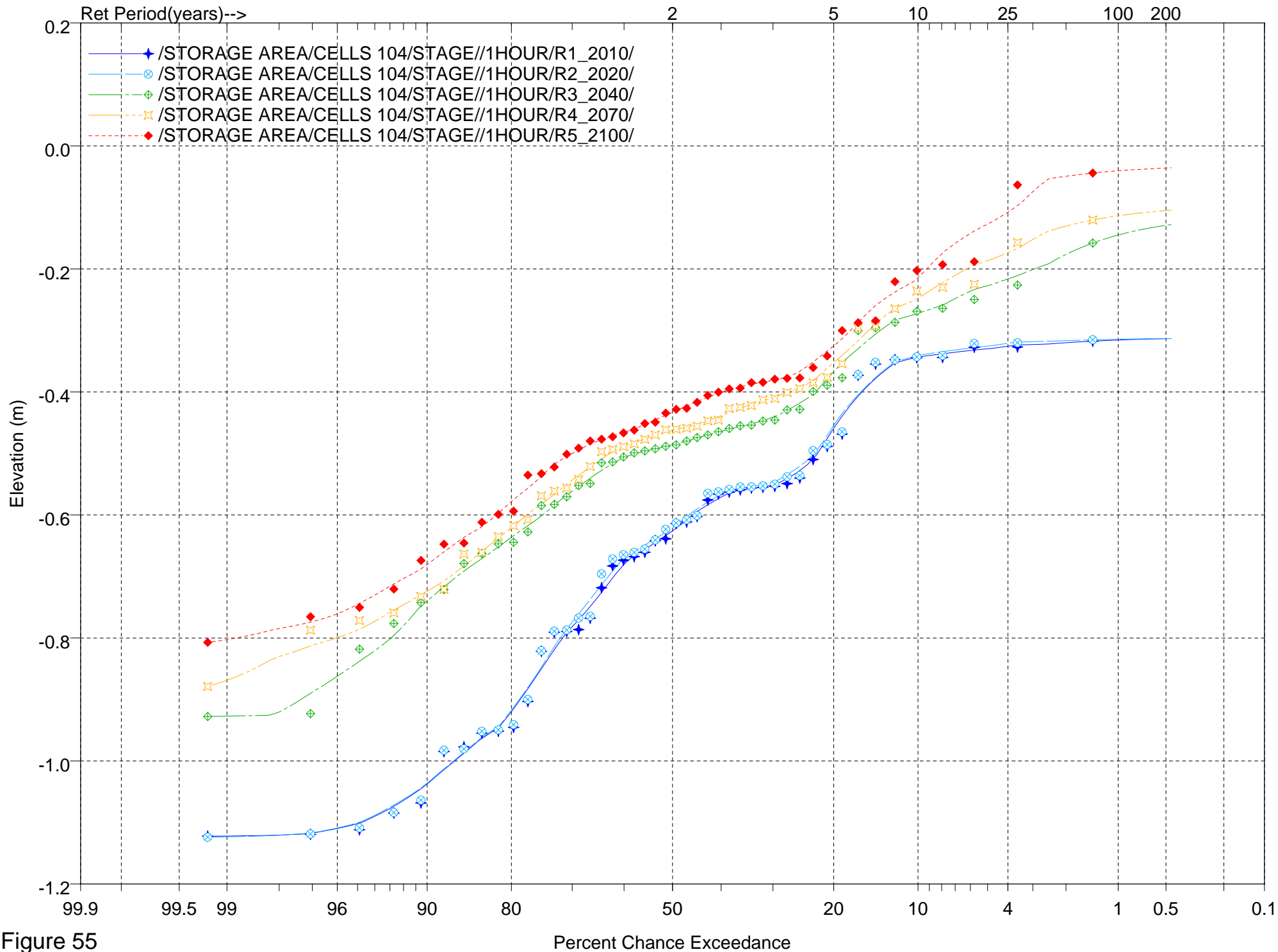


Figure 55

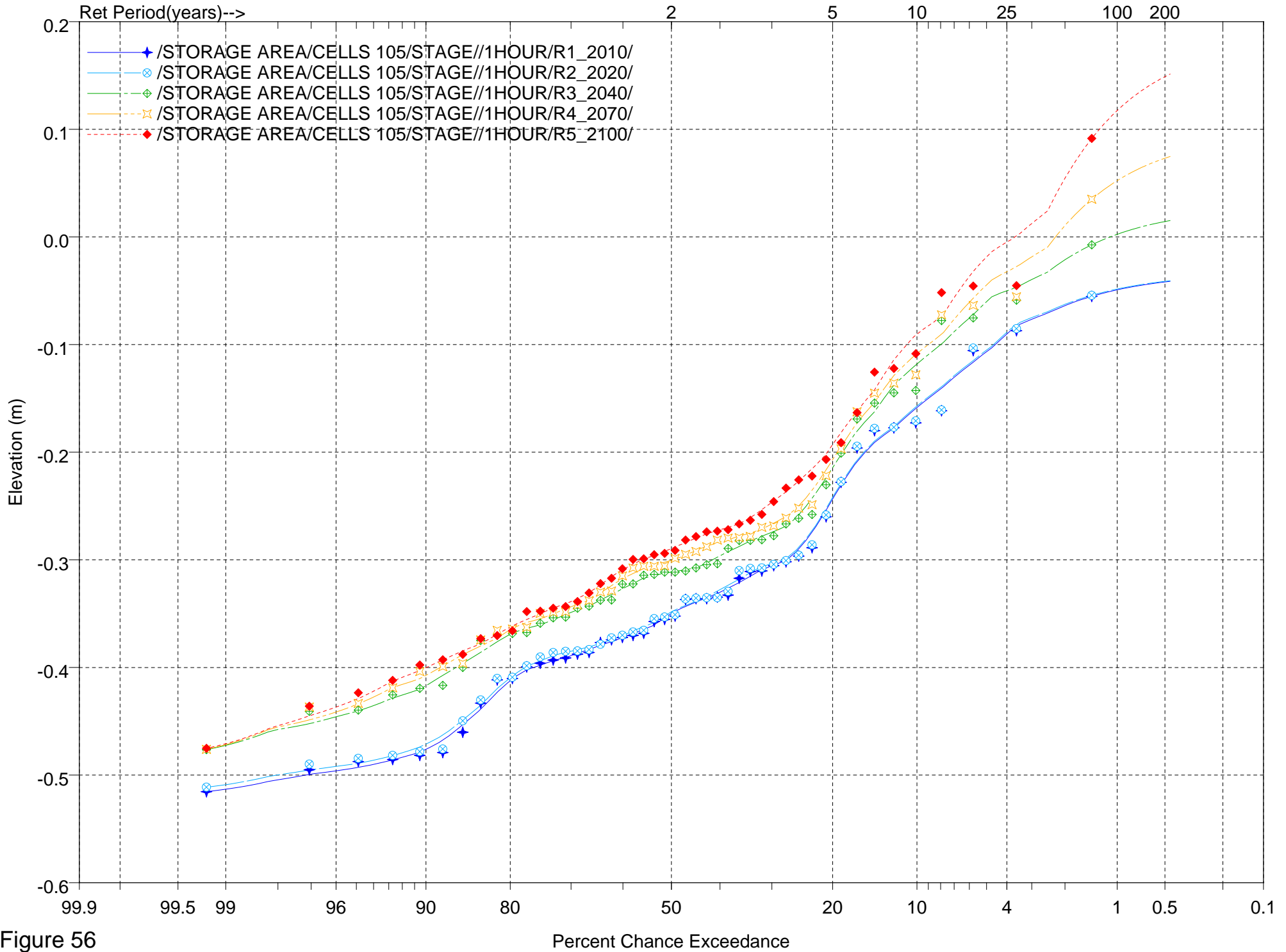


Figure 56

Percent Chance Exceedance

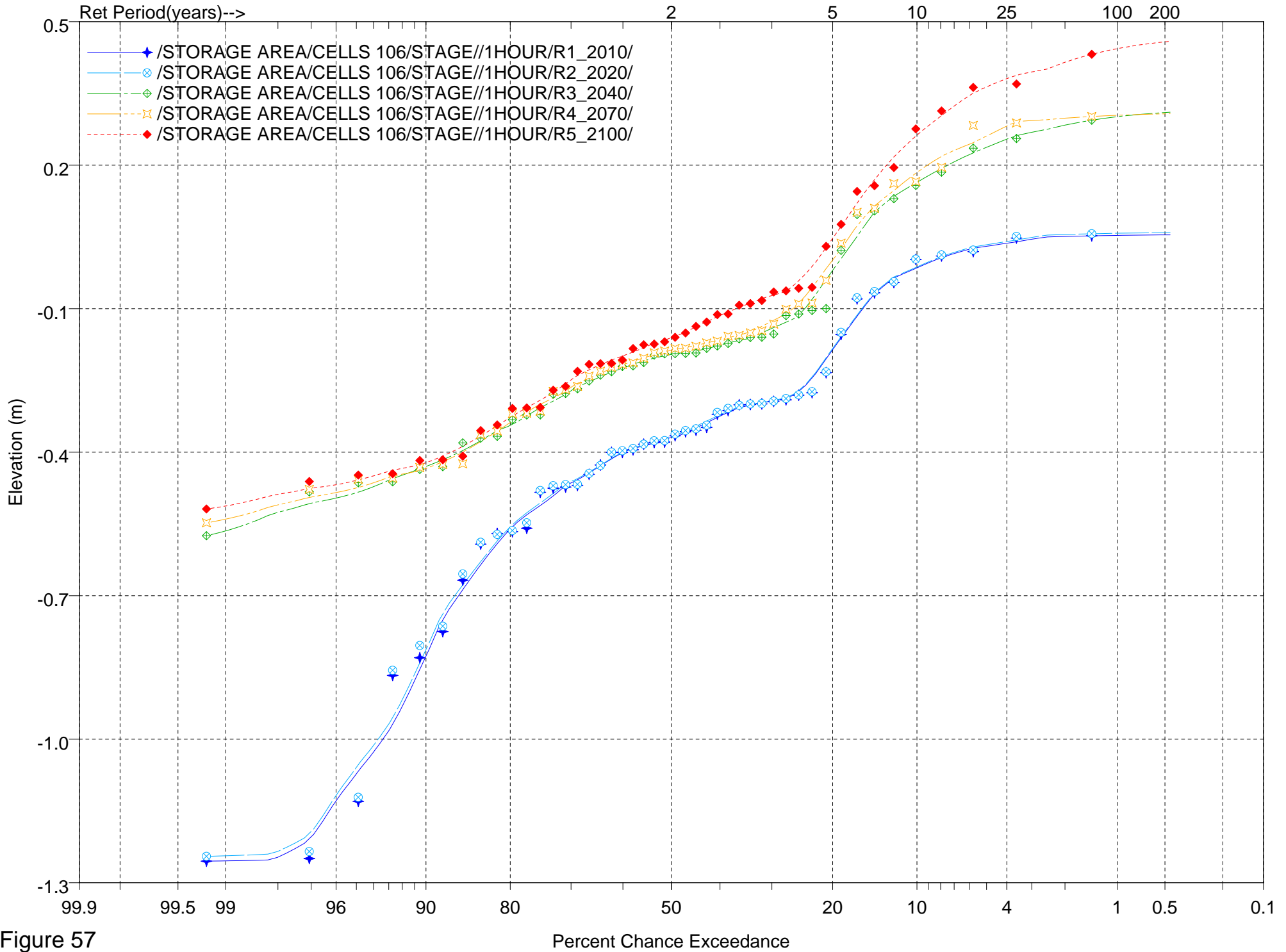


Figure 57



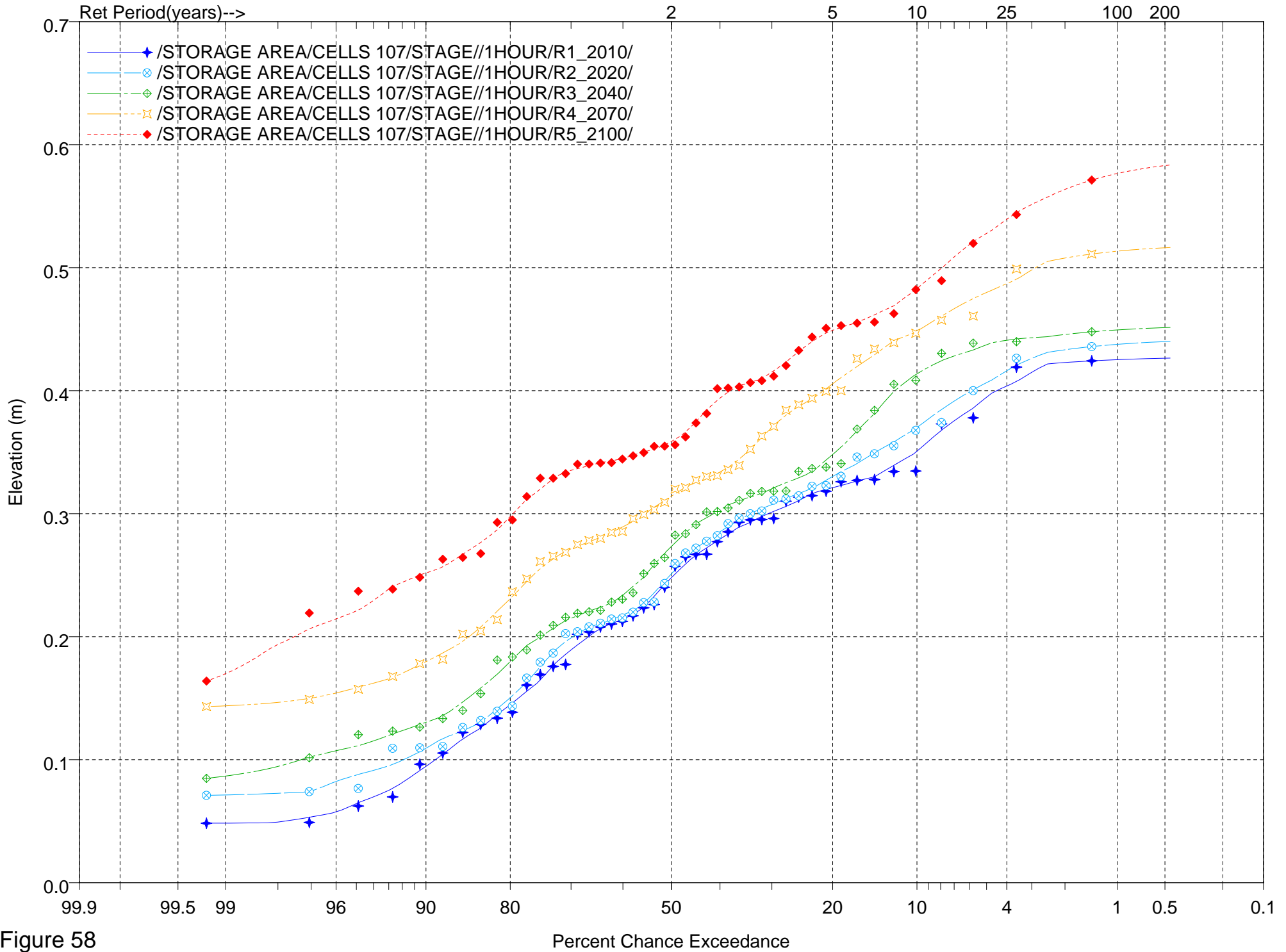


Figure 58

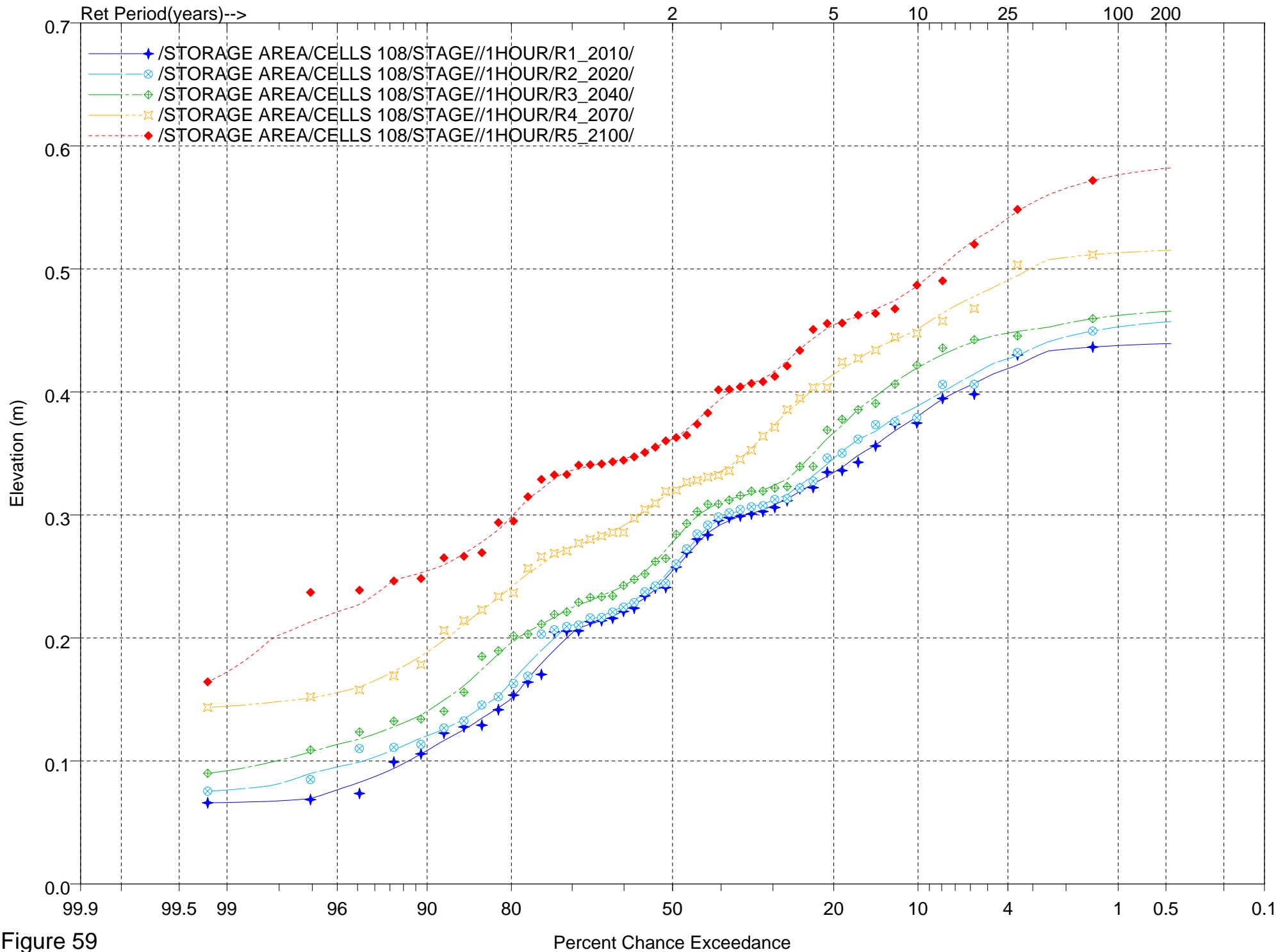


Figure 59

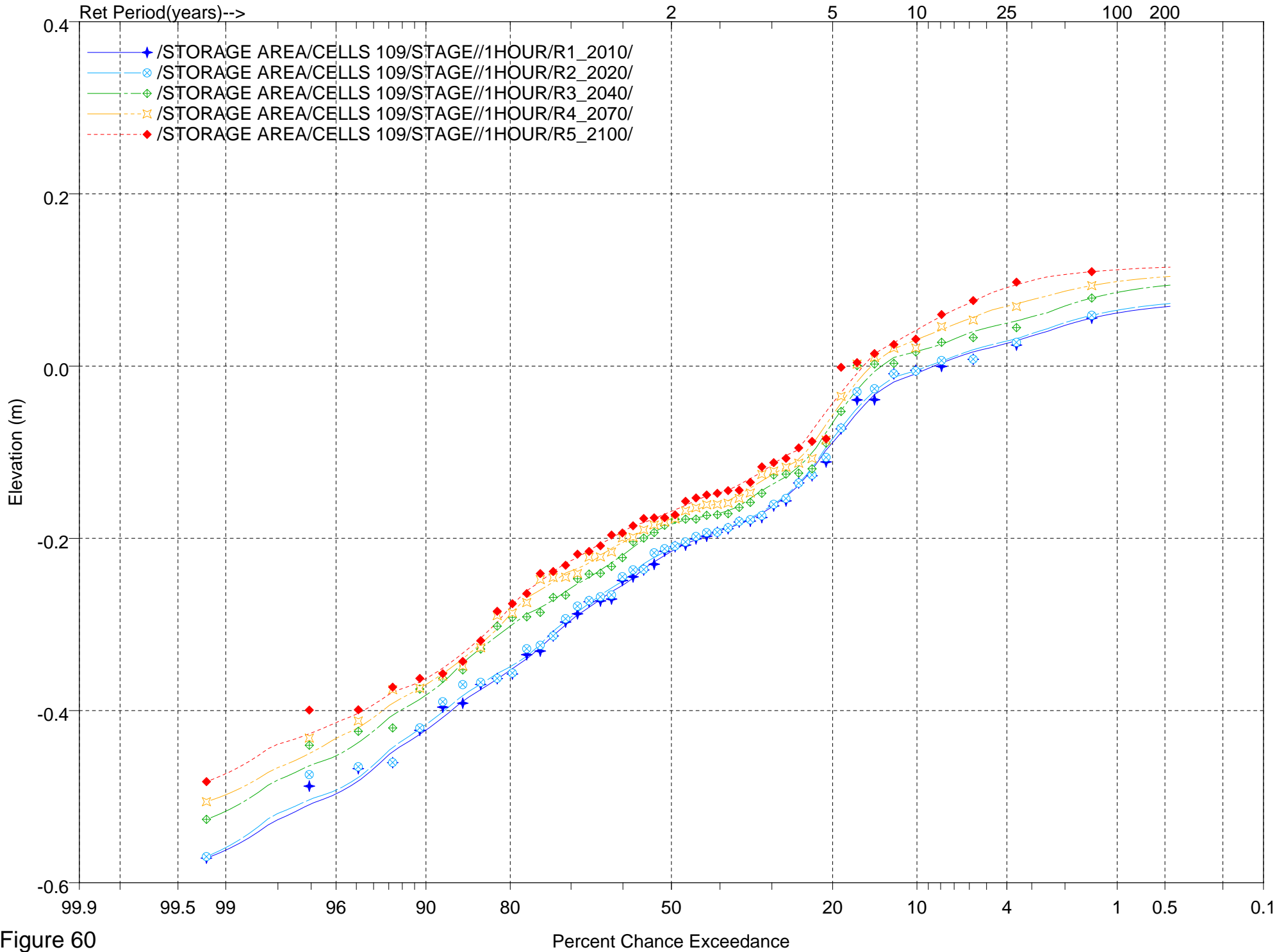


Figure 60

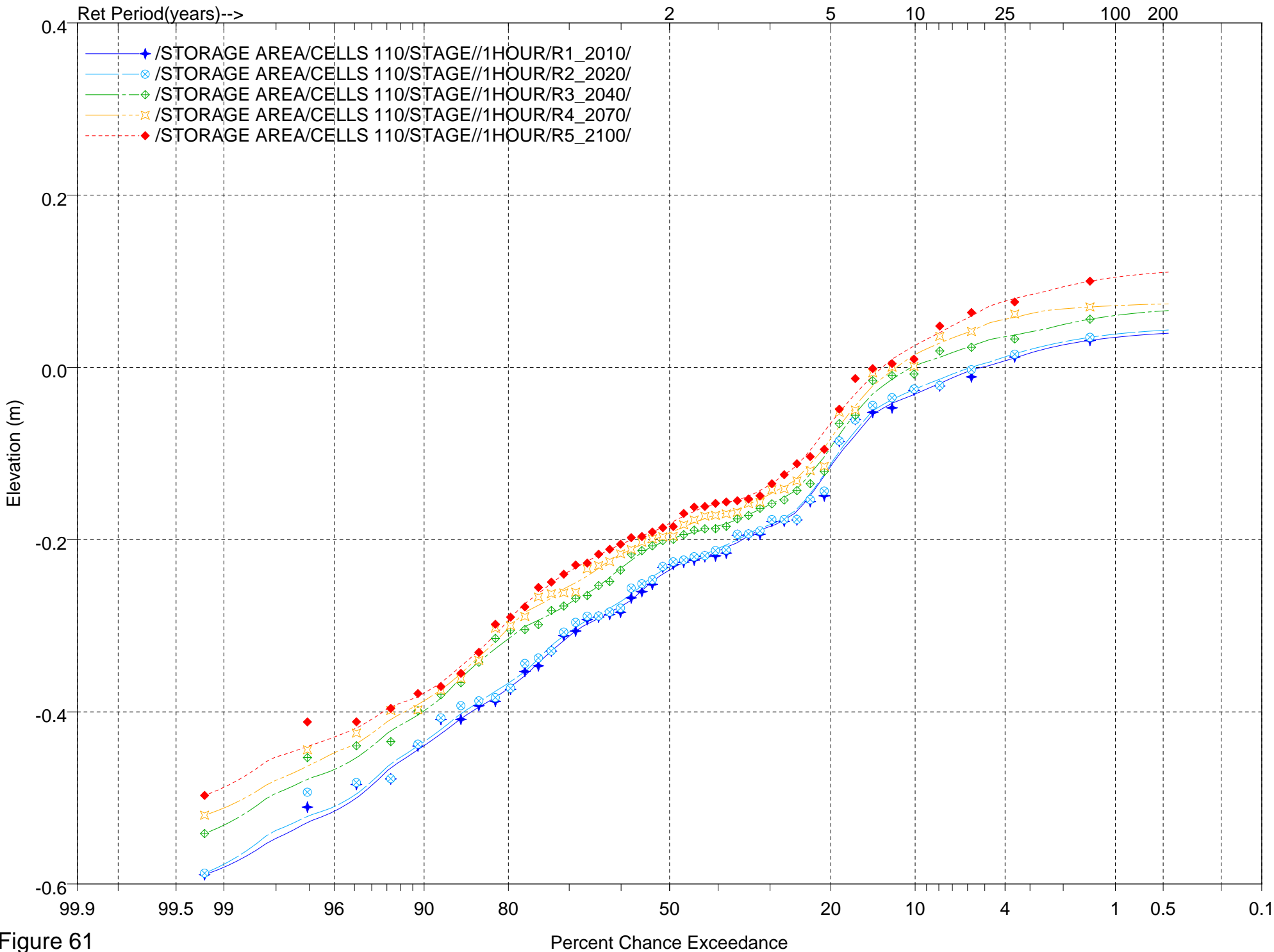


Figure 61

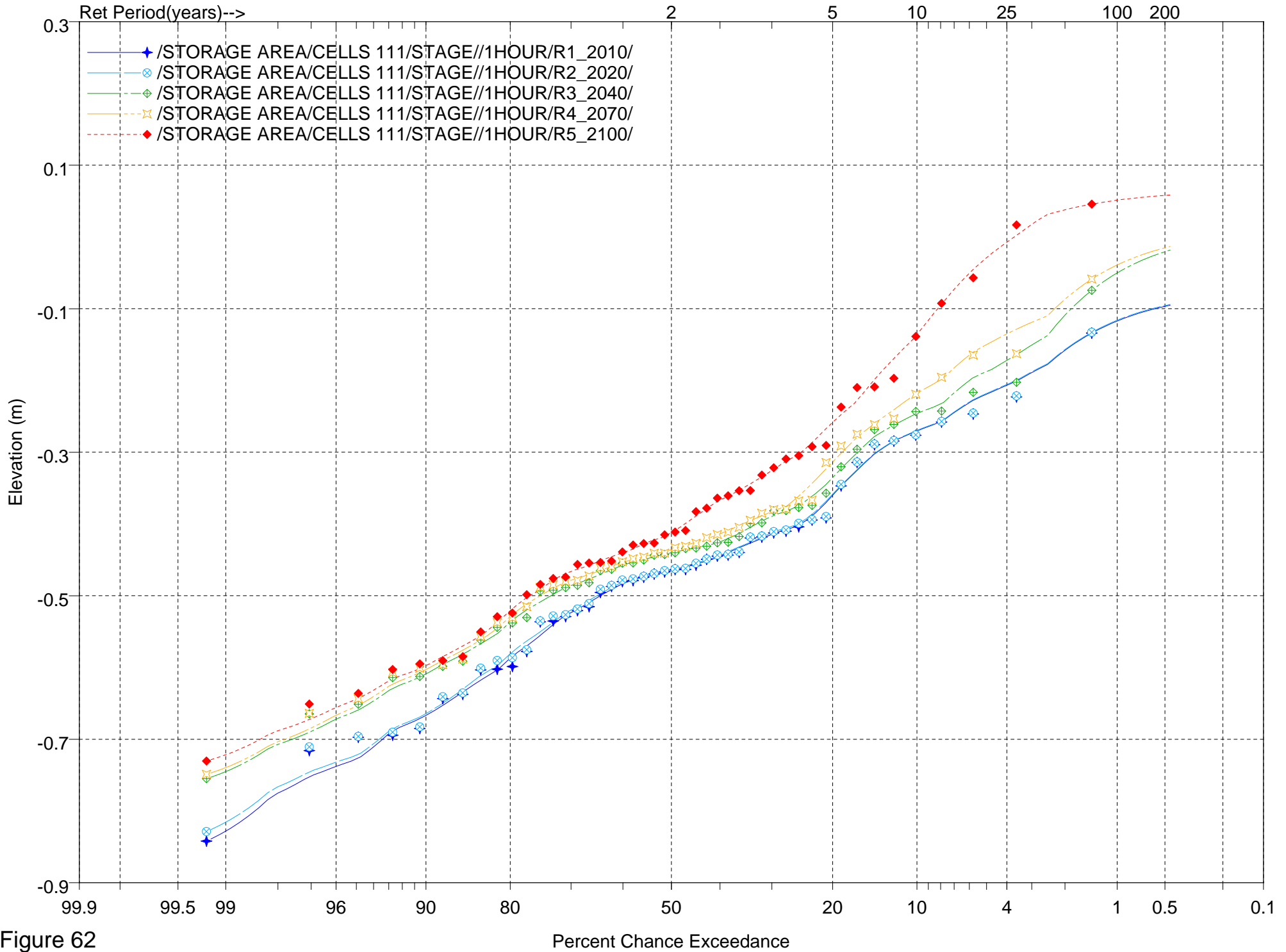


Figure 62

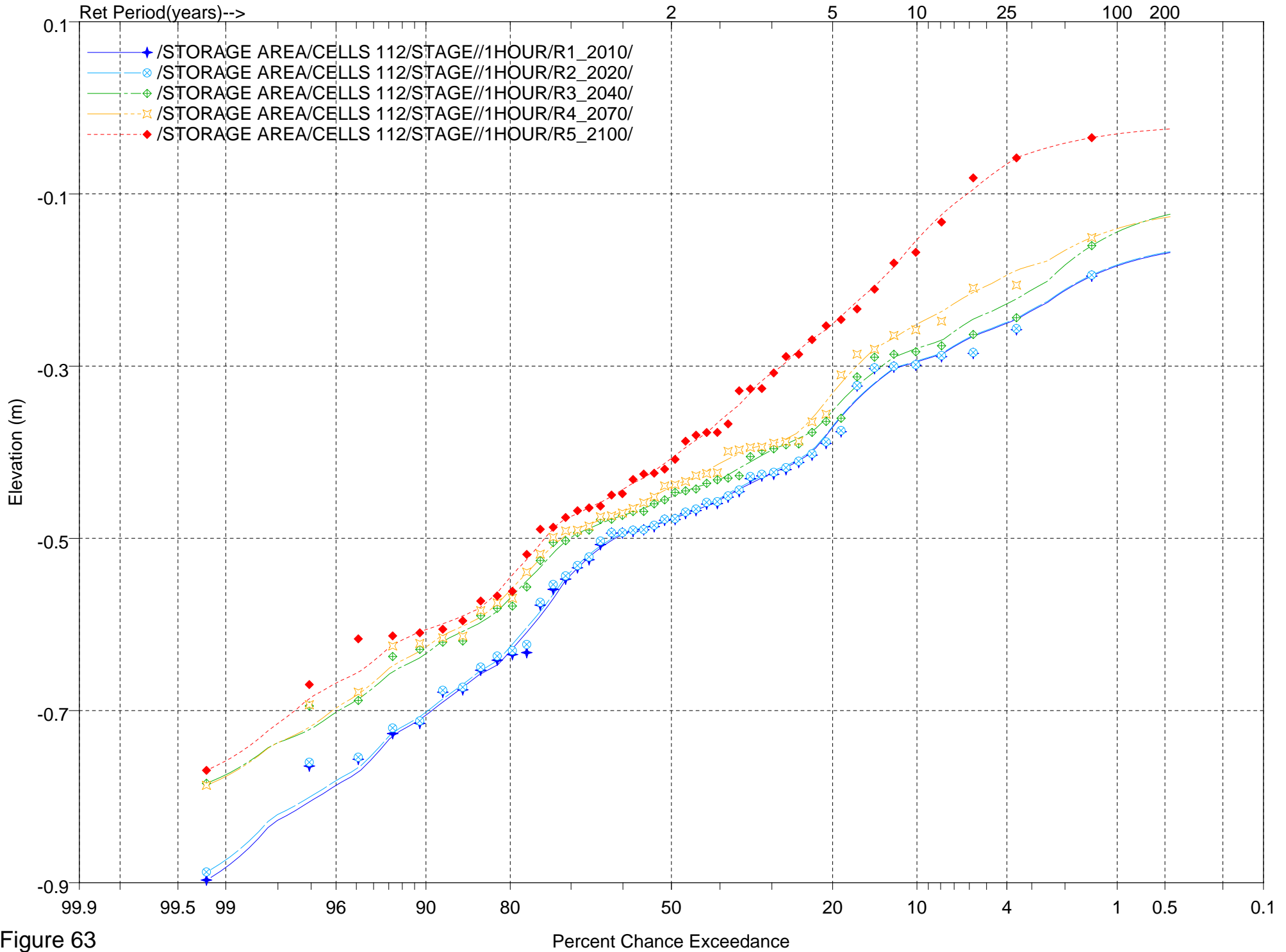


Figure 63

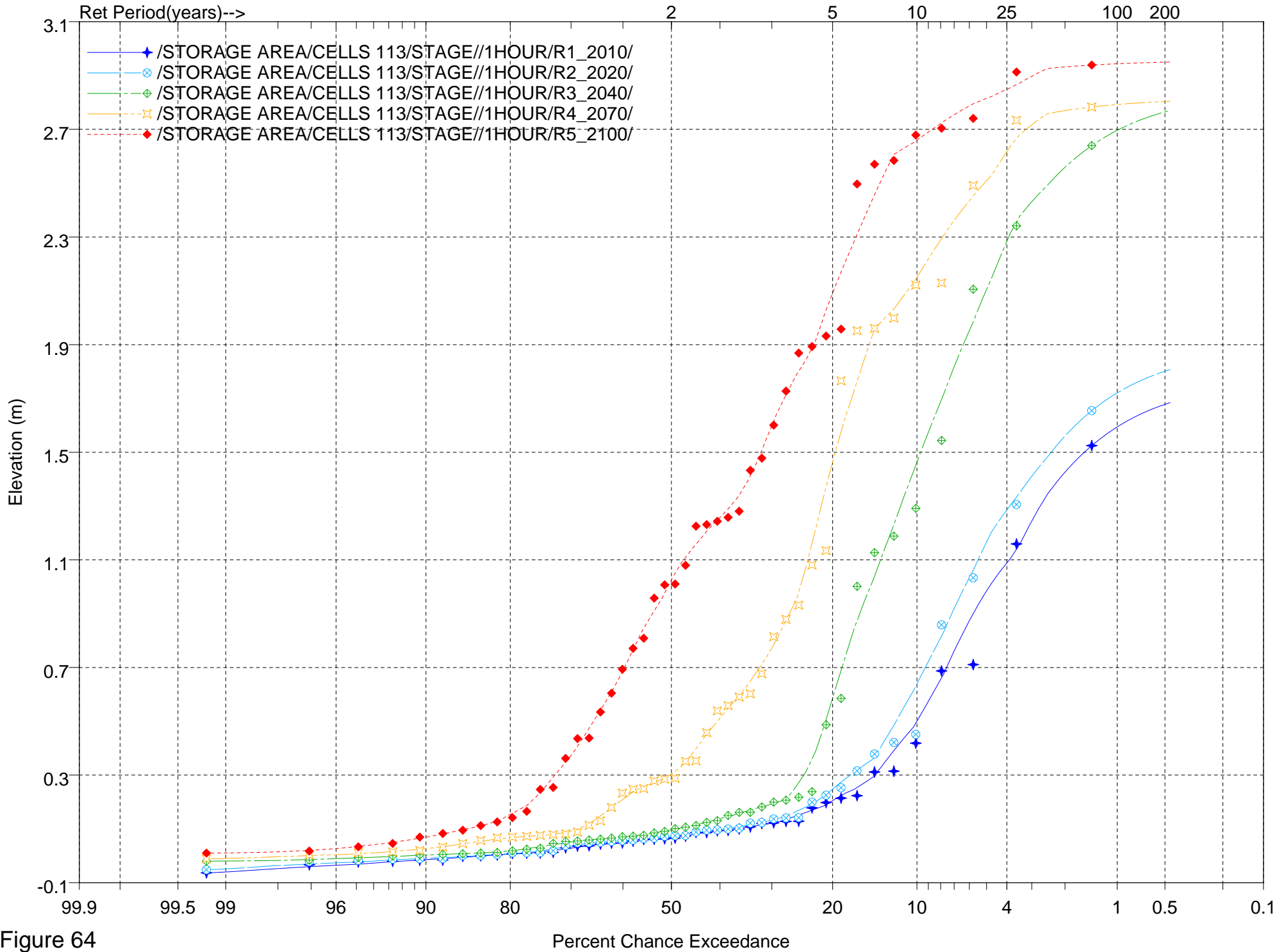


Figure 64

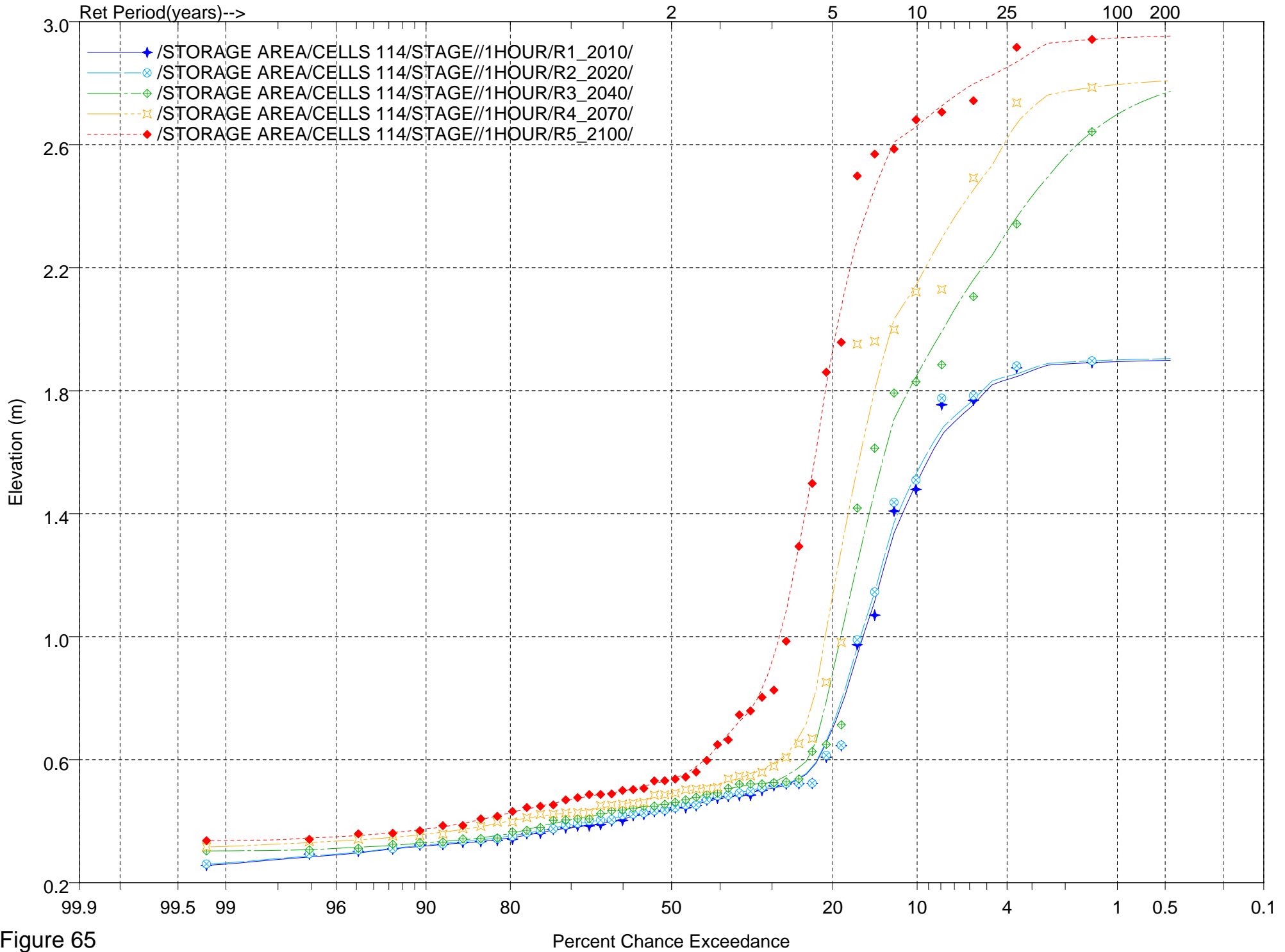


Figure 65



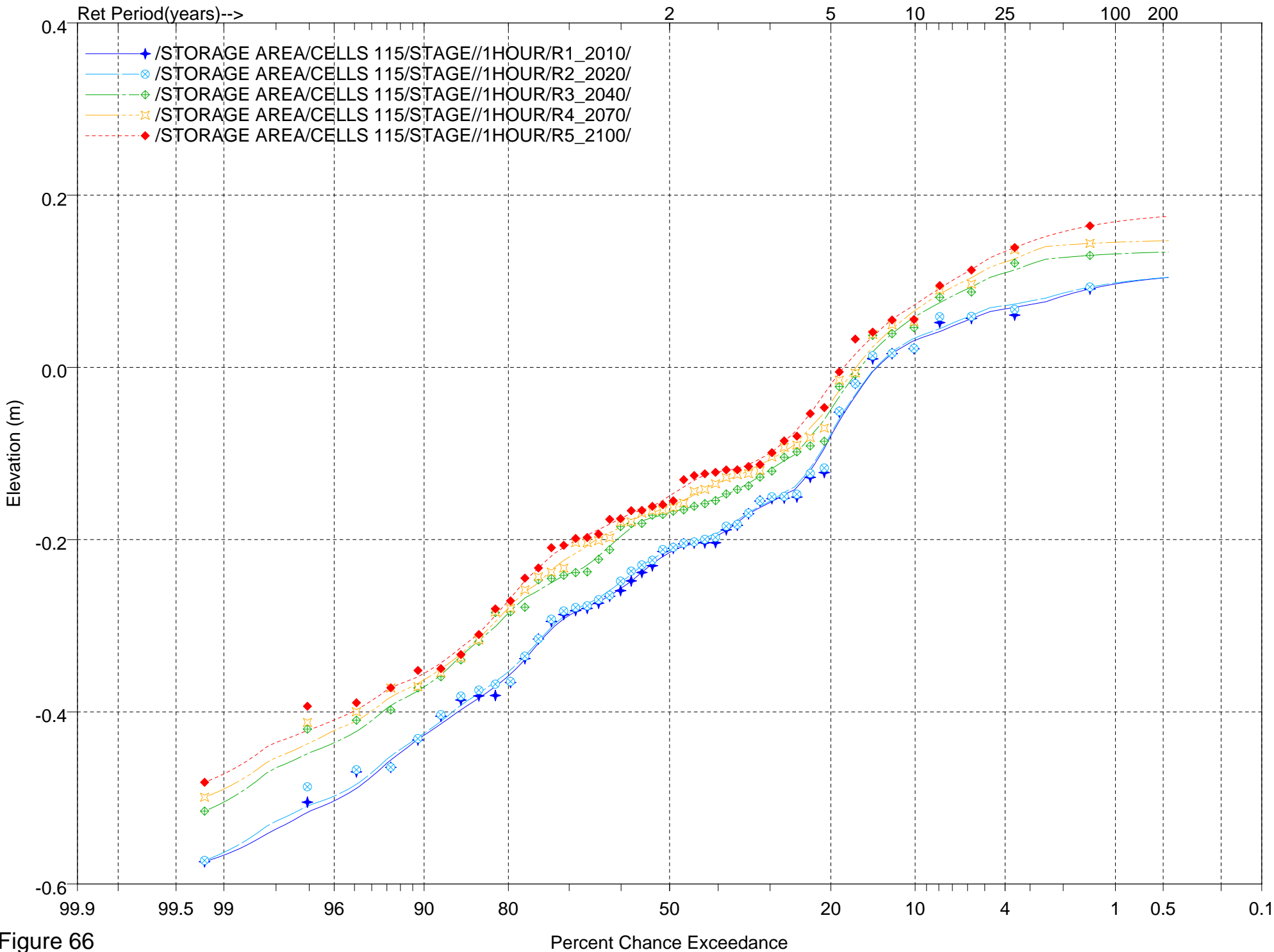


Figure 66

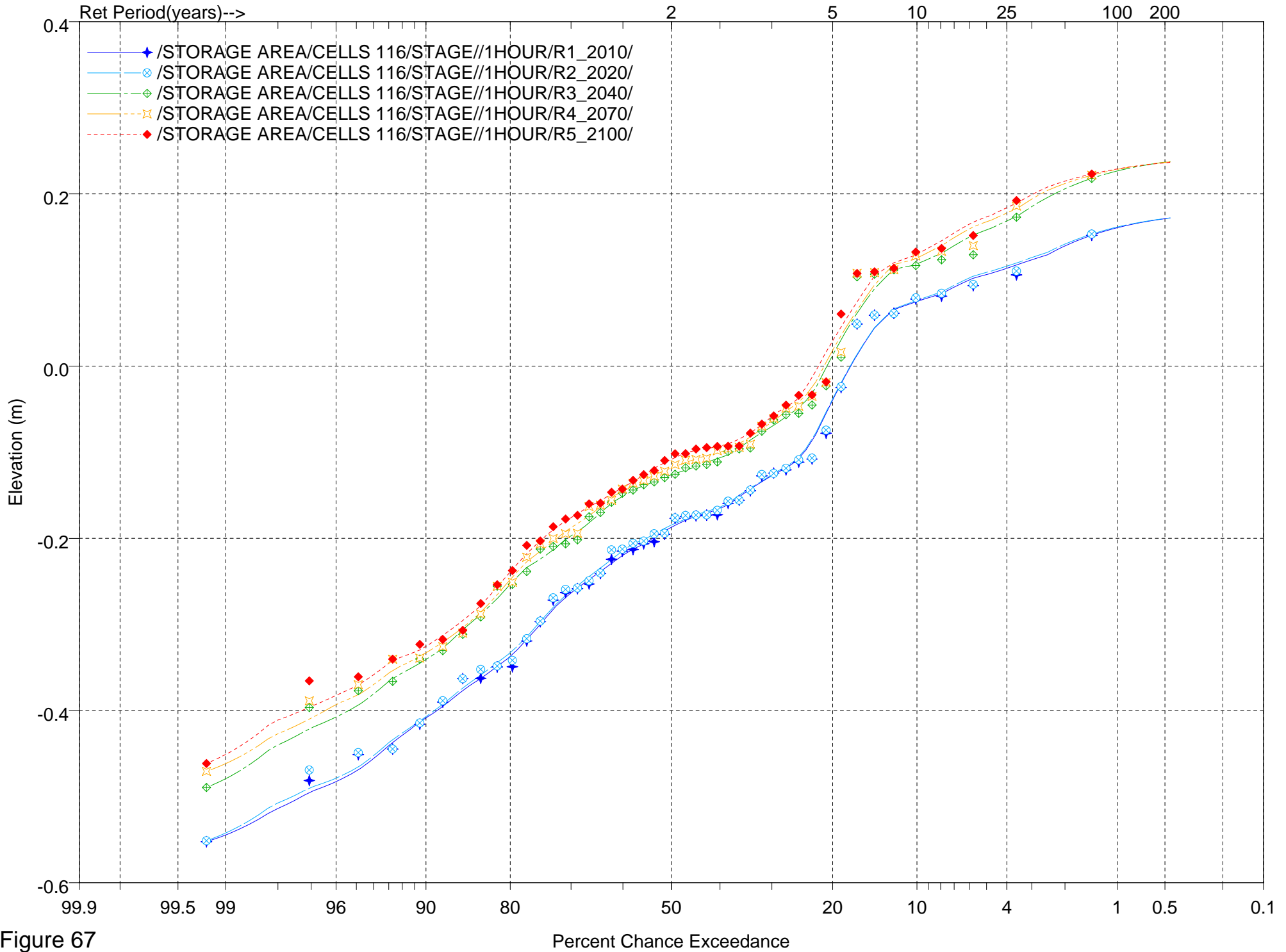


Figure 67

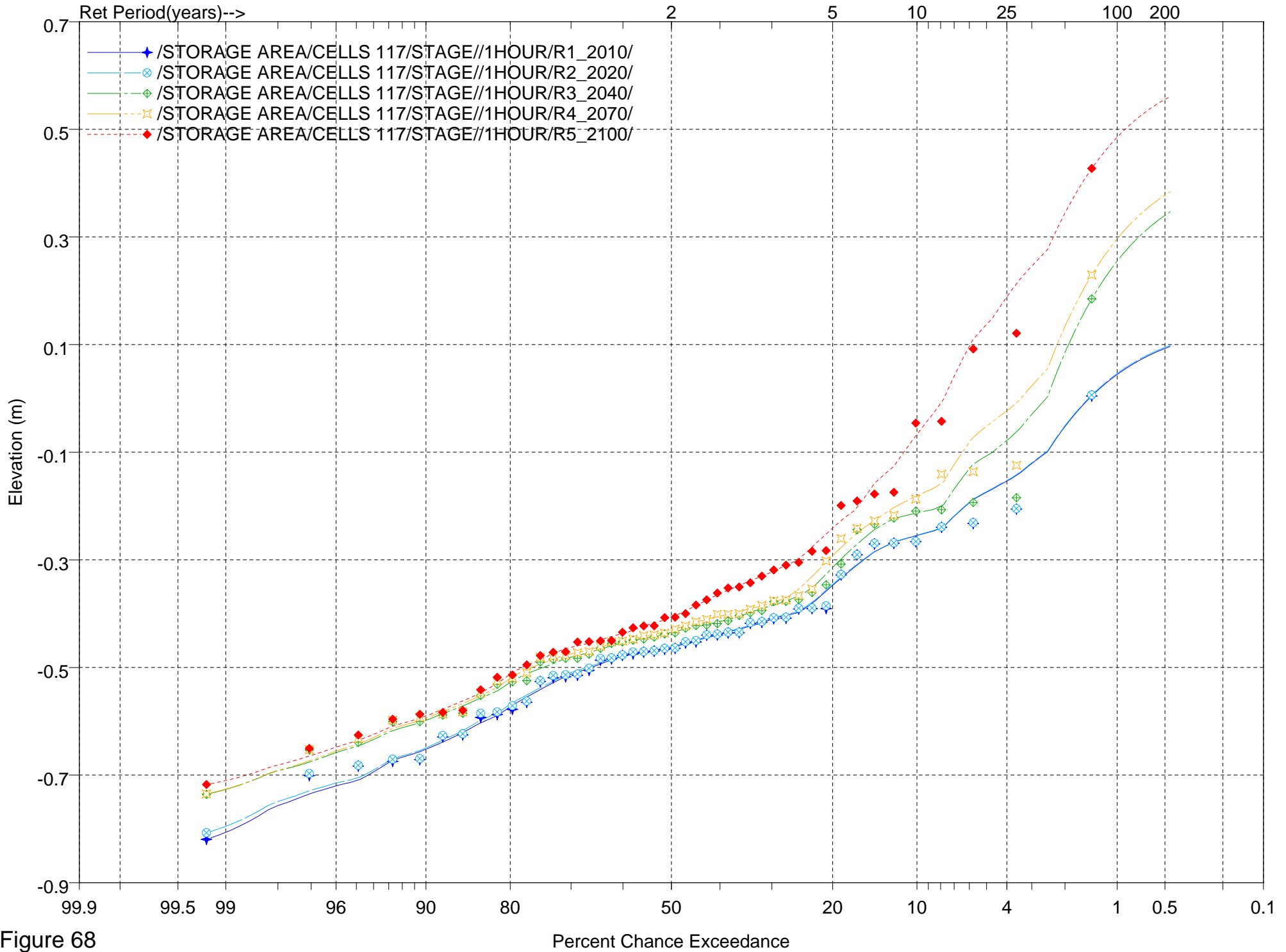


Figure 68

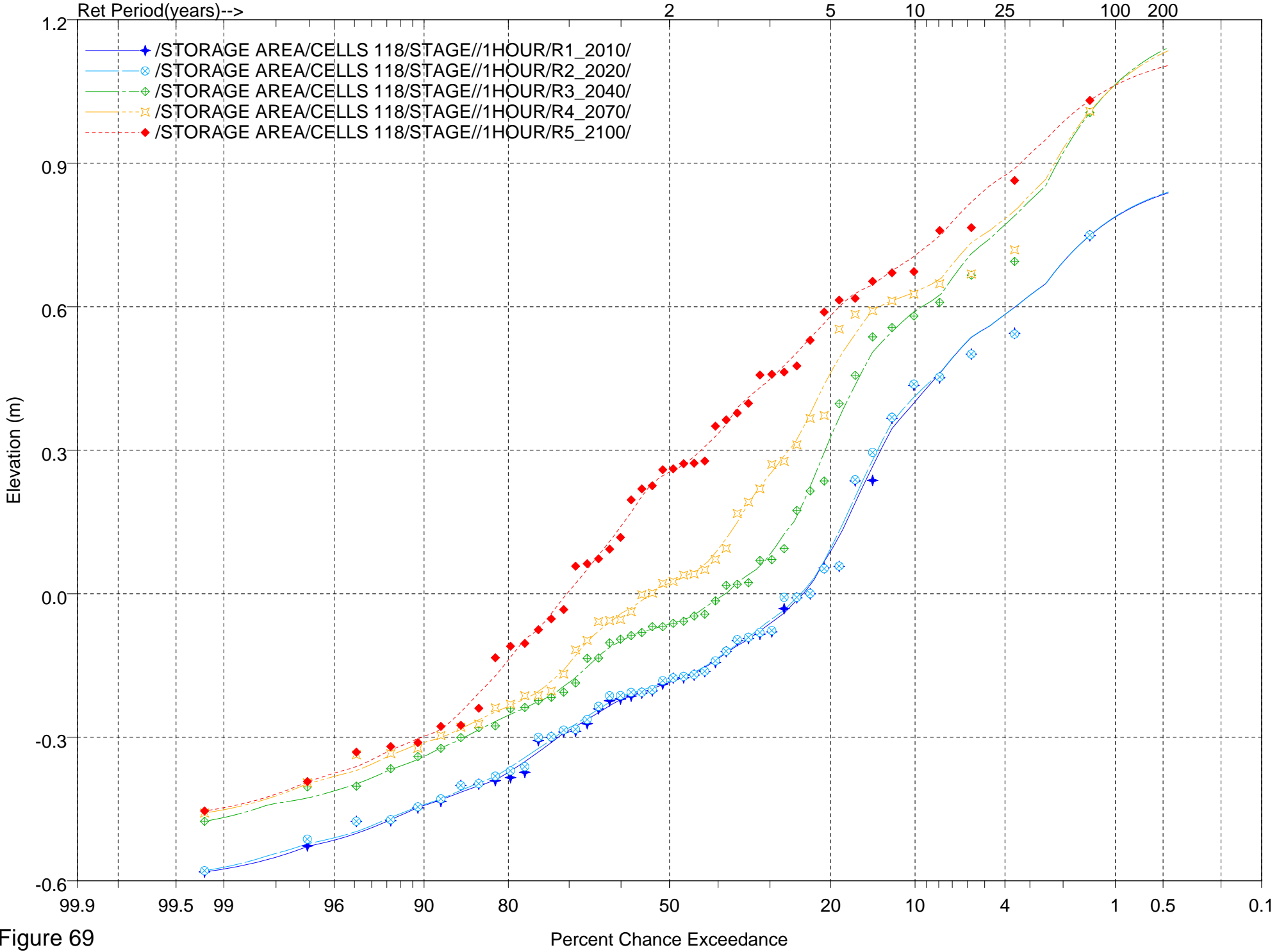


Figure 69

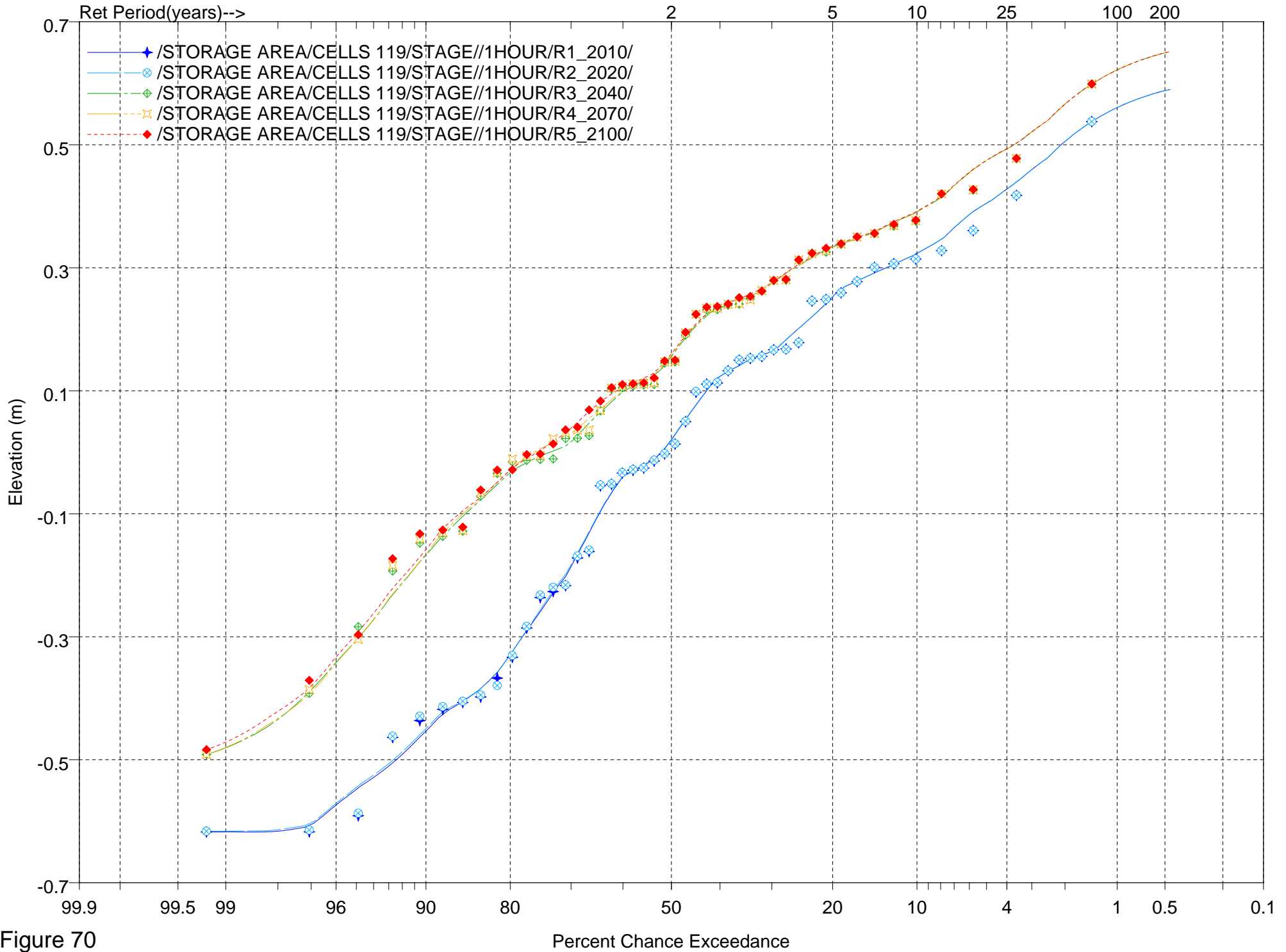


Figure 70

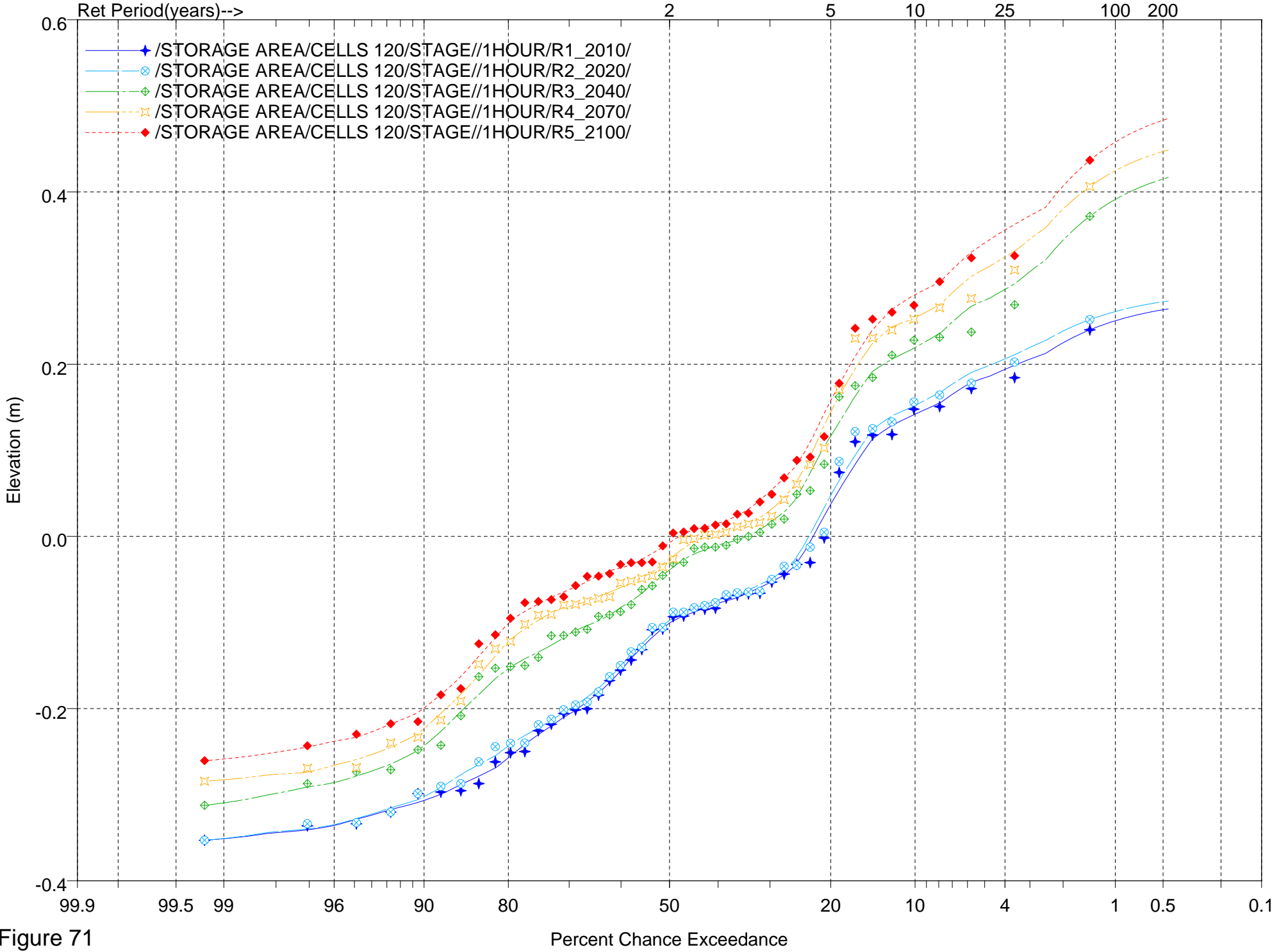


Figure 71

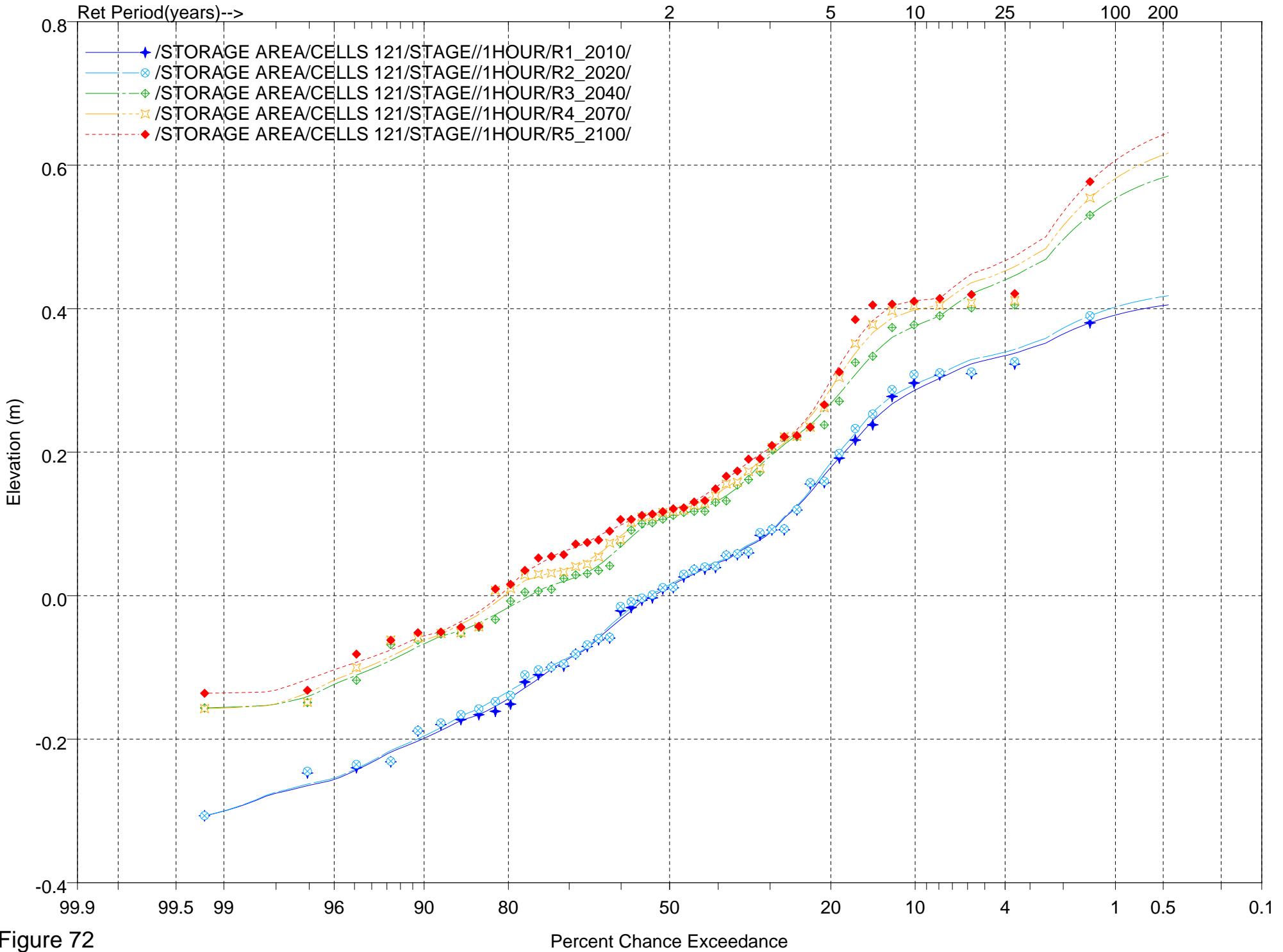


Figure 72

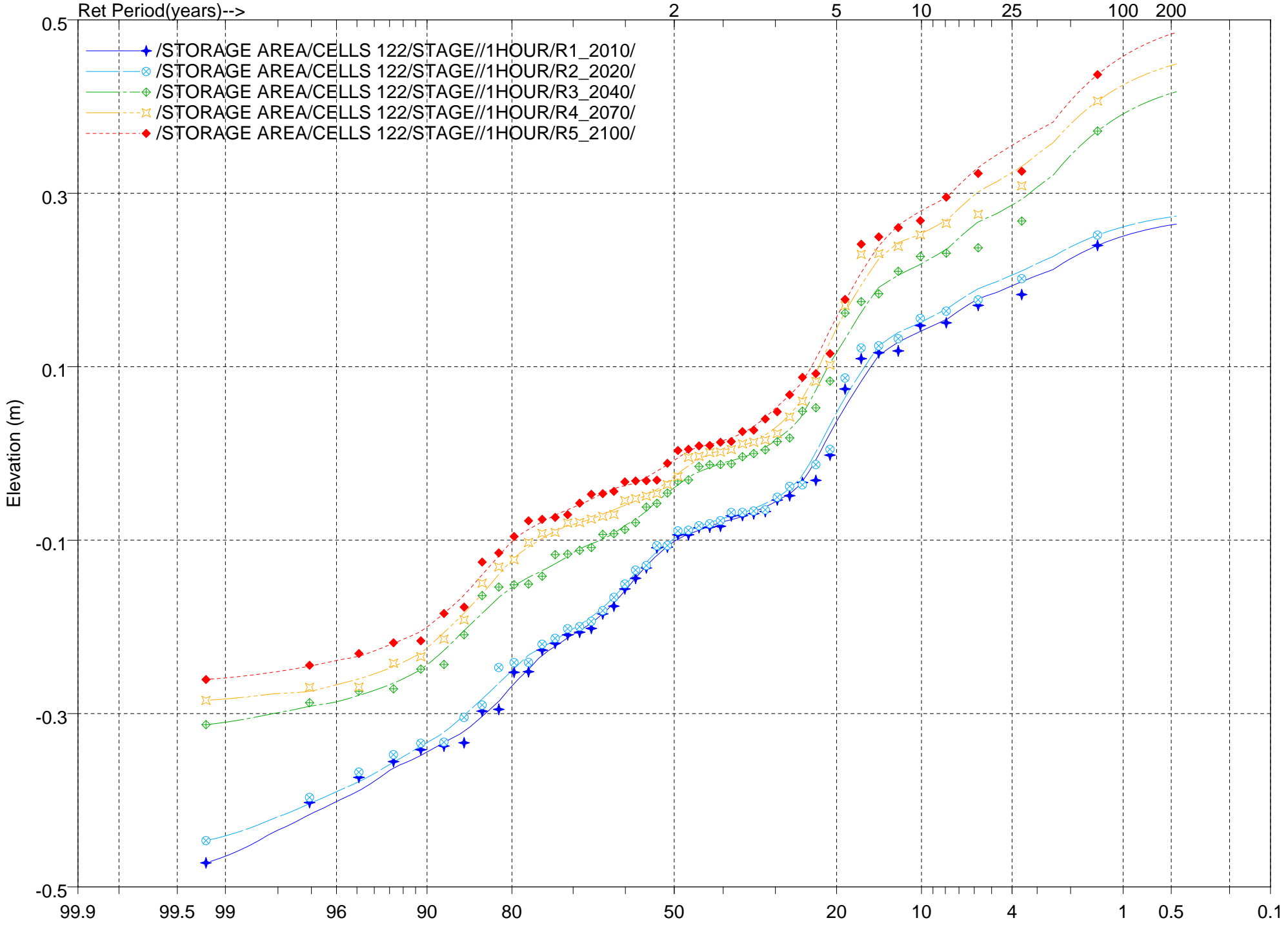


Figure 73



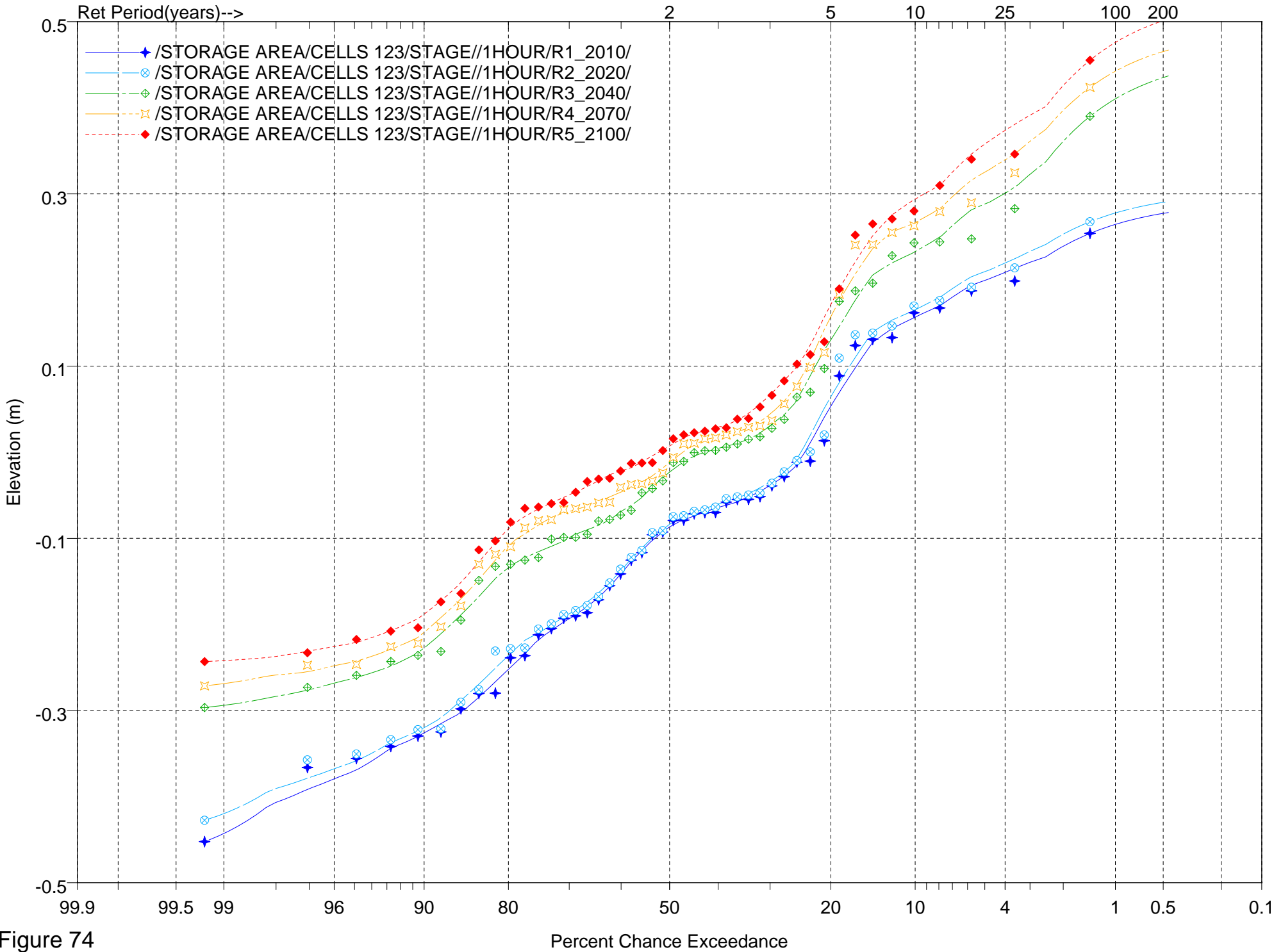


Figure 74

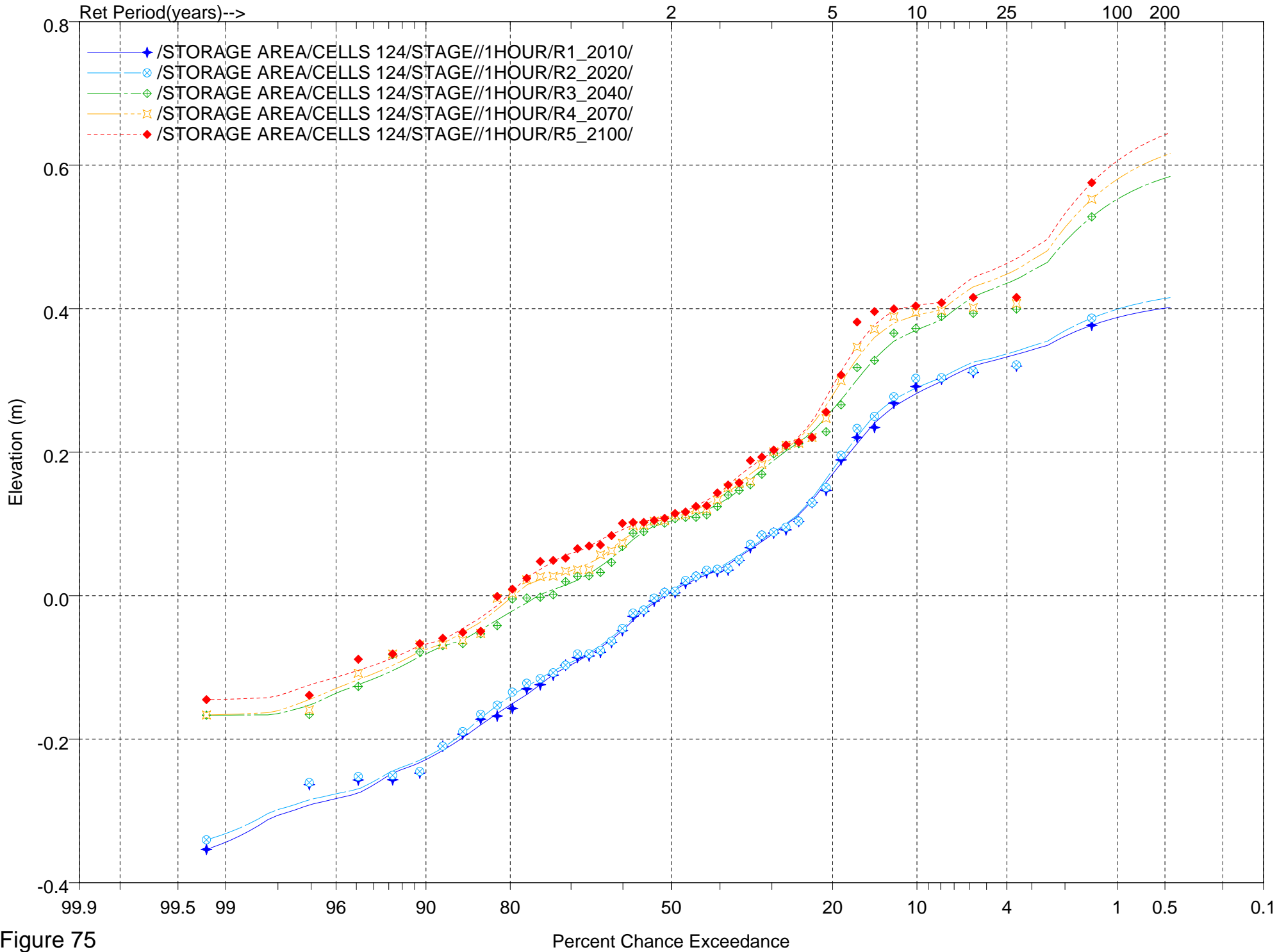


Figure 75

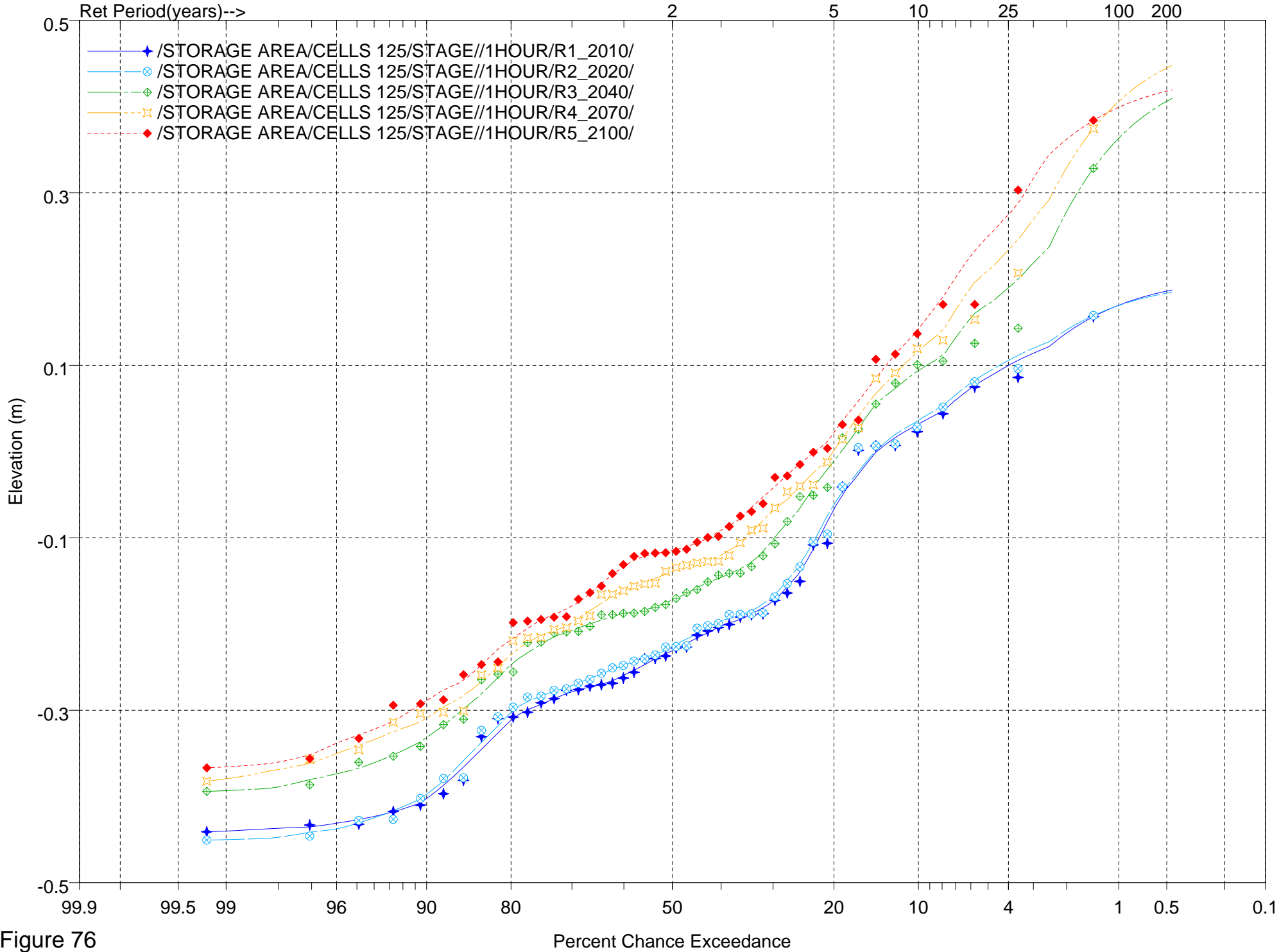


Figure 76

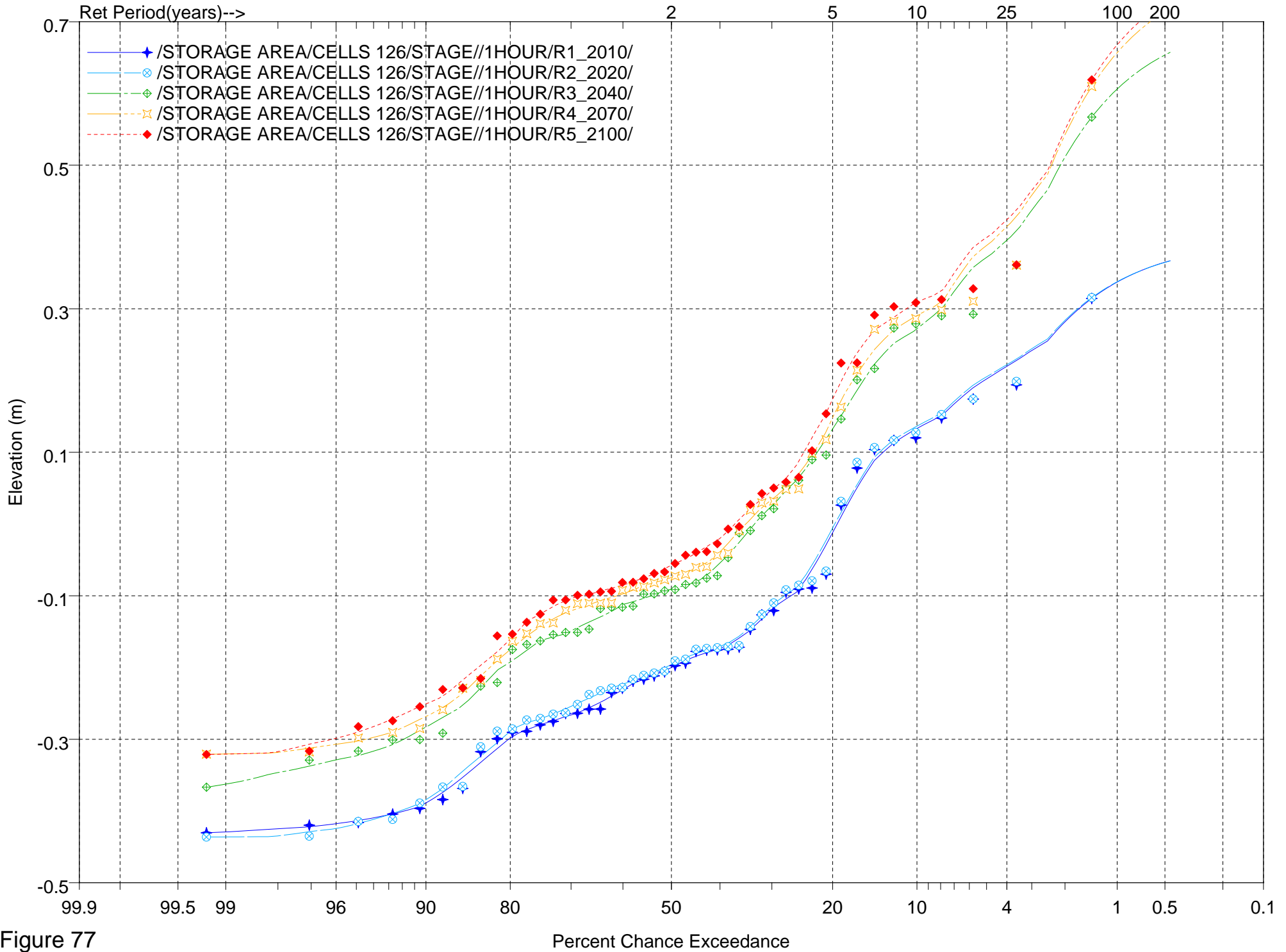


Figure 77

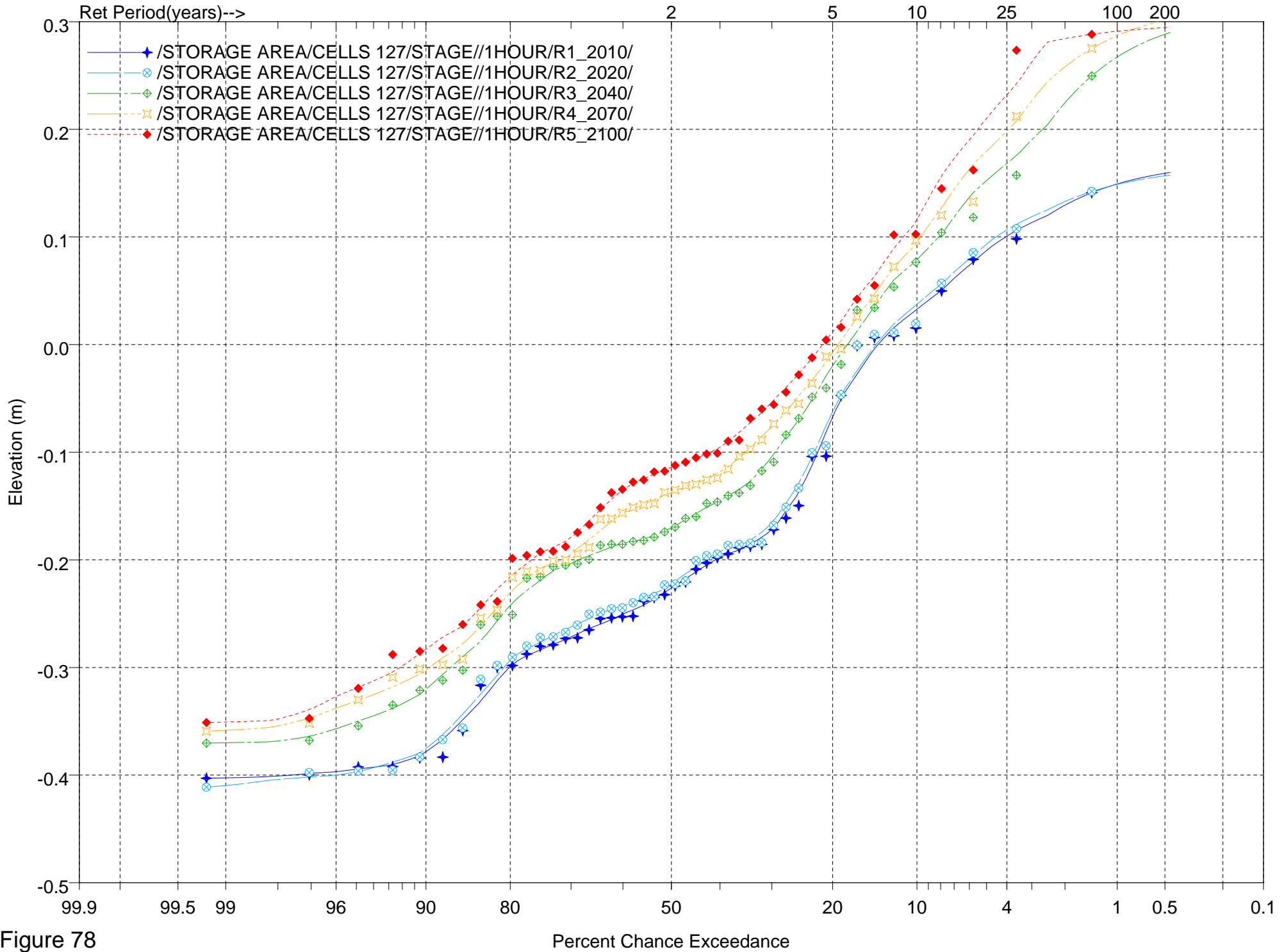


Figure 78

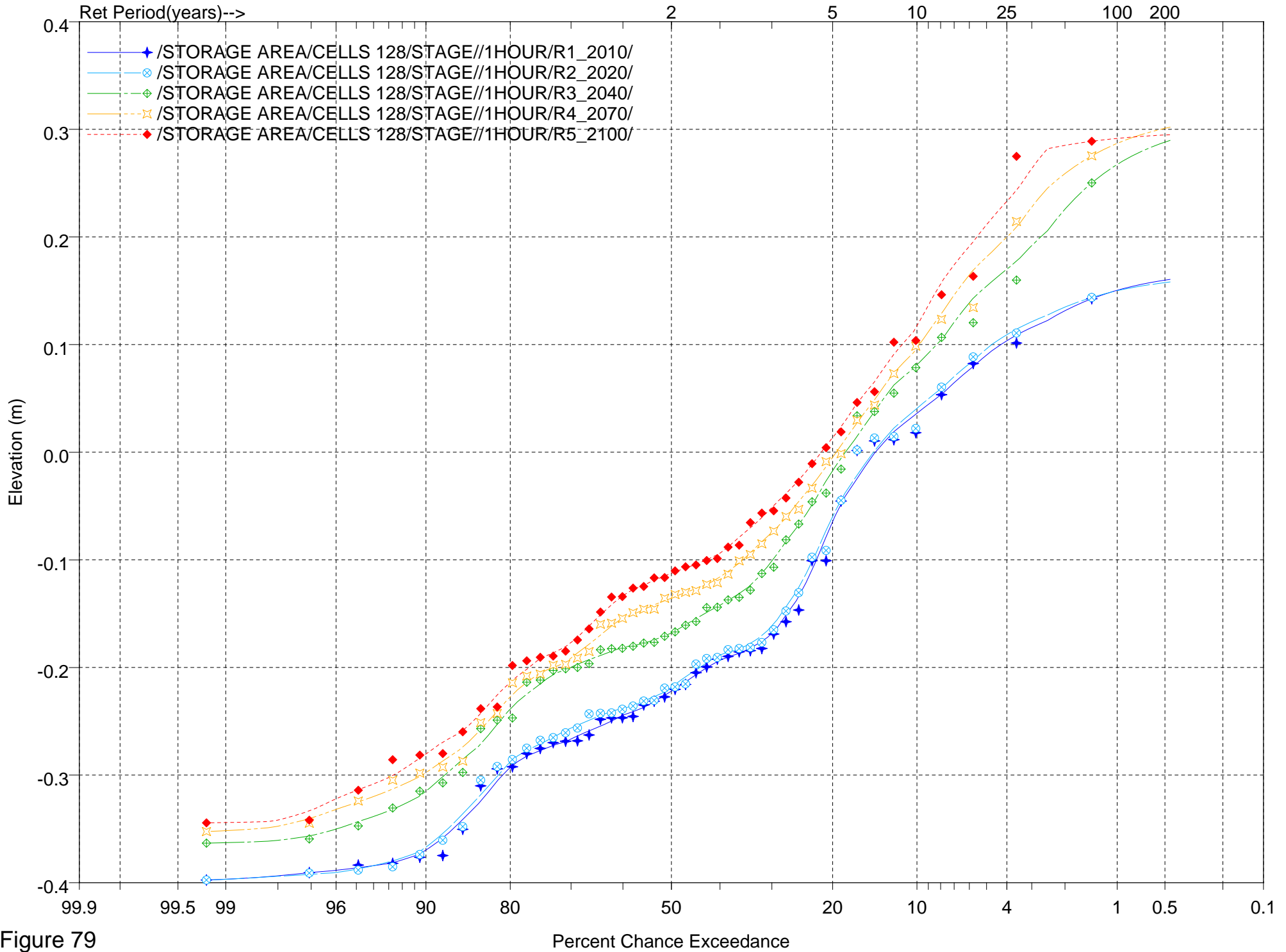


Figure 79

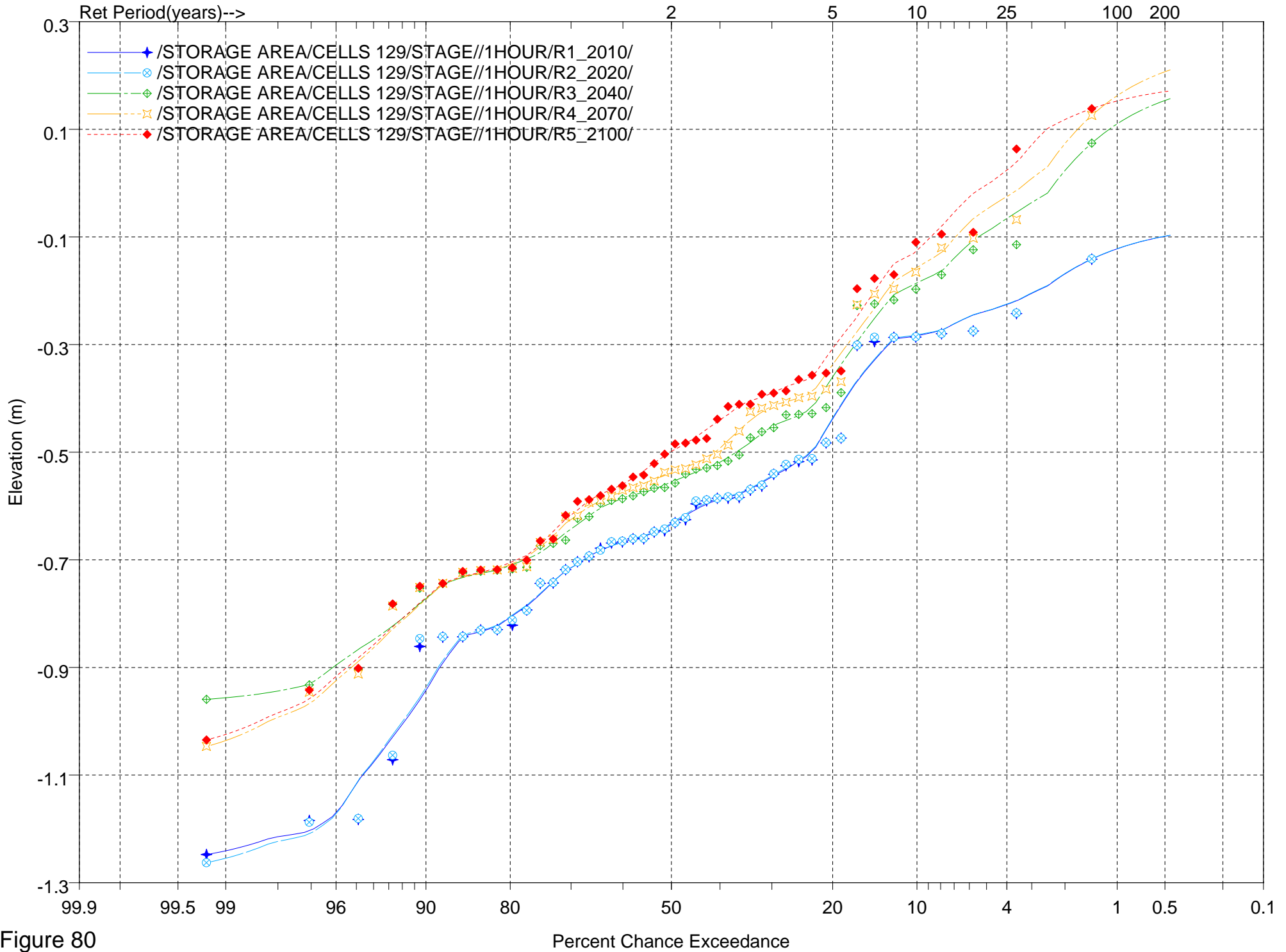


Figure 80

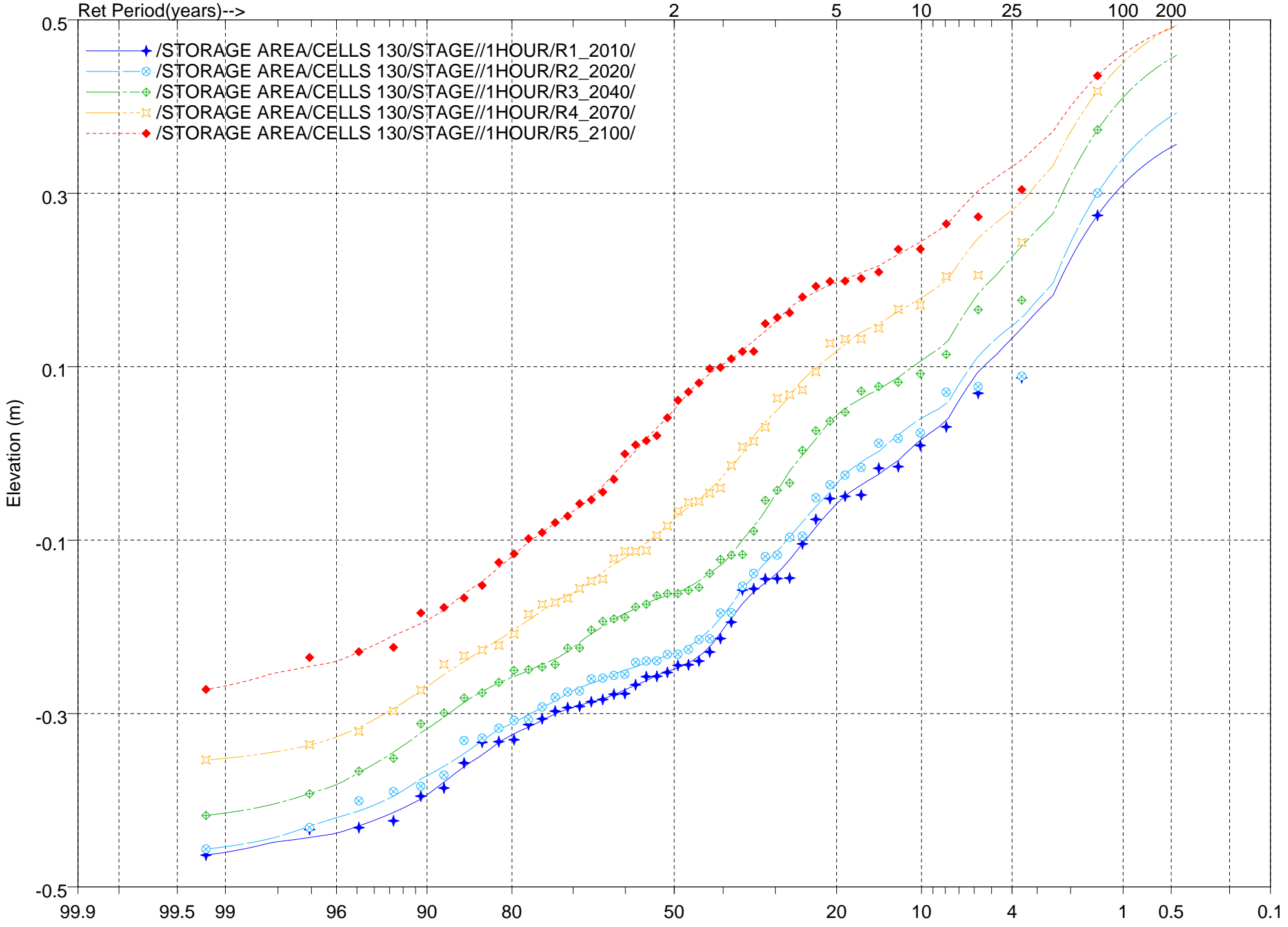


Figure 81

Percent Chance Exceedance



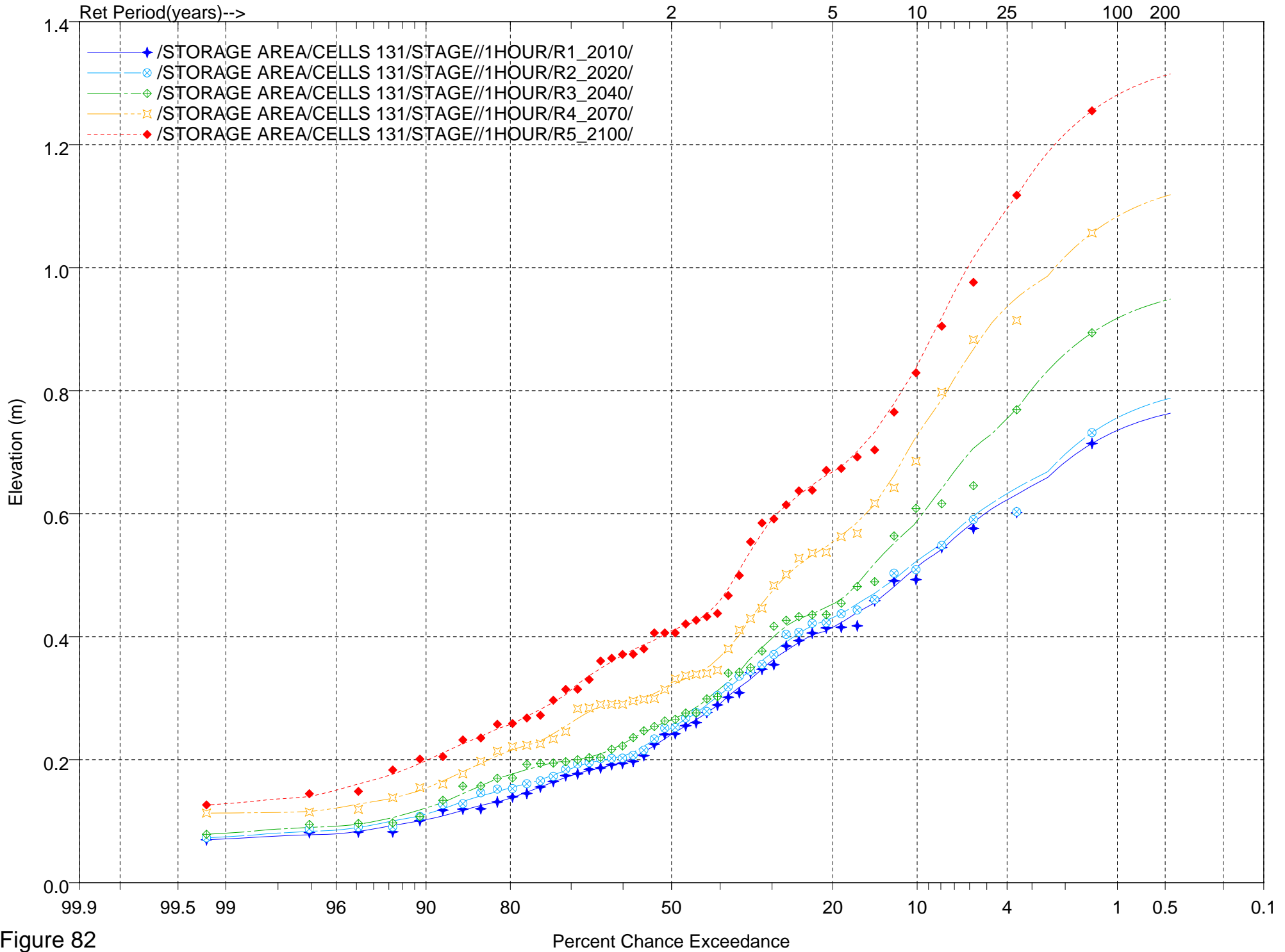


Figure 82

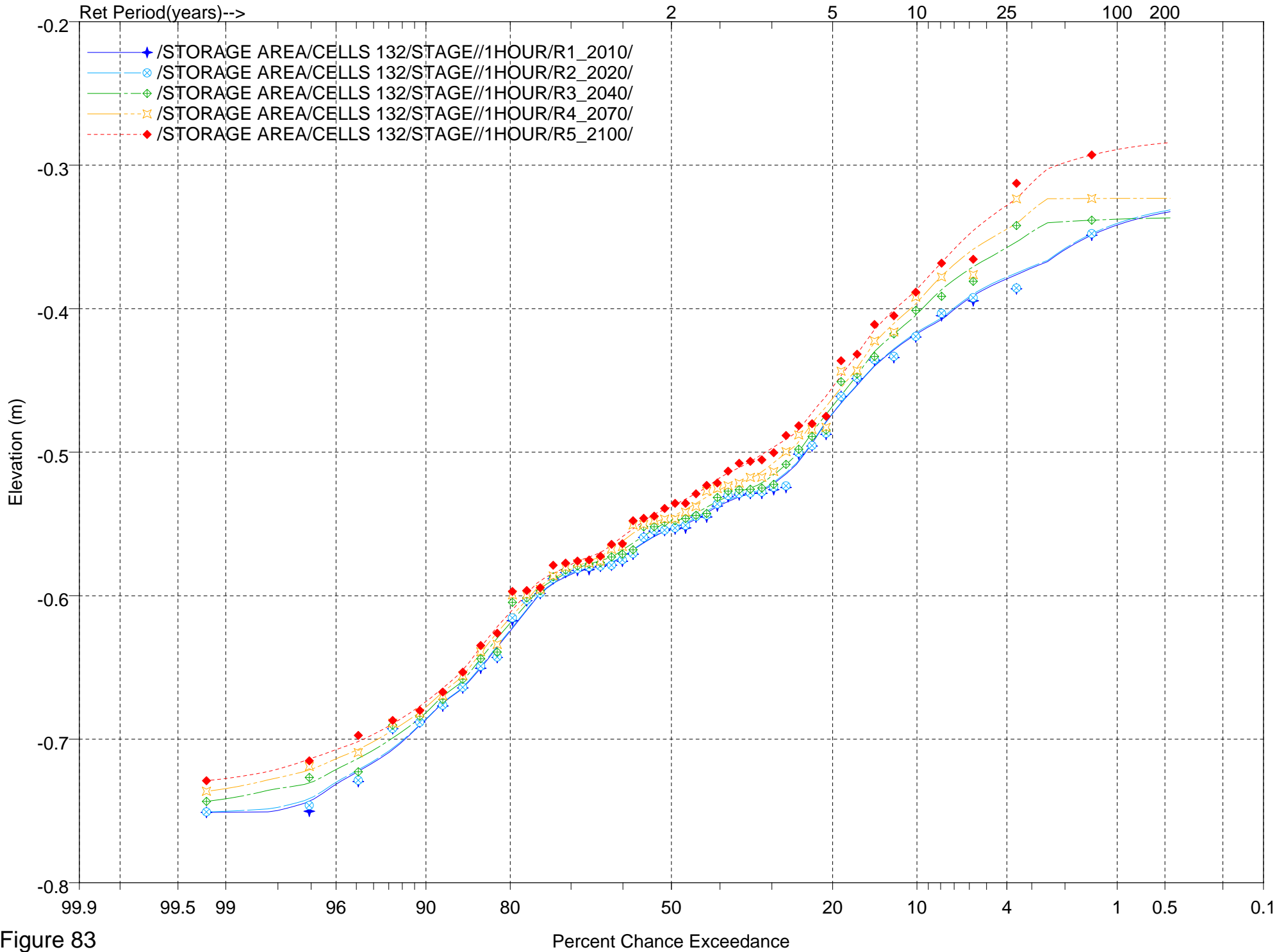


Figure 83

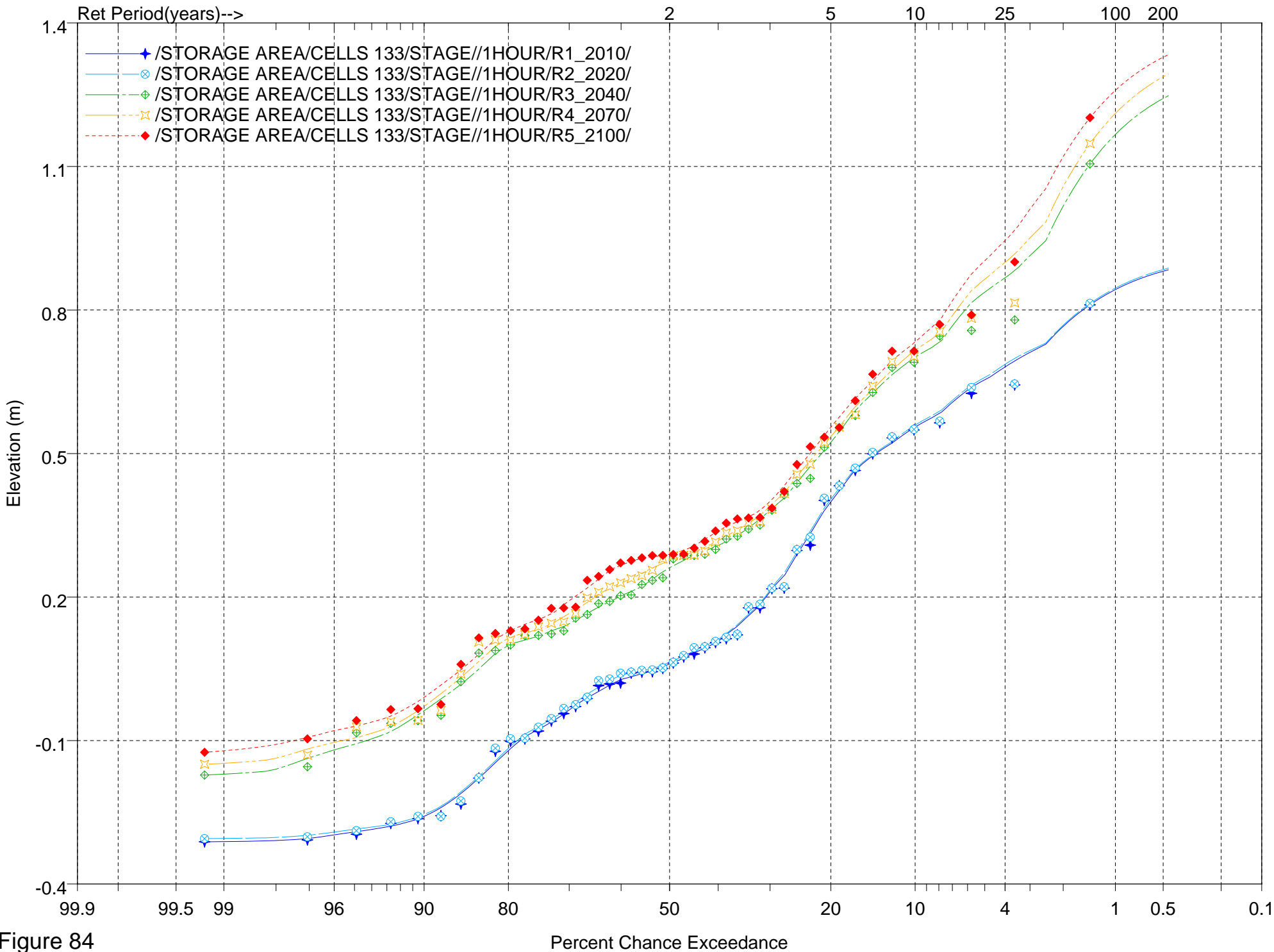


Figure 84

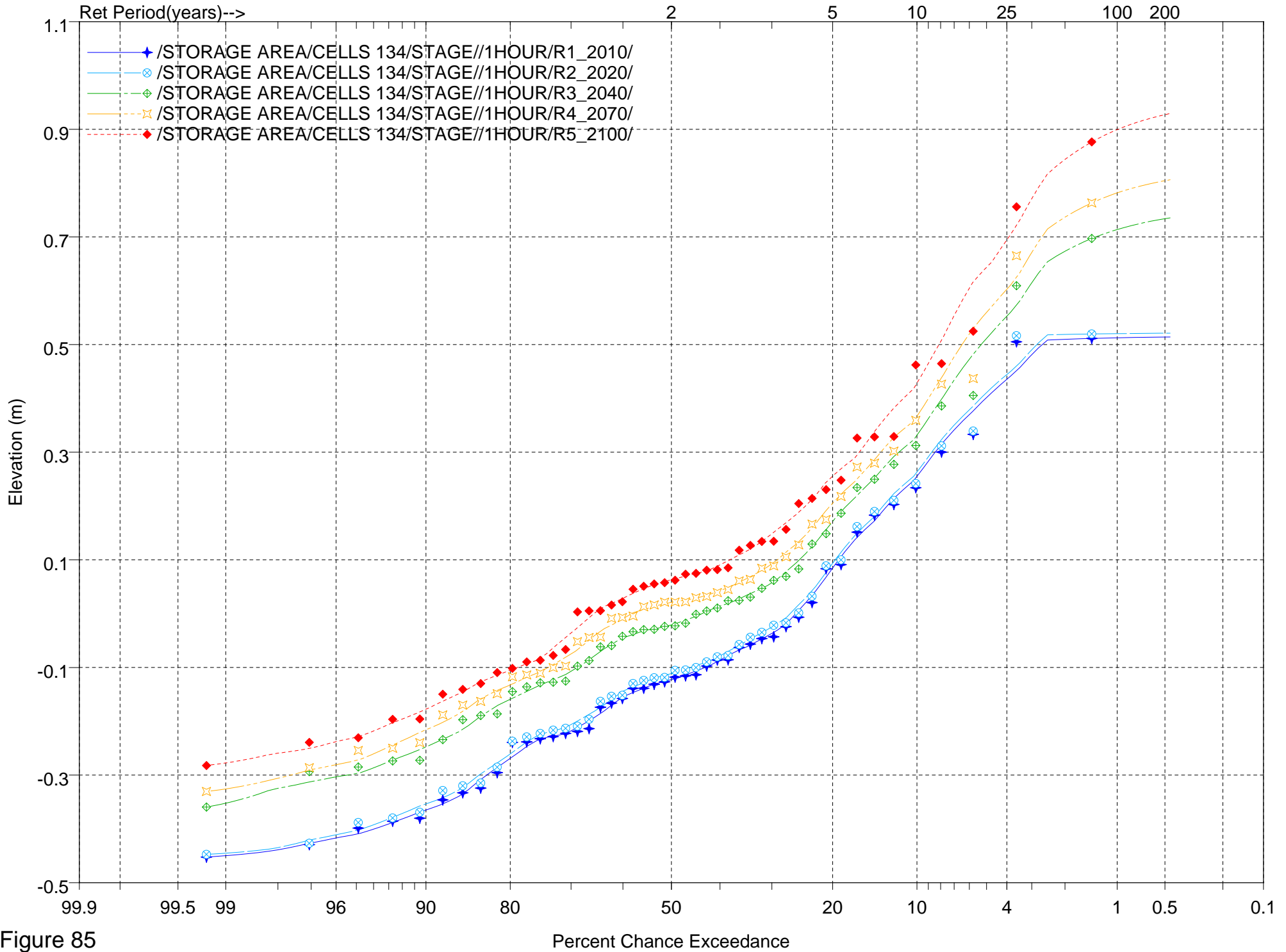


Figure 85

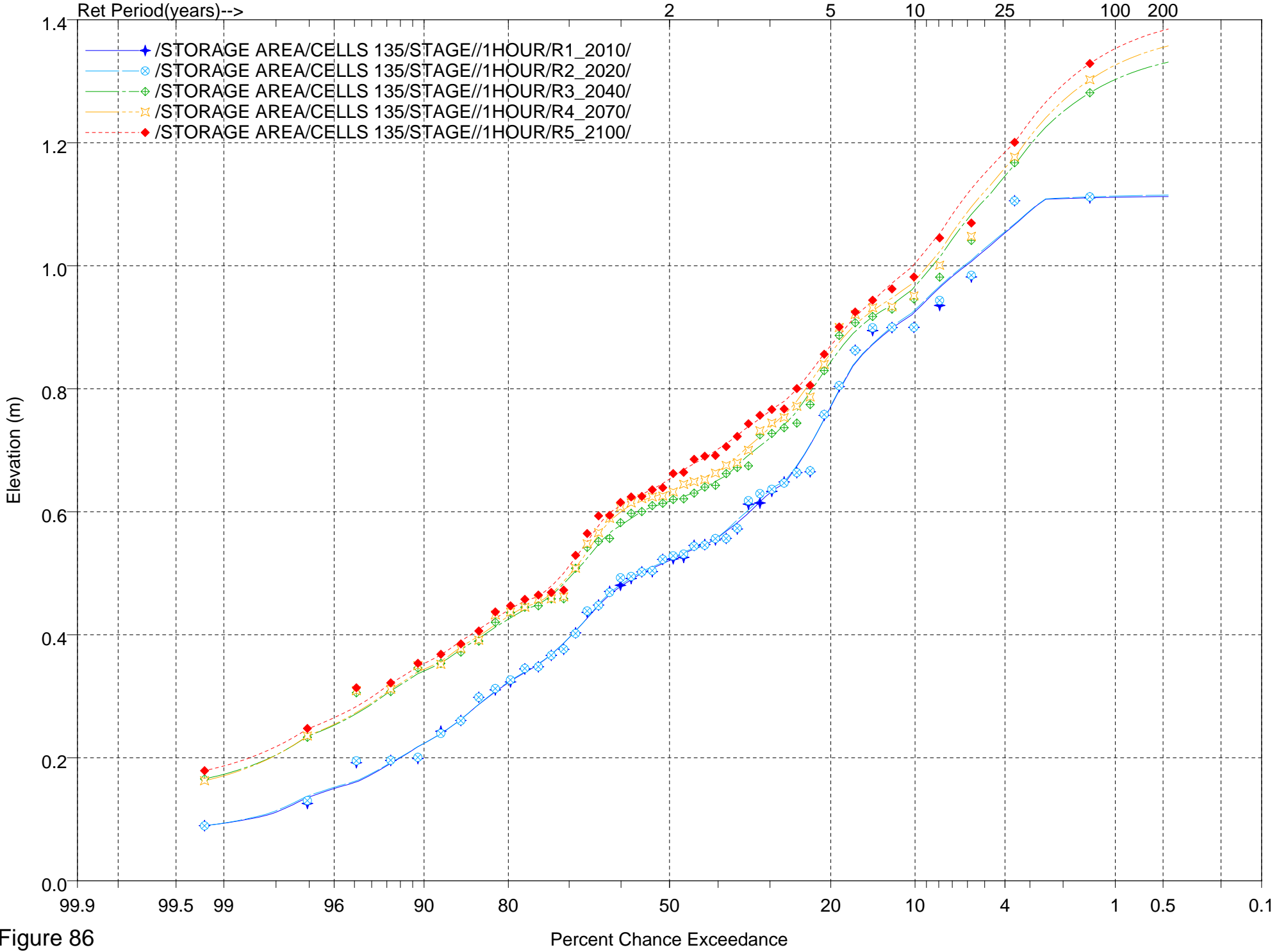


Figure 86

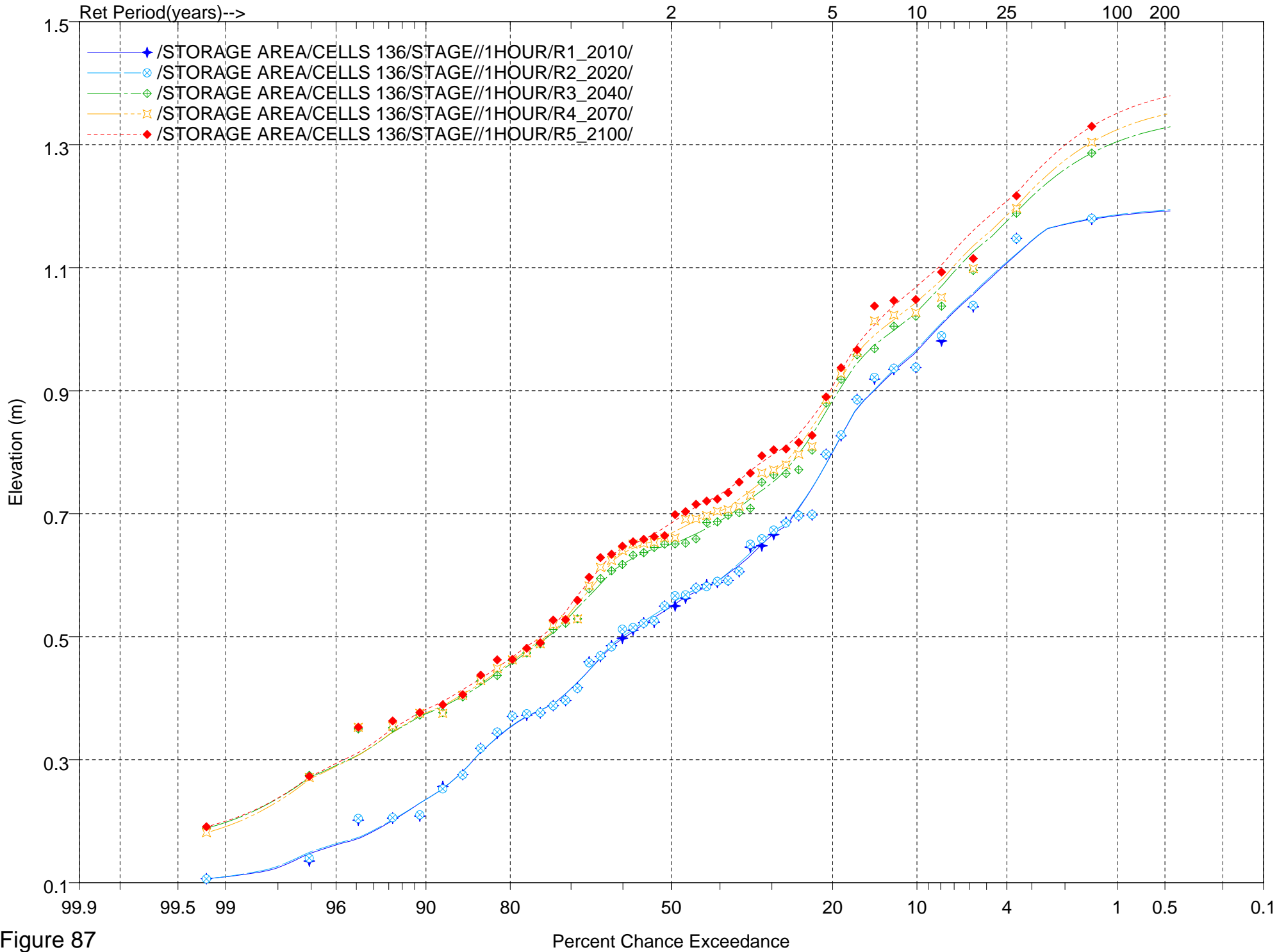


Figure 87

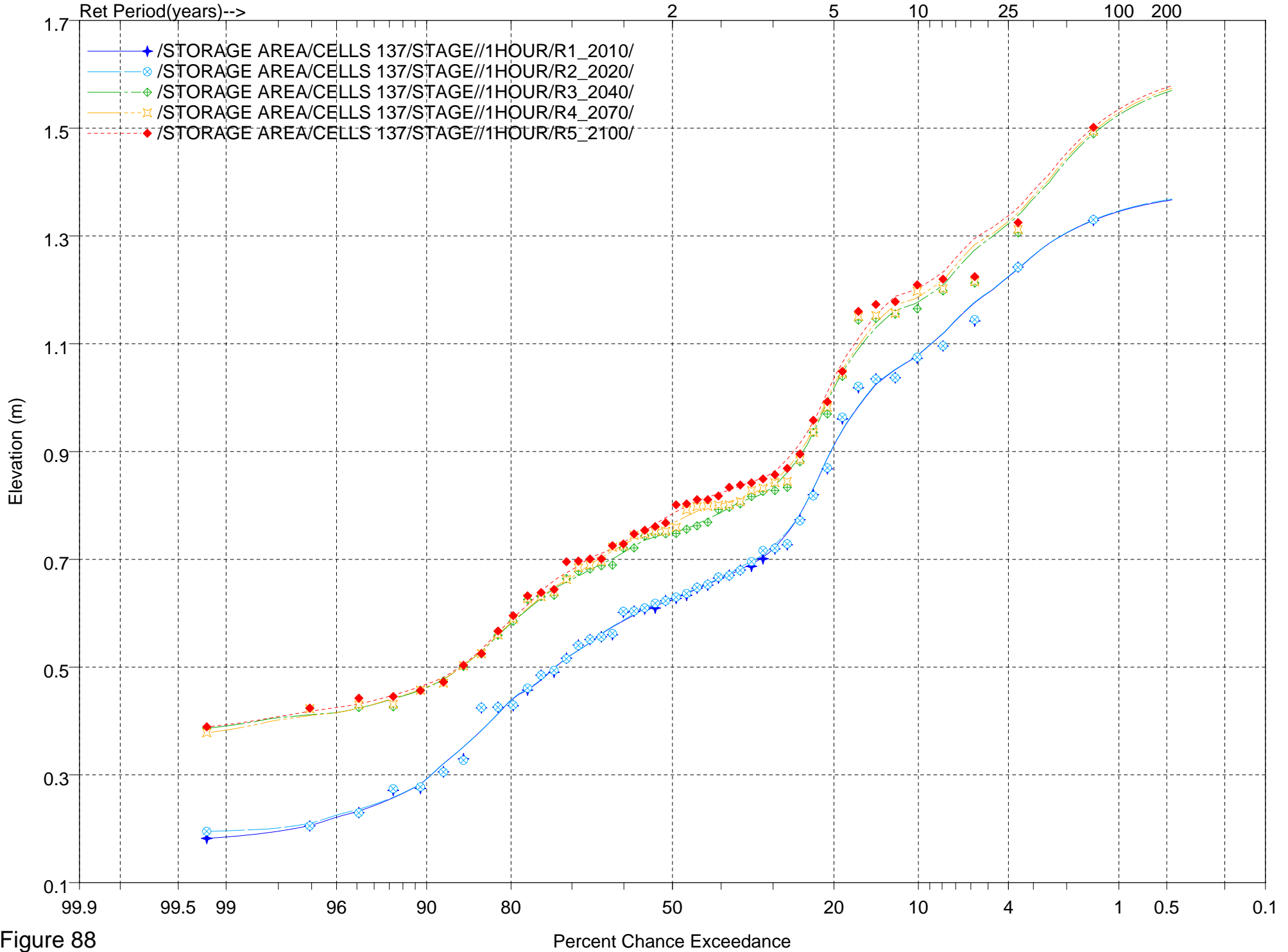


Figure 88

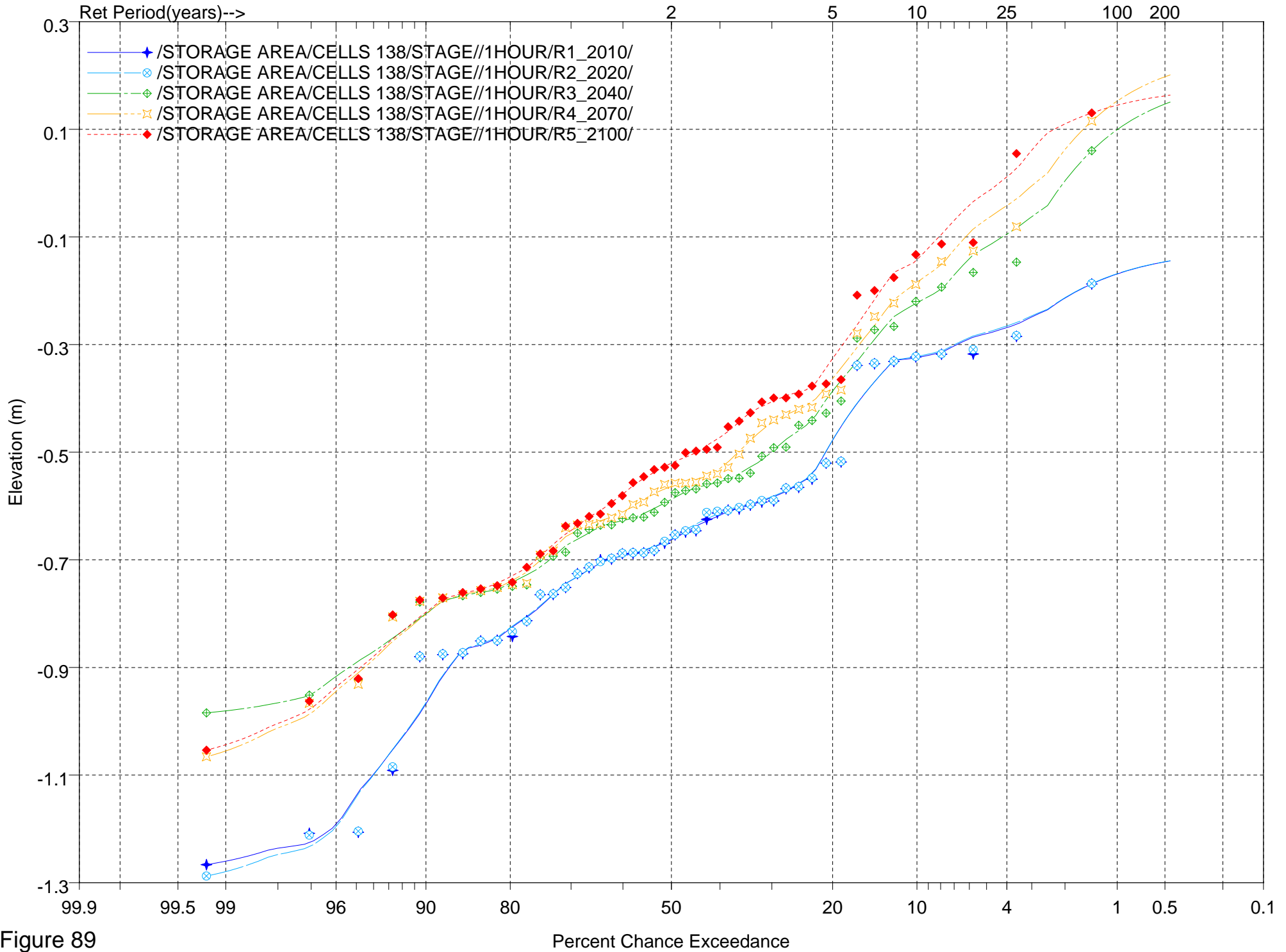


Figure 89



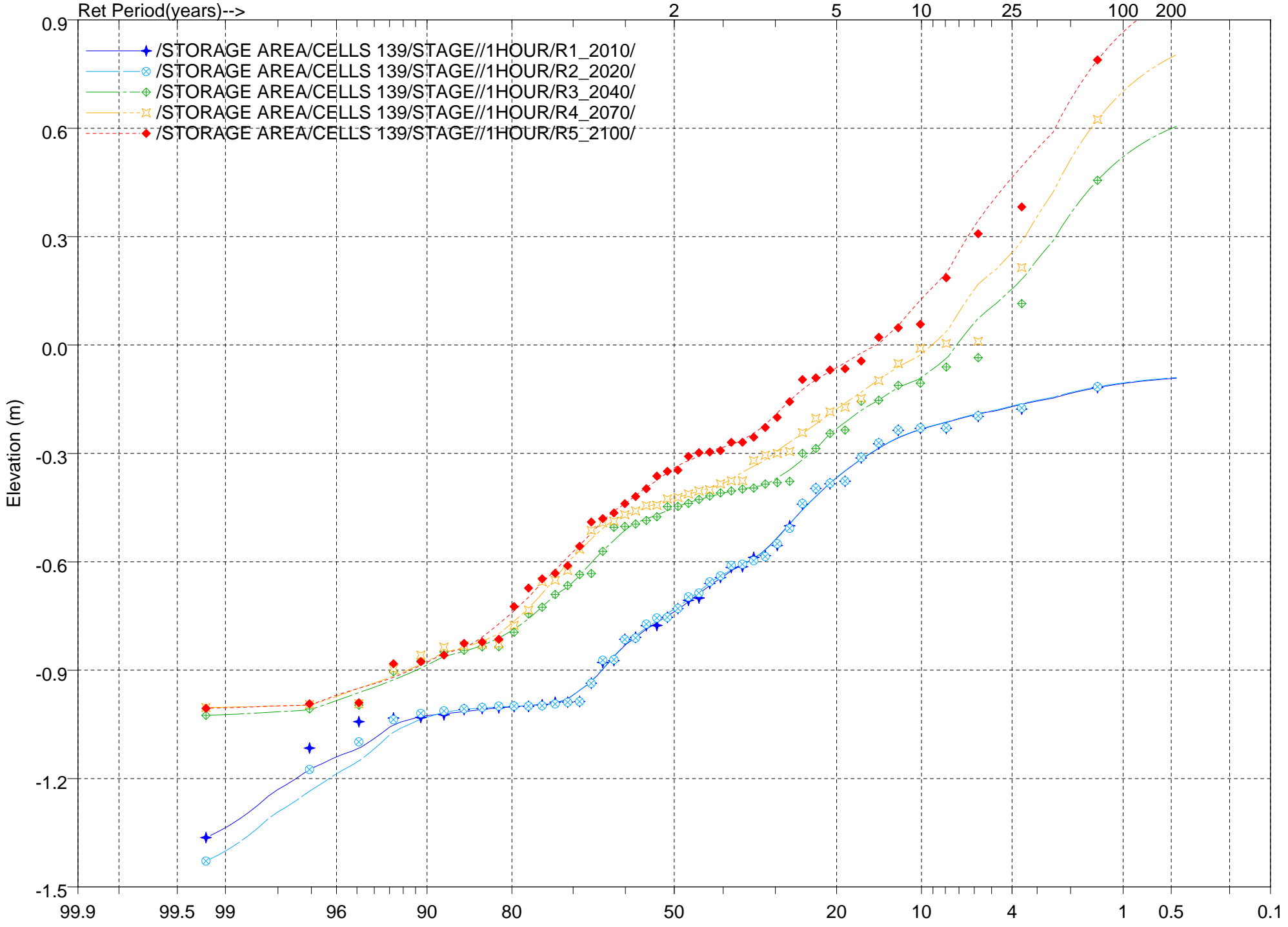


Figure 90

Percent Chance Exceedance

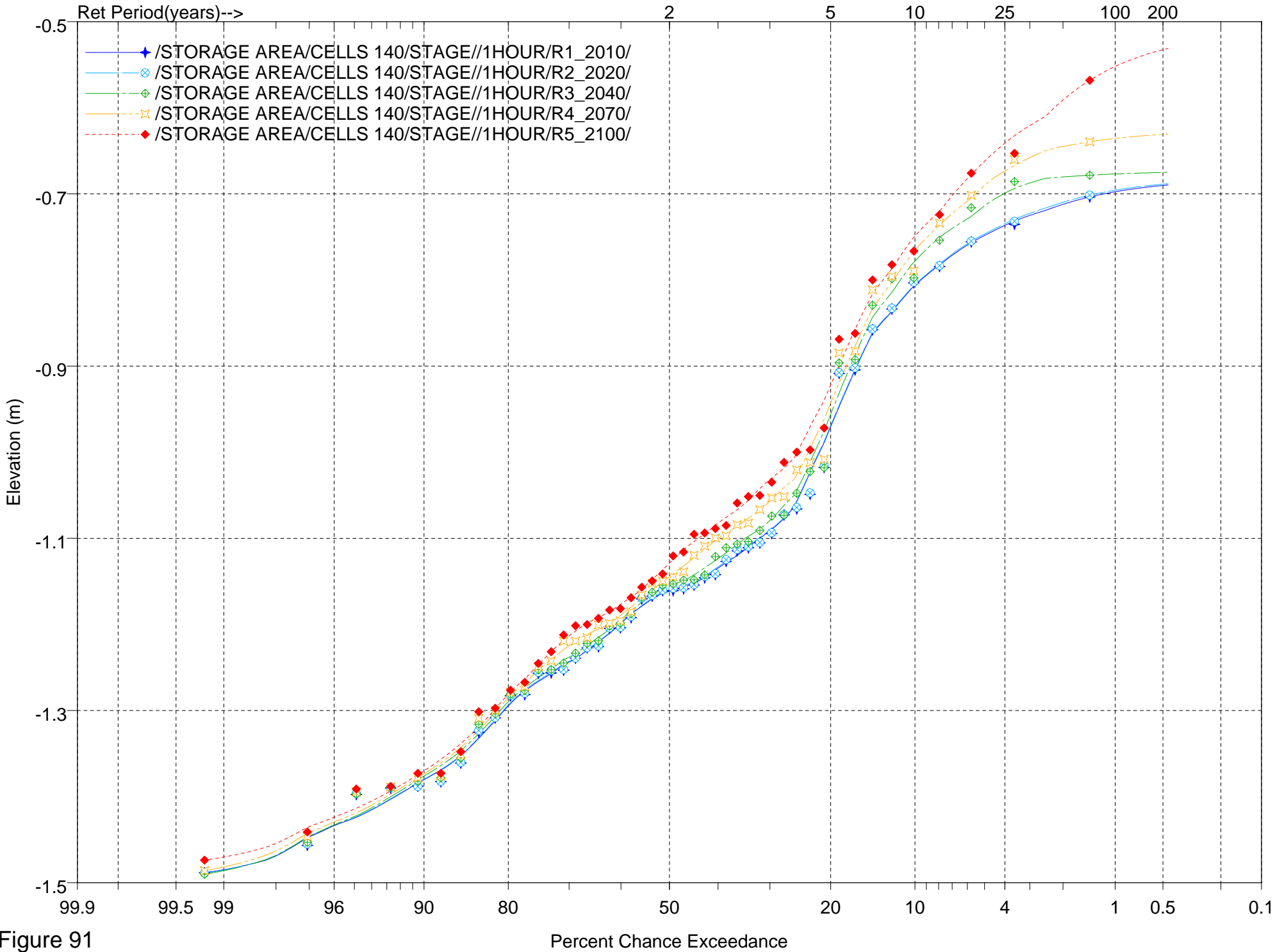


Figure 91

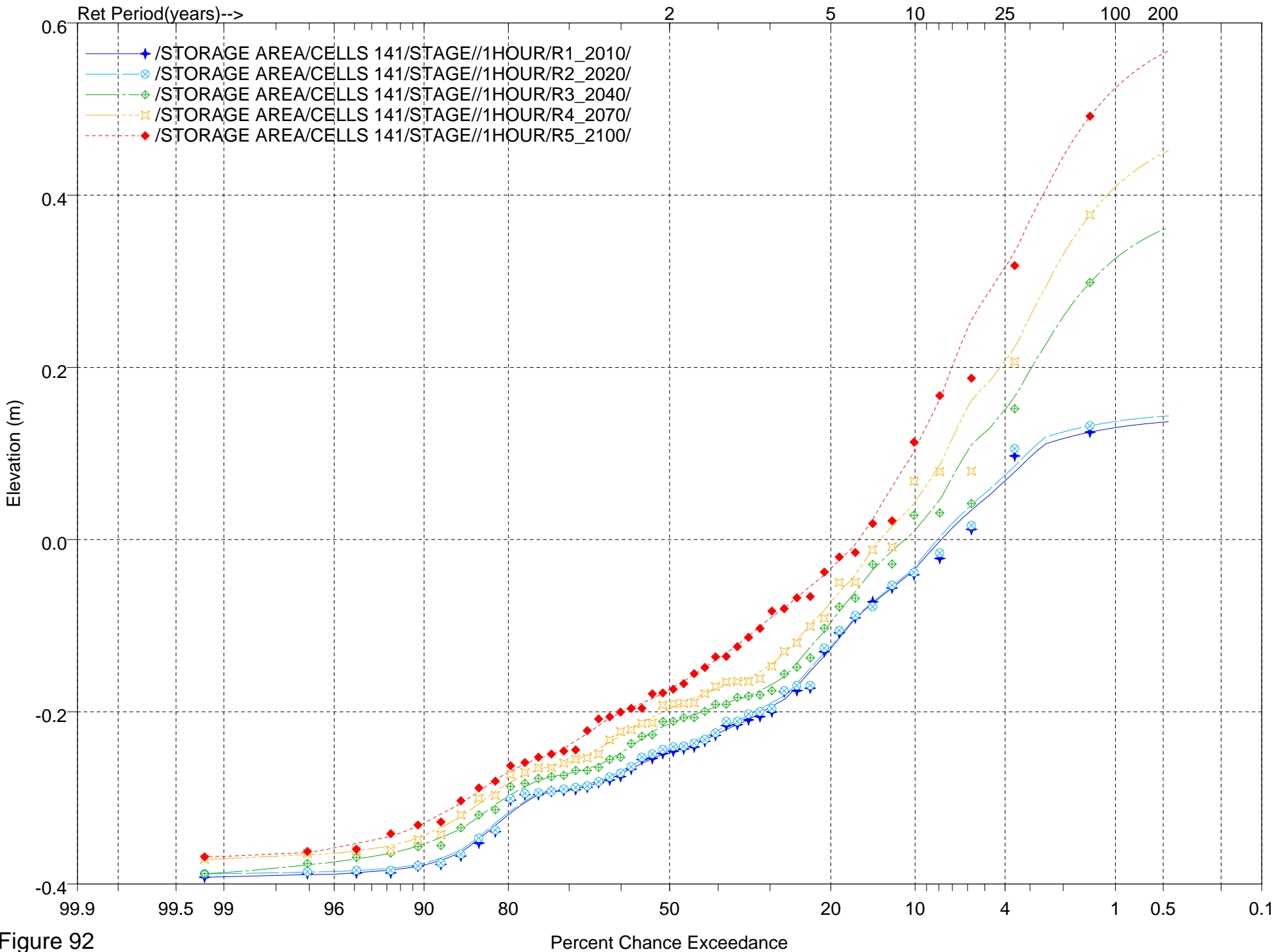


Figure 92

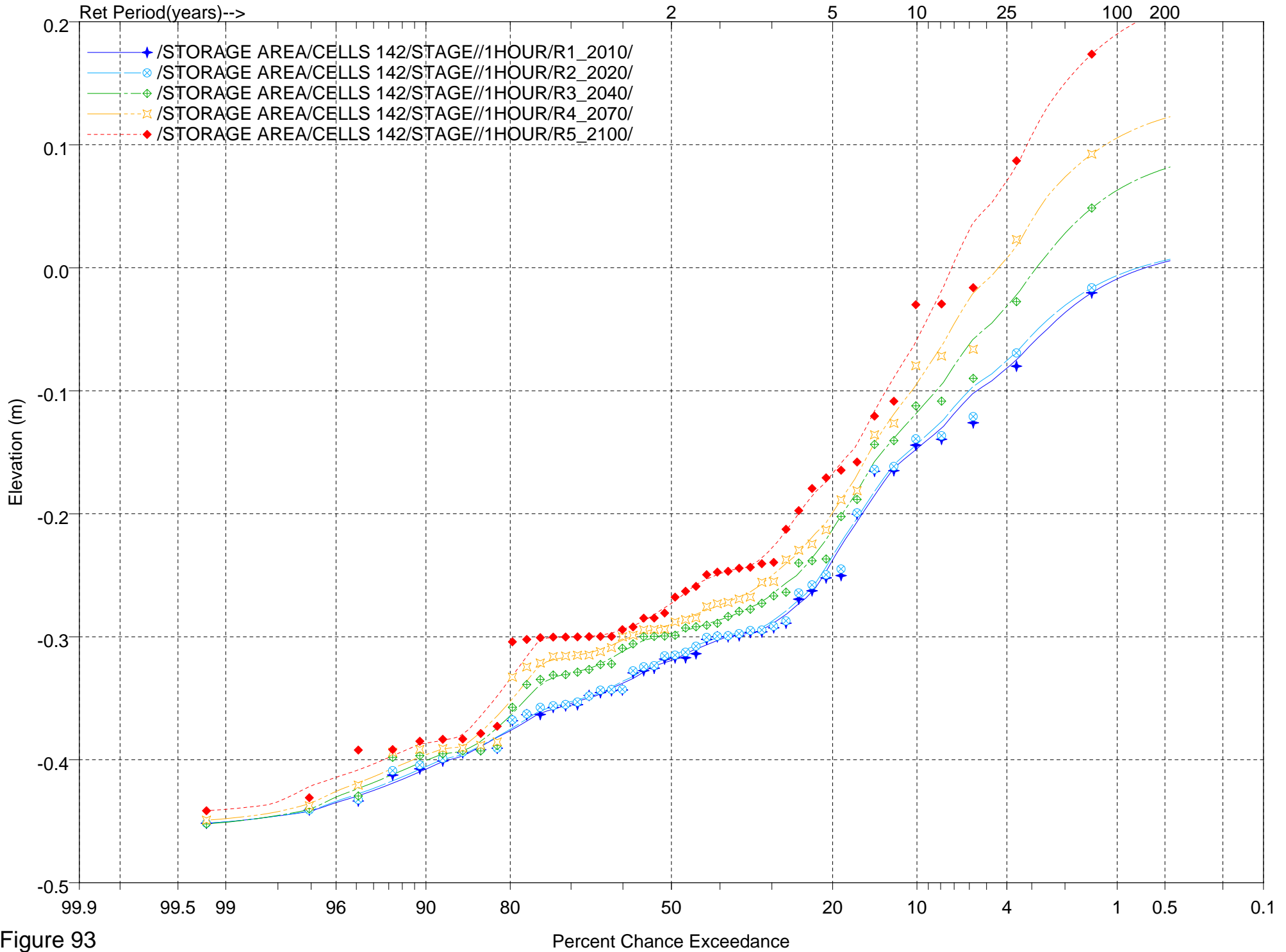


Figure 93

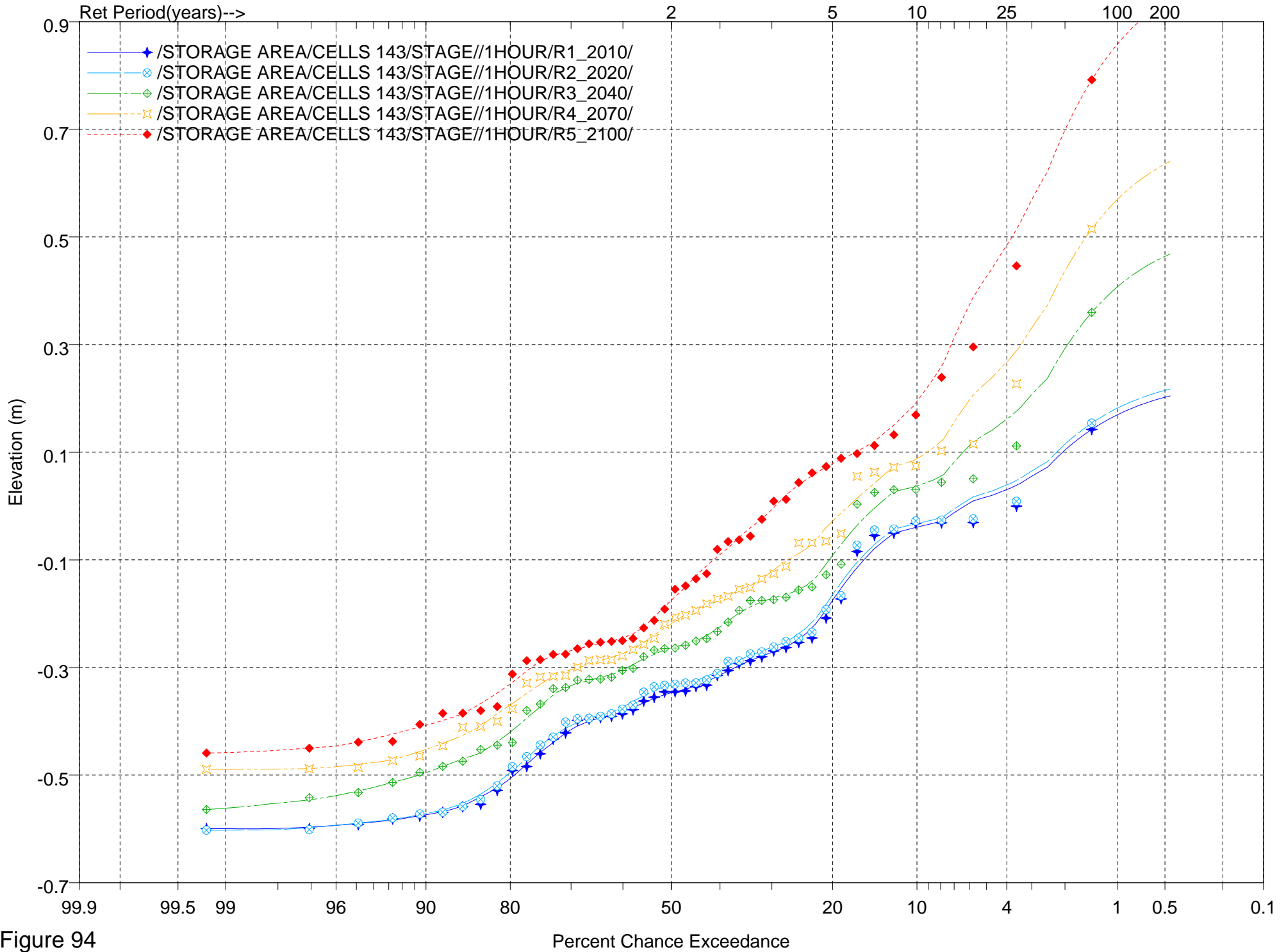


Figure 94

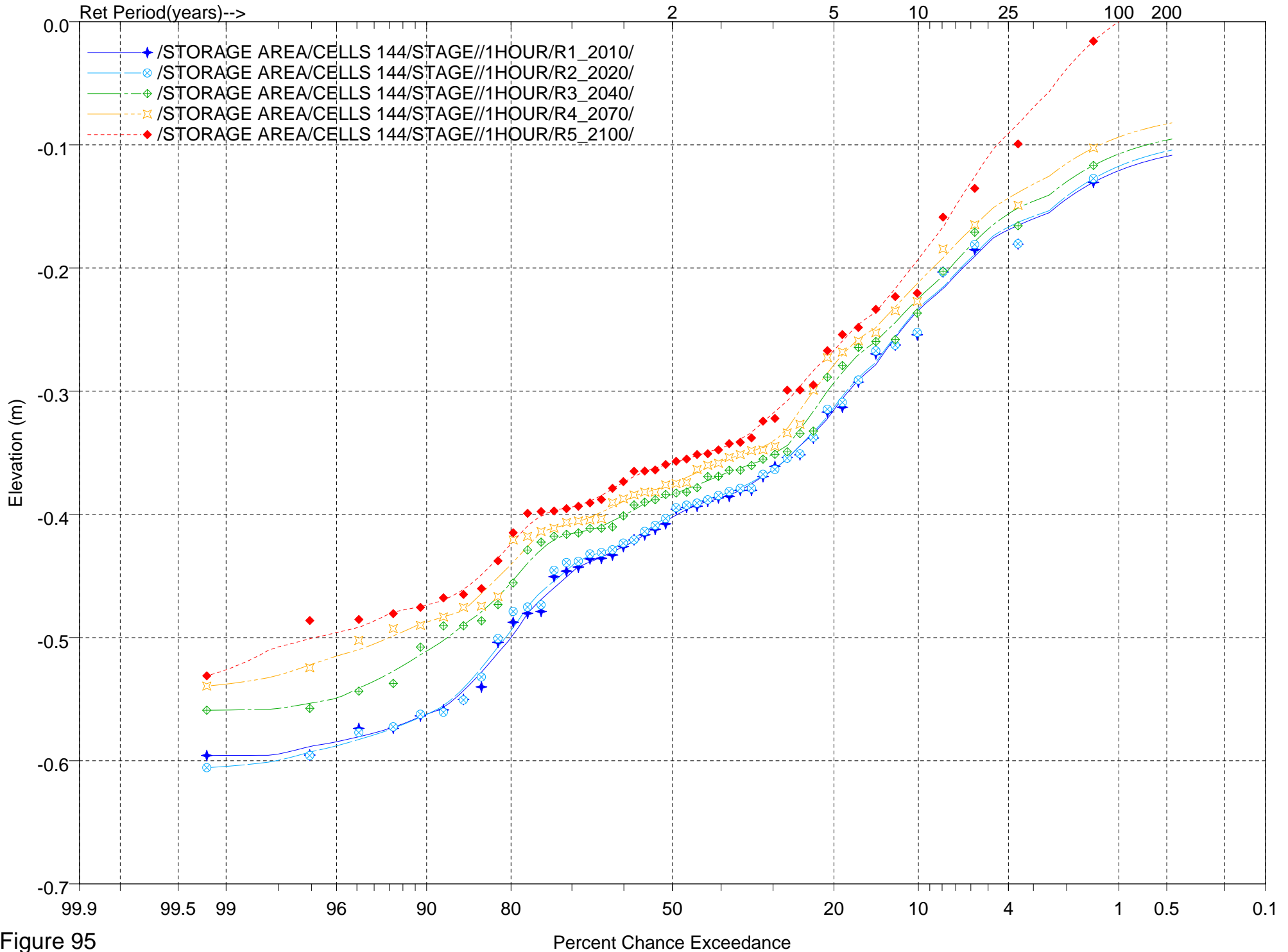


Figure 95

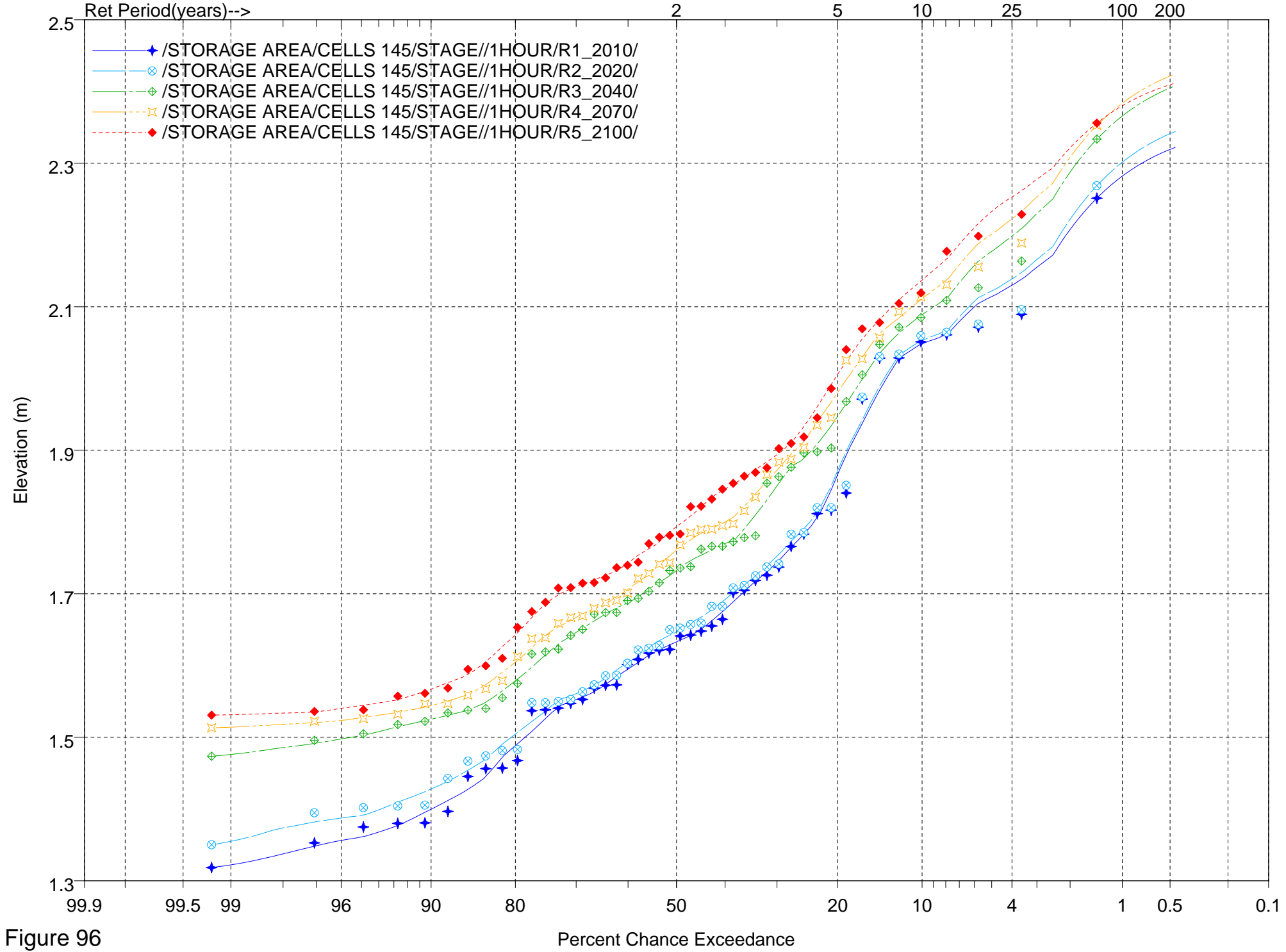


Figure 96

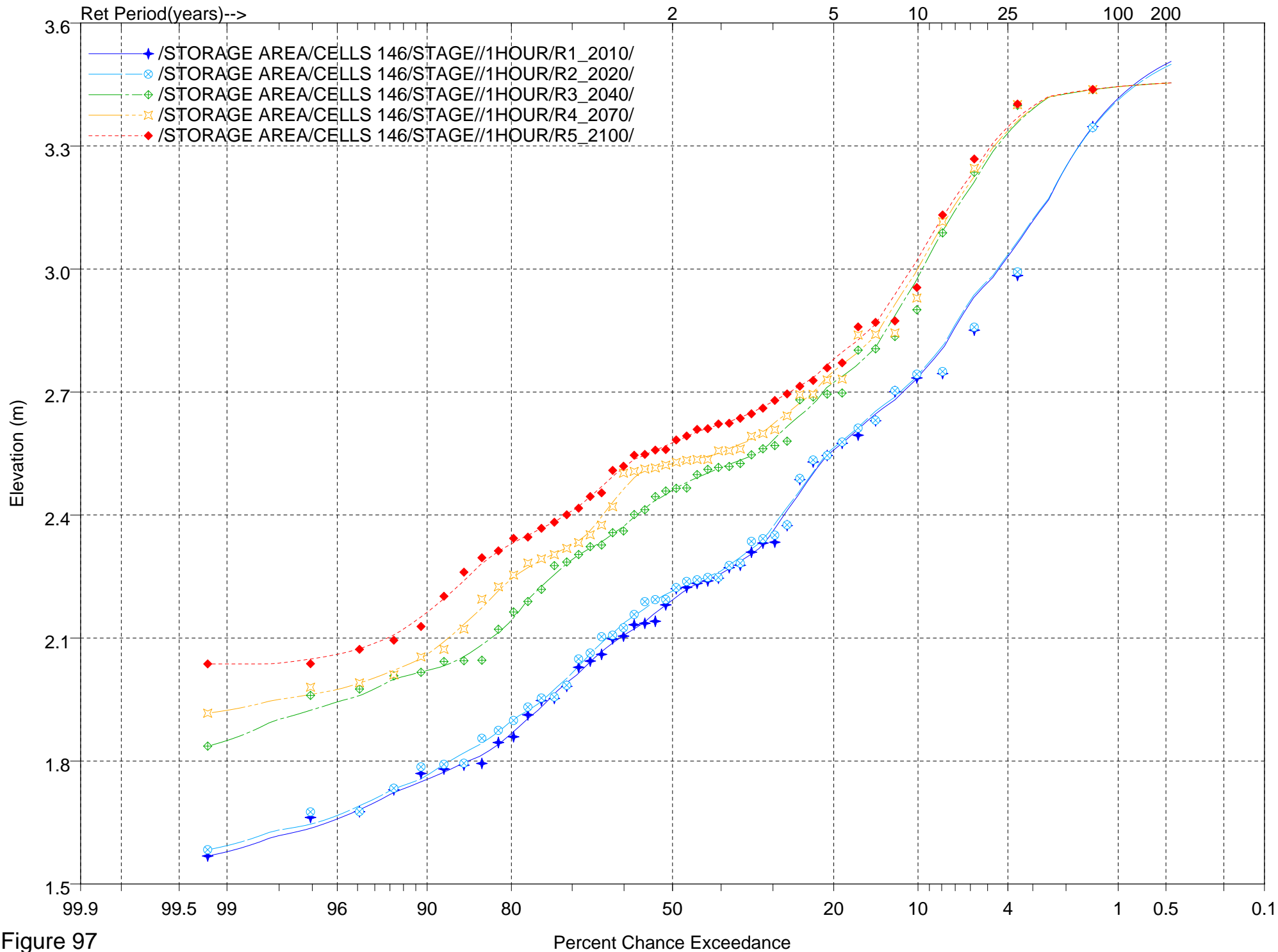


Figure 97



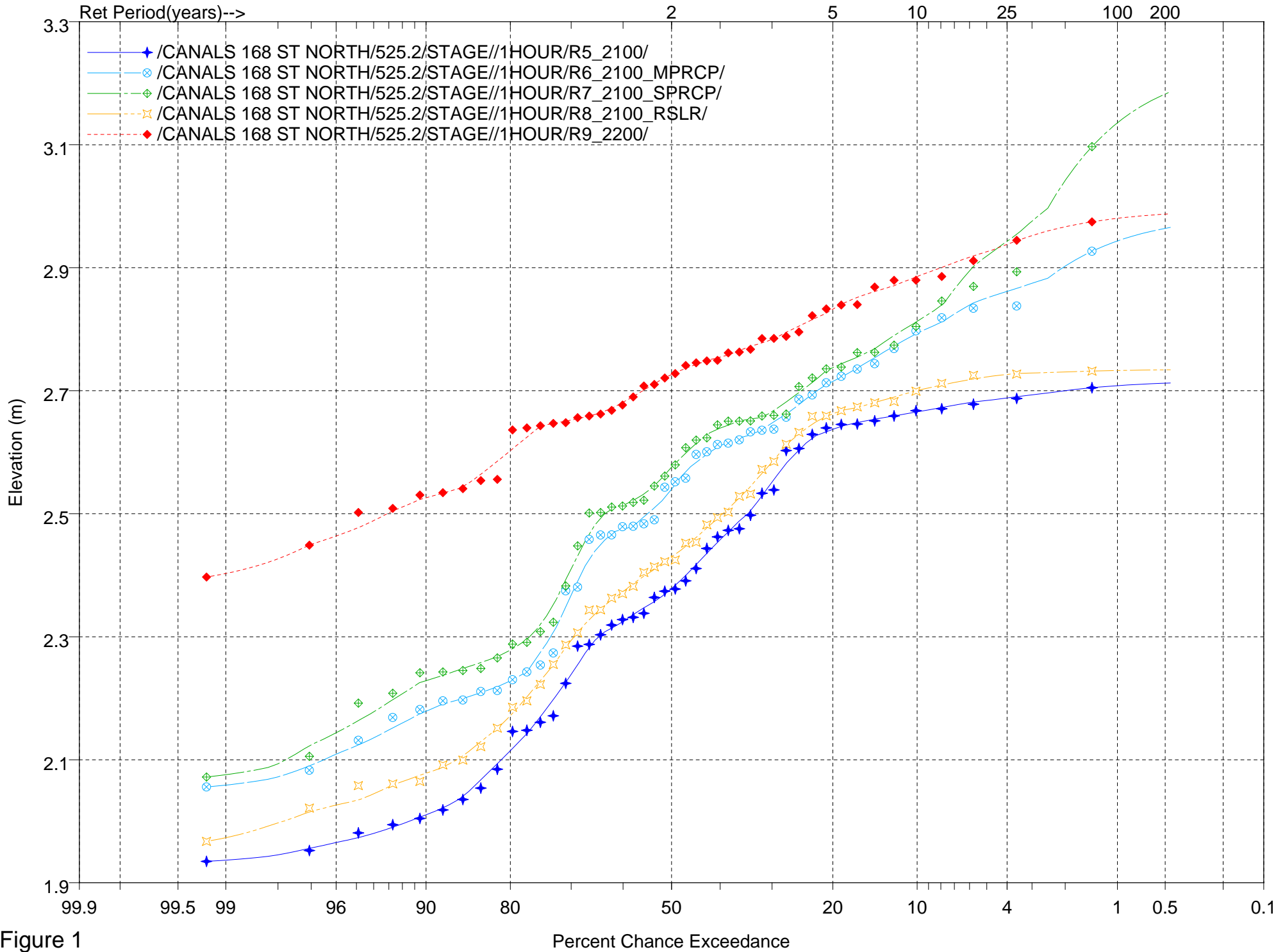


Figure 1

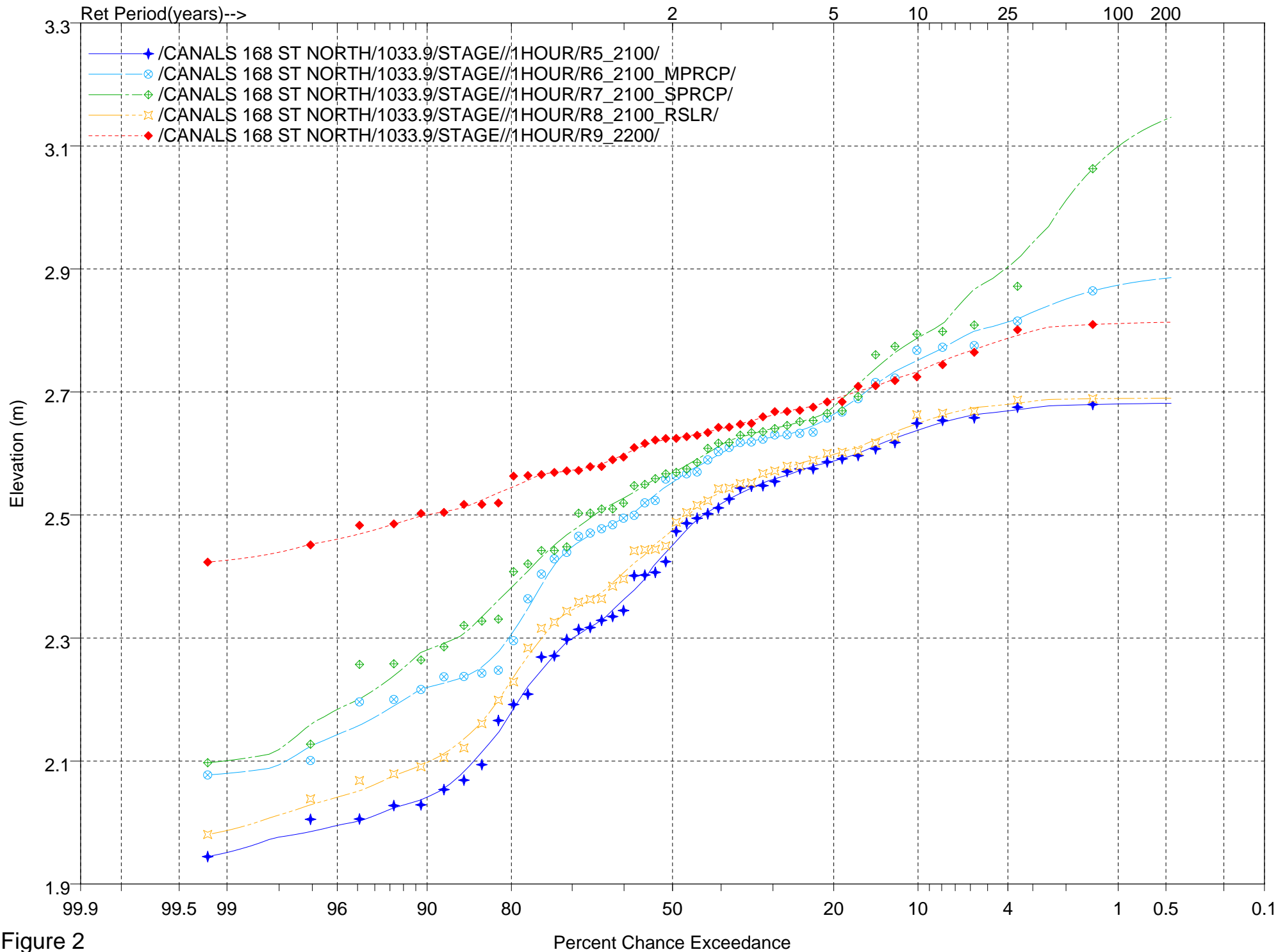


Figure 2

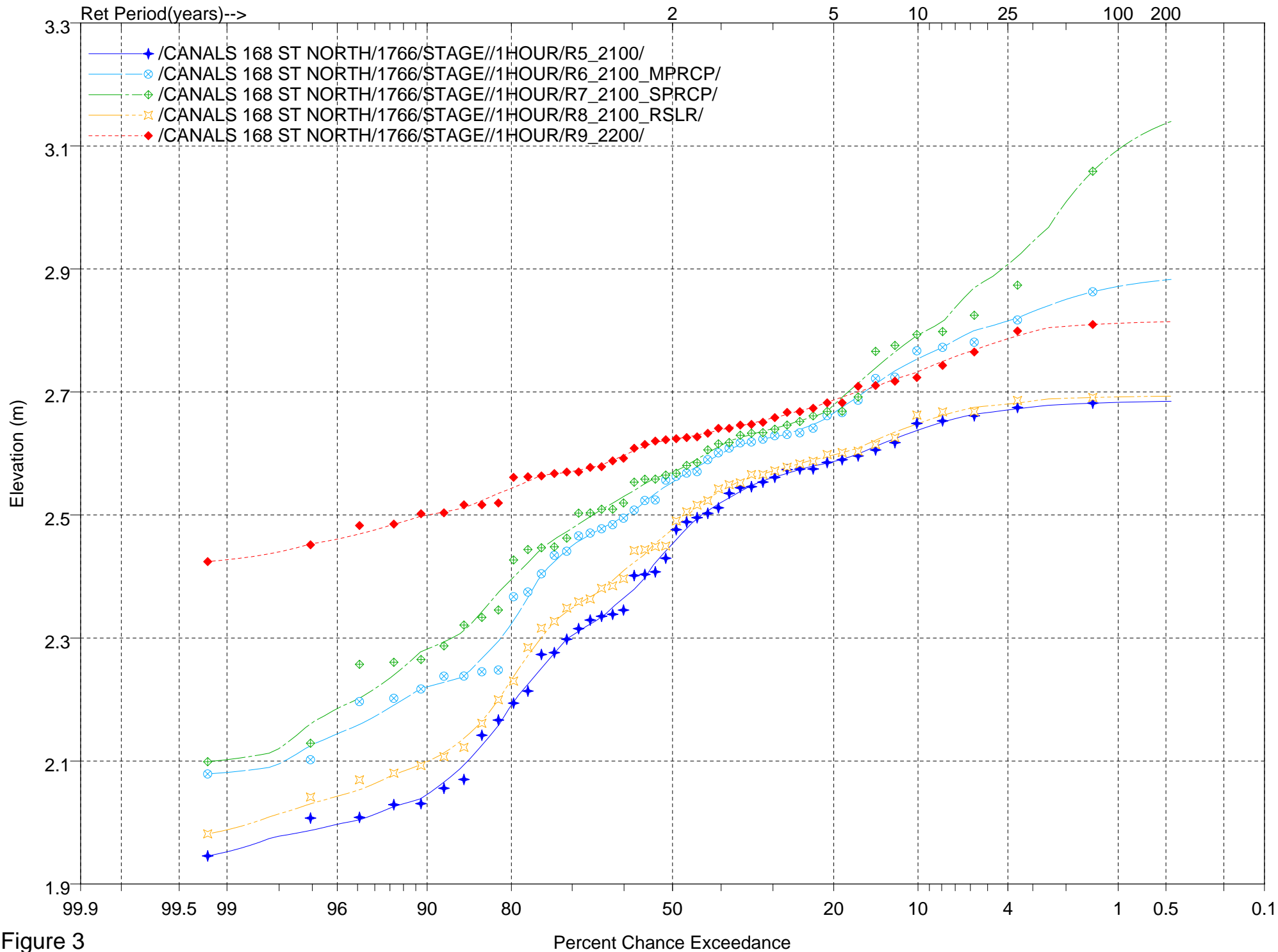


Figure 3

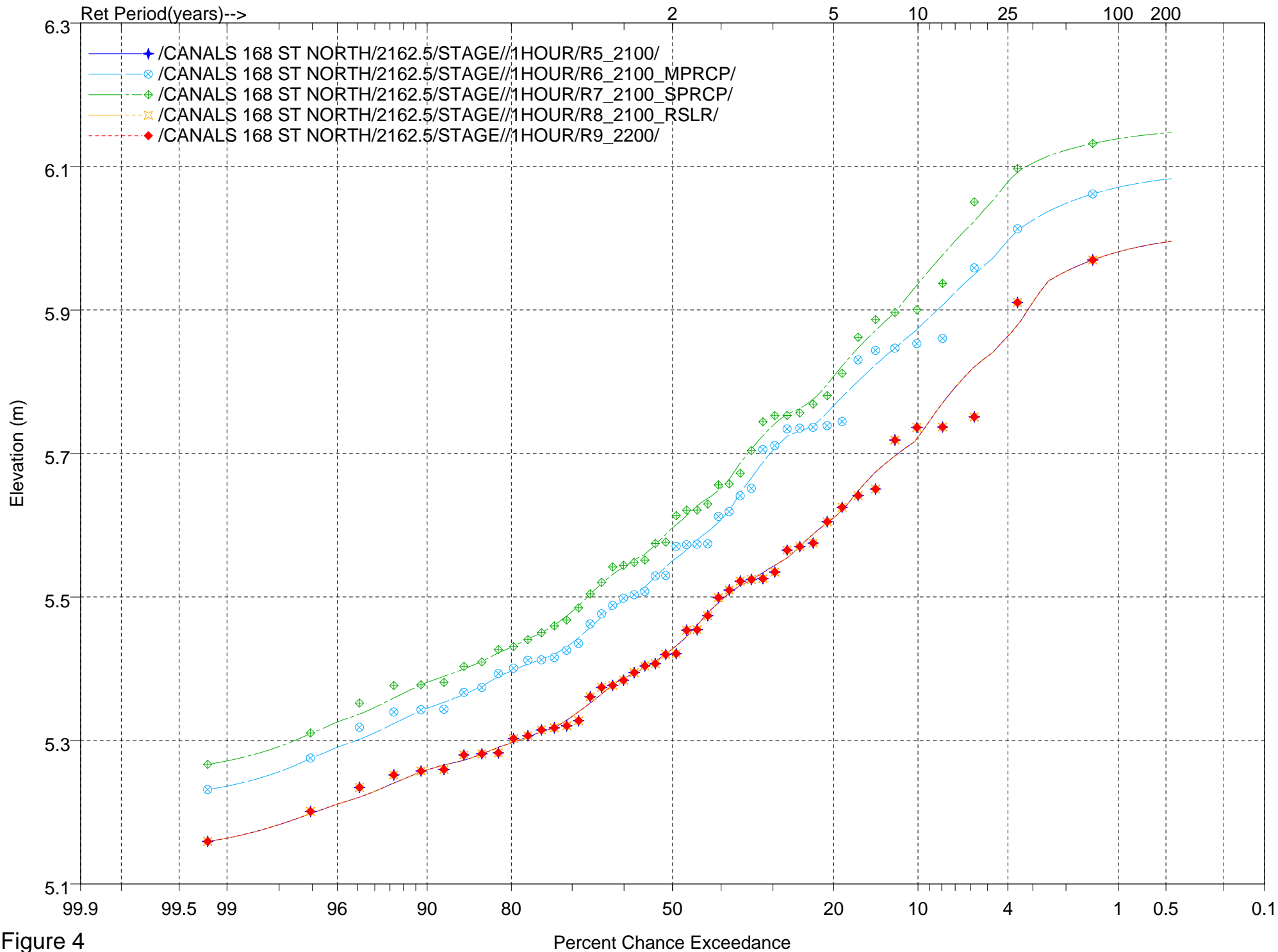


Figure 4

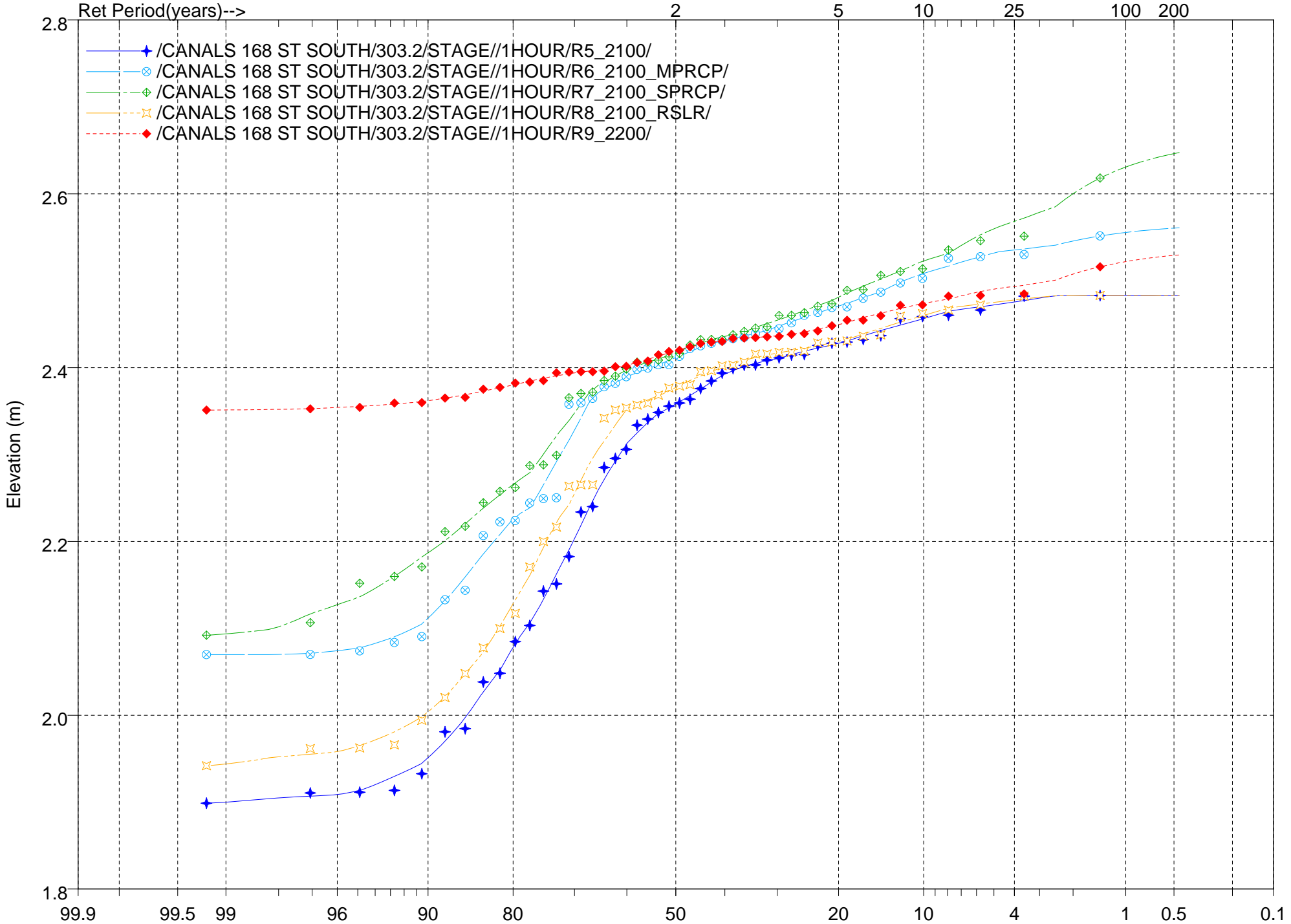


Figure 5

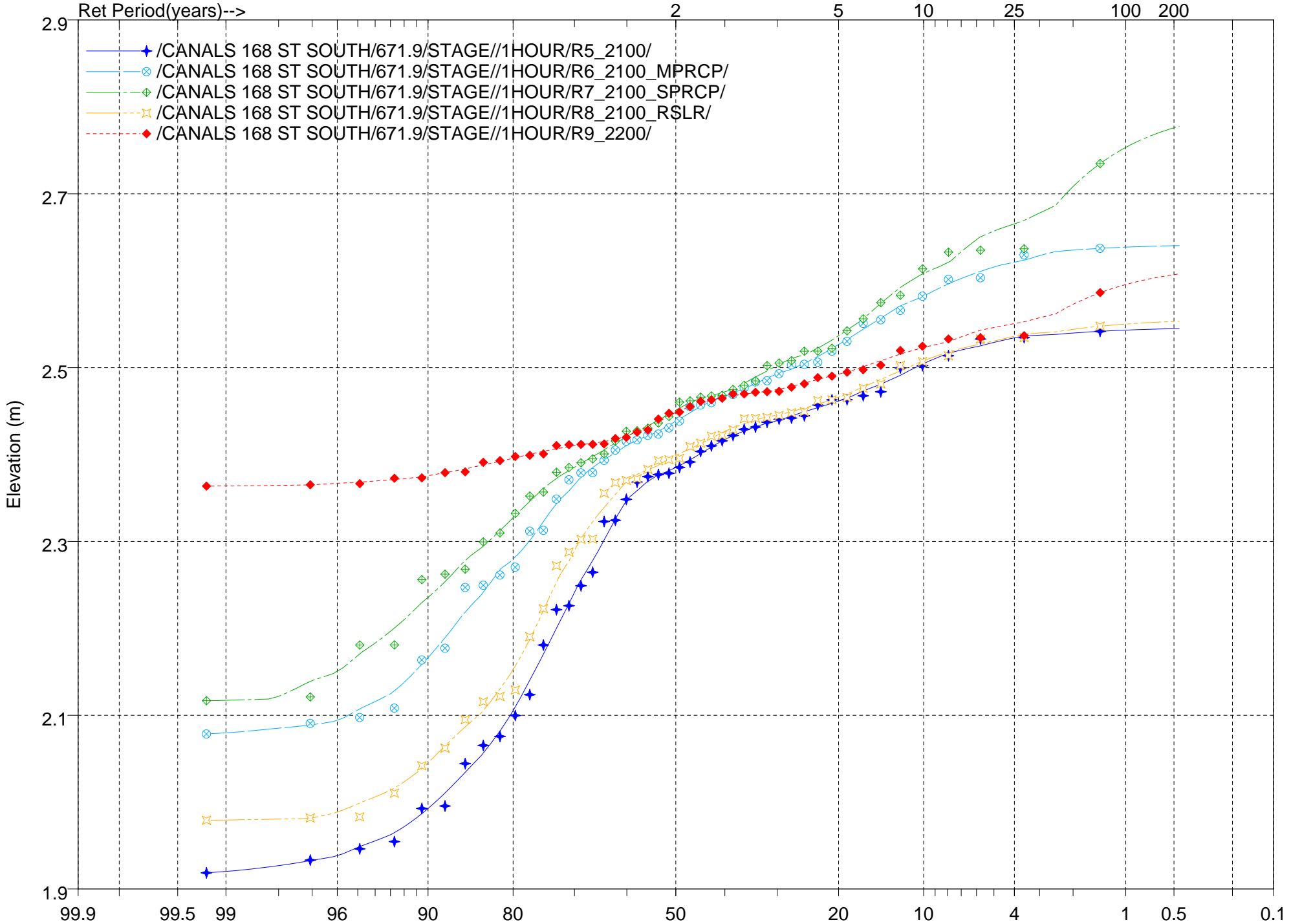


Figure 6

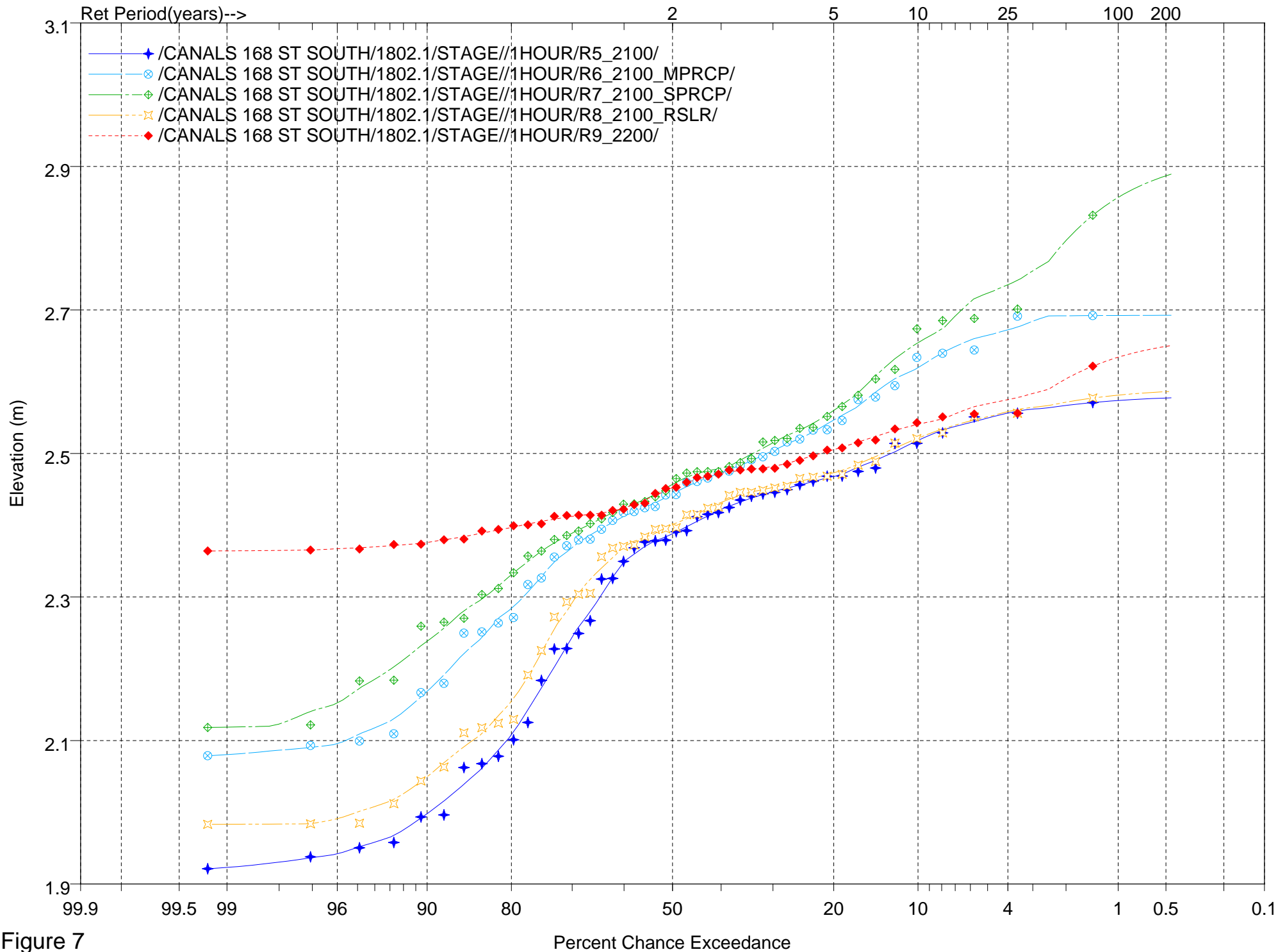


Figure 7

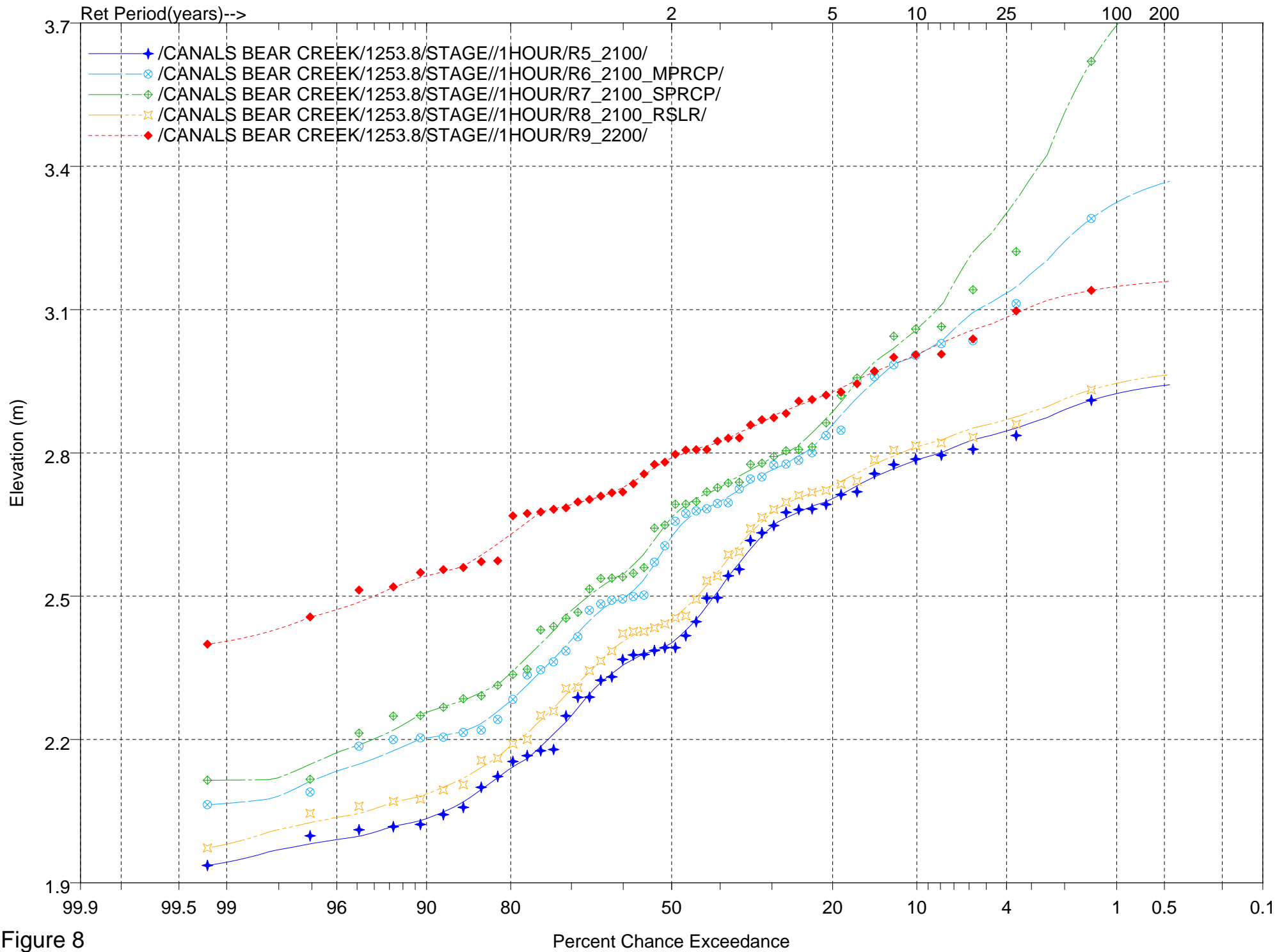


Figure 8



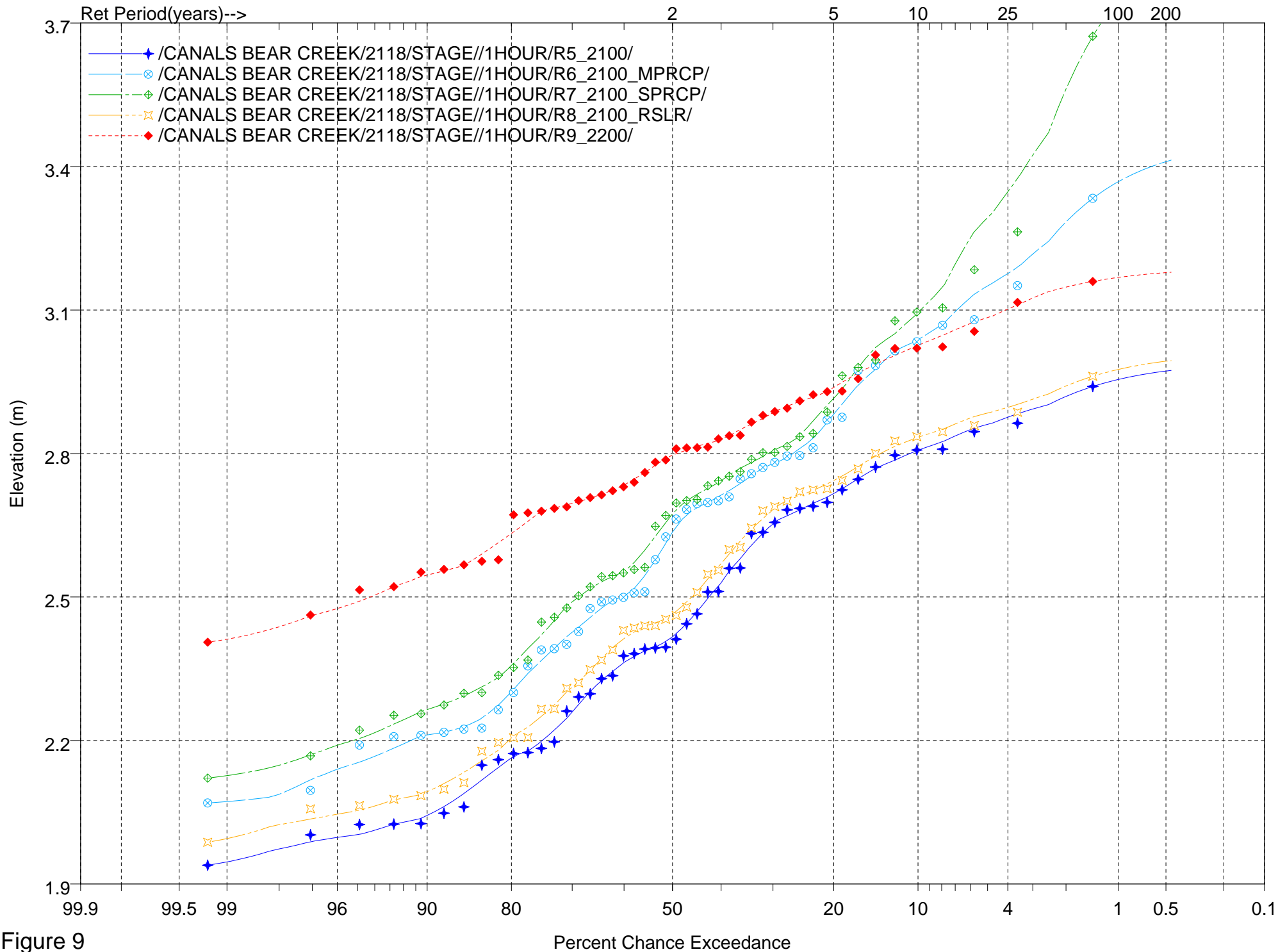


Figure 9

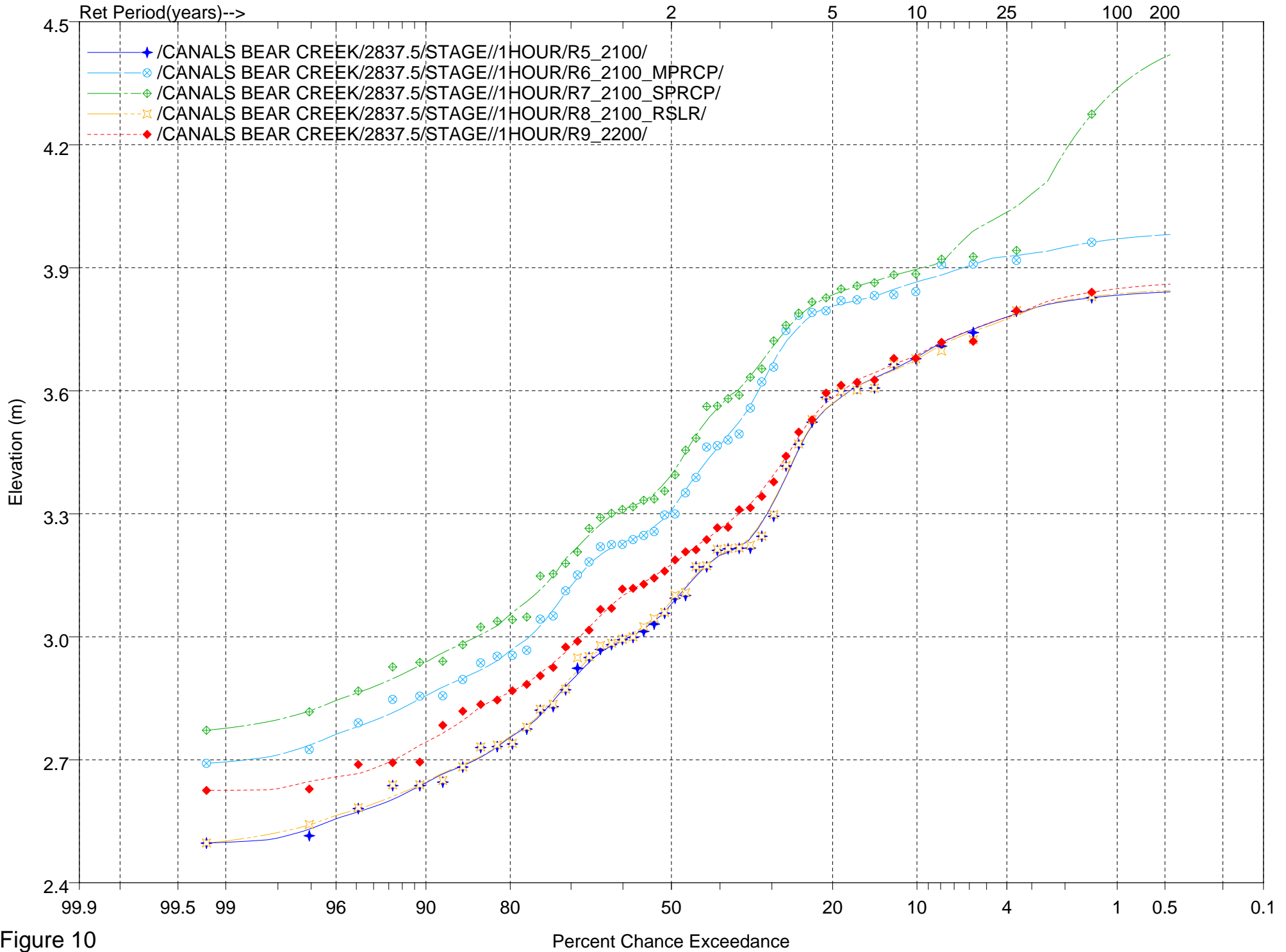


Figure 10

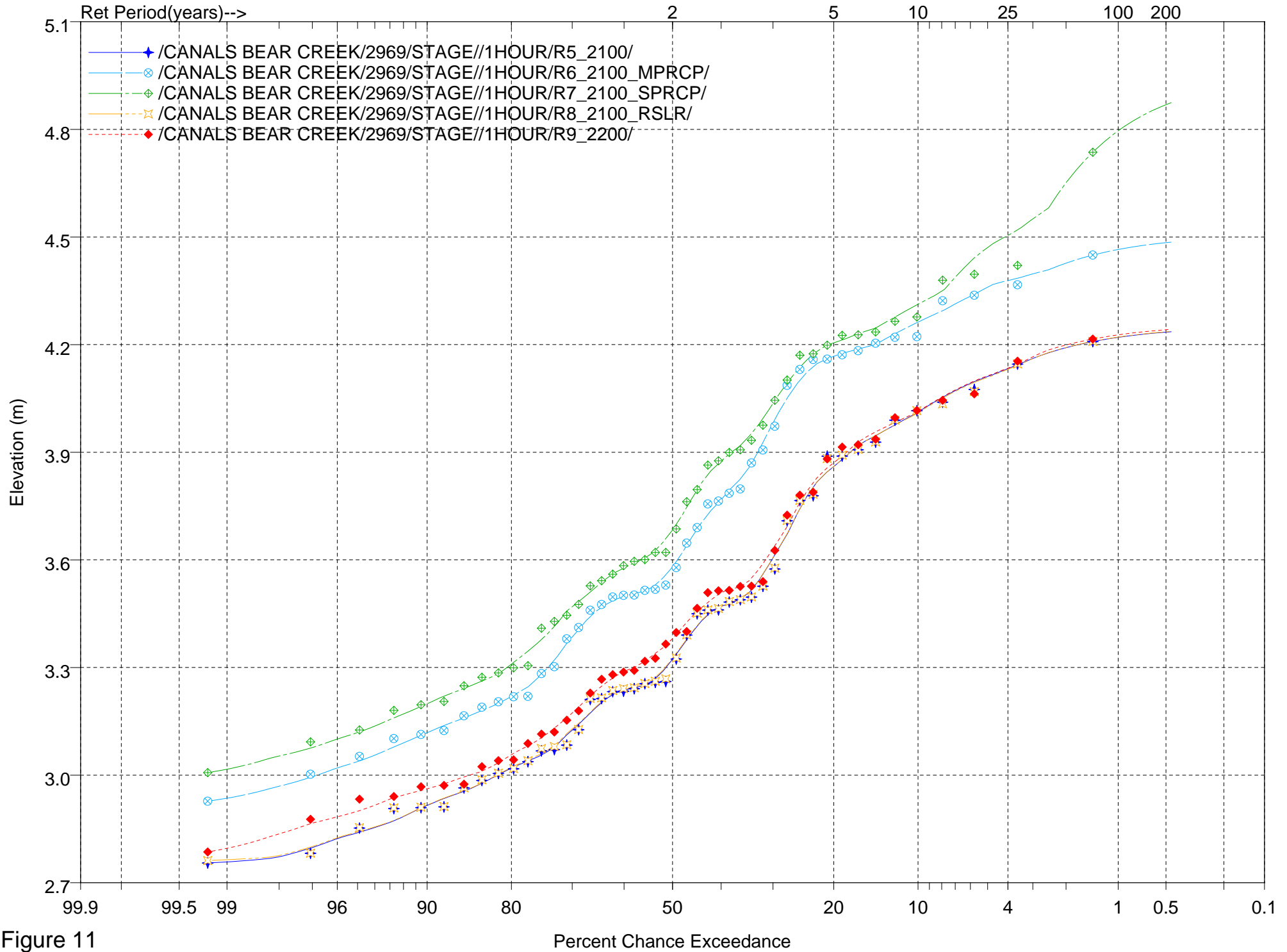


Figure 11

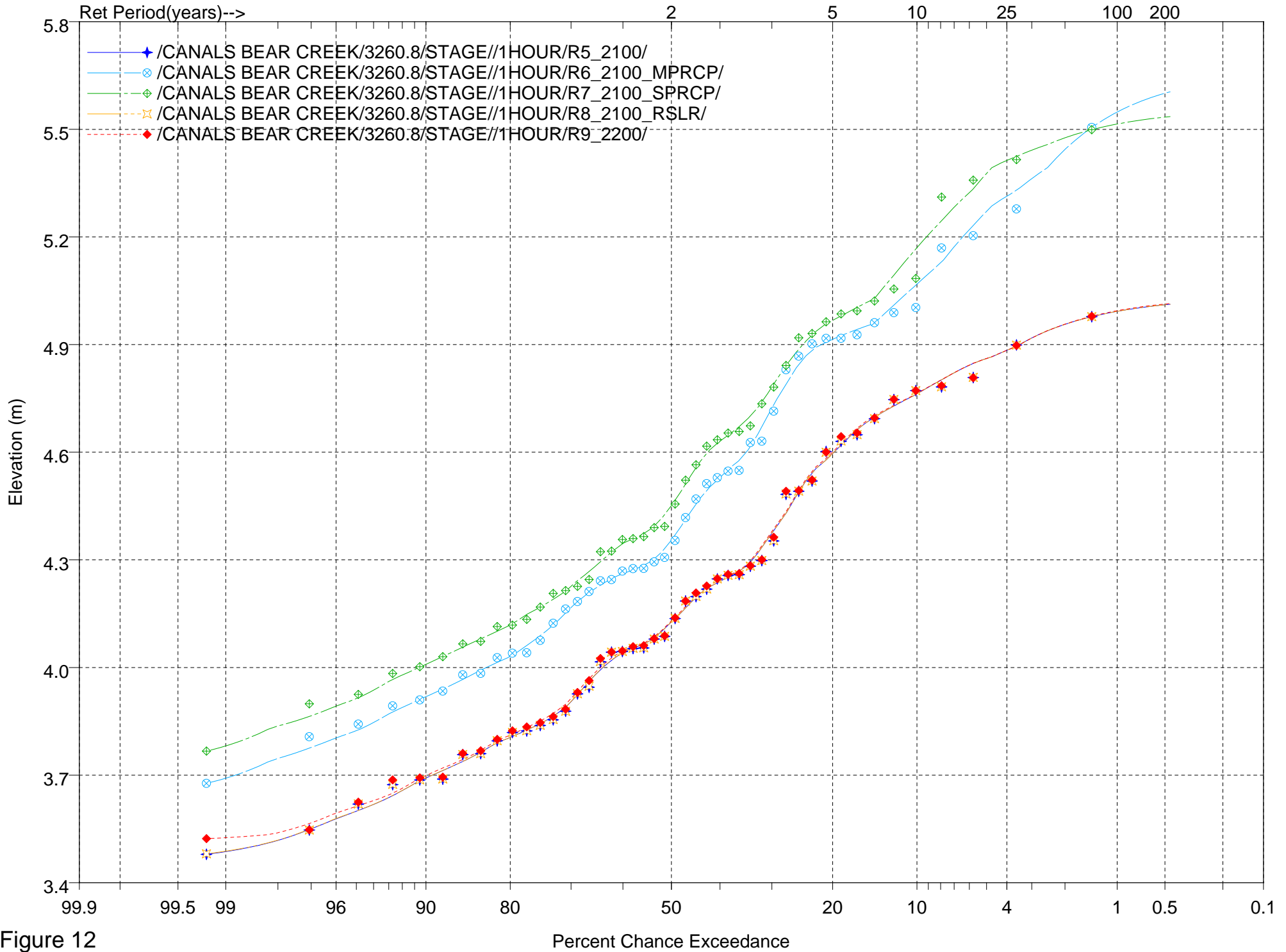


Figure 12

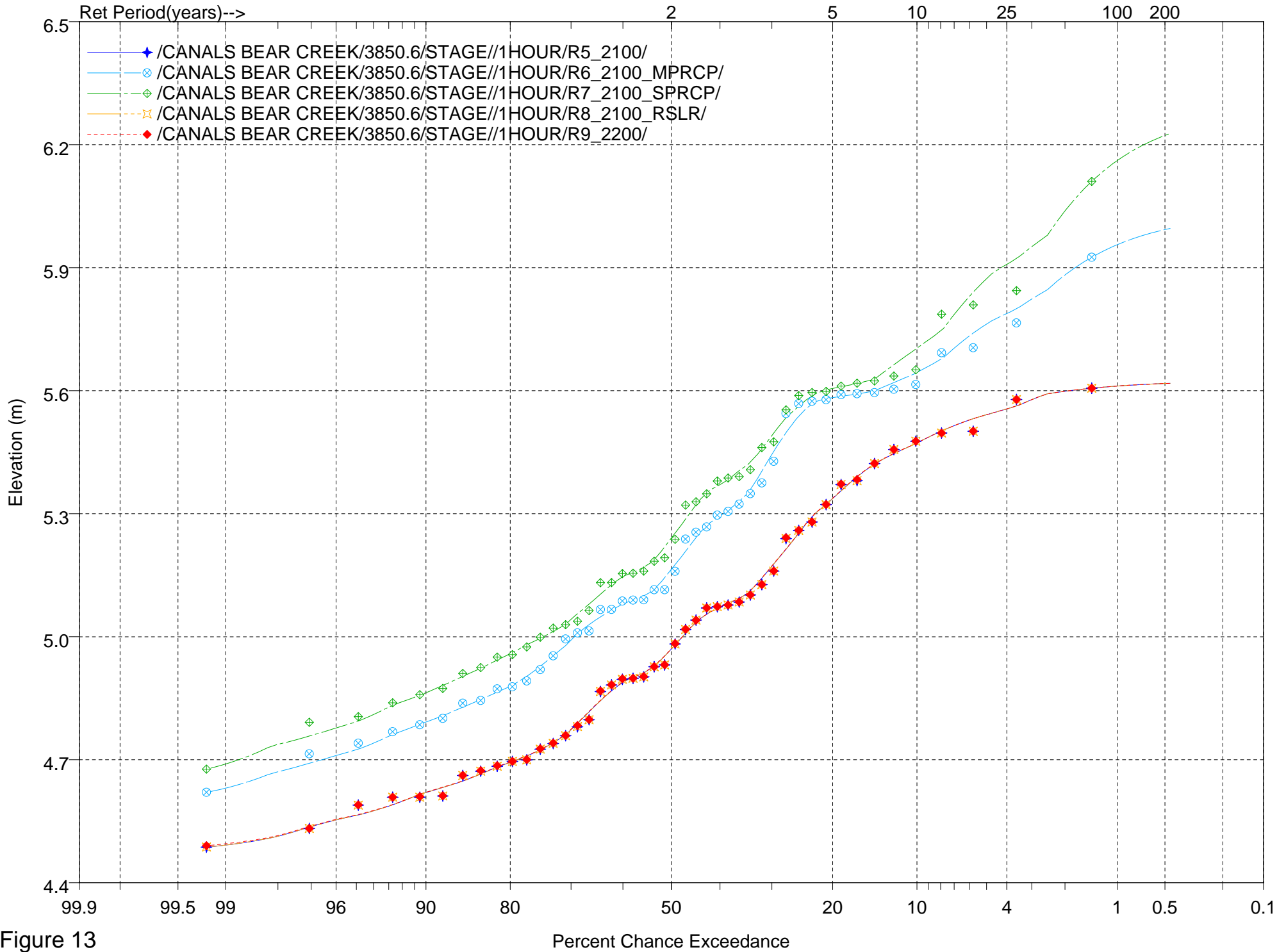


Figure 13

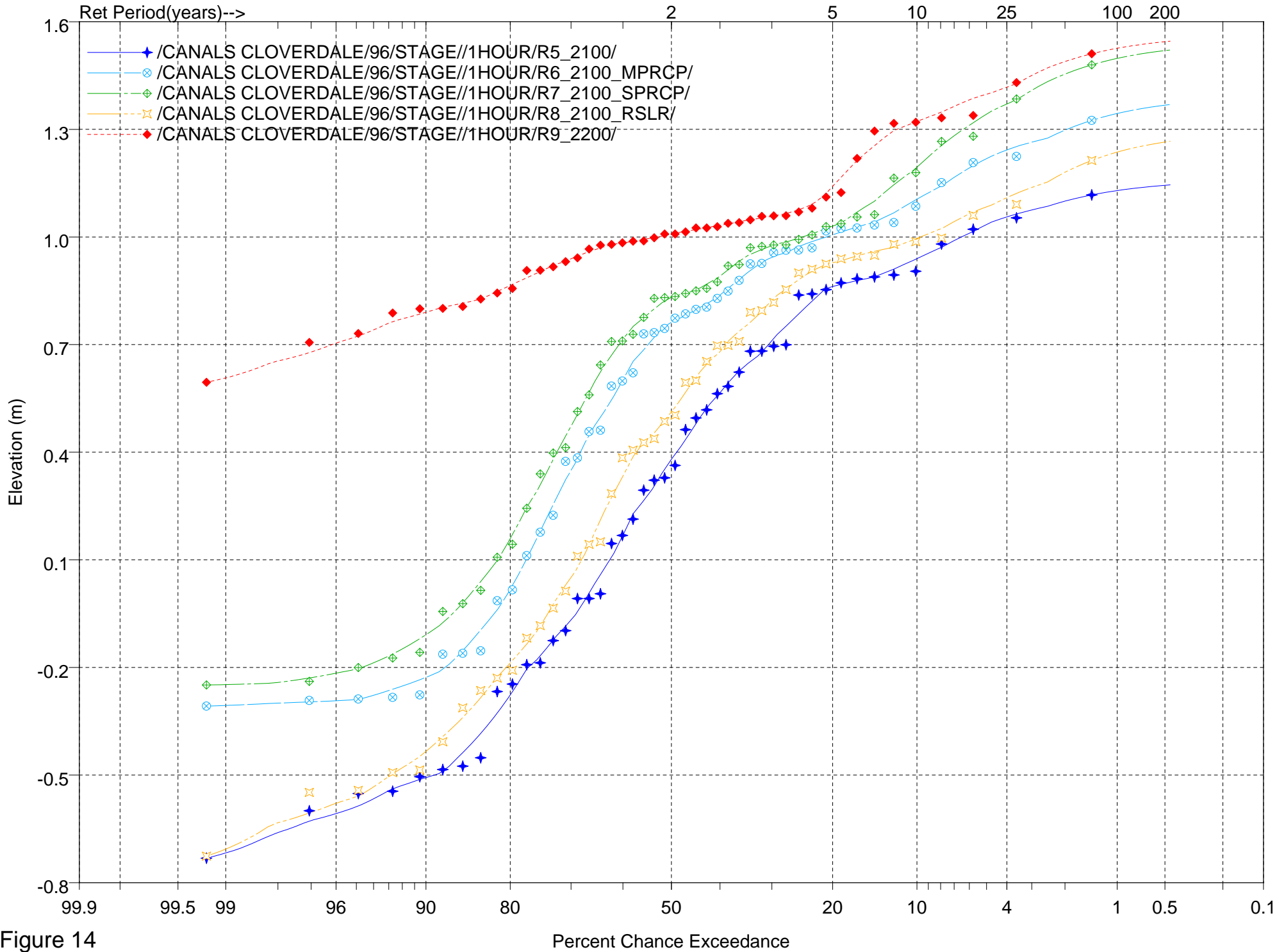


Figure 14

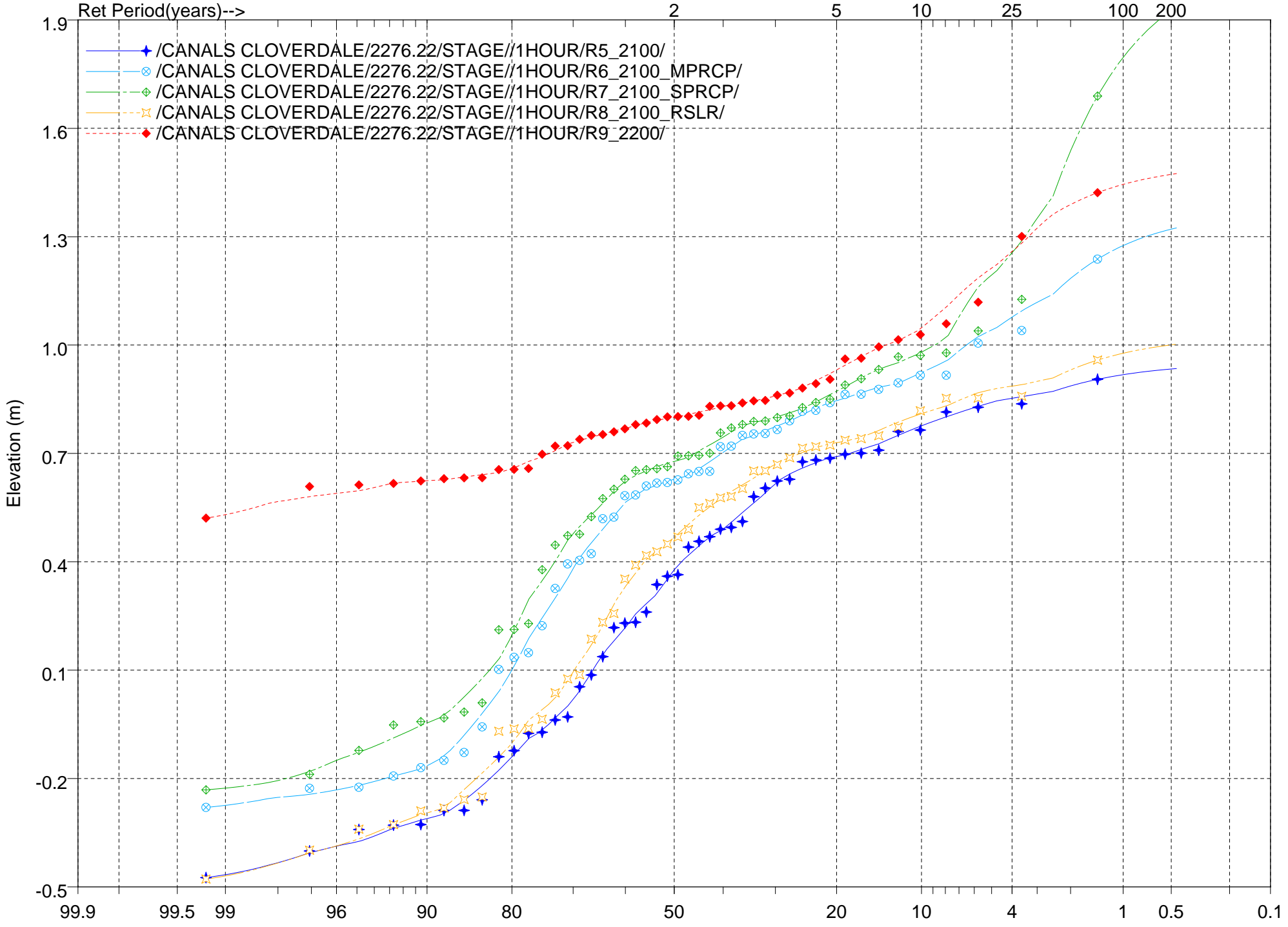


Figure 15

Percent Chance Exceedance

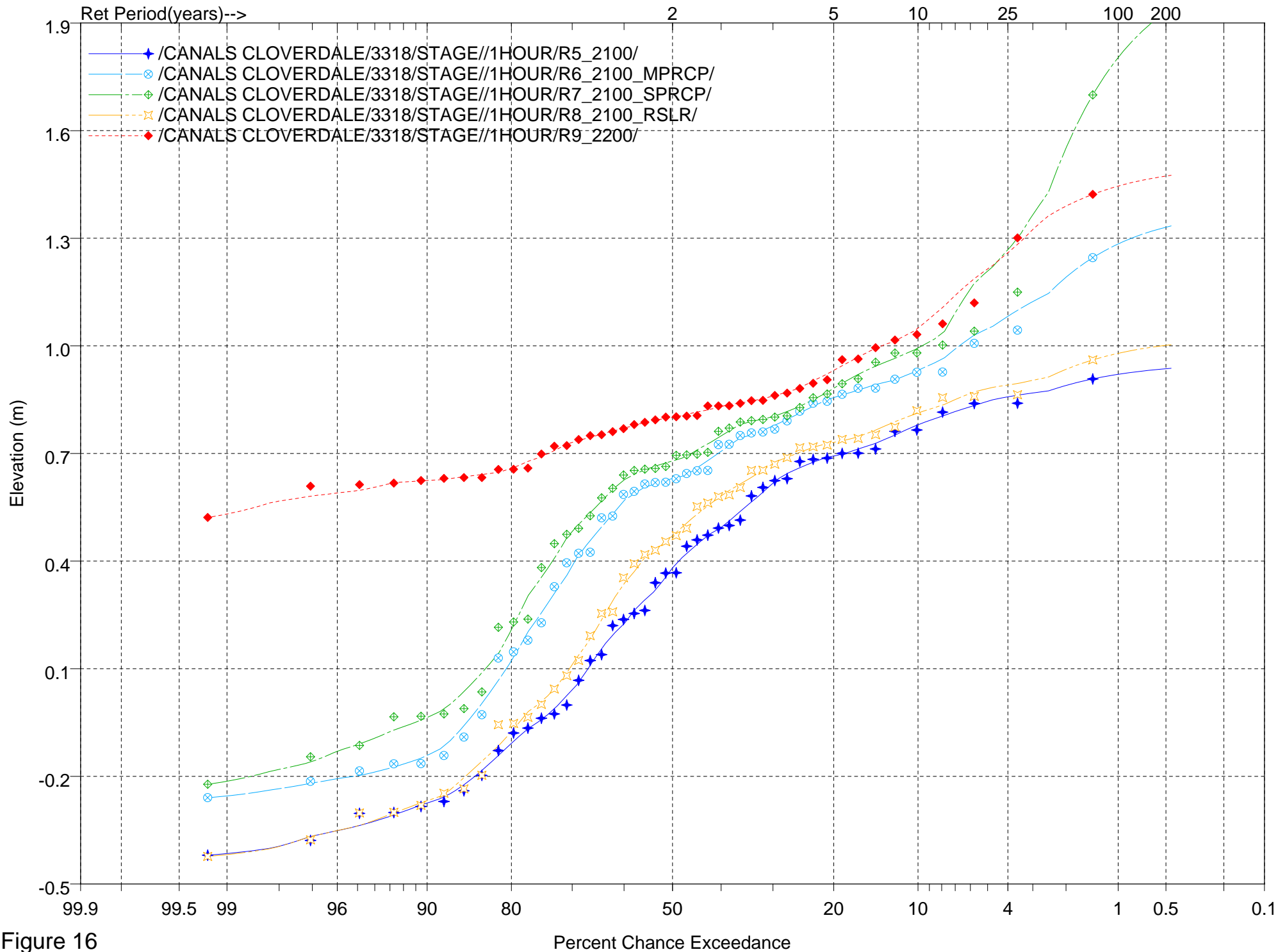


Figure 16



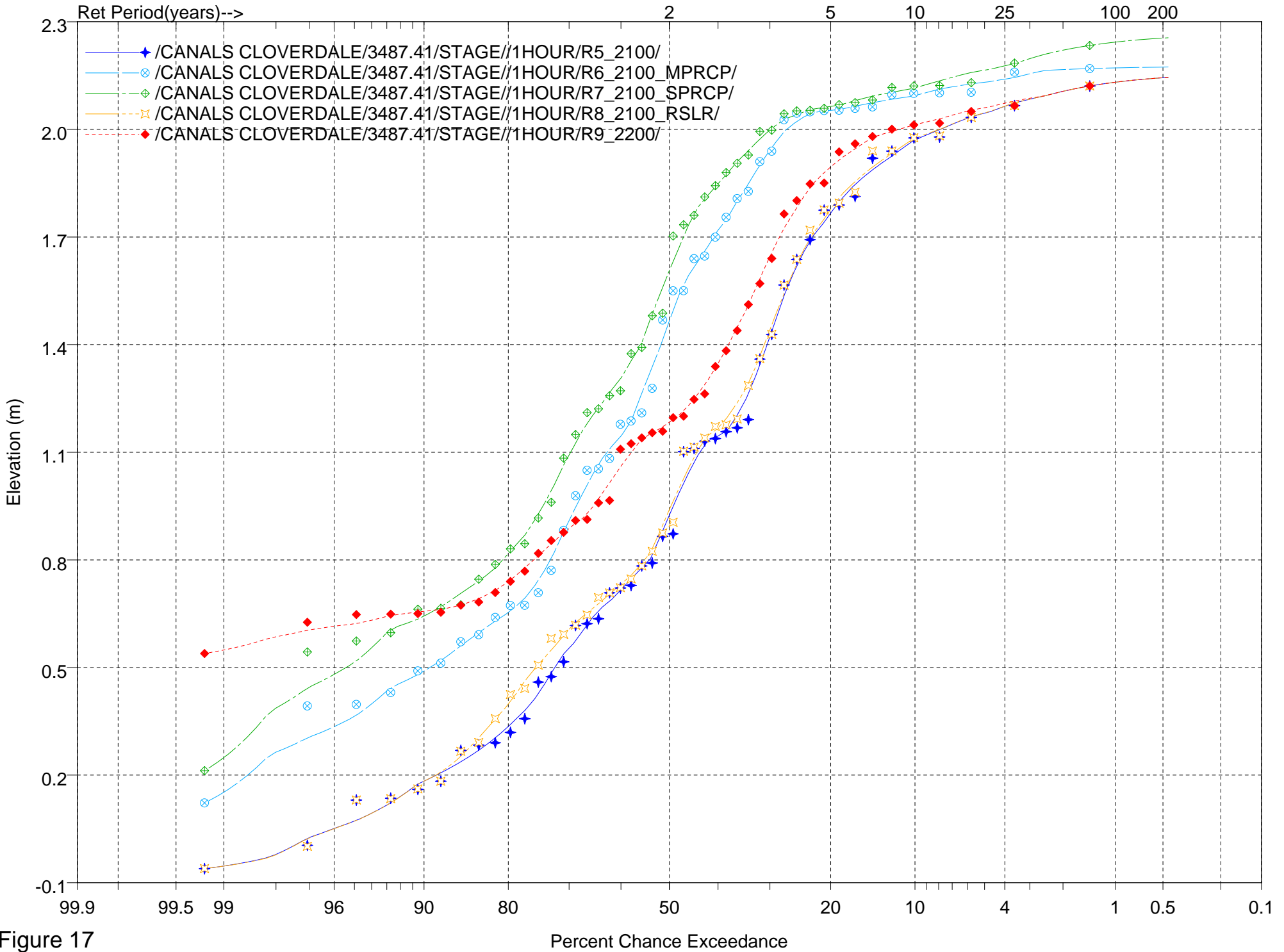


Figure 17

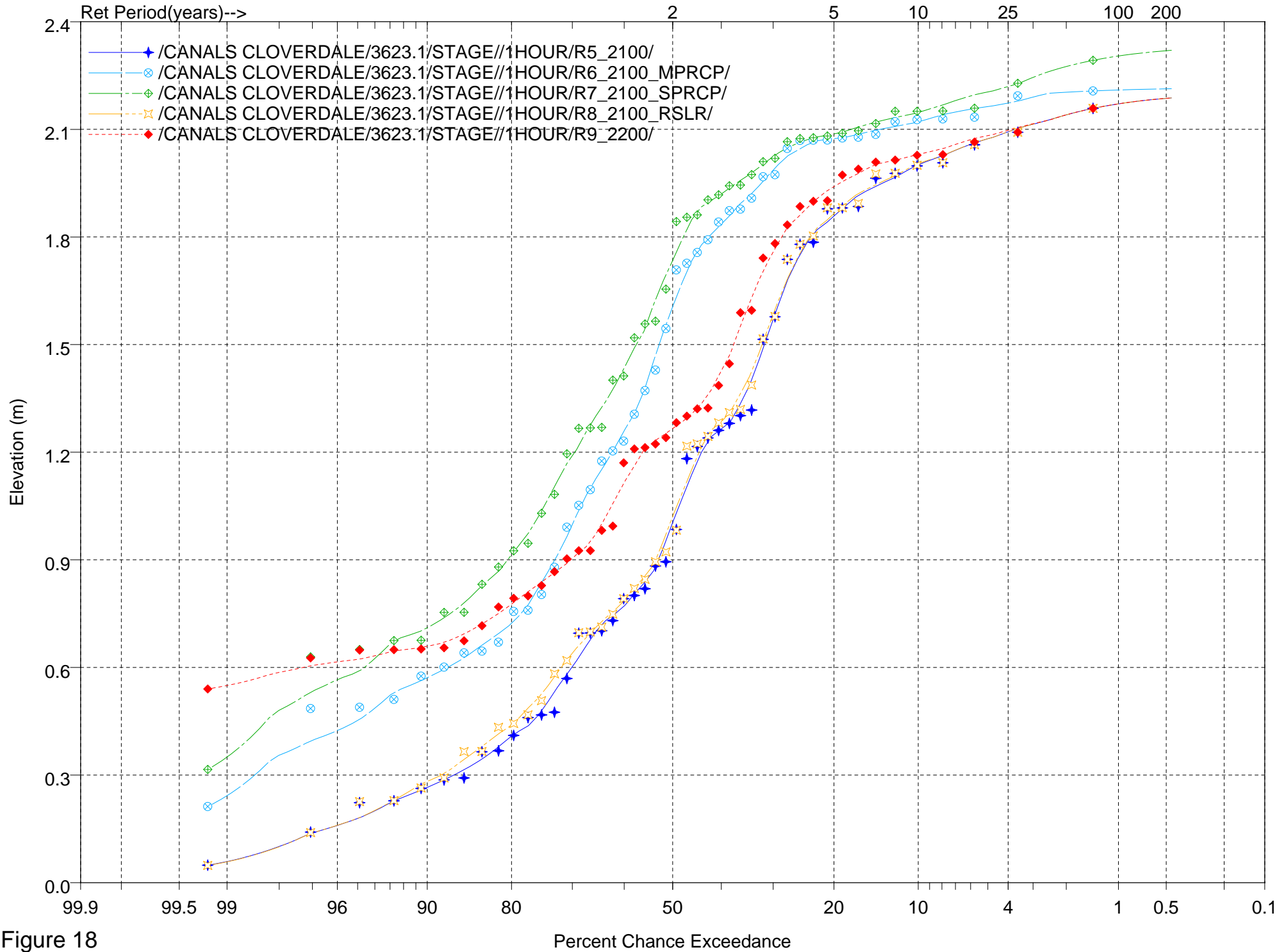


Figure 18

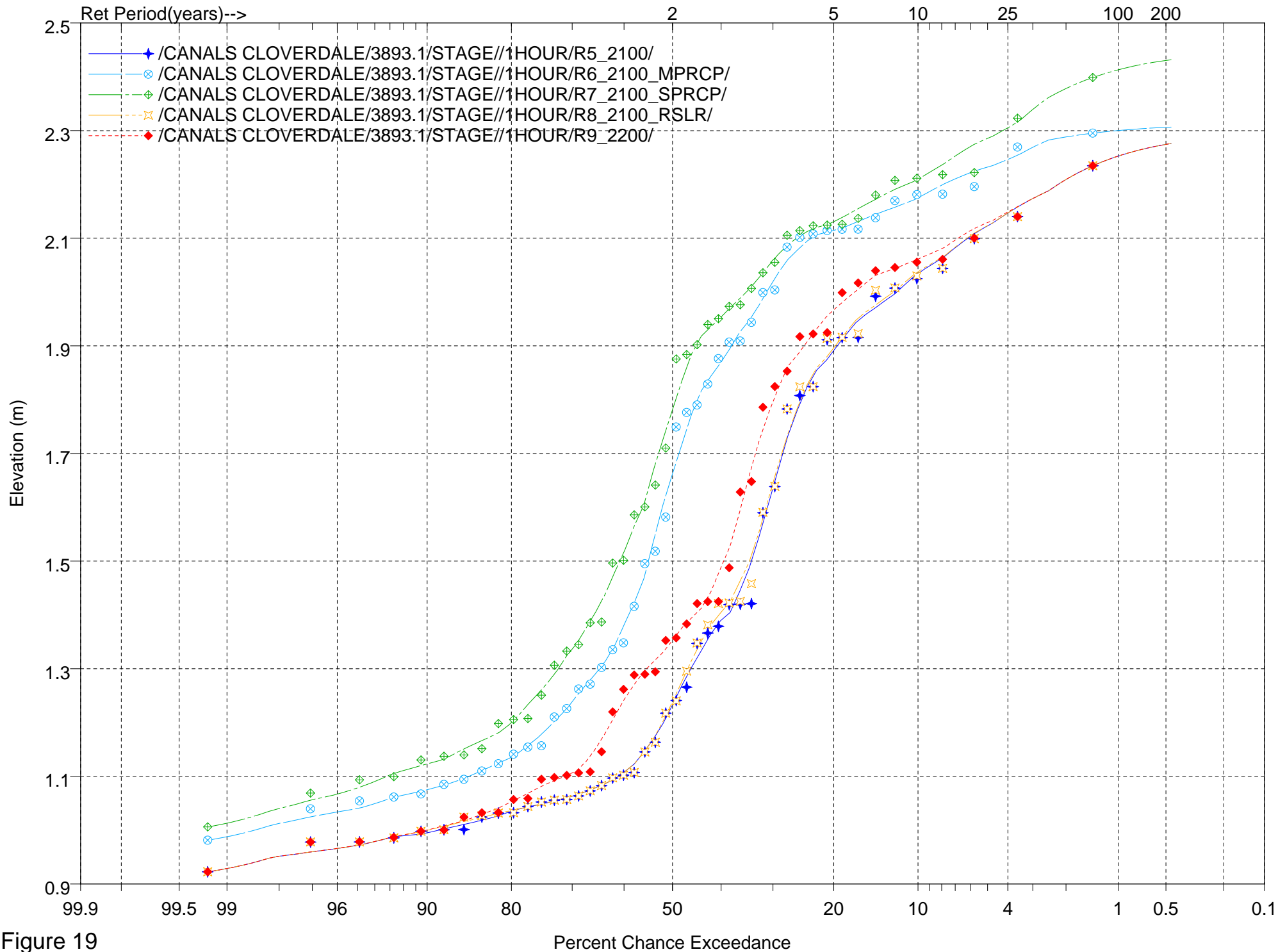


Figure 19

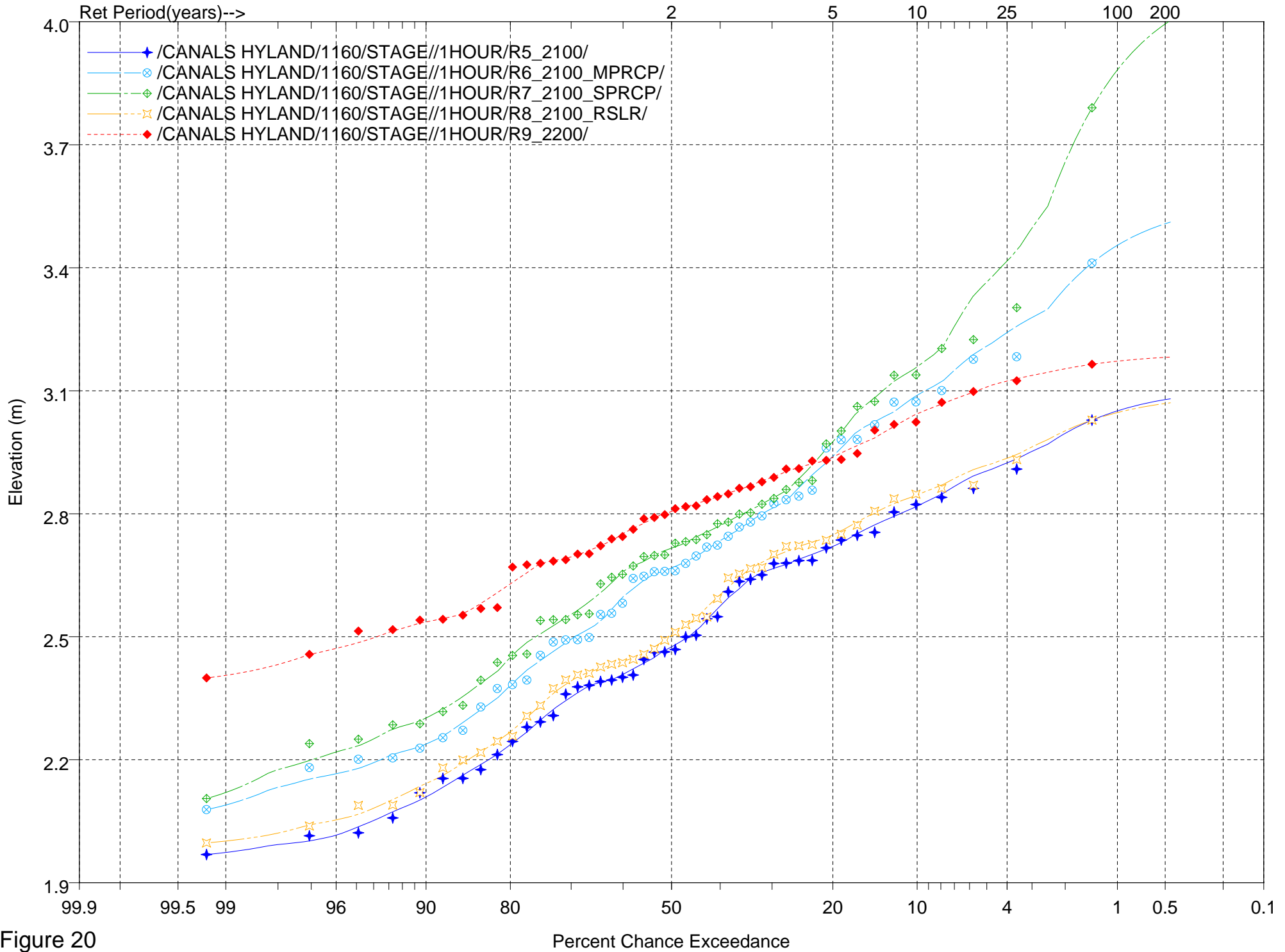


Figure 20

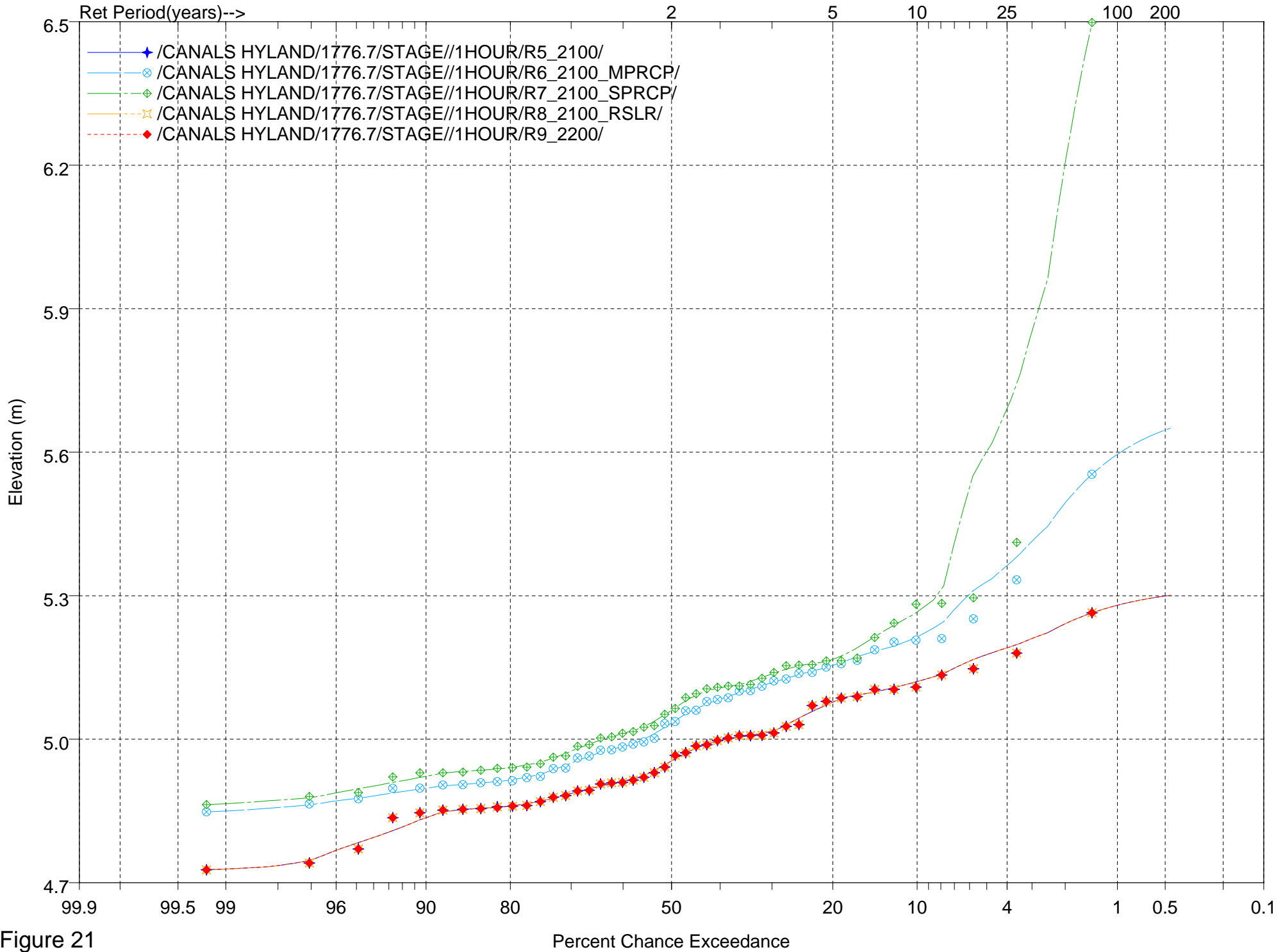


Figure 21

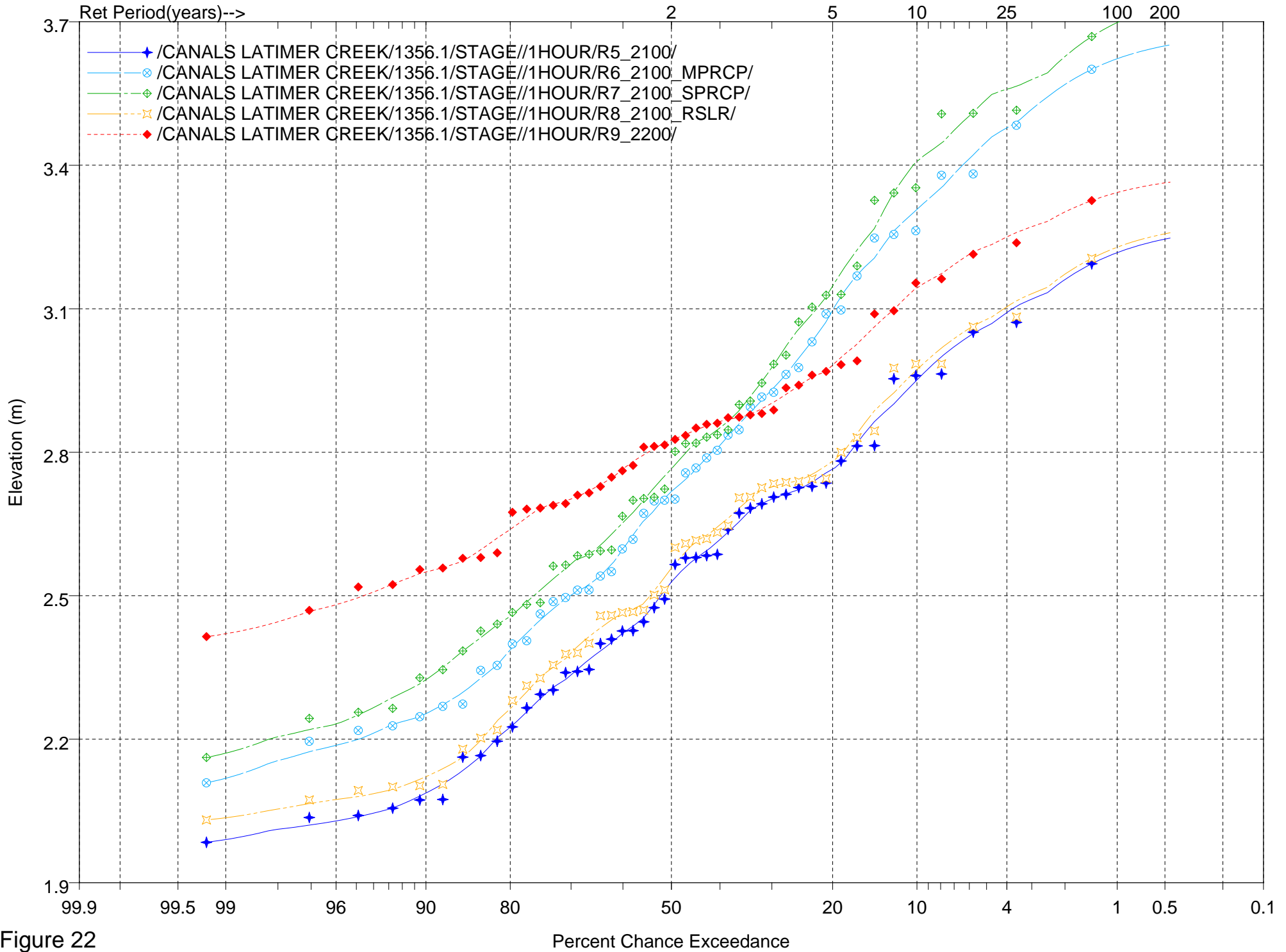


Figure 22

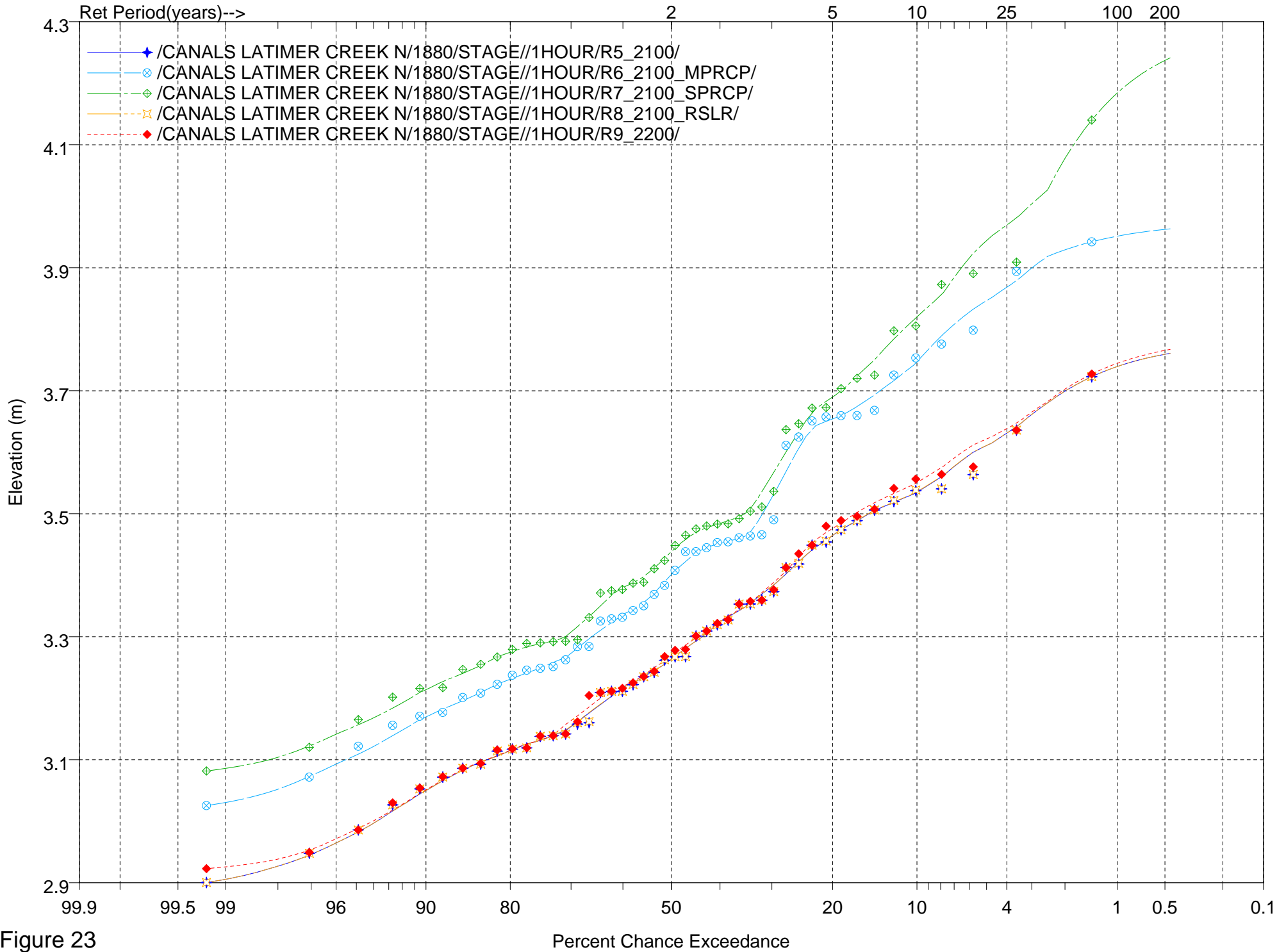


Figure 23

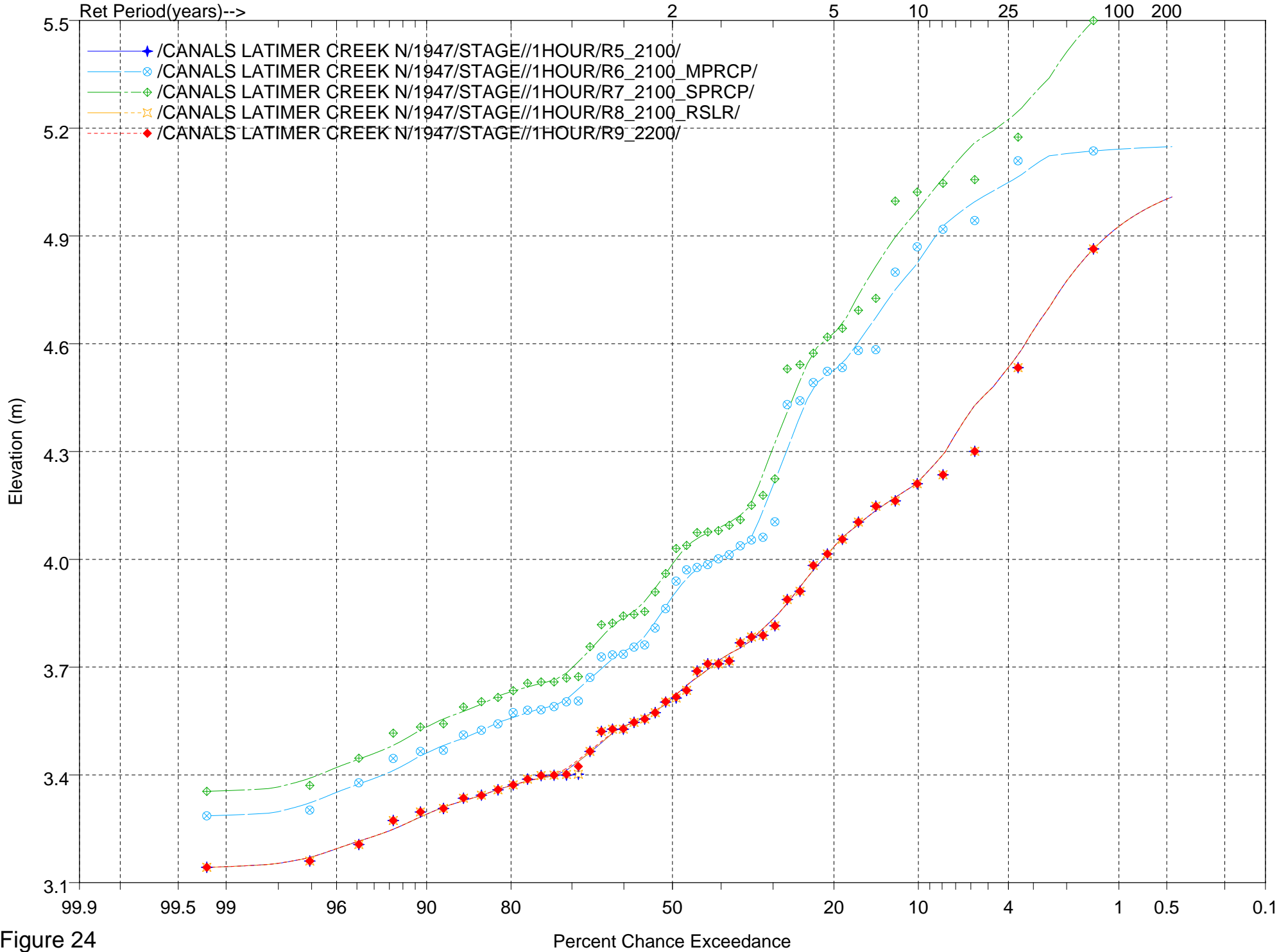


Figure 24



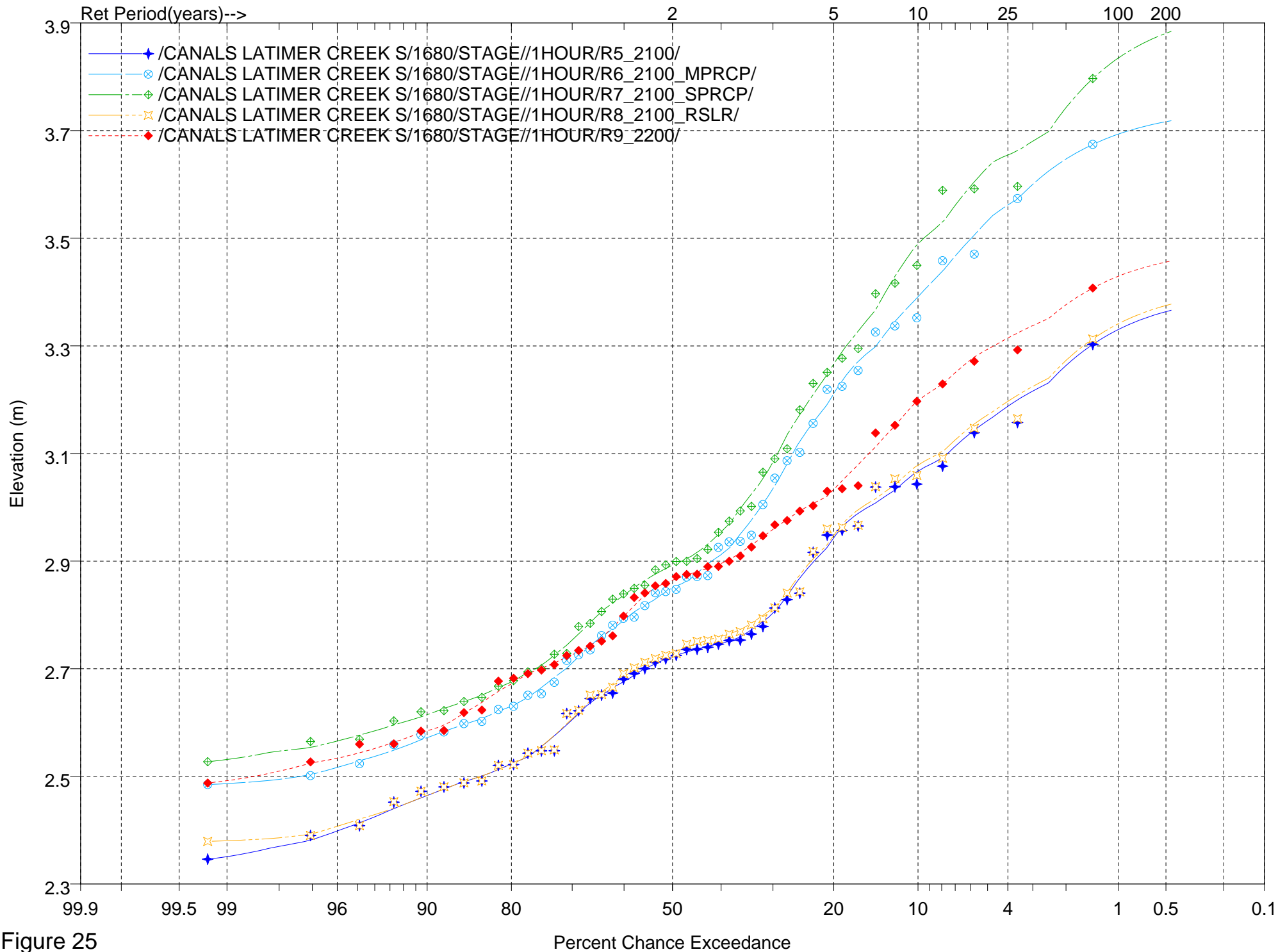


Figure 25

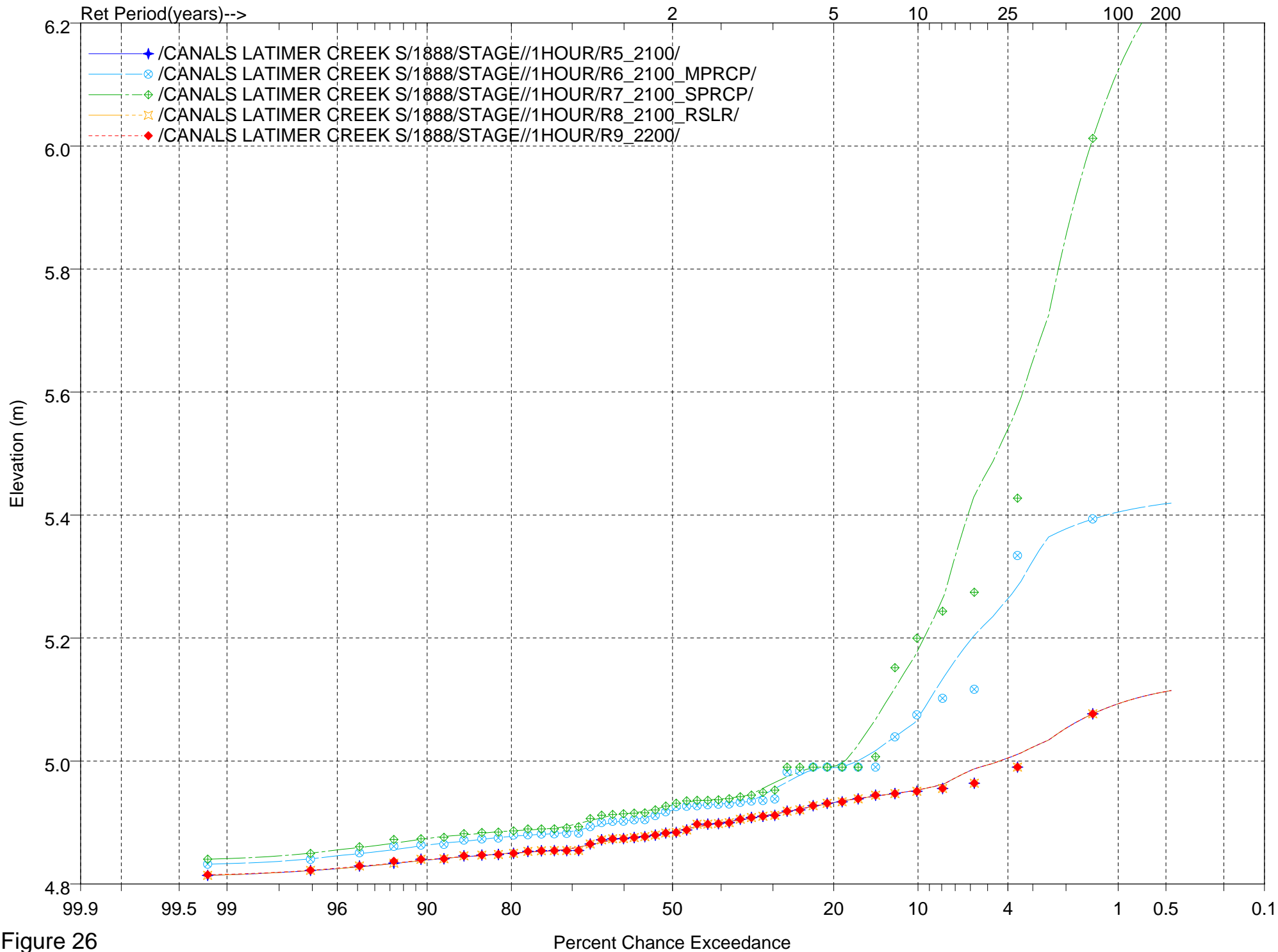


Figure 26

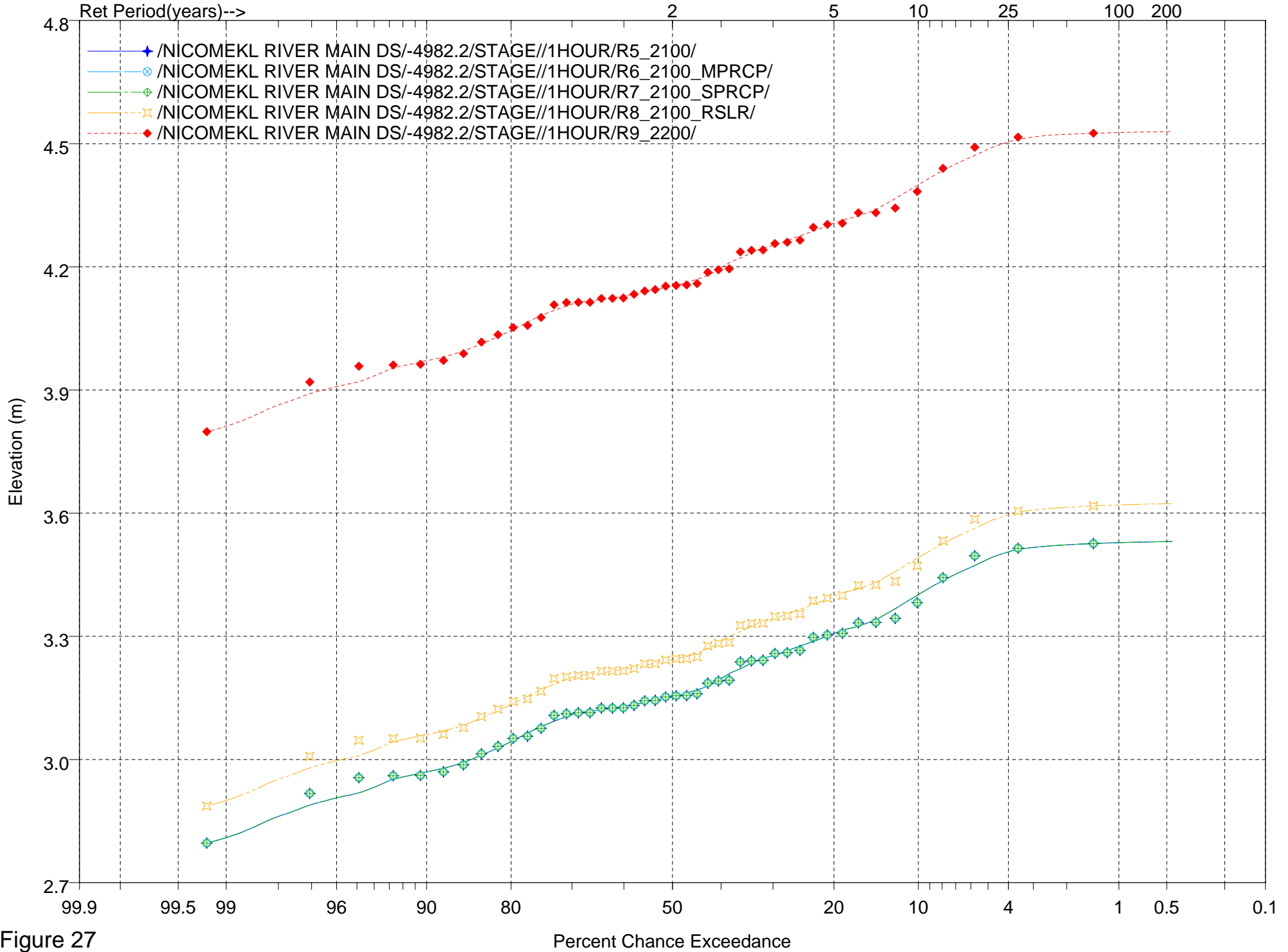


Figure 27

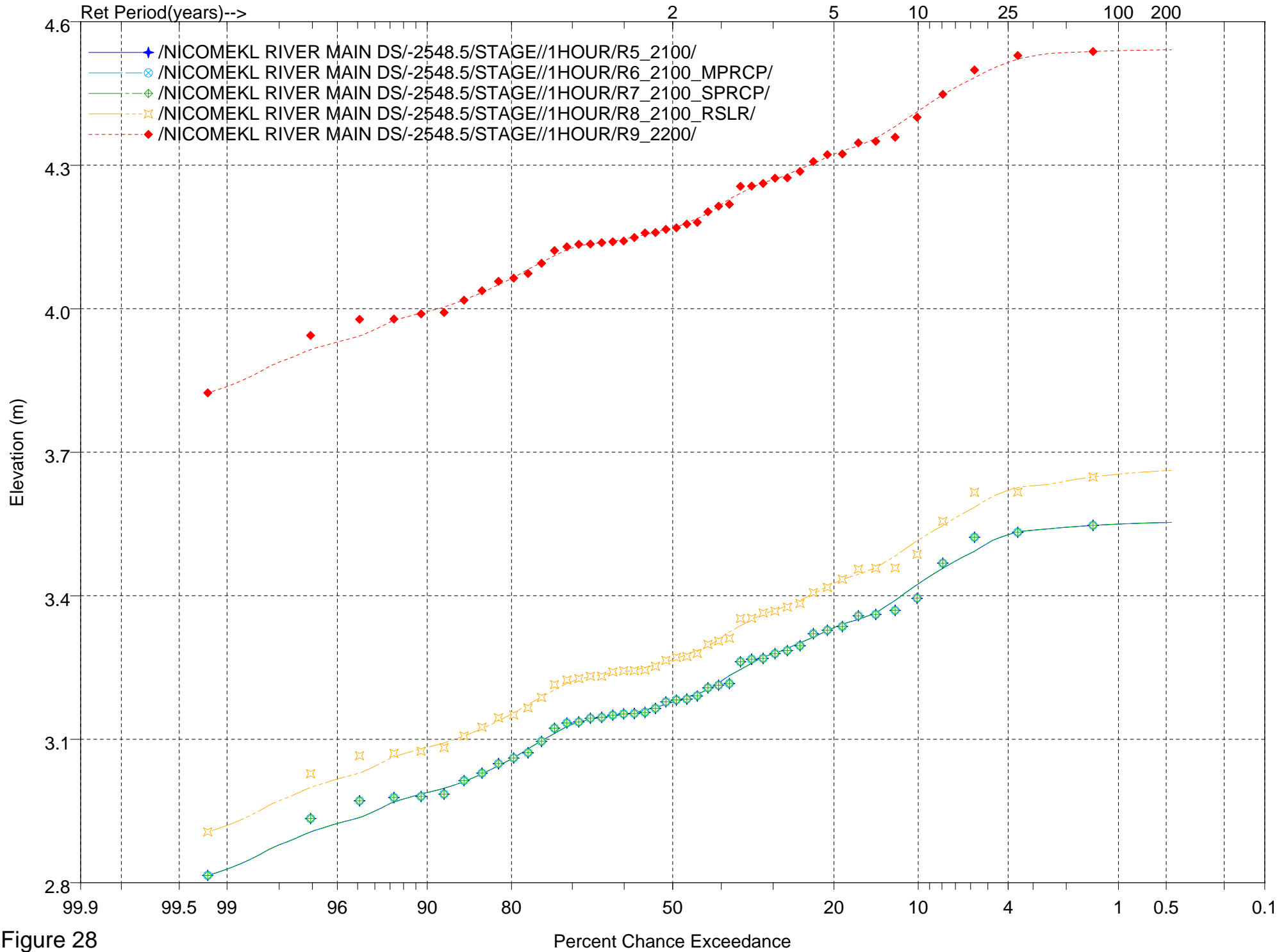


Figure 28

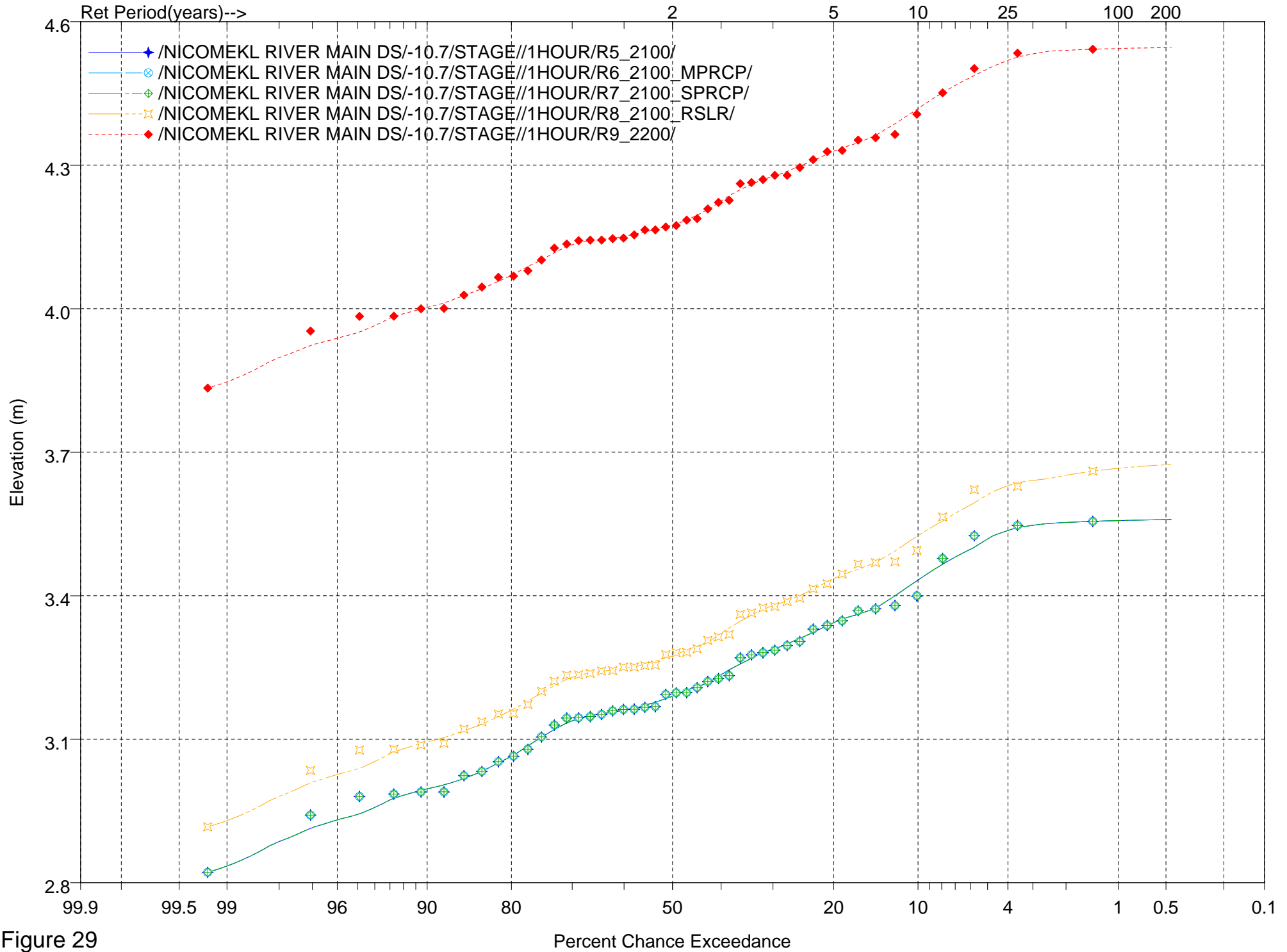


Figure 29

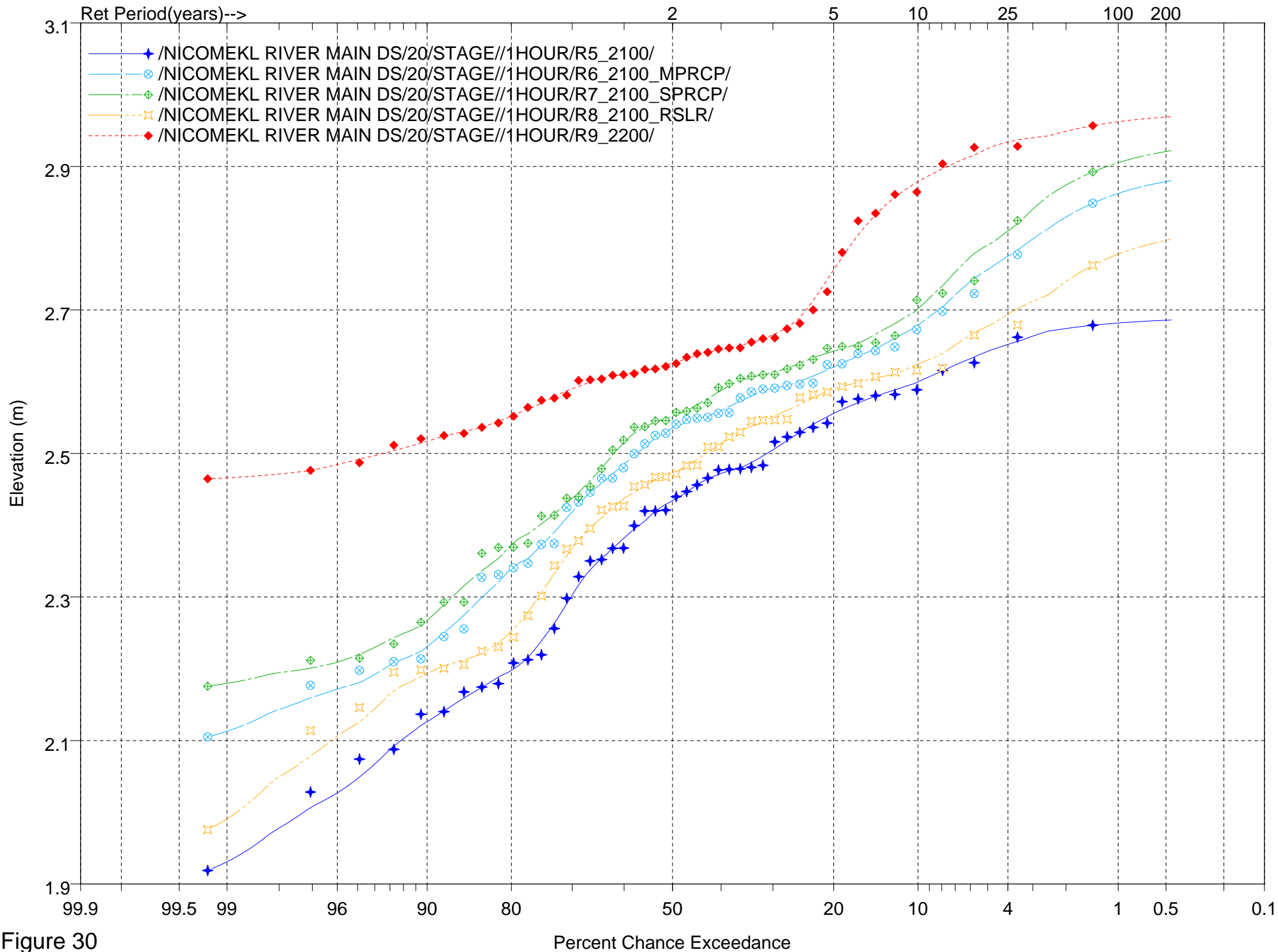


Figure 30

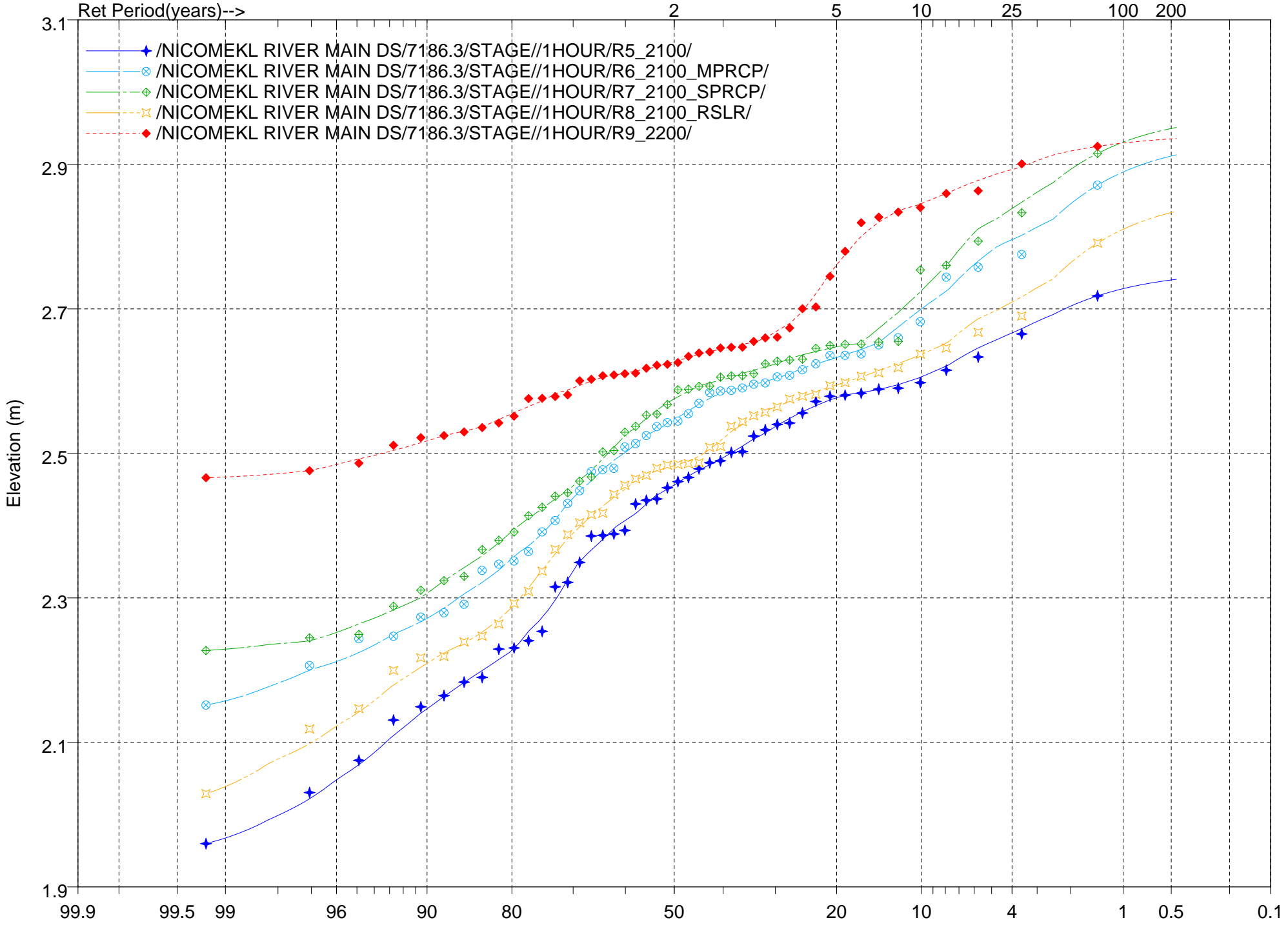


Figure 31

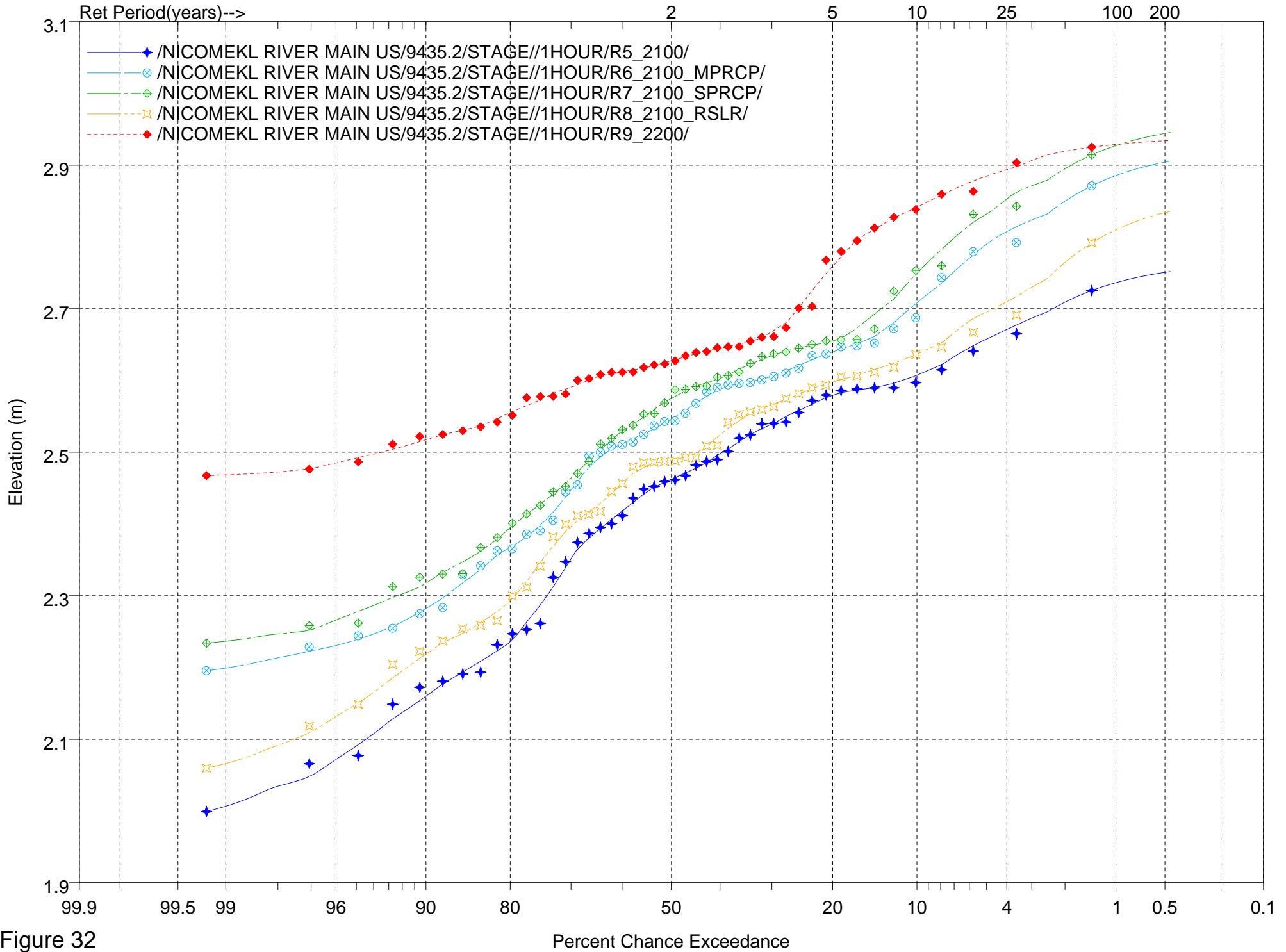


Figure 32



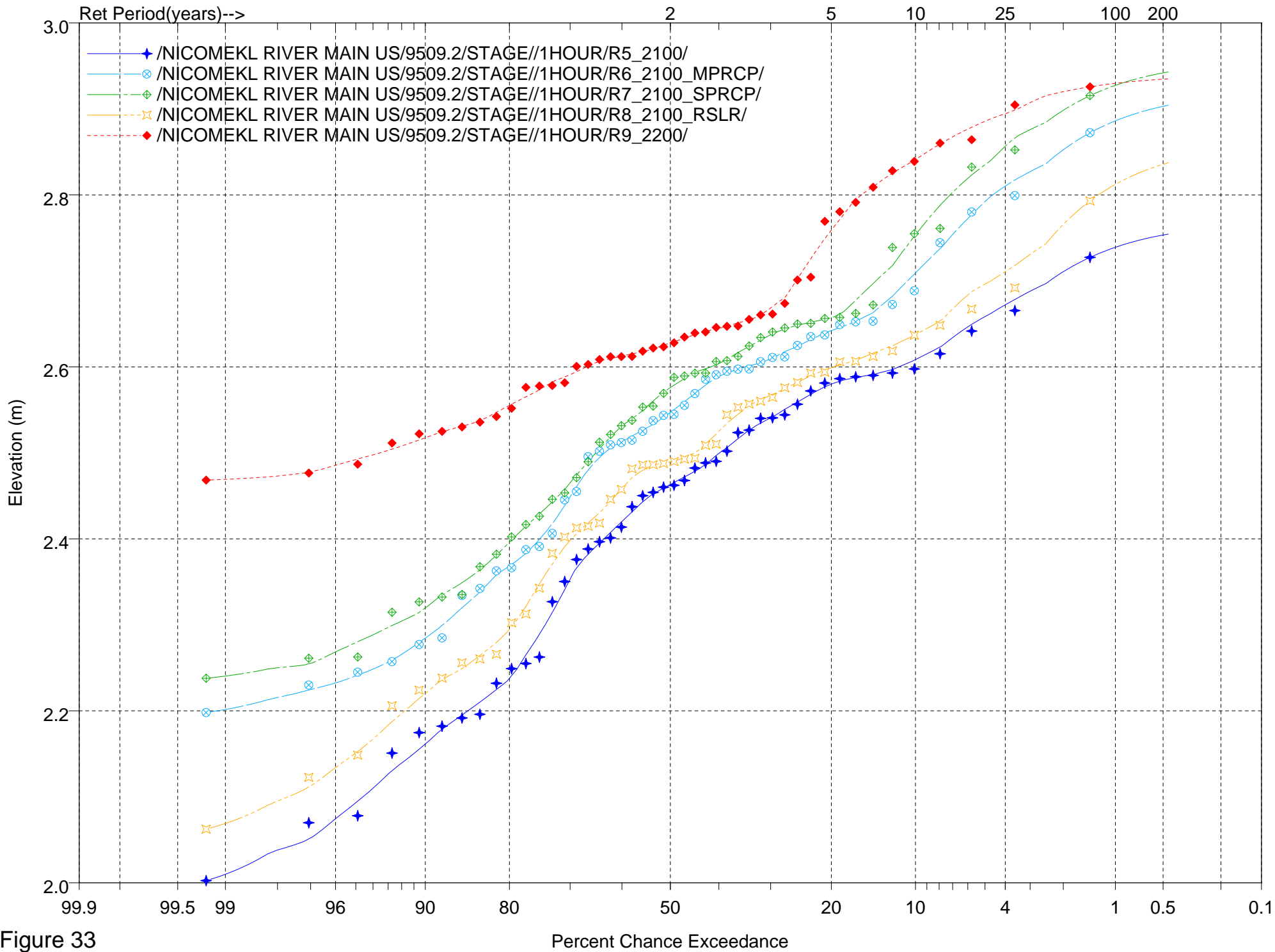


Figure 33

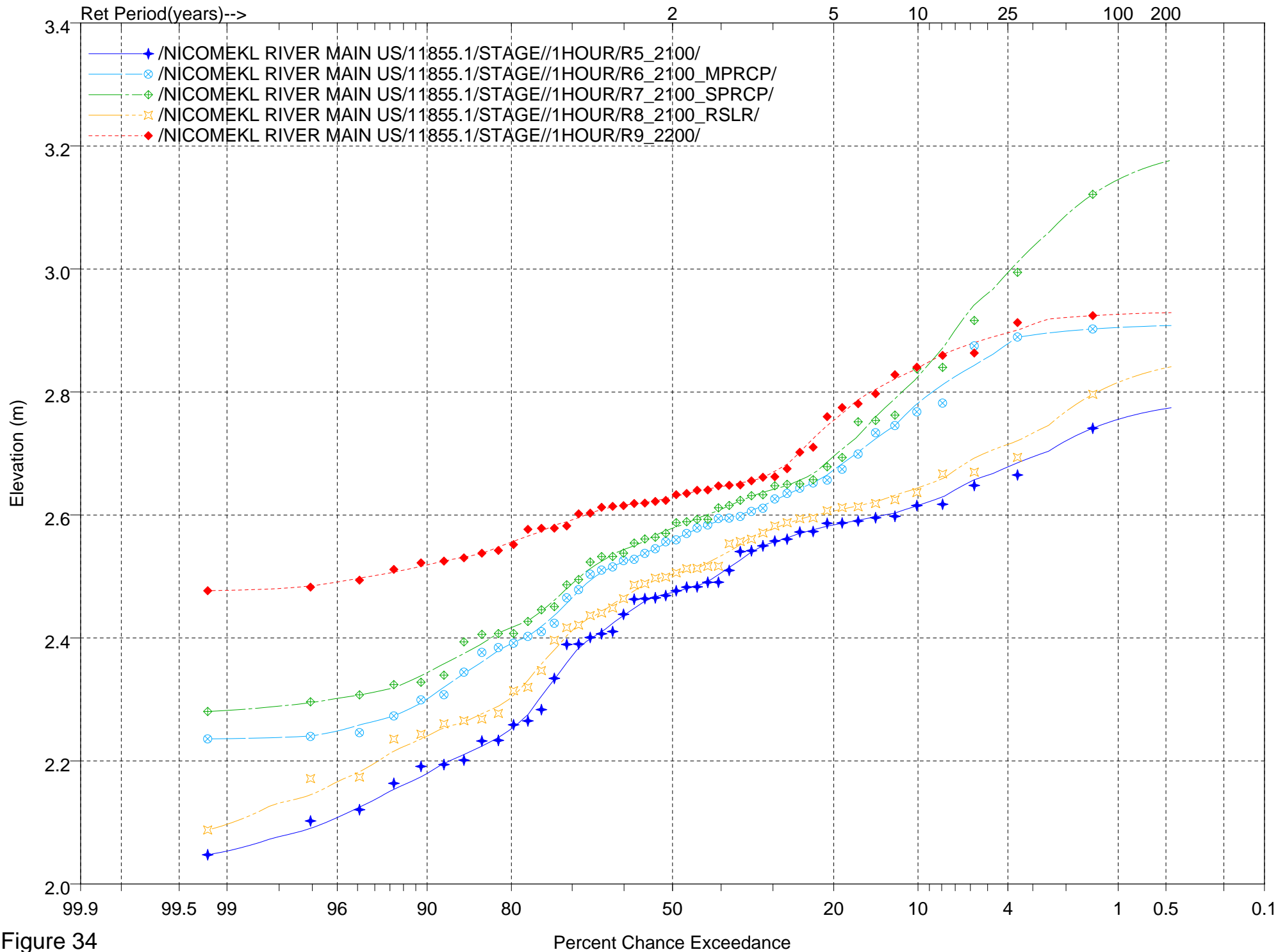


Figure 34

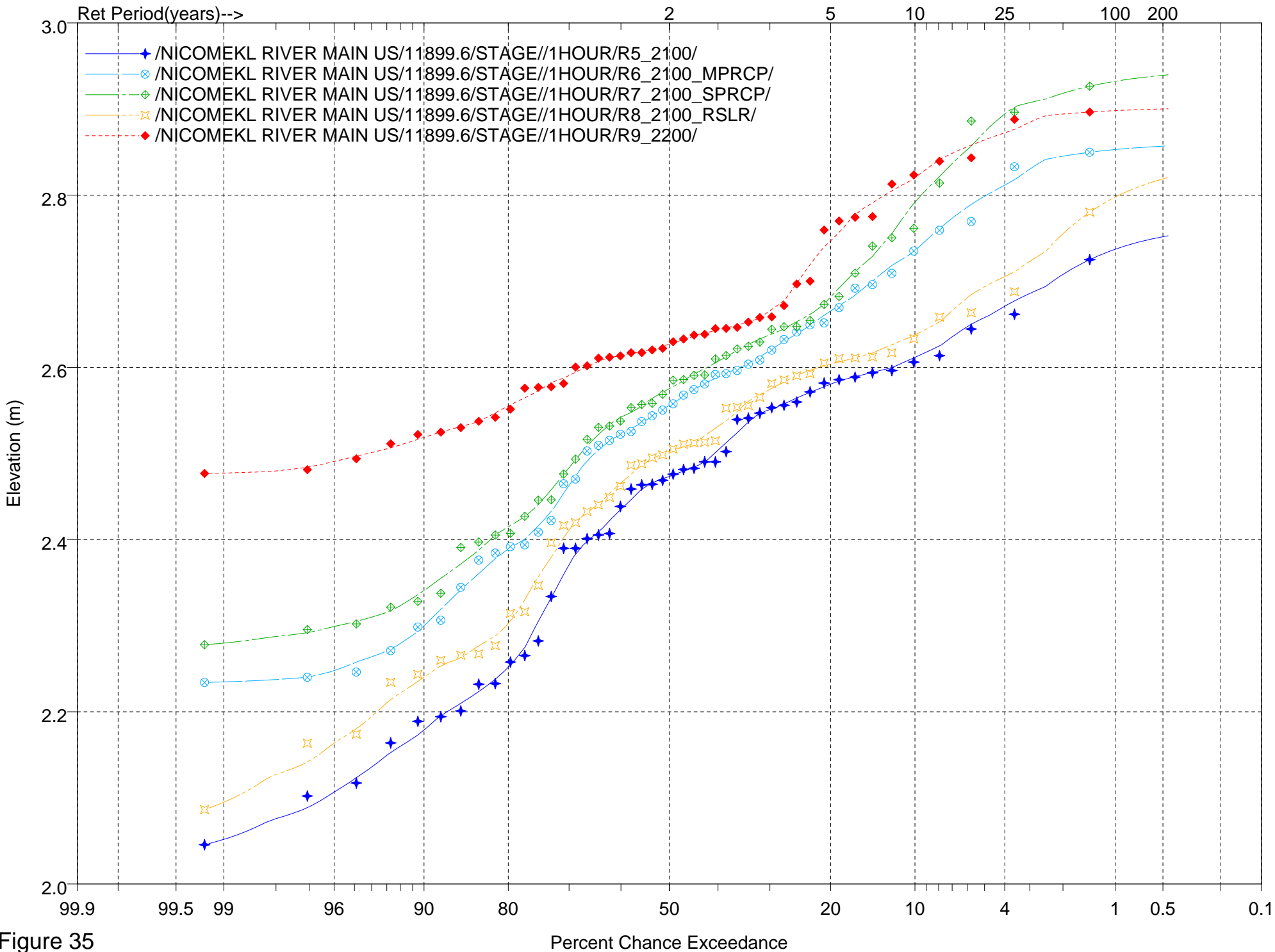


Figure 35

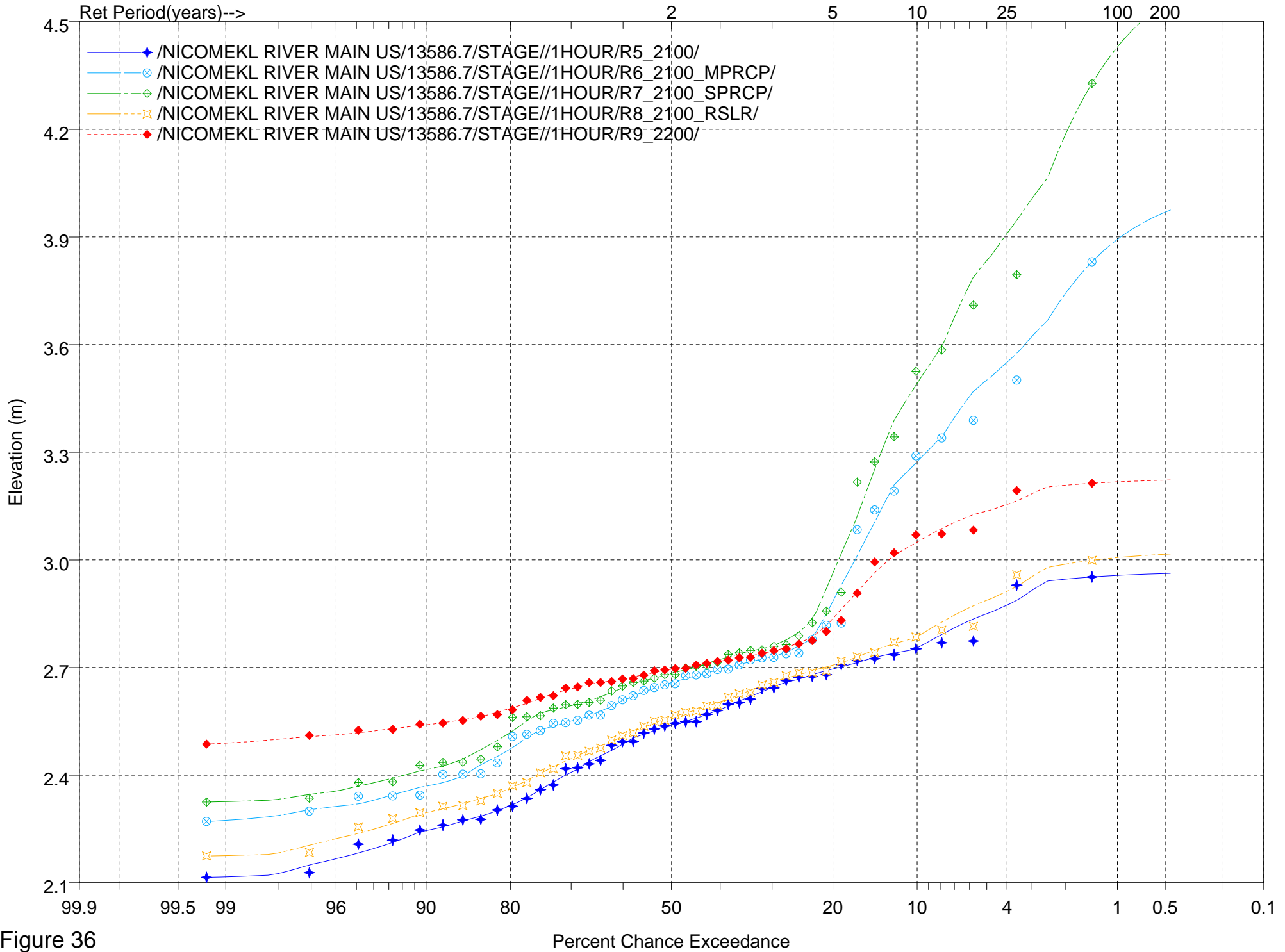


Figure 36

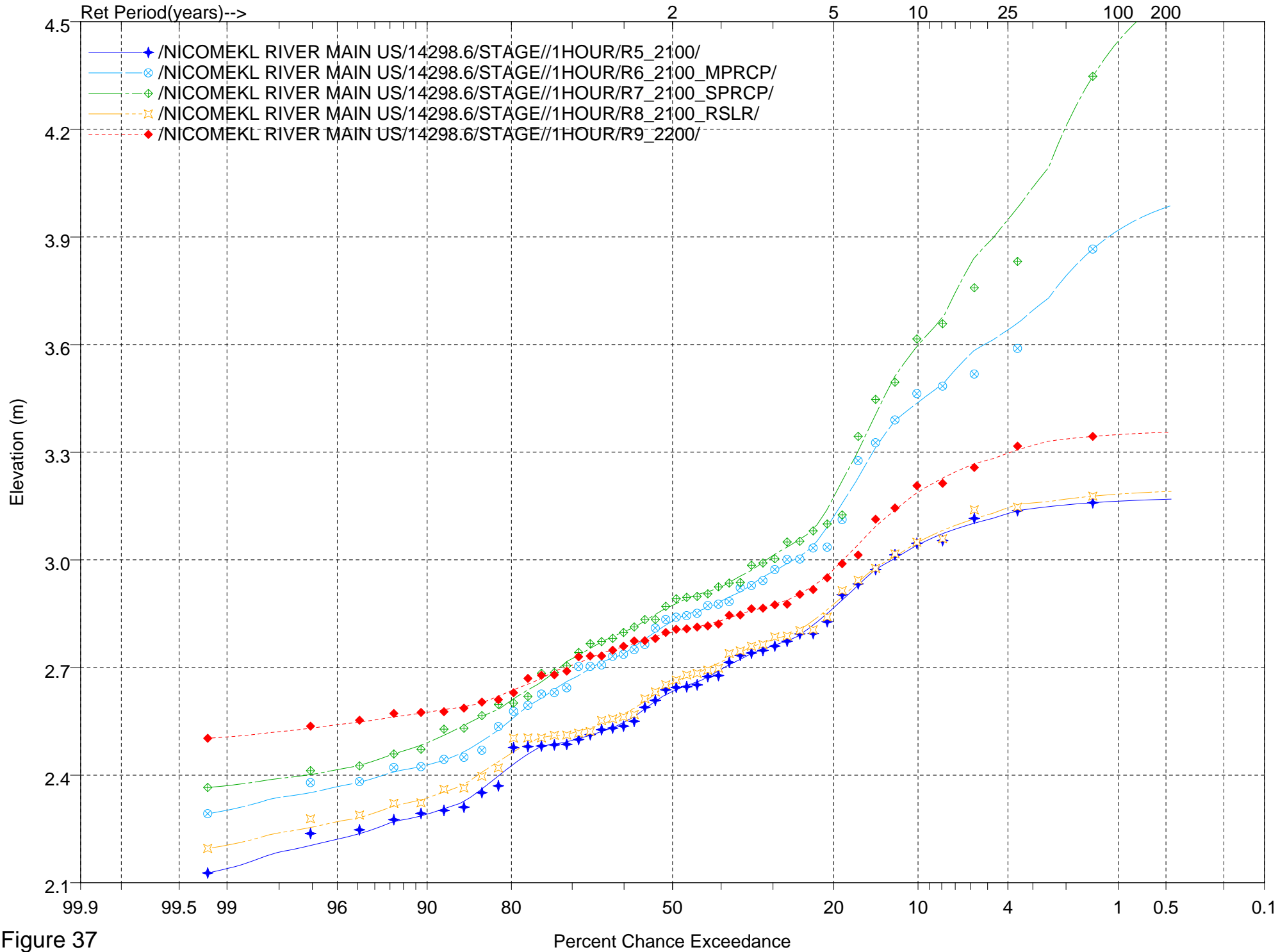


Figure 37

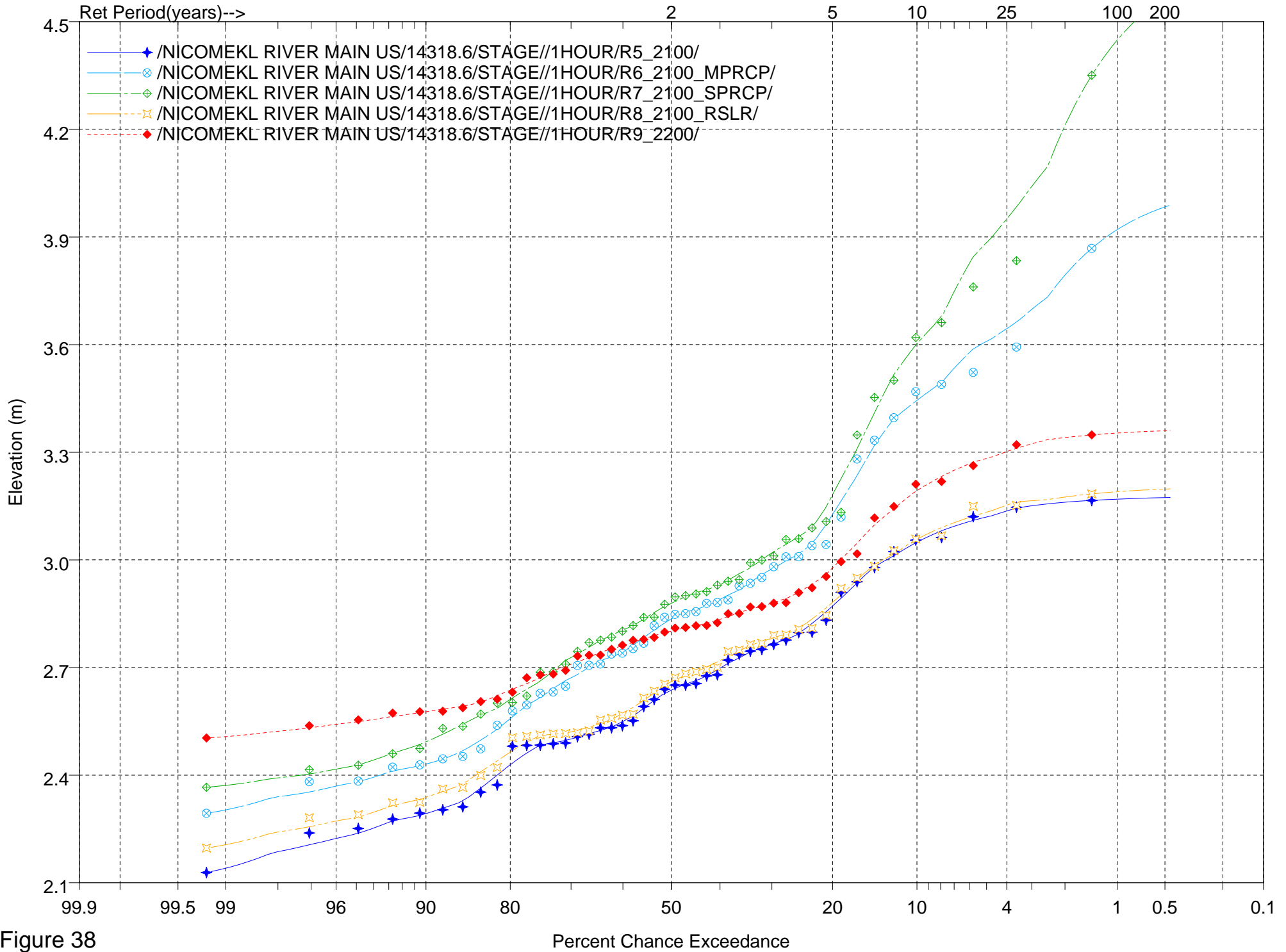


Figure 38

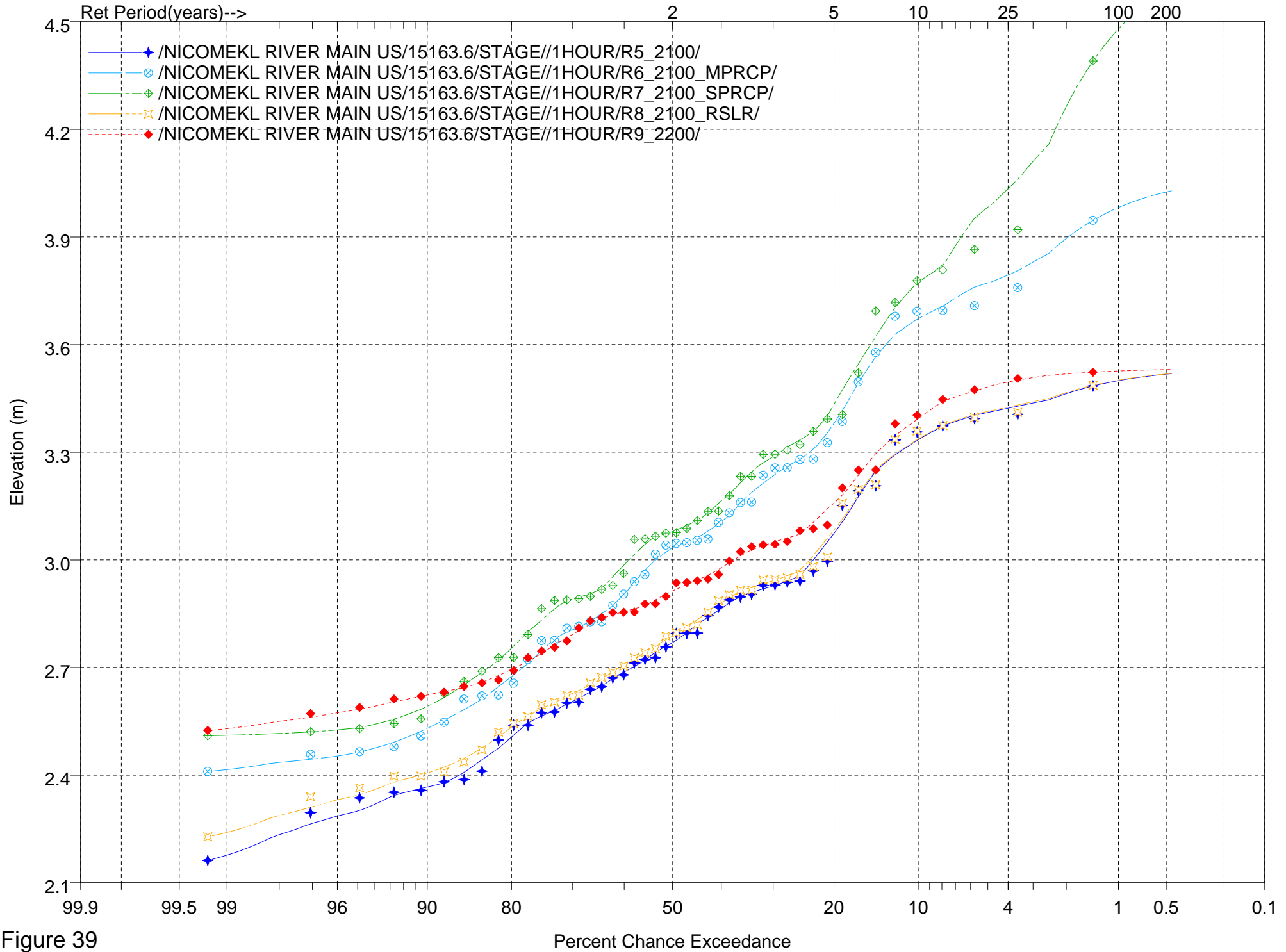


Figure 39

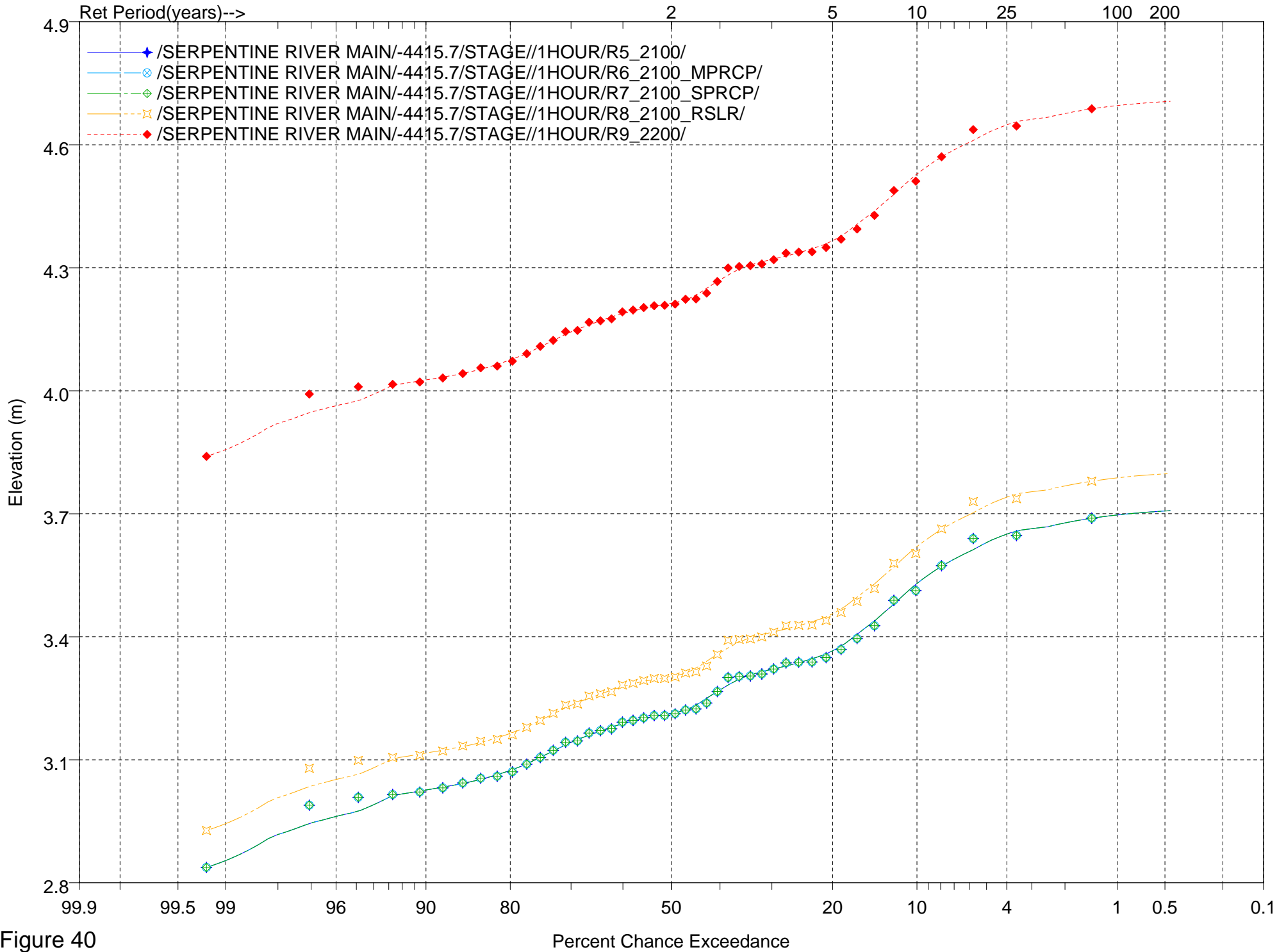


Figure 40



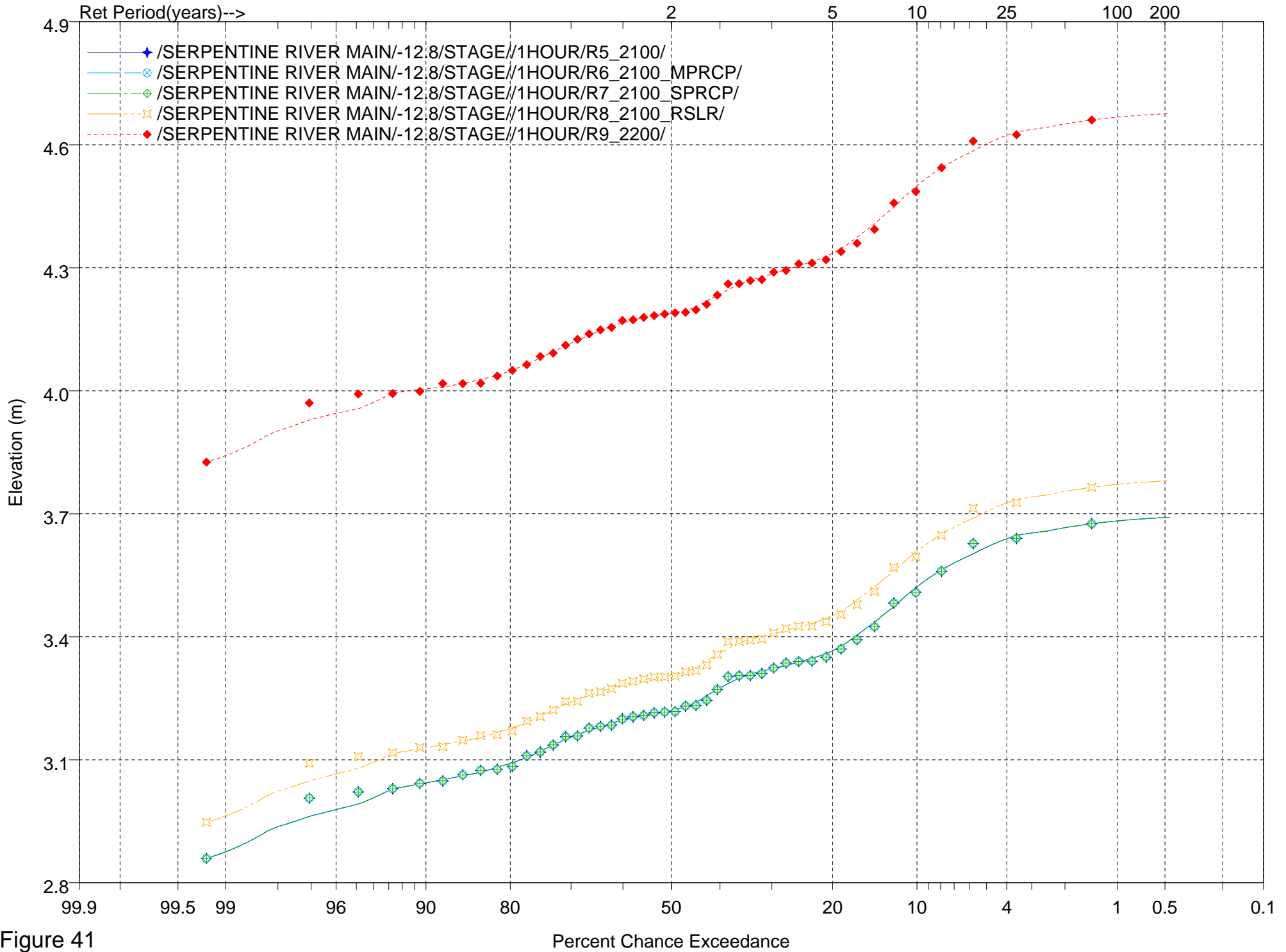


Figure 41

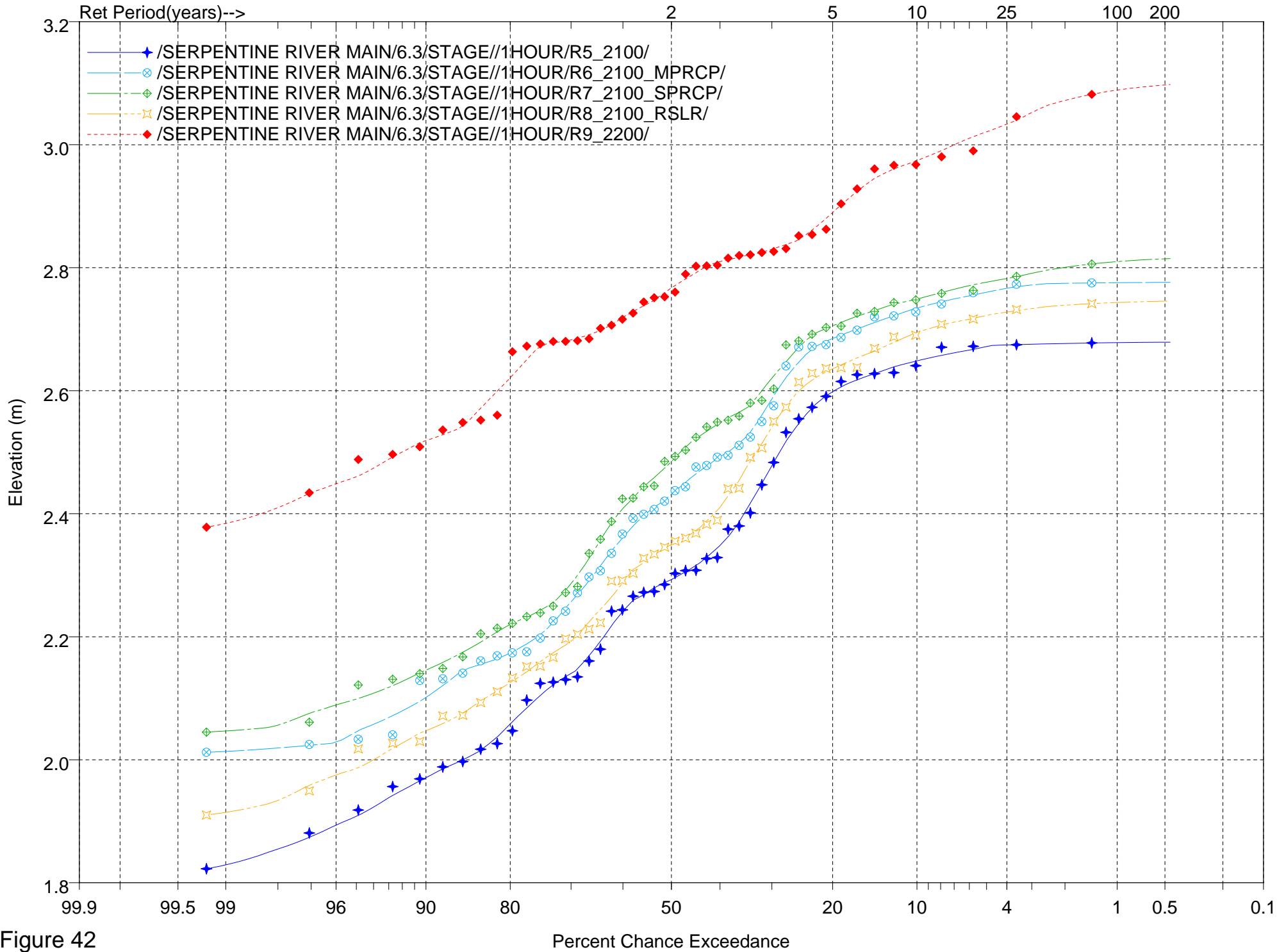


Figure 42

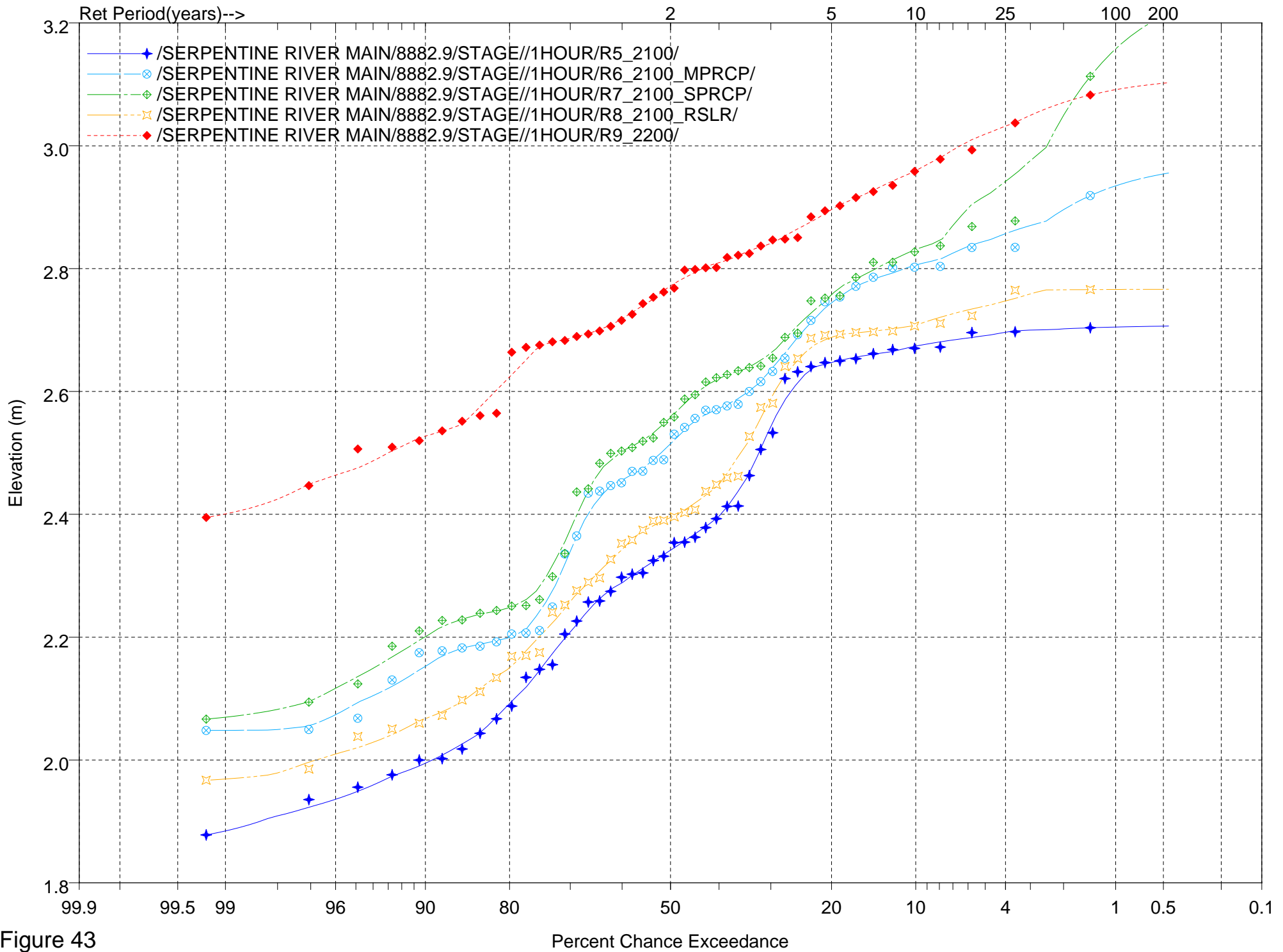


Figure 43

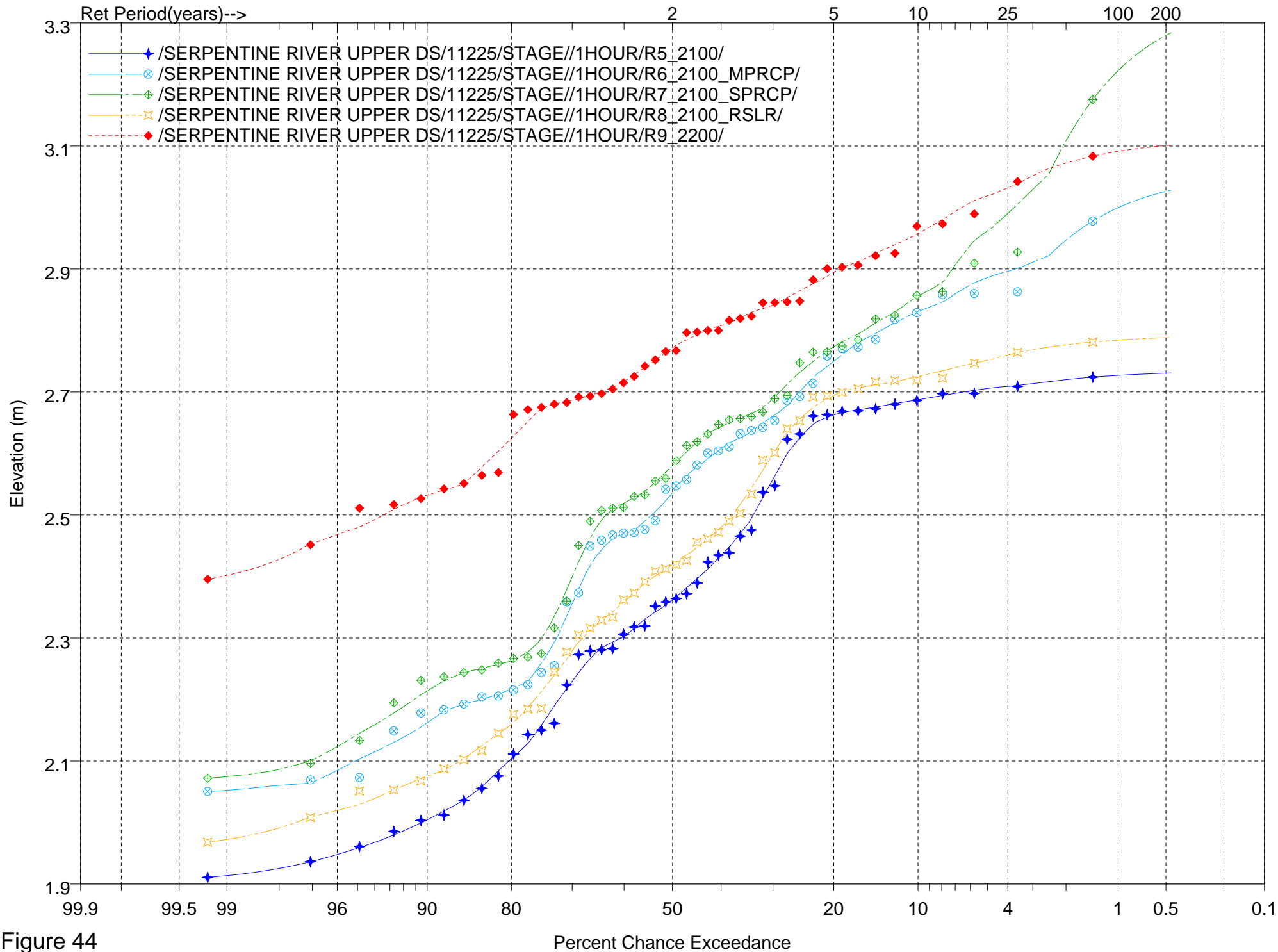


Figure 44

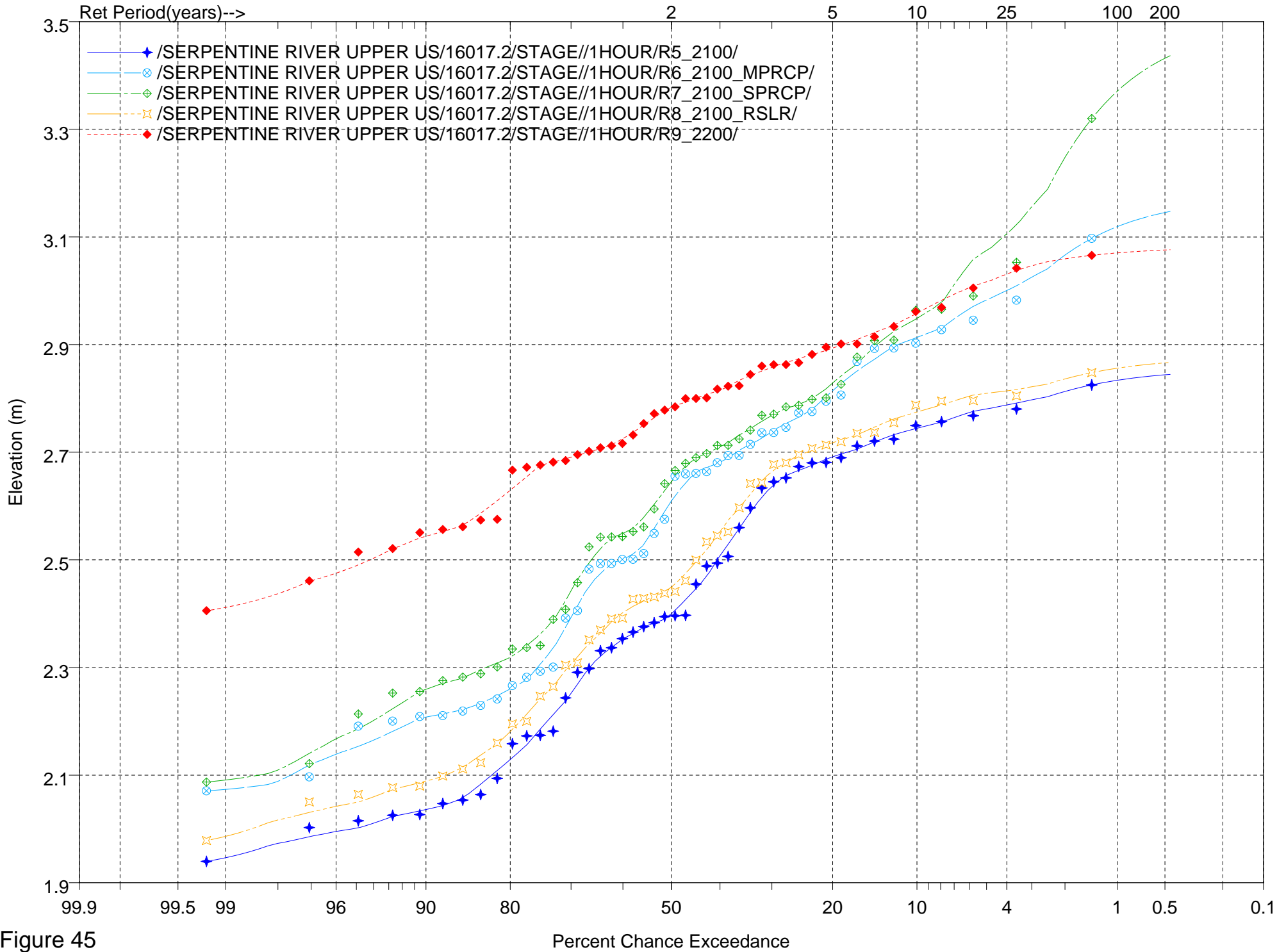


Figure 45

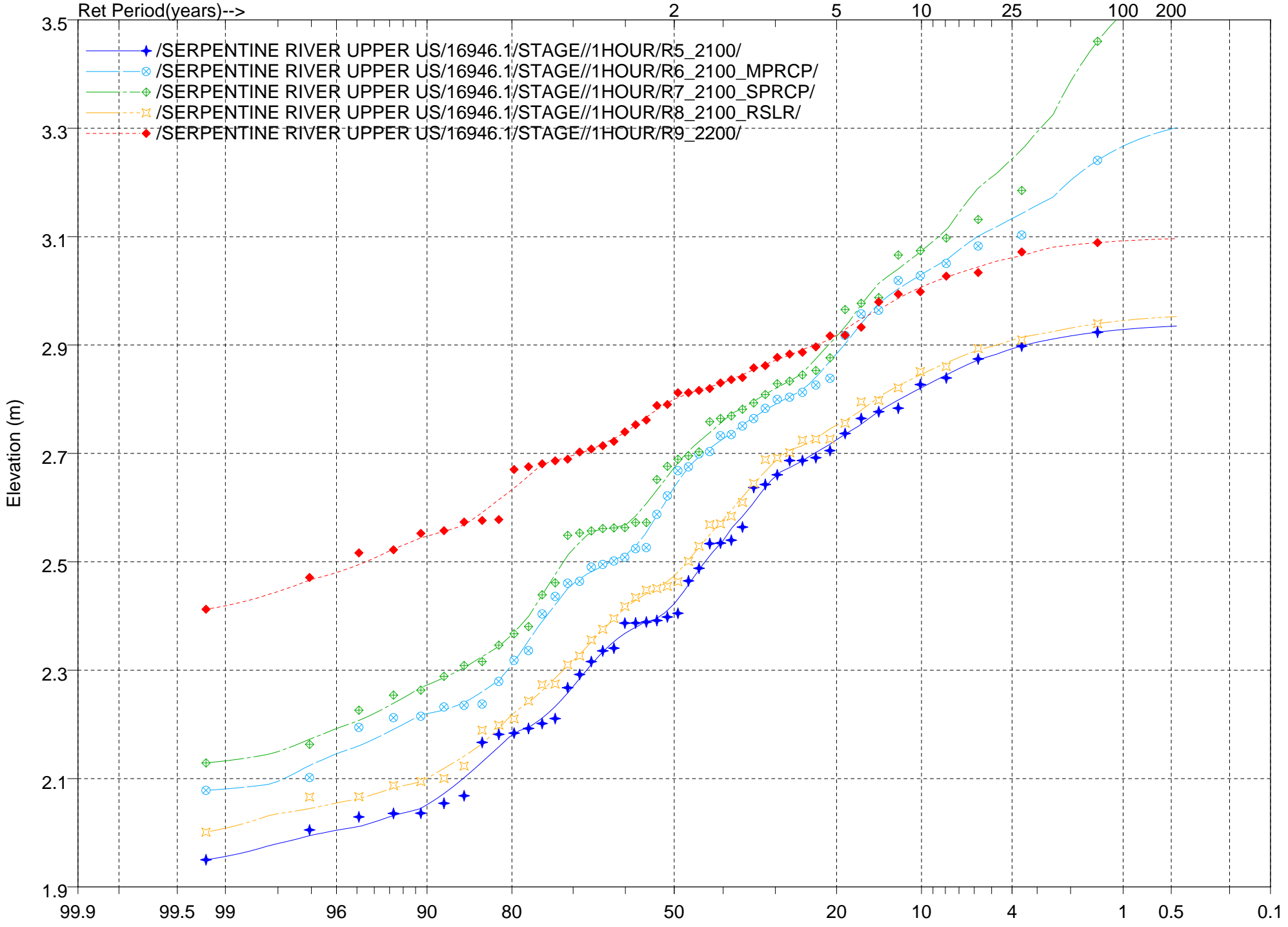


Figure 46

Percent Chance Exceedance

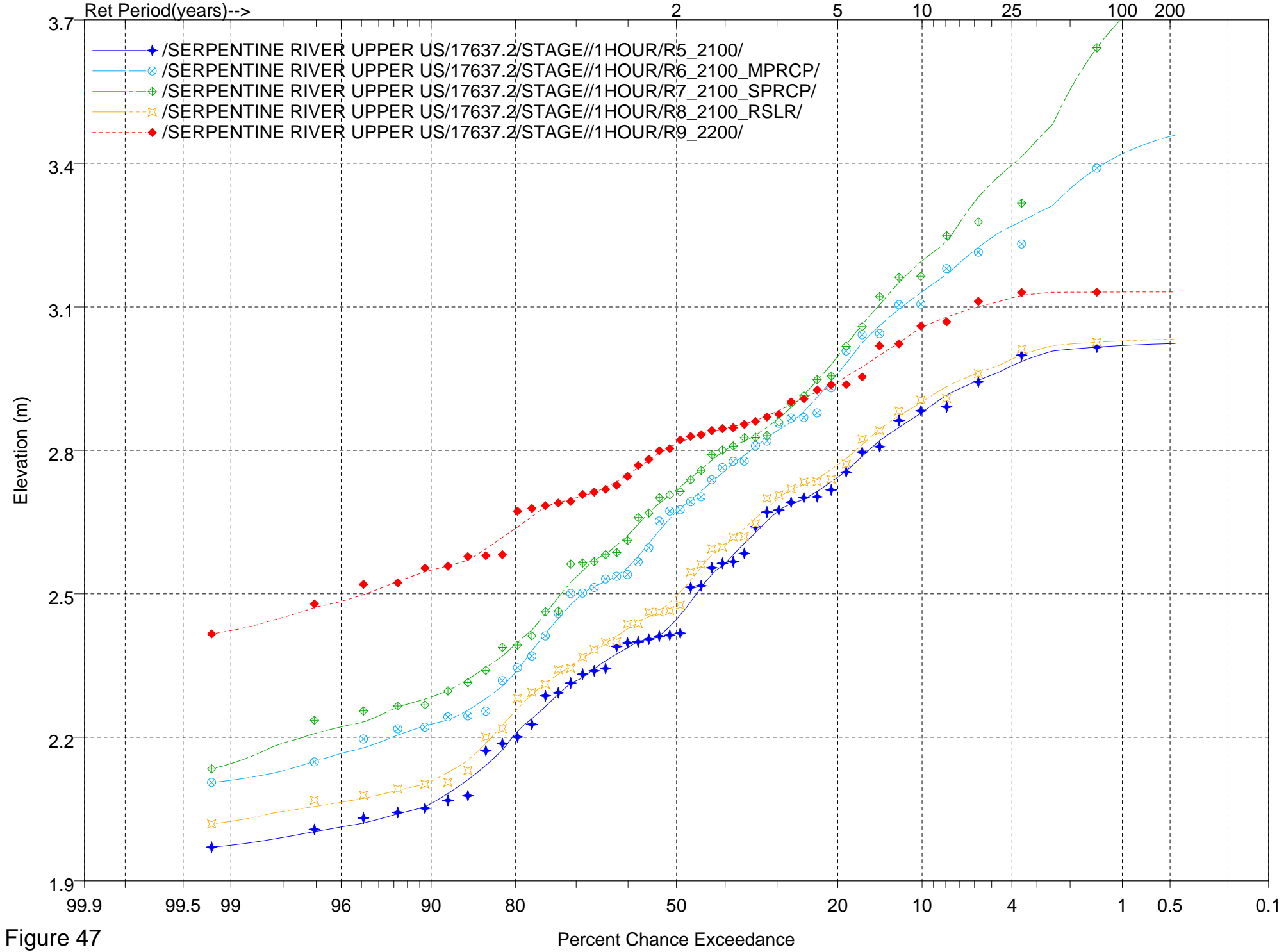


Figure 47

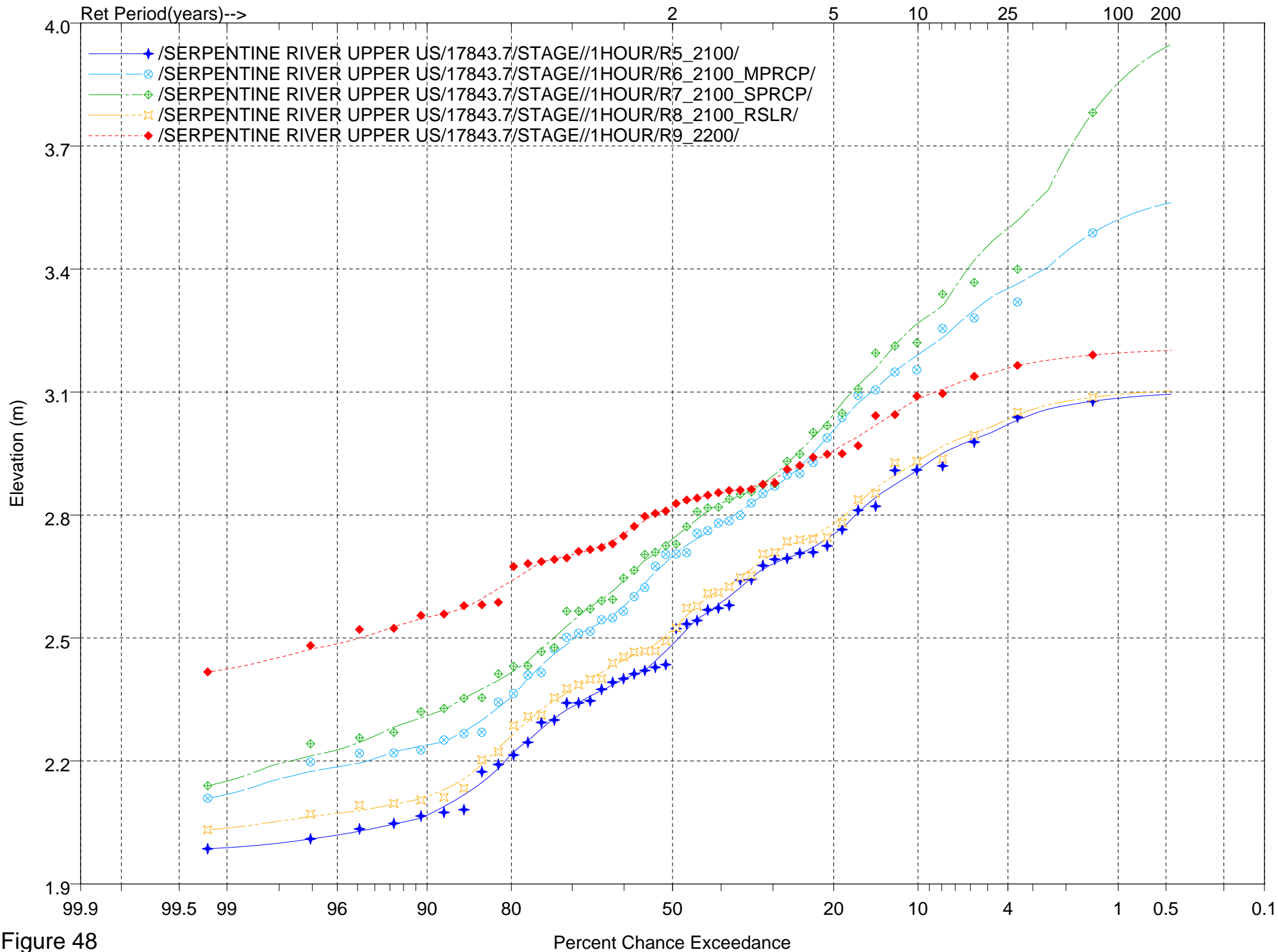


Figure 48



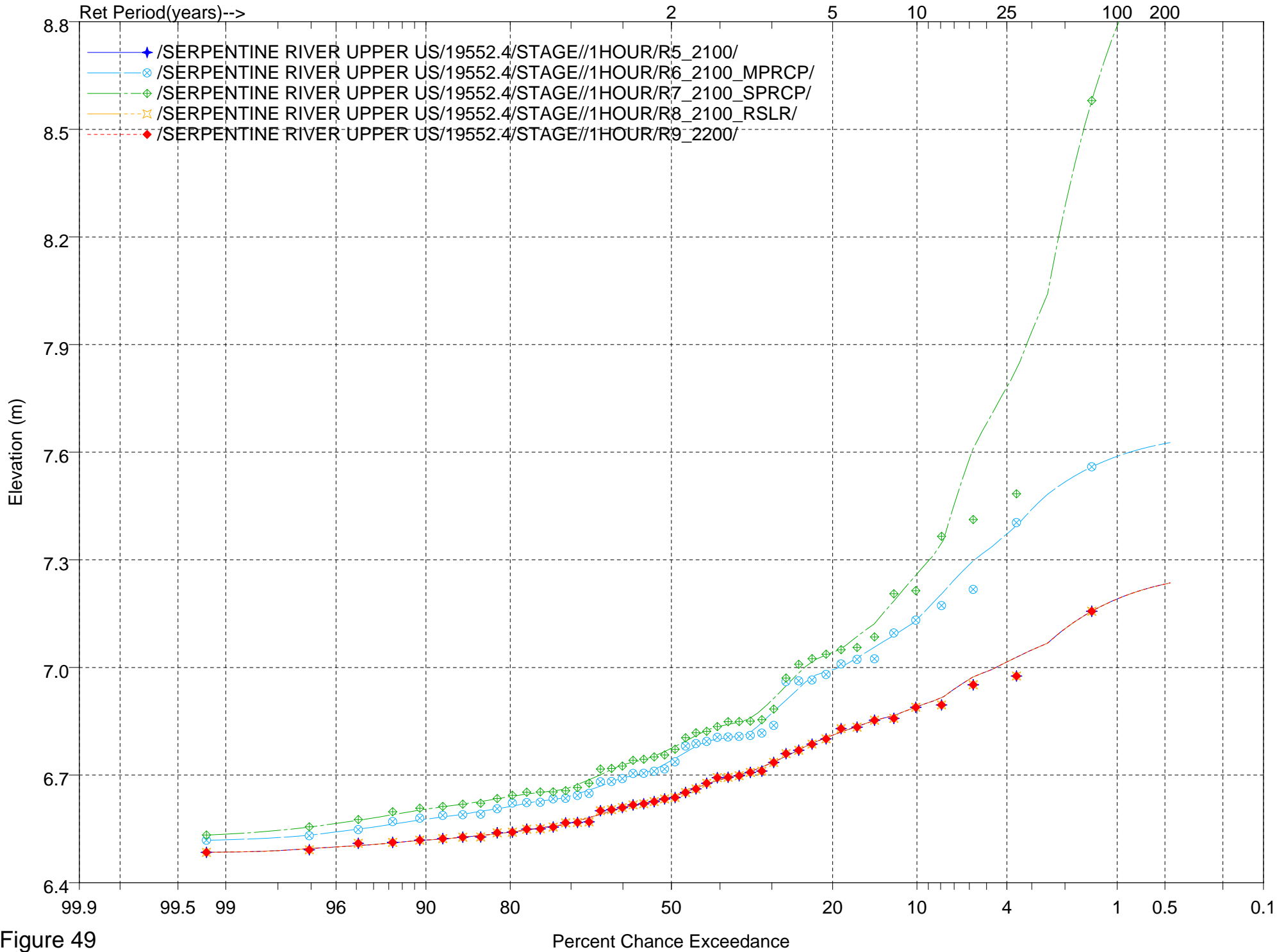


Figure 49

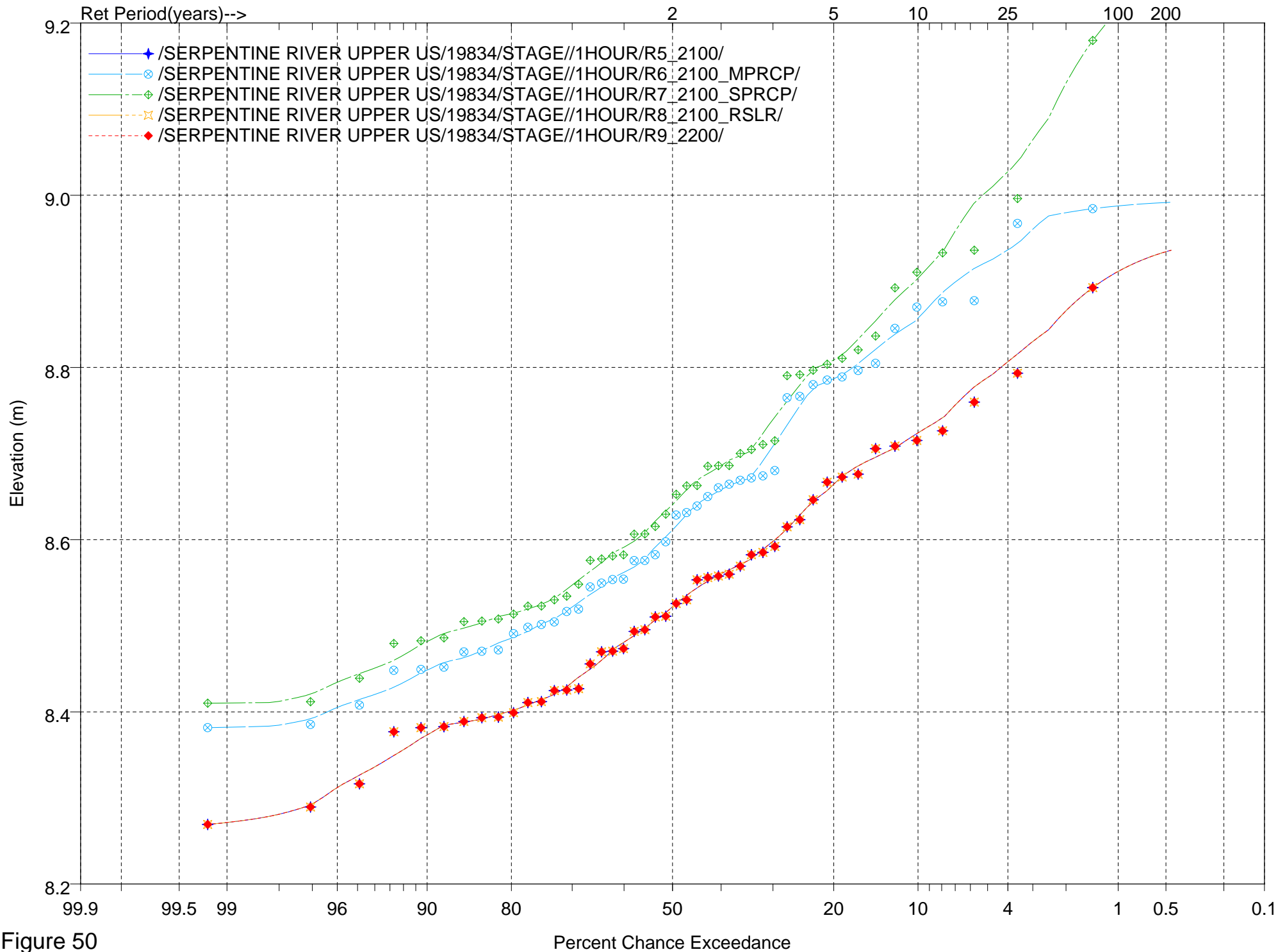


Figure 50

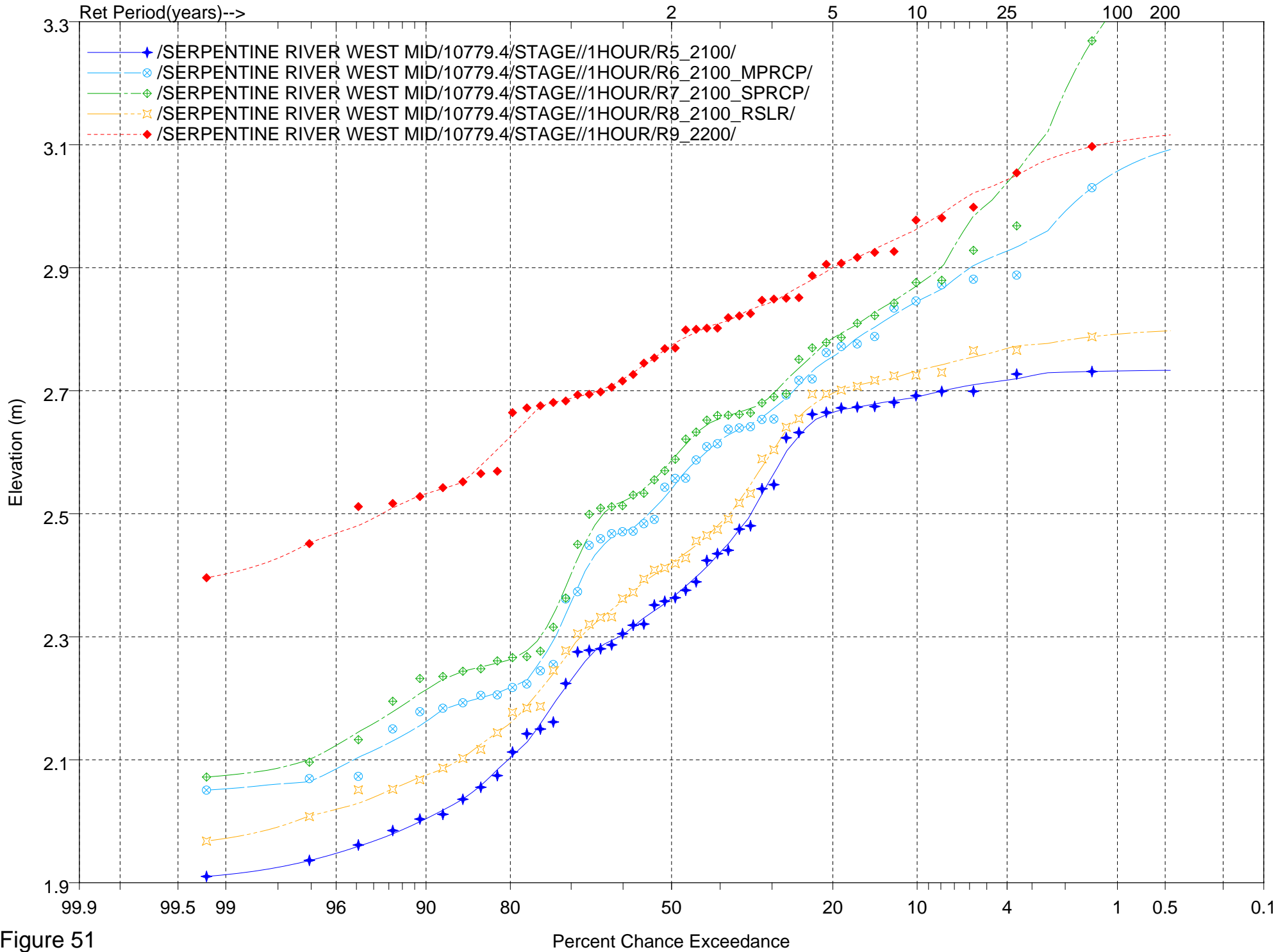


Figure 51

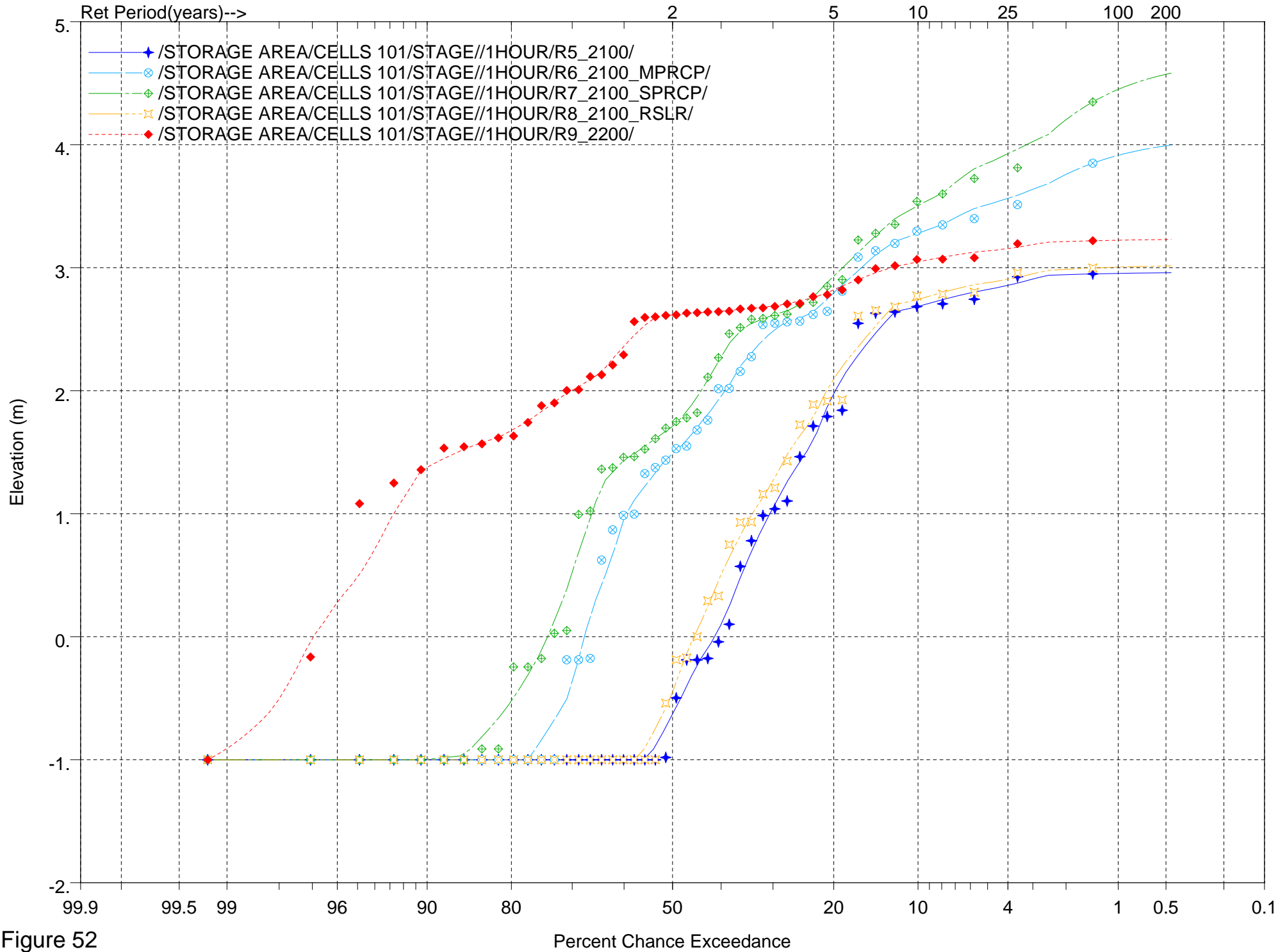


Figure 52

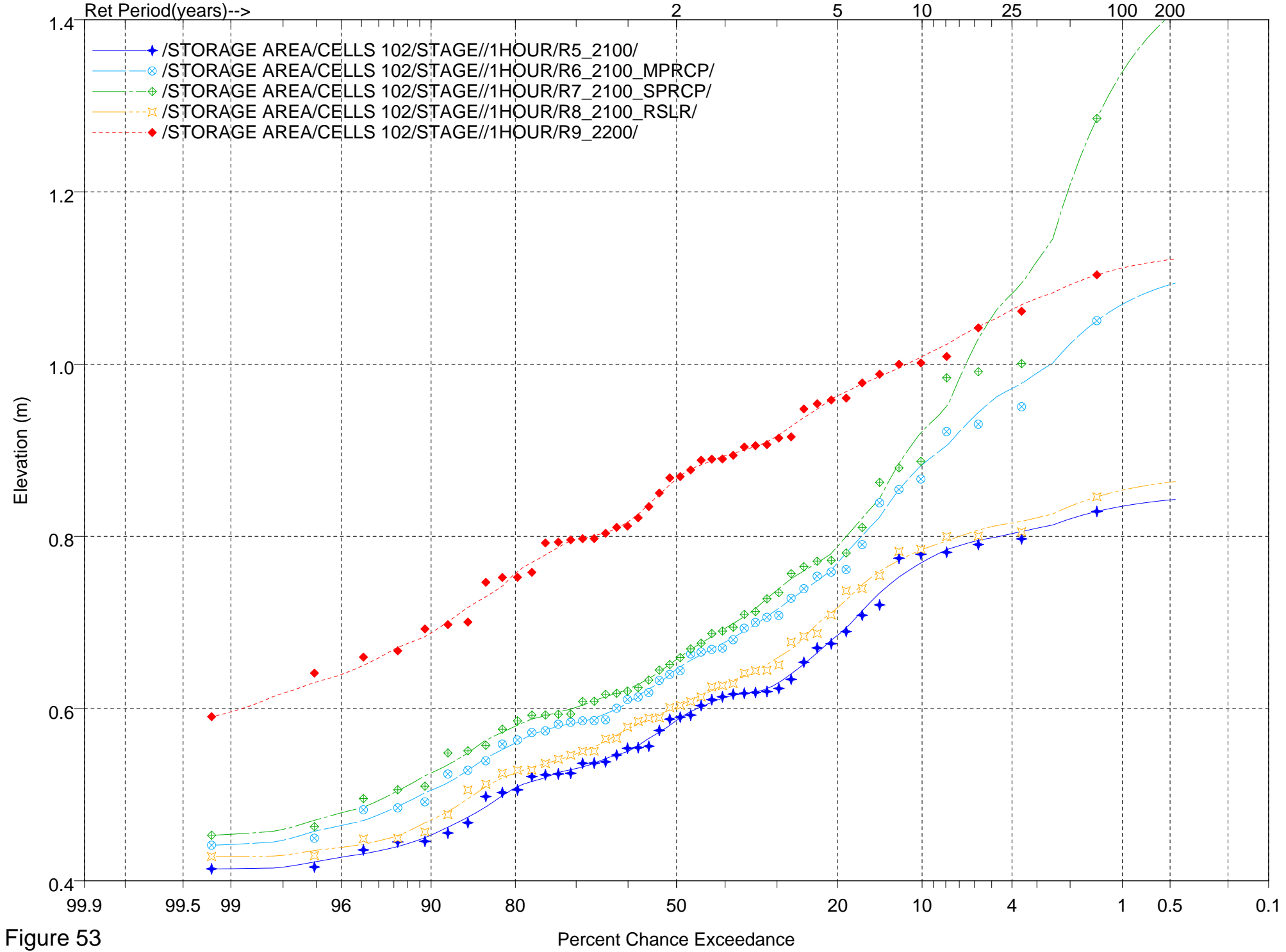


Figure 53

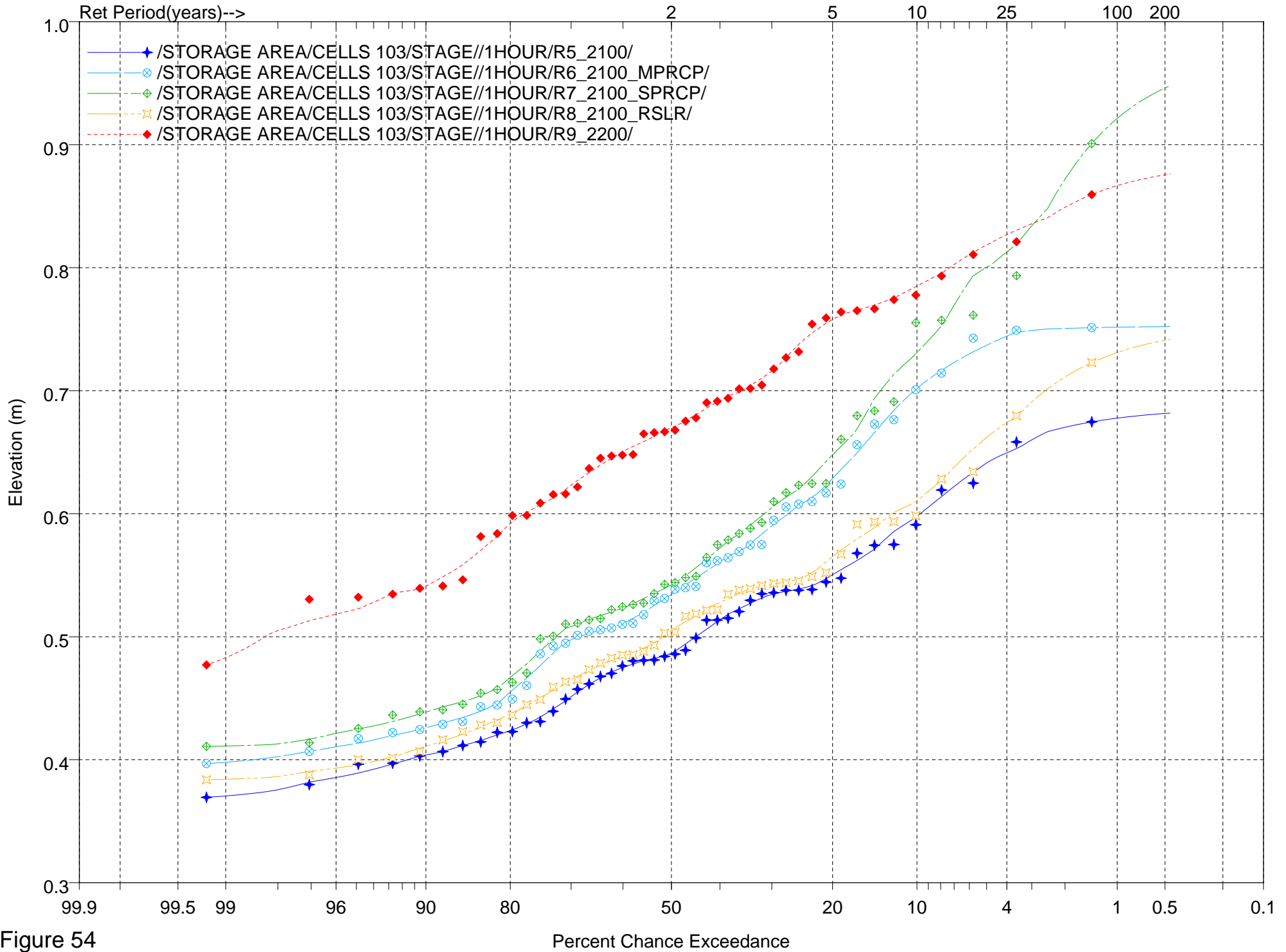


Figure 54

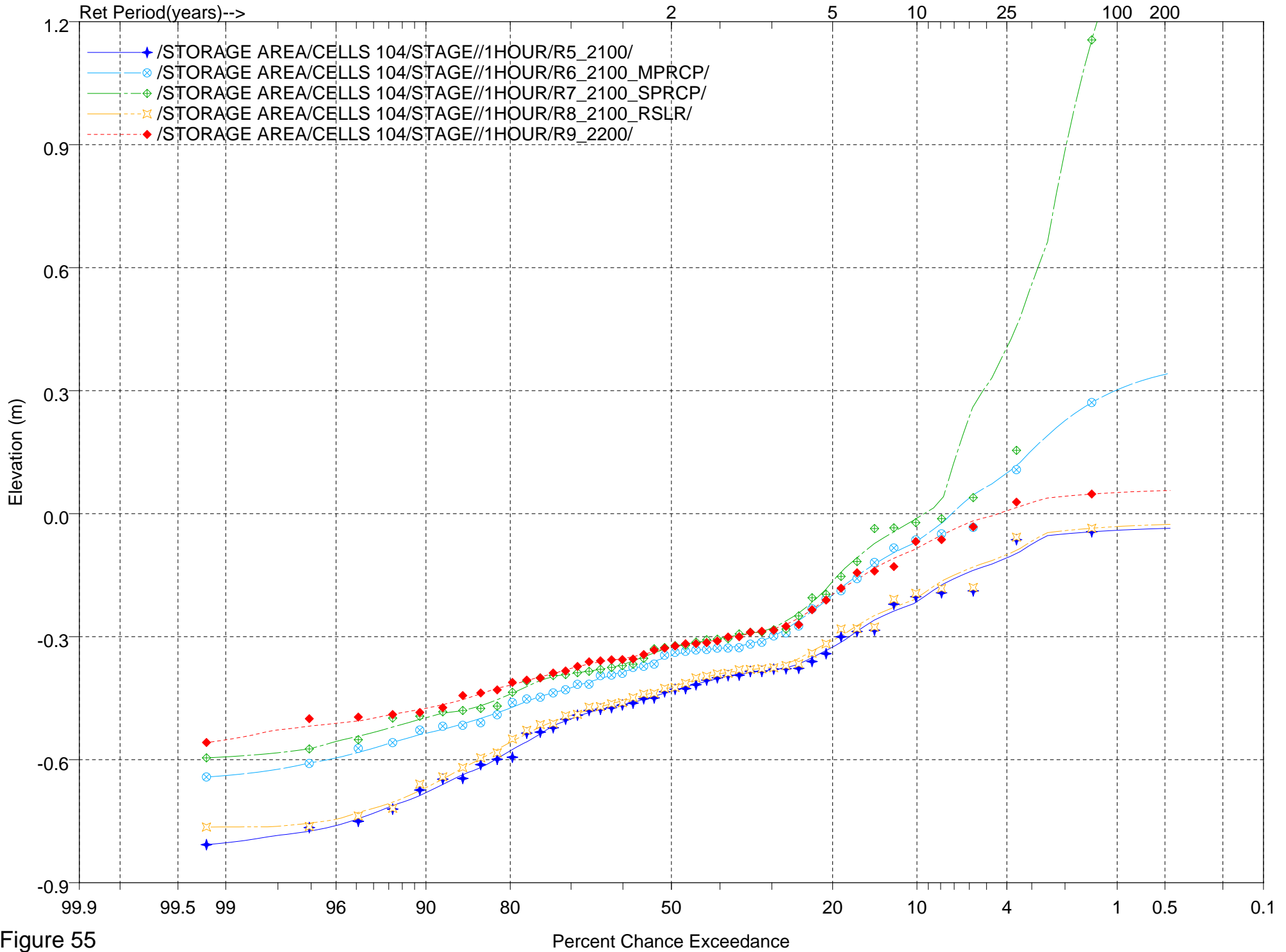


Figure 55

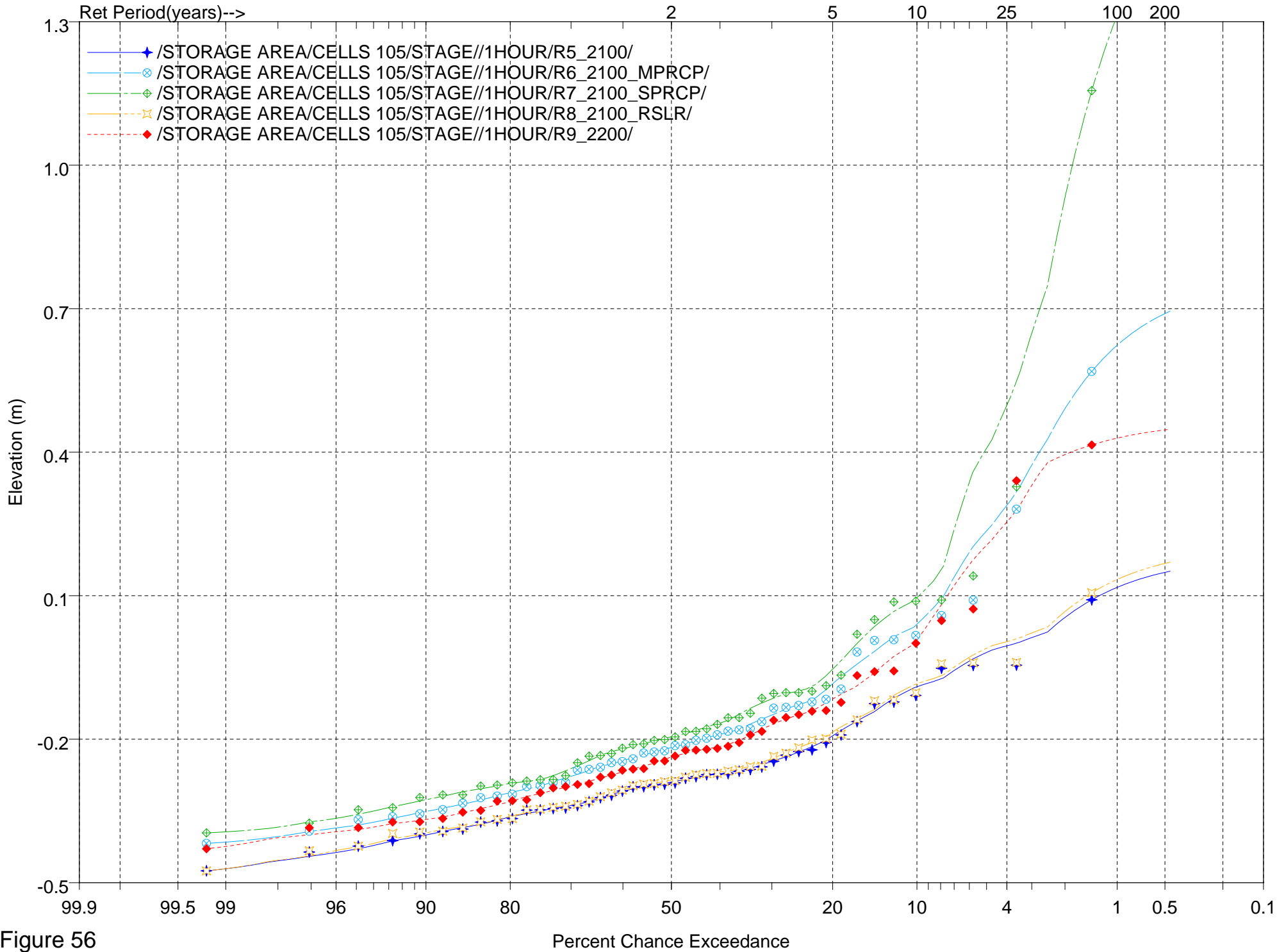


Figure 56



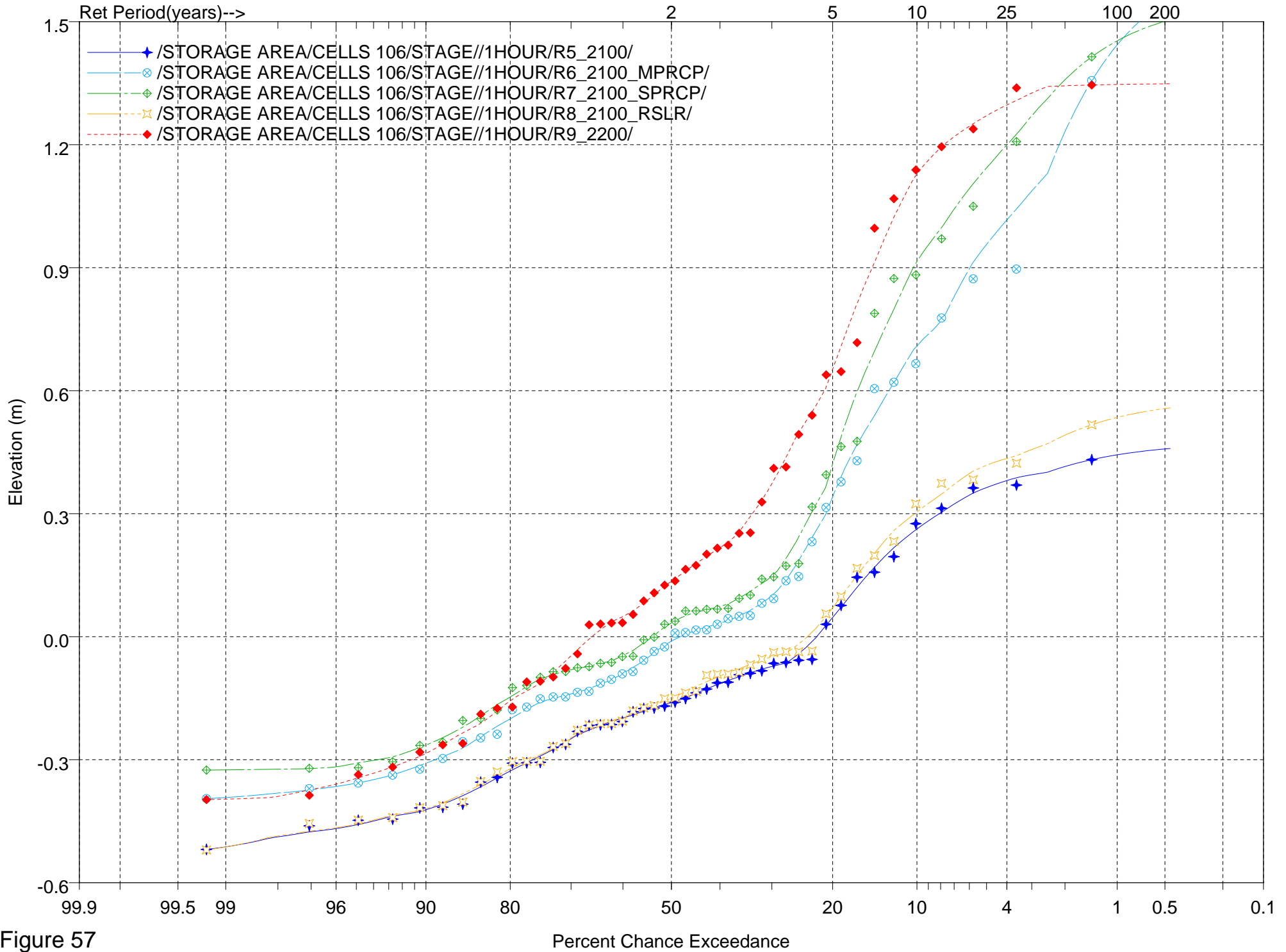


Figure 57

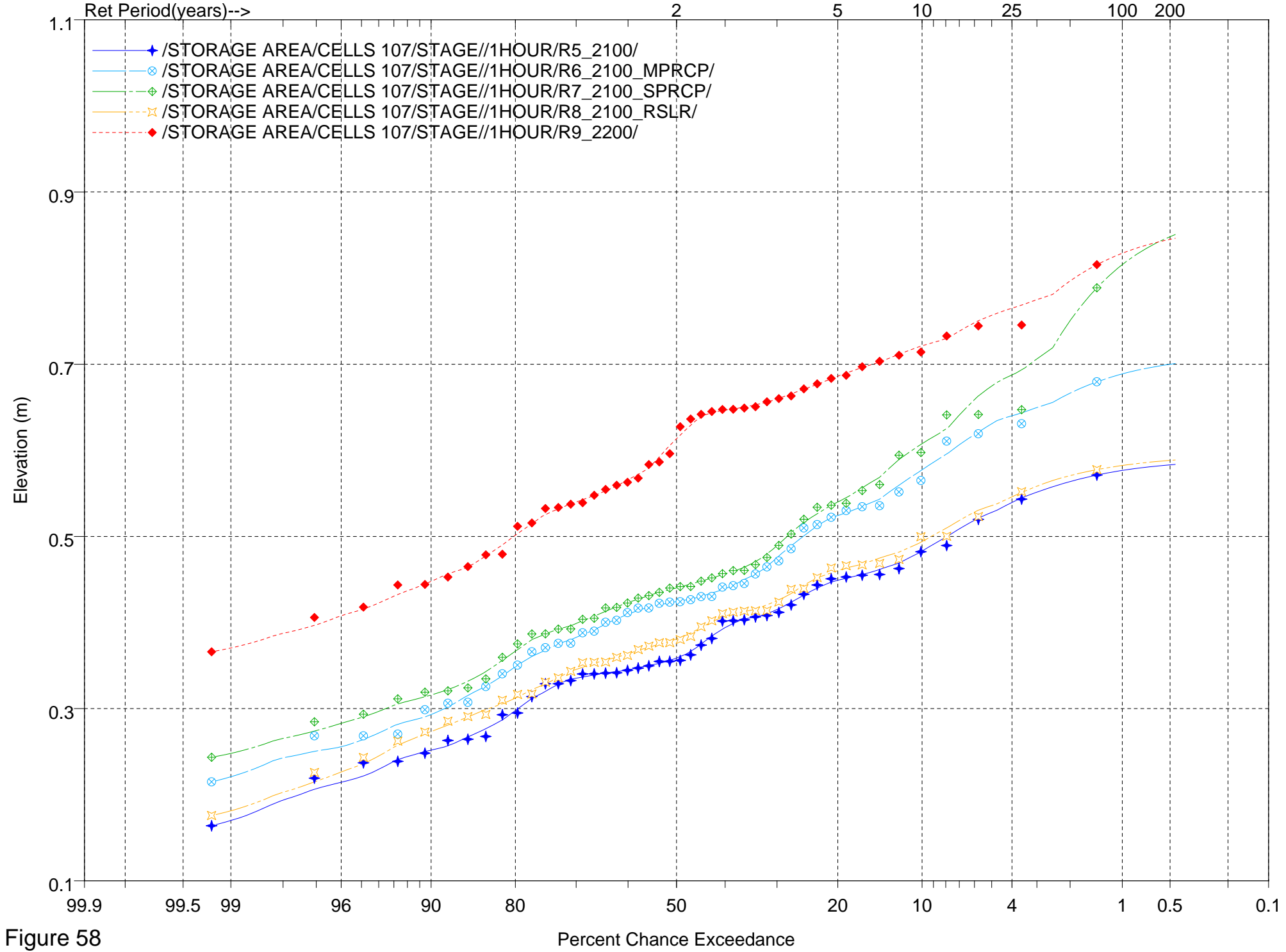


Figure 58

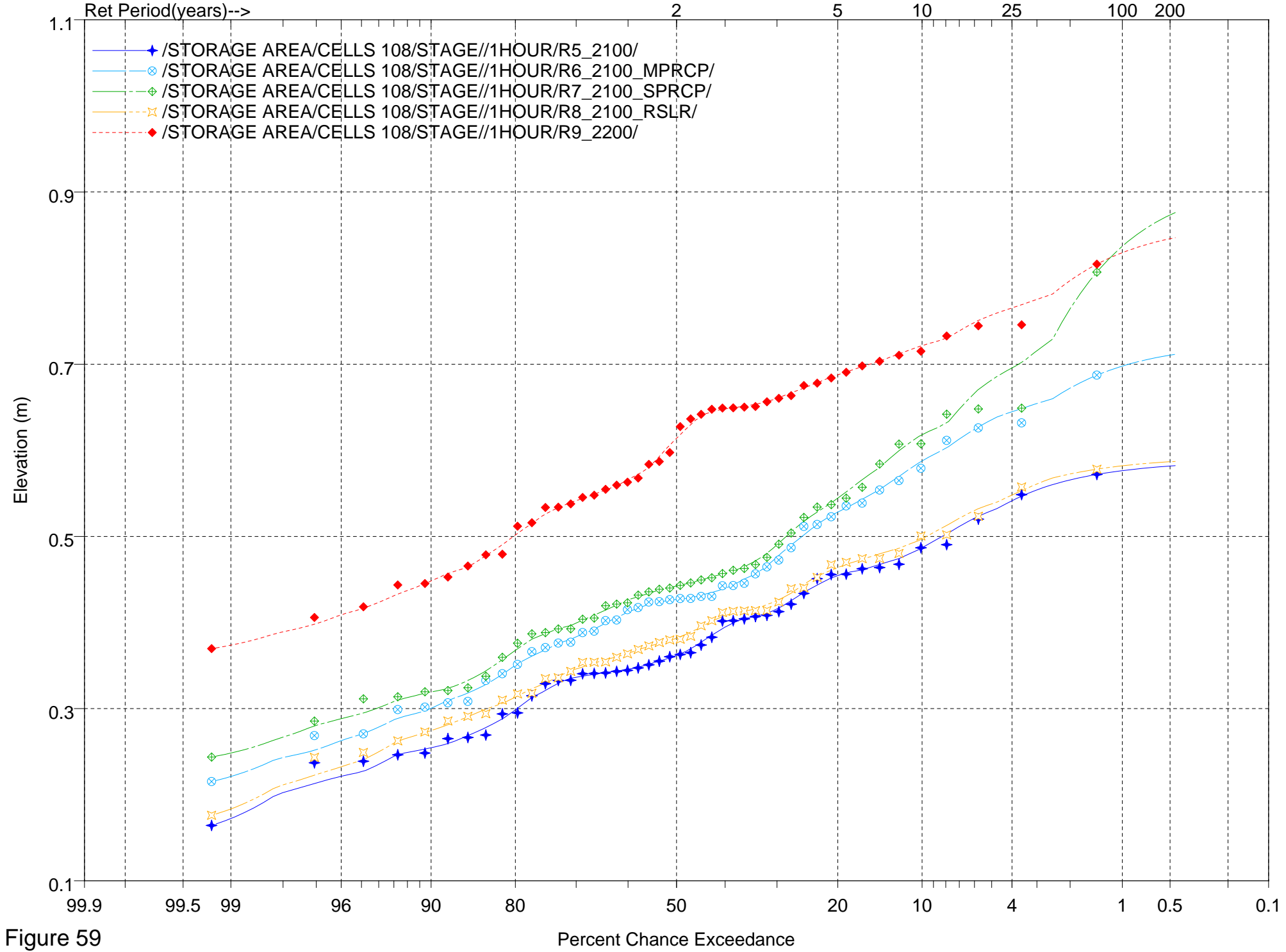


Figure 59

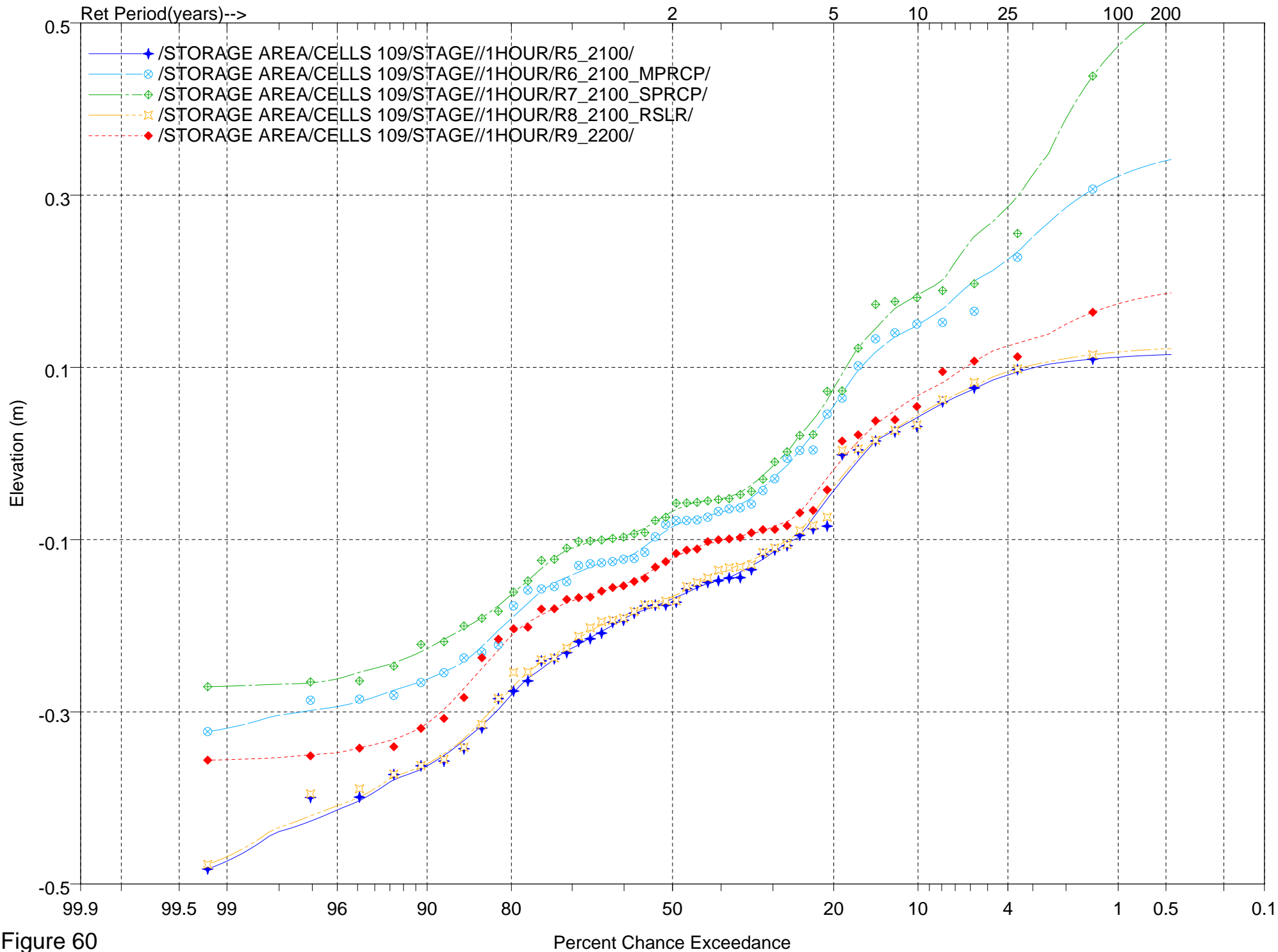


Figure 60

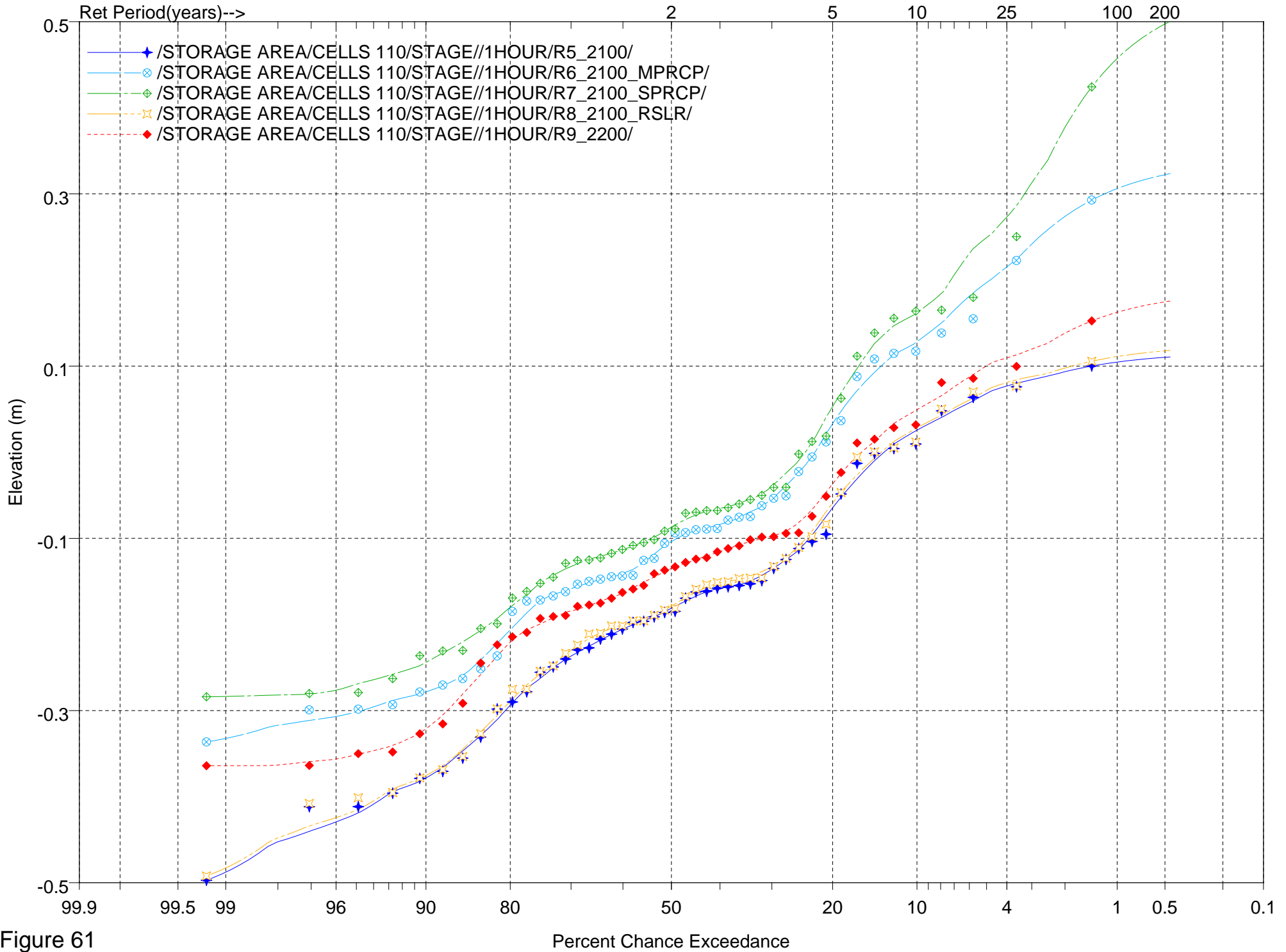


Figure 61

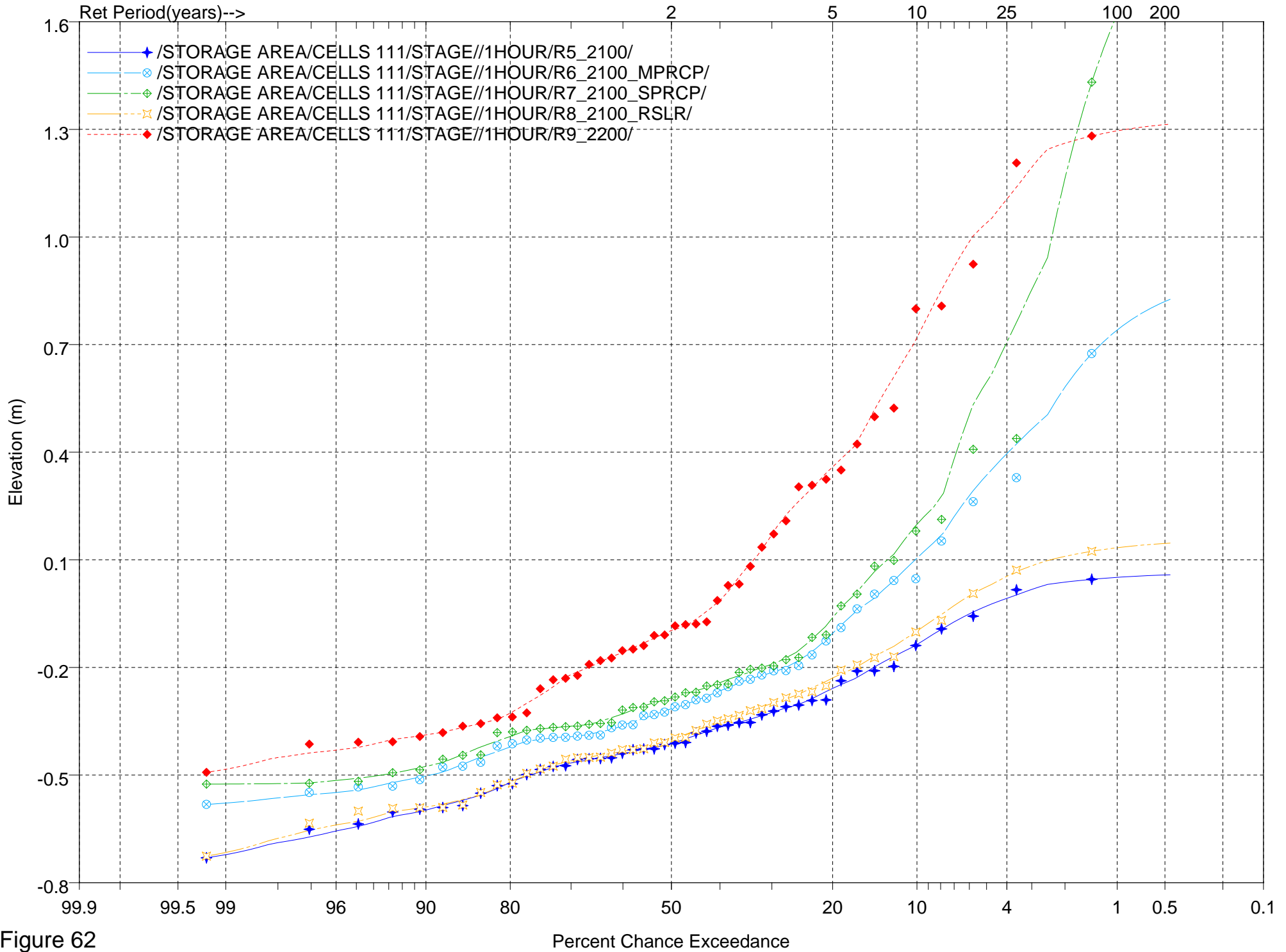


Figure 62

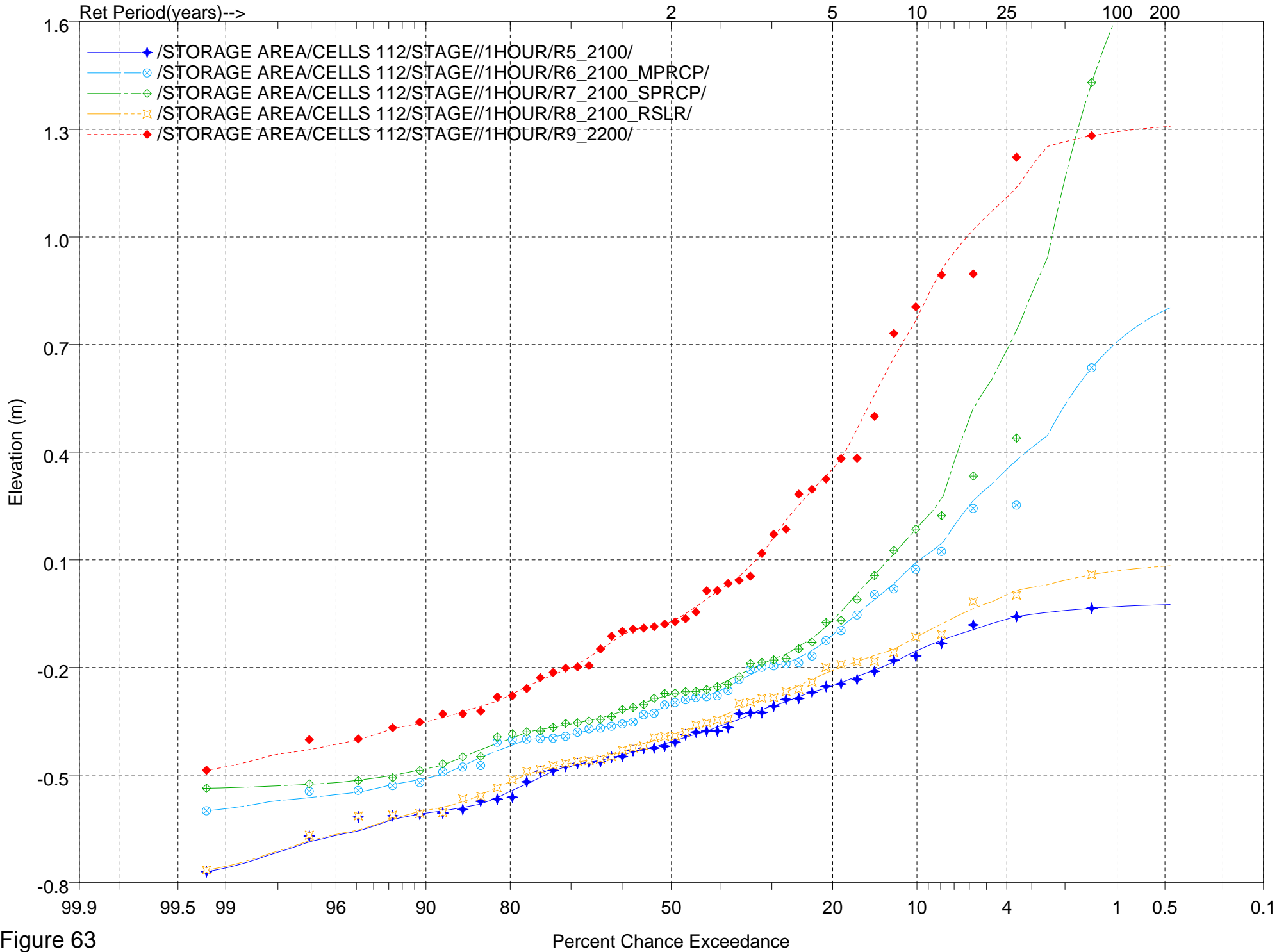


Figure 63

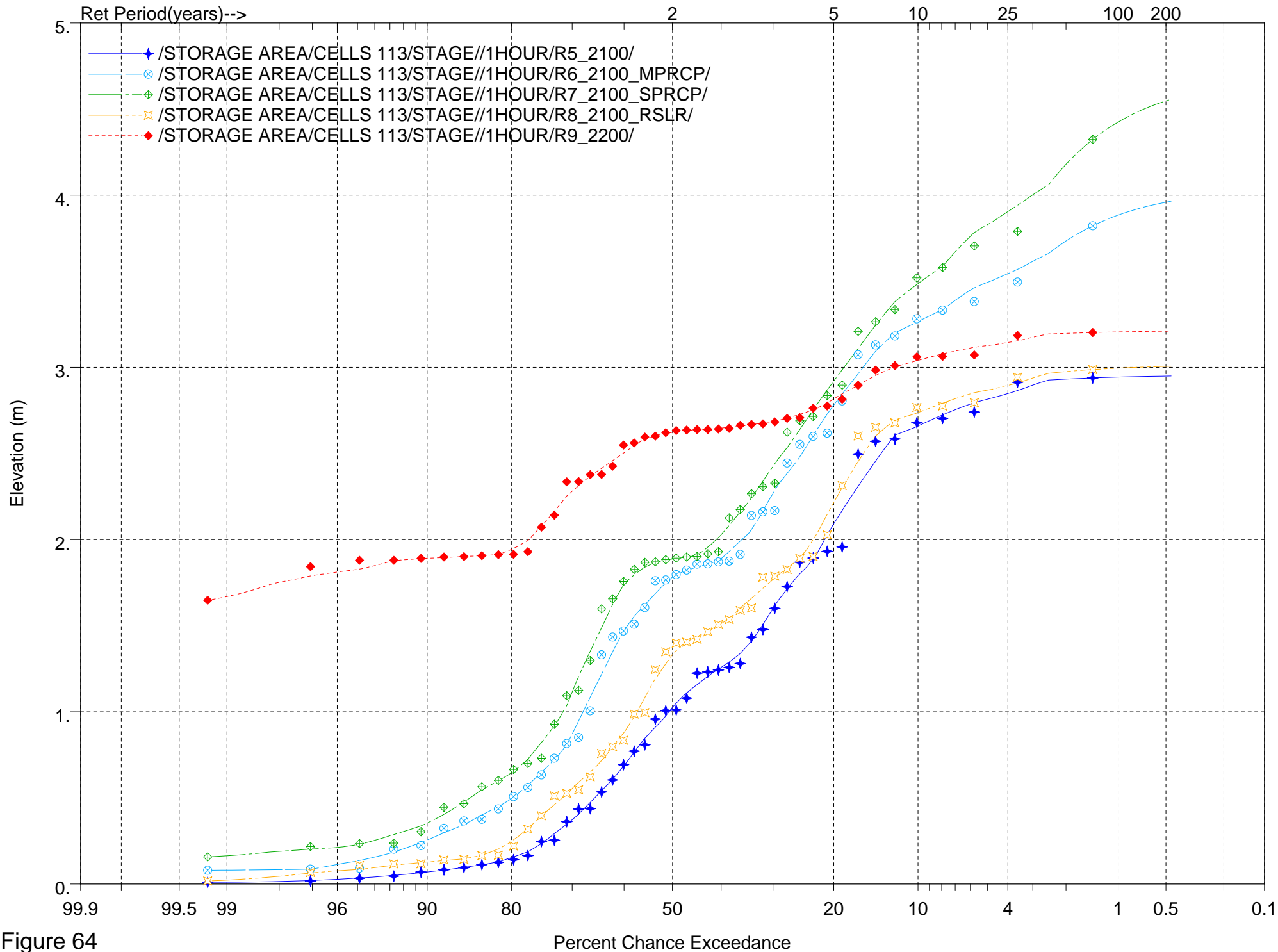


Figure 64



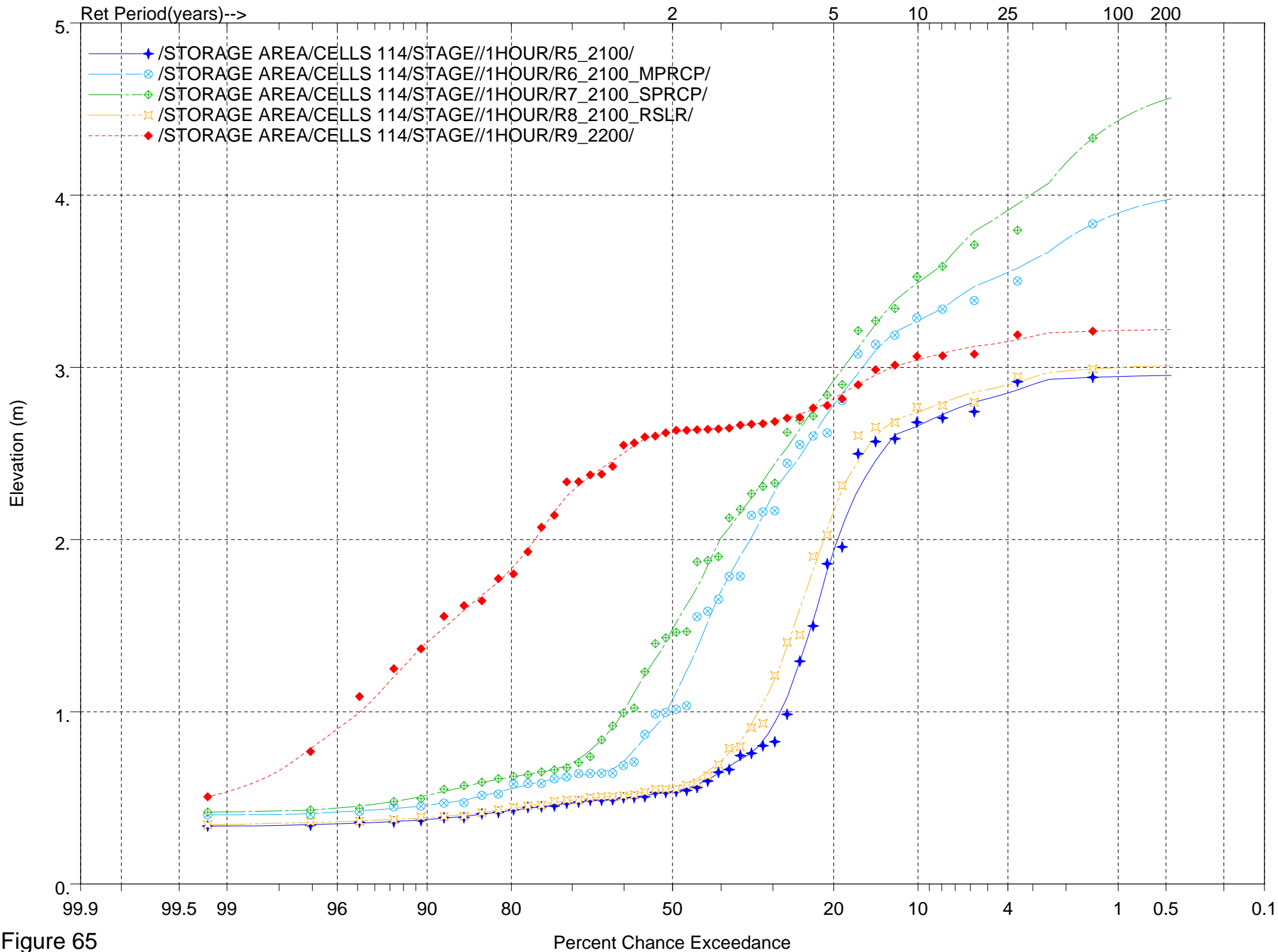


Figure 65

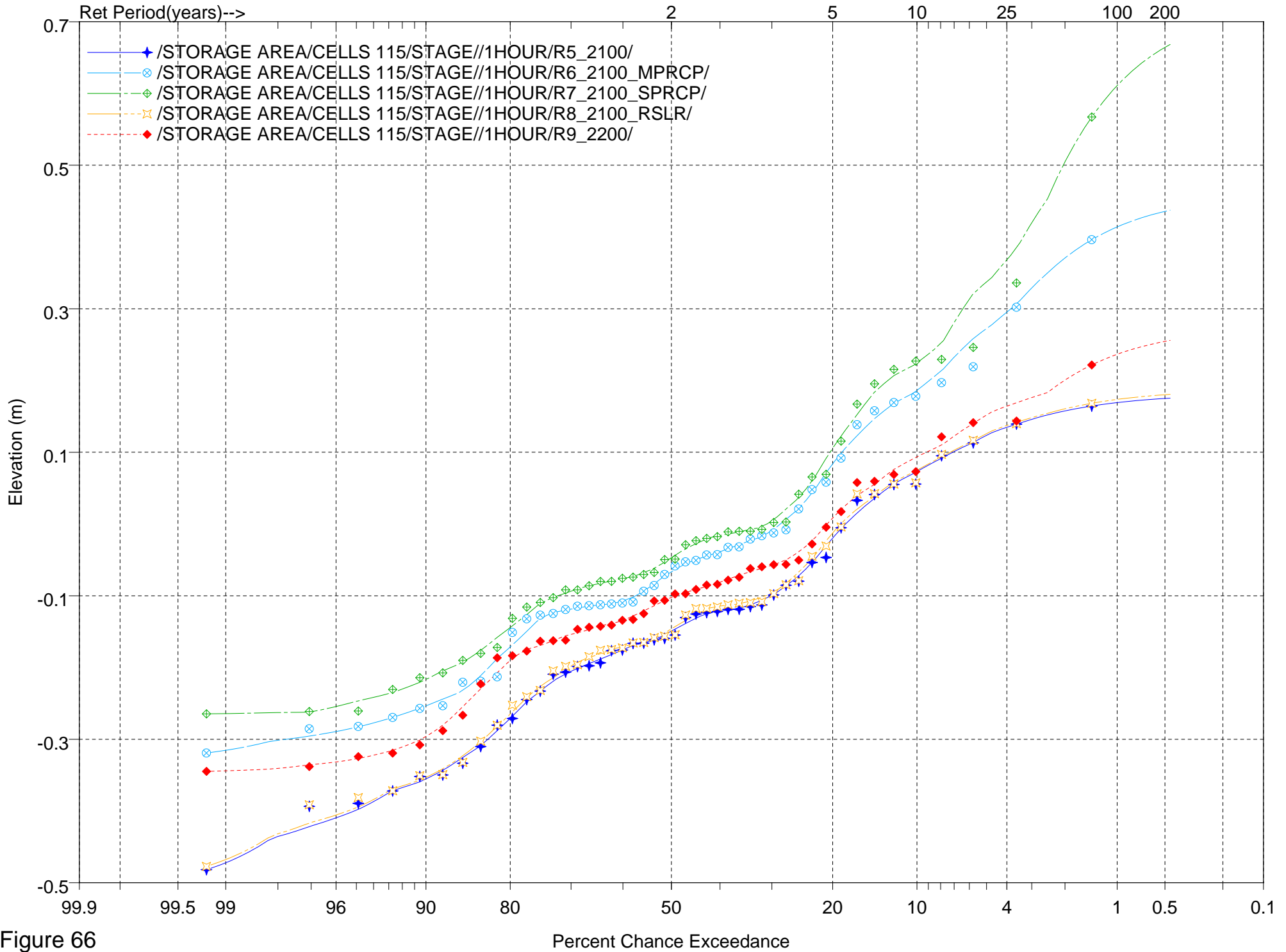


Figure 66

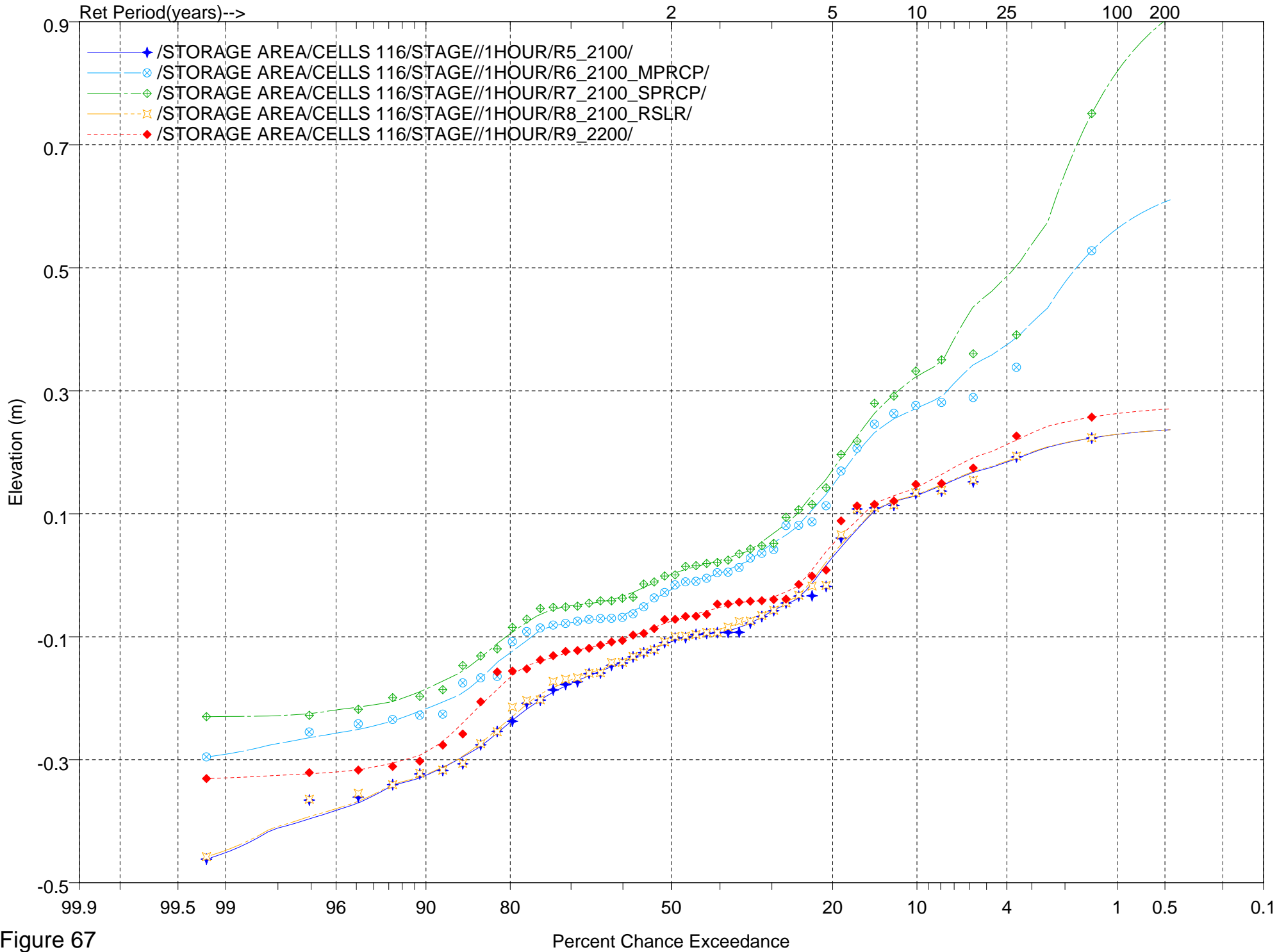


Figure 67

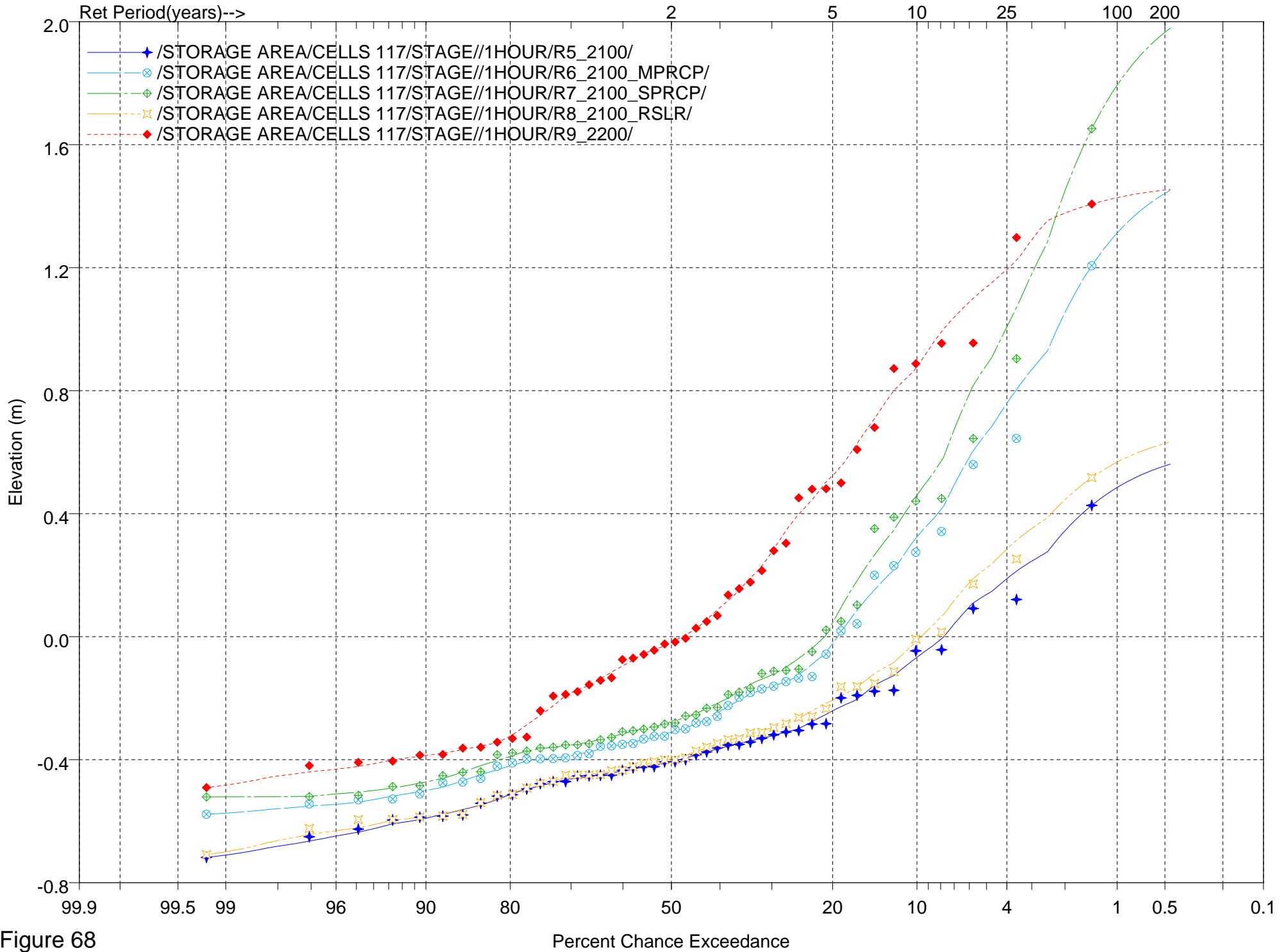


Figure 68

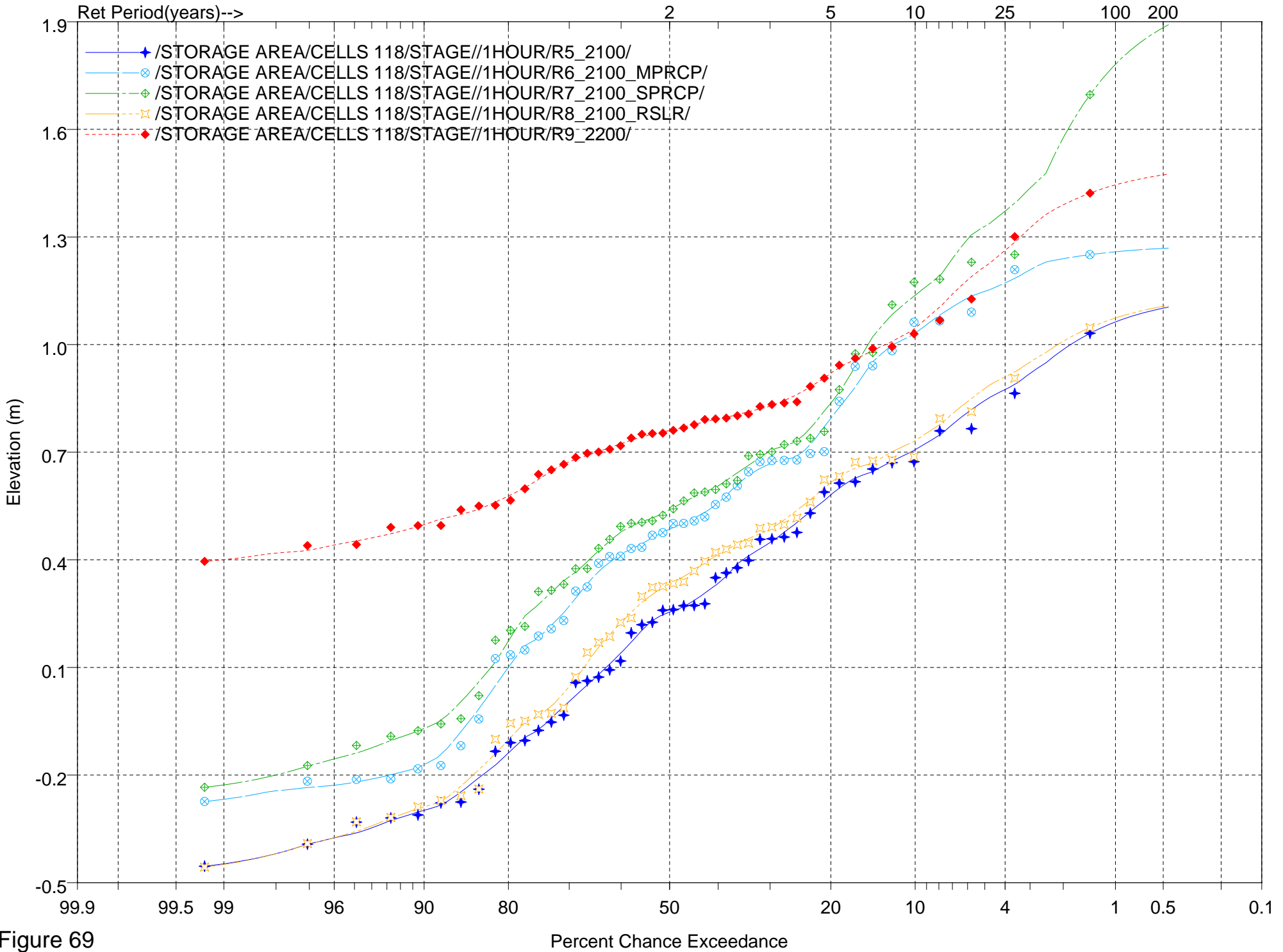


Figure 69

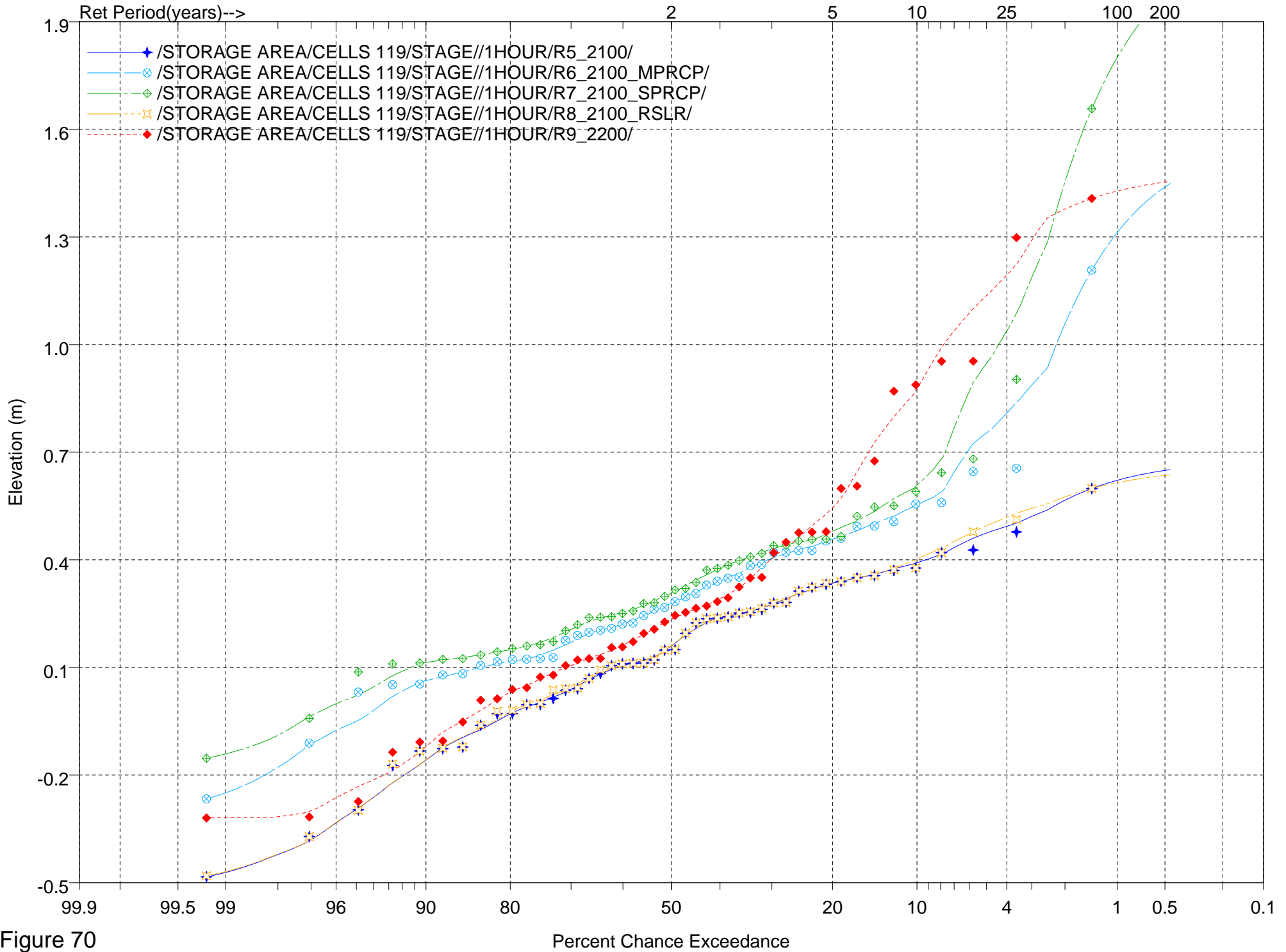


Figure 70

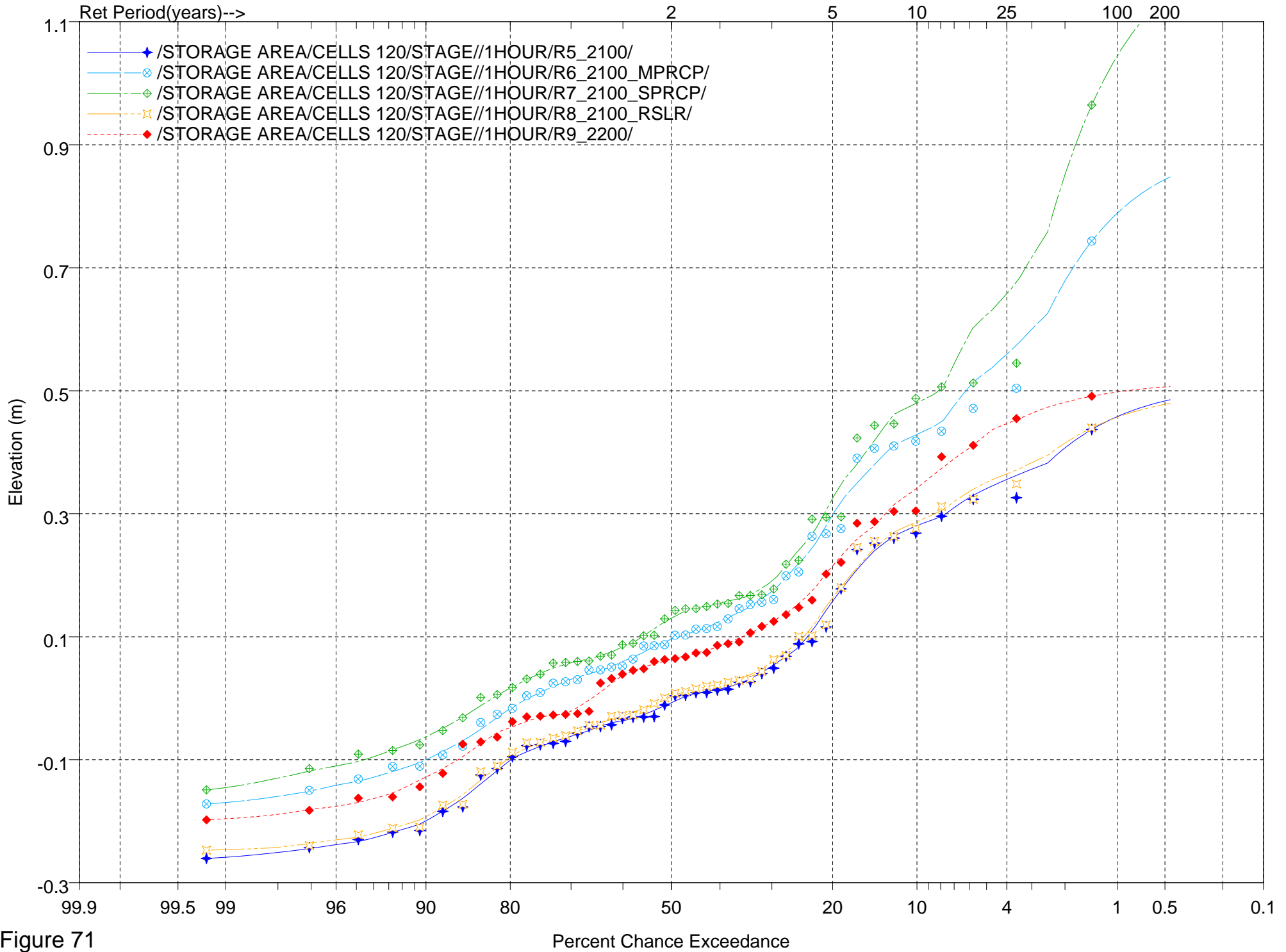


Figure 71

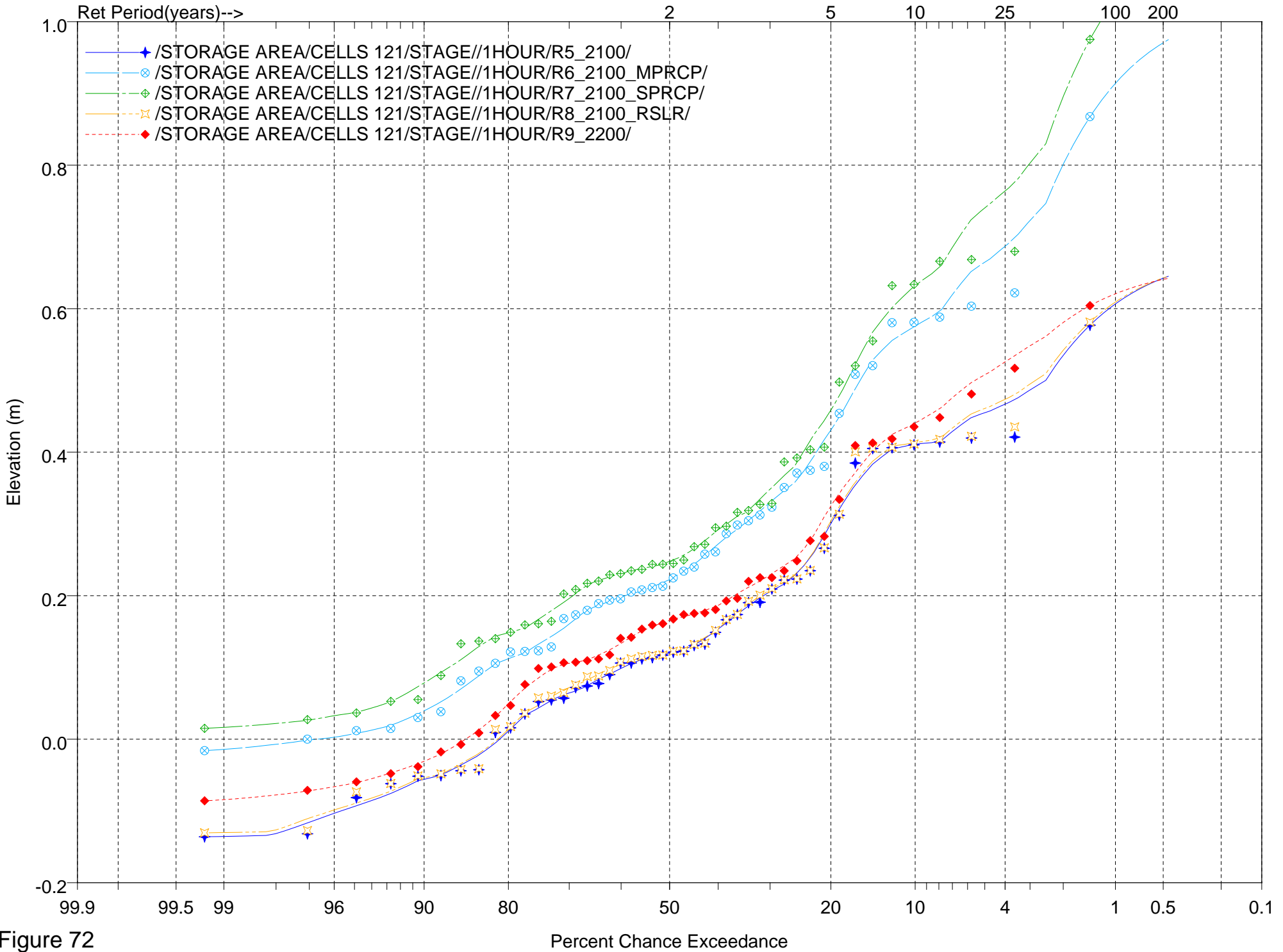


Figure 72



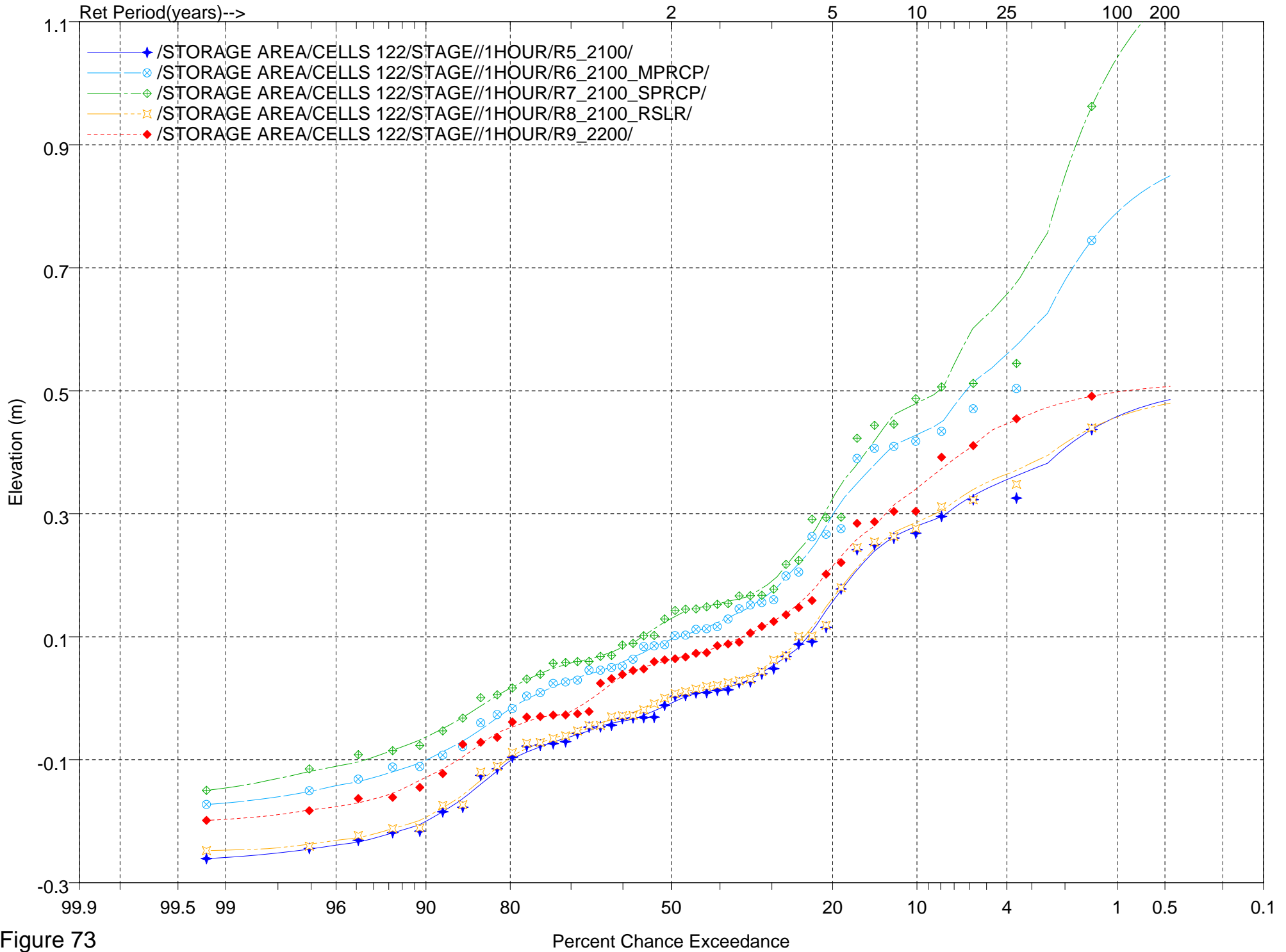


Figure 73

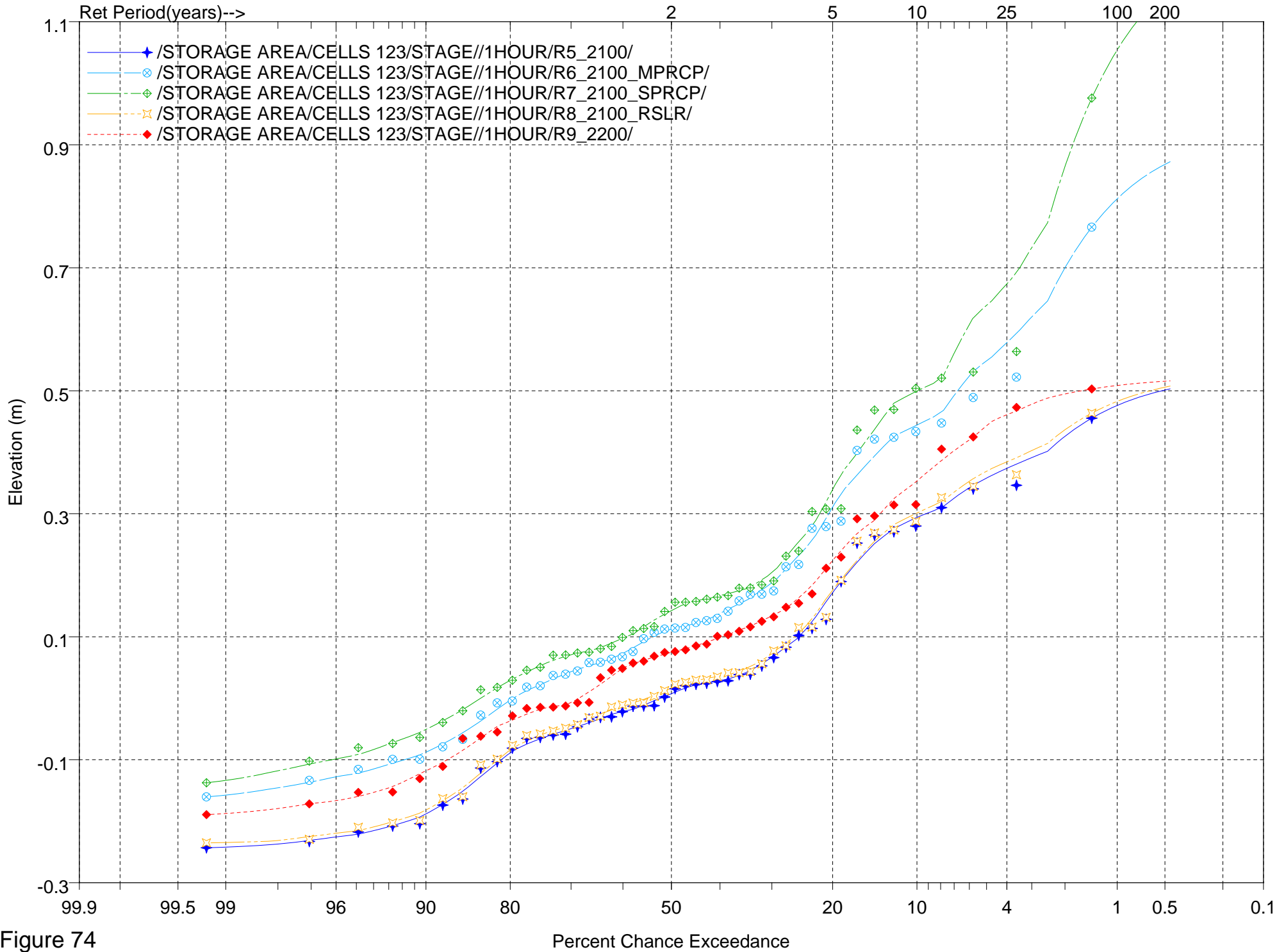


Figure 74

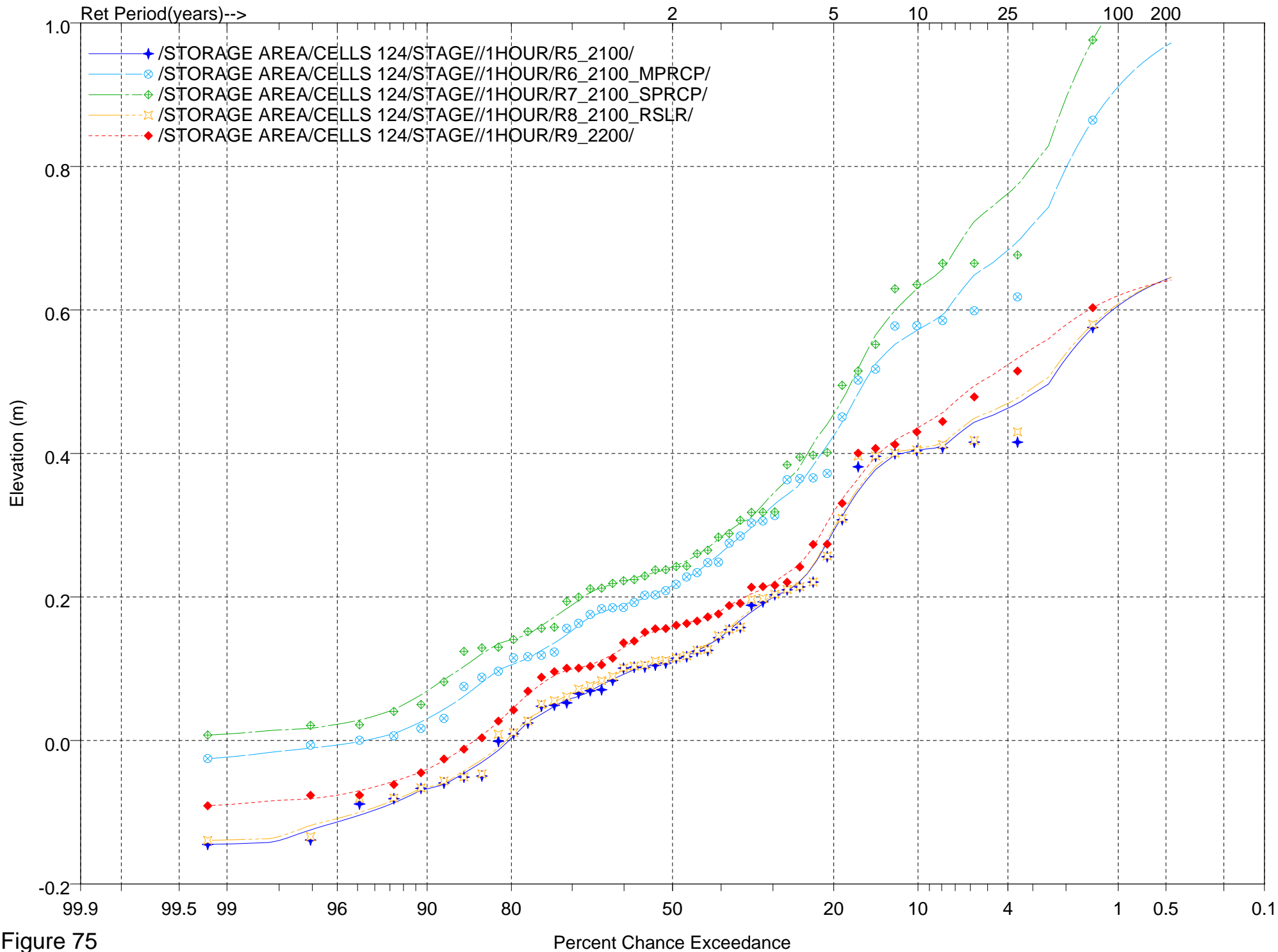


Figure 75

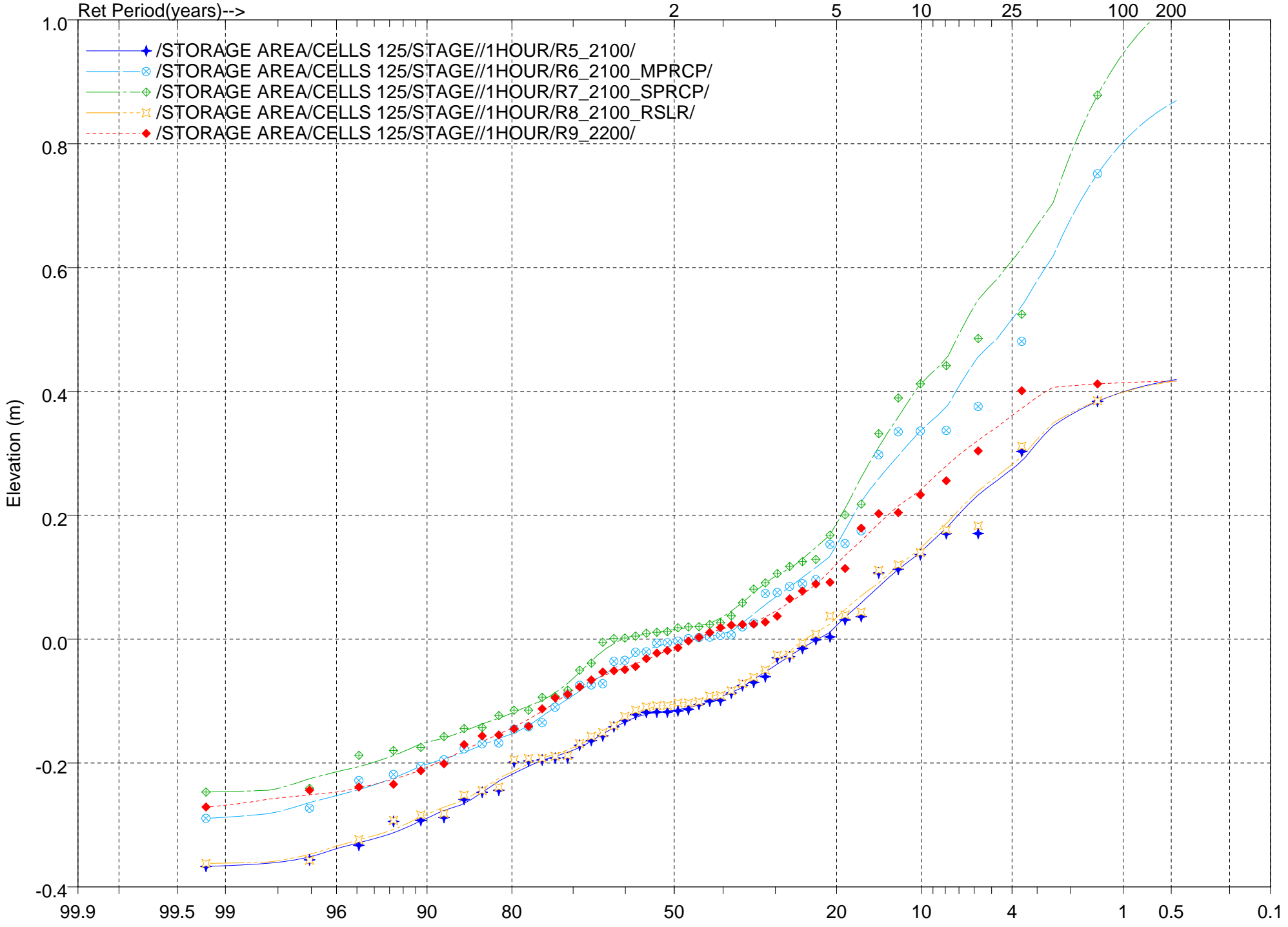


Figure 76

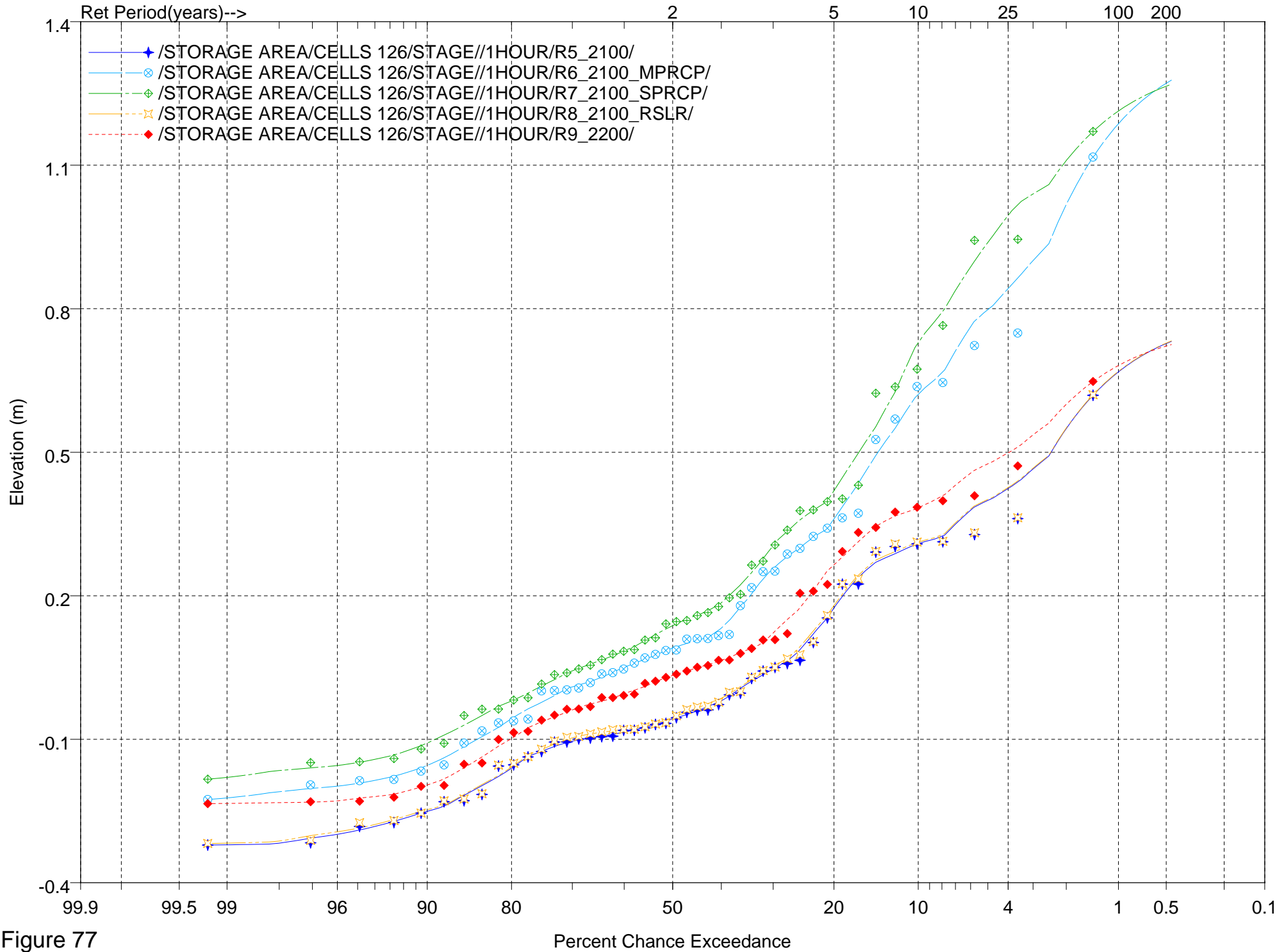


Figure 77

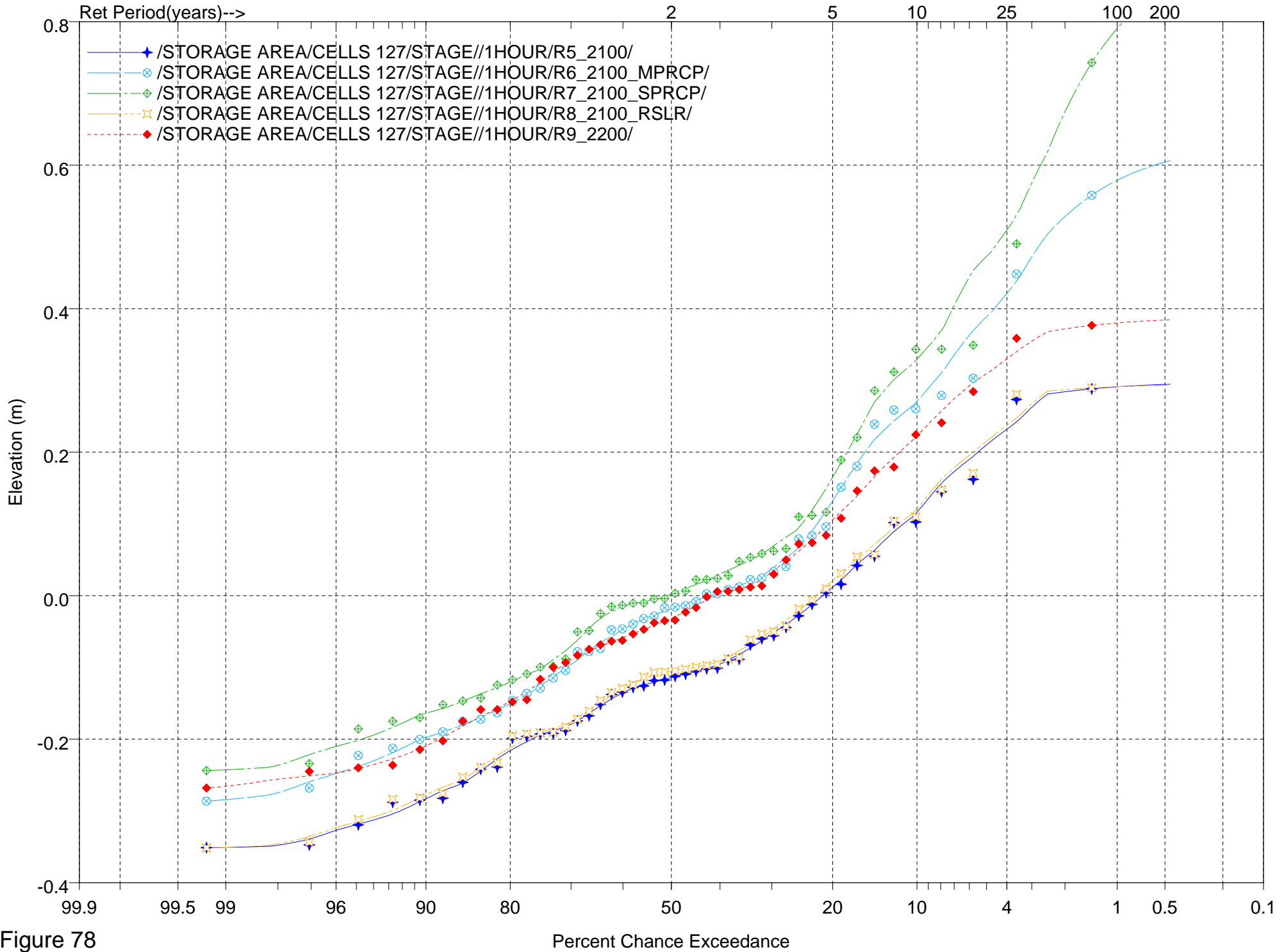


Figure 78

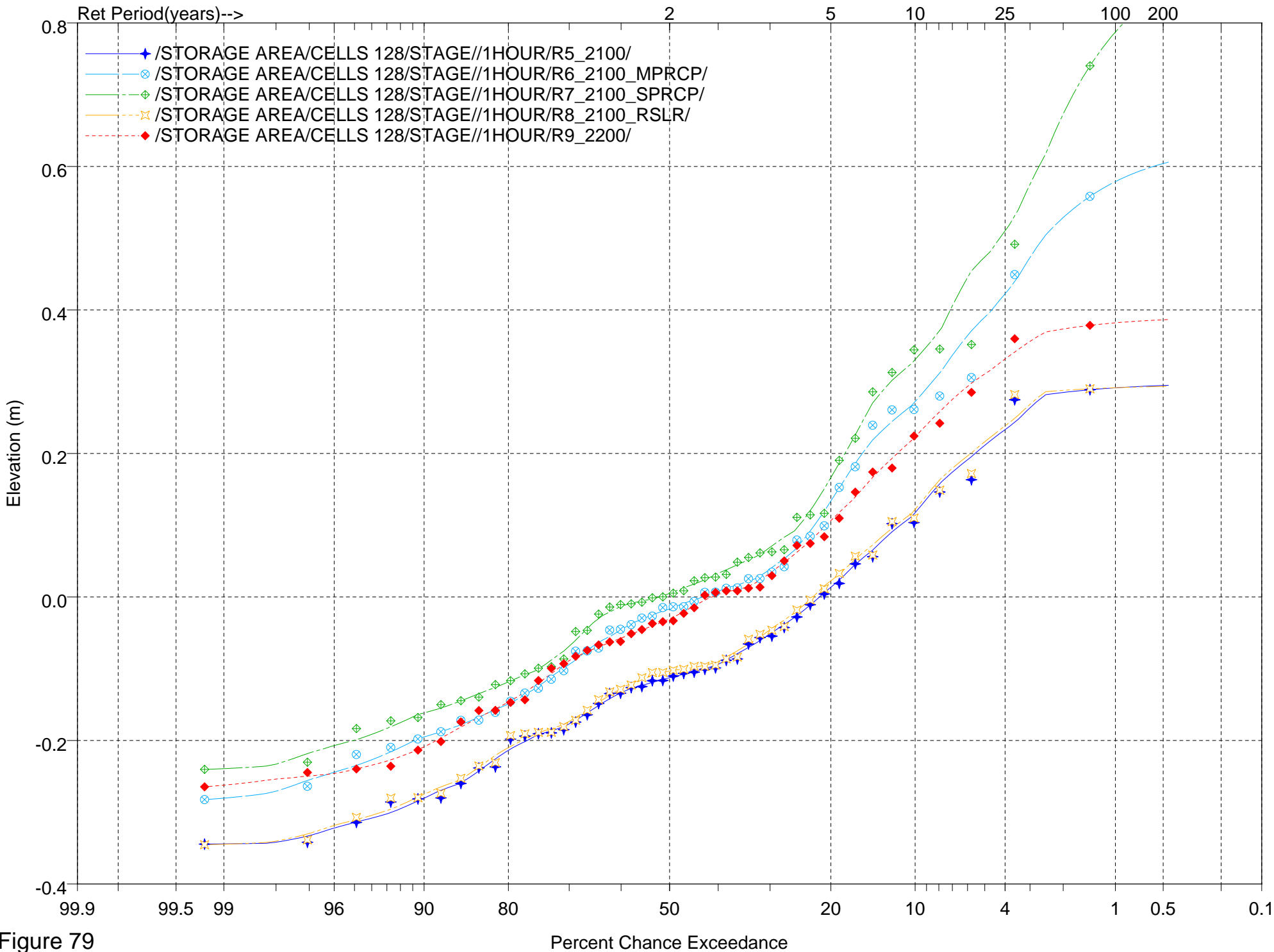


Figure 79

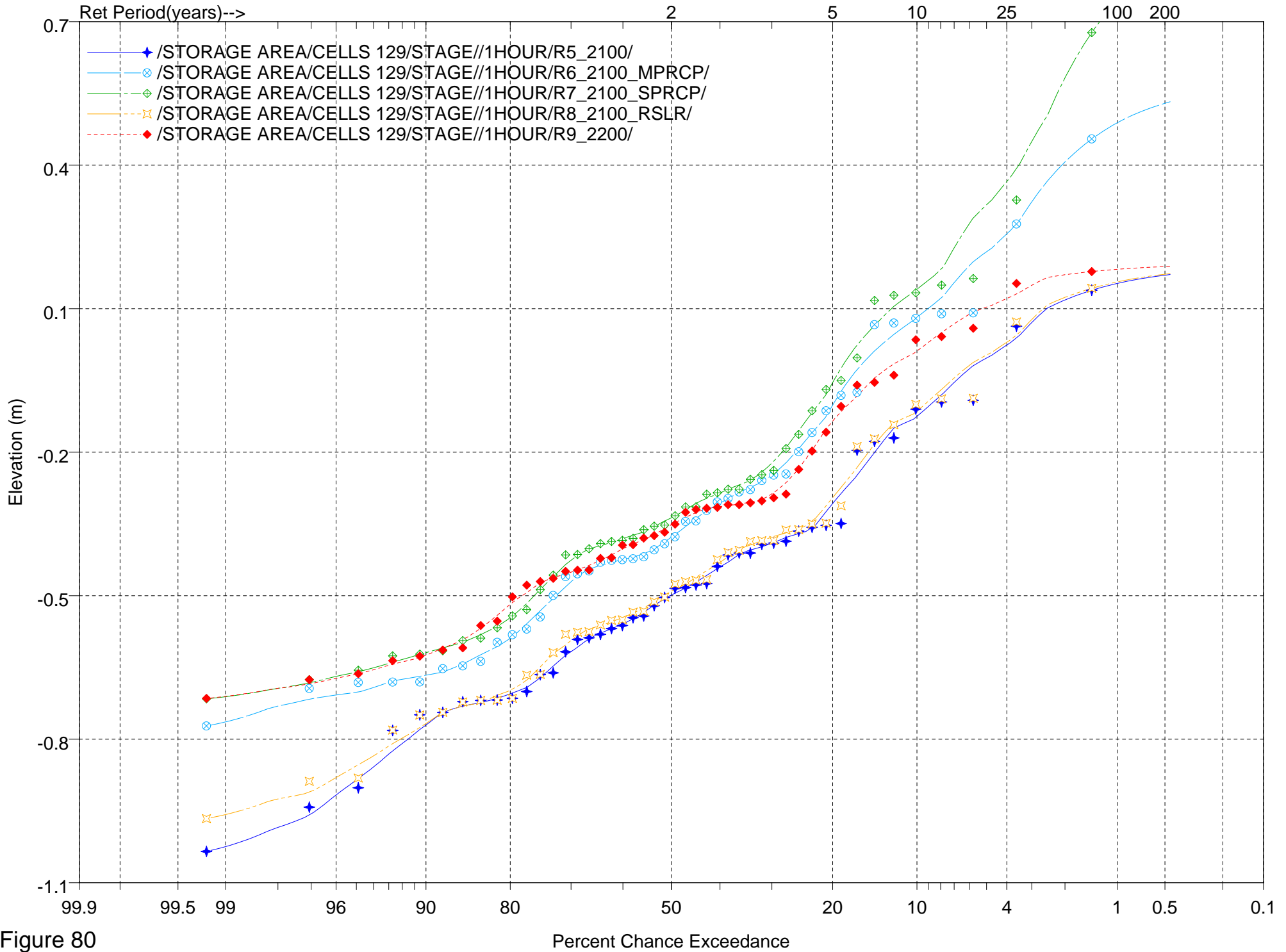


Figure 80



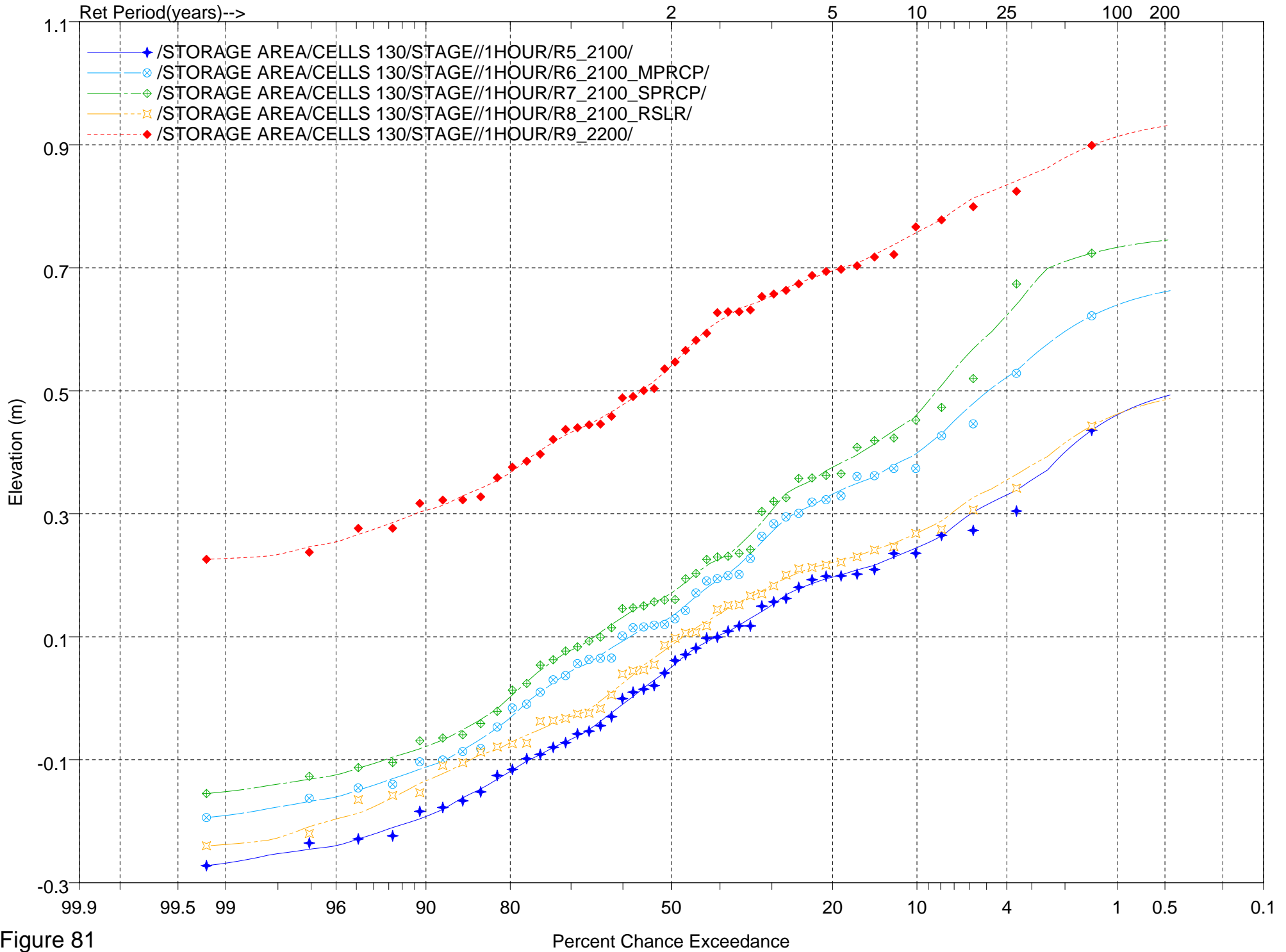


Figure 81

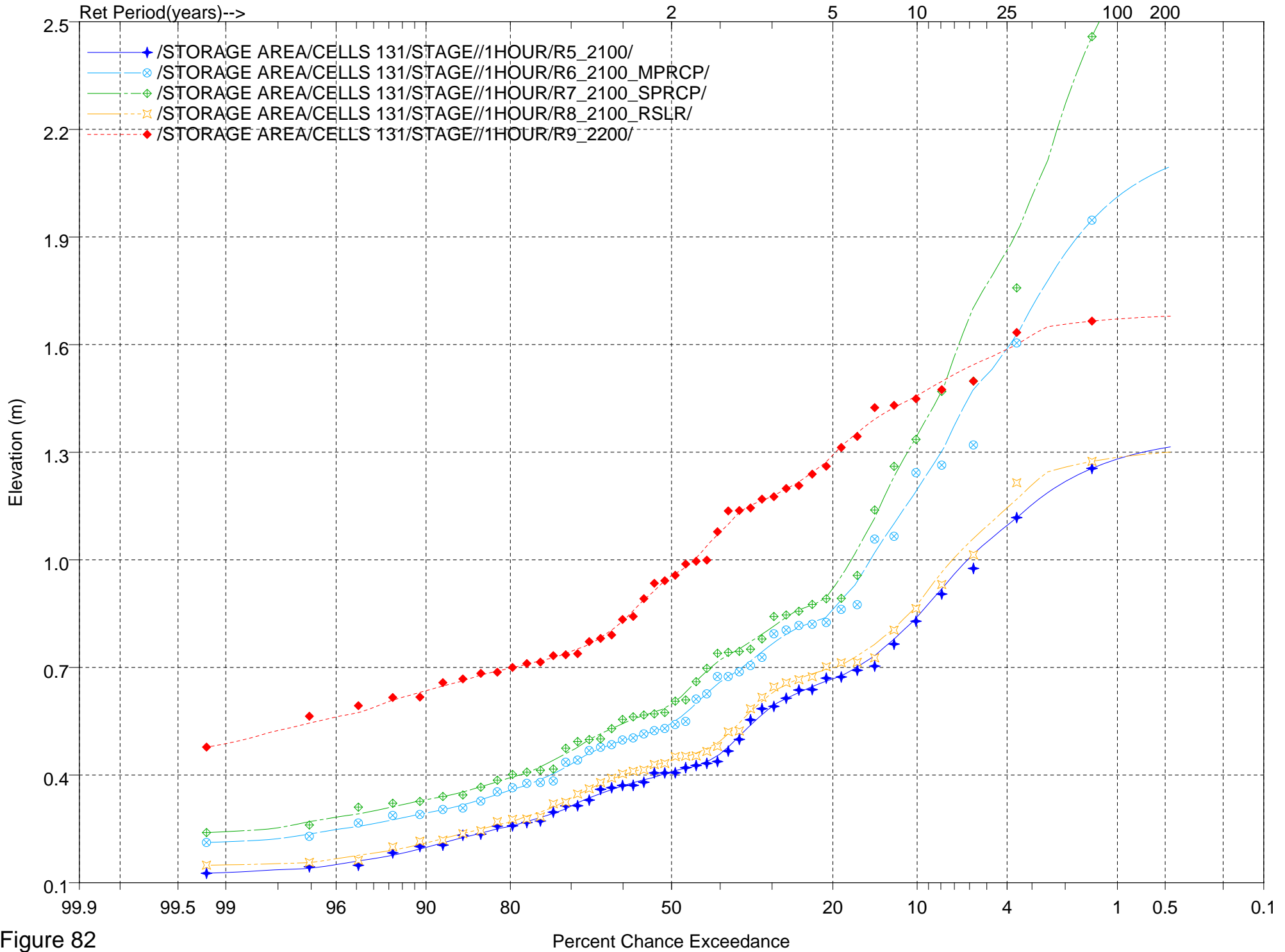


Figure 82

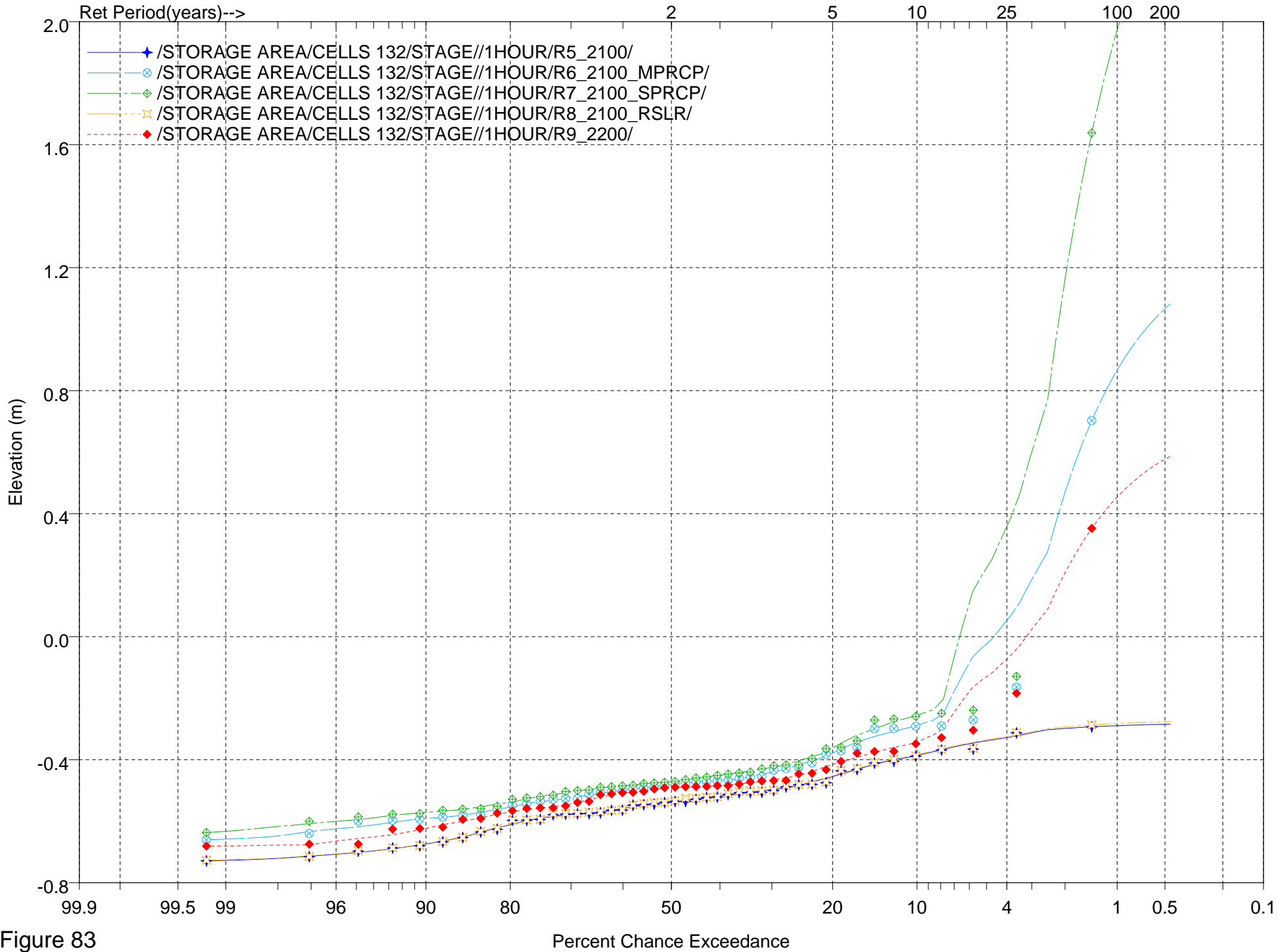


Figure 83

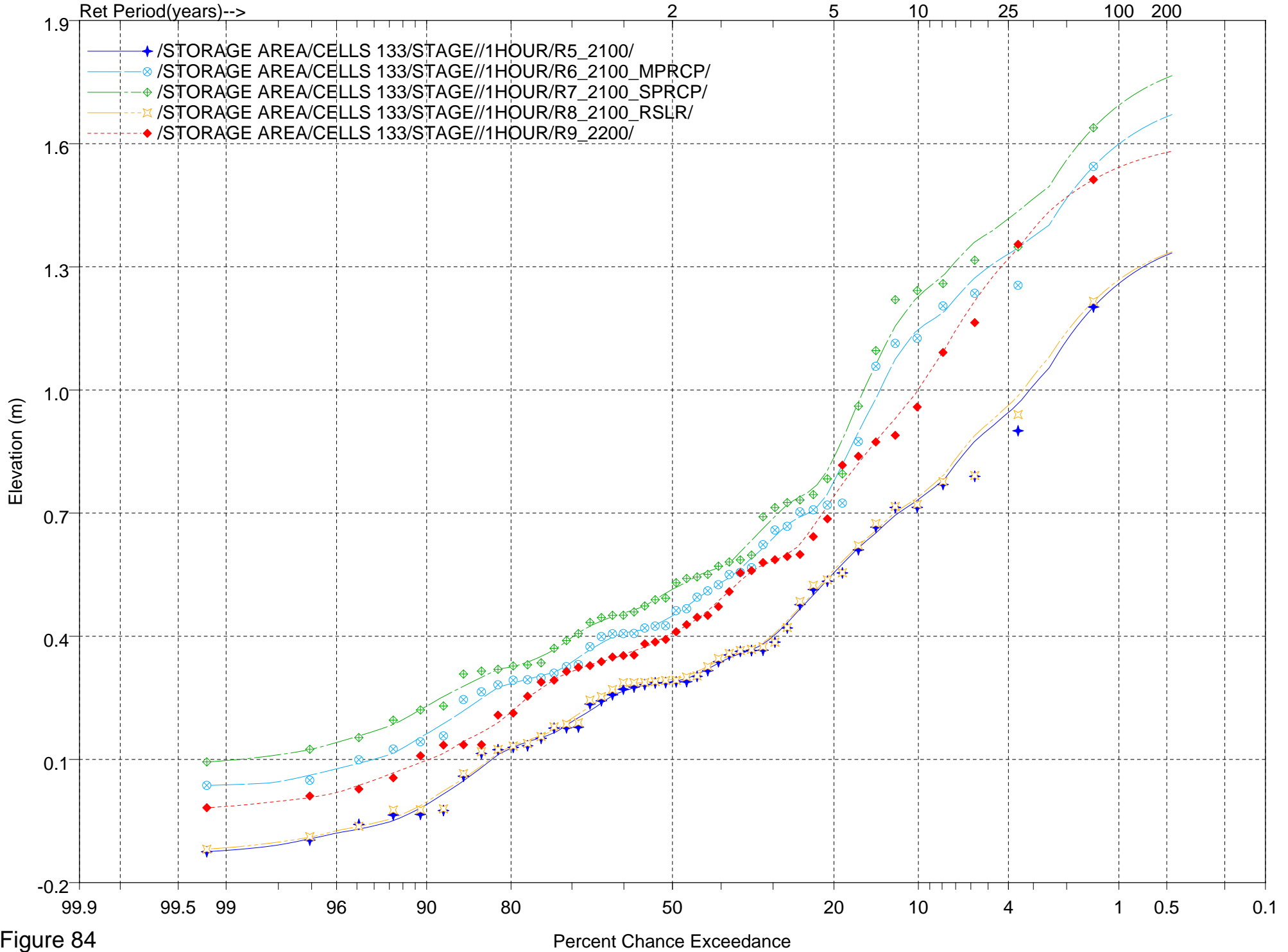


Figure 84

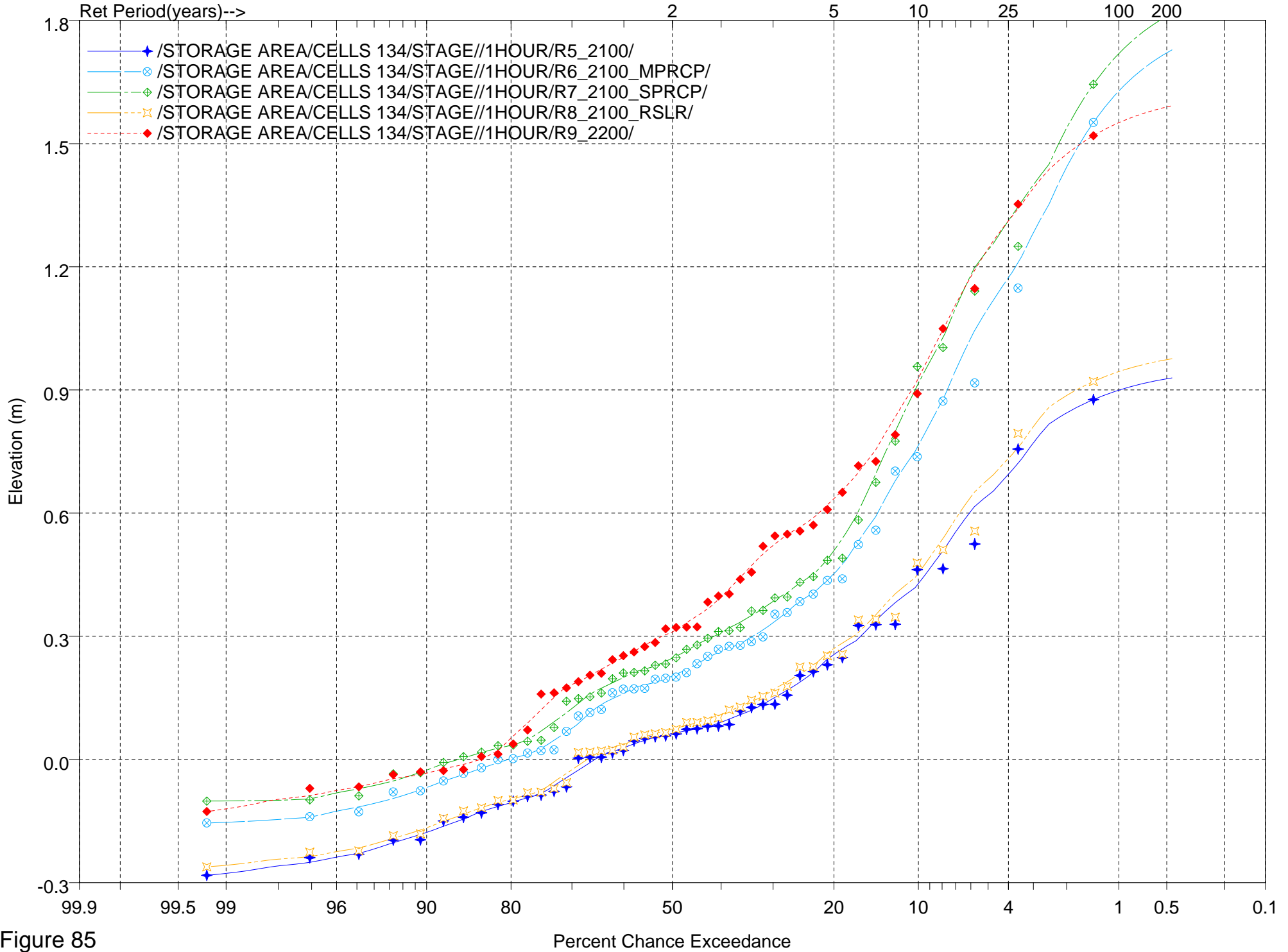


Figure 85

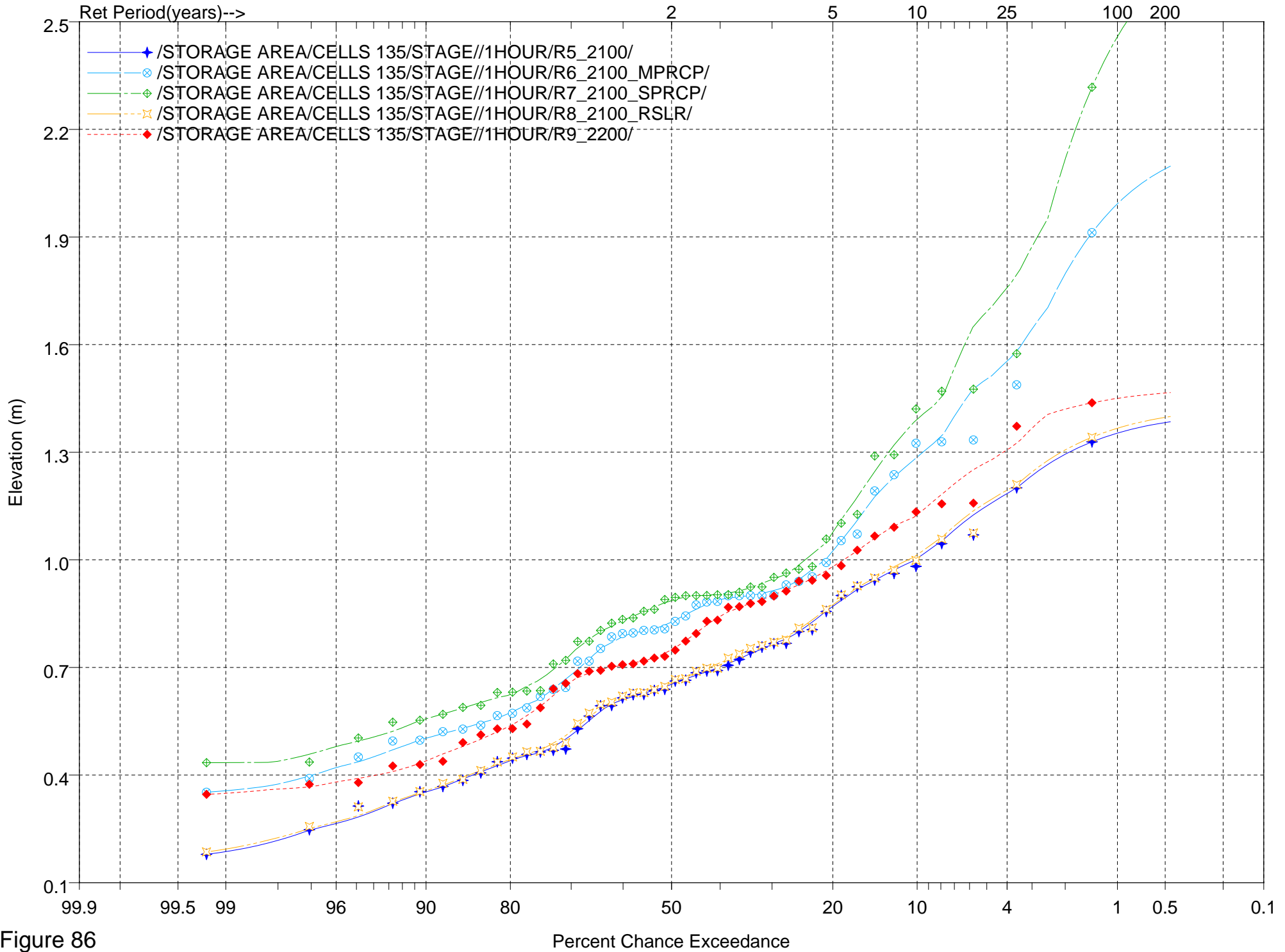


Figure 86

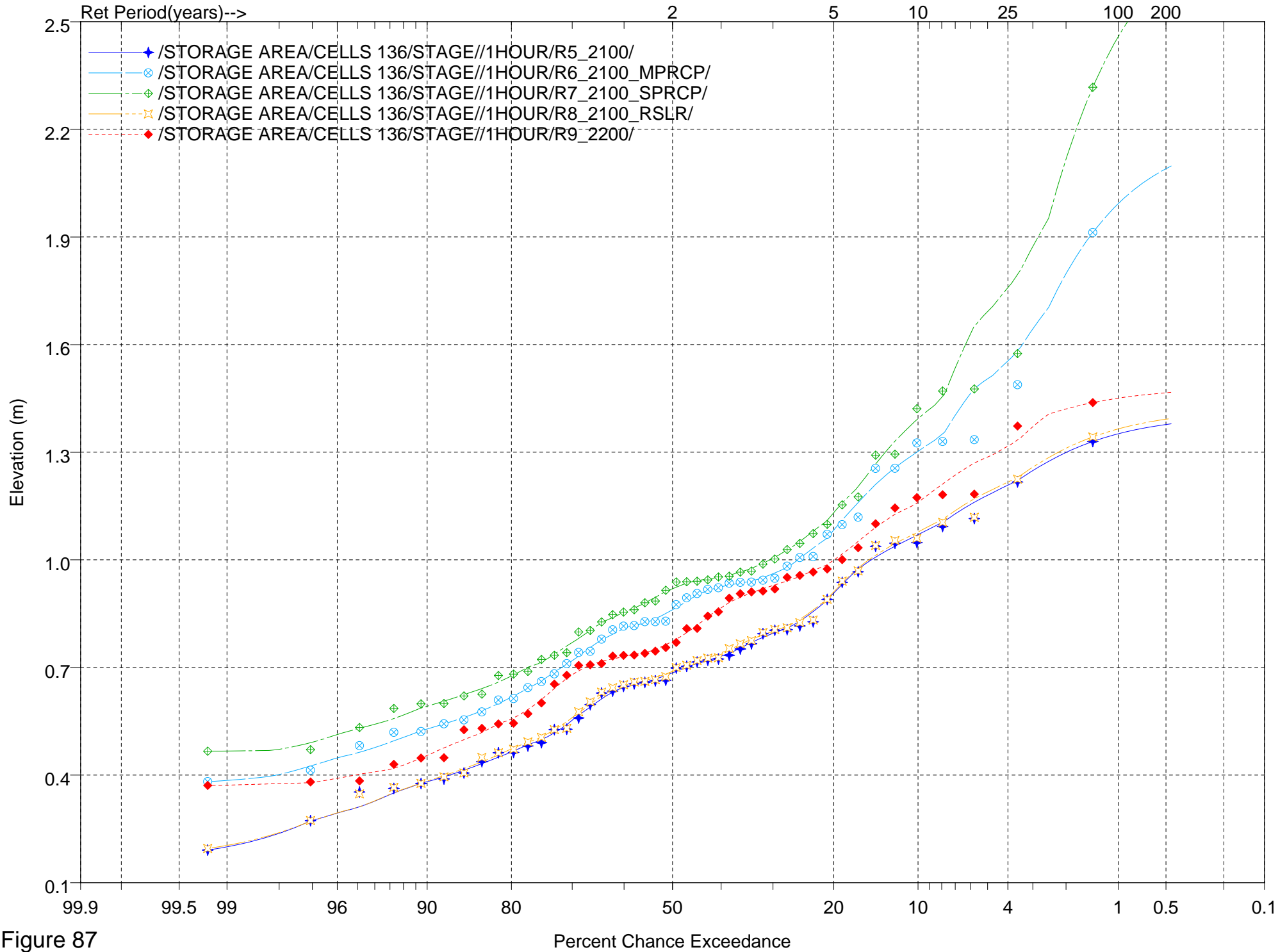


Figure 87

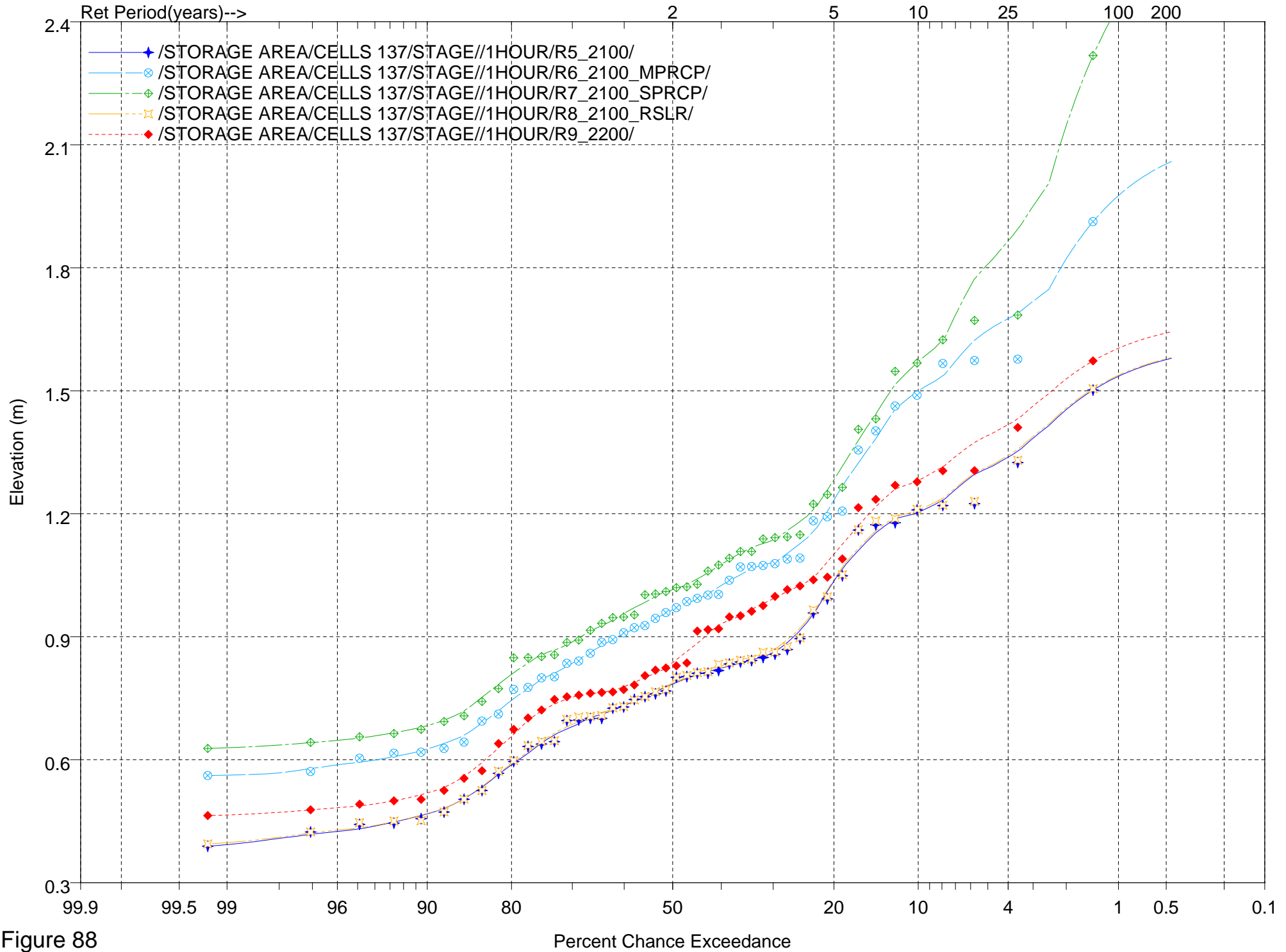


Figure 88



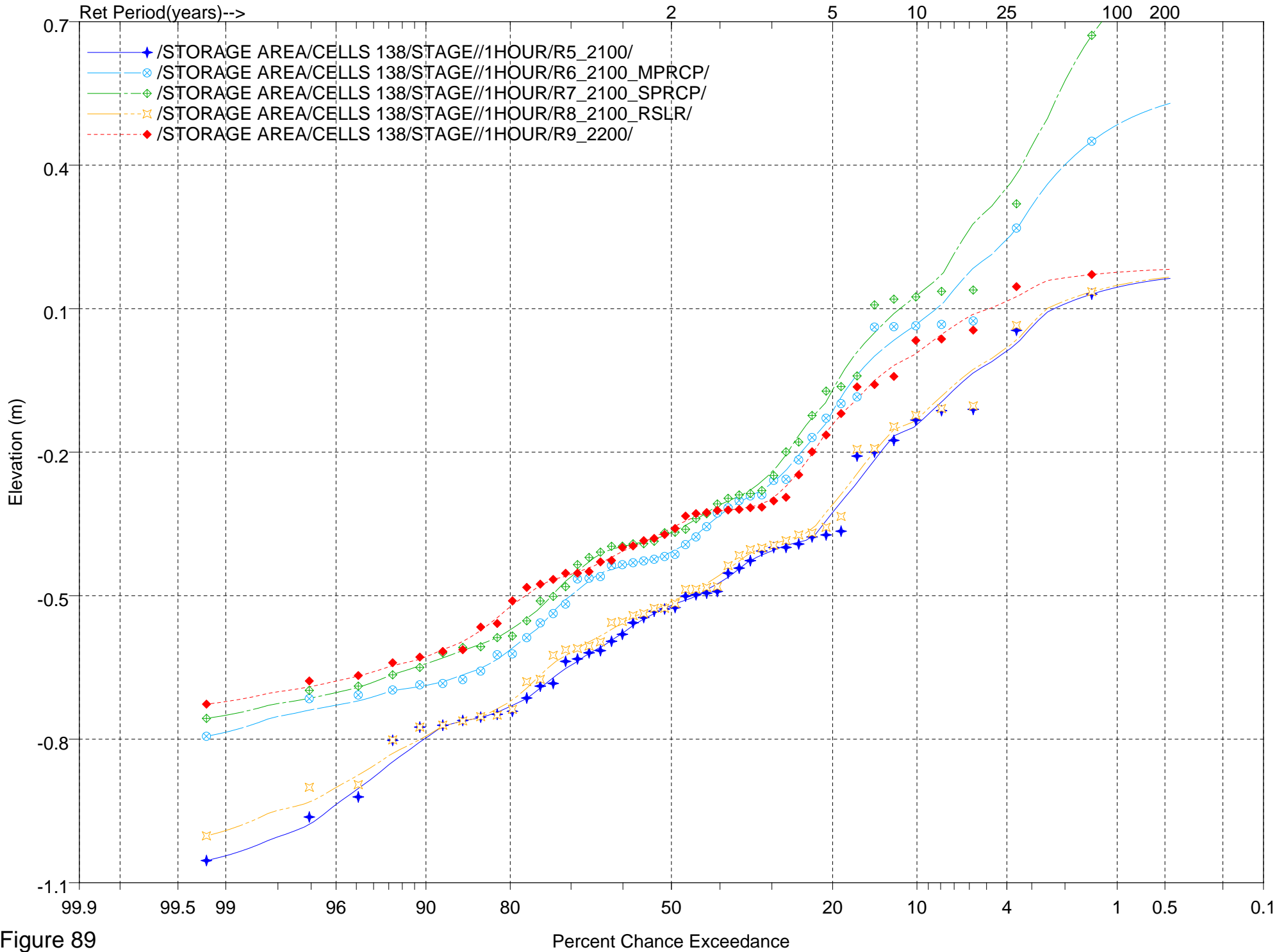


Figure 89

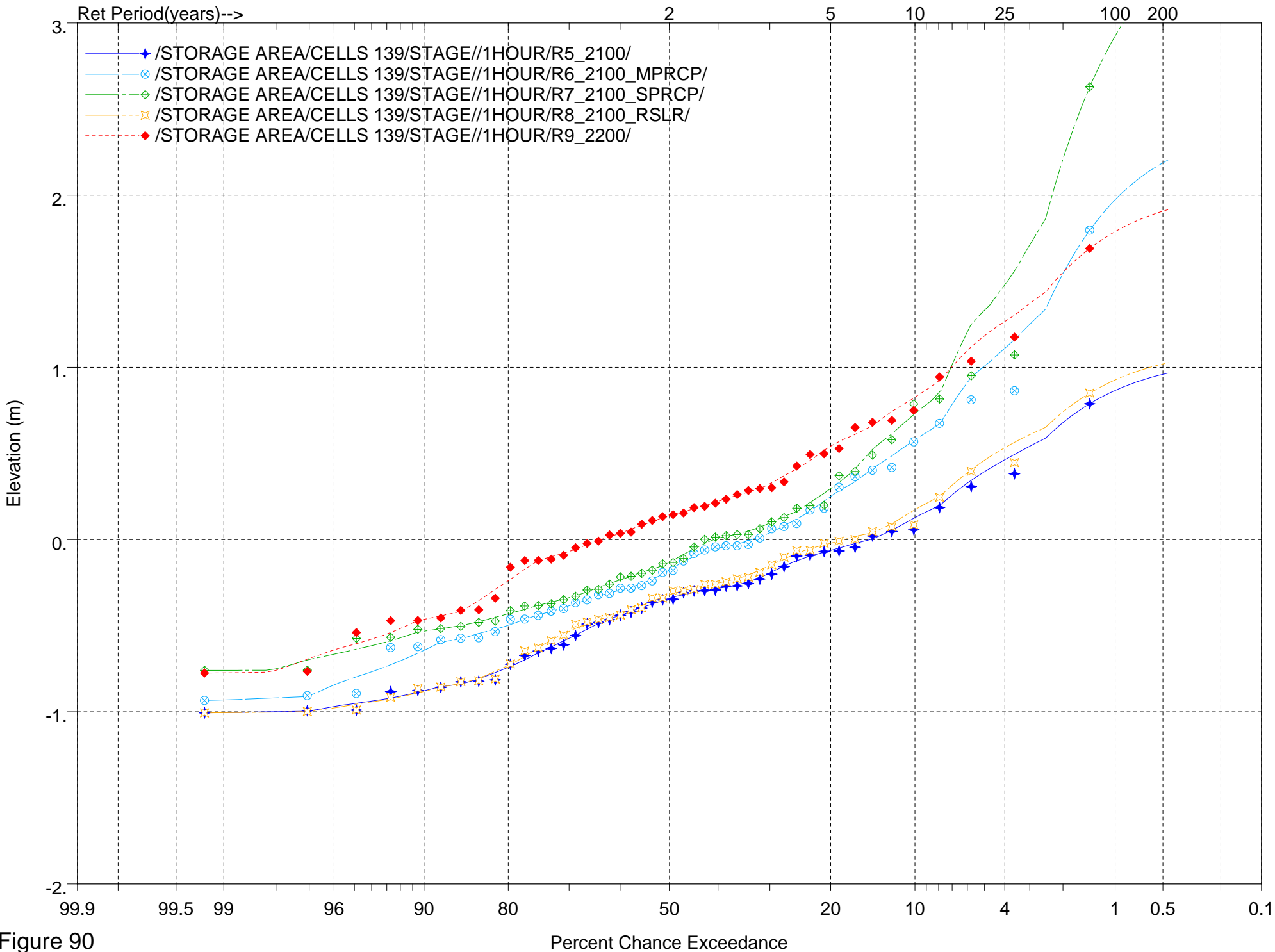


Figure 90

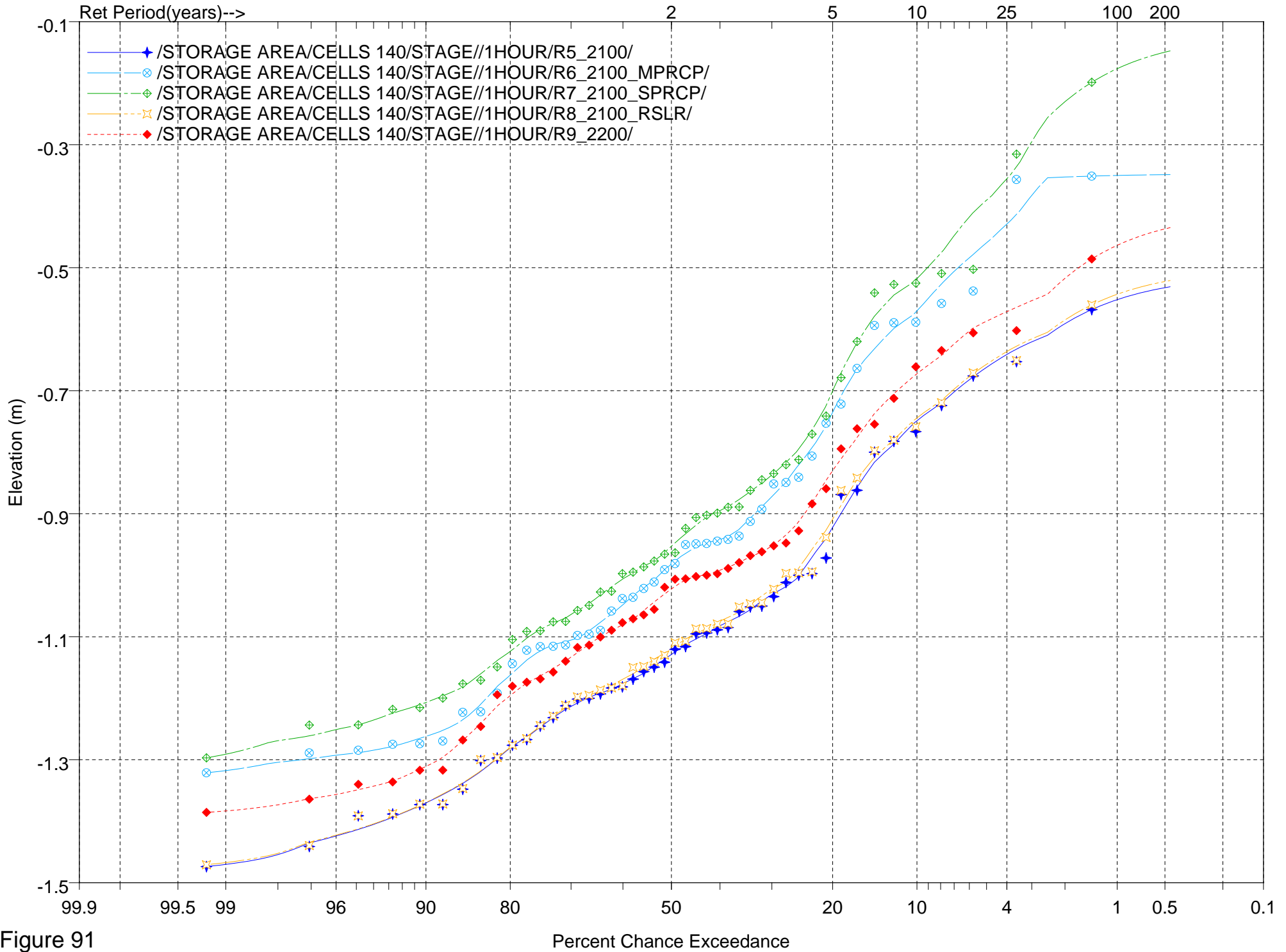


Figure 91

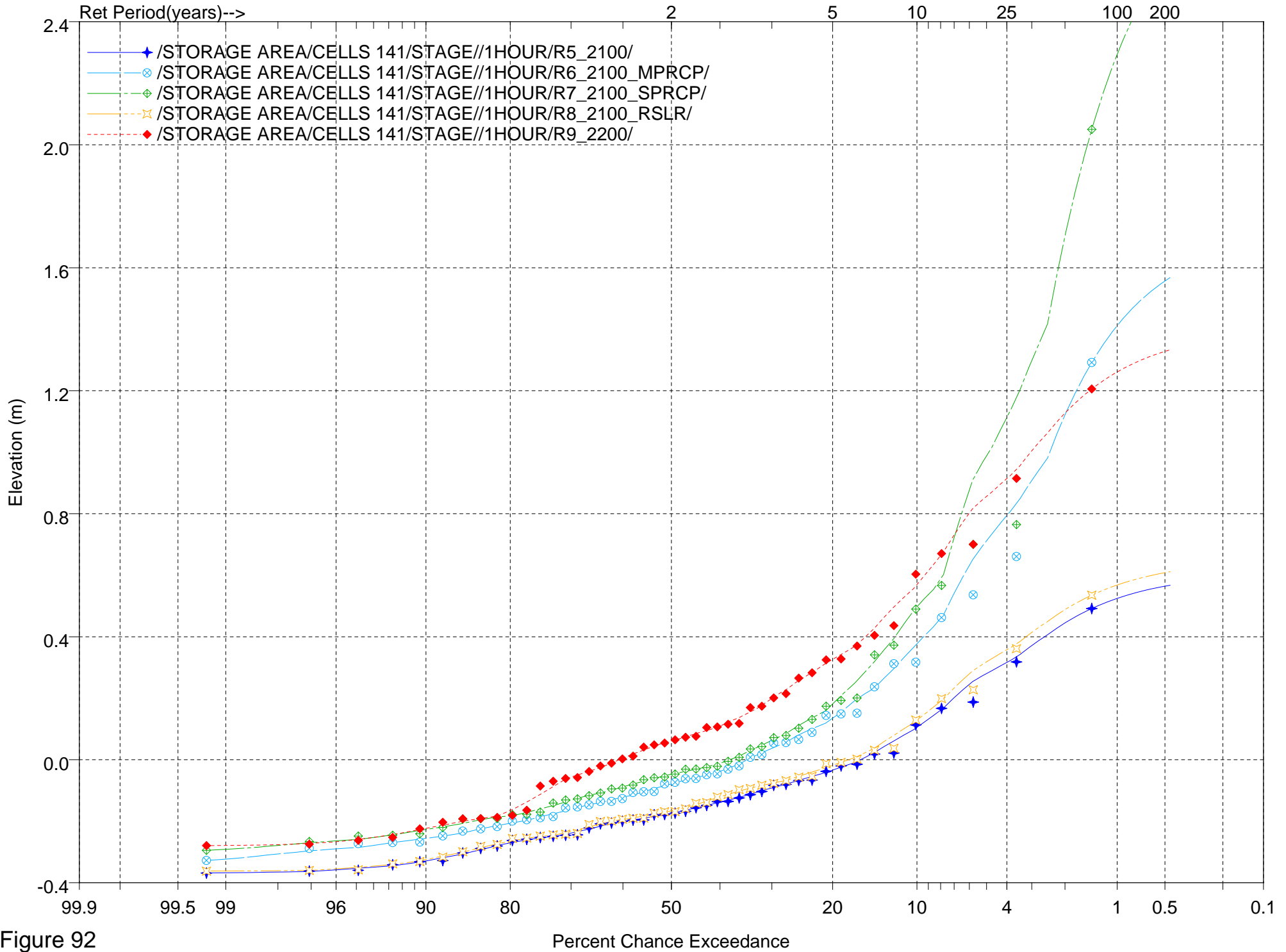


Figure 92

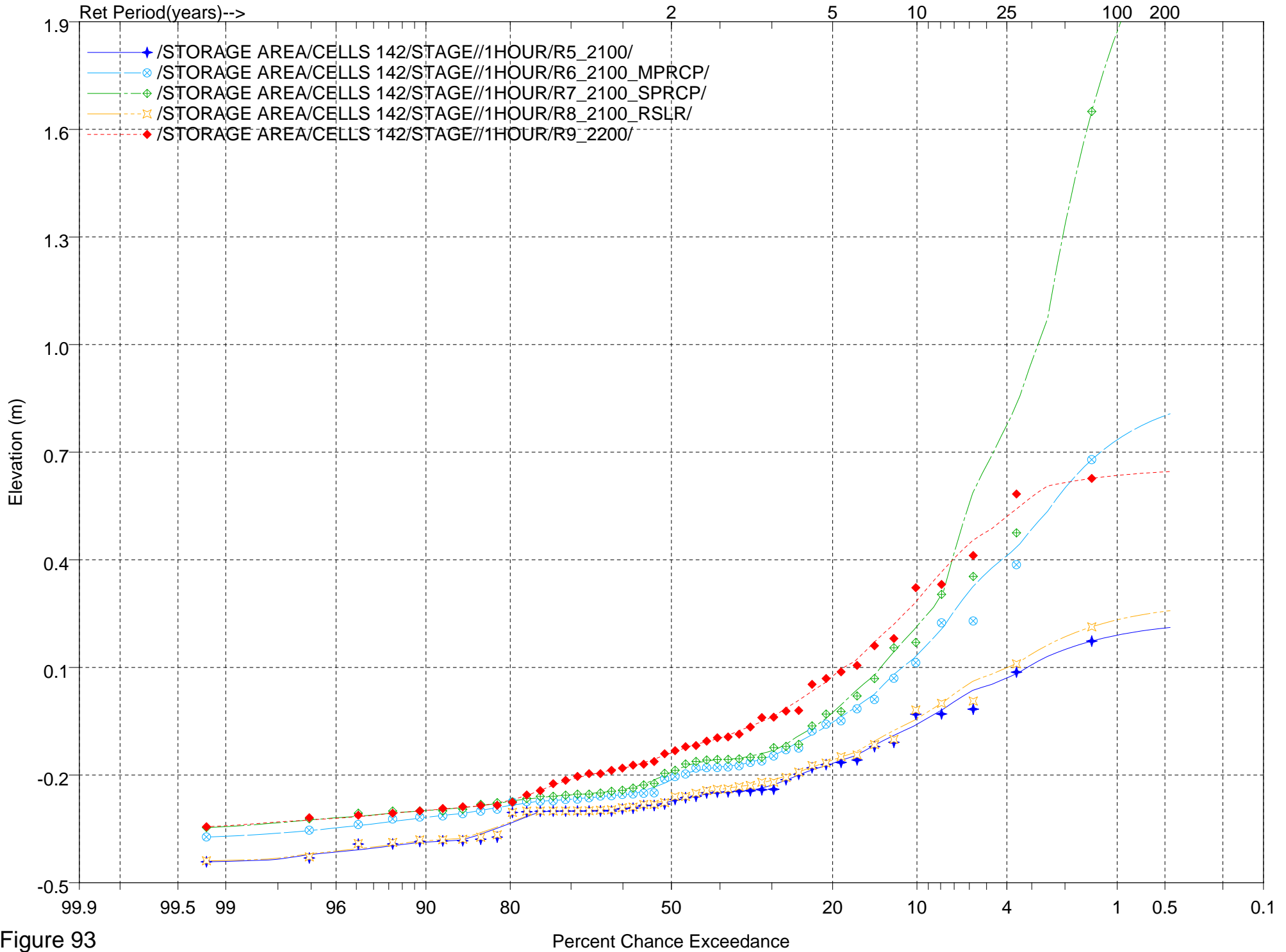


Figure 93

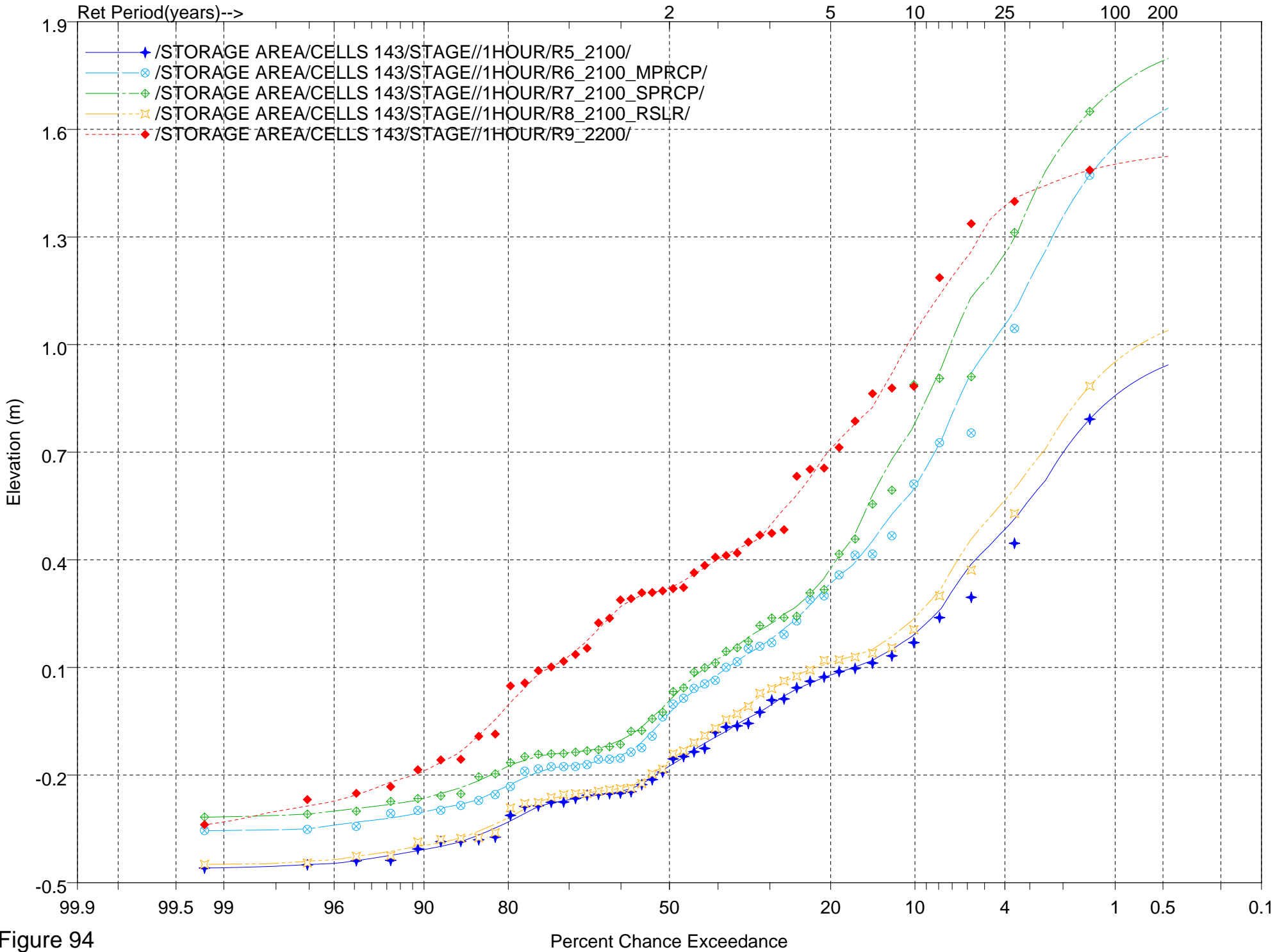


Figure 94

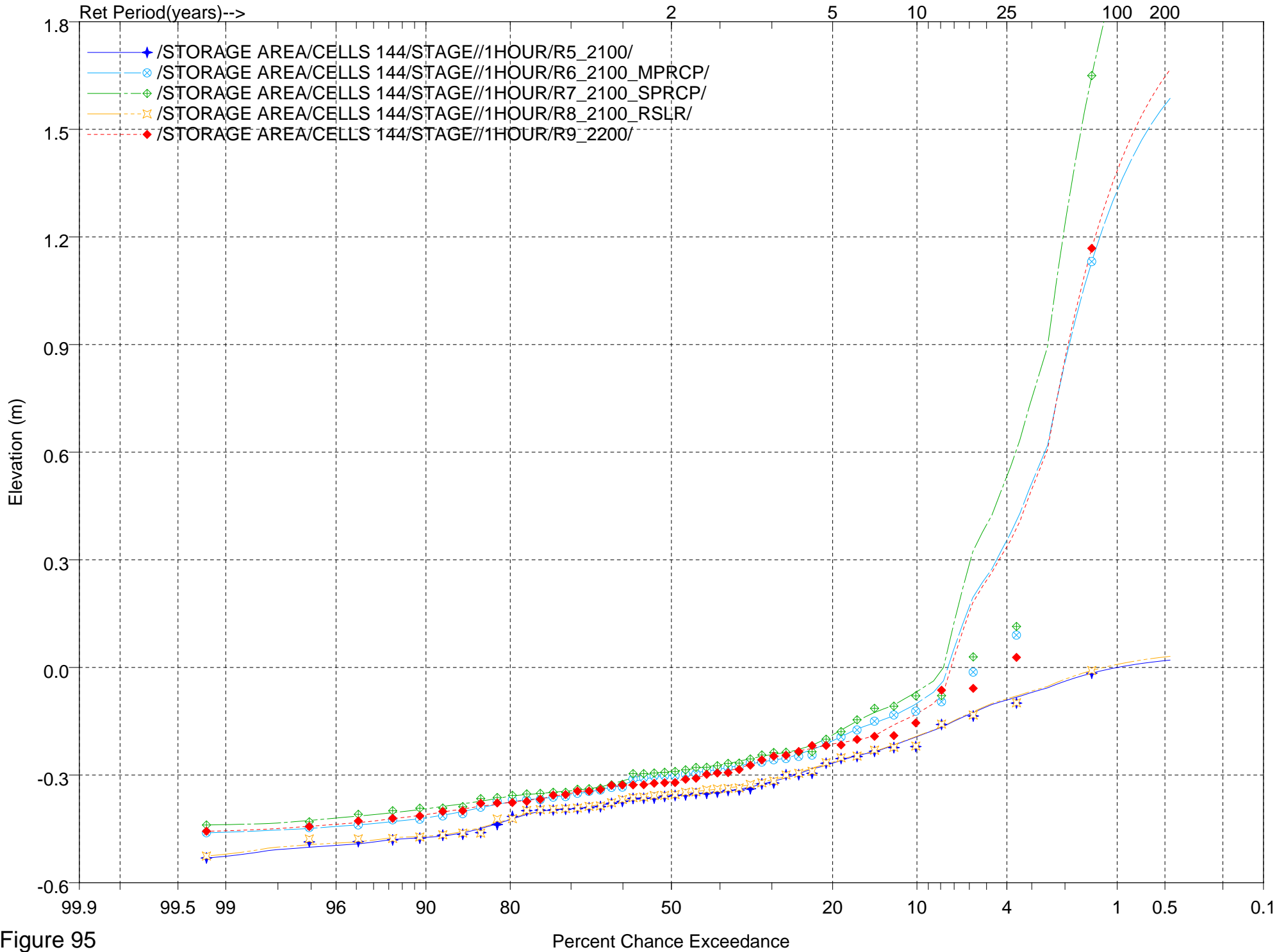


Figure 95

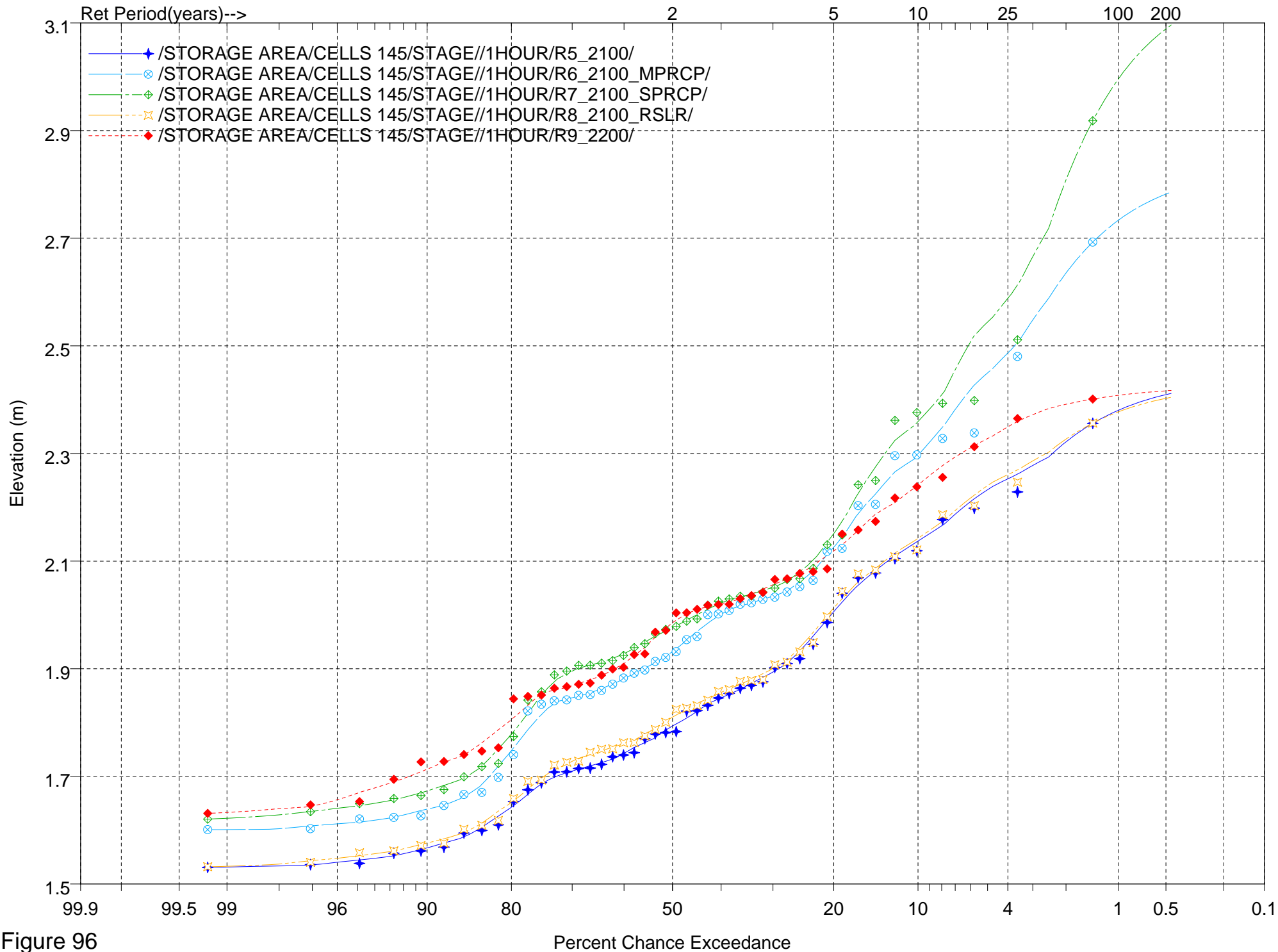


Figure 96



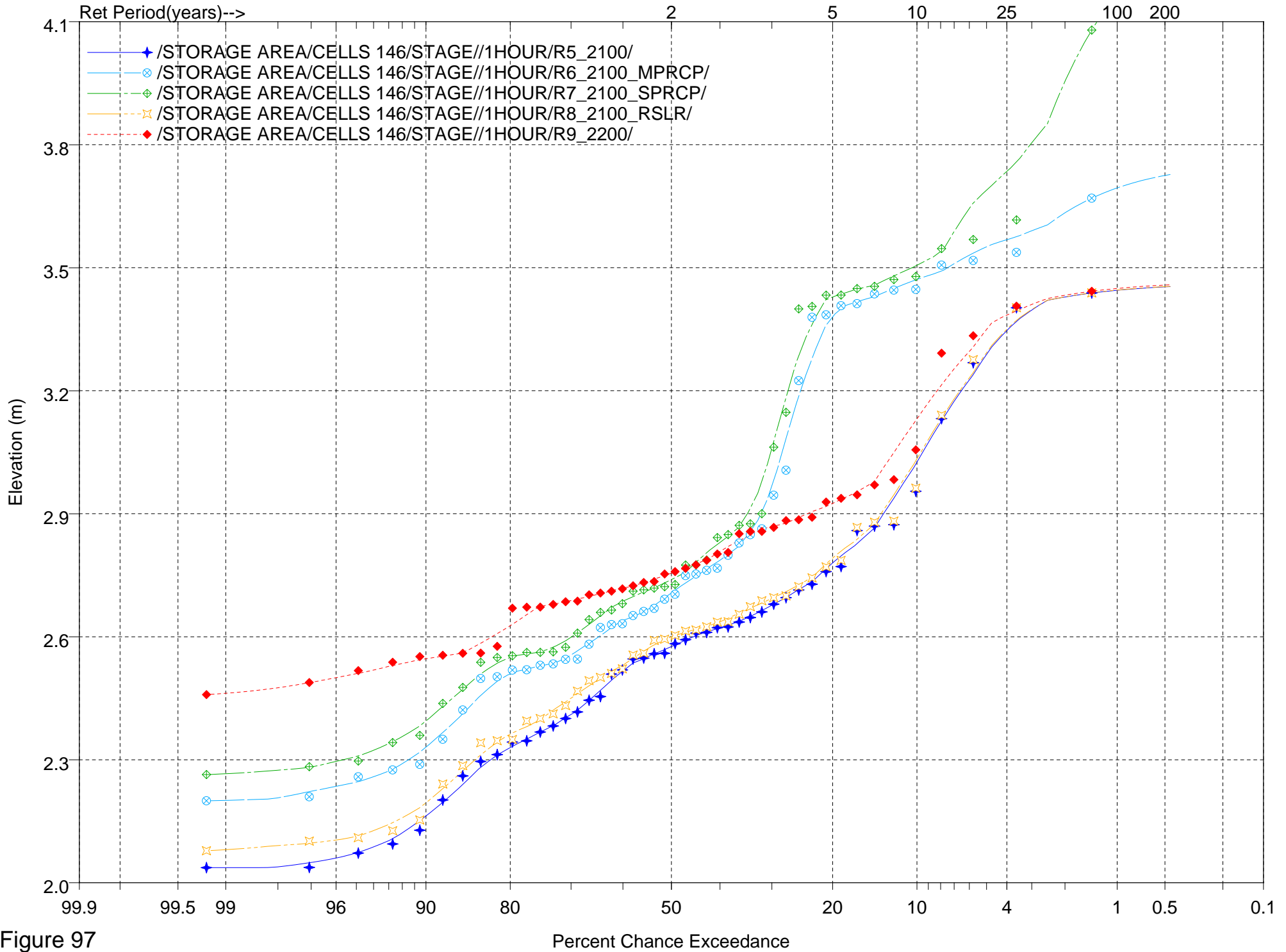
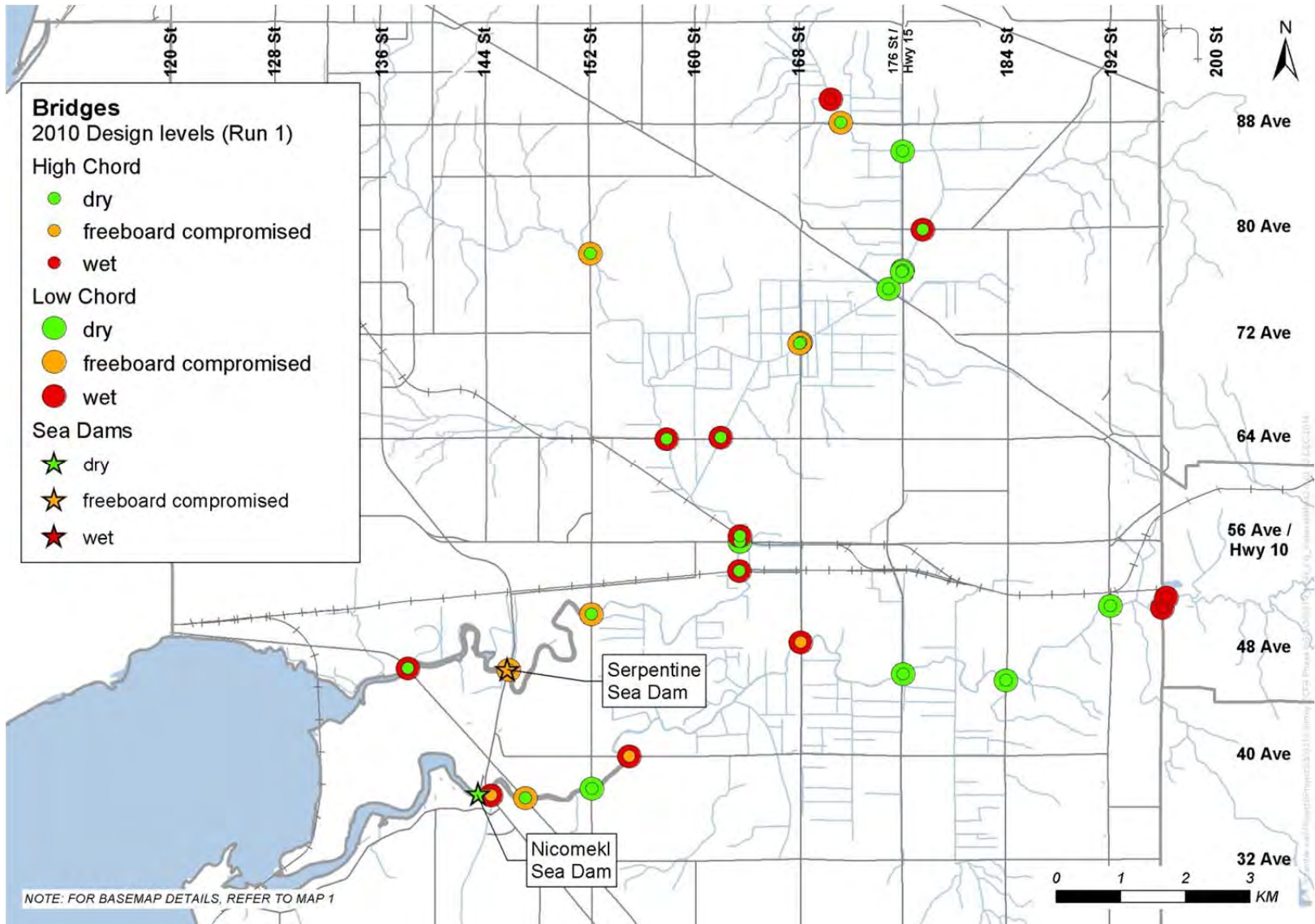
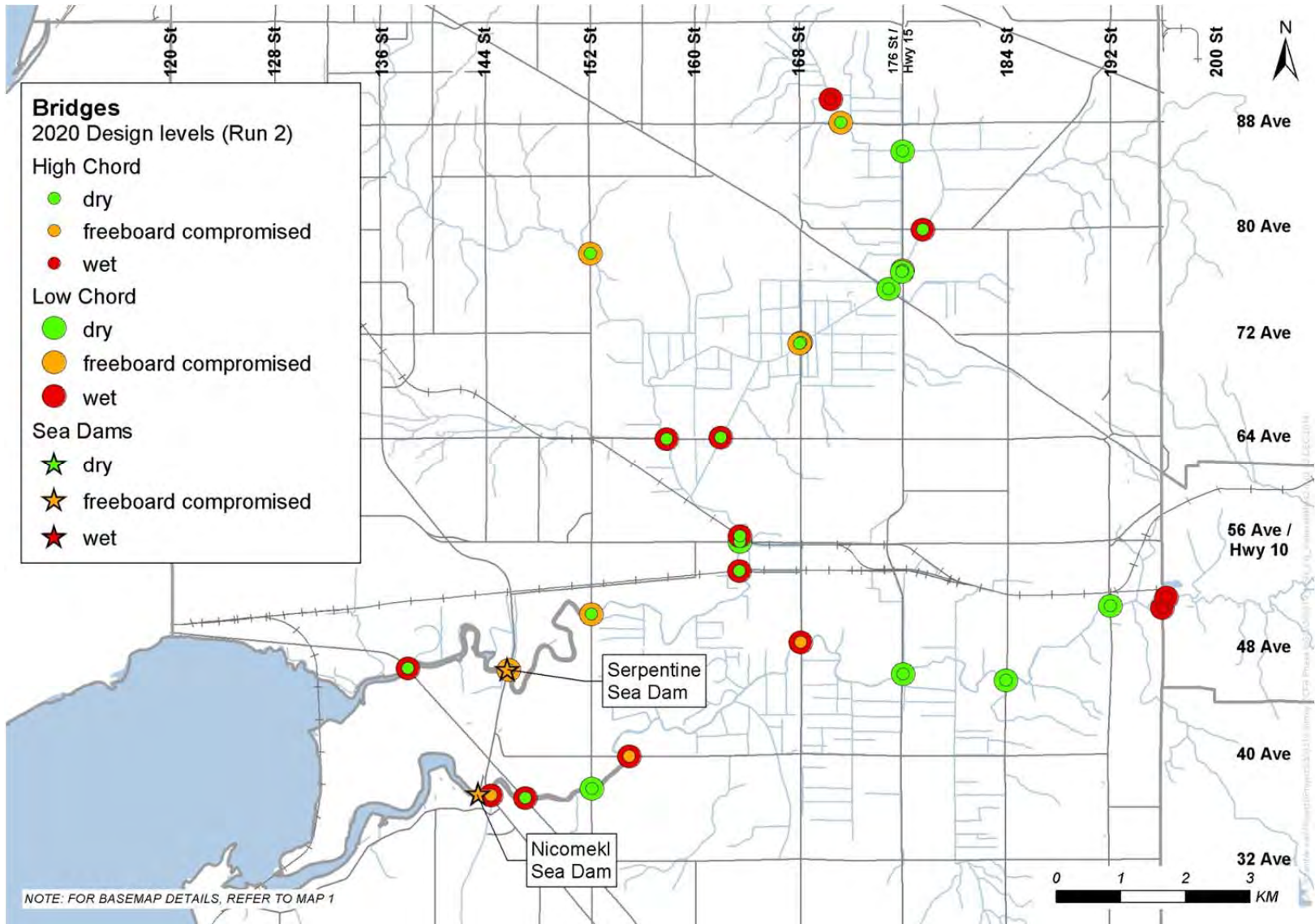


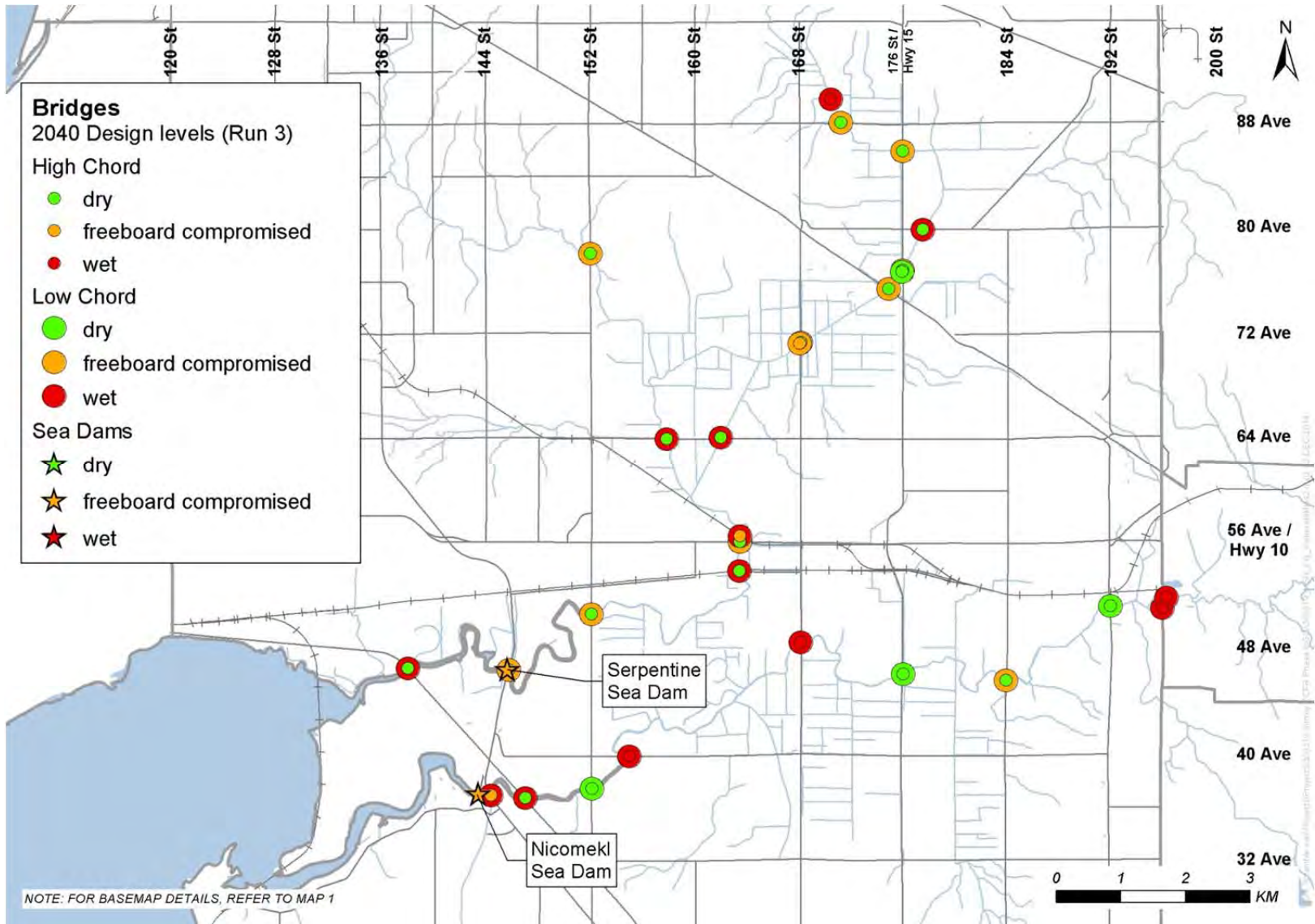
Figure 97

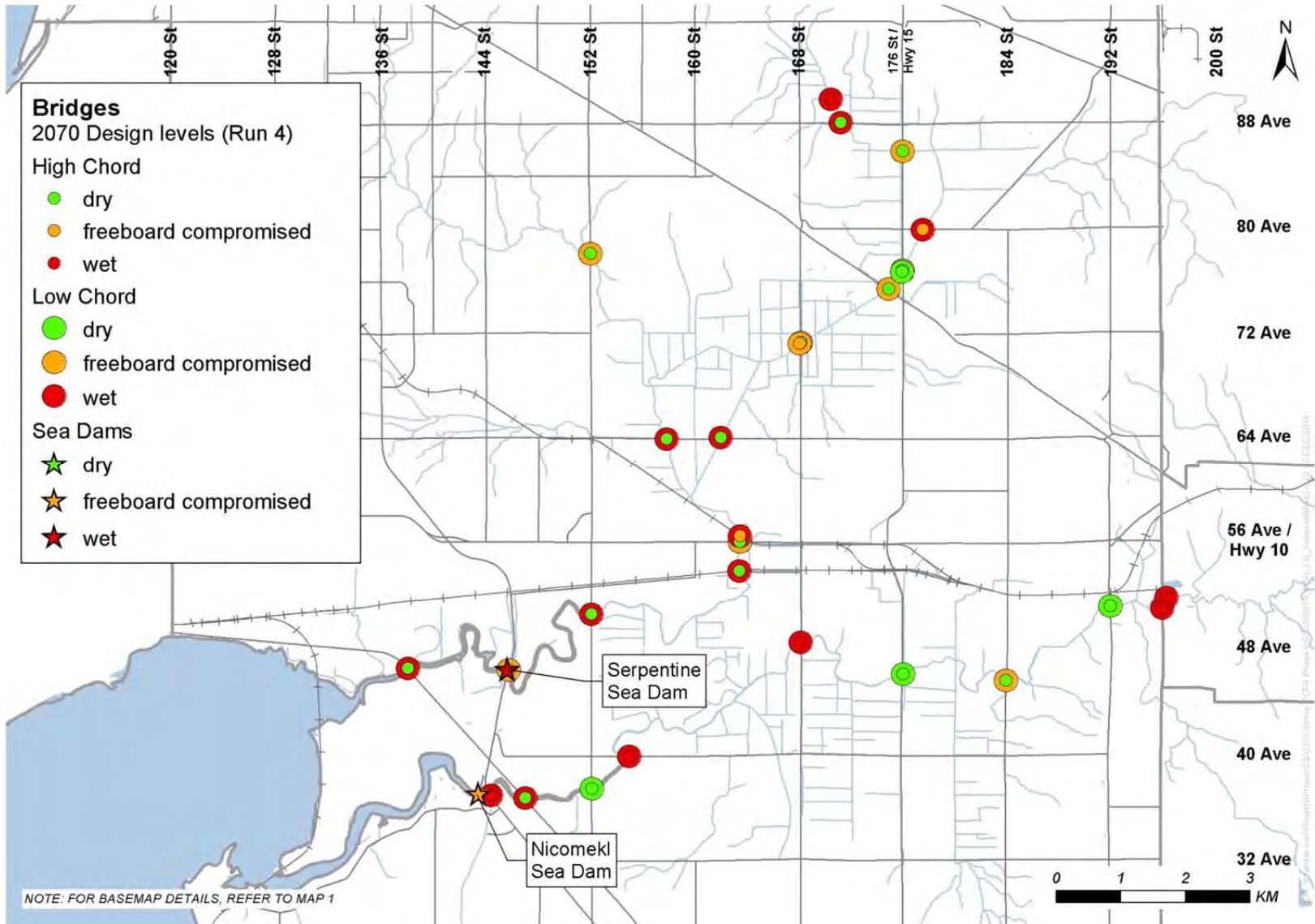
## **APPENDIX F**

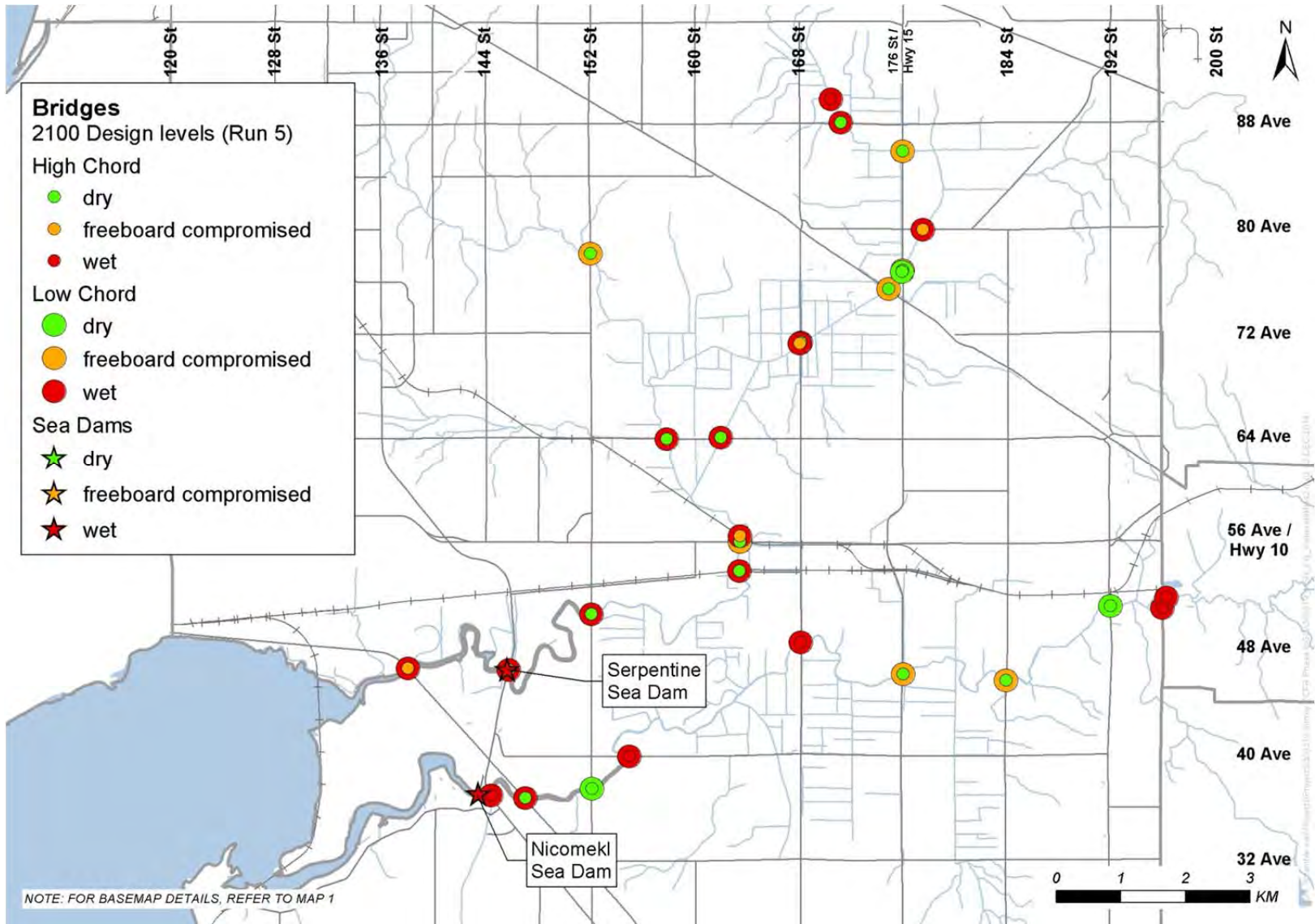
Vulnerability Assessment

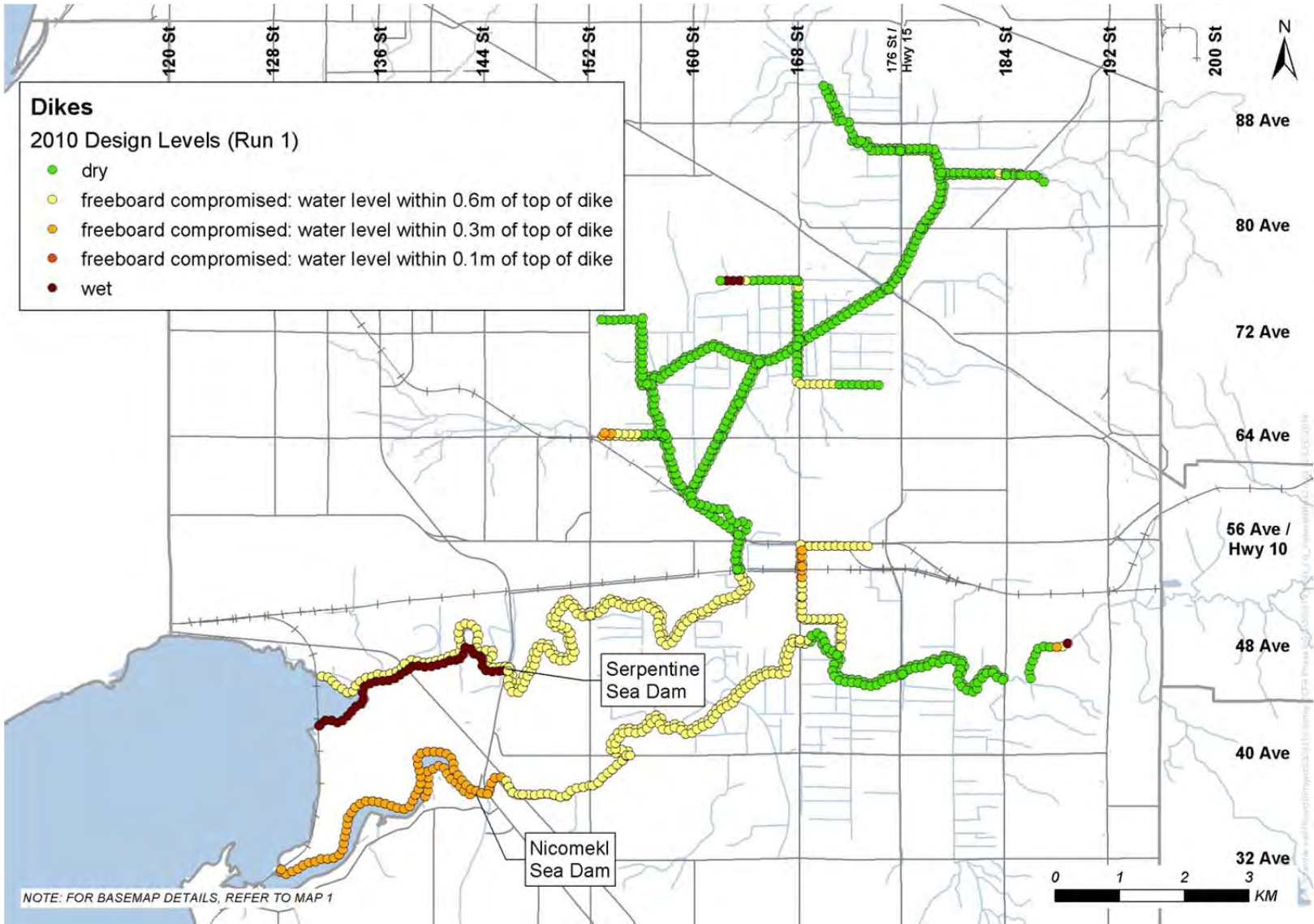




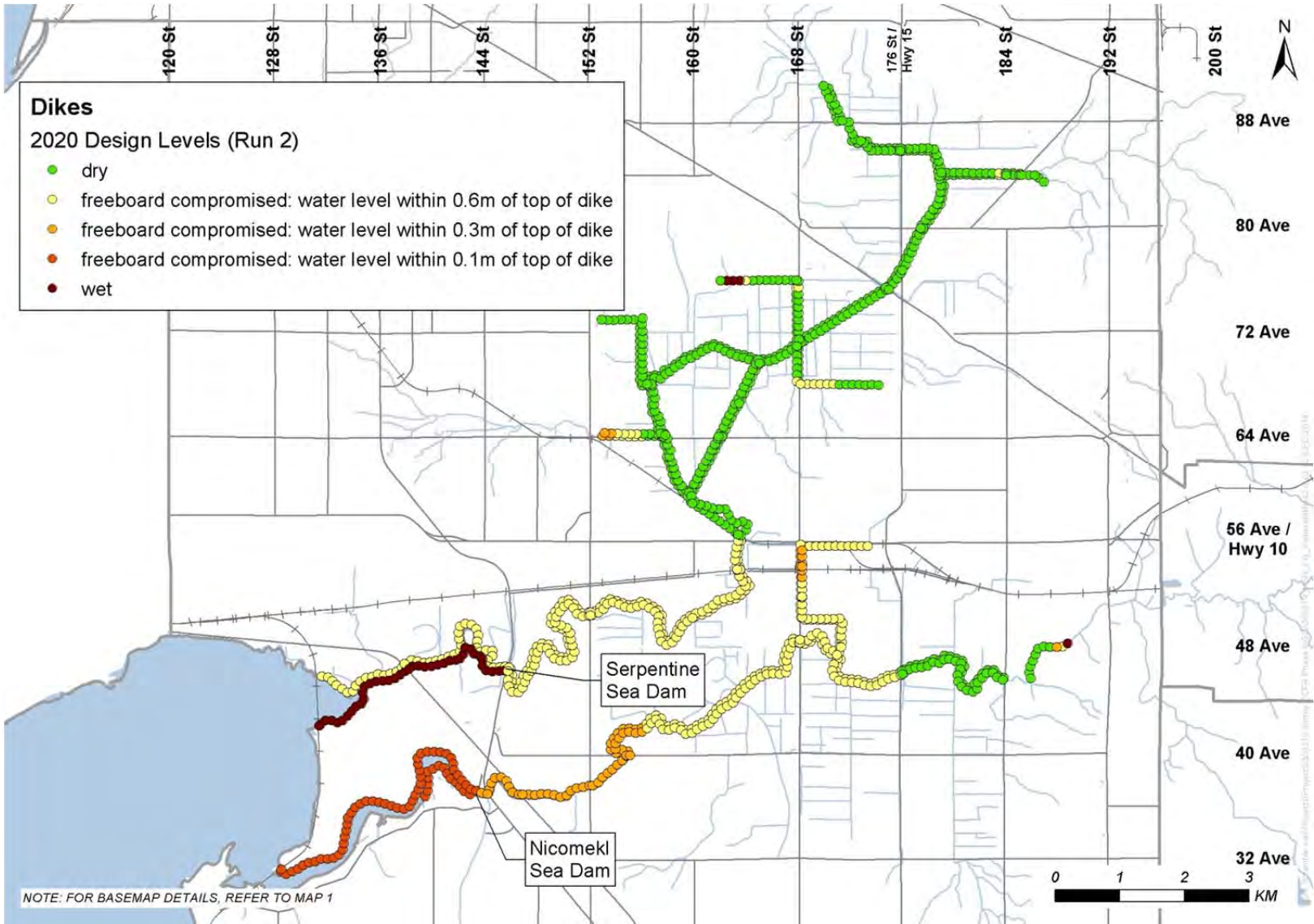


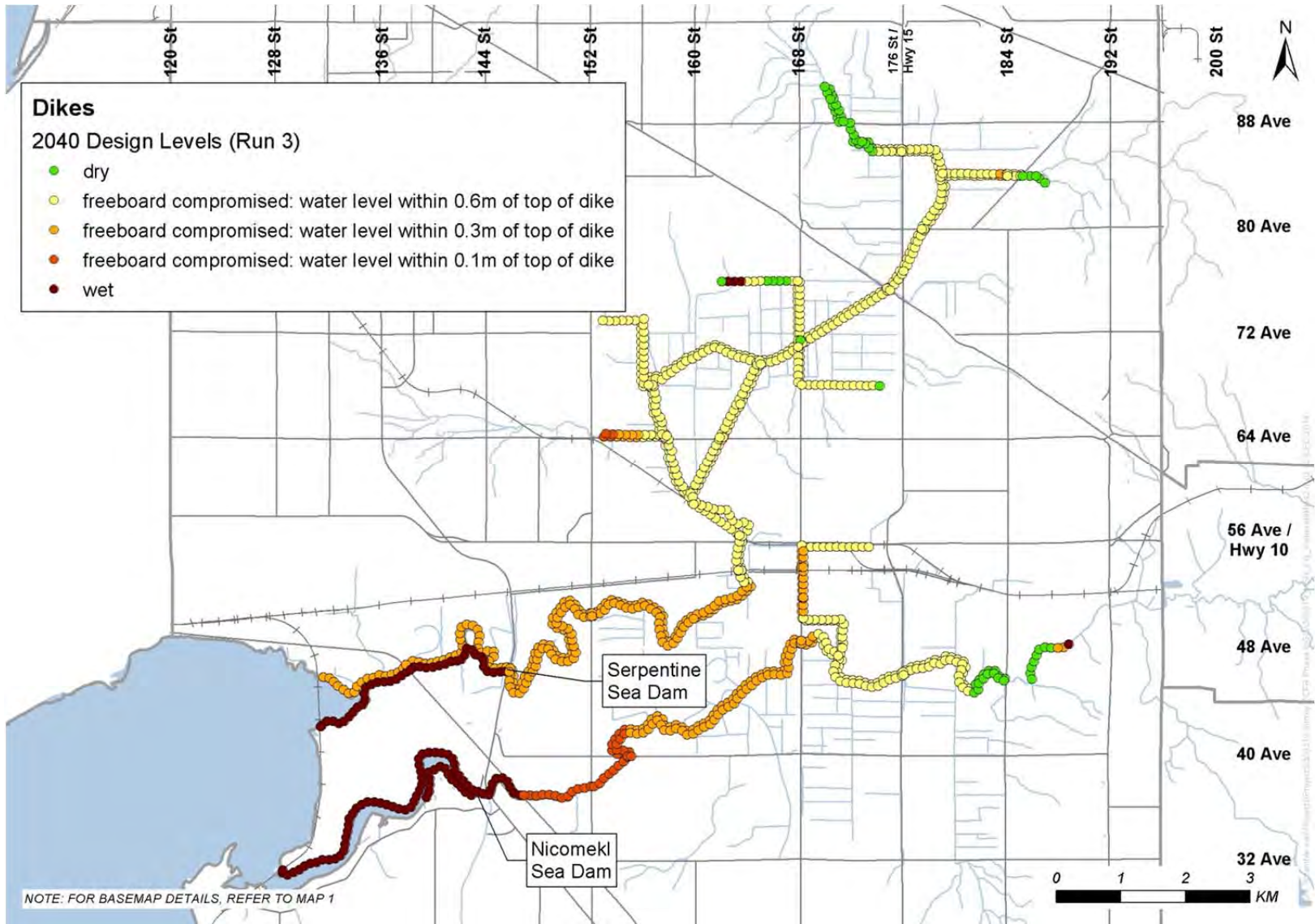


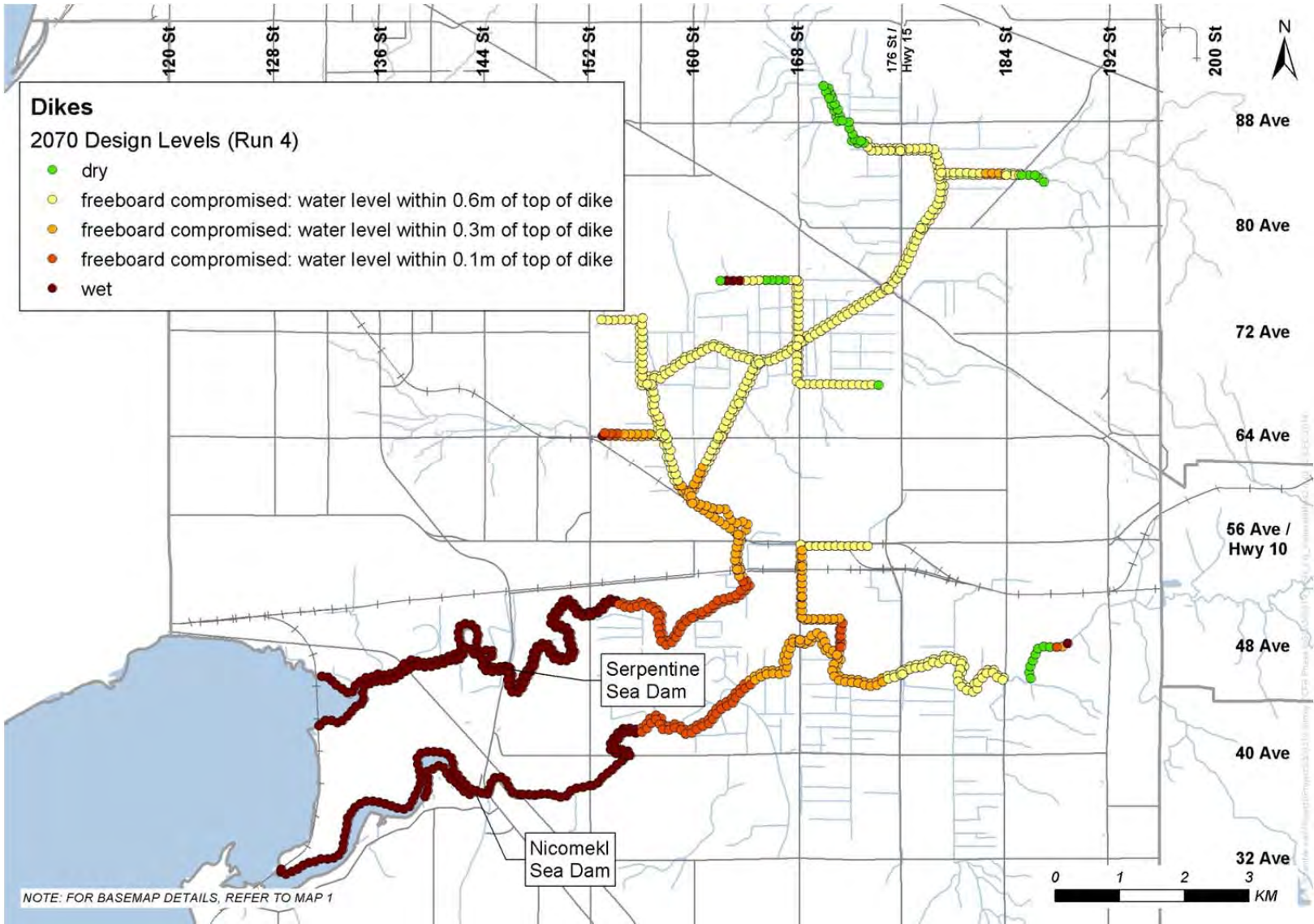


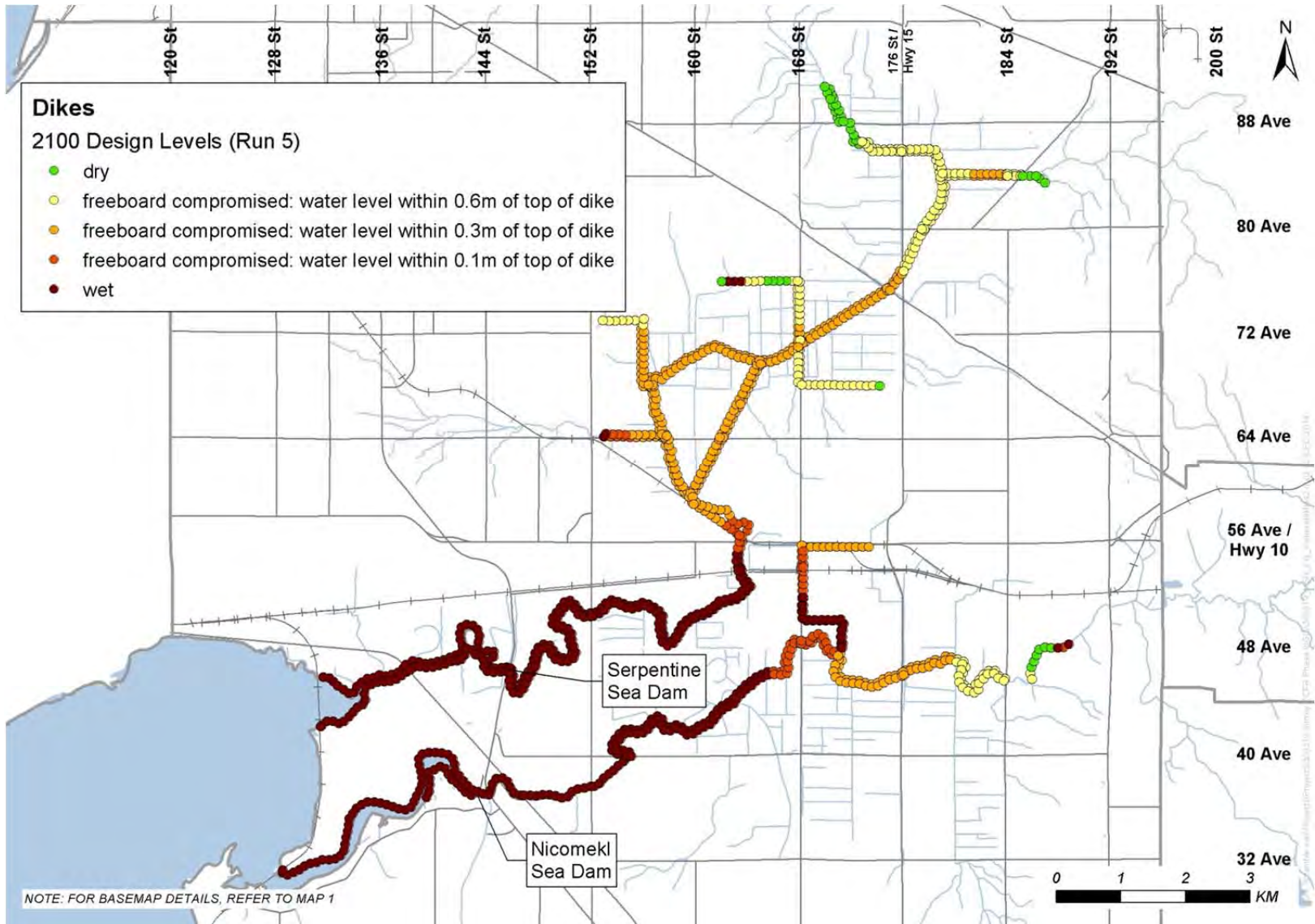


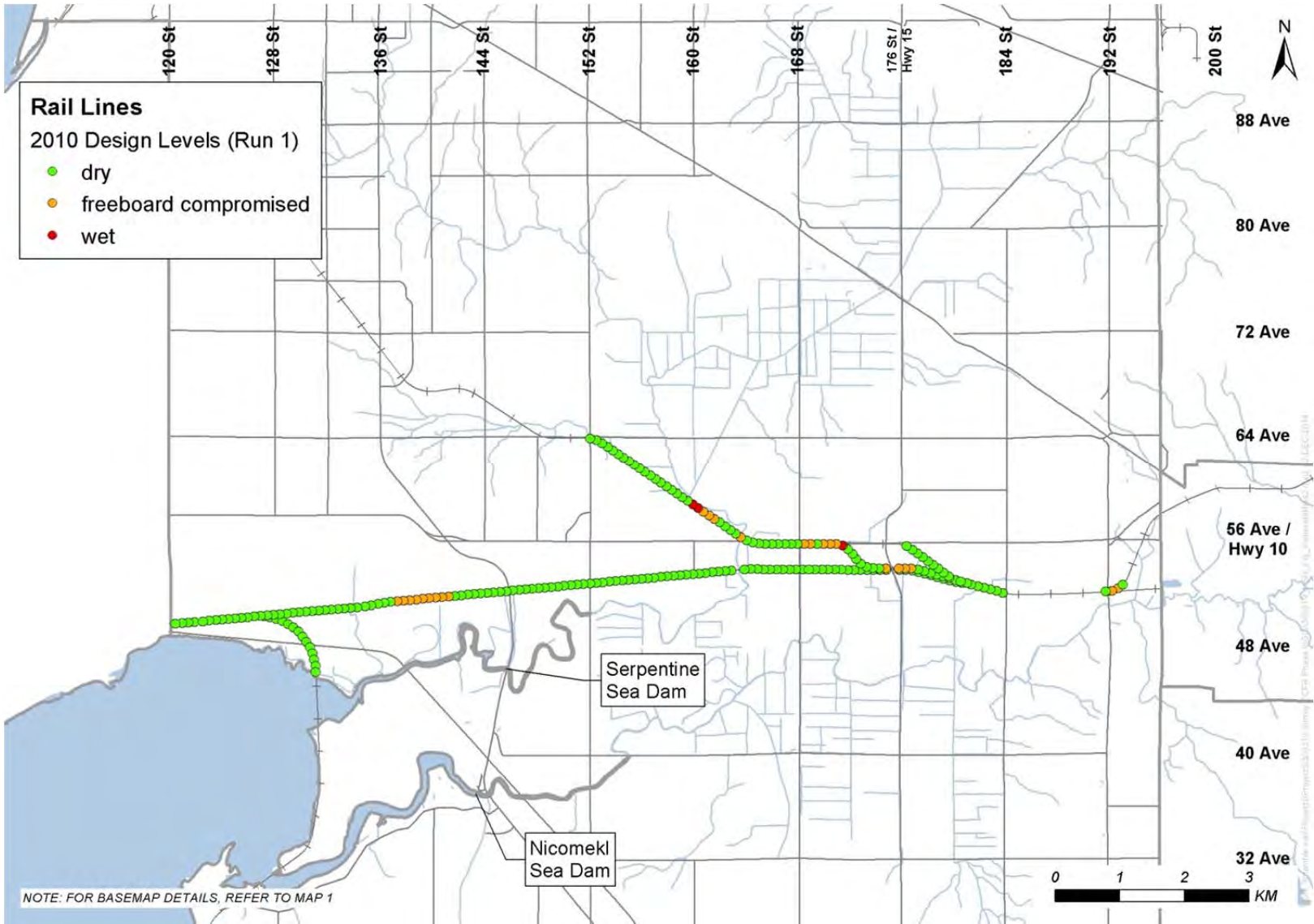


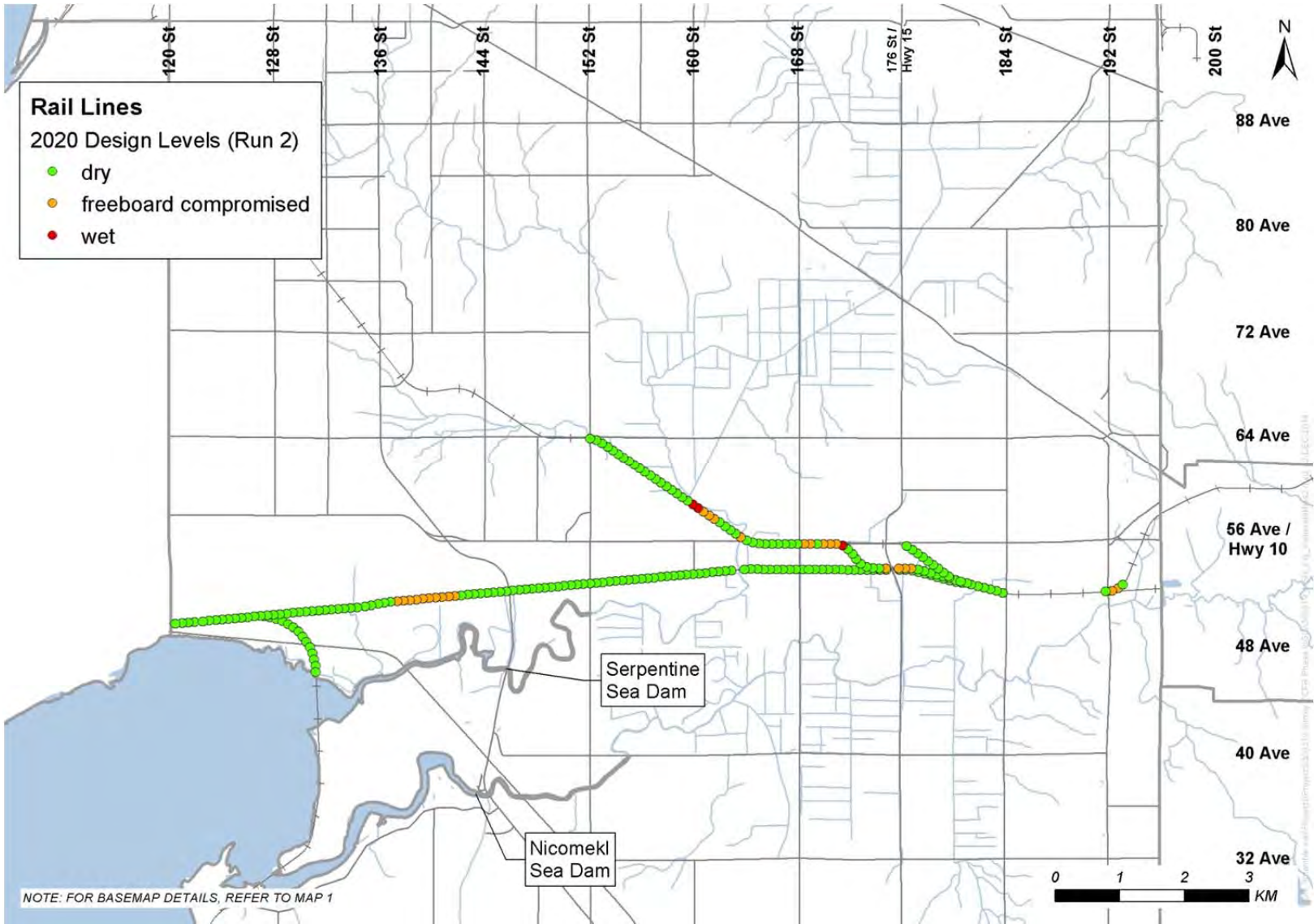


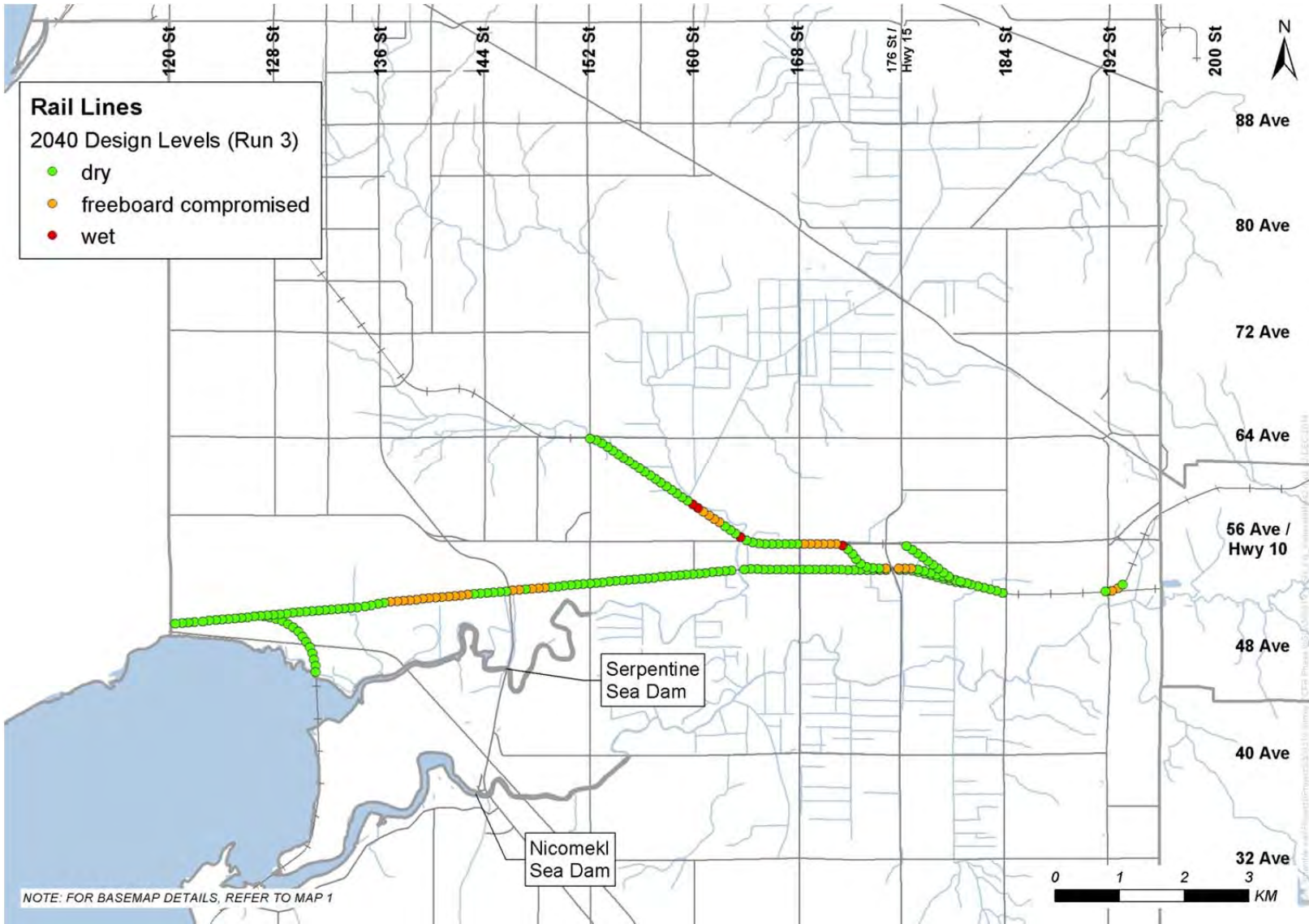


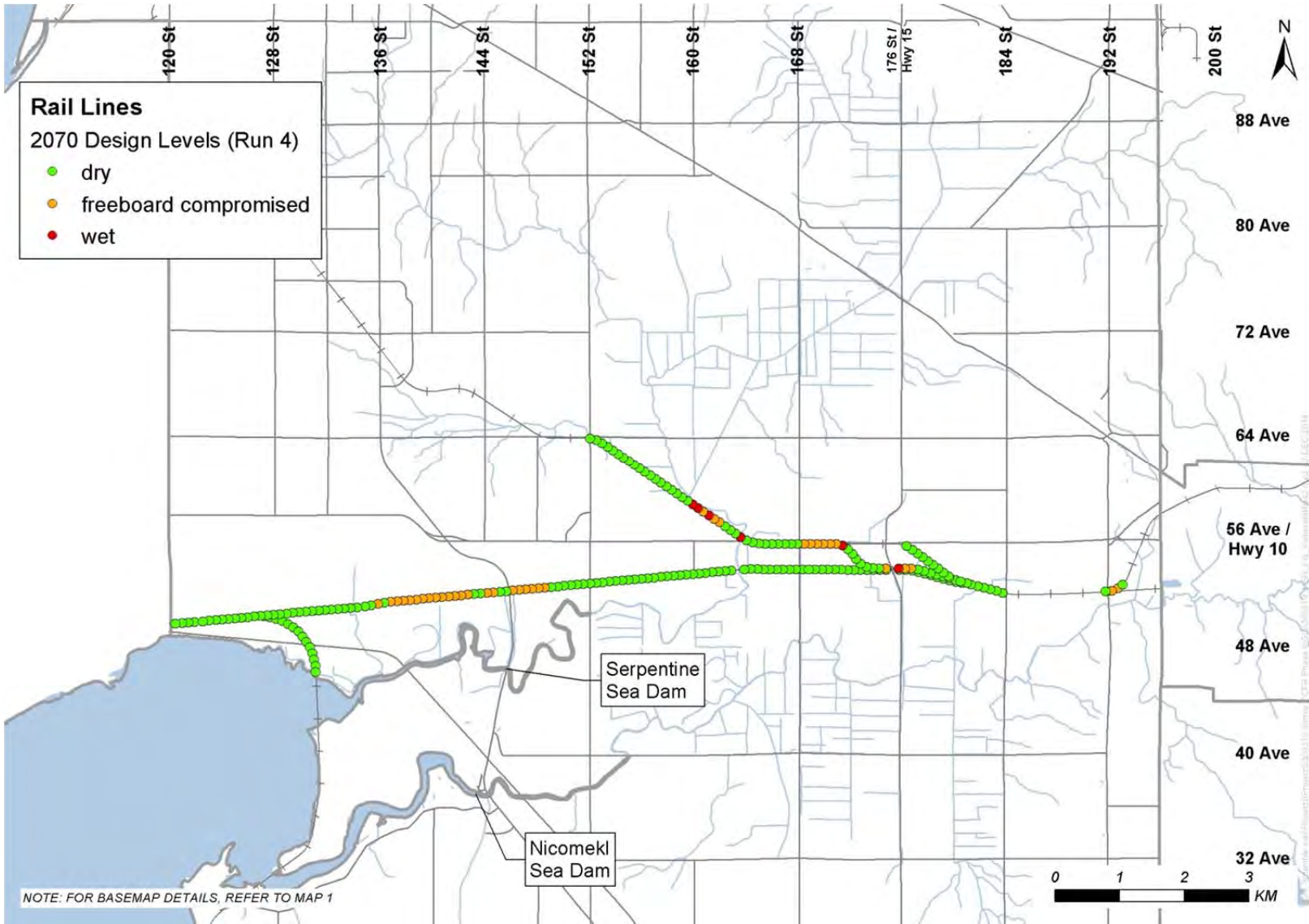




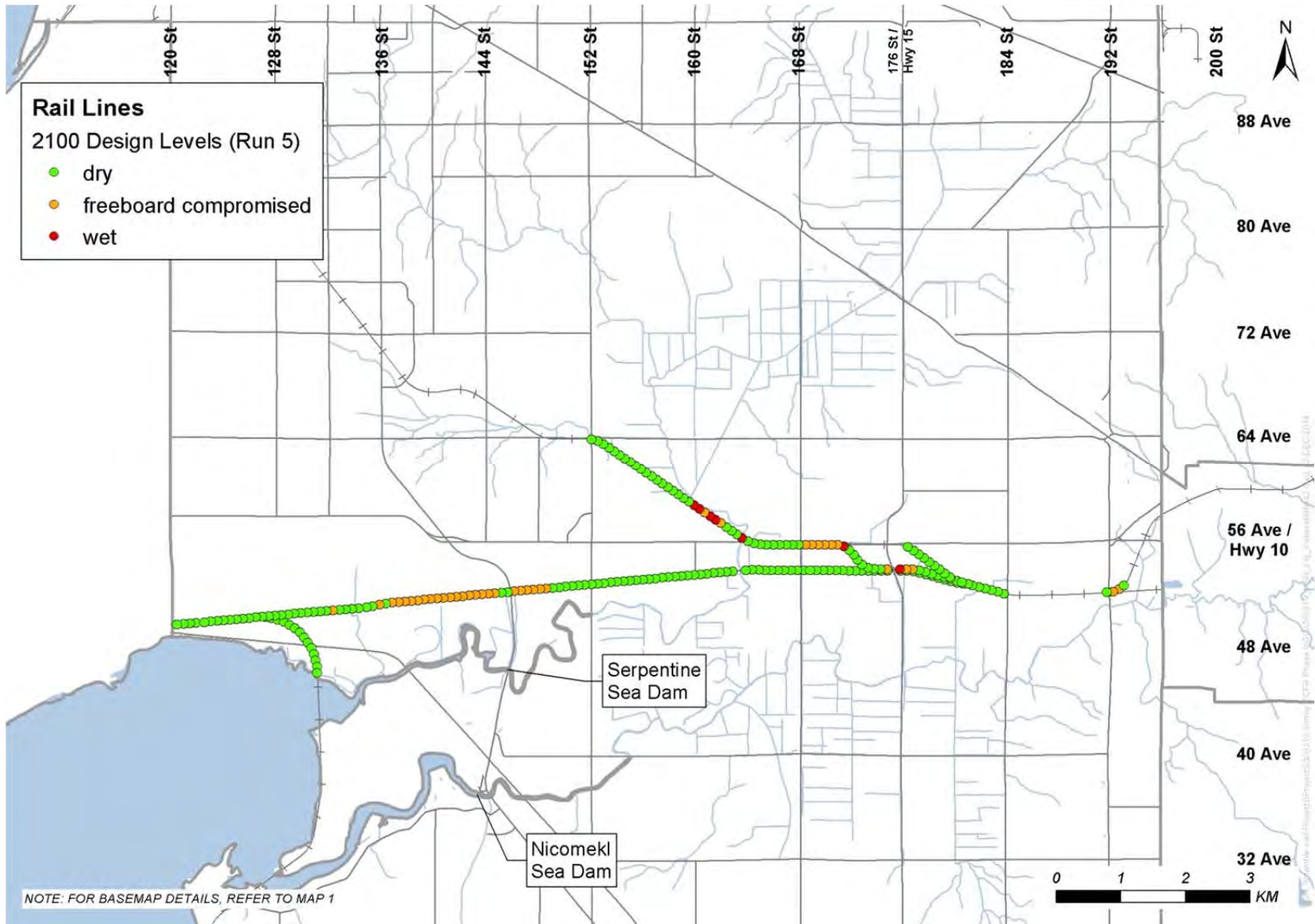


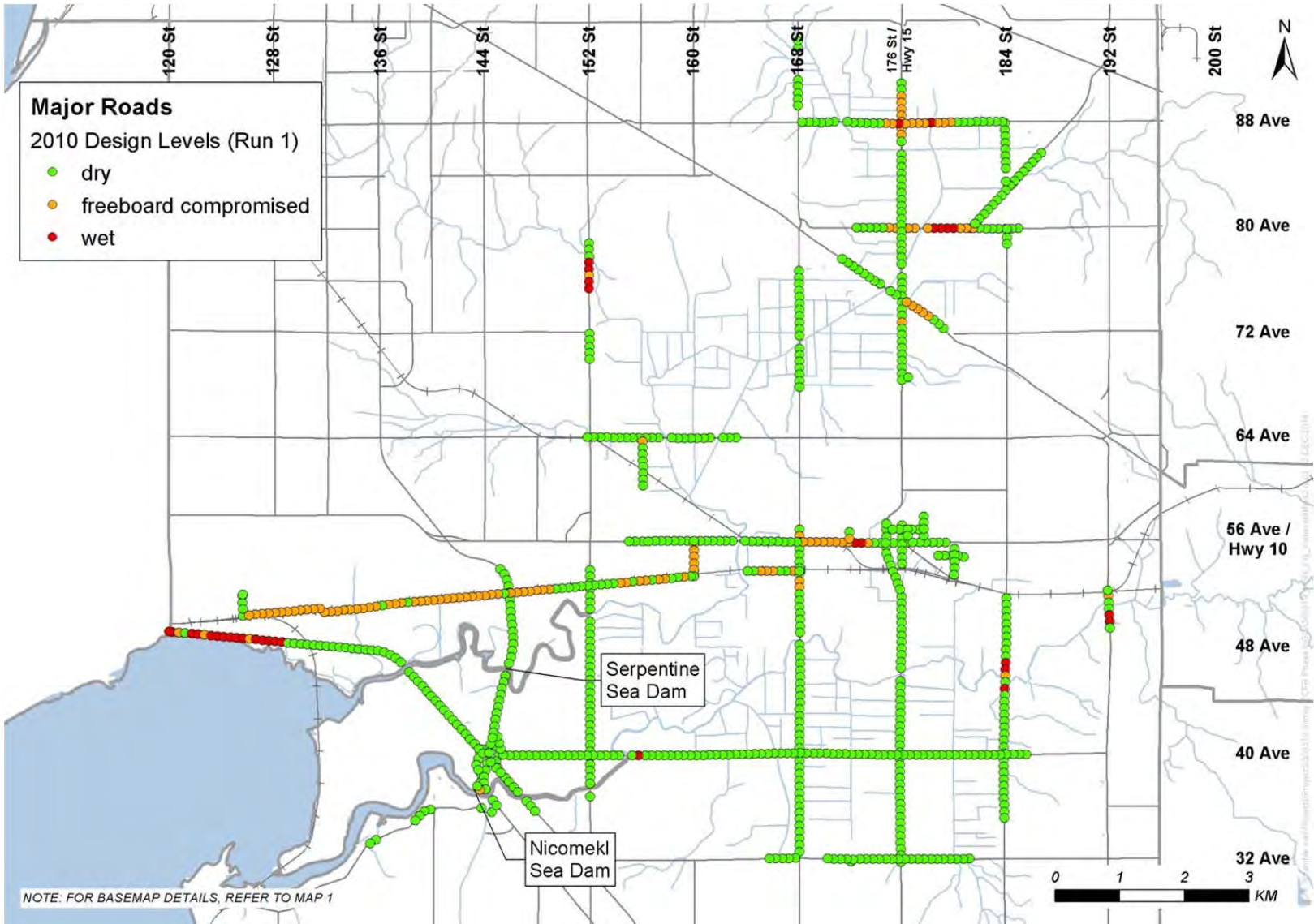


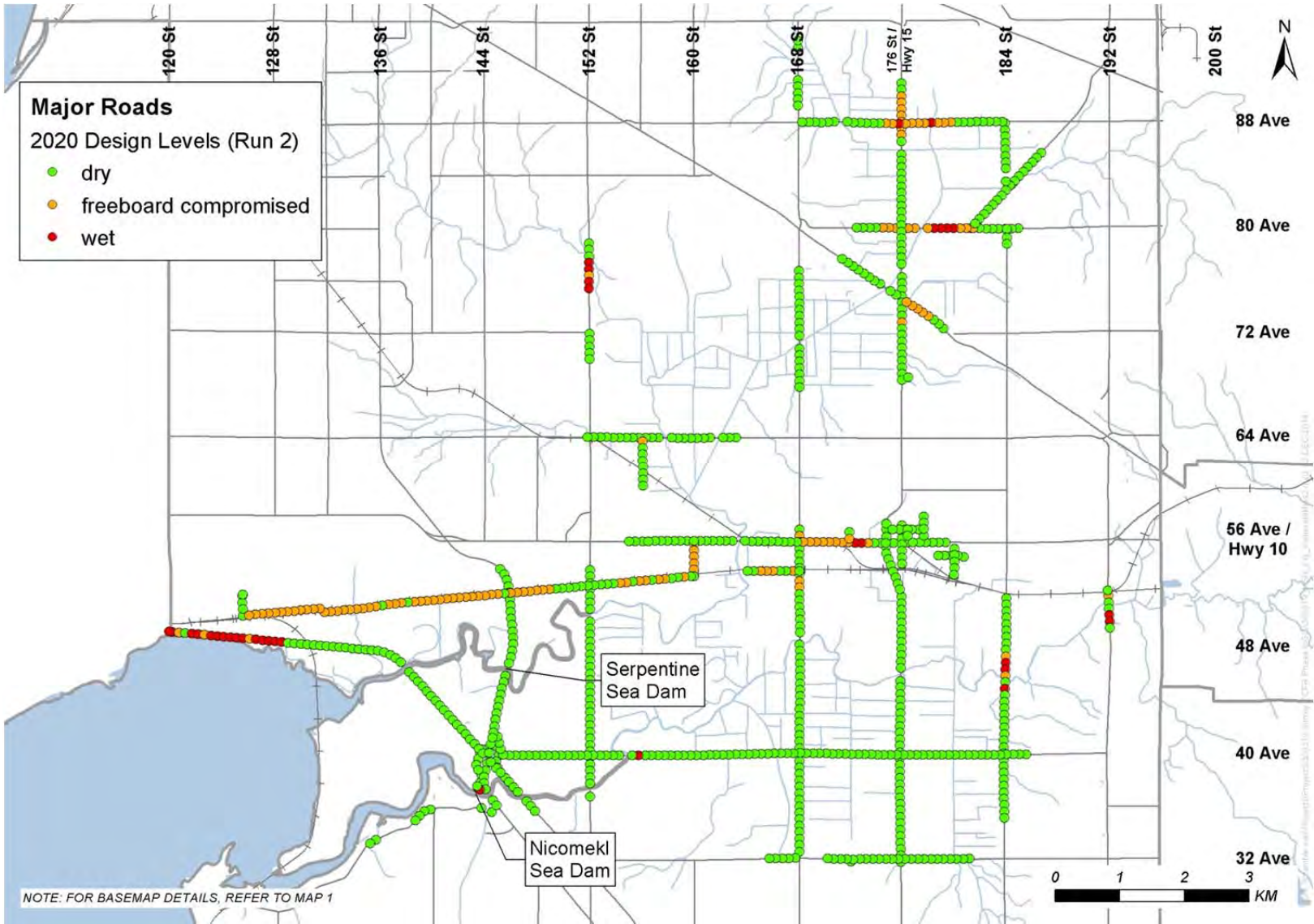


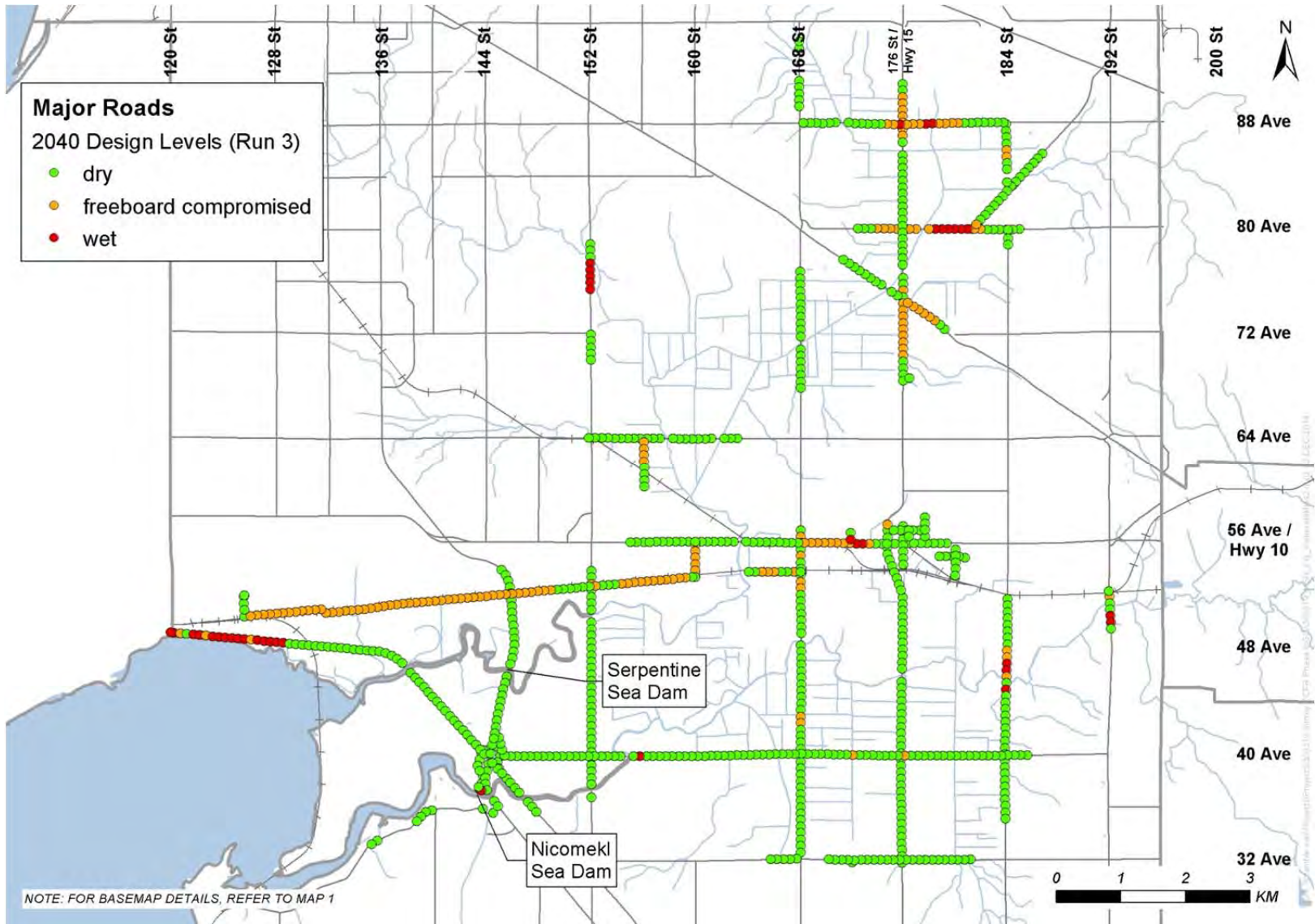


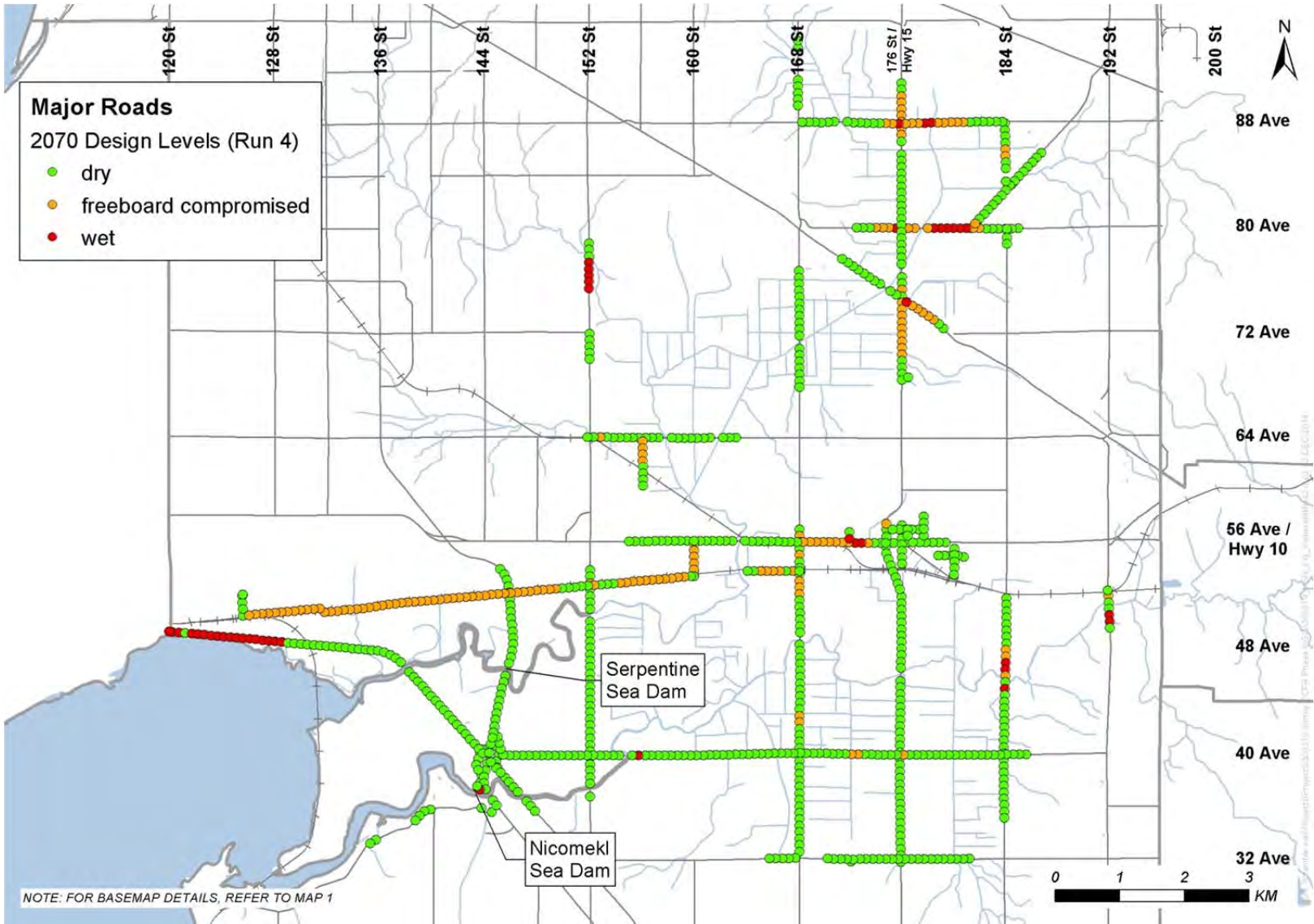


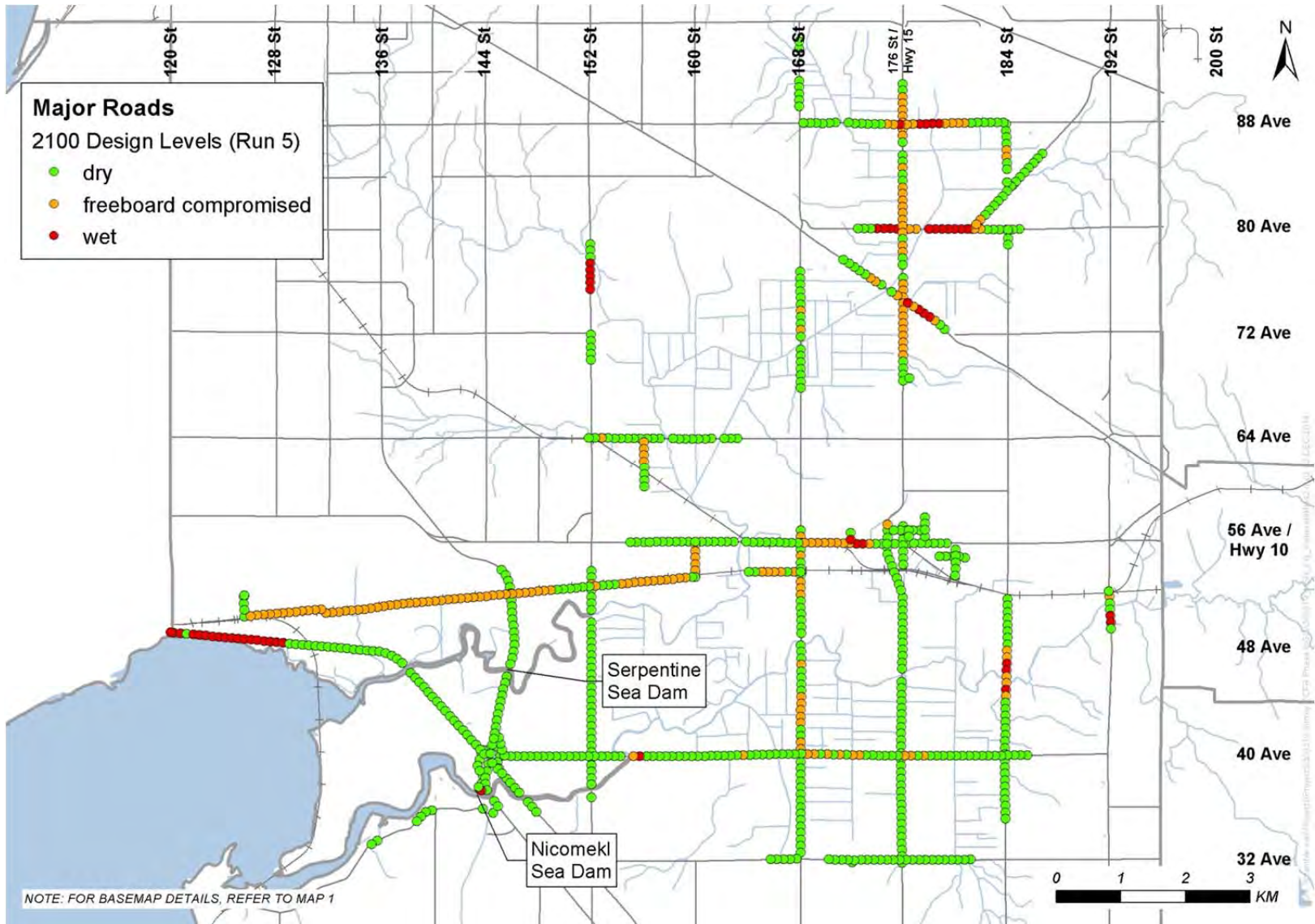








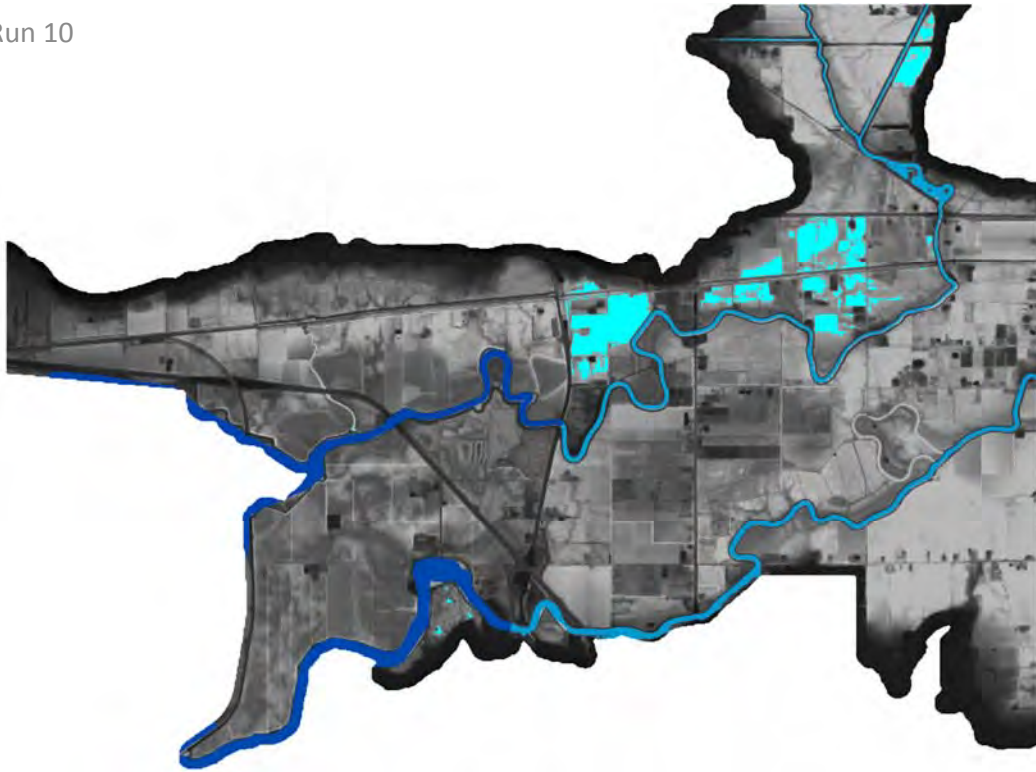




## **APPENDIX G**

Dike Breach Modelling

Run 10



Water Surface Elevation, T = 00:00:00

Run 10



Water Surface Elevation, T = 00:15:00



Run 10



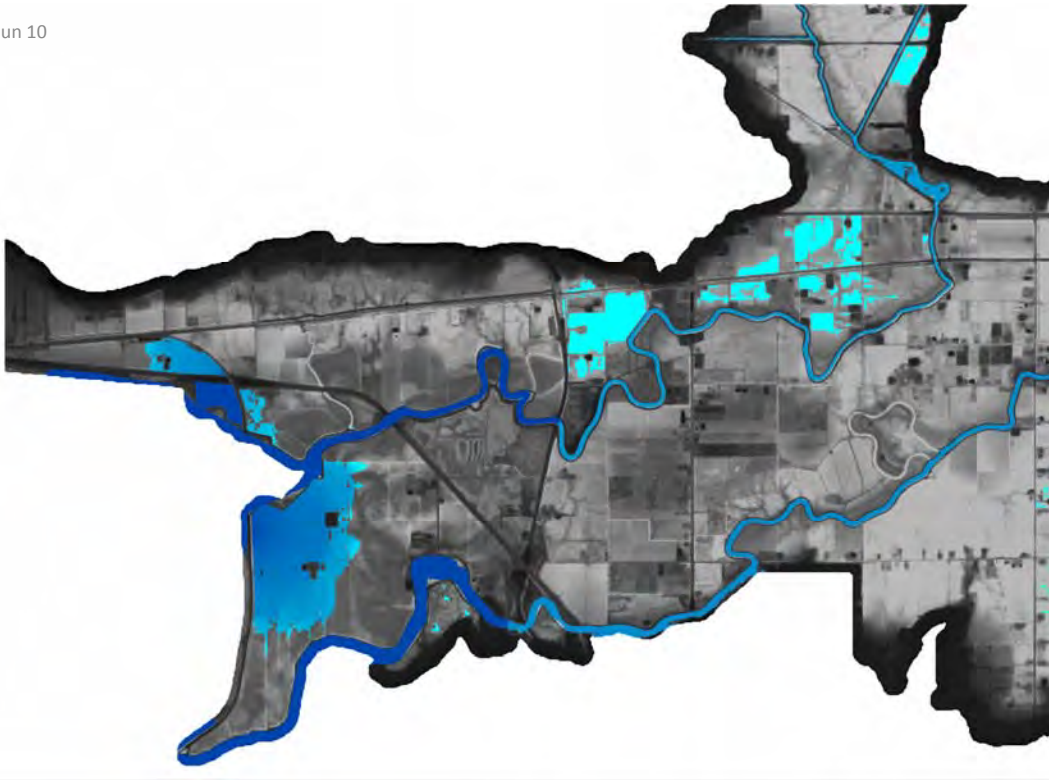
Water Surface Elevation, T = 00:30:00

Run 10



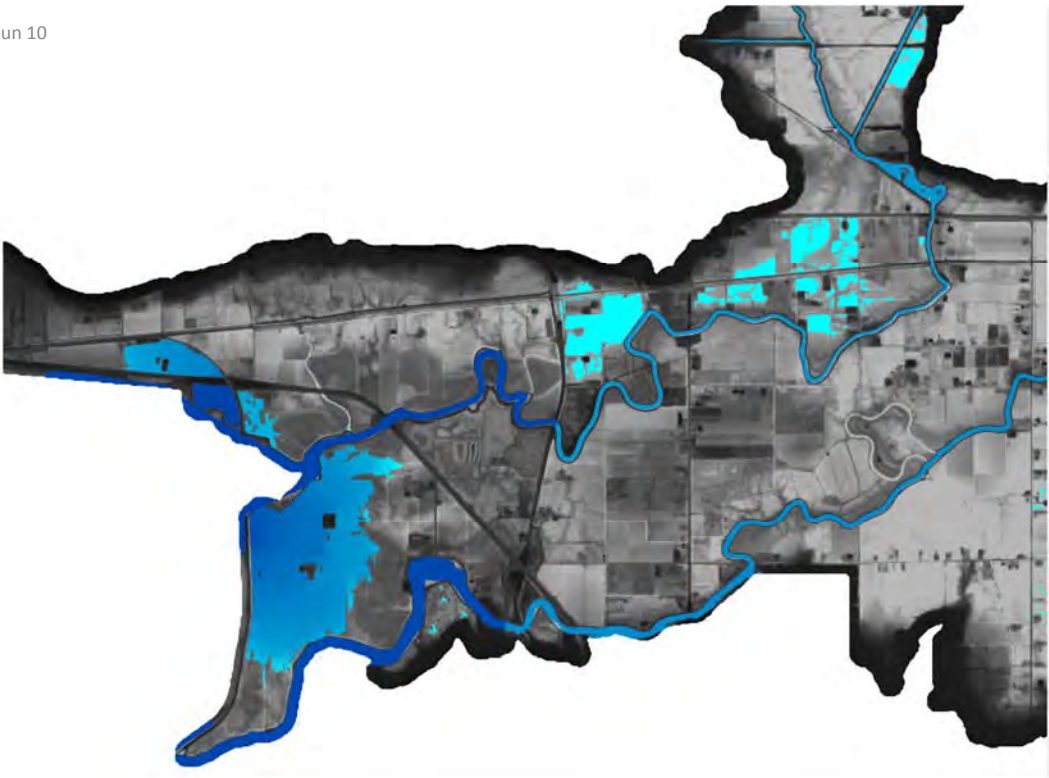
Water Surface Elevation, T = 00:45:00

Run 10



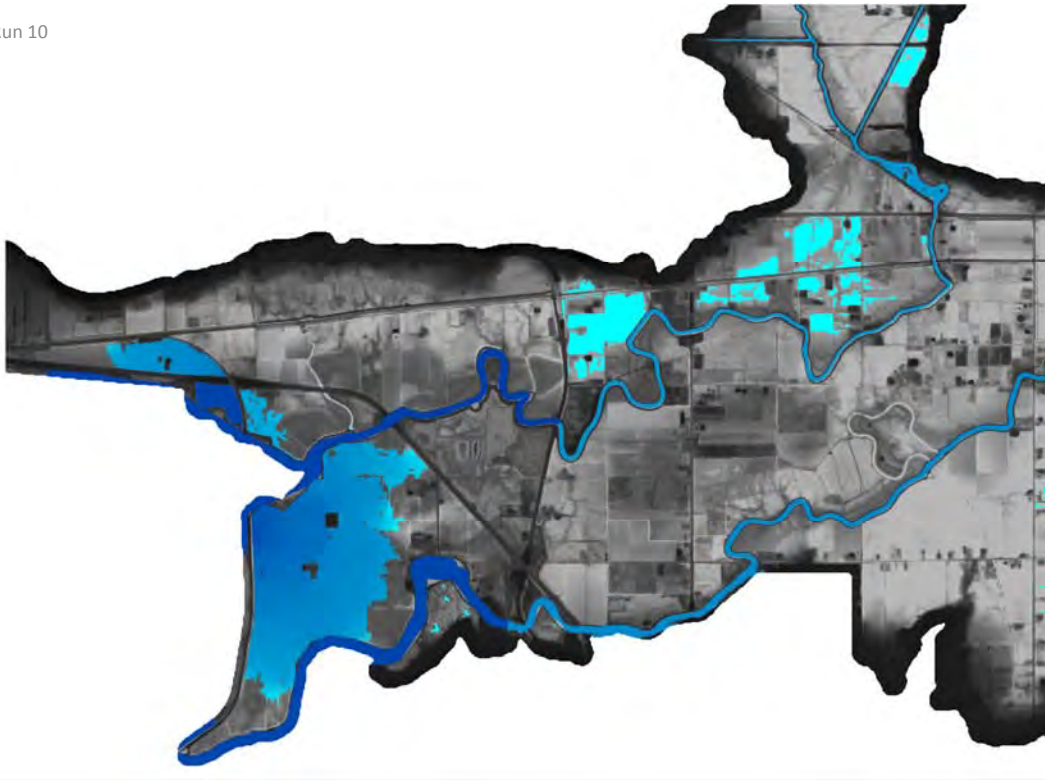
Water Surface Elevation, T = 01:00:00

Run 10



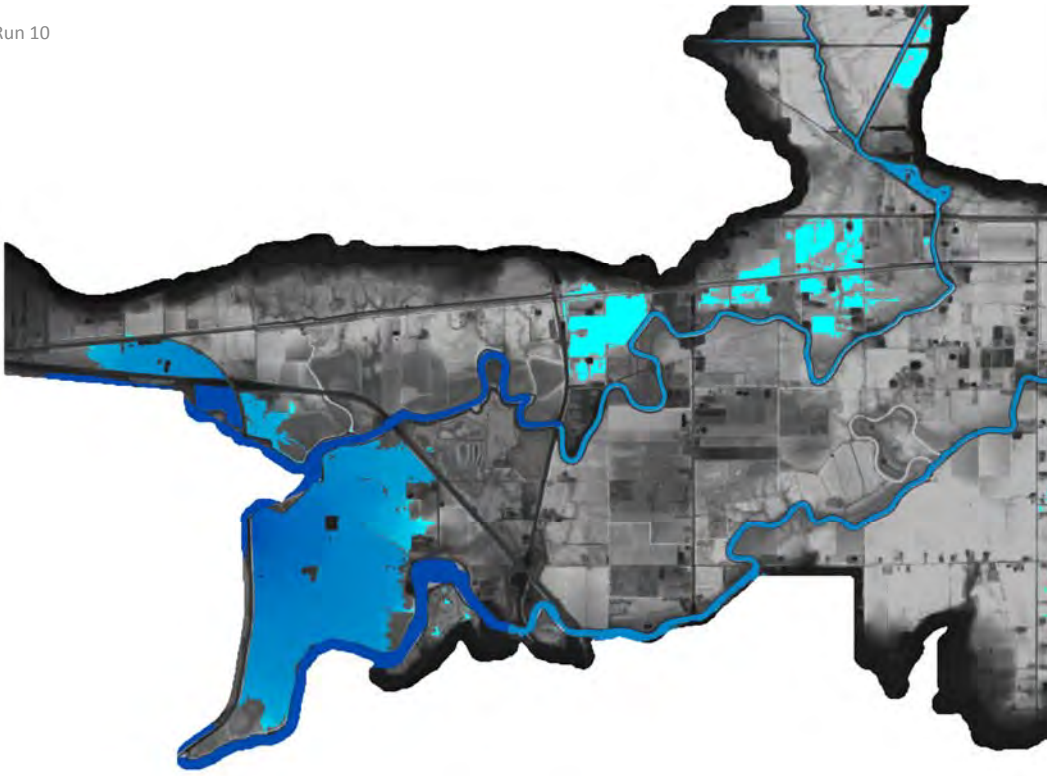
Water Surface Elevation, T = 01:15:00

Run 10



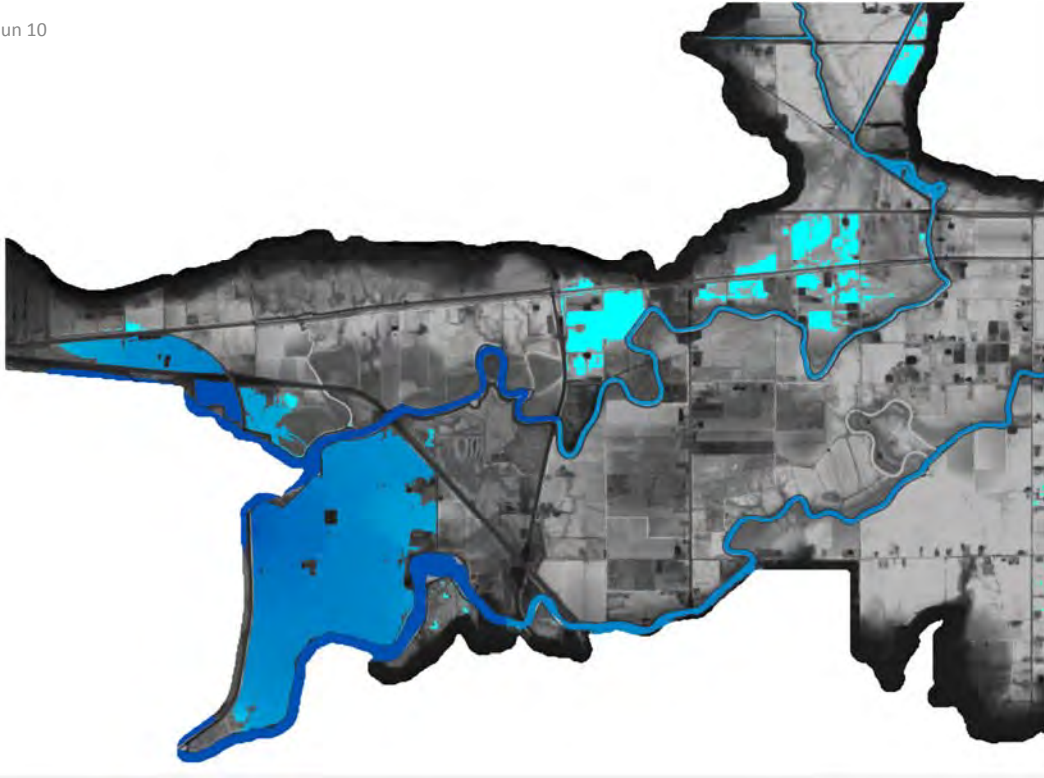
Water Surface Elevation, T = 01:30:00

Run 10



Water Surface Elevation, T = 01:45:00

Run 10



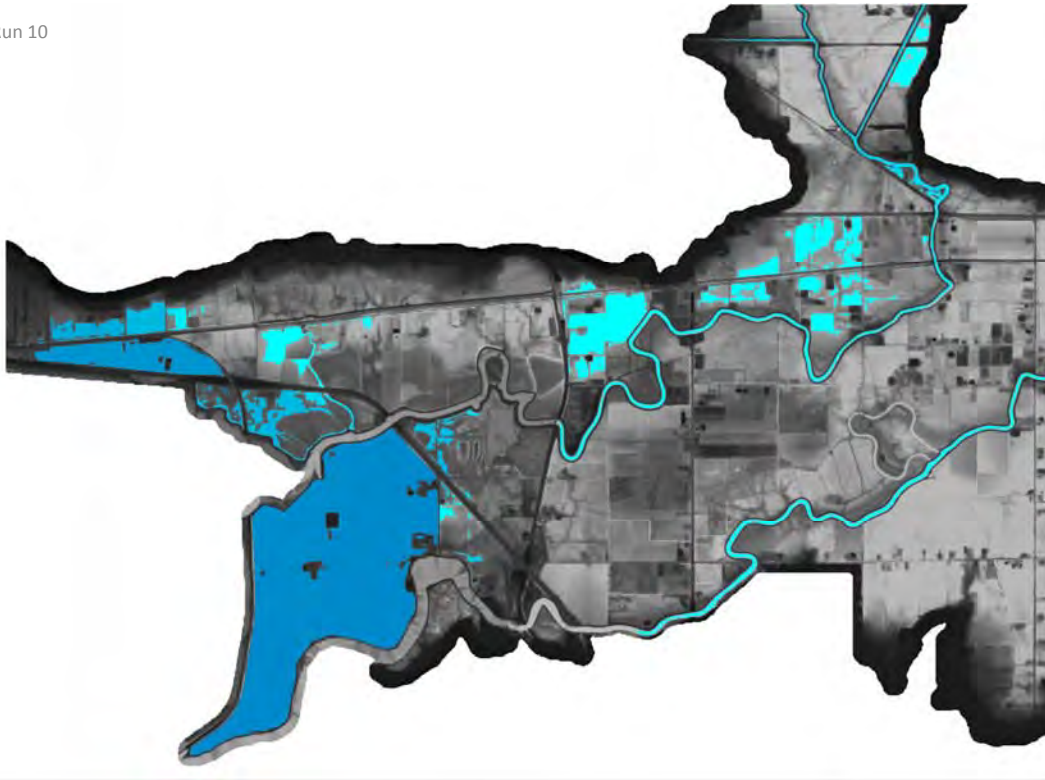
Water Surface Elevation, T = 02:00:00

Run 10



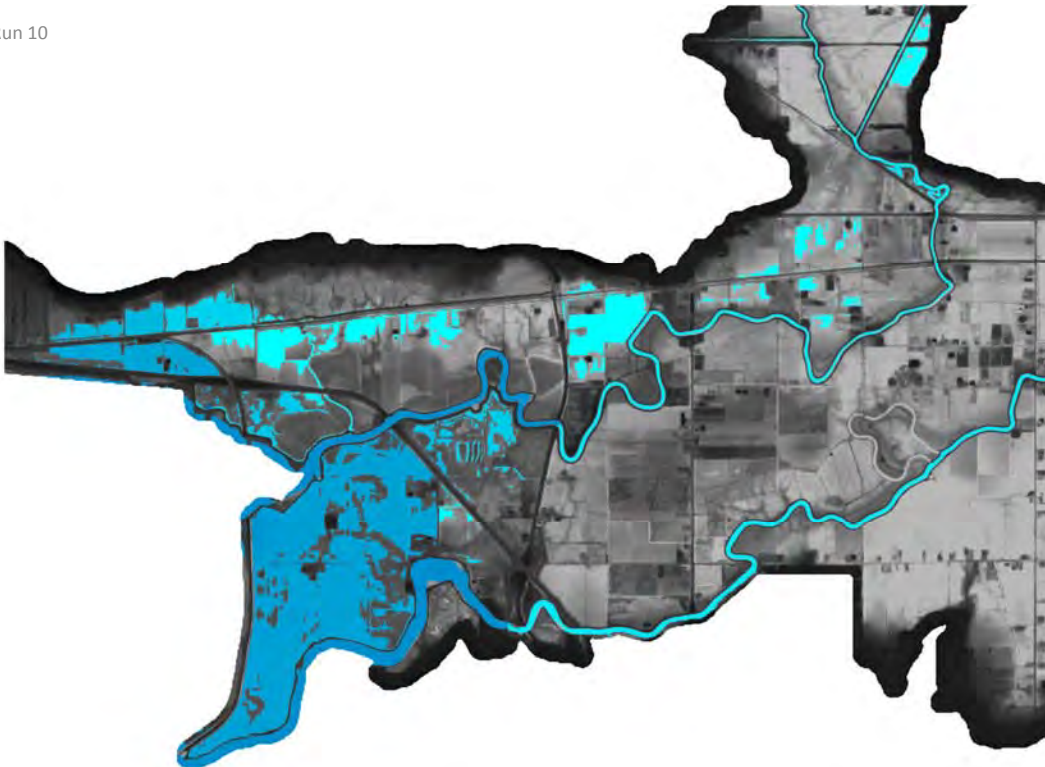
Water Surface Elevation, T = 03:00:00

Run 10



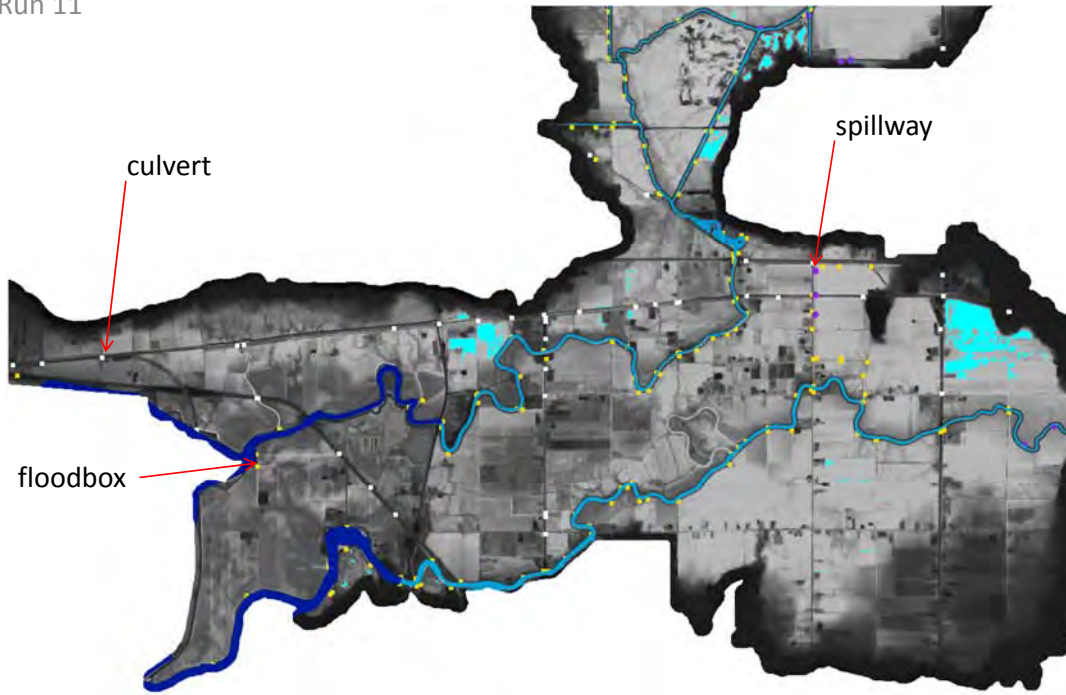
Water Surface Elevation, T = 08:00:00

Run 10



Water Surface Elevation, T = 23:00:00

Run 11



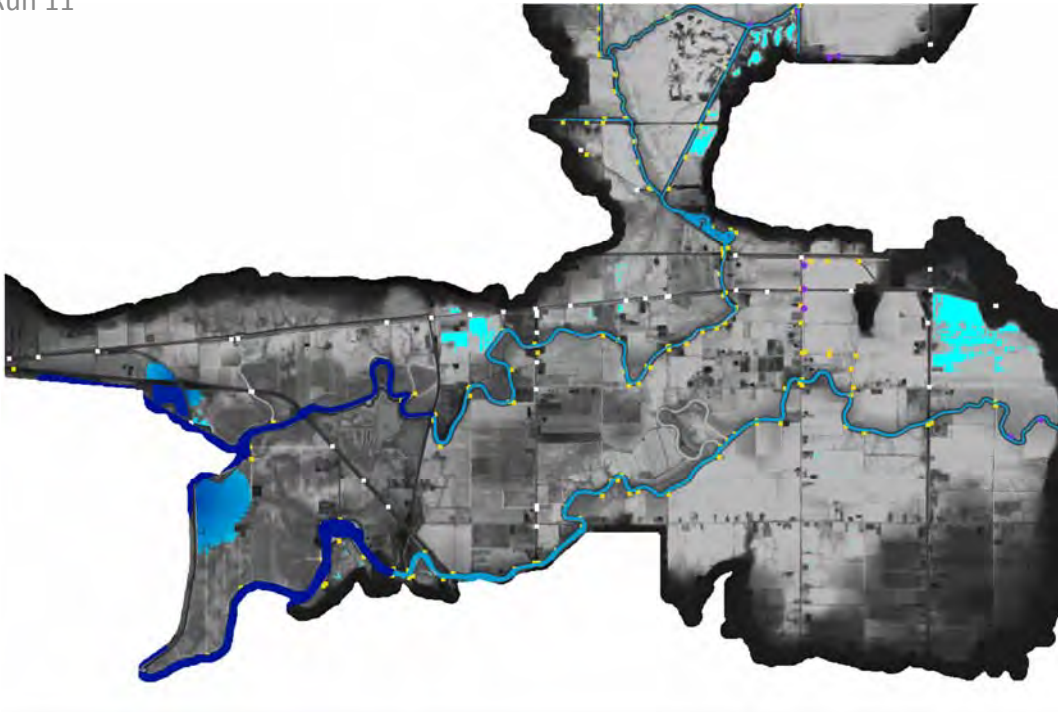
Water Surface Elevation, T = hh:mm:ss

Run 11



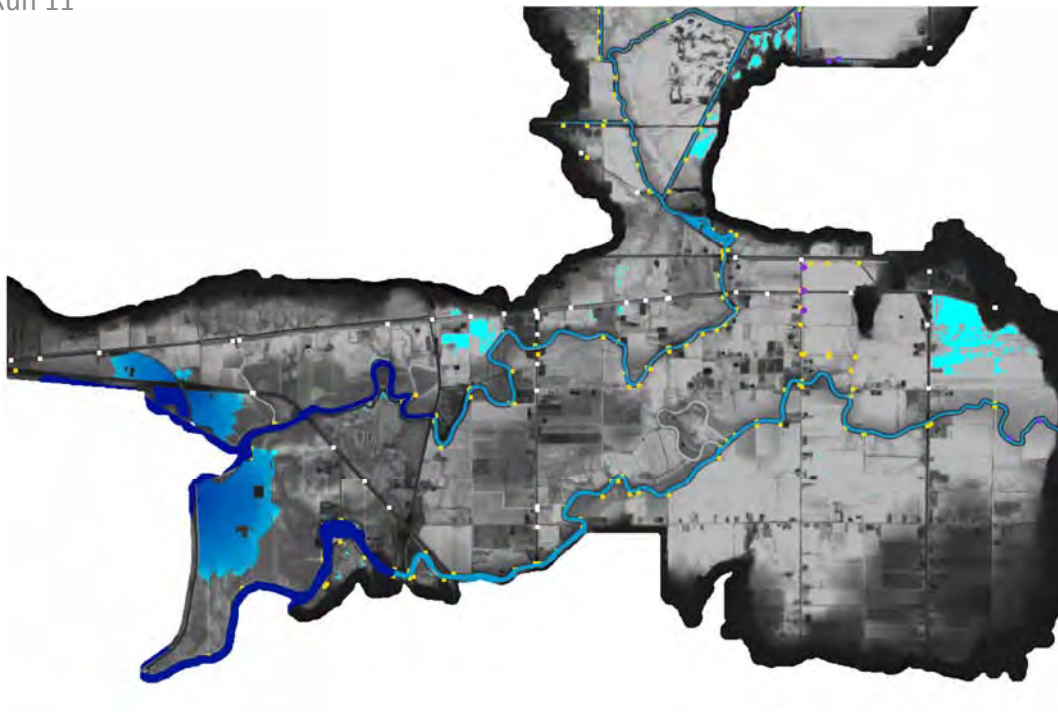
Water Surface Elevation, T = 00:15:00

Run 11



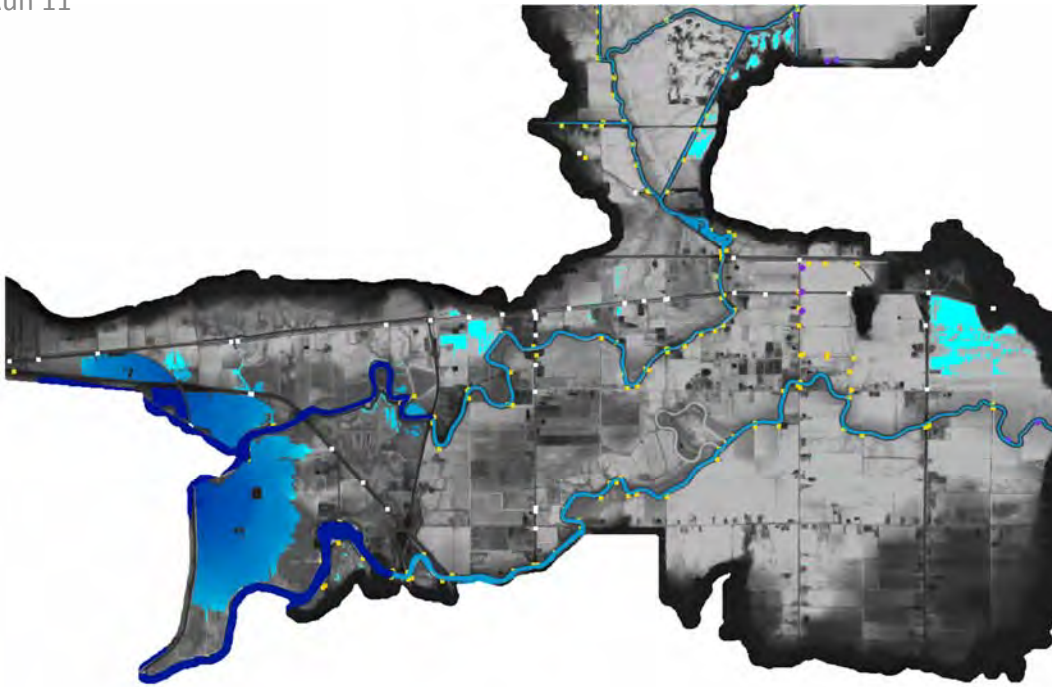
Water Surface Elevation, T = 00:30:00

Run 11



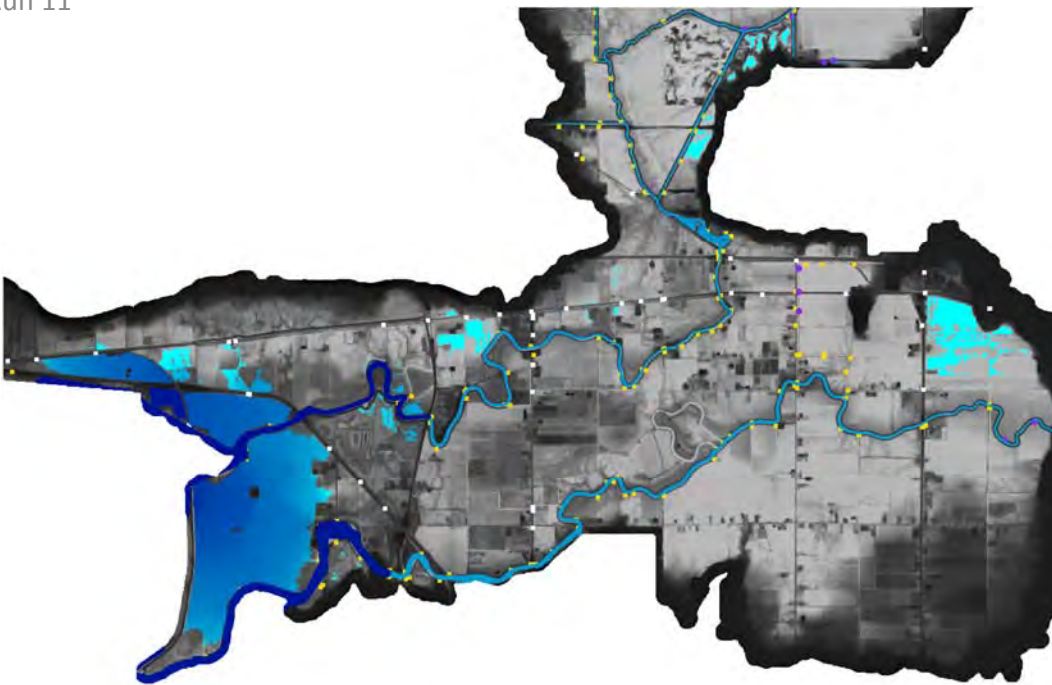
Water Surface Elevation, T = 00:45:00

Run 11



Water Surface Elevation, T = 01:00:00

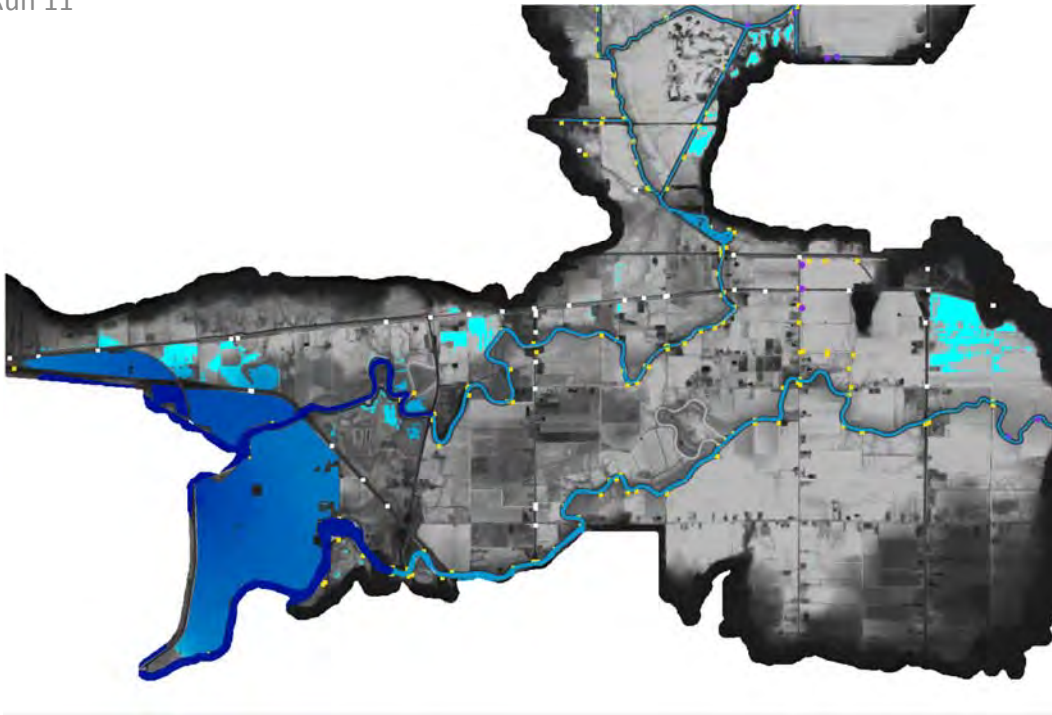
Run 11



Water Surface Elevation, T = 01:15:00

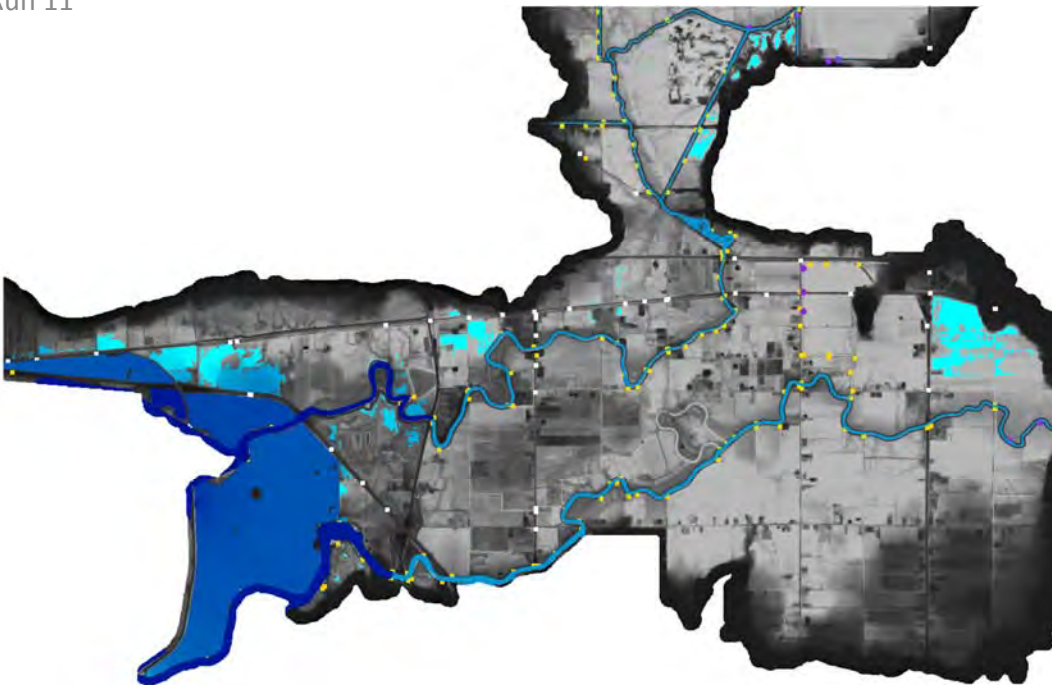


Run 11



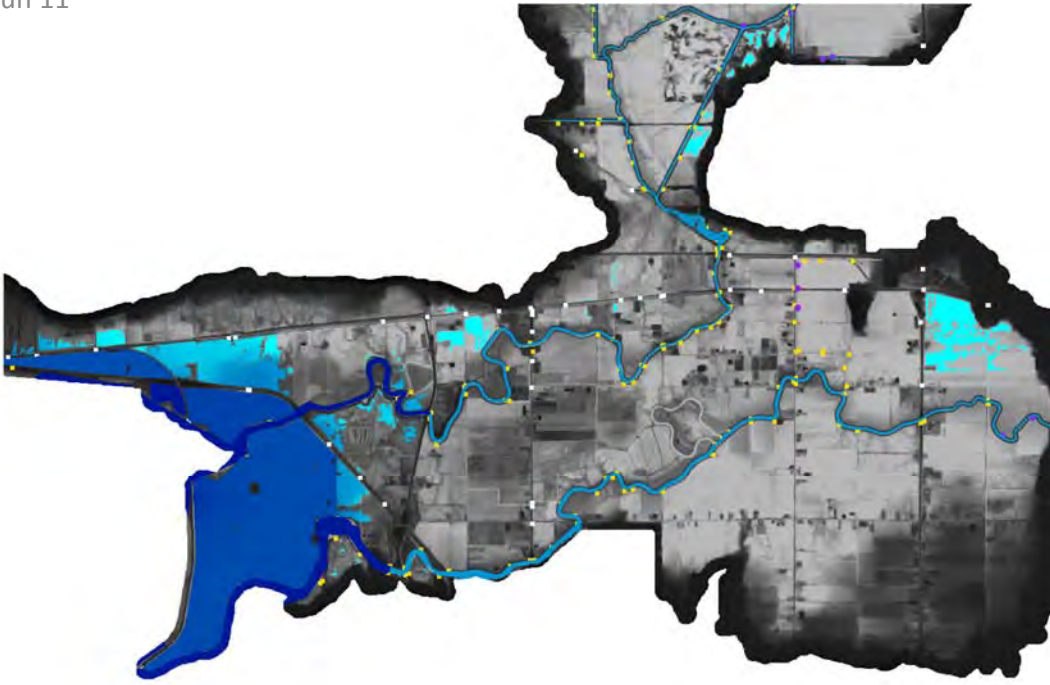
Water Surface Elevation, T = 01:30:00

Run 11



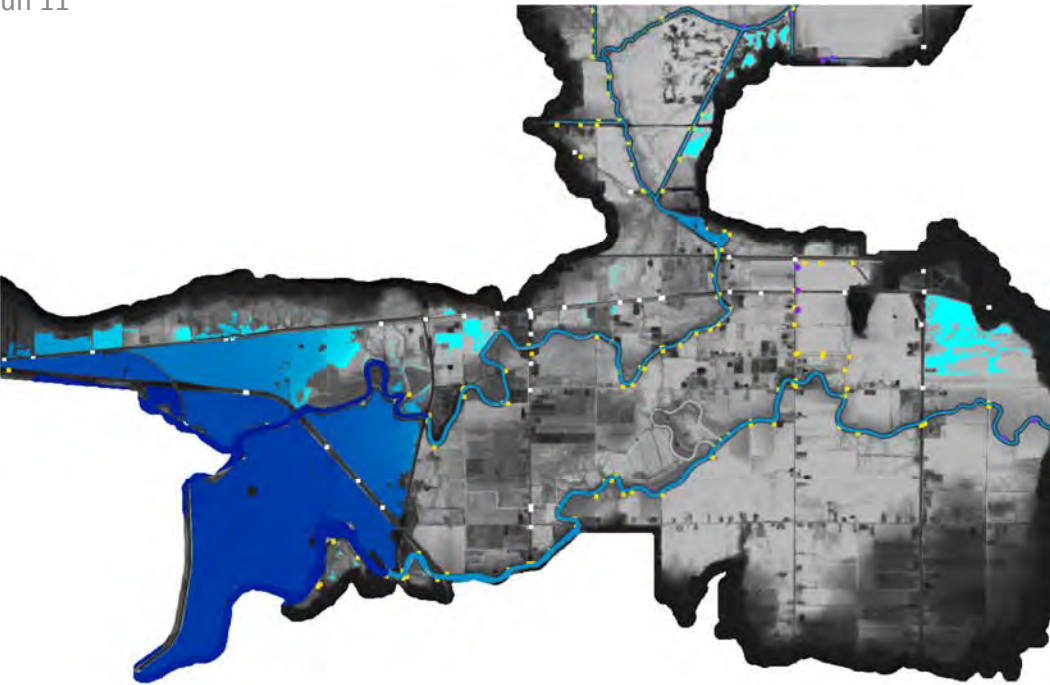
Water Surface Elevation, T = 01:45:00

Run 11



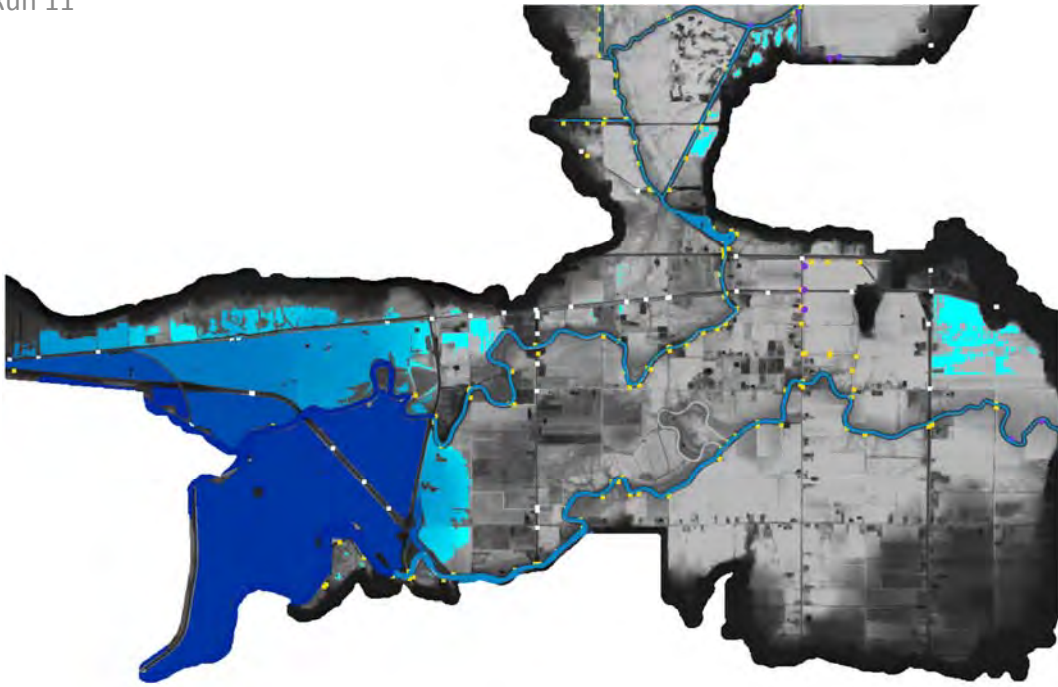
Water Surface Elevation, T = 02:00:00

Run 11



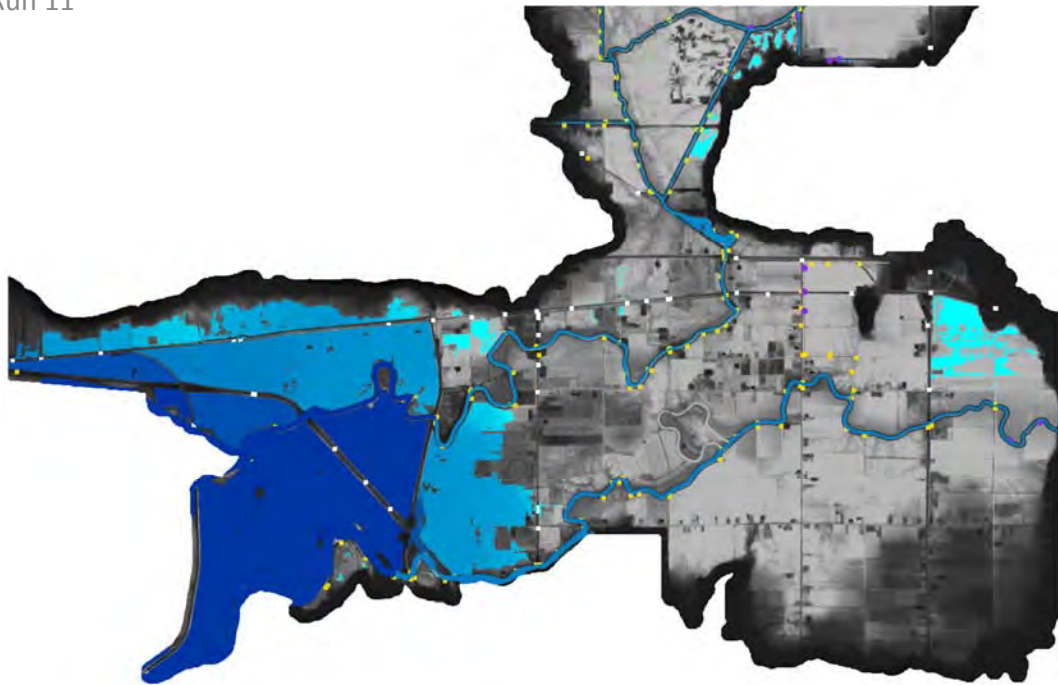
Water Surface Elevation, T = 03:00:00

Run 11



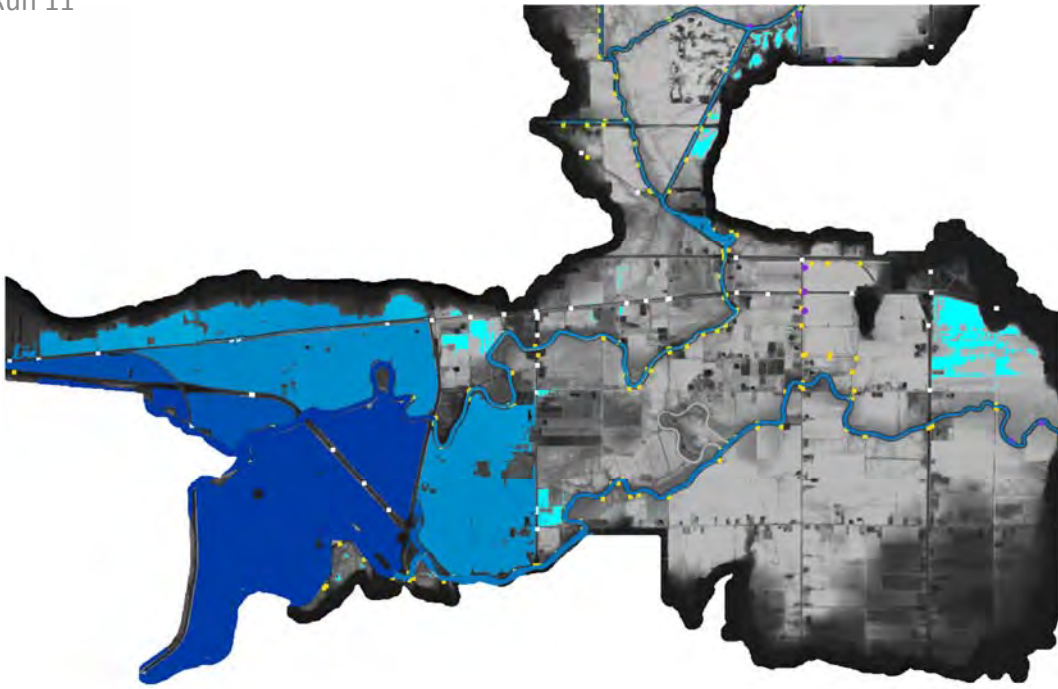
Water Surface Elevation, T = 04:00:00

Run 11



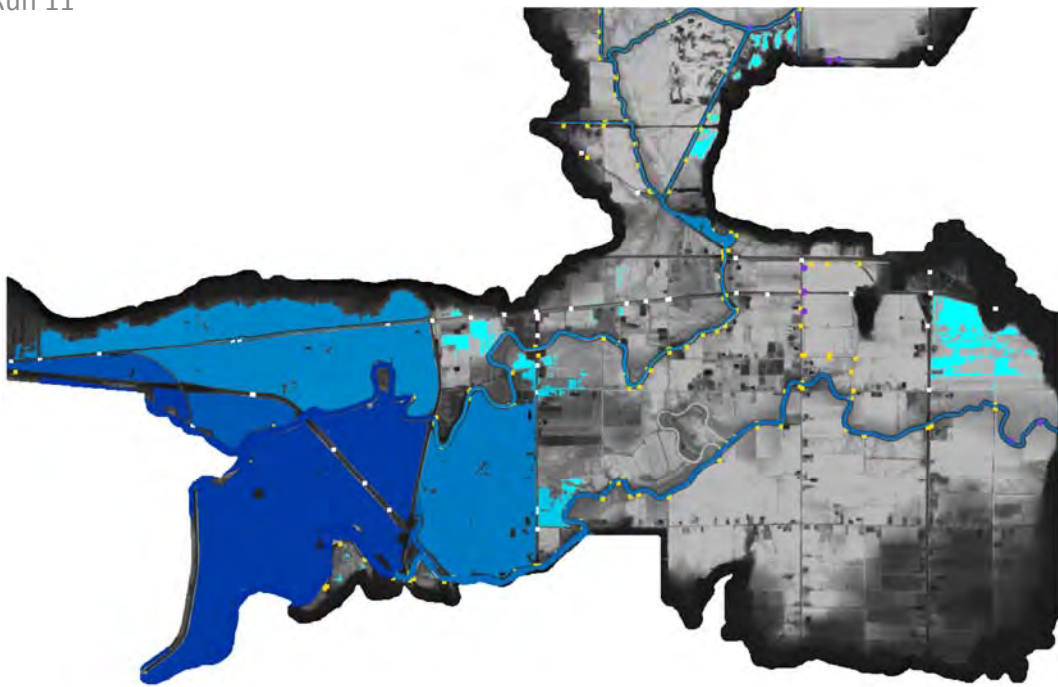
Water Surface Elevation, T = 05:00:00

Run 11



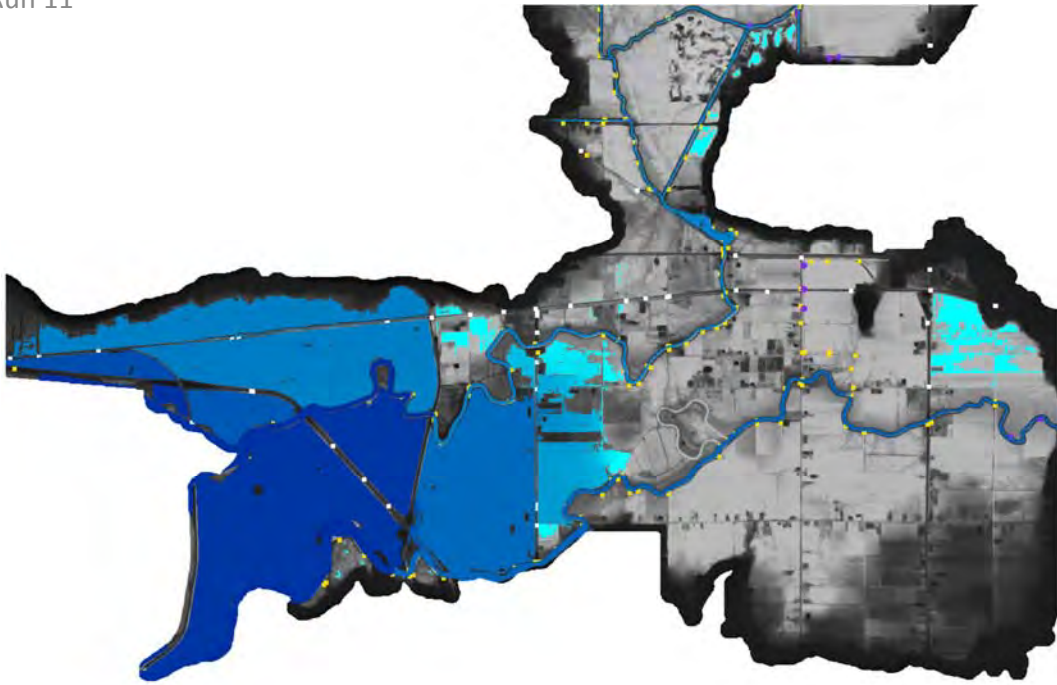
Water Surface Elevation, T = 06:00:00

Run 11



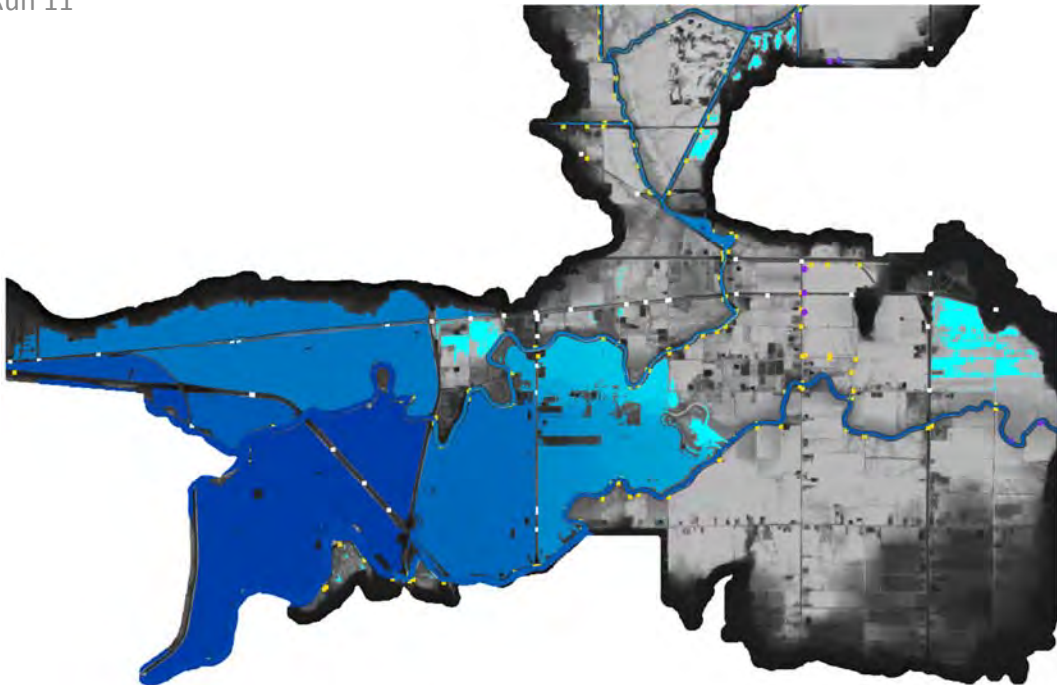
Water Surface Elevation, T = 08:00:00

Run 11



Water Surface Elevation, T = 10:00:00

Run 11



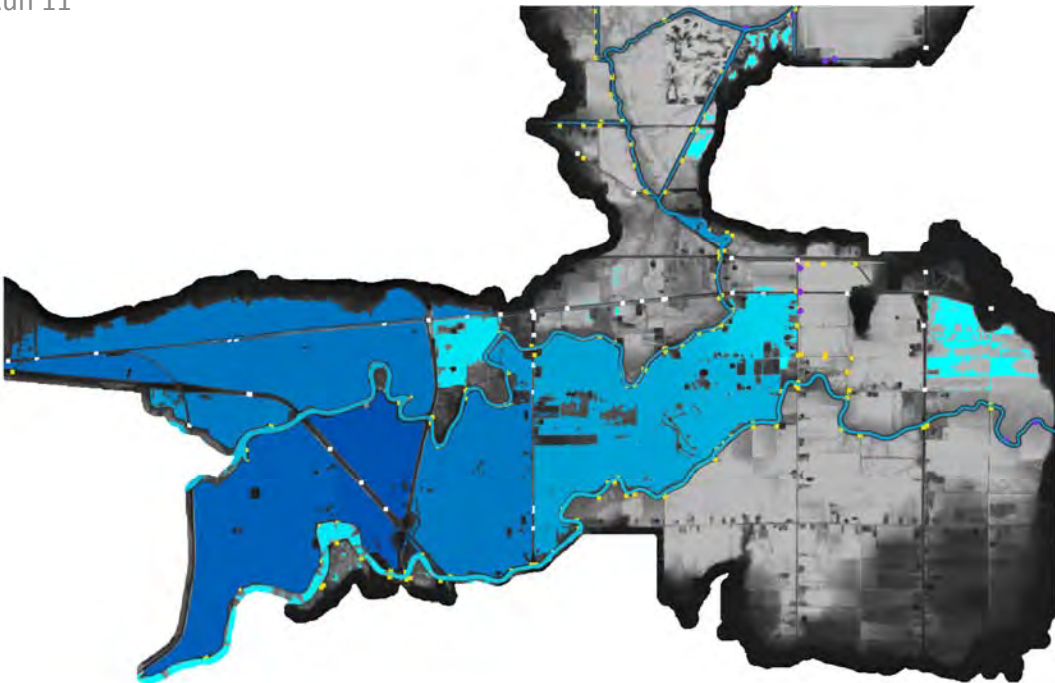
Water Surface Elevation, T = 12:00:00

Run 11



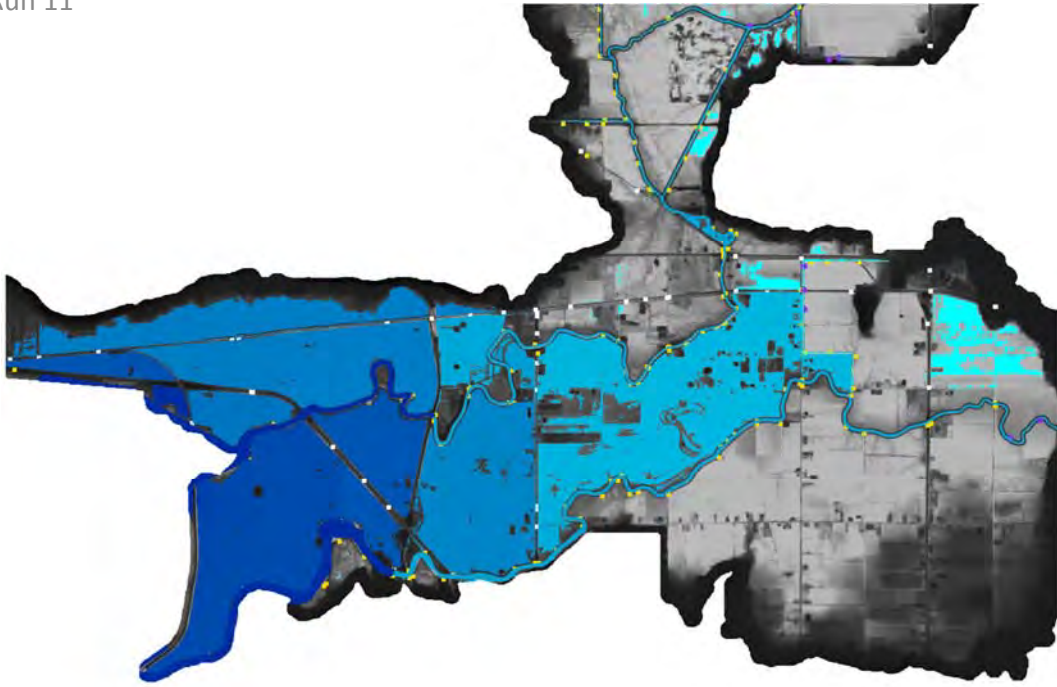
Water Surface Elevation, T = 14:00:00

Run 11



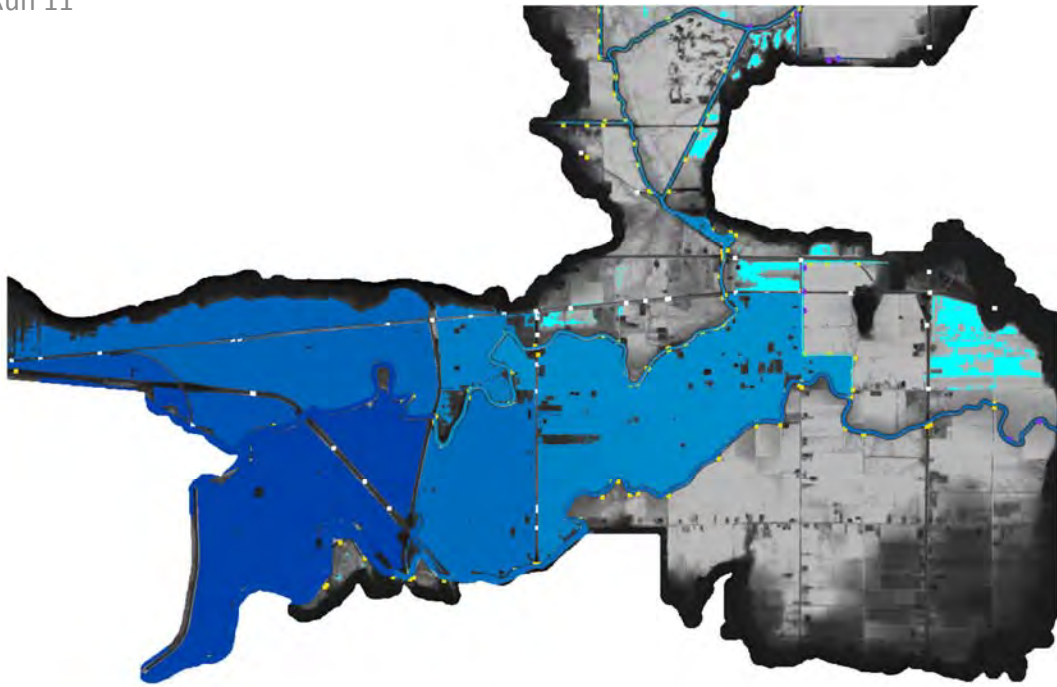
Water Surface Elevation, T = 16:00:00

Run 11



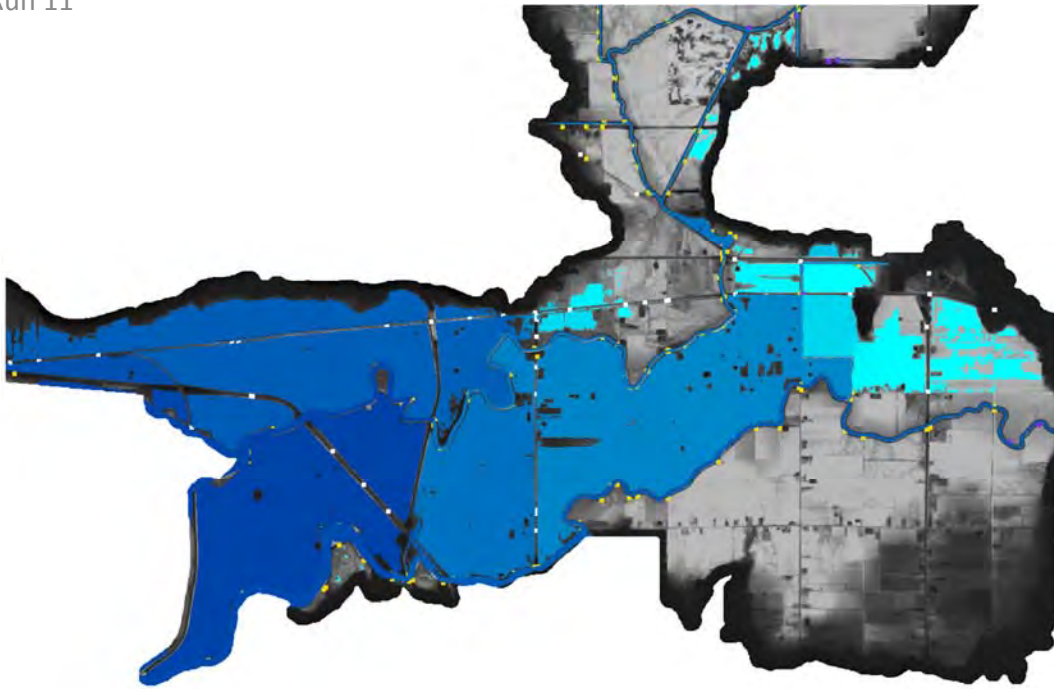
Water Surface Elevation, T = 24:00:00

Run 11



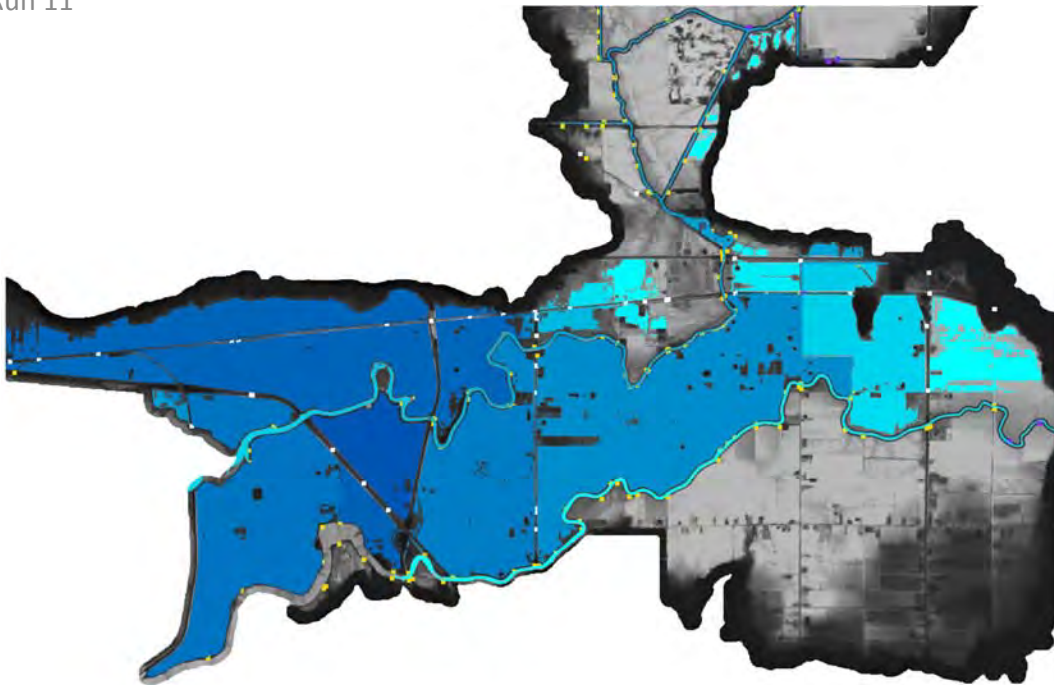
Water Surface Elevation, T = 30:00:00

Run 11



Water Surface Elevation, T = 36:00:00

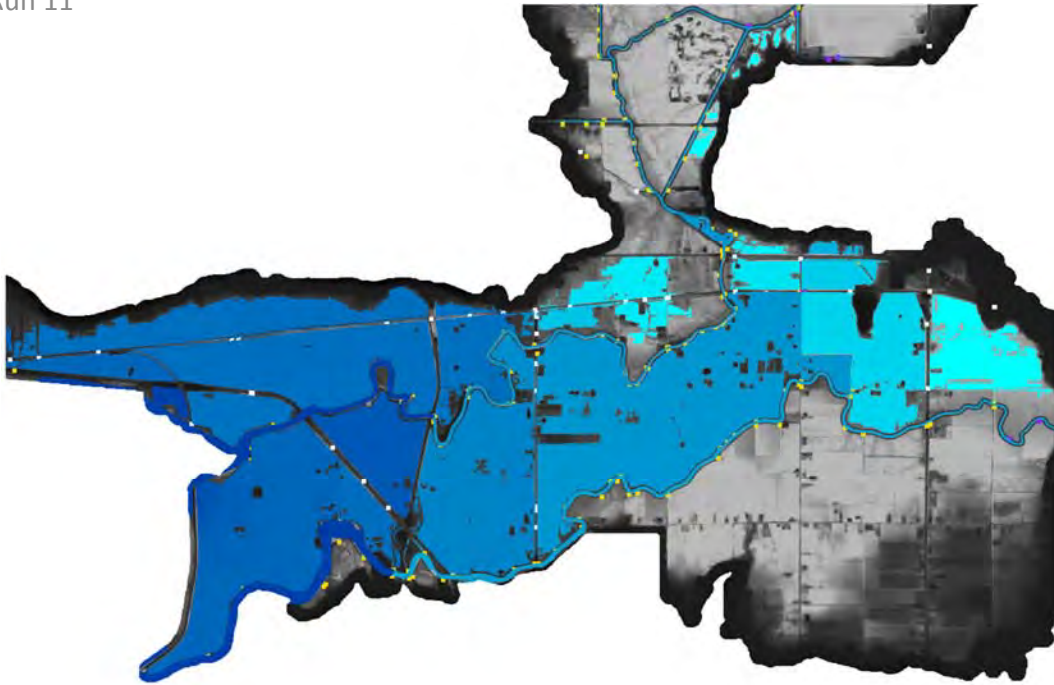
Run 11



Water Surface Elevation, T = 42:00:00

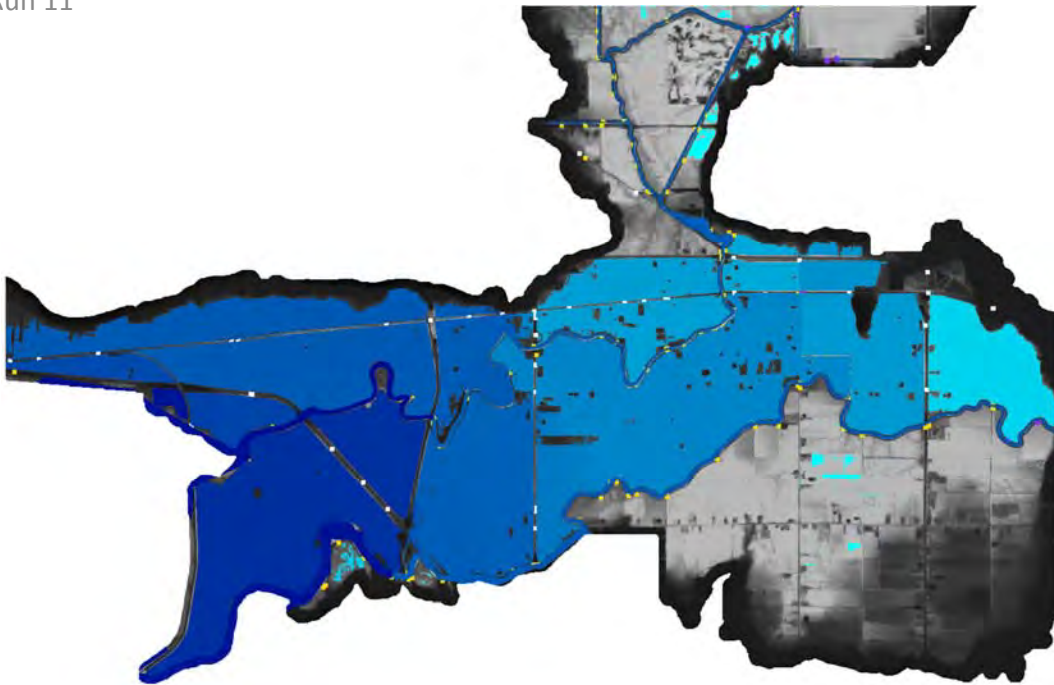


Run 11



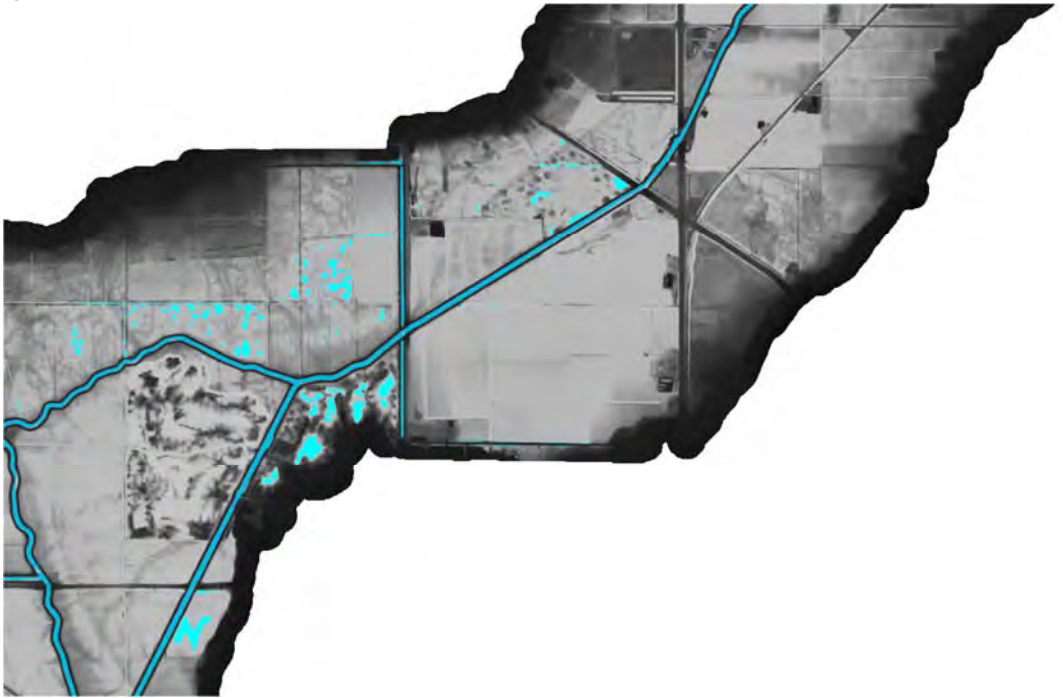
Water Surface Elevation, T = 48:00:00

Run 11



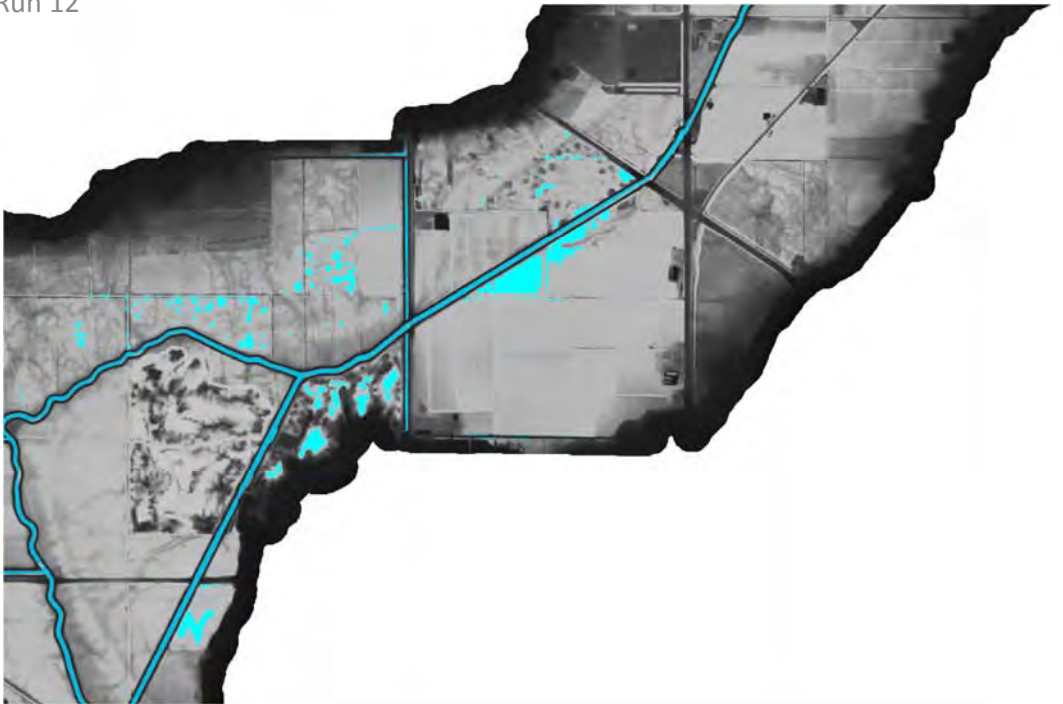
Water Surface Elevation, Peak Values

Run 12



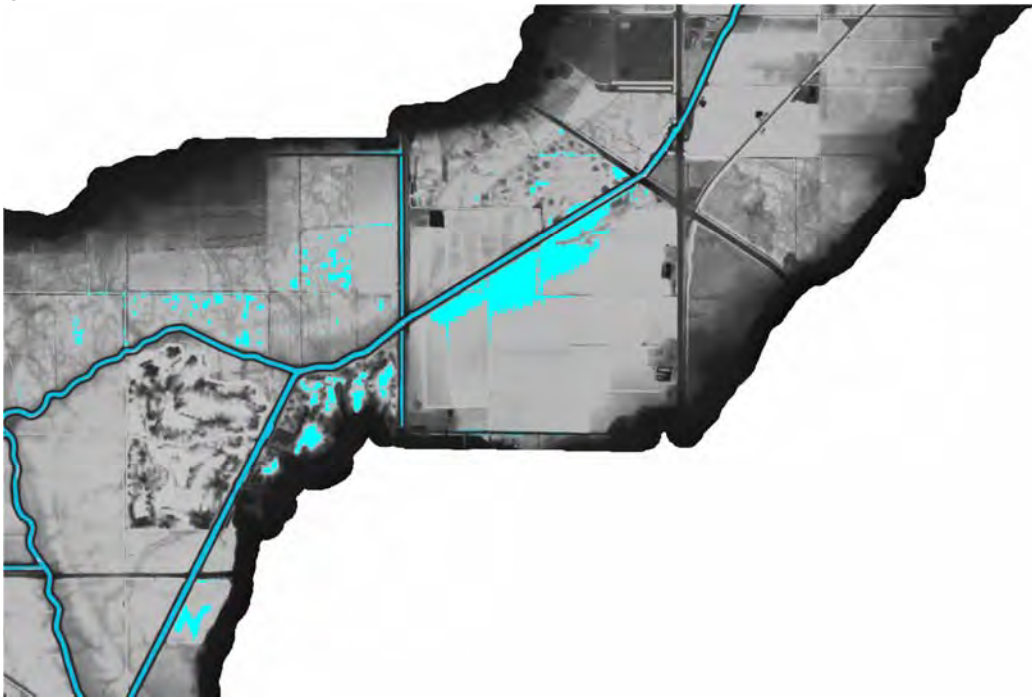
Water Surface Elevation, T = hh:mm:ss

Run 12



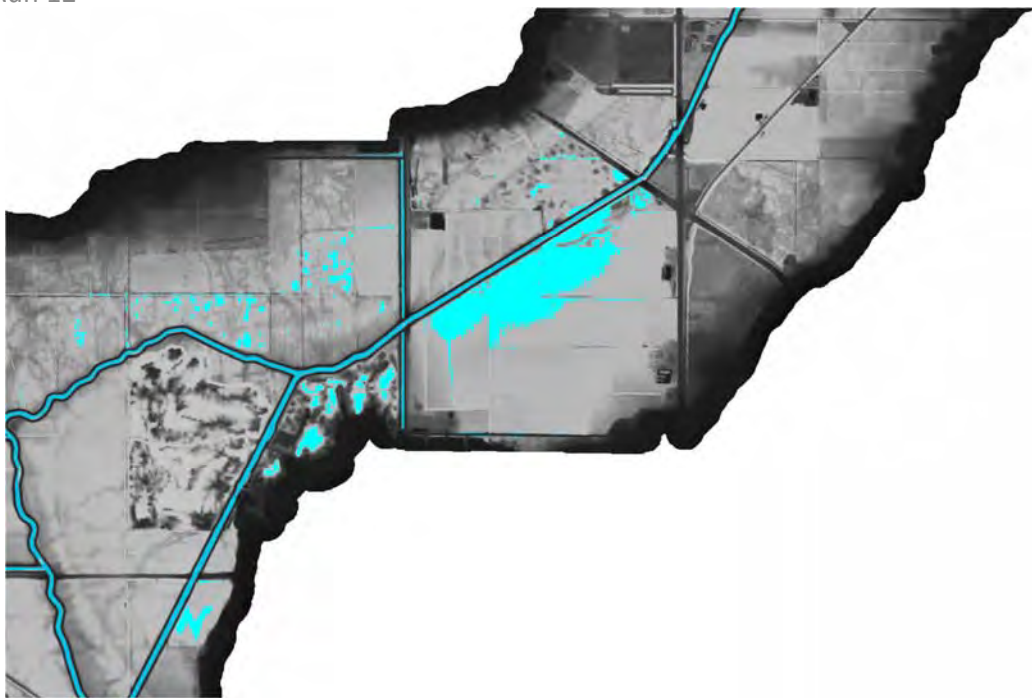
Water Surface Elevation, T = 00:15:00

Run 12



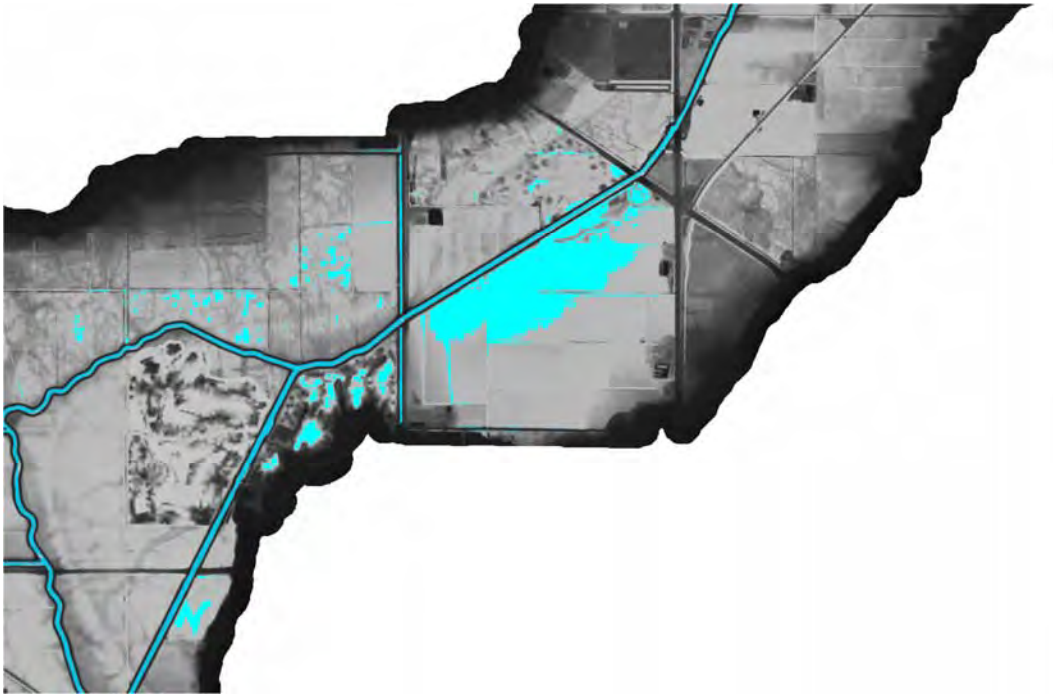
Water Surface Elevation, T = 00:30:00

Run 12



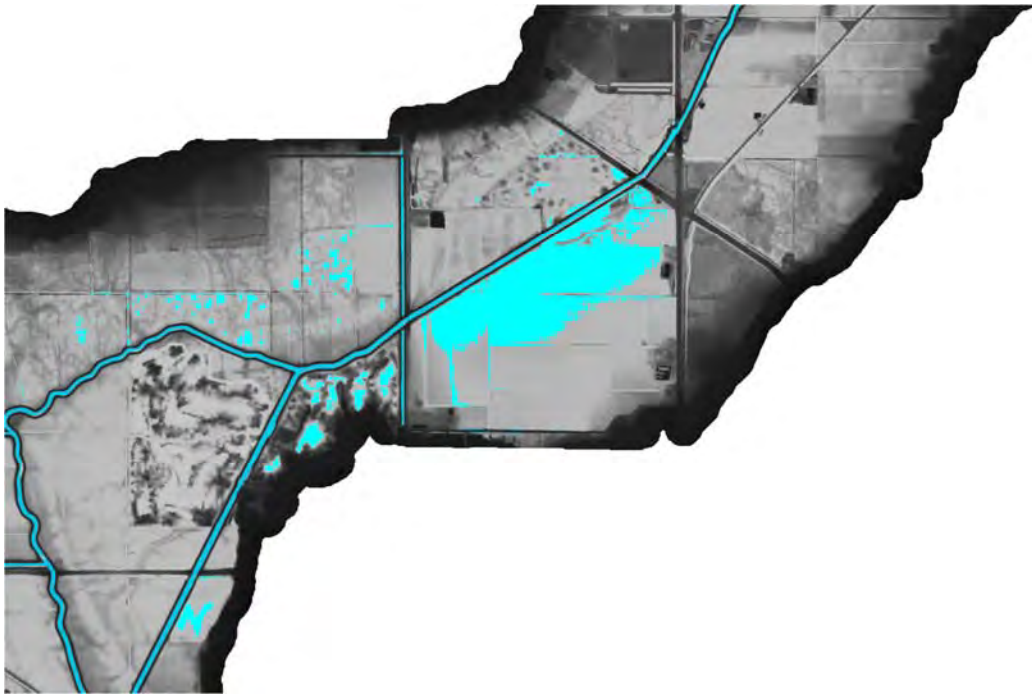
Water Surface Elevation, T = 00:45:00

Run 12



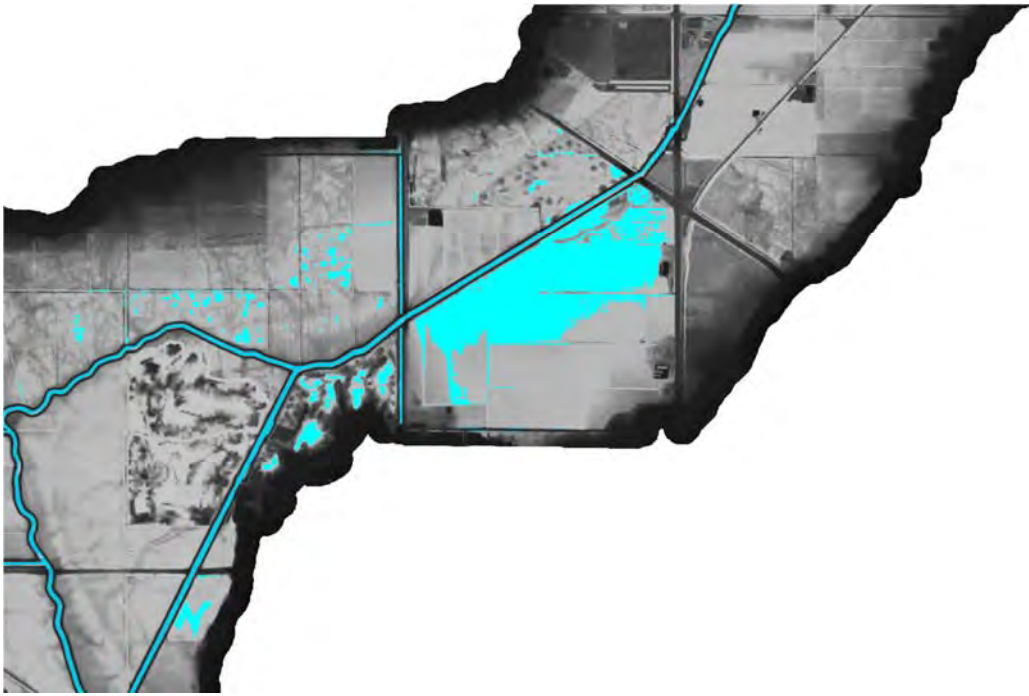
Water Surface Elevation, T = 01:00:00

Run 12



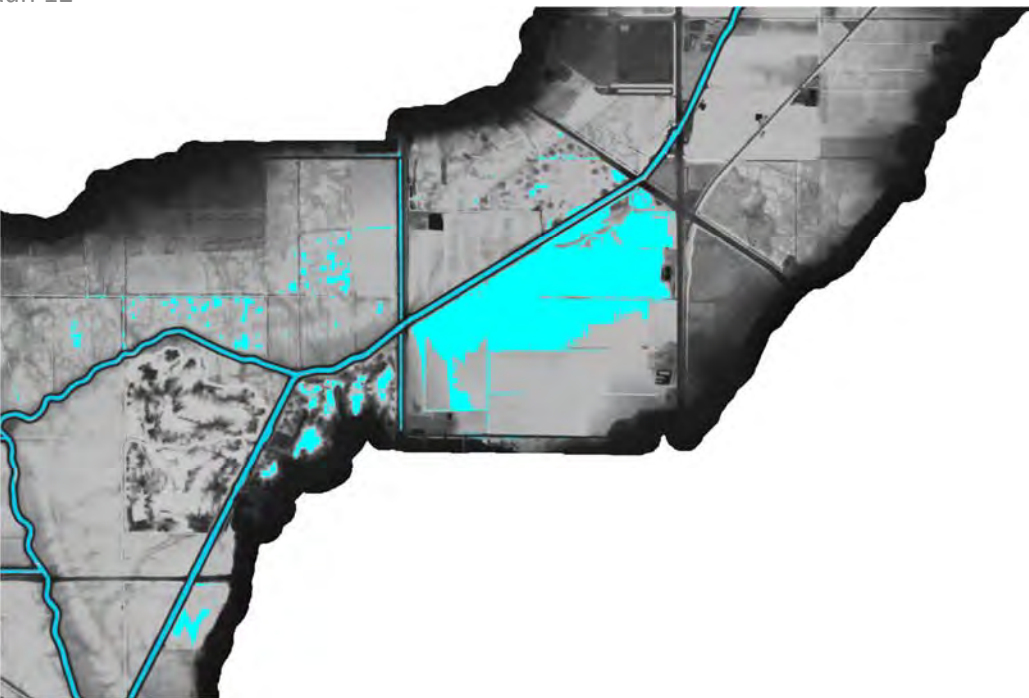
Water Surface Elevation, T = 01:15:00

Run 12



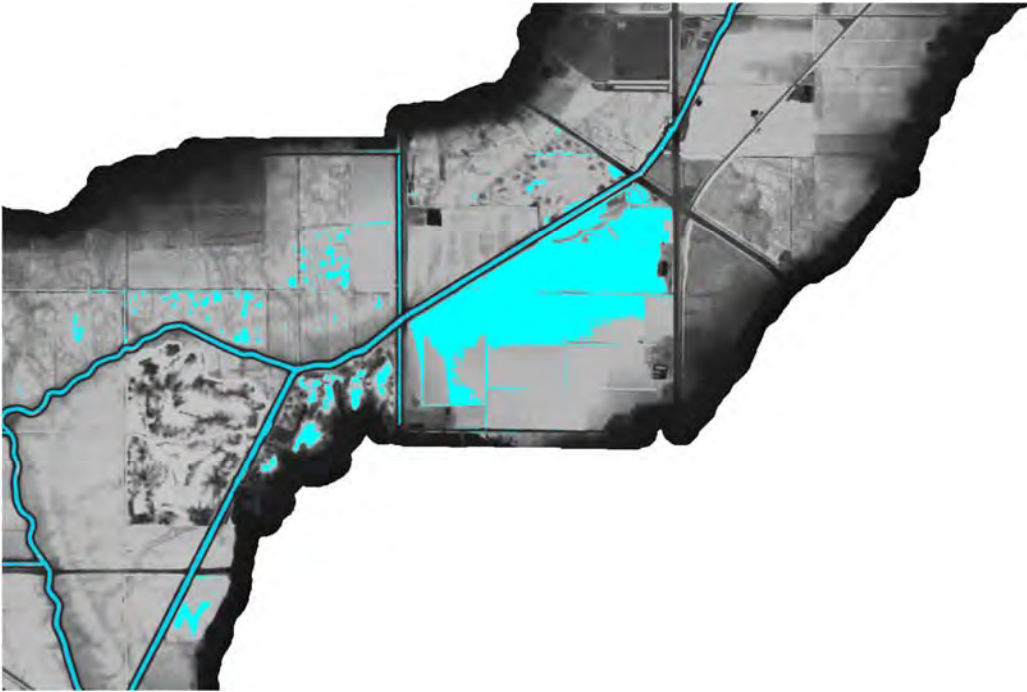
Water Surface Elevation, T = 01:30:00

Run 12



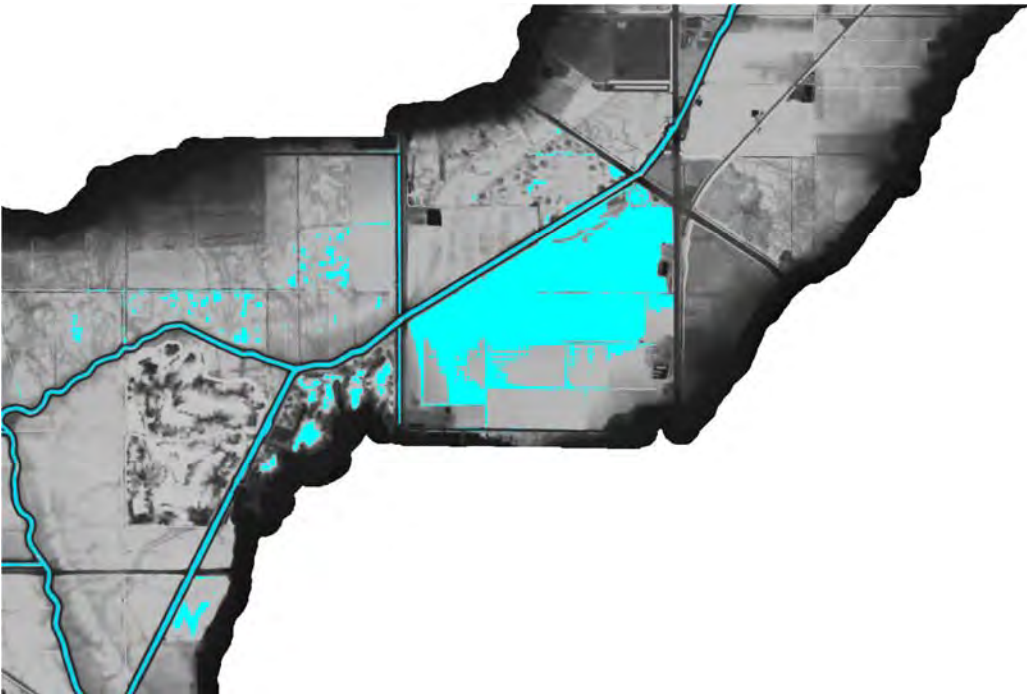
Water Surface Elevation, T = 01:45:00

Run 12



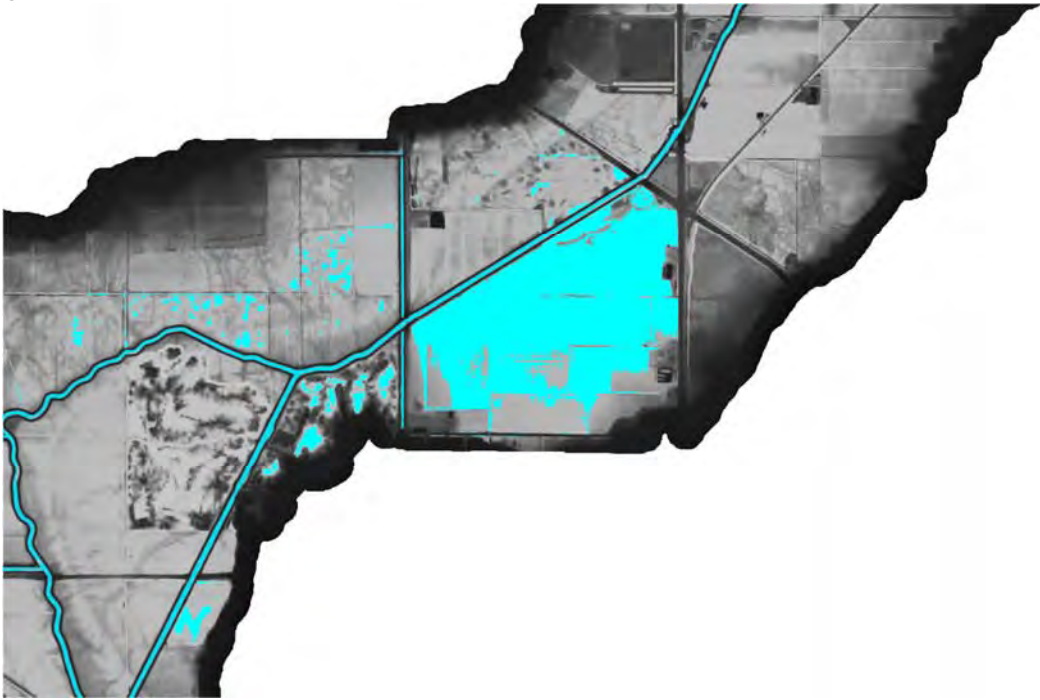
Water Surface Elevation, T = 02:00:00

Run 12



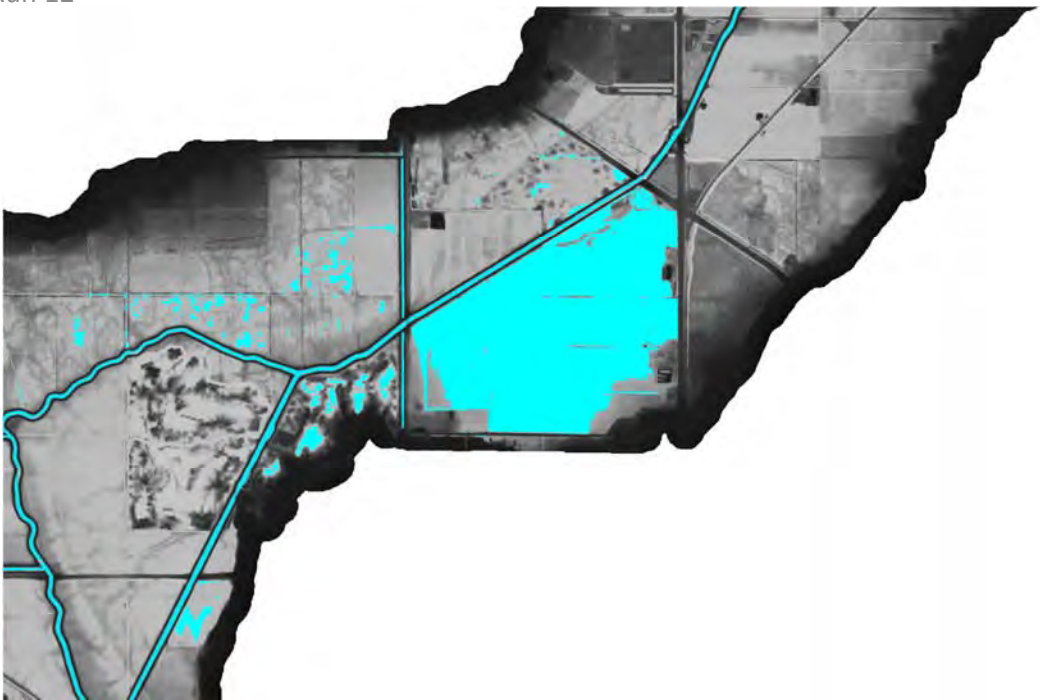
Water Surface Elevation, T = 03:00:00

Run 12



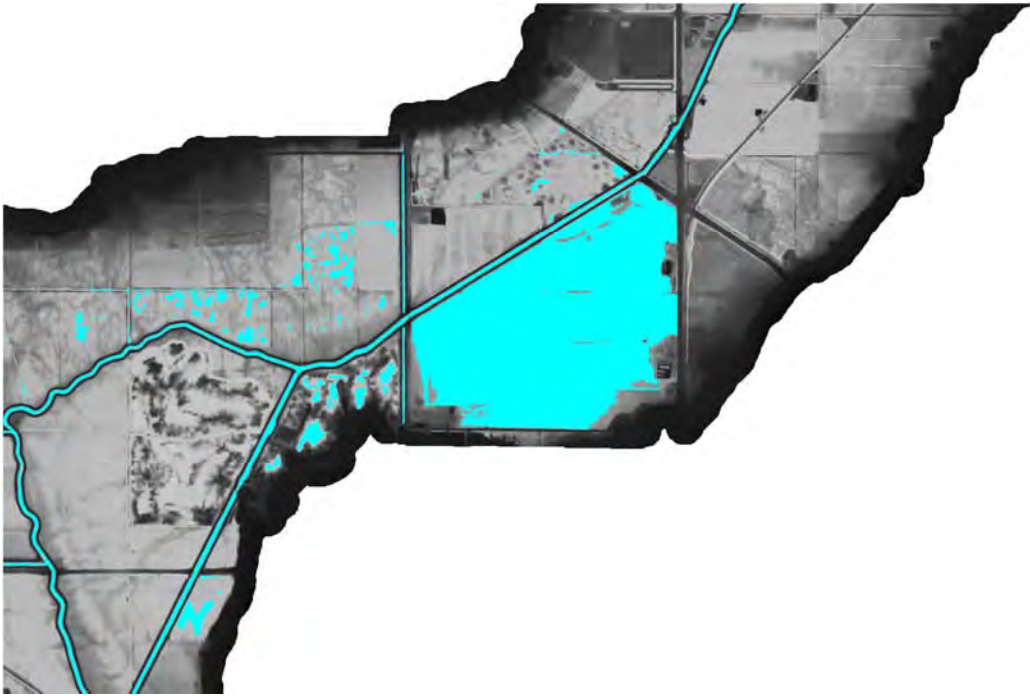
Water Surface Elevation, T = 04:00:00

Run 12



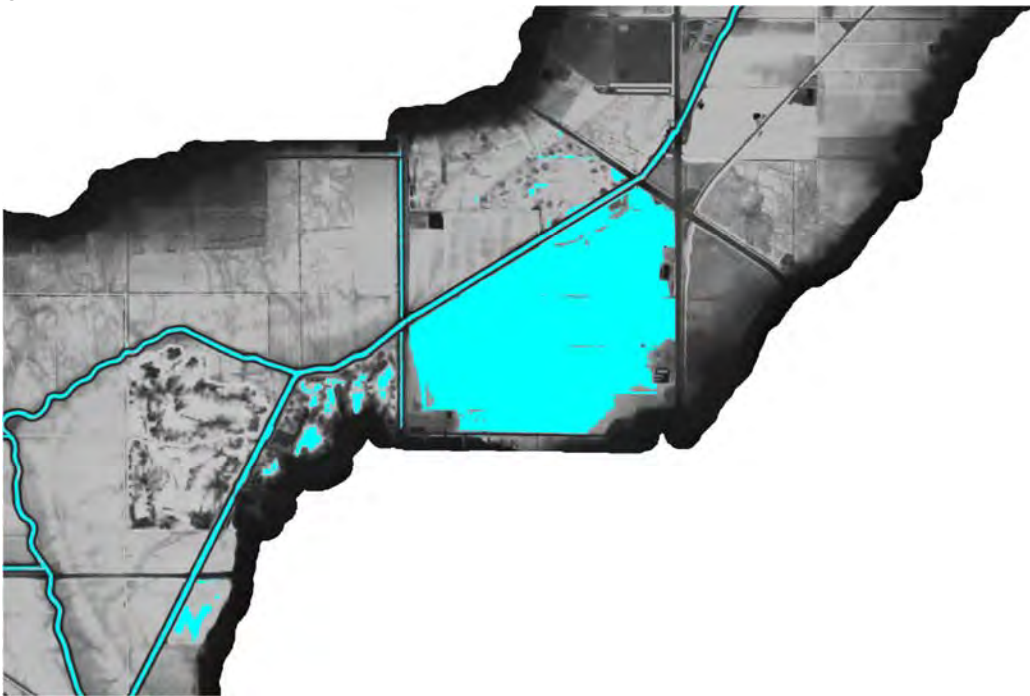
Water Surface Elevation, T = 06:00:00

Run 12



Water Surface Elevation, T = 10:00:00

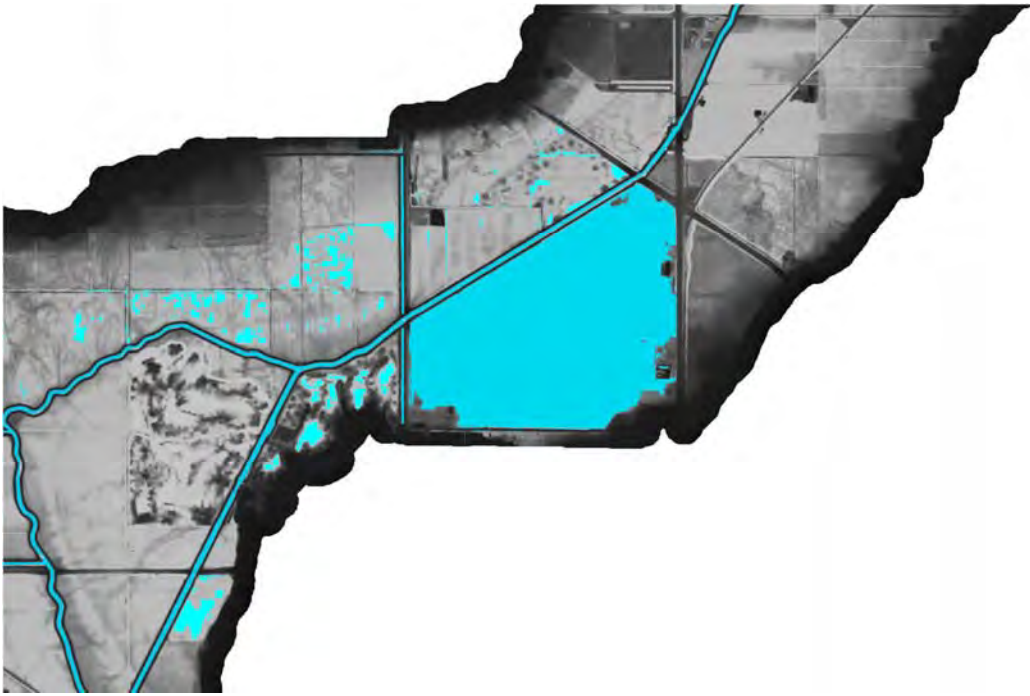
Run 12



Water Surface Elevation, T = 16:00:00



Run 12



Water Surface Elevation, T = 48:00:00